Inês Marina Soares Loureiro

Evaluation of *Trypanosoma brucei* asparagine synthetase A and ribose 5-phosphate isomerase B as potential drug targets

Tese do 3º Ciclo de Estudos Conducente ao
Grau de Doutoramento em Ciências Farmacêuticas -
Microbiologia

Trabalho realizado sob a orientação de:

Professora Doutora Anabela Cordeiro-da-Silva (Professora Associada com Agregação da Faculdade de Farmácia da Universidade do Porto, Porto, Portugal)

Doutora Joana Tavares (Investigadora do Instituto de Biologia Celular e Molecular, Porto, Portugal)

Professor Doutor Nilanjan Roy (Director de Ashok & Rita Institute of Integrated Study & Research in Biotechnology and Allied Sciences, Gujarat, India)

Janeiro, 2015

This work was performed at the Parasite Disease Group of the Institute for Molecular and Cell Biology (IBMC, Porto, Portugal) in collaboration with the Protein Crystallography Group of the IBMC, and mRNA turnover in trypanosomes Group of the Zentrum für Molekulare Biologie der Universität Heidelberg (ZMBH, Heidelberg, Germany). The author has received financial support though an individual Doctoral fellowship credited br the Foundation for Science and Technology (FCT, Portugal) with the reference SFRH/BD/64528/2009. The experimental research performed in this work has received financial support from FEDER funds through the Operational Competitiveness Program – COMPETE and by National Funds through FCT under the project PEst-C/SAU/LA0002/2011. The research leading to these results has also received funding from the European Community's Seventh Framework Programme under grant agreement No.602773 (Project KINDReD; Kinetoplastid Drug Development: strengthening the preclinical pipeline; HEALTH-F3-2013-602773). The COST Actions CM0801 "New drugs for neglected diseases" and CM1307 "Targeted chemotherapy towards diseases caused by endoparasites" and TRICONT project under ERA-NET New INDIGO have also contributed for this work.

Author's declaration

Under the terms of the "Decreto-lei nº 216/92, de 13 de Outubro", is hereby declared that the author afforded a major contribution to the conceptual design and technical execution of the work, interpretation of the results and manuscript preparation of the published articles included in this dissertation.

Under the terms of the "Decreto-lei nº 216/92, de 13 de Outubro", is hereby declared that the following original articles/communications were prepared in the scope of this dissertation.

SCIENTIFIC PUBLICATIONS

Articles in international peer-reviewed journals

In the scope of this dissertation

Loureiro I, Faria J, Clayton C, Macedo-Ribeiro S, Santarém N, Roy N, Santarém N, Cordeiro-da-Silva A*, Tavares J* (2015) Ribose 5-Phosphate Isomerase B Knockdown Compromises *Trypanosoma brucei* Bloodstream Form Infectivity. PLoS Negl Trop Dis 9(1): e3430. doi:10.1371/journal.pntd.0003430;

Loureiro I, Faria J, Clayton C, Ribeiro SM, Roy N, Santarém N, Tavares J*, Cordeiro-da-Silva A* (2013) Knockdown of Asparagine Synthetase A Renders *Trypanosoma brucei* Auxotrophic to Asparagine. PLoS Negl Trop Dis 7(12): e2578. doi:10.1371/journal.pntd.0002578.

Publications outside the scope of the thesis

Moreira D*, Santarém N*, **Loureiro I**, Tavares J, Silva AM, Amorim AM, Ouaissi A, Cordeiro-da-Silva A, Silvestre R. Impact of continuous axenic cultivation in *Leishmania infantum* virulence. PLoS Negl Trop Dis. 2012 Jan 24;

Neves BM, Silvestre R, Resende M, Ouaissi A, Cunha J, Tavares J, **Loureiro I**, Santarém N, Silva AM, Lopes MC, Cruz MT, Cordeiro da Silva A. Activation of Phosphatidylinositol 3-Kinase/Akt and Impairment of Nuclear Factor-{kappa}B. Molecular Mechanisms Behind the Arrested Maturation/Activation State of *Leishmania infantum*-Infected Dendritic Cells. Am J Pathol. 2010 Oct 29;

Hoskins C, Ouaissi M, Lima SC, Cheng WP, **Loureirio I**, Mas E, Lombardo D, Cordeiro-da-Silva A, Ouaissi A, Kong Thoo Lin P. In Vitro and In Vivo Anticancer Activity of a Novel Nano-sized Formulation Based on Self-assembling Polymers Against Pancreatic Cancer. Pharm Res. 2010 Sep 25;

Tavares J, Ouaissi A, Kong Thoo Lin P, **Loureiro I**, Kaur S, Roy N, Cordeiro-da-Silva A. Bisnaphthalimidopropyl derivatives as inhibitors of *Leishmania* SIR2 related protein 1. ChemMedChem. 2010 Jan 4.

*- The authors contributed equally to the work

COMMUNICATIONS

Oral communications

"Asparagine synthetase A and Ribose 5-phosphate isomerase B: novel potential drug targets against trypanosomatids" in IPATIMUP seminars, 28/05/13, at IPATIMUP (Porto);

"Asparagine synthetase A and Ribose 5-phosphate isomerase B: novel potential drug targets against trypanosomatids" in PhD training seminars, 05/12/12, at IBMC (Porto);

"Ribose 5-phosphate isomerase B and Asparagine synthetase A: novel potencial drug targets against trypanosomatid diseases" in Workshop Antiparasitic and Antitumor drugs (*ERA–Net Meeting*), 08/09/11, at IBMC (Porto);

"Ribose 5-phosphate isomerase B and Asparagine synthetase A: novel potencial drug targets against trypanosomatid diseases" in Molecular Studies Seminar, 13/04/2011, at IBMC (Porto);

"Genetic tools for drug target discovery and validation in trypanosomatids" at Pharmacy Faculty, Porto University, 22/07/10.

Poster communications

Loureiro I, Faria J, Clayton C, Macedo-Ribeiro S, Roy N, Tavares J & Cordeiro-da-Siva A. "Ribose 5-phosphate isomerase B knockdown compromises *Trypanosoma brucei* bloodstream form infectivity" presented in I^3S Annual Meeting, 30-31st October of 2014, at the Hotel Axis Vermar, Póvoa do Varzim;

Loureiro I, Faria J, Clayton C, Macedo-Ribeiro S, Roy N, Tavares J & Cordeiro-da-Siva A. "Ribose 5-phosphate isomerase B knockdown compromises *Trypanosoma brucei* bloodstream form infectivity" presented in British Society for Parasitology Spring Meeting, 6th to 9th April of 2014, at Cambridge University;

Loureiro I, Faria J, Clayton C, Macedo-Ribeiro S, Roy N, Santarém N, Tavares J & Cordeiro-da-Siva A. "Functional characterization of asparagine synthetase A in trypanosomes" presented in EMBO YOUNG SCIENTISTS FORUM 2013, 15-16th July at IMM, Lisbon;

Loureiro I, Faria J, Clayton C, Macedo-Ribeiro S, Roy N, Santarém N, Tavares J and Cordeiro-da-Siva A. "Knockdown of Asparagine synthetase A renders *Trypanosoma brucei* auxotrophic to asparagine" presented in 2013 British Society for Parasitology Spring Meeting, 8-11th April of 2013, at Bristol University;

Loureiro I, Faria J, Tavares J, Roy N, Cordeiro da Silva A. "Ribose 5-phosphate isomerase B in Trypanosomatids" presented in I^3S Scientific Retreat, 10th to 11th May of 2012, at Hotel Axis Vermar, Póvoa de Varzim;

Loureiro I, Tavares J, Roy N, Cordeiro da Silva A. “Ribose 5-phosphate isomerase B a potential therapeutic target against trypanosomatid diseases” presented in EU India S&T Cooperation Days 2011 - Biotechnology and Health, 1st and 2nd December of 2011, in Vienna, Austria;

Loureiro I, Tavares J, Roy N, Cordeiro da Silva A. “Ribose 5-phosphate isomerase B a potential therapeutic target against trypanosomatid diseases”, presented in Workshop Antiparasitic and Antitumor drugs (*ERA–Net Meeting*), 8-9th September of 2011, at IBMC, Porto (judged *“*best poster”);

Loureiro I, Tavares J, Cordeiro da Silva A. “Ribose 5-phosphate isomerase B, a common and potential target against parasitic infections by members of the Trypanosomatidae family” presented in I3S Scientific Retreat, 5-6th May of 2011, at Hotel Axis Vermar, Póvoa de Varzim.

Acknowledgments

First, I would like to acknowledge my supervisors, Professor Anabela Cordeiro da Silva, Dr. Joana Tavares and Professor Nilanjan Roy in making this thesis possible. To Professor Anabela Cordeiro da Silva for accepting me in her lab and for had trusted me to carry out this work. I thank you for your advices, guidance and support. To Dr. Joana Tavares, for her patience, guidance and her sincere support during periods of difficulty. While I can never thank her enough, I want her to know that I am truly grateful for her supervision during my thesis. She is an example of leadership, as she continuously demonstrates excellent qualities as a teacher and researcher.

I would like also to specially acknowledge the collaboration with Dr. Christine Clayton from Zentrum für Molekulare Biologie der Universität Heidelberg (ZMBH). The opportunity of developing my research project at her laboratory was crucial for the success of my work. I thank the guidance and the sharing of knowledge. I also thank all members of this group, specially Claudia Helbig, Diana Inchaustegui and Dorothea Droll for the welcome and for contributing to a pleasant environment during my stay in Heidelberg.

I would like to thank our collaborator Professor Sandra Macedo Ribeiro from Protein Crystallography group at IBMC for their scientific contributions and valuable help to our projects. I am grateful for your sympathy.

I would like to officially thank to FCT for financing me with a personal scientific grant and to IBMC for making available all the facilities that made my work possible.

A word of acknowledgment to all members of the Parasite Disease group (including those who have left): Marisa Teixeira, Tânia Meireles, Diana Moreira, Lúcia Teixeira, Ricardo Silvestre, Vasco Rodrigues, Pedro Cecílio, Marta Silva, Daniela Barros, Patrícia Varela, Luís Gaspar, Joana Cunha, Jorge Queiroz, Mariana Resende, Sofia Costa Lima, Célia Amorim, Begoña Pérez, Sandra Pereira, Helena Ribeiro, Catarina Baptista, Joana Teixeira, Nuno Graça, David Costa, Carla Lima, Joana Maciel, Daniela Ribeiro, Inês Mesquita, Cátia Silva, Renata Costa, Fernando Augusto Vilela and João Duarte. A special thanks to Nuno Santarém (thank you for your help in molecular biology field in the beginning of my thesis), to Susana Sousa and Ana Luísa Robalo (thank you for

your friendship) and to D. Rosa Mendes (thanks for the help and readiness in providing lab equipment and ensuring good laboratory conditions).

One of the most positive aspects during this period was to have had Joana Faria as bench mate, which in the end became a great friend. I sincerely wish you all the success in the world and one day maybe we return working together. Thanks for everything.

I make an apology to my closest friends if at some point I was remiss in our friendship. I know you guys forgive me :p.

I also would like to express my endless thanks to my parents and grand-parents whose love, belief and understanding have always and will always be there for me. I thank you all for supporting me from the very beginning of my studies. Mom and dad, you are a reference to me. Diogo my little brother, of course I have not forgotten you!

Tó, I want to thank you for your unconditional support, for your optimism, for helping me to relativize the worst moments, and most importantly, for reminding me that there are other important things in life besides work. Thanks for believing in me.

O meu sincero obrigada a todos…

Abstract

Human African trypanosomiasis (HAT) is a parasitic disease confined to the African continent and is caused by the protozoan *Trypanosoma brucei* (*T. brucei*). If left untreated is usually fatal. Disease control is dependent on drug therapy, since no human vaccine is available. However, the existing therapy is far from satisfactory owing to the emergence of resistances, toxicity and its limited efficacy. Thus, the necessity to discover and validate new drug targets with the ultimate goal of discovery new compounds is explicit. In the search for parasite specific enzymes and using an *in silico* comparative genomic approach we have selected, asparagine synthetase A (AS-A) and ribose 5-phosphate isomerase B (RpiB) to undergo biochemical and genetic studies. This thesis presents the first functional characterization of these two potential therapeutic targets against *T. brucei*.

Classically AS-A enzymes, using ammonia as nitrogen donor, convert aspartate into asparagine, which is important for nitrogen homeostasis and protein biosynthesis. *T. brucei* AS-A (*Tb*AS-A) activity was proved through biochemical approaches, having the peculiarity of using both ammonia and glutamine as nitrogen donors. RNA interference (RNAi) against *Tb*AS-A did not affect bloodstream parasites growth either *in vitro* or *in vivo*. However, growth was significantly impaired only when *Tb*AS-A RNAi-induced parasites were grown in limiting asparagine environments suggesting that RNAi-mediated down-regulation of AS-A rendered *T. brucei* auxotrophic to asparagine. In conclusion, AS-A is important for bloodstream parasites growth and infectivity only when asparagine is limiting and therefore is unlikely to be suitable as a drug target since under normal physiological conditions, asparagine is available in the blood.

RpiB belongs to the non-oxidative branch of the pentose phosphate pathway, being involved in the interconversion of ribulose 5-phosphate (Ru5P) and ribose 5-phosphate (R5P). The latter is a critical metabolite precursor for *de novo* synthesis of nucleotides and nucleic acids. *In vitro* biochemical studies confirmed *T. brucei* ribose 5-phosphate isomerase (*Tb*RpiB) activity. *Tb*RpiB knockdown by RNAi affected *in vitro* growth of bloodstream forms, but more importantly parasites infectivity since mice infected with induced RNAi clones exhibited lower parasitaemia and a prolonged survival in comparison to mice infected with control parasites. Moreover, several attempts to generate double knockouts were unsuccessful. *Tb*RpiB emerges as a new potential therapeutic target against HAT that deserves further studies.

Keywords: *T. brucei* bloodstream forms, asparagine synthetase A, ribose 5-phosphate isomerase B, enzyme kinetics and RNAi

Resumo

A tripanossomíase Africana é uma doença parasitária confinada ao continente Africano sendo causada pelo protozoário *Trypanosoma brucei* (*T. brucei*). Se não for tratada é geralmente fatal. O controlo da doença está dependente de quimioterapia, uma vez que não existe nenhuma vacina. No entanto, a terapia existente está longe de ser satisfatória devido ao aparecimento de resistências, toxicidade e eficácia limitada. Assim, a necessidade de descobrir e validar novos alvos terapêuticos, com o objetivo de identificar novos compostos, é explícita. Na procura de enzimas específicas do parasita e utilizando uma abordagem comparativa do genoma foram escolhidas entre outras duas proteínas, nomeadamente asparagina sintetase A (AS-A) e ribose 5-fosfato isomerase B (RpiB) para estudos bioquímicos e genéticos. Esta tese apresenta a primeira caracterização funcional destes dois potenciais alvos terapêuticos contra o *T. brucei*.

Classicamente as enzimas AS-A utilizam amônia como dador de azoto na conversão de aspartato em asparagina, sendo este aminoácido importante para a homeostasia do azoto e para a síntese proteica. A atividade da AS-A de *T. brucei* (*Tb*AS-A) foi comprovada através de estudos bioquímicos e revelou a particularidade de usar tanto amônia como glutamina como dadores de azoto. RNA de interferência (RNAi) contra *Tb*AS-A não afetou, nem *in vitro* nem *in vivo*, o crescimento das formas sanguíneas do parasita. No entanto, o crescimento foi significativamente comprometido quando os parasitas com RNAi induzido contra *Tb*AS-A foram submetidos a condições limitantes em asparagina, sugerindo que a subexpressão da AS-A pelo RNAi torna o parasita auxotrófico para a asparagina. Em conclusão, a AS-A é importante para o crescimento e infetividade das formas sanguíneas do parasita apenas quando a quantidade de asparagina extracelular é limitada, e por isso é improvável que venha a constituir um alvo terapêutico uma vez que em condições fisiológicas a asparagina está disponível no sangue.

A RpiB pertence ao ramo não oxidativo da via das pentoses fosfato, estando envolvida na interconversão de ribulose 5-fosfato (Ru5P) e ribose 5-fosfato (R5P). Este último é um importante precursor metabólico para a síntese *de novo* de nucleótidos e ácidos nucleicos. Estudos bioquímicos *in vitro* confirmaram a atividade enzimática da ribose 5-fosfato isomerase de *T. brucei* (*Tb*RpiB). A diminuição dos níveis de expressão desta enzima por RNAi afetou o crescimento das formas sanguíneas *in vitro*, mas mais importante afetou a infetividade dos parasitas, uma vez que ratinhos infetados com clones RNAi induzidos apresentaram parasitemias menores e sobrevivências

prolongadas quando comparados com ratinhos infetados com parasitas controlo. Além disso, diversas tentativas para obtenção de duplos knockout não foram bem sucedidas. *Tb*RpiB surge como um novo potencial alvo terapêutico contra a trypanossomíase Africana, que merece ser alvo de mais estudos.

Palavras-chave: Formas sanguíneas de *T. brucei*, asparagina sintetase A, ribose 5-fosfato isomerase B, cinética enzimática e RNAi

Table of contents

Index of figures

Figure 22. Alternative pathways to generate R5P bypassing the oxidative PPP. (A) The path from D-ribose to R5P in *E. coli*. RbsA a cytoplasmic ATPase, RbsC a membrane permease, RbsB the periplasmic ribose binding protein, RbsD is a mutarotase, that converts the pyranose form of ribose to the furanose form, and RbsK or ribokinase binds specifically the α-furanose form of ribose for its phosphorylation leading to R5P. (B) Ribose-1P synthesis within *Plasmodium* infected erythrocytes. (C) The light-independent reactions of carbon fixation in the Calvin cycle share enzymes and reactions with the PPP and glycolysis. (D) Yeast Shb17 feeds carbon into the non-oxidative PPP. The cells were fed with glucose labelled selectively at the 6-position with carbon 13 (6-^{13}C-glucose). Flux through Shb17 into S7P can be measured using [6-$^{13}C_1$]-glucose. [6-$^{13}C_1$]-glucose leads to [7-$^{13}C_1$]-S7P when S7P is made via the oxidative PPP or the non-oxidative PPP. However, when S7P is produced from SBP via Shb17, a fraction of the S7P pool is doubly labelled: [1,7-$^{13}C_2$]-S7P. This labelling pattern was observed preferentially when yeast cells were grown on media that decreased their need for NADPH (e.g. by providing them with lipids). Abbreviations: G6P, glucose-6-phosphate; F6P, frutose 6-phosphate; FBA or *fba*, fructose biphosphate aldolase; GAPDH, glyceraldehyde 3-phosphate dehydrogenase; GAP, glyceraldehyde 3-phosphate; DHAP, dihydroxyacetone phosphate; TPI, triosephosphate isomerase; E4P, erythrose 4-phosphate; SBP, sedoheptulose-1,7-bisphosphate; S7P, sedoheptulose 7-phosphate; *shb17* or SH17BPase, sedoheptulose-1,7-bisphosphatase; *tal*, transaldolase; TK or *tkl*, transketolase; RPI or *rki1*, ribose phosphate isomerase; *rpe1*, ribose phosphate epimerase; R5P, ribose 5-phosphate; Ru5P, ribulose 5-phosphate; Xu5P, xylulose 5-phosphate; PGK, phosphoglycerate kinase; PRK, phosphoribulokinase; hPNP, human purine nucleoside phosphorylase; PfPNP, purine nucleoside phosphorylase; Ino, inosine; Hxt, hypoxanthine; RBC, red blood cell; PV, parasitophorous vacuole; MTI, methylthioinosine. [Adapted from (Clasquin et al, 2011; Downie et al, 2008; Roos, 2007; Stincone et al, 2014)]. ……..... 162

Abbreviations list

4-PEH	4-phospho-D-erythronohydroxamic acid
6-PGDH	6-phosphogluconate dehydrogenase
6-PGL	6-phosphogluconolactonase
aaMϕ	alternatively activated macrophage
AAR	amino acid response
AAT	amino acid transporter
AdoMet	S-adenosylmethionine
AdoMetDC	S-adenosylmethionine decarboxylase
AGO1	first Argonaute protein
FBA or ALD	fructose-1,6-bisphosphate aldolase
AMP	adenosine monophosphate
AP-1	adaptin complex-1
APC	antigen-presenting cells
APOL1	trypanolytic toxin apolipoprotein L1
AS	asparagine synthetase
AS-A	asparagine synthetase type A
AS-B	asparagine synthetase type B
ATF4	transcription factor 4
ATP	adenosine triphosphate
BARP	brucei alanine rich protein
caMϕ	classically activated macrophage
cAMP	cyclic adenosine monophosphate
CARE	C/EBP-ATF response element
CATT	card agglutination test for trypanosomiasis
CD	cluster of differentiation
cKO	conditional knockout
CNS	central nervous system
CSF	cerebrospinal fluid
CTC	capillary centrifugation technique
dcAdoMet	decarboxylated *S*-adenosylmethionine
DCL	dicer-like enzyme
DHEA	dehydroepiandrosterone
DHFR	dihydrofolate reductase

DHFR-TS	dihydrofolate reductase-thymidylate synthase
dKO	double knockout
DNA	deoxyribonucleic acid
dsRNA	double-stranded RNA
dTMP	deoxythymidine-monophosphate
dUMP	deoxyuridine-monophosphate
EA	epiandrosterone
E. coli	*Escherichia coli*
eIF2α	eukaryotic initiation factor-2 alpha
ELISA	enzyme-linked immunosorbent assay
EP	glutamate-proline repeats
EMP70	endosomal membrane protein 70
ENO	enolase
ESAG	expression site-associated gene
G6PDH	glucose-6-phosphate dehydrogenase
GAPDH	glyceraldehyde-3-phosphate dehydrogenase
GCN2	general control non-depressible 2
GIP-sVSG	glycosylinositolphosphate attached to the shed VSG
GLP-1	golgi/lysosomal protein-1
GPEET	glycine-proline-glutamate-glutamate-threonine repeats
GPI	glycosylphosphatidylinositol
GPI–PLC	glycosylphosphatidylinositol-phospholipase C
GR	glutathione reductase
GSH	glutathione
HAPT1	high affinity pentamidine transporter
HAT	human African trypanosomiasis
H_4F	tetrahydrofolate
H_2F	dihydrofolate
HK	hexokinase
H_2O_2	hydrogen peroxide
HPR	haptoglobin-related protein
IFN-γ	interferon-gamma
Ig	immunoglobulin
IL	interleukin
ISG	invariant surface glycoprotein

LAPT1	low affinity pentamidine transporter
LDL	low-density lipoproteins
L. donovani	*Leishmania donovani*
M1	macrophage type 1
M2	macrophage type 2
mAECT	miniature anion-exchange centrifugation technique
MAPK	mitogen-activated protein kinase
MCA4	metacaspase 4
MFST	major facilitator superfamily transporter
mRNA	messenger RNA
mTOR	mammalian target of rapamycin
M. tuberculosis	*Mycobacterium tuberculosis*
$NADP^+$	nicotinamide adenine dinucleotide phosphate
NADPH	nicotinamide adenine dinucleotide phosphate hydrogen
NF-kB	nuclear factor kappa-B
NECT	nifurtimox/eflornithine combination therapy
NK	natural killer
NMR	nuclear magnetic resonance
ODC	ornithine decarboxylase
P2	purine transporter 2
p67	major lysosomal glycoprotein
PADs	proteins associated with differentiation
PAMPs	pathogen-associated molecular patterns
PARP	procyclic acidic repetitive protein
PDB	Protein Data Bank
PCR	polymerase chain reaction
PERK	protein kinase RNA-like endoplasmic reticulum kinase
PFK	phosphofructokinase
PGAM	phosphoglycerate mutase
PKA	protein kinase A
PKR	protein kinase R
PPP	pentose phosphate pathway
PTR1	pteridine reductase 1
PYK or PGK	phosphoglycerate kinase
RISC	RNAi-induced silencing complex

RIT-seq	RNA interference target sequencing
RNA	ribonucleic acid
RNAi	RNA interference
RNI	reactive nitrogen intermediates
ROS	reactive oxygen species
R5P	ribose 5-phosphate
RPE	ribose 5-phosphate epimerase
Rpi	ribose 5-phosphate isomerase
RpiA	ribose 5-phosphate isomerase type A
RpiB	ribose 5-phosphate isomerase type B
Ru5P	ribulose 5-phosphate
SIF	stumpy induction factor
siRNA	small interfering RNA
SIT	sterile insect technique
sKO	single knockout
Spd	spermidine
SpdSyn	spermidine synthase
SpmSyn	spermine synthase
SRA	serum resistance-associated
ssRNA	single-stranded RNA
STAT1	signal transducers and activators of transcription 1
TAL	transaldolase
T. brucei	*Trypanosoma brucei*
T. b. brucei	*Trypanosoma brucei brucei*
T. b. gambiense	*Trypanosoma brucei gambiense*
T. b. rhodesiense	*Trypanosoma brucei rhodesiense*
TbHpHbR	*T. brucei* haptoglobin–haemoglobin receptor
TBVs	transmission blocking vaccines
TCA	tricarboxylic acid cycle
T. cruzi	*Trypanosoma cruzi*
Tet	tetracycline
TGF-β	transforming growth factor beta
TgsGP	*T. b. gambiense*-specific glycoprotein
Th cells	T helper cells
Tip-DC	TNF/iNOS-producing dendritic cell

TK or TKL	transketolase
TLF1	trypanosome lytic factor 1
TLF2	trypanosome lytic factor 2
TLR	toll-like receptor
TPI	triosephosphate isomerase
TR or TryR	trypanothione reductase
Trx	thioredoxin
TrxR	thioredoxin reductase
TryS	trypanothione synthetase
TS	thymidylate synthase
$T(SH)_2$	trypanothione
VSG	variant surface glycoprotein
WBC	white blood cells
WHO	World Health Organization

Chapter I

Human African trypanosomiasis

1 Historical perspective

Human African trypanosomiasis (HAT), also known as African sleeping sickness, is considered a third world country disease, circumscribed throughout time in the African continent. HAT was first described around the 14th century, but only in the beginning of the 20th century, the population was decimated in Africa central areas (Louis & Simarro, 2005; Steverding, 2008). It was at that moment, when Sir David Bruce (Figure 1A) discovered *Trypanosoma brucei (T. brucei)* as the cause of Nagana disease (1895), and provided conclusive evidence that is transmitted by tsetse flies (1903) (Bruce, 1895; Cox, 2004; De Raadt, 1976). As a result local authorities set up control measures, which progressively controlled the disease, reaching a minimum of 4,435 cases declared in Africa, in 1964. Later on, the presence of social instability, conflicts and insecurity led the disease to resurge in the 1980s and 1990s, reaching an estimated 300,000 cases. Control programs were reinforced and, as a result, since 2000, the number of notified cases has been decreased, falling since 2009 to below 10,000 new reported cases (Figure 1B) (Franco et al, 2014). Besides the fact that human cases have been declining in the past decade, the lack of full-scale screening programs associated with poor diagnostic tools (Wastling & Welburn, 2011), results in under-diagnosed and under-reported cases, which is likely to be at least threefold higher than the measured value (Phillips, 2012).

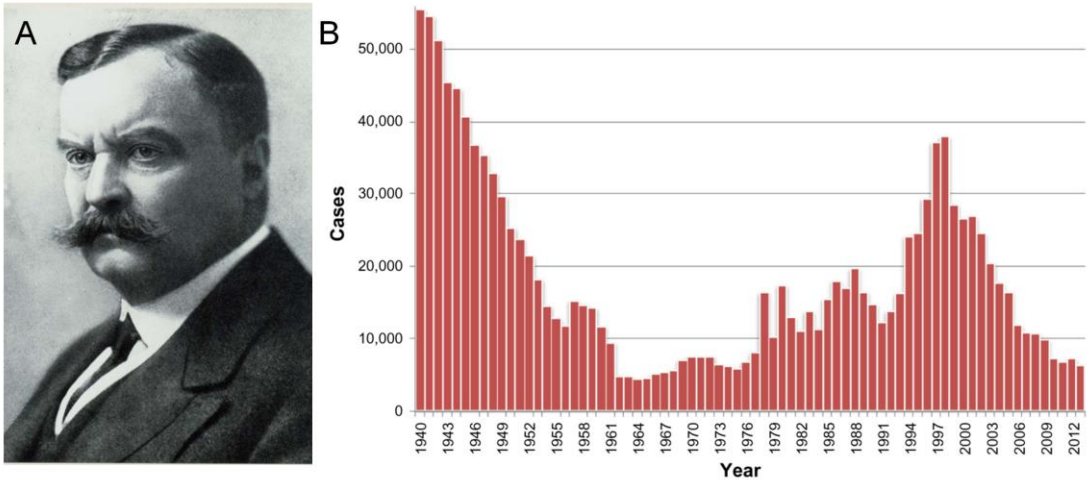

Figure 1. HAT historical features. (A) Sir David Bruce. (B) Total number of new cases of HAT reported to the World Health Organization (WHO), 1940-2013. [Adapted from (Franco et al, 2014; Steverding, 2008)].

2 Causative agent

The causative agent of HAT, *T. brucei*, is an extracellular flagellated protozoan parasite, which belongs to the Family Trypanosomatidae within the Order Kinetoplastida (Figure 2A). There are three *T. brucei* subspecies, of which two are human infective, *Trypanosoma brucei gambiense* (*T. b. gambiense*) and *Trypanosoma brucei rhodesiense* (*T. b. rhodesiense*), and one non-infective for humans, *Trypanosoma brucei brucei* (*T. b. brucei)*, therefore routinely used in laboratories (Barrett et al, 2003). Different to humans, Nagana disease in animals result from infections with *T. congolense*, *T. vivax* or *T. b. brucei* (Steverding, 2008). Gambiense HAT, caused by *T. b. gambiense*, is considered an anthroponotic disease with a minor role for animal reservoirs, while rhodesiense HAT, induced by *T. b. rhodesiense*, is regard as a zoonotic disease, affecting mainly animals; humans are only accidental hosts. Unlike *T. b. rhodesiense* infections, in which non-human vertebrates are the primary reservoir and represent <5% of HAT cases, *T. b. gambiense* infections represent >95% of the cases (Solano et al, 2013). *T. b. gambiense* is classed in two different groups, that differ in genotype and phenotype (Balmer et al, 2011; Gibson, 1986; Gibson et al, 1980; Hide et al, 1990; Jamonneau et al, 2004; Mehlitz et al, 1982; Paindavoine et al, 1986; Tait et al, 1984; Truc & Tibayrenc, 1993; Zillmann et al, 1984). Group one ("true-gambiense") is less genetically diverse and displays low virulence in rodents, while group two ("non-gambiense") is more genetically diverse, able to infect rodents and shows biological and genetic similarities to *T. b. rhodesiense* and *T. b. brucei* (Gibson, 1986).

3 Geographical distribution

T. b. gambiense infections are found in West and Central sub-Saharan Africa, while *T. b. rhodesiense* causes infections in East sub-Saharan Africa (Figure 2B) (Barrett et al, 2003). The geographic barrier of the two forms of the disease coincides with the Rift Valley, with *T. b. gambiense and T. b. rhodesiense* present at the west and east side of the valley, respectively (Franco et al, 2014). Although some patients are occasionally reported outside Africa (Lejon et al, 2003a), 36 sub-Saharan African countries are still considered the endemic areas for HAT. Currently, there are approximately 300 gambiense HAT foci within 24 sub-Saharan Africa countries (Angola, Benin, Burkina Faso, Cameroon, Chad, Central African Republic, Congo, Côte d'Ivoire, Democratic Republic of the Congo, Equatorial Guinea, Gabon, Gambia, Ghana, Guinea, Guinea Bissau, Liberia,

Mali, Niger, Nigeria, Senegal, Sierra Leone, South Sudan, Togo, Uganda), and around 60 foci of rhodesiense HAT in 13 African countries (Botswana, Burundi, Ethiopia, Kenya, Malawi, Mozambique, Namibia, Rwanda, Swaziland, Tanzania, Uganda, Zambia, and Zimbabwe) (Franco et al, 2014). Curiously, Uganda is the only country where the two subspecies co-exist, however there still remains a spatial separation between the subspecies, mainly due to the different climatic and vegetative conditions required by the two species (Berrang-Ford et al, 2010).

4 Vector

HAT is transmitted through the bite of an infected tsetse fly (genus *Glossina*) (Figure 2C). Similarly to *T. brucei* subspecies, the different tsetse flies species are related to different habitats. Thirty-one species have been described, however in nature, infections are carried almost exclusively by *Glossina palpalis* (for *T. b. gambiense*; distributed in the Atlantic coast from Senegal to Angola*), Glossina morsitans* (for *T. b. rhodesiense;* located mainly in East Africa) and *Glossina fuscipes* (for both; present in central Africa from Cameroon and Congo to the Rift Valley) (Franco et al, 2014). Both female and male flies are able to transmit the parasite, however some tsetse flies species are refractory to infection by specific trypanosome species, and even when susceptible, the parasites population can suffer a pronounced reduction in the insect midgut. These facts point the tsetse fly as a low competent vector (Molyneux, 1980). In general tsetse flies are able to adapt to host availability, odor stimuli and visual factors are probably involved in the finding of a suitable host (Tirados et al, 2011). Sexual reproduction in insect salivary glands is not obligatory in trypanosomes but is an important event yielding the possibility of genetic exchange and rapid transmission of important characteristics, such as drug resistance and virulence (Peacock et al, 2014; Peacock et al, 2011). Genetic exchange is relatively frequent in *T. b. rhodesiense*, but it is more sporadic in *T. b. gambiense* (Koffi et al, 2007).

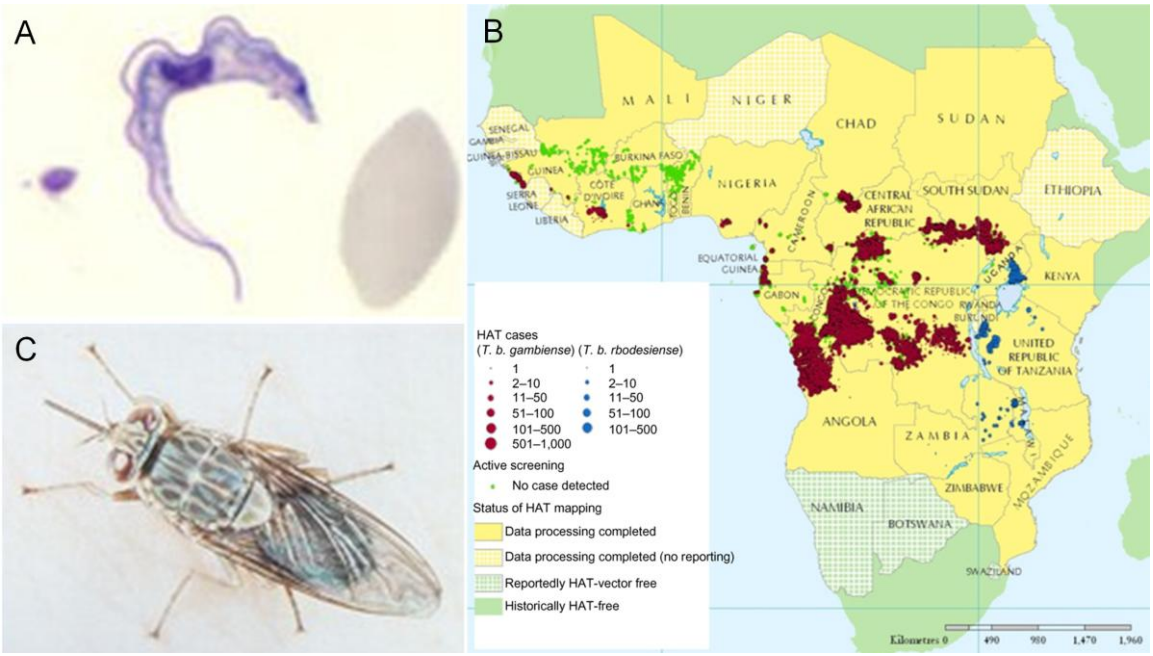

Figure 2. HAT causative agent, vector and geographical distribution. (A) *T. brucei* in thin blood smears stained with Giemsa. (B) Geographic distribution of HAT; cases reported from 2000–2009. (C) A close up of a tsetse fly. [Adapted from (CDC, 2012; Franco et al, 2014)].

5 Clinical features

Clinically HAT evolves in two stages. The first, known as early or haemato-lymphatic stage, is defined by the presence of parasites in the lymph and blood systems, while the second, named as late or meningo-encephalitic stage, is characterized by the active invasion of trypanosomes in the central nervous system (CNS). The duration of the first stage depends on the *T. brucei* subspecies involved and varies from few weeks to months in acute *T. b. rhodesiense* infections, or from several months to years in chronic *T. b. gambiense* infections (Franco et al, 2014). After inoculation, the formation of a trypanosomal chancre, characterized by local erythema, oedema, heat, tenderness and a lack of any suppuration (Malvy & Chappuis, 2011), arises in about 50% of rhodesiense infections, but is rarely formed in gambiense infections. After 3–4 weeks, the chancre usually heals with overlying desquamation, sometimes with altered pigmentation (Barrett et al, 2003). In *T. b. rhodesiense* infections, which present poor demarcation between stages, pancarditis with congestive heart failure, pericardial effusion, and pulmonary oedema can cause fatalities. In contrast, *T. b. gambiense* infections show a more insidious development (Barrett et al, 2003). The first stage is characterised by general

malaise, intermittent fever, headache, severe pruritus with scratching, skin lesions, mobile or rubbery lymphadenopathies, oedema of the face and extremities and, to a lesser extent, myocarditis, splenomegaly or hepatomegaly (Malvy & Chappuis, 2011). In the second stage general malaise worsens, headaches become more severe and patient sleep pattern is altered. Later this stage culminates in coma, severe organ failure and eventually death (Barrett et al, 2003).

6 Parasite life cycle

Inoculation in the mammalian host of infective metacyclic forms, covered with a variant surface glycoprotein (VSG), begins with the bite of an infected tsetse fly vector (Figure 3A). Actually, *T. brucei* parasites change the composition of the insect saliva, in a way that increases vector-host contact frequency and enhances the probability of parasite transmission (Van Den Abbeele et al, 2010). Once inside the host, the metacyclic trypanosomes proliferate at the site of inoculation and then transform into slender forms, as they are carried by the draining lymph nodes to the bloodstream, where they replicate by binary fission (Vickerman, 1985). When parasitaemia in the host increases, the long slender trypomastigotes (proliferative forms) release a soluble factor, stumpy induction factor (SIF), via a quorum sensing mechanism, which triggers their differentiation into short stumpy forms (non-proliferative forms) (Mony et al, 2014). Stumpy forms, which do not divide, are crucial for limiting parasitaemia within the host, and subsequent differentiation to procyclic forms when taken into a tsetse vector. During vector blood meal, stumpy forms expressing VSG are ingested and primed to differentiate into procyclic forms. This priming appears to involve production of a group of carboxylate transporters called proteins associated with differentiation (PADs) (Dean et al, 2009). The temperature, pH and citrate or cisaconitate in the tsetse midgut seem to trigger for stumpy to procyclic differentiation (Brun & Schonenberger, 1981; Czichos et al, 1986). Procyclic trypanosomes express a surface coat of procyclic acidic repetitive protein (PARP or procyclins) which includes two classes of procyclins, EP (a form of procyclin rich in Glu-Pro repeats) and GPEET (a form of procyclin rich in Glu-Pro-Glu-Glu-Thr repeats) which are developmentally regulated (Vassella et al, 2004). After multiplication in vector midgut, procyclic trypomastigotes initiate a migration (Figure 3B), that takes them through the peritrophic matrix, along the foregut to the proventriculus, and from there onwards through the mouthparts, salivary ducts and finally into the salivary gland (Langousis & Hill, 2014). In the proventriculus, procyclic trypomastigotes undergo extensive restructuring, coupled

to an asymmetric division to produce one long epimastigote and one short epimastigote (Rotureau et al, 2012; Van Den Abbeele et al, 1999). The short epimastigote, coated with alanine rich protein (BARP), attaches to epithelial cells following arrival in the salivary gland (Urwyler et al, 2007). In order to complete the life cycle, the attached epimastigotes undergo a final transformation into free metacyclic trypomastigotes, along with the acquisition of the VSG coat, for evasion in the mammalian host (Langousis & Hill, 2014).

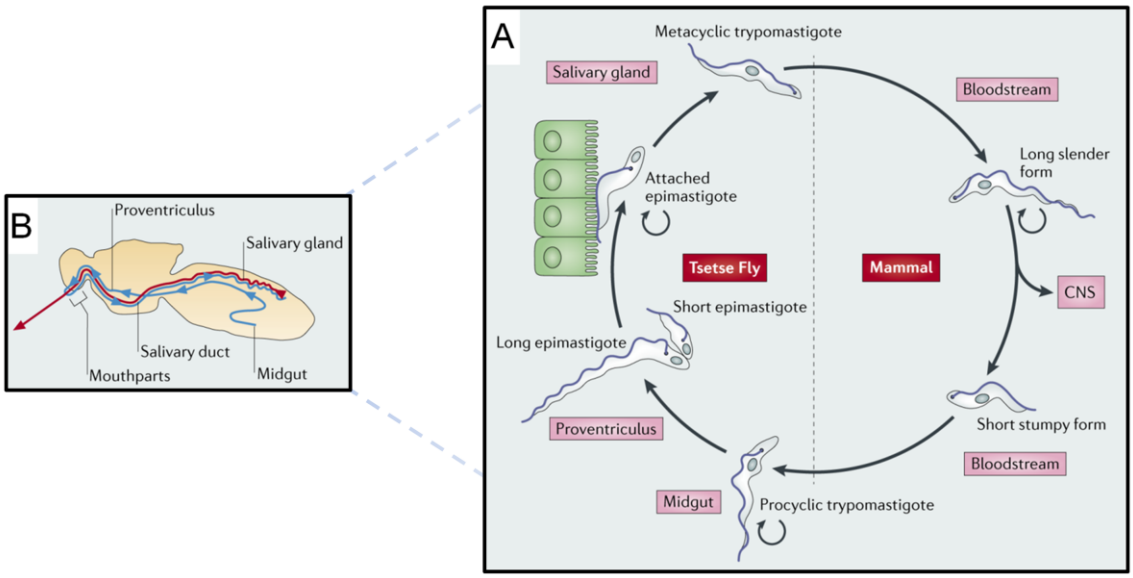

Figure 3. *T. brucei* life cycle. (A) Parasite development stages within in the mammalian host and the tsetse fly. The dividing forms that replicate via binary fission are indicated with a circular arrow. (B) Migration route of procyclic trypomastigotes within the insect. The blue line depicts the route taken from the midgut to the salivary gland and the red line indicates the route from the salivary gland to the mouthparts. [Adapted from (Langousis & Hill, 2014)].

7 Parasite-host interactions

7.1 Parasite evasion strategies

7.1.1 Variant surface glycoproteins and antigenic variation

VSGs constitute an important virulence factor throughout the mammalian infectious cycle, providing the parasite a wall of protection against the host innate and specific immune effectors (Ziegelbauer & Overath, 1993). Consistent with this, is the fact

that these molecules are codified by developmentally regulated *VSGs* genes, being silenced in the tsetse fly midgut but activated in the tsetse fly salivary glands and in the mammalian host (Tetley et al, 1987). VSGs cover the entire parasite surface. This thick coat represent up to 20% of total cell protein and is made of around 10^7 identical molecules with a conserved core structure of glycosylphosphatidylinositol (GPI) anchored in the cell membrane and, an exposed proteinacious antigen (Cross, 1975; Vickerman & Luckins, 1969) (Figure 4A). During an infection, there may be several million trypanosomes within a host, but all express one VSG at the time. The mammal immune cells recognize this VSG as foreign molecule and start to produce antibodies, which subsequently clear the parasites bearing these VSGs. However, as a result of antigenic variation from either homologous gene recombination target to the unique active VSG expression site, or of transcriptional switching between the different VSG expression sites (Horn, 2014), one "new" VSG offspring appears with a novel VSG coat, thus avoiding the specific immune response (Dempsey & Mansfield, 1983). The immune system seems not to be the trigger of this molecular mechanism once trypanosomes act in the same way even in the absence of a host defense (Doyle et al, 1980). It is currently thought that up to 30% of an African trypanosome genome is dedicated to archiving up to 2000 *VSG* genes and gene-fragments (Horn, 2014). Therefore *T. brucei* possess a broad palette of possible surfaces, which allow the cycle, of defeating one major trypanosome population with concomitant re-establishment of infection by an unrecognized sub-population, to continue "forever" leading to the host exhaustion (Baral, 2010). VSG switching operates at a frequency of approximately 1 switch/10^5 cells per population doubling (Horn, 2014). Coat exchange appears to be primarily by dilution during rapidly cell division, since recycling off and back via coupled endocytosis/exocytosis occurs slower (Seyfang et al, 1990). Antibodies clearance, low titer at least, through VSG recycling involves endocytosis at the flagellar pocket (Field & Carrington, 2009) and a vigorous directional cell motility mediated by the flagellum (Figure 4B) (Engstler et al, 2007). The shedding of VSG by GPI–phospholipase C (GPI–PLC) in dying cells is considered another strategy to deceived the immune system (Sunter et al, 2013; Webb et al, 1997) that will be further discussed.

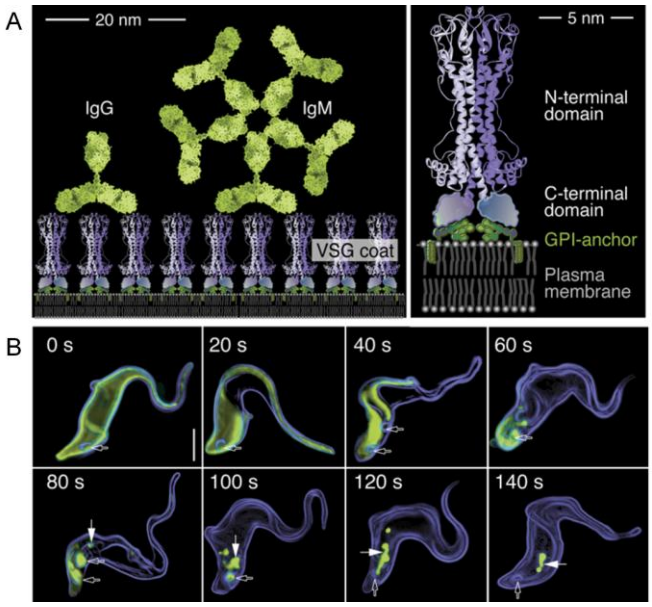

Figure 4. VSGs and host antibodies interaction. (A) Schematic representation of IgG and IgM molecules bound to the trypanosome VSG coat (left). VSG homodimer (monomers in light blue and purple) attached to the plasma membrane via GPI anchors (right). (B) Visualization of antibody removal. Cells were surface labelled with blue-fluorescent AMCA-sulfo-NHS and incubated VSG-specific IgG. Anti-VSG antibodies were detected with species-specific Alexa Fluor 488-conjugated antibodies (green). Open arrows indicate the position of the flagellar pocket, and filled arrows point the lysosome. Scale bar, 3 μm. [Adapted from (Engstler et al, 2007)].

7.1.2 Resistance to trypanosome lytic factors

Humans and some primates posses in their blood two distinct serum complexes, called trypanosome lytic factor 1 (TLF1) and 2 (TLF2), both containing the haptoglobin-related protein (HPR) and the trypanolytic toxin apolipoprotein L1 (APOL1) (Raper et al, 1999). These factors after being endocytosed are capable of killing *T. b. brucei*, but not *T. b. gambiense* or *T. b. rhodesiense* subspecies (Hajduk et al, 1989; Rifkin, 1978; Uzureau et al, 2013). TLF1 uptake occurs after HPR join haemoglobin which are then recognized by a specific TLF receptor, the haptoglobin–haemoglobin receptor (TbHpHbR) (Drain et al, 2001; Vanhollebeke et al, 2008; Widener et al, 2007), however the mechanism of TLF2 binding and uptake remains unknown, the hypothesis is that TLF2 enters via nonspecific binding to VSGs, and that the recycling of the VSG coat through the flagellar pocket would enable its uptake into the endocytic compartment (Pays et al, 2014).

In the case of *T. b. brucei* infections, the APOL1 acts once the entire TLF particle is endocytosed and trafficked to the lysosome. During endolysosomal acidification, APOL1 binds to the lysosome membrane compromising membrane integrity through anionic-pore formation (Figure 5A) (Perez-Morga et al, 2005). The loss of osmoregulation triggers lysosomal swelling, but the specific molecular mechanisms behind parasite death are still unknown (Pays et al, 2014).

Contrary to *T. b. brucei*, *T. b. rhodesiense* and *T. b. gambiense* overcome TLFs through distinct resistant mechanisms (Pays et al, 2014). *T. b. gambiense* constitutively resists normal human serum, whereas *T. b. rhodesiense* is intrinsically sensitive except when inoculated in human blood, where it acquires the ability to resist (Gibson, 2007; Xong et al, 1998). In *T. b. rhodesiense* the resistant mechanism involves a transcriptional switching of a given VSG expression site to the expression of an expression site-associated gene (*ESAG*), known as serum resistance-associated (*SRA*) (Xong et al, 1998). This gene encodes a truncated VSG, which is a GPI-anchored dimer without surface-exposed antigenic loops (Campillo & Carrington, 2003), targeted to the endolysosomal system (Stephens & Hajduk, 2011), where it binds to APOL1 (Vanhamme et al, 2003). This interaction neutralizes APOL1, probably by preventing its membrane insertion thus enabling its degradation by lysosomal cysteine proteases (Pays et al, 2014) (Figure 5B). *T. b. gambiense* uses a multifactorial defence mechanism (Figure 5C). The VSG-derived *T. b. gambiense*-specific glycoprotein (TgsGP) plays an essential role by preventing the insertion of APOL1 into endolysosomal membranes though membrane lipid stiffening. Two additional process, which both reduce intracellular levels of APOL1 are necessary for full resistance; a L210S substitution in TbHpHbR reduces APOL1 uptake, and a lower pH in early endosomes could enable faster cysteine protease-mediated digestion of APOL1 (Capewell et al, 2013; Uzureau et al, 2013).

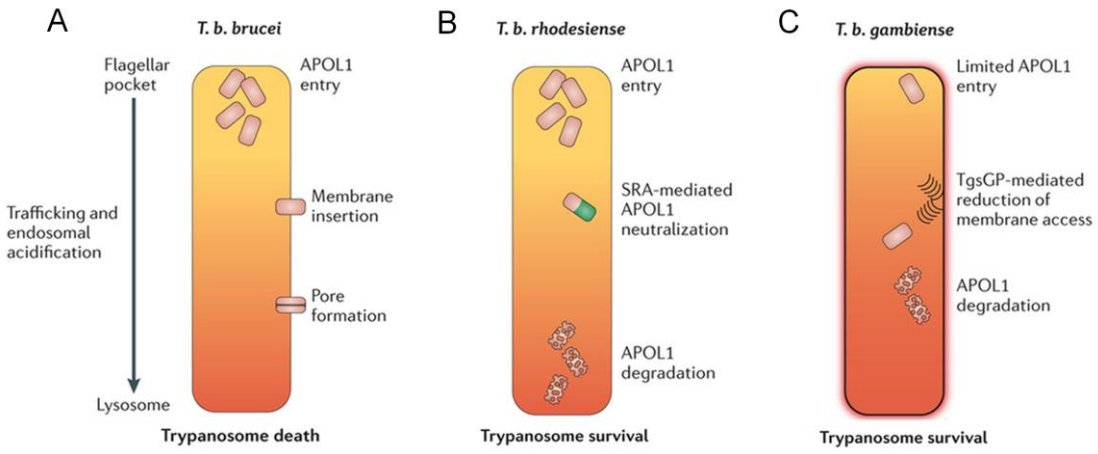

Figure 5. *T. brucei* response to APOL1. APOL1 trafficking in *T. b. brucei* (A), *T. b. rhodesiense* (B) *and T. b. gambiense* (C) subspecies. The boxes represent the endocytic compartments, and a colour gradient illustrates the endosomal acidification that takes place between the beginning (flagellar pocket), and the end (lysosome) of the endocytic pathway. [Adapted from (Pays et al, 2014)].

7.1.3 Flagellar proteins

Flagellar proteins such, GPI–PLC, calflagins, metacaspase 4 (MCA4) and ESAG4, are determinants of host–parasite interactions that modulate virulence in the mammalian host (Figure 6A and B).

GPI–PLC is a metacyclic and bloodstream form specific enzyme, located to an external linear array along the flagellum and involved on VSG release. When GPI-anchored VSG flows across the membrane into the flagellar pocket, the activated enzyme cleaves the anchor and releases VSG from the membrane, thus glycosylinositolphosphate attached to the shed VSG (GIP-sVSG) become free in blood and tissues (Hanrahan et al, 2009; Sunter et al, 2013; Webb et al, 1994). This enzyme was shown to be required for full virulence of pleomorphic trypanosomes, once mice infected with GPI–PLC null mutants have extended survival and control better the parasitaemia than the ones infected with control parasites (Webb et al, 1997).

How calflagins and MCA4 promote pathogenesis remains to be determined. Calflagins are Ca^{2+}-binding proteins that are upregulated in bloodstream parasites and localize to lipid rafts of the flagellar membrane (Emmer et al, 2009). *In vitro* these proteins are dispensable for proliferation, motility and surface-antibody clearance. However, *in vivo* studies showed attenuated parasitaemia and prolonged survival in mice infected with calflagins RNAi-induced monomorphic trypanosomes (Emmer et al, 2010). Also monomorphic *T. brucei* MCA4 null mutants have a striking virulence phenotype, that is characterized by multiple parasitaemic waves and prolonged host survival. MCA4 is a secreted and flagellum-localized bloodstream form specific protein (Proto et al, 2011).

ESAG4 is also a bloodstream form specific protein localized in the flagellar membrane. It is a member of adenylyl cyclases family that catalyze the conversion of adenosine triphosphate (ATP) to cyclic adenosine monophosphate (cAMP) (Paindavoine et al, 1992). The expression of a dominant-negative ESAG4 mutant showed not to be important *in vitro*, however the reduction in 50% of the cellular cAMP levels, leads to a reduced parasitaemia and prolonged mice survival. The proposed model is that, lysed or

phagocytosed parasites by host macrophages activate ESAG4 to produce cAMP, which, in turn, activates host protein kinase A (PKA) to inhibit trypanotoxic tumour necrosis factor alpha (TNF-α) synthesis, which enables trypanosomes to resist the early host innate immune response (Salmon et al, 2012).

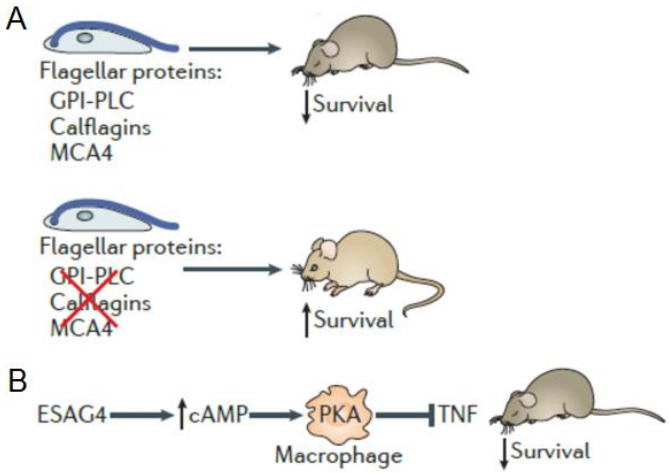

Figure 6. Flagellar proteins contribute to virulence in the mammalian host. (A) Loss of GPI–PLC, calflagins and MCA4 decreases parasite virulence and increases mice's life span. (B) *T. brucei* ESAG4 interferes with host early innate immune response promoting parasite virulence and decreases mouse survival. ESAG4 produces cAMP, which activates PKA in host macrophages to inhibit TNF-α synthesis. [Adapted from (Langousis & Hill, 2014)].

7.2 Host defense

Most of what is known to date on the host immune response directed against HAT, is derived from experimental studies, carried out in mice models, which can misrepresent what is going on in human hosts. The immune response behind this disease is still equivocal, being dependent on the parasite strain, the mouse model, or both. Moreover the major immune effectors found in one organ, might be inefficient elsewhere. To worsen, the variability of the host genotype has a huge impact on the progression of the disease, hindering the scientific community from obtaining definitive answers.

7.2.1 Innate immune response

Concerning the innate immune response against *T. brucei*, is generally accepted that trypanolytic complexes (described above in detail), complement, natural killer cells

(NK) and antigen-presenting cells (APC; macrophages and dendritic cells) are the first line of defence (Figure 7).

Although antibody mediated binding of trypanosomes, and their uptake by phagocytes does occur in the absence of complement (Ngaira et al, 1983), the latter improves the efficacy of parasite and immune-complex removal (Stevens & Moulton, 1978; Takayanagi et al, 1987). Experimental evidences suggest that both, the classical and alternative pathways of complement are activated during trypanosomiasis (Pan et al, 2006; Russo et al, 1994), however the classical pathway seems to have a more important role (Devine et al, 1986; Ferrante & Allison, 1983; Musoke & Barbet, 1977). Trypanosomes possess mechanisms to control complement-mediated lysis (Musoke & Barbet, 1977; Sheppard et al, 1978). As mentioned above, the removal of immune complexes deposited on the parasite surface occurs mainly by a hydrodynamic force generated by the parasite motility that results in the transfer of the immune complexes to the posterior pole of the cell, in which they are endocytosed (Engstler et al, 2007). Moreover, in a lower extent these parasites seem also to escape complement-mediated lysis through the shedding of VSG-antibody complexes (Seyfang et al, 1990). The role of the mannan binding lectin pathway of complement activation during trypanosome infections was never addressed. This pathway may have some relevance considering that is triggered by serum lectins and ficolins binding to the mannose residues present in the trypanosomes VSG. Moreover, this pathway activation occurs in the absence of specific antibodies, and therefore may play a crucial role in parasite clearance during the early stage of infection (Namangala, 2012).

The direct cytotoxic role of activated NK cells remains controversial and poorly documented. In resistant mice, NK cells could be one of the sources of interferon-gamma (IFN-γ) that activate naïve macrophages (M) into macrophages type 1 (M1) (also known classically activated macrophages, caMϕ), resulting in a type-I response during early stage trypanosomiasis (Namangala et al, 2007). NK cells may indirectly, through the secretion of cytokines and chemokines, be involved in parasite control, rather than by a direct trypanolytic activity (Namangala, 2012).

Macrophages and dendritic cells play a central role in the immune response as professional APCs. This function includes internalization of pathogen-associated molecular patterns (PAMPs) from trypanosomes through phagocytosis, processing of parasite antigens in the acidic compartment of the endocytic pathway, and co-stimulation and presentation of the immunogenic trypanosome peptides to antigen-specific T helper cells (Th cells) in the context of major histocompatibility complex (MHC) Class II

molecules (Dagenais et al, 2009; Namangala et al, 2000a; Shi et al, 2007). In an early *T. brucei* infection, macrophages and dendritic cells display a "classical" or pro-inflammatory activation profile, which includes production of trypanocidal molecules [reactive oxygen species (ROS), reactive nitrogen intermediates (RNI), and TNF-α], pro-inflammatory cytokines [(interleukins IL-1, IL-6 and IL-12)], and changes in functional capacity (including increased expression of MHC II and co-stimulatory molecules for APC activity) (Barkhuizen et al, 2008; Coller et al, 2003; Dagenais et al, 2009; Harris et al, 2006; Leppert et al, 2007; Lopez et al, 2008; Magez et al, 2002; Magez et al, 1998; Paulnock & Coller, 2001). There is clear evidence that unmethylated CpG deoxyribonucleic acid (DNA), released from dead or dying trypanosomes, is recognized by the host innate immune system; this toll-like receptor (TLR)-9 ligand is capable of activating macrophages *in vitro* and *in vivo* (Harris et al, 2006). Nevertheless, GPI residues of the secreted VSG are the major contributors for activation of cells of the innate immune system (Magez et al, 1998; Paulnock & Coller, 2001; Tachado et al, 1997). The GIP-sVSG binds to the type A scavenger receptor on the cell membrane (Leppert et al, 2007), and then is internalized and processed, initiating a signalling cascade, including activation of nuclear factor kappa-B (NF-kB) and mitogen-activated protein kinase (MAPK) pathways, and the expression of pro-inflammatory genes (Coller et al, 2003; Coller & Paulnock, 2001; Leppert et al, 2007; Paulnock & Coller, 2001). An additional key component of macrophage and dendritic cell activation is IFN-γ. IFN-γ binds to IFN-γR, generates the formation and phosphorylation of signal transducers and activators of transcription 1 (STAT1) homodimers, activating downstream pro-inflammatory genes (Leppert et al, 2007). The relative timing of innate immune cells exposure to GIP-sVSG and to IFN-γ is critical for the ability of cells to become activated for APC functions and, for macrophages, to kill the parasites. If there is coincident exposure to significant levels of both IFN-γ and GIP-sVSG (that may occur in early infection with activated NK cells releasing IFN-γ in response to IL-12 (not yet confirmed experimentally) (Namangala, 2012), or later with IFN-γ derived from T cells during activation of the adaptive immune response), increasing cellular activation and transcription of pro-inflammatory genes occurs (Coller et al, 2003; Lopez et al, 2008), controlling early parasite growth within host tissues. However, if cells are exposed to GIP-sVSG prior to, or in the absence of sufficient levels of IFN-γ, STAT1 is not phosphorylated and the production of trypanocidal factors as well as APC functions are inhibited (Coller et al, 2003; Dagenais et al, 2009). These events likely occur as the infection progresses, when increasing numbers of parasites release GIP-sVSG prior to sufficient activation of new Th1-cell responses for the production of IFN-γ.

Therefore, the interplay and timing of parasite and host factors are critical for the control of the parasite burden in host tissues and for regulation of host immune responses. Nevertheless, during the early stage of infection, type I cytokine responses are observed in both susceptible and resistant mice.

7.2.2 Adaptive immune response

The process of innate resistance and acquired immunity are interdependent, in which some cells, like macrophages, play a dual role, as initiators of acquired responses and as effectors component of cell-mediated immunity (Figure 7). As mentioned before, innate immune cells establish an initial pro-inflammatory response at the early stage of the infection. These pro-inflammatory molecules activate lymphocytes, mainly cluster of differentiation (CD)8^+ T cells, to produce IFN-γ, the principal activator of caMϕ. IFN-γ production could also result from a direct interaction between parasite products such as the trypanosome-derived lymphocyte-triggering factor with $CD8^+$ T cells (Olsson et al, 1991). Even though, the current paradigm is that VSG-specific Th1 cells and IFN-γ regulate the core component of host resistance for this parasitic infection (Schleifer et al, 1993). Immature $CD4^+$ T lymphocytes are activated by exposure to antigen-MHC II complexes on APCs to produce a highly polarized type 1 cytokine response (Dagenais et al, 2009; Drennan et al, 2005; Schleifer et al, 1993; Schopf et al, 1998). However, later in the disease, the host can set a type 2 immune response to alleviate parasite-elicited pathology. The trypanosomes may also induce the production of Th2 cytokines and regulatory T-cell activation that results in increased production of IL-10 and transforming growth factor beta (TGF-β), both of which suppress an exaggerated protective Th1 responses and hence promote parasite survival (Magez et al, 2007; Namangala et al, 2008; Wei & Tabel, 2008). Therefore a type 1 cellular inflammatory response may be shifted to a type 2 response, characterized by type 2 cytokines (IL-4, IL-10 and IL-13) (produced via $CD4^+$ Th2 cells), which activate macrophages to become alternatively activated (aaMφ) and promote B cell maturation into IgG1 (Kaushik et al, 2000; MacLean et al, 2001; Namangala et al, 2000b; Sternberg et al, 2005; Uzonna et al, 1999). This environment promotes parasite neutralization and allows the infection to proceed into chronic phase with minimal pathological manifestations (Baetselier et al, 2001). Actually, the activation of an anti-inflammatory response is beneficial for both, the parasite, and at a certain time to the host. In one hand there is an increase in arginase activity, leading to the production of L-ornithine, a parasite growth factor, on the other hand the depletion of

L-arginine (the substrate of NO synthase) leads to a decrease in the levels of cytotoxic NO (Vincendeau et al, 2003). Moreover, a control of the host pathology is observed, through the control of exacerbated inflammatory response, leading to a longer survival of the host and thus increasing parasite transmission probability. In resistant mice model, this switch in cytokine profile is described during the late/chronic stages of infection, presumably restricting prolonged and exaggerated inflammatory responses (Namangala et al, 2009). On the contrary, early mortality in highly susceptible mice is caused by enhancement of TNF-α due to exacerbated macrophage activation, excessive INF-γ production, and a systemic inflammatory syndrome (Shi et al, 2003; Shi et al, 2006b) (Figure 7).

Regarding the humoral response, *T. brucei* infection triggers the production of immunoglobulin (Ig)M and IgG antibodies. An important feature is the dramatic increase of trypanosome-specific and non-specific Ig production induced by cytokine activation of B cells (Malvy & Chappuis, 2011). The trypanosome-specific antibodies are protective since they mediate parasite clearance, except for the subset of parasites with renewed VSG (as described above in detail). Some antibodies are also raised against auto-antigens, resulting from aberrant non-specific polyclonal activation of B cells (Hudson et al, 1976; Kobayakawa et al, 1979; Williams et al, 1996). These elements contribute to collateral tissue damage and immunosuppression. Later in the infection, B-cells become suppressed or exhausted, resulting in a total absence of IgG responses and a strongly reduced IgM response (Semballa et al, 2004). As the infection progresses, B cell lymphopoiesis is shut down in the bone marrow and compensatory extramedullary B lymphopoiesis is truncated by apoptosis of transitional B cells thus preventing replenishment of mature marginal zone and follicular B cell compartments in the spleen. *In vitro* experiments suggest that living trypanosomes induce cell death in transitional B cells through a contact-dependent mechanism, although the mechanism of *T. brucei*-induced transitional B cell depletion *in vivo* remains to be fully elucidated (Bockstal et al, 2011).

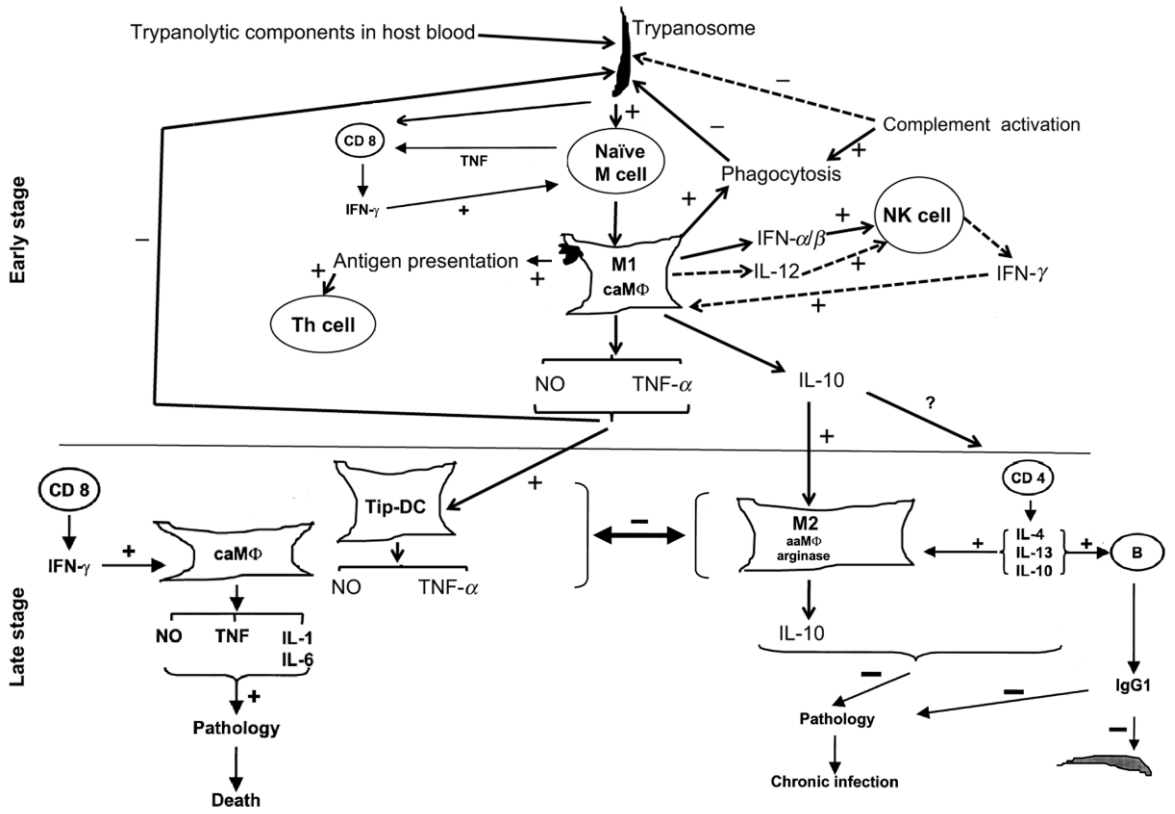

Figure 7. A model for induction of protection *versus* pathogenesis during *T. brucei* infections. Abbreviations: naïve M cell, naïve macrophage; M1 or caMϕ, classically activated macrophage; M2 (macrophage type 2) or aaMϕ (alternatively activated macrophage); TNF/iNOS-producing dendritic cell (Tip-DC), TNF-α and inducible nitric oxide synthase producing dendritic cell; NO, nitric oxide; Th, T helper cell. Dotted line, not confirmed pathway. [Adapted from (Baetselier et al, 2001; Namangala, 2012)].

8 Diagnosis

The major reason for diagnosis is the application of appropriate therapeutic and prophylactic measures. Other reasons include the need to target and monitor vector control or eradication operations, investigations of chemotherapy efficacy and drug resistance, and pathophysiological, epidemiological and socio-economic studies. Since clinical examinations are not sufficiently specific (Chappuis et al, 2005a; Lejon & Buscher, 2005), diagnosis relies on laboratory analysis and includes a two-step approach: screening and staging (Figure 8).

Contrary to *T. b. rhodesiense* infections which typically present higher parasitaemia (Pepin & Meda, 2001), and therefore trypanosomes can be identified on a peripheral blood smear, in *T. b. gambiense* infections, the amount of parasites in the

bloodstream is generally very low. In *T. b. gambiense* HAT, the card agglutination test for trypanosomiasis (CATT) is the test of choice, once it is a fast and practical serological test. Actually is the best-adapted and most efficient screening method, that allows mass population screening in endemic areas. This test can be done on serum, capillary blood obtained from a finger prick, or blood from impregnated filter papers, and is reported to be 87–98% sensitive, and 93–95% specific (Brun et al, 2010; Magnus et al, 1978). However CATT has limitations, such as the dilutions cut-offs used may lead to false-positive results, the cross-reaction events with other parasites which may elicit false positives, and a positive result does not constitute an absolute proof of active infection, as CATT can be positive three years after treatment. Therefore, after a serological positive result, the diagnosis of certitude requires microscopic parasite observation. Once in *T. b. gambiense* infections, parasites detection in blood is very difficult, concentration methods such as the microhaematocrit centrifugation (the most used) (Woo, 1970), quantitative buffy coat (the most expensive) (Bailey & Smith, 1992), and miniature anion-exchange centrifugation (the most sensitive) techniques (Lumsden et al, 1979) should be used. Other highly sensitive serological tests, such as immunofluorescence or enzyme-linked immunosorbent assay (ELISA), are efficient for *T. b. gambiense* or *T. b. rhodesiense* antibody detection, but are generally used in non-endemic countries to screen individuals with suggestive clinical features or previous exposure (Lejon et al, 1998; Noireau et al, 1988). Polymerase chain reaction (PCR) techniques have been used to increase diagnostic accuracy. A 99% of sensitivity and a 97.7% specificity was determined for PCR on blood samples (Mugasa et al, 2012). This technique is not easily applicable for routine, however the loop-mediated isothermal amplification is a more field-adapted PCR that can be used for rapid detection of both trypanosome subspecies (Kuboki et al, 2003; Njiru et al, 2008).

Staging evaluation follows infection confirmation since its crucial to determine early or late stage of the disease in order to prescribe proper treatment. Pharmacological treatment of CNS disease is far more toxic than early stage drugs (Kennedy, 2008). Staging relies on lumbar puncture for detection of trypanosomes in the cerebrospinal fluid (CSF) and/or to count white blood cells (WBC). According to WHO criteria, the presence of trypanosomes in the CSF or WBC count of more than 5 cells/µl or increased protein content (>370 mg/L) defines second-stage disease (WHO, 1998), but there are no clear consensus on the cut-offs in WBC counts (Lejon et al, 2003b).

Present research efforts to improve diagnostic tests and to develop more precise staging techniques focus on recombinant or native trypanosome antigens, parasite antigens detection methods in blood or CSF, proteomic fingerprinting, low-tech PCR

methods, new blood or CSF markers of second-stage disease and alternative non-invasive methods for staging (Agranoff et al, 2005; Buguet et al, 2005; Deborggraeve et al, 2006; Geiger et al, 2011; Hainard et al, 2009; Hutchinson et al, 2004; Kennedy, 2010; Lejon et al, 2002; Papadopoulos et al, 2004). Further development and refinement of these approaches can be applied in the future, although they must be compared to the WHO criteria, made cheap and field adaptable.

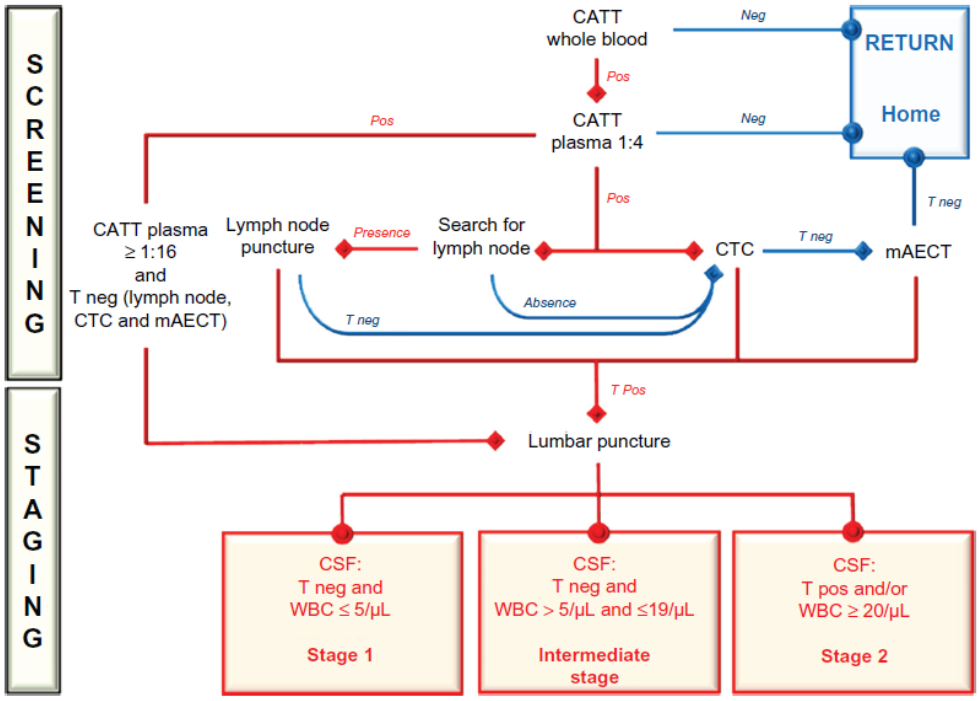

Figure 8. Decision tree for biological diagnosis and staging of *T. b. gambiense* HAT, used by a research team in Congo, from 2005 to 2009 (Buguet et al, 2009). Villagers were submitted to whole blood CATT. CATT positive (Pos) samples were tested for CATT on plasma at a 1:4 dilution. CATT plasma 1:4 negative (Neg) people were released. CATT positive suspects were examined for the presence of lymph nodes. The lymph nodes were punctured, and the fluid was examined microscopically to detect trypanosomes (T). If trypanosomes were found (T pos), the suspect was classified as being a patient. In the absence of palpable lymph nodes or of trypanosomes in lymph nodes (T neg), blood concentration techniques were undertaken. If the capillary centrifugation technique (CTC) result was negative, a new blood sample was withdrawn from a forearm vein and passed through the miniature anion-exchange centrifugation technique (mAECT). If the latter test was also negative, the suspect was released. All patients underwent staging procedures consisting of a lumbar puncture and CSF examination. CATT plasma ≥1:16 dilution

positive, people are considered as patients, and they undergo lumbar puncture, even if they are T neg in the lymph nodes and blood. Three staging possibilities are determined in CSF examination: T neg and ≤5 WBC/μL, stage 1; T neg and between 6 and 19 WBC/μL, intermediate stage; T pos and/or ≥20 WBC/μL, stage 2. [Adapted from (Bouteille & Buguet, 2012)].

9 Control strategies

Although more recently the number of HAT cases has been reduced, open economy and market globalization, with constantly increasing business travel, immigration and worker exchange, along with chances of disease migration, can contribute for HAT dissemination. Moreover, population growth, global warming and climate changes can modify the geographic distribution of parasites and vectors. The absence of an effective vaccine and a chemotherapy far from ideal call up for specific actions like, development of approaches to control vectors, identification and validation of new drug targets, development of new trypanocidal drugs, improvement in practical diagnostic techniques and improvement in understanding HAT pathophysiology (Barrett et al, 2003). Once HAT probably will not be defeated in the near future, it is imperative that international, non-governmental and philanthropic organisations and pharmaceutical companies join forces and efforts to fight this disease.

9.1 Tsetse fly control

Since there is no vaccine against HAT and chemoprophylaxis is not recommended due to the toxicity of the drugs, the only preventive measure is the reduction of tsetse fly bites. Vector control has been a way to limit rhodesiense HAT although, it was only recently applied in gambiense HAT (Solano et al, 2013). During the colonial era, many efforts were used to break the tsetse transmission cycle, as large tracts of land were cleared of vegetation and wild mammals that could act as a reservoir of *T. b. rhodesiense* were destroyed (Allsopp, 2001; Schofield & Maudlin, 2001). Besides being effective, such methods are not employed today. Synthetic insecticides were the next major approach in transmission control. Ground and aerial insecticides spraying have had considerable success, although ecological considerations now limit indiscriminate use of insecticides (Grant, 2001). Moreover these processes are not only costly, but are also labour and management intensive. Another useful way of control, but on a much smaller scale,

implies tsetse traps and target. The flies are attracted to visual cues provided by large expanses of blue or black cloth and chemical clues such as acetone, a tsetse-attracting component of cow's breath that can be used in the traps. Actually, the odour-baited traps and the insecticide-coated animal reservoir on which tsetse flies feed, have been very useful (Hargrove et al, 2000). More recently, the sterile insect technique (SIT), which involves the release of sterile flies into wild populations to compete with natural males, was very publicised (Vreysen, 2001). As a matter of fact, this strategy contributed to tsetse eradication from the island of Unguja (Zanzibar) in 1994 (Vreysen et al, 2000). The enormous costs and the large numbers of irradiated sterile males needed makes this control method unfavourable (Rogers & Randolph, 2002). Nowadays, investigations are underway to identify factors that influence parasite transmission as a way to intervene at the level of the fly. There is still a huge deficit in what is known on tsetse biology, which should be overcome with the purpose of bringing new techniques for vector control.

9.2 Vaccines

Vaccines are unlikely to be developed against HAT as a result of the different *T. brucei* defence strategies. In fact, several attempts have been made to come out with a vaccine, but this goal has never been achieved.

When VSGs were discovered, as the parasite main protection against the host immune system, researchers got excited to have an exposed epitope that they could purify, and use to develop a vaccine. Since early, research suggested that the VSG repertoire in injected metacyclic trypanosomes was limited to no more than a dozen VSGs (Barry et al, 1979; Crowe et al, 1983; Esser et al, 1982; Le Ray et al, 1978), some authors propose a vaccine using irradiated metacyclic trypanosomes, which resulted in promising preliminary results (Esser et al, 1982). However, the subsequent discovery of the mosaic nature of expressed VSGs in bloodstream forms, which is an "illimitable" repertoire (Hall et al, 2013; MacGregor et al, 2012; McCulloch & Horn, 2009), and the fact that the main Ig response elicited is the short lived IgM isotype, made the exposed antigen vaccination programmes fall into disuse.

As a consequence of these results, the non-variable antigen-based vaccines were begun to be thought as an alternative. In order to bind or uptake exogenous molecules, trypanosomes express a number of non- or less-variable surface antigens. The flagellar pocket is an organelle that contains conserved receptors and is involved in endocytosis/exocytosis, cell division and polarity, and immune evasion. Also, embedded

under the VSG coat are multiple copy-number of invariant surface glycoproteins (ISG). Trypanosome membrane associated trans-sialidases, that transfer sialic acid from sialylated glycoconjugates from the host cell surface to acceptor molecules on the parasite's surface, and cation pumps, important for cation homeostasis, were also taken into consideration. Moreover trypanosomes require a highly developed cytoskeleton, integral to motility, flexibility and mechanical stability. Thereby, cytoskeleton proteins constitute an interesting group of non-variable antigens, such β-tubulin, actin and microtubule-associated proteins. All these molecules were thought as possible candidates, and have been used in experimental vaccination schemes, however initial positive results obtained were a result of a general immune system boost at a nonspecific level and did not involved immune memory (Li et al, 2007; Li et al, 2009; Lubega et al, 2002; Radwanska et al, 2000; Ramey et al, 2009; Rasooly & Balaban, 2004; Silva et al, 2009). As mentioned above, *T. brucei* infections compromise host humoral immune competence resulting in the loss of B cell responsiveness (Radwanska et al, 2008), although human B-cell dysfunction might not be that severe as in mouse models (Lejon et al, 2014). This "memory" destruction appears to be permanent, explaining why the large majority of vaccines trailed up until now have shown promising initial results, but no long-term memory. Moreover, this could be a worry, not just for future trypanosome vaccination programmes, but also for vaccination programmes against many other infections.

The problems encountered with direct anti-trypanosome vaccination could be circumvented by alternative approaches such as transmission blocking vaccines (TBVs). TBVs can involve a number of strategies, (1) interruption of the parasite life cycle in the vector by targeting specific interactions required for parasite development (Maudlin et al, 1984; Nantulya et al, 1980), (2) reduce vector fitness by reducing the fecundity and survival (Kinyua et al, 2005; Nogge & Giannetti, 1980), and (3) block the parasitaemia onset in the host by reducing the parasite transmission through immunizing against exposed salivary antigens. The feasibility of TBVs is supported by a number of results obtained in other infections models (de la Fuente et al, 1998; Outchkourov et al, 2008; Saraiva et al, 2006; Willadsen et al, 1995), and therefore may be possible in trypanosomiasis. Several antigens have now been proposed as candidates for experimental TBV vaccination schemes, but it is still unclear whether TBVs can be realistically adapted to the field conditions (Magez et al, 2010).

Another alternative strategy to anti-trypanosome vaccination is the so-called anti-disease vaccine. There is a significant disparity in the disease progression in cattle infected with *T. congolense*, enabling animals to be labelled as trypanosusceptible and

trypanotolerant. The main difference between trypanosusceptible and trypanotolerant animals is that the latter are able to mount an anti-congopain IgG, an Ig produced by leucocytes of the adaptive immune response. Congopain is a cathepsin-L like cysteine protease in *T. congolense* trypanosomes and is under investigation as a vaccine candidate for cattle (Lalmanach et al, 2002). Since promising results were achieved, congopain is a realistic anti-disease vaccine option against animal trypanosomiasis, although it remains to be elucidated if vaccine-induced memory retains its protective capacity for prolonged periods of time during infection. A liposome-based GPI-vaccination strategy was also developed in order to prevent excessive immune activation upon infection. This proposal resulted in parasitaemia control, prolongation of host survival and limitation of infection-associated complications like anaemia, weight-loss and impairment in locomotion (Stijlemans et al, 2007), but again this response does not appear to involve the induction of B cell memory.

The technical procedures used during vaccination experiments can lead to misleading interpretations; timing between immunization and challenge, number of boosts, administration route, infection dose, parasite strain and animal route raise important doubts (Magez et al, 2010). Moreover, the absence of an effective vaccine in combination with the knowledge of the obstacles in HAT vaccination field, strongly justifies an improvement of existent chemotherapy, validation of new targets for drug intervention, and the discovery of efficient antiparasitic drugs.

9.3 Chemotherapy

If untreated, HAT is almost 100% fatal (Jamonneau et al, 2012). Chemotherapy is still unsatisfactory and ineffective against both stages of the disease, and for both *T. b. rhodesiense* and *T. b. gambiense* subspecies. The therapy against HAT is lengthy, costly and toxic and requires parenteral administration. There are currently four licensed treatment regimes: pentamidine, suramin, melarsoprol and eflonithine (Figure 9). Nifurtimox-eflornithine combination therapy besides being used off-license, was placed on the WHO list as an essential medicine. Only the mode of action of eflornithine is totally understood despite many of these drugs have been around for decades. All anti-trypanosomal drugs are donated to WHO by Sanofi-Aventis (pentamidine, melarsoprol and eflornithine) and Bayer Leverkusen (suramin, nifurtimox) and then distributed in the field (Bouteille & Buguet, 2012).

9.3.1 Pentamidine

Pentamidine isethionate (Pentacarinat®) is an aromatic diamidine used against first-stage disease caused by *T. b. gambiense* infection. Pentamidine is unsuitable for treatment of advanced disease, in part because serum binding and tissue retention reduces blood-brain barrier traversal (Barrett et al, 2011). Nevertheless, effective cases were reported against trypanosomiasis during the early phase of CNS involvement (Bray et al, 2003; Doua et al, 1996), despite pentamidine that does cross the blood-brain barrier is cleared by efflux transporters (Sanderson et al, 2009). It was first used in 1940s, either as a prophylactic as well as a curative agent (Bacchi, 1993). Four mg/kg are given daily, or on alternate days by intramuscular injection for 7-10 days (Sands et al, 1985). When given by intramuscular injection, site pain and transient swelling, abdominal pain and gastrointestinal problems, and hypoglycaemia (5–40%) are the most frequently reported adverse events. The drug enters principally via the purine transporter 2 (P2) aminopurine permease (Carter et al, 1995), however low and high affinity pentamidine transporters (LAPT1 and HAPT1, respectively) and a plasma membrane H^+ ATPases, HA1-3, also contribute to uptake (Alsford et al, 2012; De Koning, 2001). Pentamidine action appears to be multifactorial possibly due to the binding to DNA, in regions of the minor groove rich in adenine and thymine (Moreno et al, 2010). It is also known to collapse the mitochondrial membrane potential, and inhibit the F1F0-ATPase (Lanteri et al, 2008). Consequently, it is likely that the antitrypanosomal activity of pentamidine is the result of selective accumulation, leading to multiple deleterious effects, rather than effects on a specific ‘diamidine target’ (Delespaux & de Koning, 2007). Confirmed pentamidine failures are rare, likely due to low drug-resistance. Although massive use of pentamidine as a chemoprophylactic in the Democratic Republic of Congo may have selected for reduced sensitivity to this drug (Kayembe & Wery, 1972). Only recently through genome-scale RNA interference target sequencing (RIT-seq) screens, pentamidine loss-of-function was linked to melarsoprol-pentamidine cross-resistance (Alsford et al, 2012). The aquaglyceroporin 2 (AQP2), a membrane protein that facilitate the transport of water and small neutral solutes across membranes in several organisms, was discovered to facilitate drug accumulation and is also linked to clinical cases of resistance for both drugs (Baker et al, 2012). This was an important finding since the cross-resistance phenotype could not be explained based only in P2 and HAPT transporters.

9.3.2 Suramin

Suramin (Germanin®) is a sulphonated naphthylamine used for first-stage *T. b. rhodesiense* disease. It was discovered by Oskar Dressel and Richard Kothe at Bayer in 1916 (Haberkorn et al, 2001). Suramin is administered by intravenous injections every 3-7 days for 31 days (20mg/Kg, with a maximum of 1g per injection) (Barrett et al, 2007). Adverse drug reaction include acute and late hypersensitivity, nephrotoxicity, peripheral neuropathy, and bone marrow toxicity with agranulocytosis and thrombocytopenia (Kennedy, 2013). Suramin is selectively concentrated by trypanosomes through receptor-mediated endocytosis when conjugated with low-density lipoproteins (LDL) (Vansterkenburg et al, 1993). However, evidence for a non-LDL uptake in insect-stage cells was proposed (Pal et al, 2002). A high-throughput sequencing of a suramin-selected RNAi library identified a cohort of proteins contributing to drug efficacy (Alsford et al, 2012). In a proposed model a 75 kDa ISG (ISG75) acts as a major receptor for suramin delivering the drug into the degradative arm of the endocytic pathway. Suramin is delivered to the lysosome by either the serum protein carrier being cleaved by cathepsin-L upon reaching the lysosome, or by ISG75 being degraded at the late endosome. Once free, suramin may inhibit lysosomal enzymes and may also escape into the cytoplasm via the major facilitator superfamily transporter (MFST), resulting in inhibition of other cellular processes (Alsford et al, 2013). This large negatively-charged polyanion appears to inhibit unspecifically many positively-charged enzymes, so it is difficult to conclude which may be the determinant of drug action (Wang, 1995). More recently it was shown that this compound inhibits a number of glycolytic enzymes (Barrett et al, 2007), such as pyruvate kinase by binding the ATP site (Morgan et al, 2011). Resistance to suramin was reported in the 1950s (Barrett et al, 2007). The mechanisms for suramin resistance are not yet elucidated but may involve changes in ISG75 and in proteins of the endocytic apparatus, including AP-1 (adaptin complex-1), GLP-1 (Golgi/lysosomal protein-1), EMP70 (endosomal membrane protein 70), MFST, p67 (major lysosomal glycoprotein), and cathepsin-L (Alsford et al, 2012).

9.3.3 Melarsoprol

Melarsoprol (Mel B, Arsobal®), a melaminophenyl arsenical synthesised in 1949, is still the most powerful trypanocide available to cure both stages of *T. b. gambiense* and *T. b. rhodesiense* HAT (Friedheim, 1949). However, is the only effective drug against late

stage *T. b. rhodesiense* infections. Melarsoprol is usually administered intravenously and the recommended course is 10 days long with daily injections of 2.2 mg/kg (Schmid et al, 2005). Melarsoprol injections are extremely painful and toxic, and the most important reaction is a post-treatment reactive encephalopathy in 10% of patients, half of whom die, leading to an overall mortality of about 5% (Blum et al, 2001). Skin reactions, peripheral motoric, sensorial neuropathies and thrombophlebitis can also occur (Brun et al, 2010). The parasites lyse rapidly when exposed to melarsoprol (Meshnick et al, 1978). It is believed that melarsoprol is converted in the host to melarsen oxide, which is then transported by P2 transporter. Melarsen oxide acts mainly through the formation of a stable adduct with trypanothione [$T(SH)_2$], known as MelT, which is an inhibitor of trypanothione reductase (TR), a central enzyme of the parasite thiol/disulfide redox balance (Fairlamb, 2003; Fairlamb et al, 1989). Additionally, melarsoprol also formed adducts with lipoic acid (Fairlamb et al, 1992) and inhibits glycolysis (Van Schaftingen et al, 1987). In some *T. b. gambiense* HAT areas, melarsoprol treatment failures have already reached levels of 30% (Brun et al, 2001; Legros et al, 1999; Stanghellini & Josenando, 2001). As mentioned below in the pentamidine section, the cross-resistance to melarsoprol was firstly associated with P2 transporter, once *Tbat1* gene deletion and loss-of-function mutations were described in melarsoprol resistant strains generated in the laboratory (Bridges et al, 2007; Maser et al, 1999; Stewart et al, 2010), and the same mutations were also found in *T. brucei spp*. field isolates (Kazibwe et al, 2009; Matovu et al, 2001; Nerima et al, 2007). In addition, *Tbat1*-null trypanosomes were found to have lost the adenine-sensitive component of adenosine and melarsoprol-import (Geiser et al, 2005; Matovu et al, 2003). More recently and as already reported in pentamidine section, aquaglyceroporin 2 (AQP2) loss-of-function was linked to melarsoprol-pentamidine cross-resistance (Alsford et al, 2012).

9.3.4 Eflornithine

Eflornithine (DL-α-Difluoromethylornithine, DFMO; Ornidyl^{TM}) was developed in the 1970s (Janne et al, 1981). Due to the unacceptable toxicity of melarsoprol, eflornithine is the first line treatment for the second stage *T. b. gambiense* disease (Balasegaram et al, 2006; Chappuis et al, 2005b; Priotto et al, 2008). The use of this drug against *T. b. rhodesiense* is not advised, because this parasite is innately less susceptible (Iten et al, 1997). Eflornithine treatment is administered intravenously. The high IC_{50} and the low half-life dictate the use of large quantities of the drug (nearly 4 kg for a 50 kg patient) for

the treatment regime of 56 infusions over 14 days (Brun et al, 2010). It is logistically difficult to deliver and to administer in the rural areas leading to a continued reliance on melarsoprol in impoverished areas. Adverse drug reactions include bone marrow toxicity leading to anaemia, leucopenia, and thrombocytopenia (25–50%), gastrointestinal symptoms (10–39%), and convulsions (7%) (Burri & Brun, 2003). Eflornithine is the only drug with a well understood mode of action, which irreversibly inhibits ornithine decarboxylase (ODC) an enzyme of the polyamine pathway (Grishin et al, 1999; Poulin et al, 1992). Eflornithine is only active against *T. b. gambiense* forms of HAT possibly due to a reduced rate of ODC turnover in this subspecies (Iten et al, 1997). Surprisingly, it is the equal effective inhibition of mammalian ODC. The pronounced differences in turnover rates between host and parasite ODC have been invoked to explain selectivity (Heby et al, 2003), although and more important, is the fact that mammalian cells are able to induce high-affinity polyamine transporters in response to polyamine starvation, whereas *T. brucei* appears to have a limited capacity to scavenge polyamines present in serum (Fairlamb, 2003). ODC inhibition by eflornithine leads to an increase in levels of ornithine, *S*-adenosylmethionine (AdoMet) and decarboxylated *S*-adenosylmethionine (dcAdoMet), and a decrease in putrescine, spermidine (Spd) and $T(SH)_2$ (Bacchi & Yarlett, 1993; Fairlamb et al, 1987; Xiao et al, 2009). Spd conjugates with two molecules of GSH to form $T(SH)_2$, which protects the parasite from oxidative stress. The decrease in Spd and consequently in $T(SH)_2$ is therefore harmful for the parasites (Heby et al, 2007; Krauth-Siegel & Comini, 2008). Downstream of these metabolic changes, a generalized decrease in DNA, RNA and protein synthesis, including synthesis of VSG (Bitonti et al, 1988; Yarlett & Bacchi, 1988) and morphological and biochemical changes like differentiation into stumpy forms can occur (Giffin et al, 1986). The fact that the trypanosomes are unable to undergo antigenic variation facilitates the death of the parasites by the host immune system (Barrett et al, 2007). Concerning resistance, it appears that eflornithine is transported into trypanosomes via an amino acid transporter (*Tb*AAT6) and that the loss of this transporter result in eflornithine resistance (Baker et al, 2011; Schumann Burkard et al, 2011; Vincent et al, 2010). Whether this mechanism is also used in isolates from the field has yet to be established (Barrett et al, 2011).

A

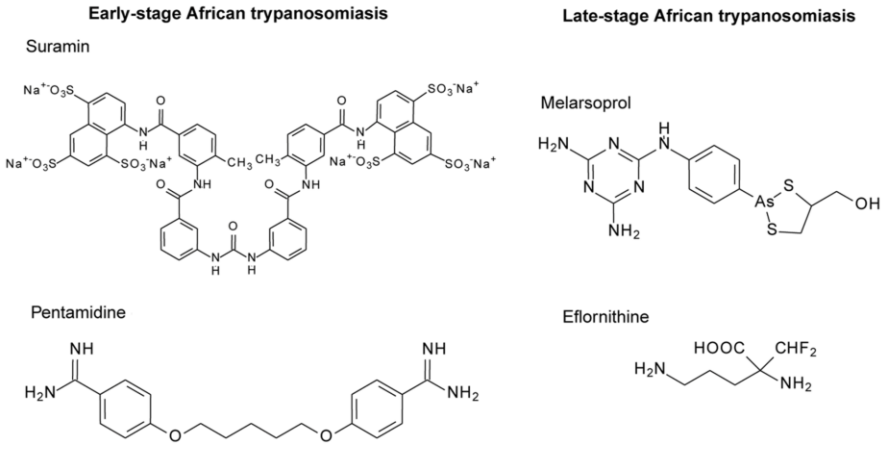

B

	Stage	Route of application	Dosing	Main adverse drug reactions
Trypanosoma brucei gambiense				
Pentamidine*	First	Intramuscular	4 mg/kg bodyweight at 24 h intervals for 7 days	Hypoglycaemia, injection site pain, diarrhoea, nausea, vomiting
Eflornithine	Second	Intravenous Infusion of >30 min	100 mg/kg bodyweight at 6 h intervals for 14 days	Diarrhoea, nausea, vomiting, convulsions; anaemia, leucopenia, and thrombocytopenia
Melarsoprol†	Second	Intravenous	2·2 mg/kg bodyweight at 24 h intervals for 10 days	Encephalopathic syndromes, skin reactions (pruritus, maculopapular eruptions), peripheral motoric (palsy) or sensorial (paraesthesia) neuropathies, thrombophlebitis
Trypanosoma brucei rhodesiense				
Suramin*	First	Intravenous	Test dose of 4–5 mg/kg bodyweight at day 1, then five injections of 20 mg/kg bodyweight every 7 days (eg, day 3, 10, 17, 24, 31); maximum dose per injection 1 g	Hypersensitivity reactions (acute, late); albuminuria, cylinduria, haematuria, peripheral neuropathy
Melarsoprol*	Second	Intravenous	Three series of 3·6, 3·6, 3·6 mg/kg bodyweight, the series spaced by intervals of 7 days; maximum dose per day 180 mg	Encephalopathic syndromes, skin reactions (pruritus, maculopapular eruptions), peripheral motoric (palsy) or sensorial (paraesthesia) neuropathies, thrombophlebitis

*Endemic countries: according to national legislature or guidelines. †Only where eflornithine is not available or where melarsoprol is first-line treatment according to national guidelines.

Figure 9. Licensed current therapies against HAT. (A) Structures of drugs used to treat early and late stage disease. (B) Table with standard treatment for HAT and main adverse reactions. [Adapted from (Brun et al, 2010; Fairlamb, 2003)].

9.3.5 Eflornithine-nifurtimox combination therapy

The new nifurtimox/eflornithine combination therapy (NECT) was advanced in 2009 (Opigo & Woodrow, 2009; Priotto et al, 2009) for the treatment of late-stage *T. b. gambiense,* after showing equivalent to better efficacy than eflornithine alone in clinical trials (Yun et al, 2010). NECT has not yet been tested against *T. b. rhodesiense* (Phillips, 2012). In combination, nifurtimox is given orally (daily dose of 15 mg/kg, three times a day for 10 days) and the eflornithine infusions are reduced in frequency (daily dose of 400 mg/kg in 14 slow infusions, every 12 hours for 7 days). The administration of the combination therapy compared to eflornithine monotherapy is much easier to implement. NETC allows the use of lower doses of each drug, being logistically easier to transport

due to the lower quantities required and the reduction in refrigeration costs (Yun et al, 2010). NECT generates adverse events, mainly abdominal pain, vomiting and headache, however, the severity of these events is relatively low compared to previous treatments, and the majority of patients treated make a good recovery (Alirol et al, 2013; Priotto et al, 2009). Nifurtimox is a 5-nitrofuran pro-drug that has been used for more than 40 years to treat Chagas disease. In trypanosomes the drug must undergo activation by nitroreduction, undertaken by NADH-dependent type I nitroreductases (Wilkinson et al, 2008). Recent evidences on the mode of action of nifurtimox showed the formation of an open chain nitrile that cause cellular death due to its interaction with a range of cellular targets (Hall et al, 2011). With regard to resistance, a genome-scale RNAi library, to screen nifurtimox and eflornithine resistance, confirmed previous findings that nitroreductase loss-of-function is the major potential mechanisms of resistance to nifurtimox (Baker et al, 2011; Wilkinson et al, 2008).

Chapter II

Discovery of targets against human African trypanosomiasis

1 Target validation

Trypanosomes are some of the earliest diverging members of the Eukaryotae and share several biochemical peculiarities that have stimulated research to discover new drug targets. In addition to the excessive toxicity of the available drugs, there is a steady loss of effectiveness due to consistently arising drug resistant parasites. Therefore is imperative the discovery and validation of new drug targets. There are some crucial points to consider for target selection, such as: absence from the host or substantially different so that it can be explored as a target; important for the survival or fitness of the pathogen; expressed in a parasite life-cycle stage suitable for drug intervention; and finally, a target that can be assayable and druggable (Barrett et al, 1999; Chawla & Madhubala, 2010; Pink et al, 2005). Target validation, through genetic and/or biochemical approaches, is the starting point of a rational course to chemotherapy.

1.1 Genetic approaches

The completion of the *T. brucei* genome project (Berriman et al, 2005) allows access to a wealth of information, available at genome databases, like GeneDB (http://www.geneDB.org) and TriTrypDB (http://tritrypdb.org). The genome databases availability combined with genetic tools, such us generation of null mutants (gene knockout) and the RNAi [messenger RNA (mRNA) knockdown, shown to occur in *T. brucei* (Ngo et al, 1998)], has allowed the discovered and validation of new drug targets.

1.1.1 Gene knockout

The gene knockout strategy requires the introduction into the parasite, usually by electroporation, of a linear DNA construct containing an antibiotic resistance gene, flanked by 5' and 3' DNA sequences from the targeted gene. The replacement of the natural gene occurs via homologous recombination. The transgenic parasites are selected through antibiotic resistance (Figure 10A) (Barrett et al, 1999). In *T. brucei*, selective gene replacement can be performed directly on procyclic forms (insect stage) or on bloodstream forms (mammalian stage). It is important to guarantee that any phenotype observed results from the deletion of the gene of interest. This is confirmed when the phenotype is restored upon target gene reintroduction (genetic complementation). Gene knockout strategies are usefull when: (1) genes can be deleted from the parasite, which

remain viable in all life-cycle stages, (2) genes can be deleted from the parasite, with little effect on viability, however switching conditions, such as changing the availability of nutrients and growth factors, can lead to cell death, (3) genes can be deleted from one life-cycle stage with little or no effect on viability but are found to be essential in another life-cycle stage, and finally (4) genes cannot be deleted from any life-cycle stage. In the latter, removal of the second copy would be lethal to the parasite, therefore a conditional knockout (cKO) can be a solution; after the first allele has been knocked out, a tetracycline (tet) regulatable copy of the gene coding sequence is inserted in the ribossomal RNA intergenic locus prior to the removal of the second endogenous allele (Figure 10B). Meaning that the second allele is effectively removed only in the presence of tet. The parasite death upon removal of tet (which represses transcription of the regulatable allele) proves undoubtedly that the gene is essential (Merritt & Stuart, 2013).

In contrast, there are other genes in which this procedure can be misleading: (1) genes that encode a protein that activates a pro-drug, (2) genes that encode a protein whose activation by a drug is toxic, (3) genes that encode an enzyme whose activity is unimportant but that is an essential building block of an essential enzyme complex (gene deletion would be lethal, but enzyme inhibition would have no significant effect), and lastly (4) gene that encode an enzyme whose autocatalytic processing is inhibited by a drug, leading to the lethal accumulation of the pro-protein (Barrett et al, 1999).

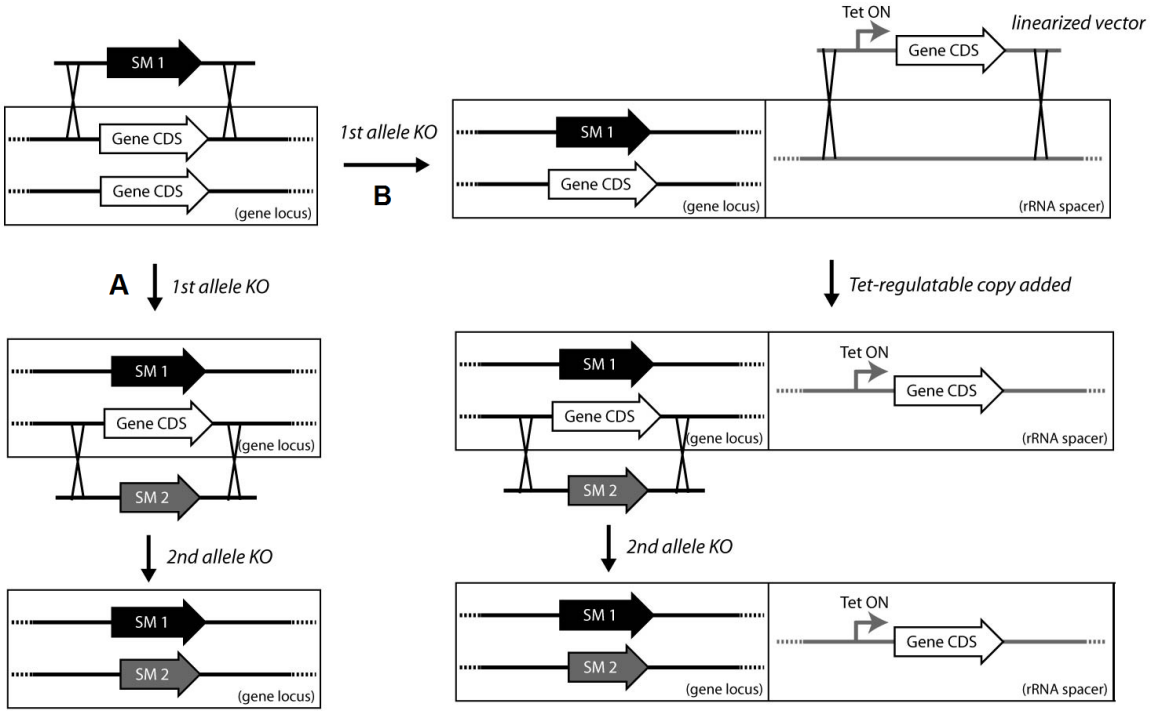

Figure 10. Gene knockout strategies. Transfection scheme to create null cell lines (A) and conditional null cell lines (B). [Adapted from (Merritt & Stuart, 2013)].

1.1.2 RNA interference

In 1998, *T. brucei* was the first protozoan parasite in which RNAi was shown to be functional (Ngo et al, 1998). RNAi purpose has been proposed to promote genome stability by silencing mobile elements and repeats (Kolev et al, 2011). The RNAi machinery comprises two dicer-like enzymes, DCL1 (cytoplasmic) and DCL2 (nuclear), which process long double-stranded RNAs (dsRNAs) into small sections of small interfering RNAs (siRNAs) (of approximately 25 nucleotides) in the cytoplasm and the nucleus, respectively (Figure 11). Nuclear *Tb*DCL2 initiates the process by targeting dsRNAs of sense and antisense transcripts from retroposons and repeats (Shi et al, 2006a). Cytoplasmic *Tb*DCL1 targets the dsRNA molecules produced by *Tb*DCL2 and any nucleic or cytoplasmic dsRNA still unprocessed (Roberts et al, 1972). RNA Interference Factor 5 (*Tb*RIF5) was very recently demonstrated to act in partnership with *Tb*DCL1 and to be necessary for cytoplasmic and not nuclear RNAi (Barnes et al, 2012). *T. brucei* first Argonaute protein (*Tb*AGO1) targets siRNAs products from both Dicers (Durand-Dubief & Bastin, 2003; Shi et al, 2009; Shi et al, 2004a; Shi et al, 2004b). Duplex siRNAs were shown to increase and avoid association with *Tb*AGO1 in the absence of *Tb*RIF4 (Barnes et al, 2012). AGO1 unwound the siRNAs fragments to form single-stranded RNAs (ssRNAs). The ssRNAs display amenable sequences that recognize specific mRNAs, which are then targeted and degraded by the RNAi-induced silencing complex (RISC). In the very beginning, it was disappointing to discover that the effect on the downregulation of the target mRNA achieved was only transient and lasted about one cell cycle. The great evolution of *T. brucei* RNAi technology was driven not only by the knowledge of the RNAi endogenous components, but also by the development of vectors for inducible and heritable expression of dsRNAs (Inoue et al, 2002; Wirtz & Clayton, 1995; Wirtz et al, 1999). RNAi is greatly used to knockdown the expression of a specific mRNA in African trypanosomes for examining the function of its protein (Inoue et al, 2002). When RNAi is used as a tool, dsRNA induces sequence-specific silencing of a query gene through degradation of the complementary RNA in the cell (Owino et al, 2008). Indeed, it circumvents the necessity of generating double knockout (dKO), which is a requirement for such studies in diploid organisms; hence it is a simpler and faster method. RNAi has been shown to occur in *T. brucei* (Ngo et al, 1998), *Trypanosoma*

congolense (Inoue et al, 2002) and *Leishmania* subgenus *Viannia* (Lye et al, 2010) but not in *Trypanosoma cruzi* (*T. cruzi*) (DaRocha et al, 2004) and *Leishmania* subgenera *Leishmania* and *Sauroleishmania* (Robinson & Beverley, 2003). However, since *T. cruzi* and *Leishmania spp.* share 76% of genes with *T. brucei* (El-Sayed et al, 2005), some data obtained from RNAi in *T. brucei* can be extrapolated to those organisms. Besides RNAi proved to be a great tool, it is important to keep in mind all the limitations inherent to this technique (Owino et al, 2008): (1) the "background" expression from the "repressed" promoters affects selection of suitable transformants (Alibu et al, 2005; Chen et al, 2003; Wang et al, 2000; Wirtz et al, 1998), (2) the development of RNAi revertants (Chen et al, 2003), (3) the variation in regulation of constructs expression due to availability of various sites for integration (Alsford et al, 2005; Biebinger et al, 1996), (4) the difficulty in generating recombinant bloodstream forms (Alsford et al, 2005), (5) the possible integration of the constructs in unanticipated regions, rather than the transcriptionally inactive rDNA locus affecting more than one protein (Motyka et al, 2004), and (6) the inability to achieve a complete abolishment of gene function (Motyka et al, 2004). Indeed, RNAi-silenced gene can elicit phenotypes similar to those of genetic null mutants, however for some cases only the full ablation of all copies can warrant the complete disruption of gene function. This is particularly true for abundant proteins or for enzymes with activity that is difficult to silence completely (Balana-Fouce & Reguera, 2007). Despite these limitations, researchers have been expanding and improving RNAi technology; from testing individual genes, passing to small-scale and genome wide RNAi screen, to finally ending up with RIT-seq (Alsford et al, 2011; Morris et al, 2002; Subramaniam et al, 2006; Wurst et al, 2009). Other milestones in RNAi technology are *in vivo* mRNA knockdown within a infection mouse model (Abdulla et al, 2008) and RNAi complementation, through introduction of an ectopic copy of a protein with the same biological function but having no more than 13 nucleotide stretches of identity (Sienkiewicz et al, 2010).

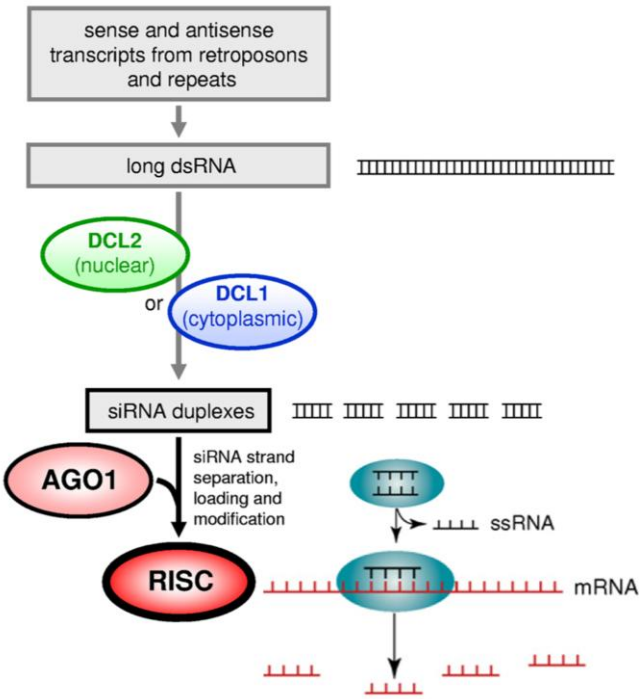

Figure 11. RNAi pathway in *T. brucei*. The two dicer-like enzymes, cytoplasmic DCL1 and nuclear DCL2, process dsRNAs into siRNAs duplexes in the cytoplasm and the nucleus, respectively. AGO1 is programmed with single stranded "guide" siRNA, following siRNA strand separation, loading and modification to form the RISC, which then cleave and degrade the target mRNA. [Adapted from (Balana-Fouce & Reguera, 2007; Kolev et al, 2011)].

1.2 Biochemical approaches

A successful protein biochemical characterization and validation has to comply with multiple factors. The expression and purification of the target protein in a soluble and active form is required in a biochemical assay. *In vitro* biochemical characterization studies require a large quantity of highly pure protein. *Escherichia coli* (*E. coli*) is the most widely used prokaryotic organism for protein production (Khow & Suntrarachun, 2012). In addition, fusion tags coupled to recombinant proteins have enabled purification of almost any protein, enhancing protein yield and solubility as well as promoting proper folding of the target protein (Arnau et al, 2006; Esposito & Chatterjee, 2006). The most frequently used fusion tags are the affinity tags; exogenous residues that bind strongly to a chemical ligand or antibody. This high affinity enables a high degree of purification of the target protein. Proteins in which native purification strategies cannot be achieved, denaturing purification conditions have to be used. However the protein's native state and its

functional capacity is not always achieved subsequent to denaturation, as a result of insufficient refolding (Kathir et al, 2005). The acquisition of the active protein is followed by the development and optimization of a functional assay to determine the best working conditions for the target (Sidoli et al, 2006). After the establishment of a functional assay, biochemical assays are used for kinetic studies (Cleland, 1967). The fundamental concept of enzyme kinetics is conveyed by Michaelis-Menton, which allows the measure of the catalytic constants (K_m, V_{max} and k_{cat}) (Cleland, 1967). This can in turn be used to characterize the type of inhibition by which a drug inhibits the enzyme activity (competitive, uncompetitive and non-competitive inhibition), and to determine the inhibitory constant (K_i) and the inhibitory concentration that reduces enzyme activity by 50% (IC_{50}) (Robertson, 2005; Swinney, 2004). Confirmed enzyme inhibitory compounds are subsequently tested for cytotoxicity in the cells, before a compound is regarded as a good lead. The value of the inhibitor can be limited by the lack of understanding how and where it binds to the target protein. Without these data, it can be difficult to improve potency, evaluate specificity, and fully explain cellular phenotypes resulting from drug treatment. Methods to identify the binding site of the inhibitor include structural studies (X-ray crystallography (Hassell et al, 2007), nuclear magnetic resonance (NMR) spectroscopy (Pellecchia et al, 2008), computational docking (Mobley & Dill, 2009), and photo-crosslinking (Robinette et al, 2006)). Mutagenesis studies are frequently used to validate the binding sites suggested by the methods described above (Claustre et al, 2002). The high throughput screening of chemical libraries, was a huge step to speed the finding of inhibitors and allows a rapidly screen of existing compounds. With the latter, financial constrains involved in drug development are reduced, which is frequently cited as a major reason for not pursuing drug development programmes against diseases of developing world (Barrett et al, 1999).

2 Targeting attractive metabolic pathways

The overall metabolism in eukaryotes is considerable conserved, however a substantial variability can be noted in enzymatic characteristics, pathways, cellular compartments and regulatory mechanisms when species are compared. Notably, *T. brucei* presents a number of features that are distinct/absent from those seen in other organisms, including mammalian cells. *T. brucei* has appealing metabolic pathways and unusual biological features that have been studied for drug target validation and to rationally design therapeutic drugs (Gull, 2002).

2.1 Polyamine metabolism

The enzymes belonging to the polyamine pathway are required for polyamines synthesis, which play pivotal roles in protein/nucleic acid synthesis and cell proliferation/differentiation, and in the synthesis of the unique redox-cofactor, $T(SH)_2$, crucial for the antioxidant defenses of parasites (Willert & Phillips, 2008). ODC catalyzes the first step in the polyamines biosynthesis, through decarboxylation of ornithine to putrescine (Figure 12). S-Adenosylmethionine decarboxylase (AdoMetDC) generates dcAdoMet, which serves as the aminopropyl group donor for Spd and spermine (Spm) synthesis. The latter reactions are catalyzed by Spd synthase (SpdSyn) and Spm synthase (SpmSyn), respectively. Interestingly, *T. brucei* has different features compared to human polyamine metabolism; (1) ODC and AdoMetDC have long half-lives, (2) appears to lack SpmSyn, and (3) exhibits negligible putrescine and uptake capacity (Heby et al, 2007; Heby et al, 2003) (Figure 12). *T. brucei* ODC knockout cell lines require exogenous putrescine for proliferation (Li et al, 1996). When null mutants of bloodstream forms were injected into mice, the parasites were unable to multiply and were quickly cleared from the blood (Li et al, 1998). Not surprisingly, was that ODC knockdown also led to cell death (Xiao et al, 2009). Nowadays, ODC is used in the field as drug target against HAT. As mentioned in the chemotherapy section, eflornithine interacts irreversibly with ODC and is the reference drug for the neurological stage of *T. b. gambiense* HAT (Grishin et al, 1999; Poulin et al, 1992). AdoMetDC is protein is activated by heterodimer formation with a catalytically dead homolog termed prozyme, found only in trypanosomatids (Willert et al, 2007). The generation of inducible AdoMetDC RNAi and prozyme cKOs in the mammalian blood stage led to a reduction in Spd and $T(SH)_2$ pools, and parasite death (Willert & Phillips, 2008). Inhibitors of AdoMetDC have also been shown to be potent trypanocidals (Bacchi et al, 1996). The functional importance of SpdSyn was also disclosed in bloodstream forms, using a tetracycline-inducible RNAi system. Down-regulation of the corresponding mRNA correlated with a decrease in intracellular Spd levels and cessation of growth (Taylor et al, 2008; Xiao et al, 2009). All these results show undoubtedly that the polyamine metabolism is a very appealing pathway for drug development. Comparative modeling and site-directed mutagenesis studies indicate that sufficient differences exist in the structures of the polyamine biosynthetic enzymes. Therefore it is possible to design structure-based inhibitors that will selectively kill the parasites while exerting minimal or at least tolerable effects on mammalian host (Heby et al, 2007).

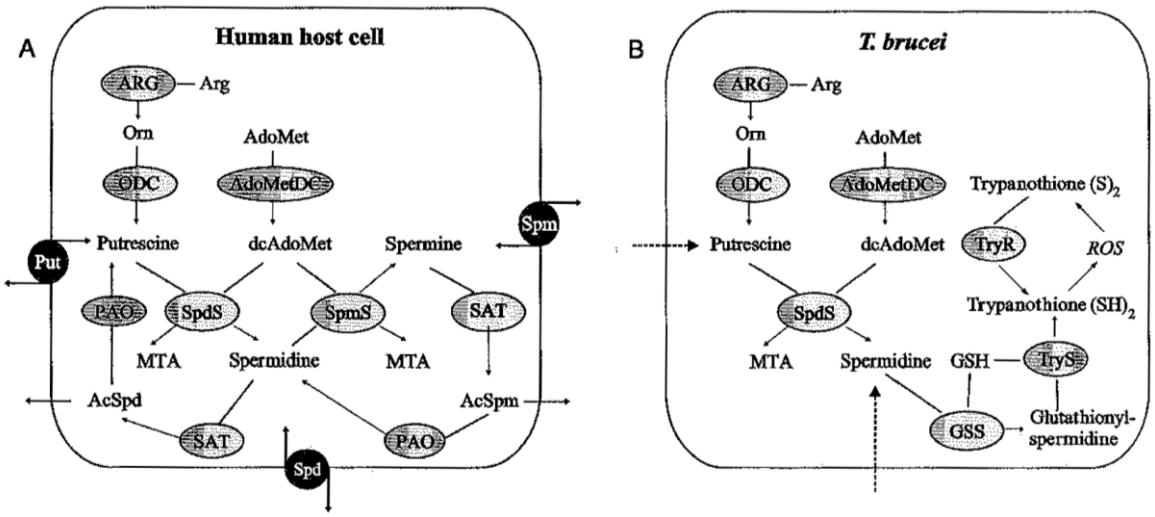

Figure 12. Human host cell and *T. brucei* polyamine pathways. (A) Polyamine pathway in mammalian cells. (B) Polyamine and $T(SH)_2$ biosynthetic pathway in *T. brucei* parasites. Abbreviations: ARG, arginase; AdoMet, S-adenosylmethionine; AdoMetDC, S-adenosylmethionine decarboxylase; SAT, N^1-acetyltransferase specific for spermidine and spermine; dcAdoMet, decarboxylated S-adenosylmethionine; MTA, methylthioadenosine; AcSpd, acetylated spermidine; AcSpm, acetylated spermine; ODC, ornithine decarboxylase; PAO, polyamine oxidase; Put, putrescine; Spd, spermidine; SpdSyn, spermidine synthase; Spm, spermine; SpmSyn, spermine synthase; GSH, glutathione; GSS, glutathionylspermidine synthase; ROS, reactive oxygen species; TryR, trypanothione reductase; TryS, trypanothione synthetase. [Adapted from (Heby et al, 2007)].

2.2 Thiol metabolism

In most eukaryotic organisms the glutathione (GSH)/glutathione reductase (GR) and thioredoxin (Trx)/thioredoxin reductase (TrxR) systems, maintain the intracellular thiol redox homeostasis (Lillig & Holmgren, 2007; Shelton et al, 2005). *T. brucei* genome sequencing project revealed absence of genes encoding for GR and TrxR (Berriman et al, 2005). Nevertheless, redox homeostasis in *T. brucei* is efficiently regulated since they can successfully withstand the oxidative burst during host infection and perfectly adapt to the different metabolic and environmental conditions imposed by their digenetic life-cycle (Krauth-Siegel & Comini, 2008). Actually, this microorganism possesses a unique redox metabolism that is based on $T(SH)_2$ (Fairlamb et al, 1985) and nicotinamide adenine dinucleotide phosphate hydrogen (NADPH)-dependent TR (Fairlamb & Cerami, 1992;

Krauth-Siegel et al, 2003). *T. brucei* trypanothione synthetase (TryS) catalyzes the entire synthesis of $T(SH)_2$ from GSH and Spd (Oza et al, 2003). The absence of the $T(SH)_2$ system in mammals, the lack of a functional redundancy within the parasite thiol system together with the sensitivity of trypanosomes against oxidative stress render the components of this metabolism attractive drug targets (Krauth-Siegel & Comini, 2008). The relevance of the $T(SH)_2$ system has been corroborated genetically [e.g. TR cKO caused increased hydroperoxide sensitivity, arrest of proliferation and loss of virulence (Krieger et al, 2000), and TryS suppression through RNAi and cKO, decreases $T(SH)_2$ levels concomitant with impairment of parasite proliferation and viability (Comini et al, 2004; Wyllie et al, 2009)]. Chemical validation studies regarding this pathway can also be seen in the literature. As an example, TR inhibitors were identified and did not block the closest mammalian homolog, the GR (Eberle et al, 2009; Eberle et al, 2011; Spinks et al, 2009). However, their efficacy in infection models turned out to be disappointing because redox metabolism of the parasite was not affected at all, unless TR was titrated down to less than 5% of normal (Krieger et al, 2000), a residual activity that is hard to permanently sustain *in vivo* by any reversible inhibitor. Therefore, recent efforts focus on irreversible TR inhibitors, which may raise concerns regarding the pronounced selectivity that is mandatory for this kind of inhibition (Flohe, 2012). Nevertheless, TR inhibition has been used in the field for the treatment of late stage *T.b. rhodesiense* infection, through the use of melarsoprol (Fairlamb et al, 1989). TryS chemical validation was achieved with inhibitors obtained from a high-throughput screening, leading to predictive metabolic impairments and parasites death (Torrie et al, 2009).

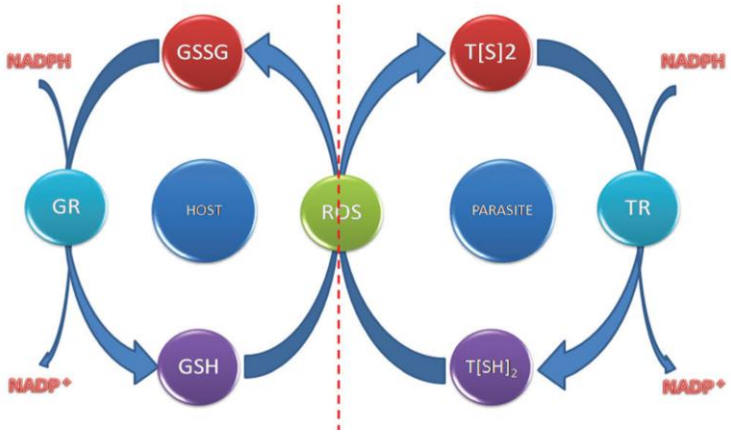

Figure 13. Simplistic representation of GSH and $T(SH)_2$ mediated redox homeostasis in mammalian host and *T. brucei* parasites. Detoxification of ROS is accomplished by a cascade derived from $T(SH)_2$/TR and GSH/GR in parasites and mammalian host,

respectively, with NADPH as the primary electron source. [Adapted from (Paul et al, 2014)].

2.3 Glycosomes and energy metabolism

T. brucei compartmentalize several important metabolic systems such as glycolysis, pentose phosphate pathway (PPP), fatty acids beta-oxidation, and ether-lipid, isoprenoid and purine/pyrimidine biosynthesis in their peroxisomes which are designated glycosomes (Michels et al, 2006). The enzymatic content of these organelles may vary considerably within the life-cycle, in particular, during differentiation between bloodstream and procyclic forms (Michels et al, 2006). This unique glycosome compartmentalization and their large phylogenetic distance with the mammalian hosts provides the parasite with unique features (Chawla & Madhubala, 2010). The glycolytic enzymes compartmentalization within the glycosome was shown to be essential (Bakker et al, 2000; Furuya et al, 2002). Contrary to other organisms in which glycolysis has negative feedback loops to prevent the autocatalytic pathway from losing control [e.g., inhibition of hexokinase (HK) by glucose 6-phosphate (Newsholme et al, 1967) and phosphofructokinase (PFK) by phosphoenolpyruvate (Blangy et al, 1968)], *T. brucei* lacks feedback regulation (Nwagwu & Opperdoes, 1982). Without compartmentalisation, ATP produced in the latter steps of the pathway would be accessible in the first steps causing a turbo explosion within the pathway and death by accumulation of toxic intermediates (Haanstra et al, 2008). In fact, the rate of glucose transport is the main regulator of glycolysis (Haanstra et al, 2011). In contrast to procyclic forms, which contain an extended glycolytic pathway catalyzing the aerobic fermentation of glucose to succinate (Figure 14) (Bochud-Allemann & Schneider, 2002; Coustou et al, 2003), in bloodstream forms, glycolysis of host glucose provides the sole source of carbon for ATP production (Clayton & Michels, 1996; Michels et al, 2006; Tielens & Van Hellemond, 1998). In bloodstream forms, not only the glycolytic enzymes have structural differences compared with their mammalian counterparts, but also the exclusively dependence on glycolysis for ATP production due to a reduced mitochondrial function, present a series of targets for potential therapeutic development (Coley et al, 2011) (Figure 14). Indeed, plasma membrane glucose transporter, as well as the pyruvate transporter that is responsible for the efflux of the trypanosome's glycolytic end-product into the blood, have been chemically validated as drug targets (Bakker et al, 1999; Seyfang & Duszenko, 1991; Wiemer et al, 1995). The genetic validation as drug targets, has been obtained by RNAi

and cKO experiments for the following glycosomal enzymes, HK (Albert et al, 2005; Chambers et al, 2008), PFK (Albert et al, 2005; Kessler & Parsons, 2005), fructose-1,6-bisphosphate aldolase (ALD) (Caceres et al, 2010), triosephosphate isomerase (TPI) (Helfert et al, 2001), and glyceraldehyde-3-phosphate dehydrogenase (GAPDH) (Caceres et al, 2010), as well as for the other enzymes involved in glycolysis but not present in the glycosomes, such as phosphoglycerate mutase (PGAM) (Albert et al, 2005), enolase (ENO) (Albert et al, 2005) and phosphoglycerate kinase (PYK) (Albert et al, 2005). Also chemical validation has been pursued for several enzymes of the glycolytic pathway, such as HK1 (Chambers et al, 2008; Dodson et al, 2011; Sharlow E, 2011; Sharlow et al, 2010; Willson et al, 2002), PFK (Brimacombe et al, 2014; Nowicki et al, 2008; Walsh et al, 2010), ALD (Azema et al, 2006), GAPDH (Aronov et al, 1999), PYK (Drew et al, 2003) and ENO (de A S Navarro et al, 2007).

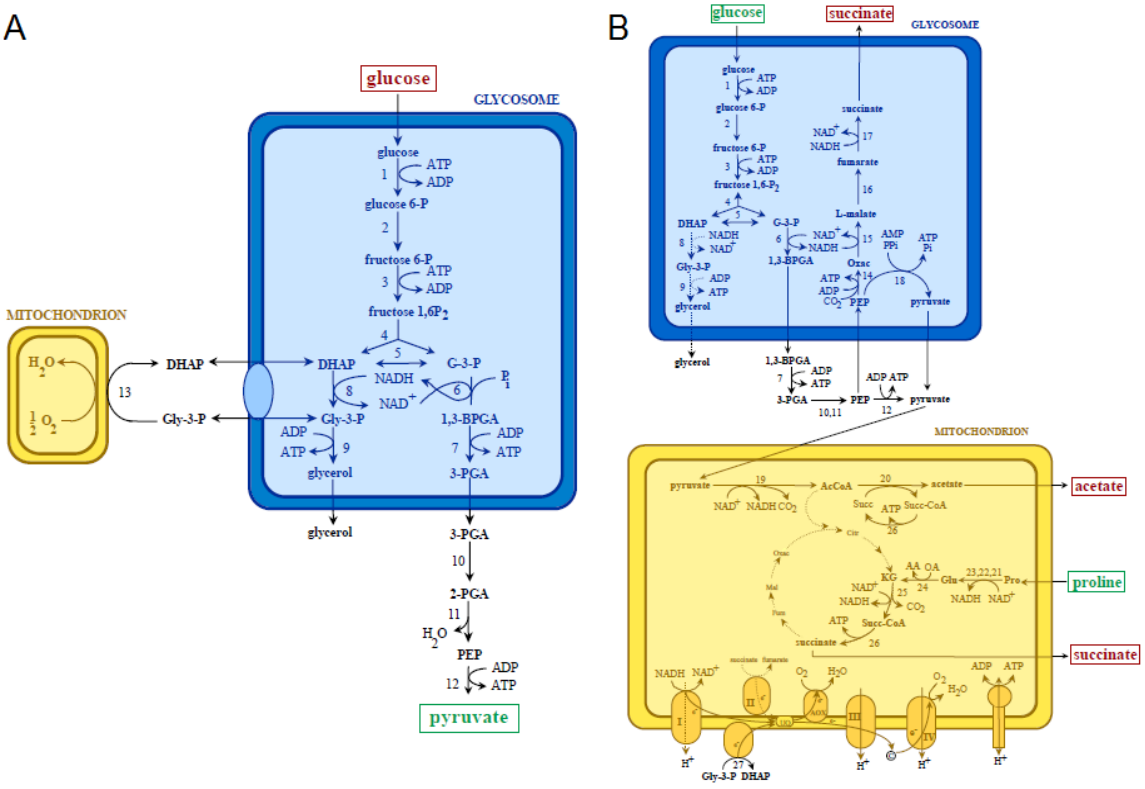

Figure 14. The energy metabolism of bloodstream (a) and procyclic (b) *T. brucei* foms. Enzymes: 1, hexokinase; 2, glucose-6-phosphate isomerase; 3, phosphofructokinase; 4, aldolase; 5, triosephosphate isomerase; 6, glyceraldehyde-3-phosphate dehydrogenase; 7, phosphoglycerate kinase; 8, glycerol-3-phosphate dehydrogenase; 9, glycerol kinase; 10, phosphoglycerate mutase; 11, enolase; 12, pyruvate kinase; 13, glycerol-3-phosphate

oxidase; 14, phospho*enol*pyruvate carboxykinase; 15, L-malate dehydrogenase; 16, fumarase; 17, fumarate reductase; 18, pyruvate phosphate dikinase; 19, pyruvate dehydrogenase complex; 20, acetate:succinate CoA transferase; 21, proline oxidase; 22, Δ'-pyrroline-5-carboxylate reductase; 23, glutamate semialdehyde dehydrogenase; 24, glutamate dehydrogenase; 25, α-ketoglutarate dehydrogenase; 26, succinyl CoA synthetase; 27, FAD-dependent glycerol-3-phosphate dehydrogenase. Abbreviations: AA, amino acid; AcCoA, acetyl-CoA; 1,3-BPGA, 1,3- bisphosphoglycerate; c, cytochrome c; Citr, citrate; DHAP, dihydroxyacetone phosphate; Fum, fumarate; G-3-P, glyceraldehydes 3-phosphate; Glu, glutamate; Gly-3-P, glycerol 3-phosphate; KG, α-ketoglutarate; Mal, malate; OA, 2-oxoacid; Oxac, oxaloacetate; PEP, phospho*enol*pyruvate; 3-PGA, 3-phosphoglycerate; Succ, succinate; Succ-CoA, succinyl CoA; UQ, ubiquinone. Substrates and secreted end-products are indicated in green and red boxes. Enzymes involved in reactions represented by dashed lines are present, but experiments indicated that no significant fluxes occurred through these steps. [Adapated from (Hannaert et al, 2003a)].

2.4 Lipid metabolism

The uniqueness of parasites lipid metabolism provides a number of enzymes that have been proven to be valid targets for the development of novel chemotherapeutics (Lee et al, 2007; van Hellemond & Tielens, 2006). *T. brucei* has two ways to supply itself with fatty acids: acquire fatty acids from the host or synthesize its own fatty acids *de novo* (Smith & Butikofer, 2010). There is a significant difference between the energy required for fatty acid synthesis compared to uptake, explaining why uptake is likely preferred over fatty acid synthesis pathway. However, when the host fatty acid supply is insufficient, the parasite must then synthesize its own fatty acids (Lee et al, 2006). Fatty acid synthesis in trypanosomes comprises at least two pathways, the fatty acid elongase pathway of the endoplasmic reticulum that serves as the major pathway for synthesis (Lee et al, 2006), and a minor pathway in the mitochondria that catalyzes the synthesis of mitochondrial fatty acids (Guler et al, 2008; Stephens et al, 2007). A number of well-known fungi lipid metabolism inhibitors appeared to be also effective against *T. brucei*, as thiolactomycin (and its derivatives) was shown to inhibit type II fatty acid biosynthesis (Jones et al, 2004).

Particularly important to the parasite is phosphatidylinositol, which is a ubiquitous phospholipid that functions as a precursor for cell signaling molecules and provides the basic building block used in GPI anchor biosynthesis. As mentioned before GPI-anchored proteins form a surface coat, known as VSG, which protects the parasite from host

immune response (Hong & Kinoshita, 2009). Some enzymes involved in phosphatidylinositol and GPI synthesis were already validated as targets (Martin & Smith, 2006; Smith et al, 2001). Also a number of natural products that inhibit fatty acid biosynthesis in other parasites have been shown to kill *T. brucei in vitro* (Karioti et al, 2007; Tasdemir et al, 2005; Tasdemir et al, 2007). Myristate is a key component of the *T. brucei* GPI-anchor, and is synthesized by a set of elongase enzymes. The essentiality of these enzymes was demonstrated using RNAi (Lee et al, 2006). N-myristoyltransferase, an enzyme responsible for attachment of myristate to the GPI anchor, showed to be essential for parasite viability based on the same knockdown approach (Price et al, 2003). Homology modelling using crystallographic information from fungal N-myristoyltransferase inhibitors, which also inhibited the trypanosomal enzyme (Bowyer et al, 2008; Panethymitaki et al, 2006), was employed to rational design new *T. brucei* selective inhibitors (Sheng et al, 2009). More recently, pyrazole sulfonamides constituted lead compounds for N-myristoyltransferase inhibition (Frearson et al, 2010).

The synthesis of sphingolipids within the fatty acid metabolism was shown to be critical to *T. brucei* viability. The sphingolipid content and biosynthetic capabilities of parasitic protozoa have drawn attention due to the potential for new chemotherapeutic targets. A key enzyme of sphingolipid biosynthesis pathway is sphingolipid synthase, which has recently been identified and shown to be essential for *T. brucei* survival by RNAi and by chemical inhibition using aureobasidin A (Mina et al, 2009; Sheng et al, 2009). Intracellular degradation of sphingomyelin, which is the main sphingolipid in *T. brucei*, is achieved by sphingomyelinases. *T. brucei* conditional null mutant demonstrates that the neutral sphingomyelinase activity is essential for growth and survival, causing VSG trafficking to be impaired (Young & Smith, 2010).

Protein prenylation through the attachment of farnesyl to proteins is an important regulatory mechanism for signal transduction. The enzyme responsible for this process, protein farnesyltransferase was shown to be a good target (Ali et al, 1999) and was used in screening efforts to identify leads for medicinal chemistry, including a series of tetrahydroquinolines active against *T. brucei* (Eastman et al, 2006).

2.5 Folate metabolism

Folate is an essential cofactor in the biosynthesis of DNA and aminoacids. The inhibition of its metabolism leads to alterations of cell replication and function. *T. brucei* parasites do not have a *de novo* pathway for the synthesis of pteridines (folate and

biopterins) and rely on salvage from the host (Ferrari et al, 2013). They depend on specific transporters for folate and biopterin and in enzymes involved in the biosynthesis of reduced folate, [thymidylate synthase (TS), dihydrofolate reductase (DHFR), and pteridine reductase 1 (PTR1)], which is an essential cofactor for the synthesis of the deoxythymidine-monophosphate (dTMP) necessary for DNA synthesis (Figure 15). TS catalyzes the reductive methylation of deoxyuridine-monophosphate (dUMP) to dTMP, using the cofactor N^5,N^{10}-methylene tetrahydrofolate as a carbon donor and reducing agent. DHFR restores the tetrahydrofolate (H_4F) pool through the NADPH dependent reduction of the dihydrofolate (H_2F) previously produced. In higher plants and protozoa, such as in *T. brucei*, the DHFR and TS activities are achieved by a single bifunctional enzyme, dihydrofolate reductase-thymidylate synthase (DHFR-TS) (Gamarro et al, 1995). PTR1 belongs to the family of short-chain dehydrogenases/reductases, and reduces both folate and biopterin (Robello et al, 1997). Therefore, bifunctional DHFR-TS is specific for folate, while PTR1 reduces both folate and biopterin (Figure 15). DHFR-TS has been chemically and genetically validated as key drug targets (Sienkiewicz et al, 2008). Although a clear chemical scaffold, for a focused lead discovery, have not been yet identified, validation data is sufficiently compelling to warrant efforts to exploit *T. brucei* DHFR as a target (Jacobs et al, 2011). PTR1 knockdown resulted in *T. brucei* loss of viability and virulence in cultures and animal models (Sienkiewicz et al, 2010). Chemical studies attempting to screen PTR1 inhibitors are present in the literature. Aminobenzothiazole and aminobenzimidazole were identified as PTR1 selective inhibitors but showed limited ability to inhibit *T. brucei* growth *in vitro* (Mpamhanga et al, 2009). Apparently other studies have also failed to obtain highly potent PTR1 inhibition and trypanocidal activity in culture (Spinks et al, 2011; Tulloch et al, 2010). Discover the basis for this limitation will be essential to any future efforts. It has been suggested that the inhibition of both enzymes, DHFR-TS and PTR1, would fully arrest the pathway's metabolic function, and the structural differences between trypanosomatids PTR1/DHFR-TS and their mammalian congeners are pronounced enough to enable selective inhibition towards an efficacious and safe therapy (Ferrari et al, 2013).

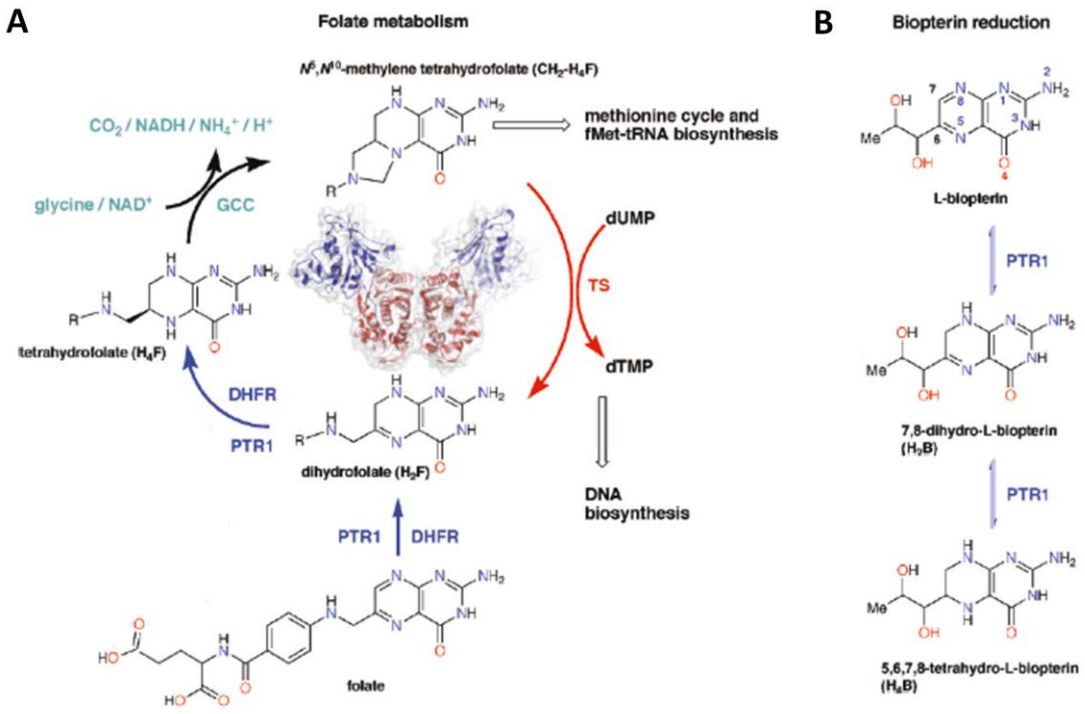

Figure 15. Folate and biopterin reduction in *T. brucei*. (A) Folate reduction catalyzed by both DHFR and PTR1 enzymes. DHFR-TS [Protein Data Bank (PDB) code 2H2Q] is shown in the center of the cycle with DHFR and TS domains colored blue and red, respectively. (B) Two-stage reduction of biopterin catalyzed by PTR1. [Adapted from (Tulloch et al, 2010)].

3 Exploiting the pentose phosphate pathway

As already mentioned, glucose is the only energy source for *T. brucei* bloodstream forms. Besides glycolysis, glucose is also metabolized by PPP. Despite less investigated than glycolysis, it is becoming clear that PPP plays a crucial role in the metabolism of many parasitic protozoa and in their relationship with the host's (Barrett, 1997). In most organisms, the PPP is localized in the cytosol, however in trypanosomatids, including *T. brucei* this pathway can be splited between the cytosol and the glycosomes (Hannaert et al, 2003a). PPP takes part of the carbohydrate metabolism and is important to maintain carbon homeostasis, to provide precursors for nucleotide and amino acid biosynthesis and to supply reducing molecules to defeat oxidative stress. PPP is divided into an oxidative and a non-oxidative branch (Figure 16). The oxidative PPP is considered unidirectional, and converts glucose-6-phosphate into ribulose 5-phosphate (Ru5P) and NADPH, whereas the bidirectional non-oxidative branch metabolizes glycolytic

intermediates yielding R5P (Stincone et al, 2014). The enzymes belonging to this pathway present marked differences from human enzymes, either in structure and/or kinetics, which make them suitable candidates as targets and allow the design of specific inhibitors (Comini et al, 2013).

3.1 Oxidative branch

The oxidative branch includes three steps for the synthesis of Ru5P, with the concomitant production of two moles of NADPH per mole of glucose 6-phosphate consumed (Figure 16) (Barrett, 1997).

Glucose-6-phosphate dehydrogenase (G6PDH; EC1.1.1.49) catalysis the first step of the PPP; glucose 6-phosphate is oxidised to 6-phospogluconolactone, while nicotinamide adenine dinucleotide phosphate ($NADP^+$) is reduced to NADPH (Glaser & Brown, 1955). G6PDH from trypanosomatids share about 50% identity with the human ortholog (Comini et al, 2013). This enzyme is predominantly distributed in the cytosol with a minor fraction compartmentalized in glycosomes (Duffieux et al, 2000; Heise & Opperdoes, 1999; Opperdoes & Szikora, 2006). RNAi mediated reduction of the G6PDH level in bloodstream forms validates genetically this enzyme as a drug target, due to the deleterious phenotype observed [growth arrest and reduced tolerance to hydrogen peroxide (H_2O_2)]. The steroids dehydroepiandrosterone (DHEA) and epiandrosterone (EA) were found to inhibit the enzyme with *K*i values about 6-fold lower than those reported for the human enzyme. Moreover viability assays confirmed the toxic effect of both steroids on cultured *T. brucei* bloodstream forms (Cordeiro et al, 2009). The specific action of steroids against G6PDH was confirmed recently using transgenic cell lines (Gupta et al, 2011).

In the second step, the enzyme 6-phosphogluconolactonase (6-PGL; EC3.1.1.31) hydrolyses 6-phospogluconolactone into 6-phosphogluconate (Duffieux et al, 2000; Miclet et al, 2001). About 85% of 6-PGL is found in the cytosol and 15% in the glycosomes, thus showing a dual localization (Duclert-Savatier et al, 2009). *T. brucei* 6-PGL crystal structure has been recently resolved, in the absence and presence of ligands (Delarue et al, 2007; Duclert-Savatier et al, 2009), which allows a detailed mechanistic characterization of the enzyme. The low amino acid identity (below 20%) with the human ortholog predicts important structural differences (Comini et al, 2013), however the essentiality of 6PGL has not yet been addressed.

Lastly, 6-phosphogluconate is oxidised and decarboxylated to Ru5P by 6-phosphogluconate dehydrogenase (6-PGDH; EC1.1.1.44), while again reducing $NADP^+$ to NADPH (Dickens & Glock, 1951). This protein is predominantly cytosolic, with a small glycosomal component in procyclics (Heise & Opperdoes, 1999). 6-PGDH from kinetoplastids exhibits low amino acid sequence identity (less than 35%) with its mammalian counterpart (Barrett, 1997; Comini et al, 2013). *T. brucei* 6-PGDH three-dimensional structure has been determined and compared against the sheep liver enzyme (Phillips et al, 1998). Despite the low protein sequence identity between both enzymes, a high conservation in the overall structure and in the residues directly engaged in substrate and coenzyme binding was observed. Several secondary residues surrounding the substrate-binding site and others bridging the C-terminal tail on the coenzyme binding site, differed significantly in identity and in structural arrangement and were proposed to account for the different affinities of substrate/coenzyme and inhibitors (Adams et al, 1994; Comini et al, 2013). Deletion of *T. brucei* 6-PGDH, leads to the accumulation of 6-phosphogluconate which inhibits phosphoglucose isomerase and consequently glycolysis (Hanau et al, 2004). The relevance of 6-PGDH for *T. brucei* was first revealed through cytotoxic studies using several substrate and cofactor analogues, as well as high-energy intermediates and transition-state analogues in inhibition studies (Dardonville et al, 2004; Dardonville et al, 2003). Some hydroxamate derivatives of D-erythronic acid, analogues of the high-energy intermediate, were found to be potent and selective inhibitors of the parasite enzyme (Dardonville et al, 2004). From this study the compound 2,3-*o*-isopropylidene-4-erythrono hydroxamate showed to be a potent inhibitor, however does not have trypanocidal activity due to its poor membrane permeability. Therefore phosphate prodrugs have been developed to circumvent this aspect. The class of aryl phosphoramidate prodrugs of 2,3-*o*-isopropylidene-4-erythrono hydroxamate showed high trypanocidal activity and a good correlation between activities with their stability in mouse blood (Ruda et al, 2010b). More recently, a novel “virtual fragment screening” approach, in which the structure of the *Lactococcus lactis* 6-PGDH (almost identical to *T. brucei*) was used as docking template, allowed the discovery of some compounds with good IC_{50} against *T. brucei* 6-PGDH (Ruda et al, 2010a).

To sum up, the oxidative branch is therefore crucial once it supplies cells with Ru5P, a precursor of the non-oxidative PPP, and with NADPH an essential reducing agent involved not only in many biosynthetic reactions, including *de novo* lipid synthesis, but also in protecting cells against oxidative stress by regenerating GSH (Comini et al, 2013).

3.2 Non-oxidative branch

In the non-oxidative part, the formed Ru5P can be converted either to R5P or to xylulose 5-phosphate. Thereafter two enzymes, transketolase (TKT) and transaldolase (TAL), are responsible for the relative complex interconversion reactions between R5P/xylulose 5-phosphate and glycolytic intermediates glyceraldehyde 3-phosphate/fructose 6-phosphate via reshuffling of monophosphate sugars (Figure 16) (Stincone et al, 2014). Through the sharing of these intermediates, TKT and TAL act as a bridge between glycolysis and the PPP. Moreover they connect to sedoheptulose 7-phosphate which is synthesized also by other sources, thus representing a glycolysis-independent entry and exit point into/from the non-oxidative PPP (Stincone et al, 2014).

Rpi (EC 5.3.1.6) converts Ru5P into R5P and the other way around. This enzyme is classified into type A (distributed in mammals, fungi and some bacteria) or B (restricted to some bacteria and protozoa). The absence of type B Rpi in mammalians and the significant structural divergence between both enzymes have raised interest on trypanosomal RpiB. Both *T. cruzi* and *Leishmania donovani* (*L. donovani*) Rpi have been suggested as potential drug targets, although genetic and chemical validation are still lacking (Kaur et al, 2012; Stern et al, 2007). The competitive inhibitor analogous of the isomerization intermediate, 4-phospho-D-erythronohydroxamic acid (4-PEH), was shown to be the best inhibitor against RpiB (Roos et al, 2005; Stern et al, 2007). However, it also strongly inhibits type A enzyme (Roos et al, 2005) and its antiparasitic activity is still unclear.

The ribose 5-phosphate epimerase (RPE; EC 5.3.1.4) interconverts Ru5P and xylulose 5-phosphate. In *T. brucei* RPE activity was detected in procyclics, but not in parasites isolated from mice (Cronin et al, 1989), which therefore does not qualify as potential target against HAT.

TKT (EC 2.2.1.1) is an enzyme capable of catalysing two distinct reversible reactions that involved the transfer of two carbon atoms: (i) from xylulose 5-phosphate to R5P, producing glyceraldehyde 3-phosphate and sedoheptulose 7-phosphate, and (ii) from xylulose 5-phosphate to erythrose 4-phosphate to generate glyceraldehyde 3-phosphate and fructose 6-phosphate, using thiamine diphosphate as a cofactor (Schenk et al, 1998). The structure of the human TKT was determined (Mitschke et al, 2010), and at least two residues involved in the binding of the cofactor and substrate (Gln189 and Lys260) are not conserved in trypanosomatids (Comini et al, 2013). Although, TKT null procyclics showed a remarkable alteration in the metabolic profile, did not exhibit any *in*

vitro growth or morphological phenotype (Stoffel et al, 2011). Additionally, TKT activity was shown repressed in bloodstream stages (Cronin et al, 1989), suggesting TKT is not a good drug target.

TAL (EC 2.2.1.2) transfer a three-carbon fragment, dihydroaxyacetone, from sedoheptulose 7-phosphate to glyceraldehyde 3-phosphate, producing fructose 6-phosphate and erythrose 4-phosphate. The backward reaction is also catalyzed by this enzyme (Comini et al, 2013). TAL was detected in the cytosol of *T. brucei* bloodstream forms (Cronin et al, 1989), however its role was never addressed. Once these forms present a defective non-oxidative branch, including an absence of TKT activity whose products constitute substrates for TAL, TAL protein can be disregarded as a drug target candidate (Comini et al, 2013).

In resume, the non-oxidative PPP has recently started to receive more attention, and in fact deserves further investigation once supplies parasites with R5P, to form the RNA and DNA backbone, and erythrose 4-phosphate, a precursor of aromatic amino acids and vitamin B6 (Stincone et al, 2014).

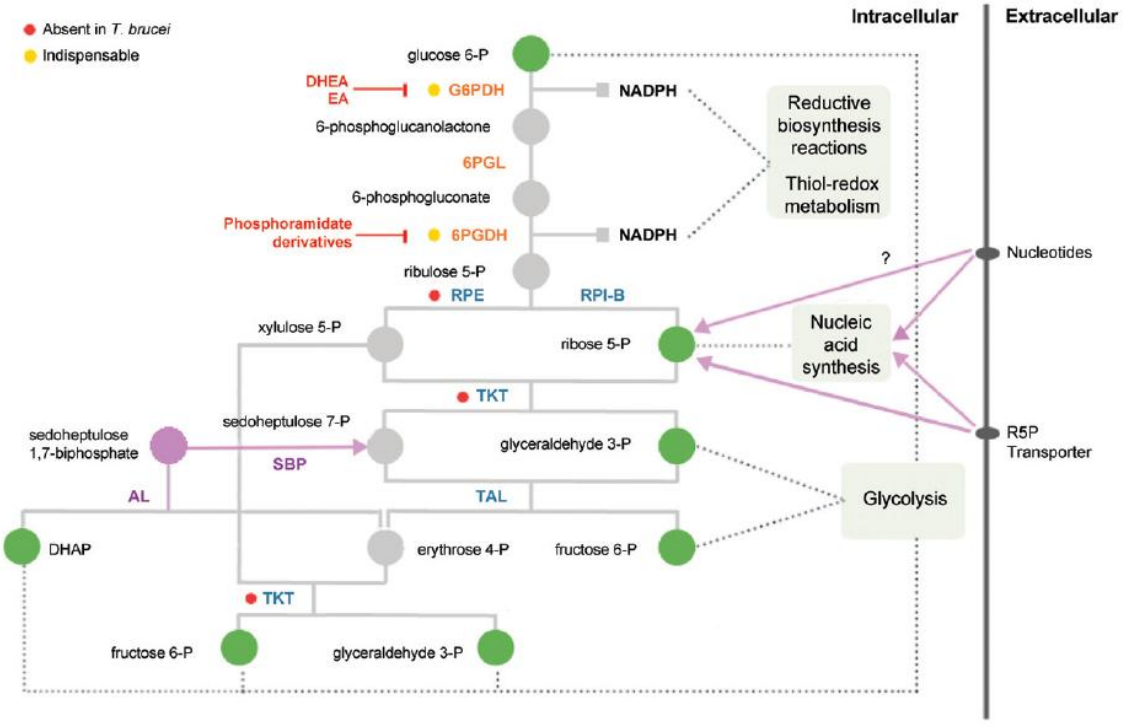

Figure 16. Scheme of the PPP in *T. brucei*: components, biological relevance, and inhibitors. The substrates and products of the PPP that are shared with other metabolic pathways are labelled with a green dot. Characterized enzyme inhibitors are shown in red. The enzymes of the oxidative and non-oxidative phase of the PPP are in orange and blue,

respectively. Salvage pathways for R5P are in lilac. Enzymes absent in infective *T. brucei* are marked with red dot. Enzymes of proved indispensability are indicated with yellow dot. [Adapted from (Comini et al, 2013)].

4 Exploiting asparagine metabolic pathway

Asparagine is a non-essential amino acid, meaning it can be synthesized from central metabolic pathway intermediates and is not required in the diet. This amino acid is frequently involved in protein active or binding sites (Snijder et al, 2001; Vernet et al, 1995) and additionally, asparagine (N)-linked glycosylation of proteins is a fundamental and extensive post-translational modification that results in the covalent attachment of an oligosaccharide onto asparagine residues of polypeptide chains (Schwarz & Aebi, 2011). Asparagine has a high nitrogen/carbon ratio and it is therefore linked to nitrogen homeostasis and protein biosynthesis. Moreover, the removal of this amino acid by L-asparaginase is widely used in chemotherapeutic protocols for treatment of acute lymphoblastic leukemia (Richards & Schuster, 1998). All these facts explain the growing biochemical and genetic studies of enzymes related with asparagine metabolism.

Two major pathways called tRNA-dependent and independent are involved in asparagine metabolism. In addition, organisms may also uptake asparagine from the exterior (Min et al, 2002) (Figure 17). Different environmental and physiological conditions can modulate the synthesis and import of asparagine (Benko et al, 1969; Hunter & Segel, 1971; Hunter & Segel, 1973; Pall, 1970; Zheng & Haselkorn, 1996). Actually some cells rely on extracellular asparagine to reach the total requirements of this amino acid. Examples of cells that must import asparagine, include asparagine auxotrophs (usually not found in nature and result from genetic manipulation, being unable to growth in minimal medium unless asparagine is added to the culture (Jones, 1978; Min et al, 2002; Qian et al, 2013; Reitzer & Magasanik, 1982; Willis & Woolfolk, 1975)), and leukemia cells which exhibit a particularly low level of asparagine and therefore are sensitive to exogenous asparagine depletion (Rizzari et al, 2013).

Very few data is available in literature concerning asparagine metabolism and transport in *T. brucei*. The ever-changing environments during *T. brucei* life cycle leads to a variable repertoire of transporters on their surfaces (Berriman et al, 2005; Besteiro et al, 2005). Trypanosomes have in their flagellar pockets a high rate of endo and exocytosis, and of transporters required for the uptake of many essential nutrients (Field & Carrington, 2009). RNAi against *T. brucei* AATP1 characterized this protein as a transporter of small

neutral amino acids, with the following order of affinity: L-threonine > L-serine > glycine > L-alanine > L-cysteine > L-asparagine (Ebikeme, 2007). Asparagine is the only *Tb*AATP1 specific amino acid with a hydrophilic side group and, consequently is the least specific, however, its side group is small enough to be recognised by this transporter. Nevertheless the apparent high level of redundancy in amino acid transporters suggests that blocking them would not cause detriment to the parasites (Ebikeme, 2007).

4.1 t-RNA dependent reactions

Aminoacyl-tRNA synthetases are central enzymes in protein translation, providing the charged tRNAs needed for appropriate construction of peptide chains. These enzymes catalyze a two-step reaction whereby an ATP and amino acid molecule enter the active site, forming an aminoacyl-adenylate intermediate followed by the esterification of the amino acid to the end of the tRNA, forming the final 'charged' aminoacyl-tRNA (Pham et al, 2014). The synthesis of Asn-tRNA^{Asn} is made through direct and/or indirect tRNA aminoacylation reactions of the tRNA dependent pathway (Figure 17A). In the presence of a discriminating asparaginyl-tRNA synthetase, (EC 6.1.1.22) a canonical aminoacylation occurs forming Asn-tRNA^{Asn} (Min et al, 2002). However, half of the prokaryotes, including bacteria and archaea do not use a full complement of 20 canonical aminoacyl-tRNA synthetases enzymes to synthesize aminoacyl-tRNA for protein synthesis (Blaise et al, 2011). In these cases, a non-discriminating aspartyl-tRNA synthetase (EC 6.1.1.23) generates the misacylated Asp-tRNA^{Asn} species which are amidated to the correctly charged Asn-tRNA^{Asn} by the Asp-tRNA^{Asn} amidotransferase (EC 6.3.5.6), using preferentially glutamine over asparagine or ammonium chloride as amide donor (Blaise et al, 2011; Tumbula et al, 2000). Non-discriminating forms are most commonly found in organisms lacking asparaginyl-tRNA synthetase, therefore the combination of non-discriminating aspartyl-tRNA synthetase and Asp-tRNA^{Asn} amidotransferase provides the sole route for Asn-tRNA^{Asn} biosynthesis (Curnow et al, 1998; Roy et al, 2003). Rarely, a given bacterium will encode for both discriminating and non-discriminating forms (e.g. *Thermus thermophilus* and *Deinococcus radiodurans*) (Becker & Kern, 1998; Curnow et al, 1998). Phylogenetic and experimental analysis suggest that asparaginyl-tRNA synthetase evolved from an ancestral aspartyl-tRNA (Figure 17B) (Feng et al, 2005; Raczniak et al, 2001; Roy et al, 2003; Shiba et al, 1998; Tumbula-Hansen et al, 2002; Woese et al, 2000; Wolf et al, 1999). The evolutionary trend appears that horizontal gene transfer has allowed some indirect pathways to be supplanted by direct ones, and not the

reverse (Szathmary, 1999), which might in part be due to the arguably greater efficiency of the direct pathways. As a matter of fact, selectivity is a major issue because the human genome encodes for 36 aminoacyl-tRNA synthetases that have eukaryotic and bacterial origins (Pham et al, 2014). It is a challenge to avoid potential cytotoxicity in aminoacyl t-RNA synthetase inhibition. Strategies to circumvent host toxicity include exploitation of bacterial-type aminoacyl-tRNA synthetase where the human homologue is divergent, as is the case of *Leishmania* asparaginyl t-RNA synthetase (Gowri et al, 2012), or exploitation of parasite-specific modifications (Bour et al, 2009). Asparaginyl-tRNA synthetase has been a long-standing drug target in *Brugia malayi*, a nematode which causes lymphatic filariasis (Pham et al, 2014). In *T. brucei* mammalian stage parasites, the knockdown of mRNA encoding asparaginyl-tRNA synthetase (Tb927.4.2310) resulted in a severe *in vitro* growth defect showing that this enzyme is essential for the parasite, however drugability studies are not yet available (Kalidas et al, 2014).

4.2 t-RNA independent reactions

AS catalyzes direct reactions of asparagine synthesis within the t-RNA independent pathway, performing the ATP-dependent conversion of aspartic acid to asparagine, employing either glutamine or ammonia as the nitrogen source (Figure 17A). There are two unlinked genes, *asnA* and *asnB*, that encode for mechanistically distinct enzymes (Nakamura et al, 1981; Scofield et al, 1990).

The *asnA* gene encodes type A enzyme (EC 6.3.1.1; putative Tb927.7.1110 in *T. brucei*) in prokaryotes, archaea and protozoan parasites (Blaise et al, 2011; Blattner et al, 1997; Gowri et al, 2012; Nakamura et al, 1981; Reitzer & Magasanik, 1982; Sugiyama et al, 1992). AS-A forms asparagine through two steps: the β-carboxylate group of aspartate is first activated by ATP to form an aminoacyl-AMP, before its amidation by a nucleophilic attack with an ammonium ion (Blaise et al, 2011). This type A enzyme is considered strictly ammonia-dependent (Cedar & Schwartz, 1969a; Cedar & Schwartz, 1969b; Reitzer & Magasanik, 1982). Structural studies (Blaise et al, 2011; Nakatsu et al, 1998), coupled with sequence analysis (Wolf et al, 2001), site-directed mutagenesis experiments (Gatti & Tzagoloff, 1991; Hinchman et al, 1992), phylogenetic and biochemical data (Blaise et al, 2011; Roy et al, 2003) show that AS-A derives from the aspartyl t-RNA synthetase ancestor (Figure 17B). It was hypothesized that aspartyl t-RNA synthetase ancestor gene duplicated, with one copy leading to the archaeal aspartyl t-RNA synthetase and the other undergoing a second gene duplication. One gene of this second

duplication gave rise to asparaginyl-tRNA synthetase, while the second copy evolved to the archaeal AS-A. To do so, the latter, firstly lost its anticodon binding domain and secondly rearranged its catalytic site, leading to loss of capacity to aminoacylate $tRNA^{Asp}$ while acquiring the ability to activate the β-carboxylate of aspartate. Archaeal AS-A was then horizontally transferred from archaea to bacteria, where it evolved into the current AS-A (Blaise et al, 2011). Till now AS-A was suggested as a drug target against *L. donovani* parasites (Gowri et al, 2012; Manhas et al, 2014), in *T. brucei* remains to be studied.

AS-B (EC 6.3.5.4; putative Tb927.3.4060 in *T. brucei*), encoded by *asnB* gene, is present not only in prokaryotes (Humbert & Simoni, 1980; Reitzer & Magasanik, 1982), but also in eukaryotes, including mammalian cells (Andrulis et al, 1987; Andrulis et al, 1989), yeasts (Ramos & Wiame, 1980), algae (Merchant et al, 2007), and higher plants (Coruzzi, 2003). The N-terminal of AS-B catalyzes the conversion of glutamine into glutamic acid and ammonia, and aspartate reacts with ATP in the C-terminal site, generating the intermediate β-aspartyl-AMP (Boehlein et al, 1998; Luehr & Schuster, 1985). The ammonia released in the N-terminal domain of the enzyme travels through an intramolecular tunnel connecting the active sites, and reacts with the reactive acyladenylate intermediate to produce asparagine (Huang, 2001). Glutamine is the preferred source of nitrogen for AS-B (Boehlein et al, 1994; Duff et al, 2011; Horowitz & Meister, 1972; Patterson & Orr, 1968; Ramos & Wiame, 1979; Reitzer & Magasanik, 1982), except for human enzyme that has similar affinity for glutamine and ammonia (Ciustea et al, 2005). The larger size of type B enzyme compared with A, and the additional ability of type B to use either glutamine or ammonia as the nitrogen donor have led to the speculation that *asnB* was formed by the fusion of an ancestral glutamine amidotransferase gene with an ancestral ammonia-dependent *asn* gene homologous to *asnA* (Gaufichon et al, 2013). Moreover phylogeny studies also showed homologs of glutamine-dependent AS within bacterial, eukaryal, and archaeal lineages, therefore suggesting that type B enzyme evolved before the segregation of organisms into the modern cell types (Min et al, 2002). AS-B is regarded as a potential therapeutic target in the treatment of pancreatic, ovarian, hepatic and breast tumours (Dufour et al, 2012; Lorenzi et al, 2008; Lorenzi et al, 2006; Yang et al, 2014). It is also generally accepted that the role of AS-B in leukaemic cells regarding resistance to L-asparaginase treatment may vary among genetic subtypes (den Boer et al, 2005; Stams et al, 2005), due to different AS expression. Therefore AS-B inhibition together with L-asparaginase

administration might be a new strategy for the treatment of tumours patients with high AS expression.

Regarding studies on AS inhibition, a transition state analogue of cysteine sulfoximine, N-adenylated S-methyl-L-cysteine sulfoximine was synthesized and showed to be an extremely potent slow binding inhibitor of *E. coli* type A enzyme (Koizumi et al, 1999). This inhibitor was also found to effectively inhibit type B enzymes (Boehlein et al, 2001; Gutierrez et al, 2006).

Alternative asparagine synthetic pathways were described, but apparently are not present in *T. brucei*. In higher plants and bacteria, β-cyanoalanine is hydrolyzed into asparagine by β-cyanoalanine hydratase (EC 4.2.1.65) (Brysk et al, 1969; Castric et al, 1972; Castric & Strobel, 1969; Piotrowski & Volmer, 2006), and in mouse (Maul & Schuster, 1986), rat liver (Cooper, 1977), and in plants (Ireland & Joy, 1983; Zhang et al, 2013), asparagine-oxo-acid transaminase (EC 2.6.1.14) catalysis the reverse reaction of L-asparagine and α-2-oxo-carboxylate, to produce 2-oxosuccinamate and an amino acid (Meister & Fraser, 1954).

Asparaginases (EC 3.5.1.1) catalyze the hydrolysis of asparagine into aspartate and ammonium ion. Firstly, the nucleophilic threonine attacks the carbonyl of the amide substrate to generate an acyl-enzyme intermediate, releasing ammonia. In the second step, water attacks the acyl-enzyme intermediate to produce L-aspartate (Michalska & Jaskolski, 2006). In some infections asparaginase constitutes a virulence factor, like in the case of *Campylobacter jejuni* (Hofreuter et al, 2008), *Helicobacter pylori* (Scotti et al, 2010; Shibayama et al, 2011), *Salmonella typhimurium* (Kullas et al, 2012) and *Mycobacterium tuberculosis* (Gouzy et al, 2014). Asparaginase takes part of therapeutic strategies against cancer metabolism, rather than a therapeutic target (Rizzari et al, 2013). In *T. brucei*, asparaginase does not seems to be present (Ginger, 2007).

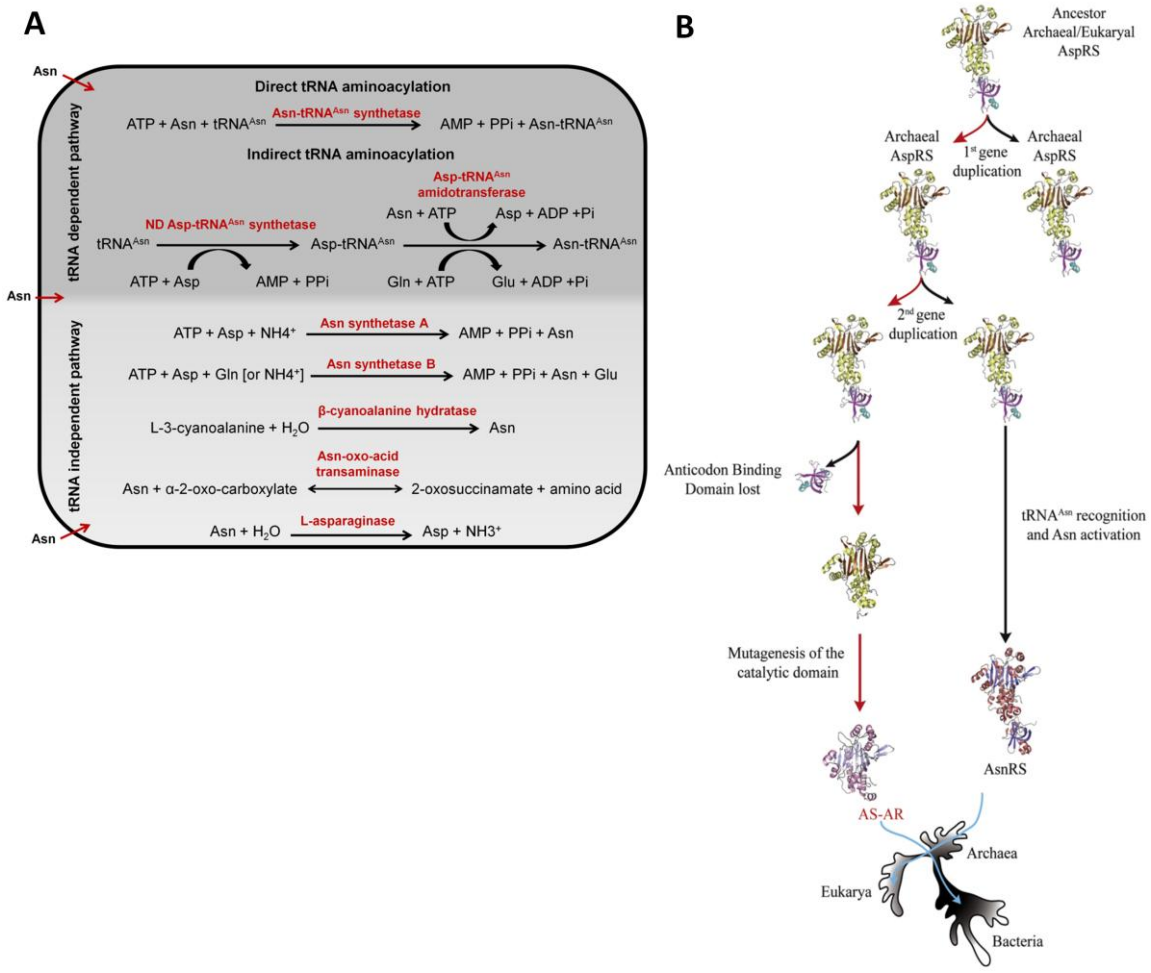

Figure 17. Enzymes involved in asparagine metabolism. (A) Asparagine consumption, synthesis and uptake. Enzymes involved in tRNA-dependent and independent pathways within asparagine metabolism are depicted. (B) Hypothetical scenario for asparaginyl-tRNA (AsnRS) and archeal AS (AS-AR) evolution. AsnRS and AS-AR derives from the same ancestor aspartyl-tRNA (AspRS). The gene of the AspRS ancestor duplicated, with one copy leading to archaeal/eukaryal AspRS and the other undergoing second gene duplication. One gene of this second duplication gave rise to AsnRS, while the second copy evolved to AS-AR through loss of the anticodon binding domain and mutations in the catalytic site. Thereafter AsnRS and AS-AR were horizontally transferred from archaea to other phylae. [Adapted from (Blaise et al, 2011)].

Chapter III

Objectives and results

1 Scope of the thesis

HAT caused by *T. brucei* parasite continues to exact a huge burden on people's lives and economy in African developing countries. Disease control is dependent on drug therapy due to the absence of a human vaccine. Nevertheless the current available drugs are of inefficient delivery, insufficient efficacy and of excessive toxicity. Moreover, the increasing resistance against the present chemotherapy imposes the discovery and validation of new drug targets to reach novel compounds (Babokhov et al, 2013). The genome sequence availability (Berriman et al, 2005) offers a unique avenue for identification of novel therapeutic targets. By using an *in silico* subtractive genomic approach, several hits came out as potential targets. AS-A and RpiB were selected based on the following criteria: i) absence of a human homologue, ii) commitment in more than one metabolic pathway, iii) "workable" size of the gene and protein, iv) availability of homologous 3D structures, and v) availability of theoretical inhibitors. The selection of a target, based on a genomic screening, implies its chemical and/or genetic validation. Therefore, the main purpose of this thesis was to evaluate genetically the functional significance of AS-A and RpiB for parasites survival and infectivity. Moreover, proteins were biochemically characterized and their subcellular localization and expression within the parasite life cycle investigated. Results section is divided in two main parts. The first part is on AS-A, an enzyme that uses ammonia as nitrogen donor for the conversion of aspartate into asparagine, which is important in nitrogen homeostasis and protein biosynthesis (Richards & Schuster, 1998). The second part provides results of RpiB, an enzyme of the non-oxidative PPP that interconverts Ru5P and R5P, playing crucial roles in carbohydrate metabolism and acid nucleic synthesis (Stincone et al, 2014). In order to functional characterize the two candidate targets, AS-A and RpiB, the specific objectives of this thesis were:

i. *In silico* analysis of the theoretical 3D protein structures;
ii. Biochemical characterization of the recombinant proteins;
iii. Study the effect of theoretical inhibitors on the enzymes activity;
iv. Analyze protein expression profiles between different parasite life cycle stages;
v. Define proteins subcellular localization;
vi. Analyze the *in vitro* and *in vivo* phenotypes of RNAi transgenic parasites.

2 Results

2.1 Knockdown of asparagine synthetase A renders *Trypanosoma brucei* auxotrophic to asparagine

Asparagine synthetase (AS) catalyzes the ATP-dependent conversion of aspartate into asparagine using ammonia or glutamine as nitrogen source. There are two distinct types of AS, asparagine synthetase A (AS-A), known as strictly ammonia-dependent, and asparagine synthetase B (AS-B), which can use either ammonia or glutamine. The absence of AS-A in humans, and its presence in trypanosomes, suggested AS-A as a potential drug target that deserved further investigation. We report the presence of functional AS-A in *Trypanosoma cruzi* (*Tc*AS-A) and *Trypanosoma brucei* (*Tb*AS-A): the purified enzymes convert L-aspartate into L-asparagine in the presence of ATP, ammonia and Mg^{2+}. *Tc*AS-A and *Tb*AS-A use preferentially ammonia as a nitrogen donor, but surprisingly, can also use glutamine, a characteristic so far never described for any AS-A. *Tb*AS-A knockdown by RNAi didn't affect *in vitro* growth of bloodstream forms of the parasite. However, growth was significantly impaired when *Tb*AS-A knockdown parasites were cultured in medium with reduced levels of asparagine. As expected, mice infections with induced and non-induced *T. brucei* RNAi clones were similar to those from wild-type parasites. However, when induced *T. brucei* RNAi clones were injected in mice undergoing asparaginase treatment, which depletes blood asparagine, the mice exhibited lower parasitemia and a prolonged survival in comparison to similarly-treated mice infected with control parasites. Our results show that *Tb*AS-A can be important under *in vivo* conditions when asparagine is limiting, but is unlikely to be suitable as a drug target.

Reprinted from PLoS Negl Trop Dis. 2013 Dec 5;7(12):e2578. doi: 10.1371/journal.pntd.0002578.

OPEN ACCESS Freely available online

PLOS | NEGLECTED TROPICAL DISEASES

Knockdown of Asparagine Synthetase A Renders *Trypanosoma brucei* Auxotrophic to Asparagine

Inês Loureiro[1], Joana Faria[1], Christine Clayton[2], Sandra Macedo Ribeiro[3], Nilanjan Roy[4], Nuno Santarém[1], Joana Tavares[1☯]*, Anabela Cordeiro-da-Silva[1,5☯]*

1 Parasite Disease Group, Instituto de Biologia Molecular e Celular da Universidade do Porto, Porto, Portugal, **2** Zentrum für Molekulare Biologie der Universität Heidelberg, DKFZ-ZMBH Alliance, Heidelberg, Germany, **3** Protein Crystallography Group, Instituto de Biologia Molecular e Celular da Universidade do Porto, Porto, Portugal, **4** Ashok and Rita Patel Institute of Integrated Study and Research in Biotechnology and Allied Sciences, New Vallabh Vidyanagar, Gujarat, India, **5** Departamento de Ciências Biológicas, Faculdade de Farmácia da Universidade do Porto, Porto, Portugal

Abstract

Asparagine synthetase (AS) catalyzes the ATP-dependent conversion of aspartate into asparagine using ammonia or glutamine as nitrogen source. There are two distinct types of AS, asparagine synthetase A (AS-A), known as strictly ammonia-dependent, and asparagine synthetase B (AS-B), which can use either ammonia or glutamine. The absence of AS-A in humans, and its presence in trypanosomes, suggested AS-A as a potential drug target that deserved further investigation. We report the presence of functional AS-A in *Trypanosoma cruzi* (*Tc*AS-A) and *Trypanosoma brucei* (*Tb*AS-A): the purified enzymes convert L-aspartate into L-asparagine in the presence of ATP, ammonia and Mg^{2+}. *Tc*AS-A and *Tb*AS-A use preferentially ammonia as a nitrogen donor, but surprisingly, can also use glutamine, a characteristic so far never described for any AS-A. *Tb*AS-A knockdown by RNAi didn't affect *in vitro* growth of bloodstream forms of the parasite. However, growth was significantly impaired when *Tb*AS-A knockdown parasites were cultured in medium with reduced levels of asparagine. As expected, mice infections with induced and non-induced *T. brucei* RNAi clones were similar to those from wild-type parasites. However, when induced *T. brucei* RNAi clones were injected in mice undergoing asparaginase treatment, which depletes blood asparagine, the mice exhibited lower parasitemia and a prolonged survival in comparison to similarly-treated mice infected with control parasites. Our results show that *Tb*AS-A can be important under *in vivo* conditions when asparagine is limiting, but is unlikely to be suitable as a drug target.

Citation: Loureiro I, Faria J, Clayton C, Ribeiro SM, Roy N, et al. (2013) Knockdown of Asparagine Synthetase A Renders *Trypanosoma brucei* Auxotrophic to Asparagine. PLoS Negl Trop Dis 7(12): e2578. doi:10.1371/journal.pntd.0002578

Editor: Alejandro Buschiazzo, Institut Pasteur de Montevideo, Uruguay

Received August 1, 2013; **Accepted** October 25, 2013; **Published** December 5, 2013

Funding: The authors received no specific funding for this study.

Competing Interests: The authors have declared that no competing interests exist.

* E-mail: jtavares@ibmc.up.pt (JT); cordeiro@ibmc.up.pt (ACdS)

☯ These authors contributed equally to this work.

Introduction

Asparagine is a naturally occurring non-essential amino acid found in many proteins. Due to its high nitrogen/carbon ratio, asparagine is likely to be linked to nitrogen homeostasis and protein biosynthesis [1]. AS is the protein involved in asparagine biosynthesis. There are two distinct types of AS, AS-A and AS-B, encoded by *asnA* and *asnB* genes, respectively. AS-A encoding genes have been reported in archaea [2,3], prokaryotes [4–7], and in the protozoan parasite *Leishmania* [8]. The AS-B encoding gene is present in prokaryotes [5,9] and also in eukaryotes, including mammalian cells [10,11], yeasts [12], algae [13], and higher plants [14]. Both types catalyze the ATP-dependent conversion of aspartate into asparagine. While AS-B can use both ammonia and glutamine (reaction B) as amide nitrogen donors [5,15–20], *Escherichia coli* (*E. coli*) AS-A was reported to be dependent strictly on ammonia (reaction A) [21,22].

A) ATP + L-aspartate + $NH4^+$ => AMP + diphosphate + L-asparagine

B) ATP + L-aspartate + L-glutamine [or $NH4^+$] => AMP + diphosphate + L-asparagine + L-glutamate

AS-A and AS-B share no sequence or structural similarities. Their three-dimensional structures provided important information concerning their distinct catalytic mechanisms [2,23–25]. AS-A exists as a dimer where each monomer has a core of eight β-strands flanked by α-helices, resembling the catalytic domain of class II aminoacyl-tRNA synthetases such as aspartyl-tRNA synthetase [24]. AS-A synthesizes asparagine in two steps: the β-carboxylate group of aspartate is first activated by ATP to form an aminoacyl-AMP, followed by amidation by a nucleophilic attack with an ammonium ion [2]. The AS-B enzyme also forms a dimer, but each monomer contains two distinct domains, each of which contains a catalytic site. The N-terminal site catalyzes the conversion of glutamine into glutamic acid and ammonia, while aspartate reacts with ATP in the C-terminal site, generating the intermediate β-aspartyl-AMP [26,27]. Similarly to other glutamine dependent amidotransferases, ammonia released in the N-terminal domain of the enzyme travels through an intramolecular tunnel connecting the active sites, and reacts with the reactive acyladenylate intermediate to produce asparagine [28].

An open reading frame encoding a putative AS-A is present in the genome of the protozoan parasites, *Trypanosoma cruzi* (*T. cruzi*) and *Trypanosoma brucei* (*T. brucei*) [29–31]. *T. cruzi* and *T. brucei* are

Author Summary

The amino acid asparagine is important not only for protein biosynthesis, but also for nitrogen homeostasis. Asparagine synthetase catalyzes the synthesis of this amino acid. There are two forms of asparagine synthetase, A and B. The presence of type A in trypanosomes, and its absence in humans, makes this protein a potential drug target. Trypanosomes are responsible for serious parasitic diseases that rely on limited drug therapeutic options for control. In our study we present a functional characterization of trypanosomes asparagine synthetase A. We describe that *Trypanosoma brucei* and *Trypanosoma cruzi* type A enzymes are able to use either ammonia or glutamine as a nitrogen donor, within the conversion of aspartate into asparagine. Furthermore, we show that asparagine synthetase A knockdown renders *Trypanosoma brucei* auxotrophic to asparagine. Overall, this study demonstrates that interfering with asparagine metabolism represents a way to control parasite growth and infectivity.

transmitted to a mammalian host through an invertebrate vector, and are responsible for Chagas disease and African sleeping sickness, respectively. Disease control is dependent on drug therapy, but treatment options are limited, both by high toxicity and recent emergence of drug resistance [32–34]. Vaccines for *T. brucei* infections are unlikely to be developed not only because of extensive antigenic variation [35], but also because infections compromise host humoral immune competence [36].

Trypanosome AS-A might be a drug target due to the absence of a homologue in humans [8]. AS-A is important in other microorganisms. For example, *asnA* is an essential gene in *Haemophilus influenzae* (DEG10050178) [37], and is strongly up-regulated in *Pasteurella multocida* during host infection [38], and when *Klebsiella aerogenes* is grown in an amino acid-limited but ammonia rich environment [5]. We therefore undertook biochemical and genetic studies of AS-A in trypanosomes to ascertain its biological role and evaluate its potentiality as drug target.

Materials and Methods

Ethics statement

All experiments involving animals were carried out in accordance with the IBMC.INEB Animal Ethics Committees and the Portuguese National Authorities for Animal Health guidelines, according to the statements on the directive 2010/63/EU of the European Parliament and of the Council. IL, JT and ACS have an accreditation for animal research given by the Portuguese Veterinary Direction (Ministerial Directive 1005/92).

Parasite culture

Procyclic and bloodstream forms of *Trypanosoma brucei brucei* Lister 427 were used. Procyclic forms were grown in MEM-Pros medium supplemented with 7.5 μg/ml hemin, 10% fetal calf serum (FCS) and 100 IU/mL of penicillin/streptomycin at 27°C, with cell densities between 5×10^5 cells/ml to $1–2\times10^7$ cells/ml. Bloodstream forms were grown in complete HMI-9 medium (supplemented with 10% FCS and 100 IU/mL of penicillin/streptomycin) [39] in vented tissue culture flasks; these cultures were diluted when cultures reached the cell density of 2×10^6/ml and incubated in a humidified atmosphere of 5% CO2, at 37°C. Bloodstream RNAi cell cultures were supplemented with 7.5 μg/ml hygromycin and 0.2 μg/ml phleomycin.

Cloning of *T. brucei* and *T. cruzi ASA* genes

T. brucei asparagine synthetase A (*TbASA*) and *T. cruzi* asparagine synthetase (*TcASA*) genes were obtained by performing PCR on genomic DNA from *Trypanosoma brucei brucei* TREU927 and *Trypanosoma cruzi* CL Brener Non-Esmeraldo-like. Fragments of the open reading frames of *TbASA* (Tb927.7.1110; chromosome Tb927_07_v4; 28861 to 289067) and *TcASA* (Tc00.1047053503 625.10; chromosome TcChr29-P; 687159–688206) were PCR-amplified using a Taq DNA polymerase with proofreading activity (Roche). The sequences of the primers were as follows: sense primer 5′ - CTAATTACATATGGGCGACGACGGTTATTC - 3′ and antisense primer 5′ - CCCAAGCGAATTCTTACAACA-AATTGTGC - 3′, sense primer 5′ - CAAT TTGCATATGACA-TCGGGAGATCC - 3′ and antisense primer 5′ - CCCAAGCA-AGCTTTCACAGCAAGGG - 3′, respectively. PCR conditions were as follows: initial denaturation (2 min at 94°C), 35 cycles of denaturation (30 s at 94°C), annealing (30 s at 45°C) and elongation (2 min at 68°C) for *Tb*AS-A, and annealing (30 s at 50°C) and elongation (2 min at 68°C) for *Tc*AS-A, and a final extension step (10 min at 68°C). The PCR products were isolated from a 1% agarose gel, purified by the Qiaex II protocol (Qiagen), and cloned into a pGEM-T Easy vector (Promega) and sent to Eurofins MWG (Germany) for sequencing.

Expression and purification of poly-His-tagged recombinant *Tb*AS-A and *Tc*AS-A

The *TbASA* and *TcASA* genes were subcloned into pET28a(+) expression vector (Novagen). The recombinant 6-His-tagged proteins were expressed in *E. coli* BL21DE3 by induction of log-phase cultures with 0.5 mM IPTG (NZYTech) for 3 h at 37°C (*Tc*AS-A) and at 18°C, overnight (O/N) (*Tb*AS-A). Bacteria were harvested and resuspended in buffer A [0.5 M NaCl (Sigma), 20 mM Tris.HCl (Sigma), pH 7.6]. The sample was sonicated and centrifuged to obtain the bacterial crude extract. The recombinant proteins were purified using Ni^{2+} resin (ProBond) and washing and elution with increasing levels (25 mM to 1 M) of imidazole (Sigma). The presence and purity of the recombinant protein in the several fractions was determined by SDS-PAGE and Coomassie staining. Dialysis was performed against PBS [137 mM NaCl (Sigma), 2.7 mM KCl (Sigma), 10 mM $Na_2HPO_4.2H_2O$ (Riedel-de Haën), 2 mM KH_2PO_4 (Riedel-de Haën) pH 7.4].

To generate rat and rabbit polyclonal antibodies against *Tb*AS-A, each animal was first immunized with 150 μg of recombinant *Tb*AS-A protein. After 2 weeks, 4 boosts with 100 μg of recombinant *Tb*AS-A were given weekly. The collected blood samples were centrifuged to obtain the serum.

Protein extracts and western blot analysis

Extracts were obtained in RIPA buffer [(20 mM Tris-HCl (Sigma) (pH 7.5), 150 mM NaCl (Sigma), 1 mM Na_2EDTA (Sigma), 1 mM EGTA (Sigma), 1% Nonidet P-40 (Sigma), 1% sodium deoxycholate (Sigma), 2.5 mM sodium pyrophosphate (Sigma), 1 mM β-glycerophosphate (Sigma), 1 mM Na_3VO_4 (Sigma)], with freshly-added complete protease inhibitor cocktail (Roche Applied Science). The total protein amount was quantified using Biorad Commercial Kit (Reagents A, B and S) and the samples were then kept at −80°C. For analysis of parasites from mice, trypanosomes were purified from mouse blood using a DE-52 (Whatman) column [40].

For Western blotting, 2 μg of recombinant *Tb*AS-A and *Tc*AS-A proteins, 10 μg of total soluble cell extract, or 1×10^7 parasites, were resolved in SDS/PAGE and transferred on to a nitrocellulose

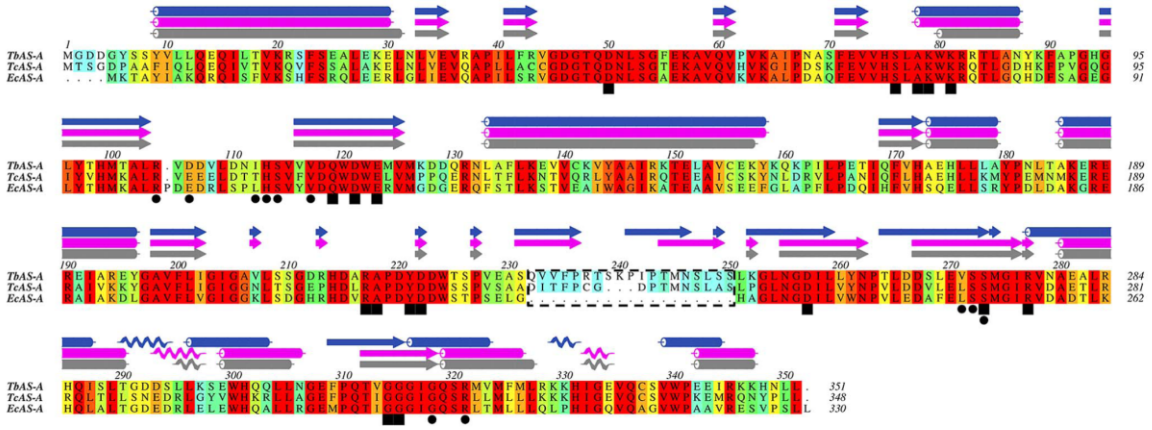

Figure 1. Multiple-sequence alignment of AS-A protein. Alignment of type A asparagine synthetase from *T. brucei* (NCBI-GeneID:3658321/Tb927.7.1110), *T. cruzi* (NCBI-GeneID:3534325/Tc00.1047053503625.10) and *E. coli* (NCBI-GeneID:948258/pdb:12AS). The residues are colored according to ALSCRIPT Calcons (Aline version 011208) using a predefined colour scheme (red: identical residues; orange to blue: scale of conservation of amino acid properties in each alignment column; white: dissimilar residues). Secondary structure elements of *Ec*AS-A crystal structure (grey) and of *Tc*AS-A (purple) and of *Tb*AS-A (blue) homology models are depicted above the alignment. In all protein sequences, asparagine (squares) and AMP binding residues (circles) were identified. The dashed box indicates a structurally divergent region.
doi:10.1371/journal.pntd.0002578.g001

Hy-bond ECL membrane (Amersham Biosciences). The membrane was blocked in 5% (w/v) non-fat dried skimmed milk in PBS/0.1% Tween-20 (blocking solution), followed by incubation with an anti-His-tag rabbit antibody (MicroMol-413) (1:5000) or a combination of an anti-*Tb*AS-A rabbit antibody (1:1000) with an anti-aldolase rabbit antibody (1:5000) in blocking solution at 4°C O/N, respectively. Blots were washed with PBS/0.1% Tween-20 (3×15 min). Horseradish peroxidase-conjugated goat anti-rabbit IgG (Amersham) (1:5000 for 1 h, at room temperature) in blocking buffer was used as the secondary antibody. The membranes were developed using SuperSignal WestPico Chemiluminescent Substrate (Pierce). ImageJ software (version 1.43u) was used for protein bands semi-quantification.

Enzyme assays

AS activity was assessed by quantification of asparagine formation [41]. The reactions were performed in a total of 150 µl of enzyme assay mixture in 85 mM Tris-HCl (Sigma) containing aspartate (Sigma), ammonia (Sigma), ATP (Sigma) and 8.4 mM Mg^{2+} (Sigma). Following incubation for set times at 37°C, enzymatic reactions were terminated by boiling 4 min, and then centrifuged at maximum speed for 30 s. 100 µl of the reaction mixture supernatant was added to 900 µl of ninhydrin 0.05% in ethanol. The resulting mixtures were boiled at 100°C for 5 min, then centrifuged for 30 s and maintained on ice. 300 µl of clear supernatant fluids were transferred to 96-well plates, and the absorbance at 340 nm determined [41]. Based on reaction linearity studies, 7.5 µg of enzyme and 15 min incubation at 37°C were selected as final conditions. To determine K_ms, the concentrations of substrates were varied in the following ranges: 1.25–20 mM (aspartate), 0.78–50 mM (ammonia) and 0.62–10 mM (ATP), while the remaining substrates concentrations were in excess ([aspartate] >20 mM, [ATP] >10 mM, and [ammonia] >50 mM). K_m for glutamine was determined using a concentration range of 1.5625–25 mM, while ATP and aspartate were maintained in excess. Measurements were performed in triplicate, and the initial rate was analyzed to obtain values of V_{max} and K_m by curve fitting using GraphPad Prism (5.0 version).

Using a query based on L-cysteine-S-sulfinic acid inhibitor [42], the ZINC database was screened using the program ROCS (version 2.3.1) to find compounds that have good shape similarity (measured by 3D Tanimoto) and similar functional group overlap to the query molecule. L-cysteine-S-sulfate (Sigma; PubChem Substance ID 24892471) was used under the following conditions: 2.5 mM aspartate, 1.25 mM ATP, 12.5 mM ammonia, and 8.4 mM Mg^{2+}. The characterization of the mechanism of inhibition consisted in the determination of K_m and V_{max} for each substrate, in the presence of four inhibitor concentrations (0.025, 0.050, 0.1 and 0.2 mM). The following substrate concentration ranges 1.25–10 and 1.25–50 mM were used for aspartate and ammonia, respectively, while to determine K_m for ATP, a range from 0.625 to 10 mM (*Tb*AS-A) or from 0.3125 to 5 mM (*Tc*AS-A) was assayed. K_i was determined by "$K_{m\ app}$ Method"[43].

AS-A protein alignments and *Tb*AS-A/*Tc*AS-A homology models

*Ec*AS-A, *Tb*AS-A and *Tc*AS-A protein alignments were performed using ClustalW [44]. Aline, Version 011208 [45], was used for editing protein sequence alignments and preparing Fig. 1. *Tb*AS-A and *Tc*AS-A homology models were obtained with SWISS-MODEL, using *Ec*AS-A crystal structure (Protein Data Bank (PDB) accession code 12AS [24]) as a template (percentage of sequence identity of 56% and 57%, respectively) [46–48]. The 3D structures were rendered in PyMOL (The PyMOL Molecular Graphics System, Version 1.3, Schrödinger, LLC).

Generation of *Tb*AS-A RNAi cell lines

The "stuffer strategy" was used to generate RNAi-mediated AS-A depletion. First, the *TbASA* fragment (amplified with a sense oligo with a BglII – SphI linker 5′ - GAGAAGATCTGCA-TGCGCGACGACGGTTATTCGTCATAC - 3′, and an anti-sense oligo with a EcoRI – SalI 5′ – CGGAATTCGTCGA-CACTCCGTTTTTCGGATTGCGGC – 3′) was cloned twice in opposite direction on either sides of a 'stuffer' fragment of the pHD1144 vector (also digested with SphI and SalI) (Fig. S1A). The

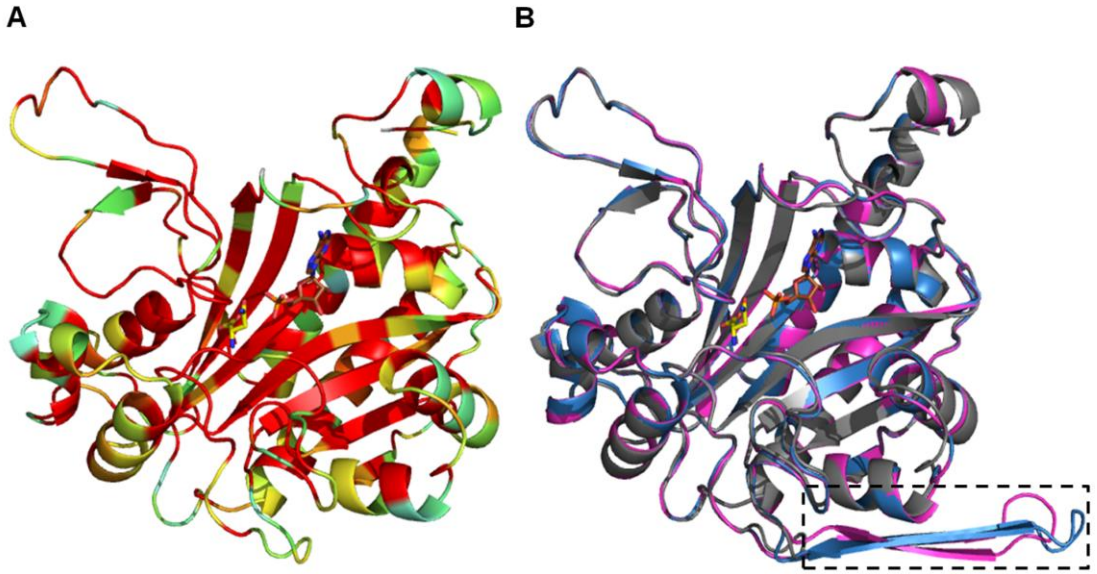

Figure 2. Homology models of AS-A from trypanosomes. (A) Ribbon representation of *Ec*AS-A colored according to the sequence similarity with *Tb*AS-A and *Tc*AS-A as shown in Fig. 1. (B) Superposition of *Ec*AS-A structure (grey) (PDB accession code 12AS), with *Tb*AS-A (blue) and *Tc*AS-A (purple) homology models (obtained from the SWISS-MODEL server, using PDB 12AS as a template). A small structurally divergent region is marked by a dashed rectangle. Ligand color schemes: asparagine is shown in yellow (oxygen, red; nitrogen blue) and AMP is shown in brown (oxygen, red; nitrogen blue; phosphorous orange).
doi:10.1371/journal.pntd.0002578.g002

resulting [(target)-stuffer-(reverse-complement target)] construct obtained through HindIII and BglII digestion, which generates a stem-loop RNA, was cloned into pHD1145 (also digested with HindIII and BglII) (Fig. S1B). The final construct was linearized with NotI and 10 µg of DNA was transfected into 2×10^7/ml bloodstream form cell line carrying pHD1313 plasmid (contains two copies of the tet repressor and a phleomycin resistance cassette) by electroporation using Amaxa Basic Parasite Nucleofector Kit (Lonza). Transcription occurs on induction with tetracycline (100 ng/ml), hence producing mRNA homologs to the target the gene. Stable individual clones were selected 5 to 7 days after transfection with 7.5 µg/ml of hygromycin.

In vitro analysis of *Tb*AS-A RNAi

To analyse growth, *T. brucei* RNAi cell line and cells expressing the tet repressor only (wt), were seeded at 2×10^5 cells/ml of complete HMI9 medium, in the presence and absence of tetracycline. Cell growth was monitored microscopically on a haemocytometer (Marienfeld) and the culture diluted back to 2×10^5 cells/ml daily. The same protocol was repeated in complete HMI9 medium with basal IMDM without asparagine, complete HMI9 medium with basal IMDM without asparagine supplemented with 6.7×10^4 nM of asparagine (levels found in human plasma [49]), and complete HMI9 medium with basal IMDM without asparagine supplemented with 1.67×10^5 nM of asparagine (levels found in normal medium).

In vivo analysis of *Tb*AS-A RNAi

Wild-type and transgenic bloodstream *T. brucei* parasites were cultured in the absence of selecting drugs (hygromycin and phleomycin) for 24 h, then tetracycline was added. After a further 48 h, parasites were inoculated in mice. For each experiment, 4 groups of BALB/c mice (6–8 weeks old, n = 4) (Harlan Laboratories, United Kingdom) were infected by intraperitoneal injection of 10^4 *T. brucei* bloodstream forms. 2 groups were injected with wt strain (with or without tetracycline) and the other 2 groups were injected with RNAi cell line (with or without tetracycline). 48 h prior infection the 2 RNAi induced groups were given doxycycline (treated with 1 mg/ml doxycycline hyclate and 5% sucrose containing water). The 2 non-induced groups were given standard water. To evaluate the virulence of RNAi induced parasites in mice with reduced plasmatic levels of asparagine, animals were treated with 50 IU of *E. coli* L- asparaginase (ProSpec-Tany TechnoGene) 48 h before injection and every 48 h. According to the literature, L-asparagine could not be detected in the blood 48 h following an intravenous injection of *E. coli* L-asparaginase, at a dose of 50 IU/mouse [50]. Mice were monitored every day for general appearance and behaviour. Parasitemia was monitored daily from the fifth day post-infection, using tail-vein blood, in a haematocytometer under a microscope. Animals with a parasitemia greater than 10^8 parasites/ml were euthanized, as previous studies had established that these levels were consistently lethal within the next 24 h.

Immunofluorescence

T. brucei bloodstream forms from log-phase cultures, with or without RNAi, were fixed in µ-Chamber 12 well (Ibidi) for 15 min, at room temperature, in PBS containing 3% p-formaldehyde, washed twice with PBS, and then permeabilized in PBS containing 0.1% of Triton X-100. Fixed cells were incubated for 60 min in PBS containing 10% FCS at room temperature (RT), in a humidified atmosphere, then washed twice with PBS/2% FCS. Cells were then incubated with primary rat or rabbit polyclonal antibody against *Tb*AS-A (1:100 and 1:5000 respectively, both

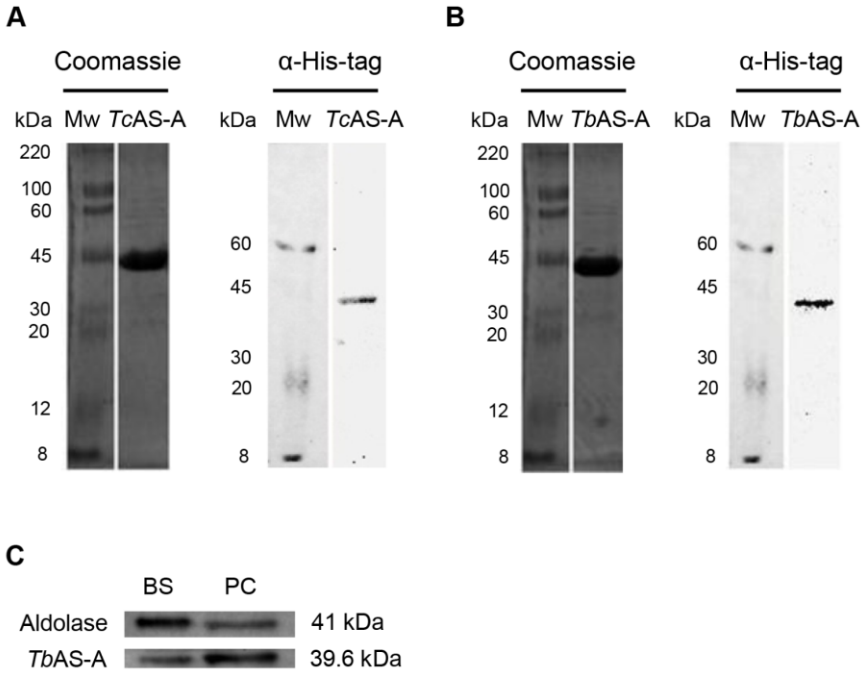

Figure 3. Analysis of purified recombinant *Tc*AS-A/*Tb*AS-A and of AS-A expression within *T. brucei* life cycle stages. Purified *Tc*AS-A (A) and *Tb*AS-A (B) recombinant proteins were analyzed using 12% SDS-PAGE and visualized using Coomassie blue staining. MW, molecular weight marker. Rabbit anti-histidine monoclonal antibody (1:1000) was used in immunoblotting assays with the *Tc*AS-A (A) and *Tb*AS-A (B) purified recombinant proteins. (C) AS-A expression within *T. brucei* life-cycle stages: 10 µg of protein from BS (bloodstream forms) and PC (procyclic forms) lysates were analysed by Western blot. Aldolase was used as a loading control. Rabbit anti-*Tb*AS-A and anti-aldolase polyclonal antibodies were used for protein detection. The results are representative of three independent experiments.
doi:10.1371/journal.pntd.0002578.g003

diluted in blocking solution) overnight at 4°C, followed by two washes with PBS/2% FCS. Subsequently, cells were incubated with Alexa Fluor 647 conjugated goat anti-rat or Alexa Fluor 488 conjugated goat anti-rabbit secondary antibodies (Molecular probes from Life technologies) (1:500 diluted in blocking solution) for 1 h at RT in an humidified atmosphere, then washed twice with PBS. Next, the slides were stained and mounted with Vectashield-DAPI (Vector Laboratories, Inc.). Images were captured using fluorescence microscope AxioImager Z1 and software Axiovision 4.7 (Carl Zeiss, Germany). Pseudo-coloring of images was carried out using ImageJ software (version 1.43u).

In case of *Tb*AS-A immunolocalization, *T. brucei* wt bloodstream forms cells were co-stained using rat anti-*Tb*AS-A antibody (1:100 diluted in blocking solution), rabbit anti-aldolase antibody (1:5000 diluted in blocking solution), anti-BiP antibody (kindly provided by Dr. Jay Bangs, 1:500 diluted in blocking solution), anti-enolase antibody (kindly provided by Dr. Paul Michels, 1:5000 diluted in blocking solution) or anti-GRASP antibody (kindly provided by Dr. Graham Warren, 1:200 diluted in blocking solution). Alexa Fluor 647 conjugated goat anti-rat (1:500) and Alexa Fluor 488 conjugated goat anti-rabbit (1:500) were used as secondary antibodies. Staining with MitoTracker Orange (Invitrogen) followed by Alexa Fluor 488 conjugated goat anti-rabbit (1:500),

Table 1. *Tb*AS-A and *Tc*AS-A kinetic parameters for aspartate, ATP and ammonia.

Species	Substrate	K_m (mM)	V_{max} $\times 10^{-3}$(mM.s^{-1})	k_{cat} (s^{-1})	k_{cat}/K_m (M^{-1}.s^{-1})
T. brucei	Aspartate	5.39±0.31	6.72±0.14	5.31±0.11	9.85×10^2
	ATP	1.80±0.32	7.88±0.48	6.22±0.38	3.46×10^3
	Ammonia	5.55±0.41	7.21±0.16	5.69±0.13	1.03×10^3
T. cruzi	Aspartate	6.45±2.05	3.09±0.40	2.41±0.32	3.74×10^2
	ATP	0.72±0.01	4.42±0.02	3.45±0.02	4.79×10^3
	Ammonia	7.75±1.55	3.14±0.21	2.45±0.17	3.16×10^2

The values are the means ± standard deviation obtained from 3 independent experiments.
doi:10.1371/journal.pntd.0002578.t001

Table 2. *Tb*AS-A and *Tc*AS-A kinetic parameters for glutamine.

Species	K_m(mM)	V_{max} ×10^{-3} (mM.s^{-1})	k_{cat}(s^{-1})	k_{cat}/K_m ($M^{-1}.s^{-1}$)
T. brucei	8.20±1.70	7.06±0.61	5.58±0.48	6.80×10^2
T. cruzi	15.33±3.66	4.33±0.53	3.38±0.41	2.20×10^2

The values are the means ± standard deviation obtained from 3 independent experiments.

doi:10.1371/journal.pntd.0002578.t002

as a secondary antibody. The labelling of parasites with MitoTracker was done by adding 250 nM to the cell culture medium (without FCS) for 30 minutes, prior to washing, fixing and staining using the protocol described above. Images were captured using the confocal microscope Leica TCS SP5II and LAS 2.6 software (Leica Microsystems, Germany). Again, image analysis was done using ImageJ version 1.43U software.

Digitonin permeabilization

For each sample condition, 1.0×10^7 bloodstream cells were washed once with cold trypanosome homogenization buffer (THB), containing 25 mM Tris (Sigma), 1 mM EDTA (Sigma) and 10% sucrose (Sigma), pH = 7.8. Just before cell lysis, leupeptin (Sigma) (final concentration of 2 µg/ml) and different digitonin (Calbiochem) quantities (final concentrations of 5, 12.5, 25, 50, 100, 150 and 200 ug/ml) were added to 500 µl of cold THB, for cell pellet resuspension. Untreated cells (0 µg/ml of digitonin) and those completely permeabilized (total release, the result of incubation in 0.5% Triton X-100) were used as controls. Each sample was incubated 60 min on ice, and then centrifuged at 2000 rpm, 4°C, for 10 min. Supernatants were transferred to new chilled tubes and 500 µl of cold THB was added to each pellet and then mixed. All fractions were analysed through Western blot as described above.

Cell cycle analysis

T. brucei bloodstream forms were analyzed by flow cytometry for DNA content following RNAi induction. Cells were collected by centrifugation and washed twice with PBS containing 2% FCS. Each 2×10^6 cells were resuspended in 1 mL of PBS/2% FCS and 3 mL of cold absolute ethanol was added while vortexing. Cells were fixed for 1 hour at 4°C and then washed twice in PBS. 1 mL of staining solution [3.8 mM sodium citrate dehydrate (Sigma), 50 µg/mL propidium iodide (Sigma), 0.5 µg/µL RNAse A (Sigma) in PBS] was added to the cell pellets and vortex. Samples were analysed by FACS (Becton Dickinson) after a incubation at 4°C for 30 min. Data was analyzed by FlowJo software (Ashland, OR).

Statistical analysis

One-way ANOVA and two-tailed Student's test were used for statistical analysis. Statistical analysis was performed using GraphPad Prism Software (version 5.0), and p values≤0.01 were considered to be statistically significant. Asterisks indicate statistically significant differences (*** $p\leq0.001$, ** $p\leq0.01$).

Results

Conservation of AS-A in trypanosomes

One open reading frame that code for a putative AS-A is present in the genomes of *T. cruzi* CL Brener Non-Esmeraldo-like and *T. brucei* TREU927 (http://tritrypdb.org) [29–31]. A protein multiple sequence alignment, performed using ClustalW [44], of AS-A from *T. brucei* (Tb927.7.1110, NCBI-GeneID:3658321), *T. cruzi* (Tc00.1047053503625.10, NCBI-GeneID:3534325) and *E. coli* (NCBI-GeneID:948258) is shown in Figure 1. The amino acid residues known to be involved in the active-site formation in *E. coli* [24] are highly conserved within the three sequences (Fig. 1). Protein alignments demonstrated 58% similarity for *Ec*AS-A *versus* *Tb*AS-A, 60% for *Ec*AS-A *versus* *Tc*AS-A, and 63% for *Tb*AS-A *versus* *Tc*AS-A.

Like *Ec*AS-A, *Tb*AS-A and *Tc*AS are predicted to be dimeric, as seen from superimposed homology models with the *Ec*AS-A crystal structure [24] (Fig. 2A). The only structurally divergent region (area marked by dashed rectangle) (Fig. 1, 2B), is present in both *Tb*AS-A (from residues Q232 to S250) and *Tc*AS-A (from residues D232 to S247), but absent in *Ec*AS-A. This region is distant from the enzyme active site and the dimer interface and its functional and structural significance are unknown. The amino acids involved in asparagine binding are all strictly conserved, while in the AMP binding pocket, the majority of the residues are conserved, except for three residues (Fig. 1). In *Ec*AS-A, E103 (D106 and E106 in *Tb*AS-A and *Tc*AS-A, respectively) and L109 (I112 and T112 in *Tb*AS-A and *Tc*AS-A, respectively) (Fig. 1) are not directly involved in polar interactions with the nucleotide base, but form part of the outer wall of the binding site [24]. The main chain of L249 in *Ec*AS-A (V271 and L268 in *Tb*AS-A and *Tc*AS-A, respectively) is directly involved in hydrogen bonds with ribose from AMP, however the different side chains of leucine and valine do not affect the shape of AMP binding site.

Trypanosome AS-A catalyze asparagine synthesis using either ammonia or glutamine as nitrogen donors

*Tb*AS-A and *Tc*AS-A coding sequences were cloned into the bacterial expression vector pET28a. Histidine-tagged fusion proteins were purified under non-denaturing conditions (Fig. 3A, B). As expected, the recombinant proteins were recognized by anti-His Tag monoclonal antibody (Fig. 3A, B). Rabbit polyclonal antibodies produced against recombinant *Tb*AS-A recognized the protein in total extracts from two different parasite developmental stages, bloodstream forms (mammalian host parasite stage) and procyclic forms (insect vector parasite stage) (Fig. 3C).

The capacities of *Tb*AS-A and *Tc*AS-A to produce asparagine from aspartate in the presence of ATP, ammonia and Mg^{2+} were determined using a specific quantitative colorimetric assay for L-asparagine [41]. The pH optimum was 7.6, with detectable activity from 6.0 to 9.0 (data not shown). Mg^{2+} was an essential co-factor for *Tb*AS-A and *Tc*AS-A (data not shown), as previously described for *Ec*AS-A [22]. We included 8.4 mM Mg^{2+} in the final reaction mixture. Lower concentrations (2, 4 and 6 mM) gave lower activity while increased concentrations (up to 16 mM) resulted in no substantial activity improvement (data not shown). *Tb*AS-A and *Tc*AS-A showed similar K_ms for aspartate and ammonia ($p>0.01$), while *Tc*AS-A showed higher K_m for ATP than *Tb*AS-A ($p=0.0042$) (Table 1). ATP is the substrate required for the generation of the β-aspartyl adenylate intermediate, which reacts with ammonia, releasing asparagine. In its absence, the reaction did not occur (data not shown). To our surprise, both *Tb*AS-A and *Tc*AS-A could also use glutamine as a nitrogen donor (Table 2). *Tb*AS-A showed higher K_m for this nitrogen donor than *Tc*AS-A, however not statistically significant ($p>0.01$). Both enzymes present higher K_m values for ammonia than for glutamine, but these differences were not statistically significant ($p>0.01$) (Table 1 and 2). *Tb*AS-A had a higher V_{max} than *Tc*AS-A, for both ammonia ($p<0.0001$) and glutamine ($p=0.0043$) dependent-activities (Table 1 and 2). *Tb*AS-A had similar catalytic

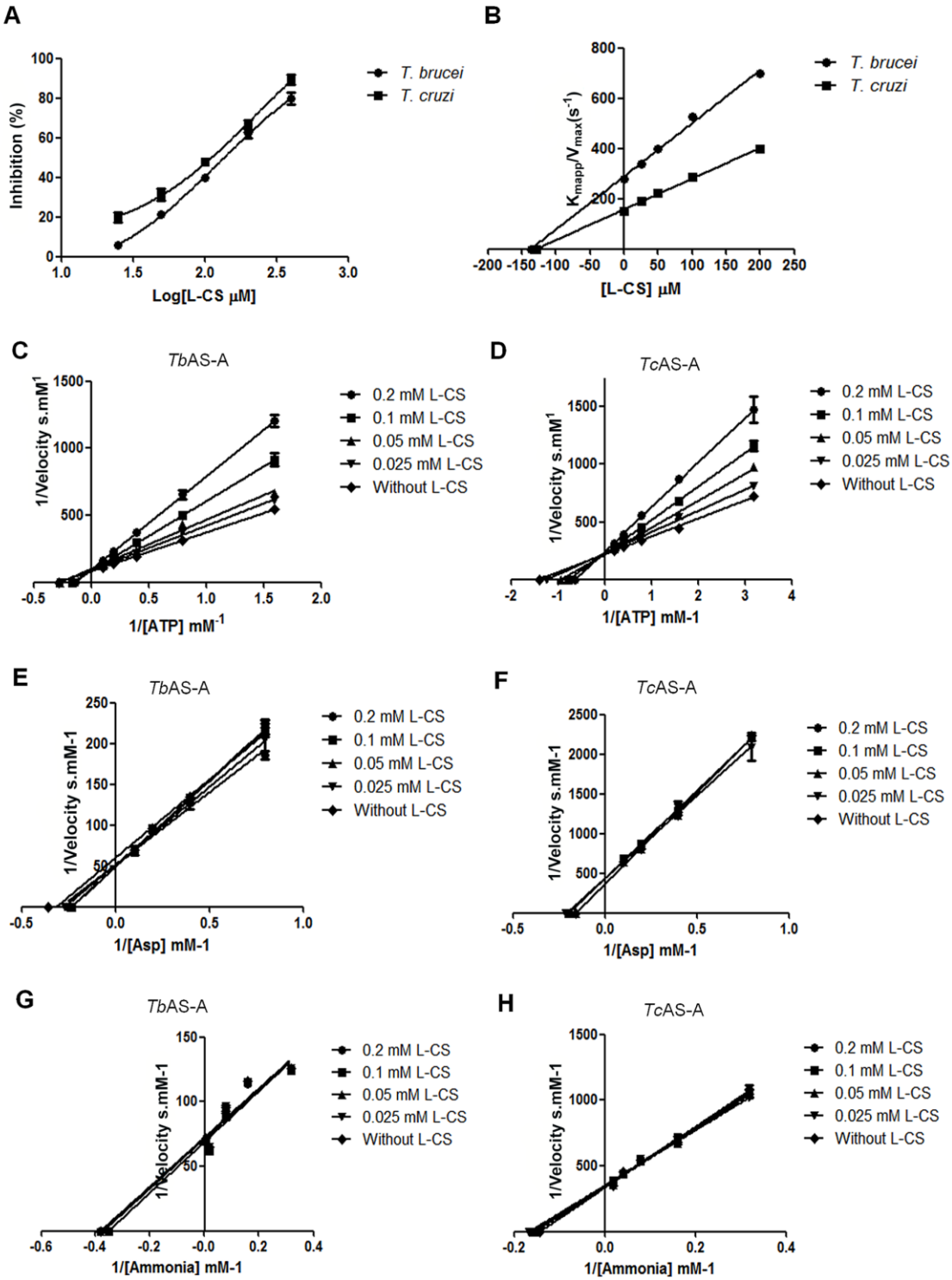
A
Inhibition (%)
Log[L-CS µM]
T. brucei
T. cruzi
B
$K_{mapp}/V_{max}(s^{-1})$
[L-CS] µM
T. brucei
T. cruzi
C
TbAS-A
1/Velocity s.mM-1
1/[ATP] mM-1
0.2 mM L-CS
0.1 mM L-CS
0.05 mM L-CS
0.025 mM L-CS
Without L-CS
D
TcAS-A
1/Velocity s.mM-1
1/[ATP] mM-1
0.2 mM L-CS
0.1 mM L-CS
0.05 mM L-CS
0.025 mM L-CS
Without L-CS
E
TbAS-A
1/Velocity s.mM-1
1/[Asp] mM-1
0.2 mM L-CS
0.1 mM L-CS
0.05 mM L-CS
0.025 mM L-CS
Without L-CS
F
TcAS-A
1/Velocity s.mM-1
1/[Asp] mM-1
0.2 mM L-CS
0.1 mM L-CS
0.05 mM L-CS
0.025 mM L-CS
Without L-CS
G
TbAS-A
1/Velocity s.mM-1
1/[Ammonia] mM-1
0.2 mM L-CS
0.1 mM L-CS
0.05 mM L-CS
0.025 mM L-CS
Without L-CS
H
TcAS-A
1/Velocity s.mM-1
1/[Ammonia] mM-1
0.2 mM L-CS
0.1 mM L-CS
0.05 mM L-CS
0.025 mM L-CS
Without L-CS

Figure 4. *T. brucei* and *T. cruzi* AS-A *in vitro* inhibition. (A) Inhibition (%) of *T. brucei* and *T.cruzi* AS-A activity by L-cysteine-S-sulfate (L-CS). (B) Plot of K_{mapp}/V_{max} *versus* L-CS concentration was established; K_i corresponds to the symmetric value of the X-axis intersection. (C-H) Plots showing the effect of different L-CS concentrations on the inverse of the initial velocity *versus* the inverse of several concentrations of ATP, aspartate or ammonia for *Tb*AS-A (C, E and G, respectively) and *Tc*AS-A (D, F and H, respectively) enzymes. Error bars indicate standard deviation of the means of two replicates and data shown are representative of three independent experiments.
doi:10.1371/journal.pntd.0002578.g004

rates for both glutamine and ammonia-dependent activities ($p>0.01$), whereas *Tc*AS-A presented a slightly higher, but not statistically significant, rate for glutamine-dependent activity ($p>0.01$) (Table 1 and 2). The high conservation of the active sites and the small amino acid differences identified in the homology models do not allow an accurate structural interpretation of the small differences observed. Indeed, these might have been due to slight differences in the proportion of protein that was correctly folded.

L-cysteine-S-sulfate, considered a putative AS-A inhibitor from a virtual screening, inhibited both enzymes, with IC_{50}s of 126 and 100 µM for *Tb*AS-A and *Tc*AS-A, respectively (Fig. 4A). For both enzymes, the kinetic characteristics suggested competition with ATP binding (Fig. 4C, D). No changes in the K_ms and V_{max}s for aspartate and ammonia were observed ($p>0.01$) (Fig. 4E, F, G, H), suggesting the inhibition is exclusively due to ATP binding interference ($p\leq0.01$) . K_i values of 137 and 128.9 µM were determined for *Tb*AS-A and *Tc*AS-A, respectively (Fig. 4B).

AS-A localizes in the cytosol of *T. brucei* bloodstream forms

The subcellular localization of *Tb*AS-A was determined by immunofluorescence and digitonin fractionation in bloodstream forms. As expected, induction of RNAi resulted in a decrease in the fluorescence intensity (Fig. S2A, B, C). *Tb*AS-A is in the cytosol, as revealed by colocalization with the cytosolic enzyme enolase [51] (Fig. 5A) and no colocalization with aldolase, BiP, GRASP or mitotracker (Fig. S3), markers for glycosomes [52],

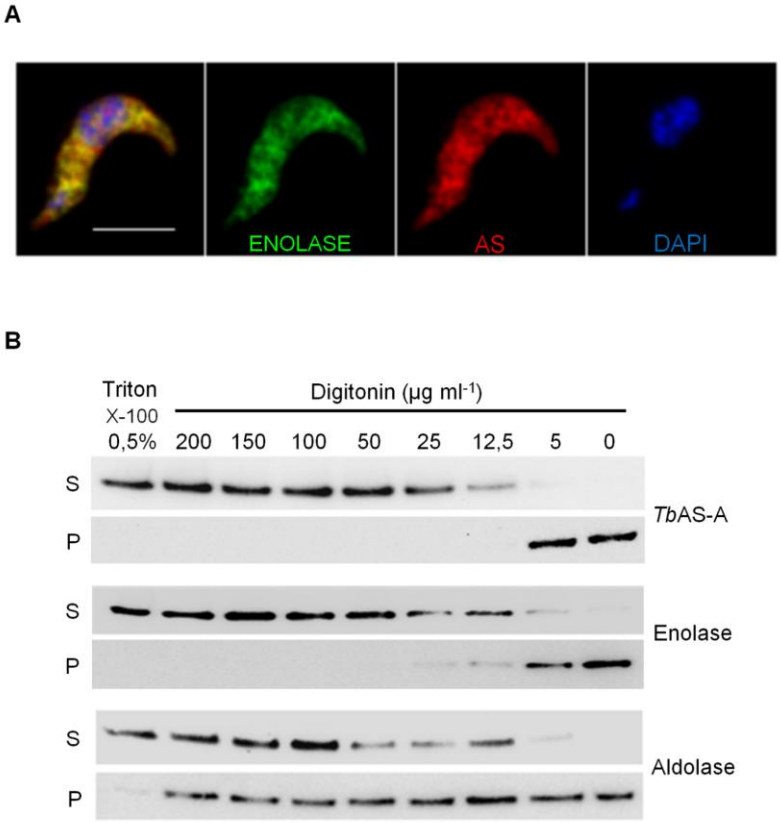

Figure 5. AS-A subcellular localization in *T. brucei* bloodstream forms. (A) Immunofluorescence analysis by confocal microscopy of *Tb*AS-A (red) and enolase (green) in bloodstream forms. DAPI locate nuclear and kinetoplast mitochondrial DNA (blue). Bar, 5 µm. Images are maximal Z-projections of 50 contiguous stacks separated by 0.1 µm. (B) For digitonin permeabilization, selected supernatant (S) and pellet (P) fractions obtained at different digitonin concentrations were subjected to Western-blot analysis and probed with rabbit antisera raised against *Tb*AS-A, enolase (cytoplasmic marker) and aldolase (glycosome marker). Data shown is representative of two independent experiments. Untreated cells (0 µg/ml of digitonin) and those completely permeabilized in Triton X-100 0.5% were used as controls.
doi:10.1371/journal.pntd.0002578.g005

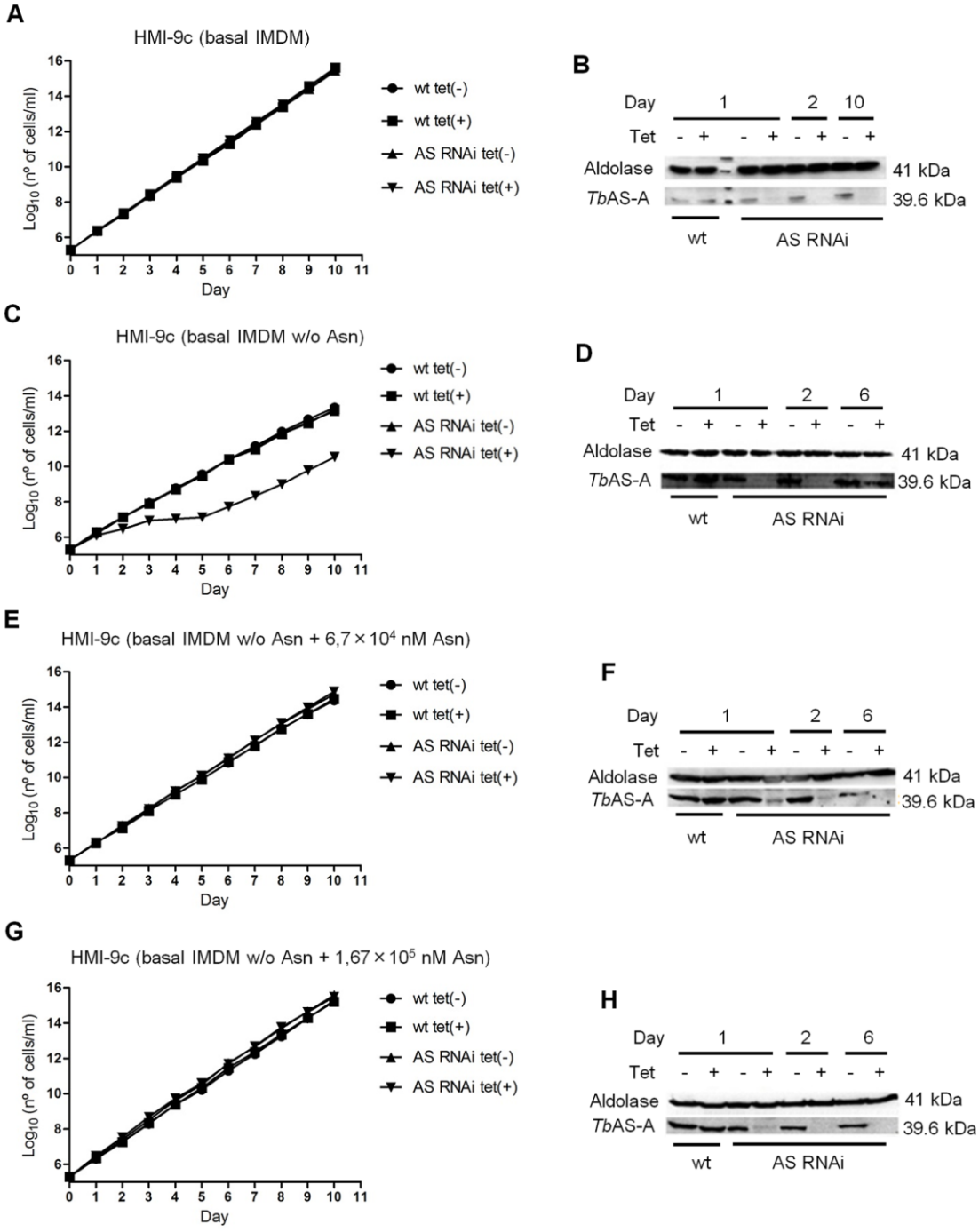

Figure 6. ***In vitro*** **effect of RNAi-mediated AS-A down-regulation in** ***T. brucei*** **bloodstream forms.** Growth curve of a wt *versus* a representative AS RNAi cell line were performed in unmodified medium [complete HMI-9 (HMI-9c) with basal IMDM] (A), modified medium [HMI-9c with basal medium without asparagine - HMI-9c (basal IMDM w/o Asn)] (C), modified medium supplemented with 6.7×10^4 nM of asparagine [HMI-9c (basal IMDM w/o Asn + 6.7×10^4 nM Asn)] (E), modified medium supplemented with 1.67×10^5 nM of asparagine [HMI-9c (basal IMDM w/o Asn + 1.67×10^5 nM Asn)] (G). Circles and squares represent wild-type growth in the absence or presence of tetracycline, respectively, while up triangles and down triangles represent clones growth in the absence or presence of tetracycline, respectively. Cumulative cell numbers are plotted as the product

of cell number and total dilution. Error bars indicate standard deviation. The effect of RNAi on the AS-A protein levels was analyzed by Western blots with extracts of noninduced tet(−), and RNAi-induced tet(+) cells, isolated from unmodified medium (B), modified medium (complete HMI-9 medium with basal IMDM without asparagine) (D), modified medium supplemented with 6.7×10^4 nM of asparagine (F), modified medium supplemented with 1.67×10^5 nM of asparagine (H). Cells were collected at day 1, 2, 6 and 10 of RNAi induction. Results are representative of three independent experiments.
doi:10.1371/journal.pntd.0002578.g006

endoplasmic reticulum [53], Golgi and mitochondria compartments [54], respectively. Controls performed with rat or rabbit pre-immune sera and secondary antibody alone, showed no detectable signal (data not shown). Digitonin fractionation also resulted in similar profiles for AS-A and enolase (cytosolic marker) and no similarity to aldolase (glycosomes marker) (Fig. 5B).

AS-A knockdown makes *T. brucei* bloodstream forms dependent on extracellular asparagine

To study the biological role of AS-A in *T. brucei* bloodstream forms, cells were stably transfected with an RNA interference plasmid construct. RNAi against asparagine synthetase A was induced in normal medium (complete HMI-9) by adding tetracycline. No difference was observed in cell proliferation between induced and non-induced cells (Fig. 6A), although AS-A protein was reduced to ≈13% of the normal level within 48 hours (Fig. 6B). When, however, the AS-A-depleted cells were grown in HMI-9 medium with only the asparagine from the fetal calf serum, growth was impaired, with an increase in the proportion of cells in G0/G1 (Fig. 6C and 7B, C). Presumably the asparagine from the serum allowed this slower growth. Levels of asparagine usually found in human serum (6.7×10^4 nM) [49], which are somewhat lower than in normal medium (1.67×10^5 nM; IMDM - Iscove's modified Dulbecco's basal medium from Gibco Invitrogen), were sufficient to overcome this defect (Fig. 6E, G). In complete HMI-9 medium, with only asparagine from the fetal calf serum, the growth defects of induced RNAi clones are abrogated at day 5 post-induction (Fig. 6C, 7D), and the percentage of cells in GO/G1 and S phases of the cell cycle return to the ones found in non-induced cells (Fig. 7A), suggesting the appearance of RNAi revertants, as is also visible on the Western blot (Fig. 6D). Similar reversion to evade lethal RNAi in trypanosomes has been seen many times before [55]. In the presence of asparagine, low AS-A levels were maintained (Fig. 6B, F and H).

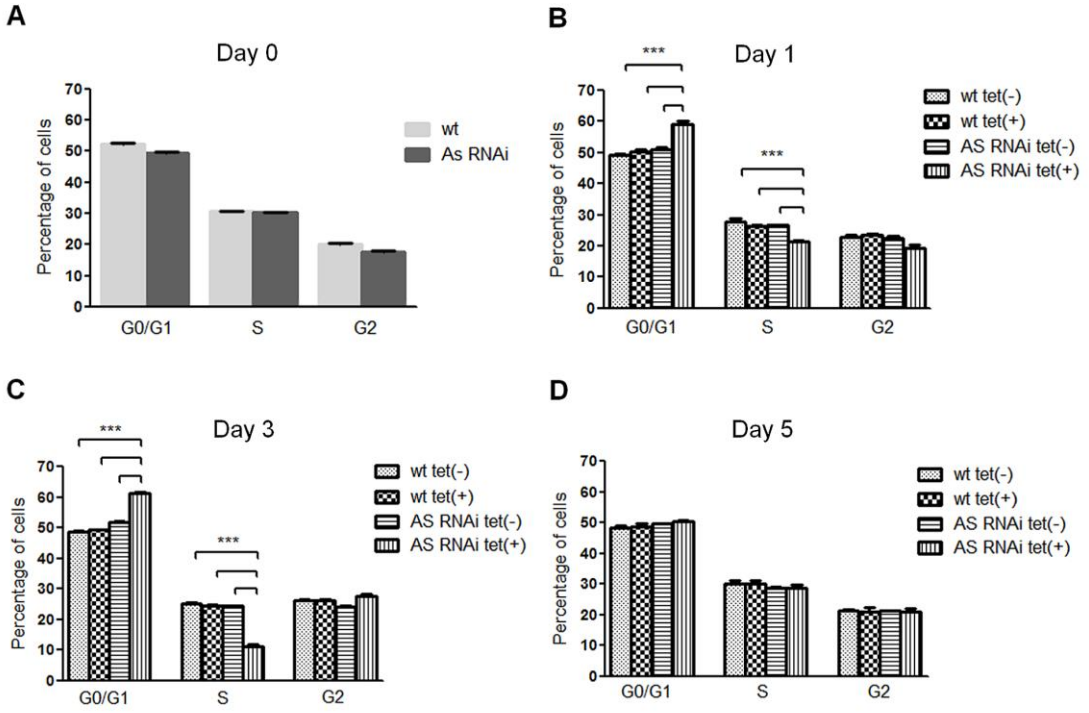

Figure 7. *In vitro* effect of RNAi-mediated AS downregulation on *T. brucei* cell cycle. DNA content of ≈2×10^6 wt and RNAi cell line parasites grown in completed HMI-9 medium with basal IMDM without asparagine, was collected before tetracycline induction, day 0 (A), and at day 1 (B), 3 (C), and 5 (D) post-induction, for cell cycle analysis. Samples were analysed by flow cytometry and the percentage of cells in each phase of the cell cycle were determined using FlowJo software. Each bar represents the average from three replicates. Error bars indicate standard deviation of these measurements. The statistics were calculated by one-way ANOVA (*** $p\leq0.001$ and ** $p\leq0.01$).
doi:10.1371/journal.pntd.0002578.g007

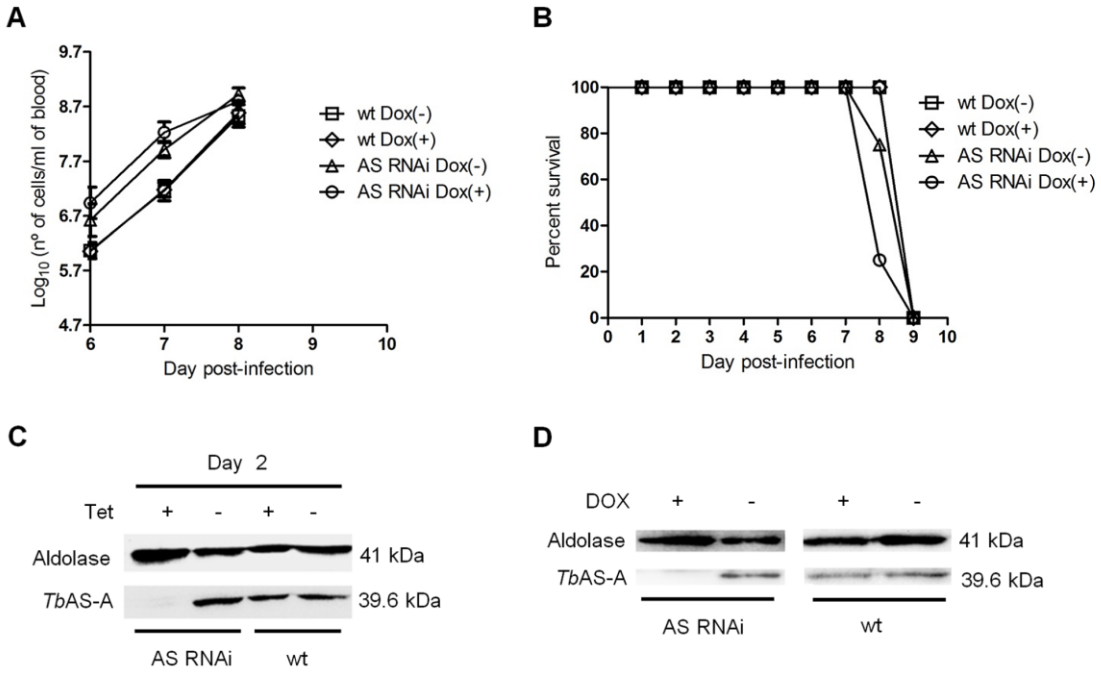

Figure 8. ***In vivo*** **effect of RNAi against** ***Tb*****AS-A.** (A) Groups of 4 mice were infected intraperitoneally, with 1×10^4 control wt parental cell line (open squares and open diamonds) or a representative AS RNAi clone (open triangles and open circles). The mice were either untreated (open squares and open triangles) or treated with 1 mg/ml doxycycline (Dox) (open diamonds and open circles) in the water supply. Parasitemia was quantified at the times indicated. Error bars indicate standard deviation of the means of three mice for wt cell lines, and four mice in the case of AS RNAi cell lines. The detection limit for this assay is 5×10^4 trypanosomes per ml of blood. Mice were euthanized when parasitemia reached 1×10^8 cells/ml. (B) Kaplan–Meier survival analysis of mice infected with wt parental cell line and AS RNAi cell line in the absence or presence of doxycycline. Data are representative of three independent experiments. Western blot analysis of the AS-A levels in trypanosomes injected in mice, after 48 h of *in vitro* tetracycline induction (C), and in trypanosomes isolated from mice, before being euthanized (D).
doi:10.1371/journal.pntd.0002578.g008

Normal *T. brucei* parasites also showed a statistically significant slower growth under conditions of asparagine limitation ($p\leq0.01$; data not shown) (compare Fig. 6C, with A, E, G). It is therefore possible that even when the parasite has AS, it also requires external asparagine for optimal *in vitro* growth.

AS-A is dispensable for *T. brucei* infectivity in mice

To test whether AS-A is important for parasite infection in a disease model, two groups of mice ($n=4$) were inoculated with the parental cell line, and other two groups with RNAi cells. Two mice groups were fed with water containing doxycycline to induce down-regulation of *Tb*AS-A, while the remaining mice were kept as non-induced controls. Within six days of inoculation, all mice from the different groups developed high levels of parasitemia (Fig. 8A), and all had to be euthanized after seven or eight days post-infection (Fig. 8B). The results confirm that the asparagine in mouse blood is sufficient to compensate for the ≈87% downregulation of AS-A (Fig. 8C, D).

To assess the contribution of blood L-asparagine *in vivo*, mice were treated with L-asparaginase [50]. L-asparaginase treatment did not affect growth of normal parasites in mice (Fig. 9A) and consequently did not extend animal survival (Fig. 9B). However L-asparaginase treatment in mice infected with *Tb*AS-A RNAi-induced parasites caused a decrease in the parasitemia (Fig. 9D), thus leading to an increase of mice survival (Fig. 9E). Even so, the infection resulted in death. As happened *in vitro*, RNAi revertants appeared during the course of infection in asparaginase-treated, but not untreated, mice (Fig. 9F). Parasites extracts from wt infected mice were used as controls (Fig. 9C).

Discussion

In this study we demonstrated that trypanosomes AS-A use both ammonia or glutamine as nitrogen donors for the ATP dependent conversion of aspartate into asparagine. Such hybrid activity was only previously demonstrated for type B enzymes, which prefer glutamine to ammonia [15–19]. The small differences in K_m of *Tb*AS-A and *Tc*AS-A for ammonia and glutamine (1.5 and 2 fold, respectively) are lower than the difference found in most AS-B enzymes, with the exception of the human enzyme, which has similar affinities for both [16–20]. Purified *E. coli* AS-A used only ammonia as the nitrogen source, and results from *Klebsiella aerogenes* also suggested that AS-A preferentially uses ammonia as substrate [5,21,22]. The conclusions for AS-A enzymes of these two Gram-negative organisms relied on both biochemical and genetic analysis, but given technical limitations at the time, and the fact that background enzyme activity was seen in the absence of both ammonia and glutamine, some re-examination in bacteria would be worthwhile. Moreover the overall K_m values of trypanosomes AS-A for aspartate, are 6 up to 20 fold higher than the ones found in the literature for prokaryotic asparagine synthetase type A [5,21,22]. *Trypanosoma* AS-A structures were not yet been solved

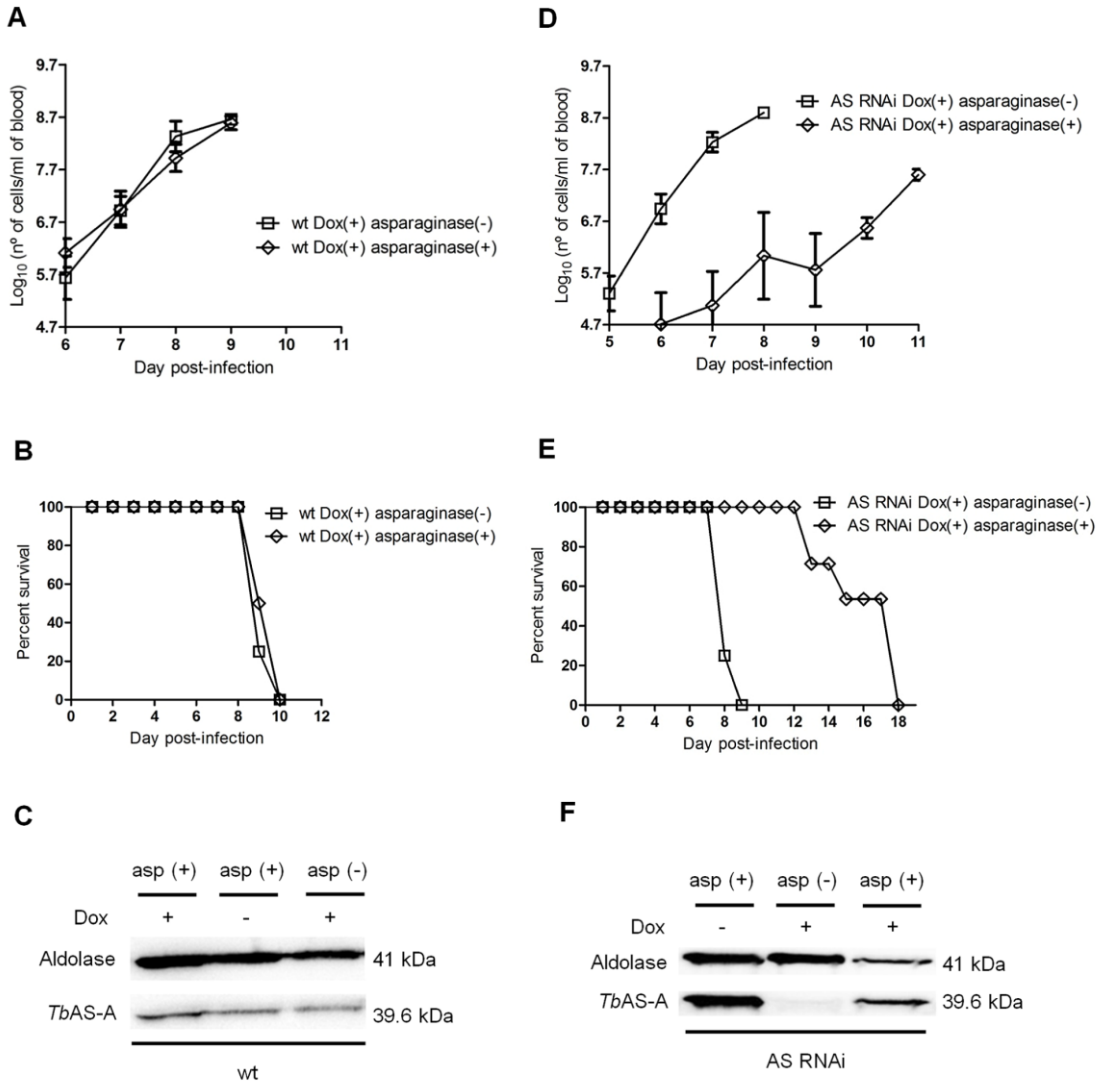

Figure 9. ***In vivo*** **RNAi against** ***Tb*****AS-A in mice undergoing** ***E. coli*** **L-asparaginase treatment.** Time course of the parasitemia of two groups of 4 mice infected intraperitoneally, with 1×10^4 of RNAi induced [using 1 mg/ml of doxycycline, Dox (+)] wt parental cell line (A) or a representative AS RNAi cell line (D) either untreated (open squares) or treated daily every 2 days (open diamonds) with 50 IU *E. coli* L-asparaginase/mouse. Parasitemia was quantified in peripheral tail blood at the times indicated. Error bars indicate standard deviation, and data are representative of two independent experiments using two different AS RNAi clones. The detection limit for this assay is 5×10^4 trypanosomes/ml of blood. Mice were culled when parasitemia reached 1×10^8 cells/ml. Kaplan–Meier survival plot of mice infected with RNAi induced wt cell line (B) or AS RNAi cell line (E) either untreated (open squares) or treated (open diamonds) with *E. coli* L-asparaginase. (F) Western blot analysis of AS-A levels in trypanosomes isolated from mice, before being euthanized. (C) Wt cell extracts, also collected when mice were culled, were use as negative control.
doi:10.1371/journal.pntd.0002578.g009

and our protein homology models are not completely enlightening, nevertheless we can speculate that such differences may result in the fact that parasite enzymes were expressed and purified as recombinant proteins in bacteria and not purified directly from trypanosomes extracts. As a consequence, differences in protein post-transcriptional processing and/or changes in protein conformation cannot be excluded.

Our results suggest that bloodstream-form parasites rely on two major sources of asparagine to ensure normal proliferation: uptake from the extracellular medium and biosynthesis by AS-A. Bloodstream form proliferation, either *in vitro* or *in vivo*, was only significantly affected when both asparagine sources were compromised. Also consistent with this idea, in the published RNAi screen, a very slight (possibly insignificant) growth disadvantage was seen in bloodstream forms depleted of AS-A [56]. In the same way, our *in vitro* results are corroborated with previous studies, as mammalian cells with low expression of AS are similarly susceptible to asparagine depletion [57–59], and asparaginase

isolated from *E. coli* and *Erwinia carotovora* act as potent anti-leukemic agents [60].

In the trypanosomes genome there is a second open reading frame (Tb927.3.4060) coding for a putative AS domain. However this is apparently not a classical AS, despite the presence of a good Pfam AS domain (PF0073) at the C-terminus. A BLASTp search using the *T. brucei* sequence revealed a variety of proteins of unknown function that aligned not only across the AS domain, but also in the N-terminal region, which contains N-terminal aminohydrolase domains. Best matches originate from extremely diverse eukaryotes including a plant, an alga, a member of the fungi and an amoeba. BLASTp against the *Saccharomyces cerevisiae* predicted proteome yielded YML096W, and the reciprocal BLASTp on the trypanosome genome indeed gave Tb927.3.4060 as best match. The function of YML096W is not known, and in a trypanosome RNAi screen no growth defect was seen for Tb927.3.4060 [56].

The capacity of trypanosomes to grow using asparagine from the extracellular environment, and the lack of growth defect when the levels of AS-A are reduced, show that only a combination therapy using both a *Tb*AS-A inhibitor and an extracellular asparagine depletor (e.g. L-asparaginase) or an asparagine transport blocker could inhibit parasite growth. This is not appropriate for African sleeping sickness treatment. A combination that absolutely required simultaneous activities of two different drugs would be wide open to resistance development, and drug combination including an intravenously-introduced enzyme is likely to be both too expensive and logistically inappropriate for treatment of African trypanosomiasis. Moreover, L-asparaginase treatment in cancer results in serious adverse events [61–63]. We therefore conclude that AS-A is not a good candidate as a sleeping sickness drug target. Its role in *Trypanosoma cruzi*, however, remains to be established.

Supporting Information

Figure S1 RNAi vectors used to generate RNAi-mediated *Tb*AS-A downregulation. (A) pHD1144 vector for stem-loop cloning (pSP72 vector with a stuffer fragment); (B) pHD1145 inducible polymerase I vector for insertion of ready-made stem-loops (pHD677 vector without a T7 promoter and with an inducible EP1 promoter and hygromycin resistance cassette, insertion into ribosomal spacer).
(TIF)

Figure S2 Validation of antibodies against *Tb*AS-A. Immunofluorescence analysis of *T. brucei* wt or a representative AS RNAi clone grown in the presence or absence of tetracycline. RNAi induced and uninduced cells were grown for 48 h, then fixed and probed with rat polyclonal anti-*Tb*AS-A (A) or rabbit polyclonal anti-*Tb*AS-A (B) antibody and co-stained with DAPI. Bars, 5 µm. Quantification of *Tb*AS-A fluorescence levels in induced cells (AS RNAi tet(+), $n = 30$) and uninduced cells (AS RNAi tet(−), $n = 30$), using the rat and the rabbit polyclonal anti-*Tb*AS-A antibodies (C). Data representative of two independent experiments using two different clones. ImageJ software (version 1.43u) was used for fluorescence quantification. p value was calculated by Student's t test (*** $p \leq 0.001$ and ** $p \leq 0.01$).
(TIF)

Figure S3 *Tb*AS-A cellular localization in *T. brucei* bloodstream forms. Immunofluorescence analysis by confocal microscopy of *Tb*AS-A (red) in bloodstream forms. Aldolase (glycosome marker), GRASP (golgi marker), BiP (endoplasmic reticulum marker) and MitoTracker (labels mitochondria) are in green. DAPI locate nuclear and kinetoplast mitochondrial DNA (blue). Bars, 5 µm. Images are maximal Z-projections of 50 contiguous stacks separated by 0.1 µm.
(TIF)

Acknowledgments

We would like to thank Dr. Jay Bangs from University of Wisconsin-Madison Medical School, USA, for providing us BiP antibody, Dr. Paul Michels from Université Catholique de Louvain, Belgium, for sending us enolase antibody and Dr. Graham Warren from Yale University School of Medicine, USA, for the GRASP antibody. We also thank Claudia Helbig for assistance in Heidelberg.

Author Contributions

Conceived and designed the experiments: IL JF JT ACdS. Performed the experiments: IL JF NS JT. Analyzed the data: IL JF SMR CC JT ACdS. Contributed reagents/materials/analysis tools: CC SMR NR. Wrote the paper: IL JF CC SMR JT ACdS.

References

1. Richards NG, Schuster SM (1998) Mechanistic issues in asparagine synthetase catalysis. Adv Enzymol Relat Areas Mol Biol 72: 145–198.
2. Blaise M, Frechin M, Olieric V, Charron C, Sauter C, et al. (2011) Crystal structure of the archaeal asparagine synthetase: interrelation with aspartyl-tRNA and asparaginyl-tRNA synthetases. J Mol Biol 412: 437–452.
3. Roy H, Becker HD, Reinbolt J, Kern D (2003) When contemporary aminoacyl-tRNA synthetases invent their cognate amino acid metabolism. Proc Natl Acad Sci U S A 100: 9837–9842.
4. Nakamura M, Yamada M, Hirota Y, Sugimoto K, Oka A, et al. (1981) Nucleotide sequence of the asnA gene coding for asparagine synthetase of E. coli K-12. Nucleic Acids Res 9: 4669–4676.
5. Reitzer LJ, Magasanik B (1982) Asparagine synthetases of Klebsiella aerogenes: properties and regulation of synthesis. J Bacteriol 151: 1299–1313.
6. Blattner FR, Plunkett G, 3rd, Bloch CA, Perna NT, Burland V, et al. (1997) The complete genome sequence of Escherichia coli K-12. Science 277: 1453–1462.
7. Sugiyama A, Kato H, Nishioka T, Oda J (1992) Overexpression and purification of asparagine synthetase from Escherichia coli. Biosci Biotechnol Biochem 56: 376–379.
8. Gowri VS, Ghosh I, Sharma A, Madhubala R (2012) Unusual domain architecture of aminoacyl tRNA synthetases and their paralogs from Leishmania major. BMC Genomics 13: 621.
9. Humbert R, Simoni RD (1980) Genetic and biomedical studies demonstrating a second gene coding for asparagine synthetase in Escherichia coli. J Bacteriol 142: 212–220.
10. Andrulis IL, Chen J, Ray PN (1987) Isolation of human cDNAs for asparagine synthetase and expression in Jensen rat sarcoma cells. Mol Cell Biol 7: 2435–2443.
11. Andrulis IL, Shotwell M, Evans-Blackler S, Zalkin H, Siminovitch L, et al. (1989) Fine structure analysis of the Chinese hamster AS gene encoding asparagine synthetase. Gene 80: 75–85.
12. Ramos F, Wiame JM (1980) Two asparagine synthetases in Saccharomyces cerevisiae. Eur J Biochem 108: 373–377.
13. Merchant SS, Prochnik SE, Vallon O, Harris EH, Karpowicz SJ, et al. (2007) The Chlamydomonas genome reveals the evolution of key animal and plant functions. Science 318: 245–250.
14. Coruzzi GM (2003) Primary N-assimilation into Amino Acids in Arabidopsis. Arabidopsis Book 2: e0010.
15. Boehlein SK, Richards NG, Schuster SM (1994) Glutamine-dependent nitrogen transfer in Escherichia coli asparagine synthetase B. Searching for the catalytic triad. J Biol Chem 269: 7450–7457.
16. Duff SM, Qi Q, Reich T, Wu X, Brown T, et al. (2011) A kinetic comparison of asparagine synthetase isozymes from higher plants. Plant Physiol Biochem 49: 251–256.
17. Ramos F, Wiame JM (1979) Synthesis and activation of asparagine in asparagine auxotrophs of Saccharomyces cerevisiae. Eur J Biochem 94: 409–417.
18. Horowitz B, Meister A (1972) Glutamine-dependent asparagine synthetase from leukemia cells. Chloride dependence, mechanism of action, and inhibition. J Biol Chem 247: 6708–6719.
19. Patterson MK Jr OG (1968) Asparagine biosynthesis by the Novikoff Hepatoma isolation, purification, property, and mechanism studies of the enzyme system. J Biol Chem 243: 376–380.

20. Ciustea M, Gutierrez JA, Abbatiello SE, Eyler JR, Richards NG (2005) Efficient expression, purification, and characterization of C-terminally tagged, recombinant human asparagine synthetase. Arch Biochem Biophys 440: 18–27.
21. Cedar H, Schwartz JH (1969) The asparagine synthetase of Escherichia coli. II. Studies on mechanism. J Biol Chem 244: 4122–4127.
22. Cedar H, Schwartz JH (1969) The asparagine synthetase of Escherhic coli. I. Biosynthetic role of the enzyme, purification, and characterization of the reaction products. J Biol Chem 244: 4112–4121.
23. Larsen TM, Boehlein SK, Schuster SM, Richards NG, Thoden JB, et al. (1999) Three-dimensional structure of Escherichia coli asparagine synthetase B: a short journey from substrate to product. Biochemistry 38: 16146–16157.
24. Nakatsu T, Kato H, Oda J (1998) Crystal structure of asparagine synthetase reveals a close evolutionary relationship to class II aminoacyl-tRNA synthetase. Nat Struct Biol 5: 15–19.
25. Nakatsu T, Kato H, Oda J (1996) Crystallization and preliminary crystallographic study of asparagine synthetase from Escherichia coli. Acta Crystallogr D Biol Crystallogr 52: 604–606.
26. Boehlein SK, Stewart JD, Walworth ES, Thirumoorthy R, Richards NG, et al. (1998) Kinetic mechanism of Escherichia coli asparagine synthetase B. Biochemistry 37: 13230–13238.
27. Luehr CA, Schuster SM (1985) Purification and characterization of beef pancreatic asparagine synthetase. Arch Biochem Biophys 237: 335–346.
28. Huang XH, HM; and Raushel, F (2001) Channeling of substrates and intermediates in enzyme-catalyzed reactions. Annual Review in Biochemistry 70: 149–180.
29. Berriman M, Ghedin E, Hertz-Fowler C, Blandin G, Renauld H, et al. (2005) The genome of the African trypanosome Trypanosoma brucei. Science 309: 416–422.
30. El-Sayed NM, Myler PJ, Bartholomeu DC, Nilsson D, Aggarwal G, et al. (2005) The genome sequence of Trypanosoma cruzi, etiologic agent of Chagas disease. Science 309: 409–415.
31. El-Sayed NM, Myler PJ, Blandin G, Berriman M, Crabtree J, et al. (2005) Comparative genomics of trypanosomatid parasitic protozoa. Science 309: 404–409.
32. Legros D, Ollivier G, Gastellu-Etchegorry M, Paquet C, Burri C, et al. (2002) Treatment of human African trypanosomiasis–present situation and needs for research and development. Lancet Infect Dis 2: 437–440.
33. Castro JA, de Mecca MM, Bartel LC (2006) Toxic side effects of drugs used to treat Chagas' disease (American trypanosomiasis). Hum Exp Toxicol 25: 471–479.
34. Alsford S, Kelly JM, Baker N, Horn D (2013) Genetic dissection of drug resistance in trypanosomes. Parasitology: 1–14.
35. MacGregor P, Szoor B, Savill NJ, Matthews KR (2012) Trypanosomal immune evasion, chronicity and transmission: an elegant balancing act. Nat Rev Microbiol 10: 431–438.
36. Radwanska M, Guirnalda P, De Trez C, Ryffel B, Black S, et al. (2008) Trypanosomiasis-induced B cell apoptosis results in loss of protective anti-parasite antibody responses and abolishment of vaccine-induced memory responses. PLoS Pathog 4: e1000078.
37. Akerley BJ, Rubin EJ, Novick VL, Amaya K, Judson N, et al. (2002) A genome-scale analysis for identification of genes required for growth or survival of Haemophilus influenzae. Proc Natl Acad Sci U S A 99: 966–971.
38. Boyce JD, Wilkie I, Harper M, Paustian ML, Kapur V, et al. (2002) Genomic scale analysis of Pasteurella multocida gene expression during growth within the natural chicken host. Infect Immun 70: 6871–6879.
39. Schlecker T, Schmidt A, Dirdjaja N, Voncken F, Clayton C, et al. (2005) Substrate specificity, localization, and essential role of the glutathione peroxidase-type tryparedoxin peroxidases in Trypanosoma brucei. J Biol Chem 280: 14385–14394.
40. Lanham SM (1968) Separation of trypanosomes from the blood of infected rats and mice by anion-exchangers. Nature 218: 1273–1274.
41. Sheng S, Kraft JJ, Schuster SM (1993) A specific quantitative colorimetric assay for L-asparagine. Anal Biochem 211: 242–249.
42. Fresquet V, Thoden JB, Holden HM, Raushel FM (2004) Kinetic mechanism of asparagine synthetase from Vibrio cholerae. Bioorg Chem 32: 63–75.
43. Kakkar T, Boxenbaum H, Mayersohn M (1999) Estimation of Ki in a competitive enzyme-inhibition model: comparisons among three methods of data analysis. Drug Metab Dispos 27: 756–762.
44. Larkin MA, Blackshields G, Brown NP, Chenna R, McGettigan PA, et al. (2007) Clustal W and Clustal X version 2.0. Bioinformatics 23: 2947–2948.
45. Bond CS, Schuttelkopf AW (2009) ALINE: a WYSIWYG protein-sequence alignment editor for publication-quality alignments. Acta Crystallogr D Biol Crystallogr 65: 510–512.
46. Arnold K, Bordoli L, Kopp J, Schwede T (2006) The SWISS-MODEL workspace: a web-based environment for protein structure homology modelling. Bioinformatics 22: 195–201.
47. Kiefer F, Arnold K, Kunzli M, Bordoli L, Schwede T (2009) The SWISS-MODEL Repository and associated resources. Nucleic Acids Res 37: D387–392.
48. Peitsch MC, Wells TN, Stampf DR, Sussman JL (1995) The Swiss-3DImage collection and PDB-Browser on the World-Wide Web. Trends Biochem Sci 20: 82–84.
49. Cooney DA, Capizzi RL, Handschumacher RE (1970) Evaluation of L-asparagine metabolism in animals and man. Cancer Res 30: 929–935.
50. Goldberg AI, Cooney DA, Glynn JP, Homan ER, Gaston MR, et al. (1973) The effects of immunization to L-asparaginase on antitumor and enzymatic activity. Cancer Res 33: 256–261.
51. Hannaert V, Albert MA, Rigden DJ, da Silva Giotto MT, Thiemann O, et al. (2003) Kinetic characterization, structure modelling studies and crystallization of Trypanosoma brucei enolase. Eur J Biochem 270: 3205–3213.
52. Clayton CE (1987) Import of fructose bisphosphate aldolase into the glycosomes of Trypanosoma brucei. J Cell Biol 105: 2649–2654.
53. Bangs JD, Uyetake L, Brickman MJ, Balber AE, Boothroyd JC (1993) Molecular cloning and cellular localization of a BiP homologue in Trypanosoma brucei. Divergent ER retention signals in a lower eukaryote. J Cell Sci 105 (Pt 4): 1101–1113.
54. He CY, Ho HH, Malsam J, Chalouni C, West CM, et al. (2004) Golgi duplication in Trypanosoma brucei. J Cell Biol 165: 313–321.
55. Chen Y, Hung CH, Burderer T, Lee GS (2003) Development of RNA interference revertants in Trypanosoma brucei cell lines generated with a double stranded RNA expression construct driven by two opposing promoters. Mol Biochem Parasitol 126: 275–279.
56. Alsford S, Turner DJ, Obado SO, Sanchez-Flores A, Glover L, et al. (2011) High-throughput phenotyping using parallel sequencing of RNA interference targets in the African trypanosome. Genome Res 21: 915–924.
57. Scotti C, Sommi P, Pasquetto MV, Cappelletti D, Stivala S, et al. (2010) Cell-cycle inhibition by Helicobacter pylori L-asparaginase. PLoS One 5: e13892.
58. Ueno T, Ohtawa K, Mitsui K, Kodera Y, Hiroto M, et al. (1997) Cell cycle arrest and apoptosis of leukemia cells induced by L-asparaginase. Leukemia 11: 1858–1861.
59. Broome JD (1963) Evidence that the L-asparaginase of guinea pig serum is responsible for its antilymphoma effects. I. Properties of the L-asparaginase of guinea pig serum in relation to those of the antilymphoma substance. J Exp Med 118: 99–120.
60. Beard ME, Crowther D, Galton DA, Guyer RJ, Fairley GH, et al. (1970) L-asparaginase in treatment of acute leukaemia and lymphosarcoma. Br Med J 1: 191–195.
61. Appel IM, Hop WC, van Kessel-Bakvis C, Stigter R, Pieters R (2008) L-Asparaginase and the effect of age on coagulation and fibrinolysis in childhood acute lymphoblastic leukemia. Thromb Haemost 100: 330–337.
62. Cohen H, Bielorai B, Harats D, Toren A, Pinhas-Hamiel O (2010) Conservative treatment of L-asparaginase-associated lipid abnormalities in children with acute lymphoblastic leukemia. Pediatr Blood Cancer 54: 703–706.
63. van den Berg H (2011) Asparaginase revisited. Leuk Lymphoma 52: 168–178.

Supplementary Figures

Figure S1

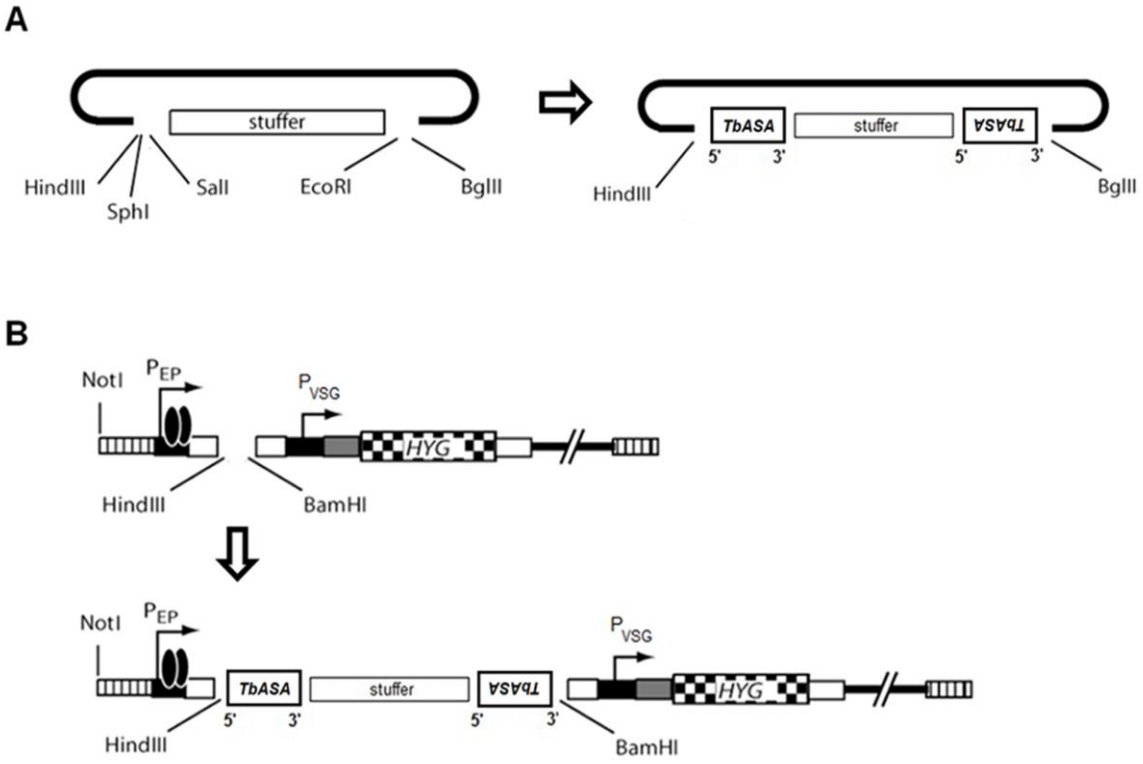

Adapted from protocol book of EMBO/TDR practical course "RNA interference and genetic manipulation in Trypanosoma brucei" provided by Christine Clayton

Figure S1. RNAi vectors used to generate RNAi-mediated *Tb*AS-A downregulation. (A) pHD1144 vector for stem-loop cloning (pSP72 vector with a stuffer fragment); (B) pHD1145 inducible polymerase I vector for insertion of ready-made stem-loops (pHD677 vector without a T7 promoter and with an inducible EP1 promoter and hygromycin resistance cassette, insertion into ribosomal spacer).

Figure S2

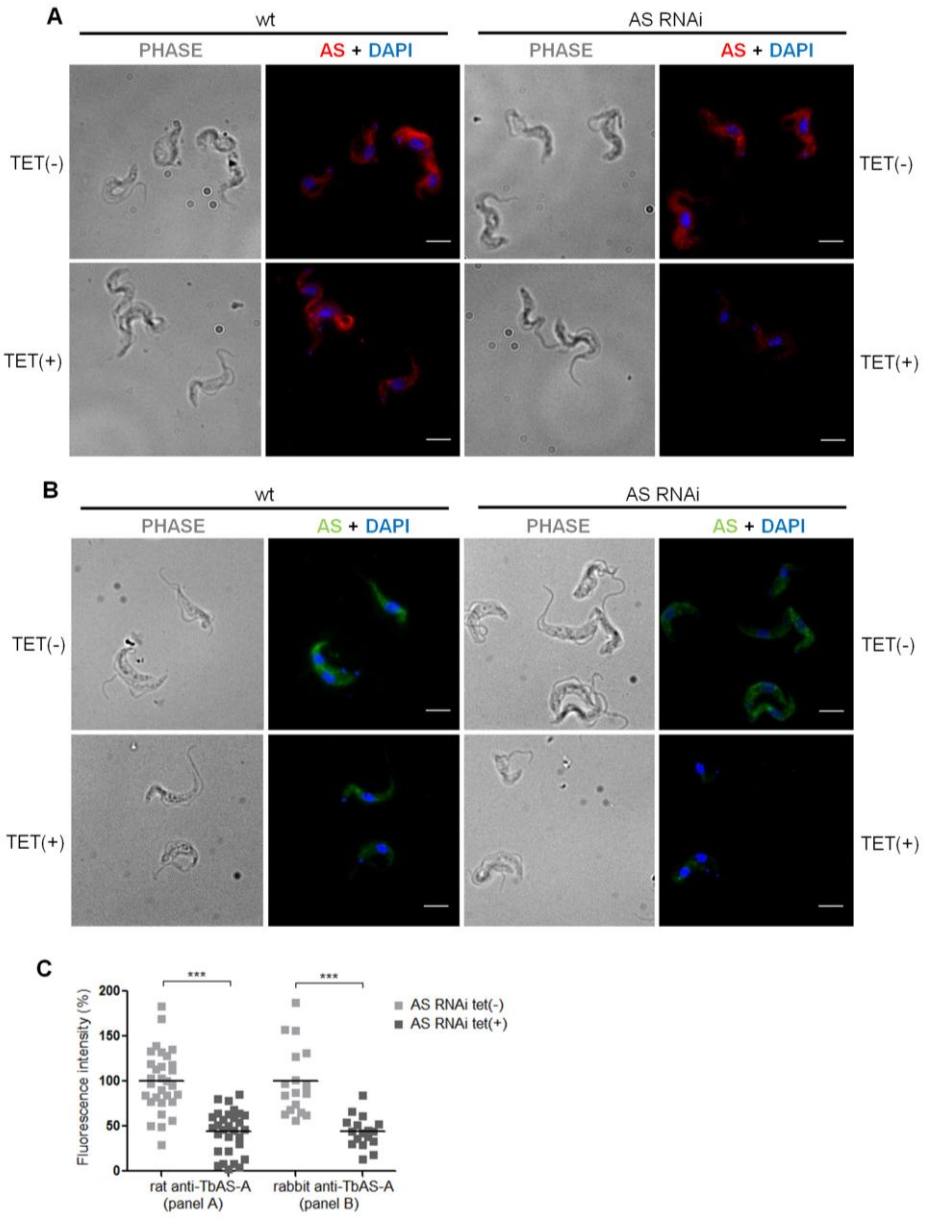

Figure S2. Validation of antibodies against *Tb*AS-A. Immunofluorescence analysis of *T. brucei* wt or a representative AS RNAi clone grown in the presence or absence of tetracycline. RNAi induced and uninduced cells were grown for 48h, then fixed and probed with rat polyclonal anti-*Tb*AS-A (A) or rabbit polyclonal anti-*Tb*AS-A (B) antibody and co-stained with DAPI. Bars, 5µm. Quantification of *Tb*AS-A fluorescence levels in induced cells (AS RNAi tet(+), n = 30) and uninduced cells (AS RNAi tet(-), n = 30), using the rat and the rabbit polyclonal anti-*Tb*AS-A antibodies (C). Data representative of two independent experiments using two different clones. ImageJ software (version 1.43u) was used for fluorescence quantification. p value was calculated by Student's t test (*** $p \leq 0.001$ and ** $p \leq 0.01$).

Figure S3

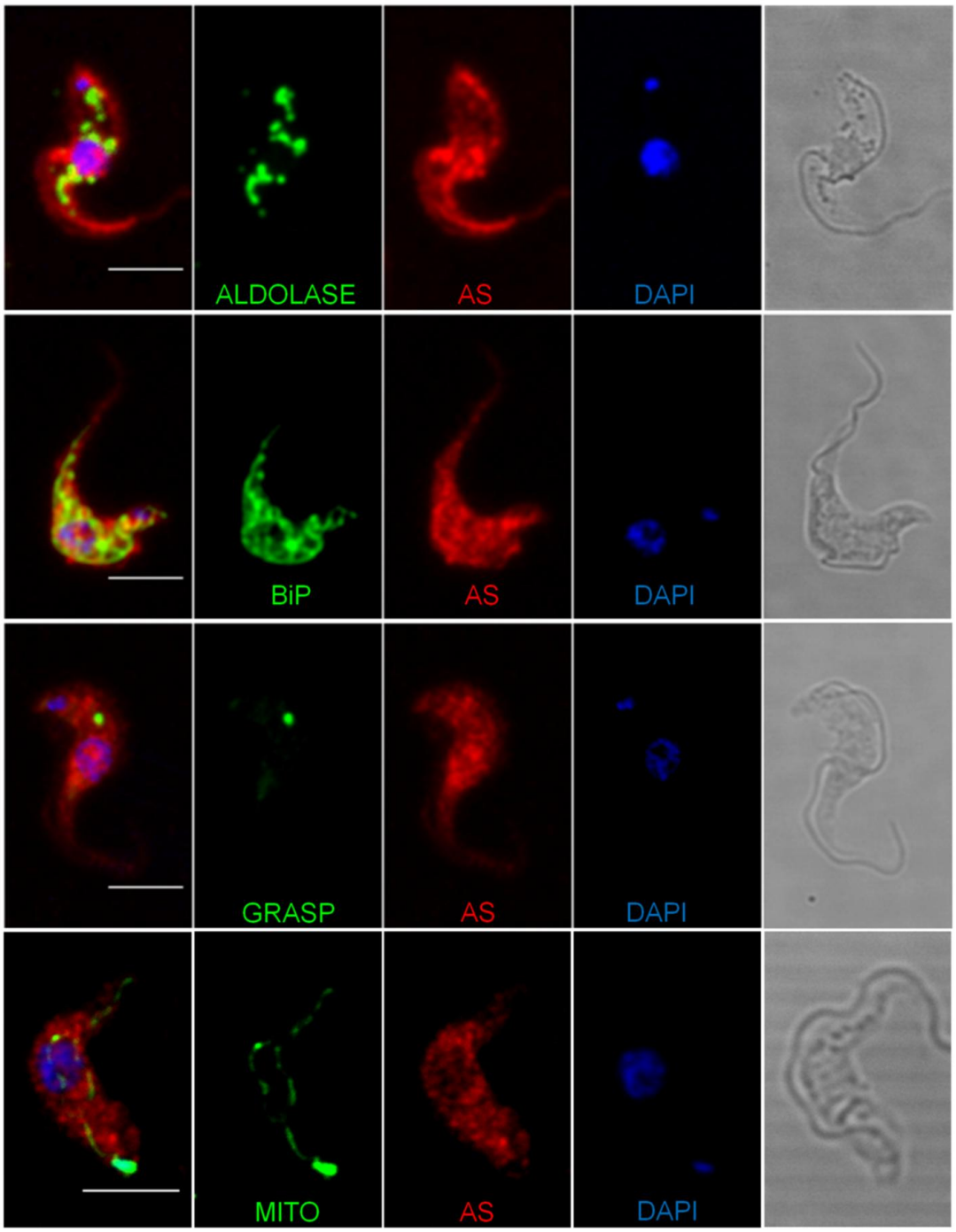

Figure S3. *Tb*AS-A cellular localization in *T. brucei* bloodstream forms. Immunofluorescence analysis by confocal microscopy of *Tb*AS-A (red) in bloodstream forms. Aldolase (glycosome marker), GRASP (golgi marker), BiP (endoplasmic reticulum marker) and MitoTracker (labels mitochondria) are in green. DAPI locate nuclear and kinetoplast mitochondrial DNA (blue). Bars, 5 µm. Images are maximal Z-projections of 50 contiguous stacks separated by 0.1 µm.

PLOS | NEGLECTED TROPICAL DISEASES

Correction: Knockdown of Asparagine Synthetase A Renders *Trypanosoma brucei* Auxotrophic to Asparagine

Inês Loureiro, Joana Faria, Christine Clayton, Sandra Macedo Ribeiro, Nilanjan Roy, Nuno Santarém, Joana Tavares, Anabela Cordeiro-da-Silva

Published: December 06, 2013 • DOI: 10.1371/annotation/eb4faa32-fc8d-43ae-ba92-f34c0c4e5052

The following information was missing from the Funding section: This work was funded by FEDER funds through the Operational Competitiveness Program – COMPETE and by National Funds through FCT – Fundação para a Ciência e a Tecnologia under the project PEst-C/SAU/LA0002/2011. IL, JF and NS were supported by fellowships from FCT reference SFRH/BD/64528/2009, SFRH/BD/79712/2011 and SFRH/BPD/BIA-MIC/118644/2010, respectively. JT is an Investigator FCT funded by National funds through FCT and co-funded through European Social Fund within the Human Potential Operating Programme. The research leading to these results has also received funding from the European Community's Seventh Framework Programme under grant agreement No.602773 (Project KINDRED). The COST Action CM0801 'New drugs for neglected diseases' and TRICONT project under ERA-NET New INDIGO have also contributed for this work. The funders had no role in study design, data collection and analysis, decision to publish, or preparation of the manuscript.

Citation: Loureiro I, Faria J, Clayton C, Ribeiro SM, Roy N, et al. (2013) Correction: Knockdown of Asparagine Synthetase A Renders *Trypanosoma brucei* Auxotrophic to Asparagine. PLoS Negl Trop Dis 7(12): 10.1371/annotation/eb4faa32-fc8d-43ae-ba92-f34c0c4e5052. doi:10.1371/annotation/eb4faa32-fc8d-43ae-ba92-f34c0c4e5052

Published: December 6, 2013

Competing interests: No competing interests declared.

2.2 *T. brucei* ribose 5-phosphate isomerase B as a promising drug target

2.2.1 Ribose 5-phosphate isomerase B knockdown compromises *Trypanosoma brucei* bloodstream form infectivity

Ribose 5-phosphate isomerase is an enzyme involved in the non-oxidative branch of the pentose phosphate pathway and catalyzes the inter-conversion of D-ribose 5-phosphate and D-ribulose 5-phosphate. Trypanosomatids, including the agent of African sleeping sickness namely *Trypanosoma brucei*, have a type B ribose-5-phosphate isomerase. This enzyme is absent from humans, which have a structurally unrelated ribose 5-phosphate isomerase type A, and therefore has been proposed as an attractive drug target waiting further characterization. In this study *Trypanosoma brucei* ribose 5-phosphate isomerase B showed *in vitro* isomerase activity. RNAi against this enzyme reduced parasites *in vitro* growth and more importantly bloodstream forms infectivity. Mice infected with induced RNAi clones exhibited lower parasitaemia and a prolonged survival compared to control mice. Phenotypic reversion was achieved by complementing induced RNAi clones with an ectopic copy of *Trypanosoma cruzi* gene. Our results present the first functional characterization of *Trypanosoma brucei* ribose 5-phosphate isomerase B, and show the relevance of an enzyme belonging to the non-oxidative branch of the pentose phosphate pathway in the context of *Trypanosoma brucei* infection.

Reprinted from PLoS Negl Trop Dis. 2015 Jan 8; 9(1): e3430. doi:10.1371/journal.pntd.0003430

OPEN ACCESS Freely available online

PLOS | NEGLECTED TROPICAL DISEASES

Ribose 5-Phosphate Isomerase B Knockdown Compromises *Trypanosoma brucei* Bloodstream Form Infectivity

Inês Loureiro[1], Joana Faria[1], Christine Clayton[2], Sandra Macedo-Ribeiro[3], Nuno Santarém[1], Nilanjan Roy[4], Anabela Cordeiro-da-Siva[1,5‡*], Joana Tavares[1‡*]

1 Parasite Disease Group, Instituto de Biologia Molecular e Celular da Universidade do Porto, Porto, Portugal, **2** Zentrum für Molekulare Biologie der Universität Heidelberg, DKFZ-ZMBH cv Alliance, Heidelberg, Germany, **3** Protein Crystallography Group, Instituto de Biologia Molecular e Celular da Universidade do Porto, Porto, Portugal, **4** Ashok & Rita Patel Institute of Integrated Study & Research in Biotechnology & Allied Sciences, New Vallabh Vidyanagar, Dist-Anand, Gujarat, India, **5** Departamento de Ciências Biológicas, Faculdade de Farmácia da Universidade do Porto, Porto, Portugal

Abstract

Ribose 5-phosphate isomerase is an enzyme involved in the non-oxidative branch of the pentose phosphate pathway, and catalyzes the inter-conversion of D-ribose 5-phosphate and D-ribulose 5-phosphate. Trypanosomatids, including the agent of African sleeping sickness namely *Trypanosoma brucei*, have a type B ribose-5-phosphate isomerase. This enzyme is absent from humans, which have a structurally unrelated ribose 5-phosphate isomerase type A, and therefore has been proposed as an attractive drug target waiting further characterization. In this study, *Trypanosoma brucei* ribose 5-phosphate isomerase B showed *in vitro* isomerase activity. RNAi against this enzyme reduced parasites' *in vitro* growth, and more importantly, bloodstream forms infectivity. Mice infected with induced RNAi clones exhibited lower parasitaemia and a prolonged survival compared to control mice. Phenotypic reversion was achieved by complementing induced RNAi clones with an ectopic copy of *Trypanosoma cruzi* gene. Our results present the first functional characterization of *Trypanosoma brucei* ribose 5-phosphate isomerase B, and show the relevance of an enzyme belonging to the non-oxidative branch of the pentose phosphate pathway in the context of *Trypanosoma brucei* infection.

Citation: Loureiro I, Faria J, Clayton C, Macedo-Ribeiro S, Santarém N, et al. (2015) Ribose 5-Phosphate Isomerase B Knockdown Compromises *Trypanosoma brucei* Bloodstream Form Infectivity. PLoS Negl Trop Dis 9(1): e3430. doi:10.1371/journal.pntd.0003430

Editor: Michael P. Pollastri, Northeastern University, United States of America

Received July 25, 2014; **Accepted** November 21, 2014; **Published** January 8, 2015

Data Availability: The authors confirm that all data underlying the findings are fully available without restriction. All relevant data are within the paper and its Supporting Information files except for the sequence of TbRpiB, TcRpiB from CL Brener Esmeraldo-like and non-Esmeraldo-like which are available from TriTrypdb.org under the accession numbers Tb927.11.8970, Tc00.1047053509199.24 and Tc00.1047053508601.119 respectively.

Funding: This work was funded by the European Community's Seventh Framework Programme under grant agreement No. 602773 (Project KINDRED). The COST Action CM1307 'Targeted chemotherapy towards diseases caused by endoparasites' and FEDER funds through the Operational Competitiveness Program – COMPETE and by National Funds through FCT – Fundação para a Ciência e a Tecnologia under the project PEst-C/SAU/LA0002/2011 have also contributed for this work. IL and JF were supported by fellowships from FCT reference SFRH/BD/64528/2009 and SFRH/BD/79712/2011, respectively. NS is supported by a fellowship from the European Community's Seventh Framework Programme under grant agreement No. 602773 (Project KINDRED). JT is an Investigator FCT funded by National funds through FCT and co-funded through European Social Fund within the Human Potential Operating Programme. The funders had no role in study design, data collection and analysis, decision to publish, or preparation of the manuscript.

Competing Interests: The authors have declared that no competing interests exist.

* cordeiro@ibmc.up.pt (ACdS); jtavares@ibmc.up.pt (JT)

‡ These authors contributed equally to this work.

Introduction

African sleeping sickness is a vector borne disease of mammals, caused by *Trypanosoma brucei* (*T. brucei*), for which the development of more effective, safe, and affordable chemotherapies remains a major goal. Vaccines are unlikely to be suitable [1–3], and therefore disease control relies exclusively on chemotherapy. The glucose-based metabolism is a key metabolic pathway for bloodstream forms, the mammalian infective stages. The absence of a fully functional mitochondrion along with a remarkable high proliferation rate makes parasites entirely dependent on glucose [4,5]. The glucose-based metabolism comprises two pathways: the glycolytic pathway and the pentose phosphate pathway (PPP). Despite using the same substrate, the pathways have different functions. Glycolysis catabolizes glucose for ATP requirements, while PPP includes an oxidative branch, mainly involved in the maintenance of cell redox homeostasis, and a non-oxidative branch in which ribose 5-phosphate is produced for nucleotide and nucleic acid synthesis. Enzymes involved in the PPP non-oxidative branch include ribose-5-phosphate isomerase, ribulose-5-phosphate epimerase, transaldolase and transketolase, and in contrast with enzymes involved in the glycolysis [6–15] or in the oxidative PPP [16,17], have been less studied. In *T. brucei*, enzymes of the non-oxidative branch downstream ribose-5-phosphate isomerase are apparently developmentally regulated [18]. Ribose 5-phosphate epimerase and transketolase activities were only detected in procyclics, the parasite form present in the insect vector. This suggests that in the mammalian host, bloodstream forms constrain sugar metabolism to the production of ribose-5-phosphate and NADPH via the oxidative phase of the

Author Summary

Within the non-oxidative branch of the pentose phosphate pathway, ribose 5-phosphate isomerase catalyzes the inter-conversion of ribose 5-phosphate and ribulose 5-phosphate. There are two types of ribose 5-phosphate isomerase, namely A and B. The presence of type B in *Trypanosoma brucei*, and its absence in humans, make this protein a promising drug target. African sleeping sickness is a serious parasitic disease that relies on limited chemotherapeutic options for control. In our study, a functional characterization of *Trypanosoma brucei* ribose 5-phosphate isomerase B is reported. Biochemical studies confirmed enzyme isomerase activity and its downregulation by RNAi affected mainly parasites infectivity *in vivo*. Overall this study shows that ribose 5-phosphate isomerase depletion is detrimental for parasites infectivity under host pressure.

PPP, most likely to meet the remarkably high proliferation rate of these parasites [19], and/or to protect themselves against a variety of reactive oxygen and nitrogen species [20,21] in a context of an *in vivo* infection.

Ribose-5-phosphate isomerase (Rpi) catalyzes the inter-conversion between ribulose-5-phosphate (Ru5P) and ribose 5-phosphate (R5P). Contrary to trypanosomatids, which have a Rpi type B (RpiB), the presence of a structurally unrelated Rpi type A (RpiA) in humans together with the adverse phenotype observed in *rpiA*$^{-}$/*rpiB*$^{-}$ knockout *Escherichia coli* (*E. coli*) [22] have led to suggest RpiB as an attractive drug target candidate that waits further characterization.

In this study, we investigate the importance of RpiB in *T. brucei* bloodstream form viability and infectivity.

Materials and Methods

Ethics statement

All experiments were carried out in accordance with the IBMC.INEB Animal Ethics Committees and the Portuguese National Authorities for Animal Health guidelines, according to the statements on the directive 2010/63/EU of the European Parliament and of the Council. IL, JT and ACS have an accreditation for animal research given from Portuguese Veterinary Direction (Ministerial Directive 1005/92).

Parasite culture

Procyclic and bloodstream *T. brucei* Lister 427 were cultivated in MEM-Pros and HMI-9 medium, respectively, as previously described [23]. Bloodstream forms containing pHD1313 [24] were maintained with 0.2 μg/ml phleomycin.

Cloning of trypanosomes *RPIB* genes

Ribose 5-phosphate isomerase B genes from *T. brucei* (*TbRPIB*) and *T. cruzi* (*TcRPIB*) were obtained by performing PCR on genomic DNA from *Trypanosama brucei* TREU927 and *Trypanosoma cruzi* CL Brener Non-Esmeraldo-like. Fragments of the open reading frames of *TbRPIB* (Tb927.11.8970; chromosome Tb927_11_v5 from 2,462,183 to 2,463,307) and *TcRPIB* (Tc00.1047053508601.119; chromosome TcChr30-P from 475,724 to 476,203) were PCR-amplified using a Taq DNA polymerase with proofreading activity (Roche). The primers were as follows: sense primer 5′ - CAATTTCCATATGACGCG-CAAGGTGGC - 3′ and antisense primer 5′ - CCCAAG-CAAGCTTCTAACAACCATTCG - 3′, sense primer 5′ - CAATTTCCATATGACGCGCCGAGTCGC - 3′ and antisense primer 5′ - CCCAAGCGAATTCTCATTTTACCCCTTTG - 3′, respectively. PCR conditions were as follows: initial denaturation (2 min at 94°C), 35 cycles of denaturation (30 s at 94°C), annealing (30 s at 40°C) and elongation (2 min at 68°C) followed by a final extension step (10 min at 68°C); initial denaturation (2 min at 94°C), 35 cycles of denaturation (30 s at 94°C), annealing (30 s at 58°C) elongation (2 min at 68°C) and a final extension step (10 min at 68°C), respectively. The PCR products were isolated from a 1% agarose gel, purified by the Qiaex II protocol (Qiagen), and cloned into a pGEM-T Easy vector (Promega) and sent to Eurofins MWG (Germany) for sequencing. All fragments were checked against the *T. brucei* and *T. cruzi* genome sequence database (http://www.genedb.org) using Blast to ensure their specificity.

Expression and purification of poly-His-tagged recombinant *Tb*RpiB and *Tc*RpiB

The *TbRPIB* and *TcRPIB* genes were excised from the pGEM-T Easy vector (using NdeI/EcoRI restriction enzyme combination), gel purified and subcloned into pET28a(+) expression vector (Novagen). The resulting constructs presented a poly-His tag (6× Histidine residues) at the N-terminal and were used to transform *E. coli* BL21DE3 cells. Both recombinant proteins were expressed by induction of log-phase cultures (500 ml; OD_{600} = 0.6) with 0.5 mM IPTG (isopropyl-β-D- thiogalactopyranoside) for 3 h at 37°C and agitation at 250 rpm/min. Bacteria were harvested by centrifugation (4000 rpm, for 40 min, at 4°C), resuspended in 20 ml of buffer A (0.5 M NaCl, 20 mM Tris.HCl, pH 7.6). The sample was sonicated, according to the following conditions: output 4, duty cycle 50%, 10 cycles with 15 s each. Centrifugation (4000 rpm, for 60 min, at 4°C) was followed to obtain the bacterial crude extract. The recombinant enzymes were purified in one step using Ni^{2+} resin (ProBond) pre-equilibrated in buffer A. The column was washed sequentially with 2–3 ml of the buffer A, 20 ml of the bacterial crude extract, 2 ml of buffer A 25 mM imidazole, 2 ml of buffer A 30 mM imidazole, 2 ml of buffer A 40 mM imidazole, 2 ml of buffer A 40 mM imidazole, 2 ml of buffer A 50 mM imidazole, 10 ml of buffer A 100 mM imidazole, 5 ml of buffer A 500 mM imidazole and 8 ml of buffer B (1 M imidazole, 0.5 M NaCl, 200 mM Tris, pH 7.6). *Tb*RpiB and *Tc*RpiB were eluted in the fractions of buffer A containing between 100 and 500 mM of imidazole. Dialysis was performed against 100 mM Tris/HCl (pH 7.6).

To generate rat polyclonal antibody against *Tb*RpiB, and rabbit polyclonal antibodies against *Tb*RpiB and *Tc*RpiB, each animal was first immunized with 150 μg of recombinant protein. After 2 weeks, 4 boosts with 100 μg of recombinant *Tb*RpiB or *Tc*RpiB were given weekly. The collected blood samples were centrifuged to obtain the sera.

Protein alignments and homology models

Multiple sequence alignments were performed in ClustalW [25] and images prepared with Aline, Version 011208 [26]. Homology models were obtained in SWISS-MODEL, using PDB accession code 3K7S as a template [27–29]. 3D structures were rendered with PyMOL (The PyMOL Molecular Graphics System, Version 1.3, Schrödinger, LLC).

Enzyme assays

*Tb*RpiB activity was assessed through *Km* determination for R5P and Ru5P, through 4-deoxy-4-phospho-D-erythronohydroxamic acid (4-PEH) (kindly provided by Dr. Laurent Salmon) inhibitory capacity against *Tb*RpiB, and through 4-PEH inhibition

mechanism characterization. Firstly, to determine the *Km* for R5P and to characterize 4-PEH-inhibition mechanism, a direct spectrophotometric method at 290 nm [30] was used, to quantify Ru5P formation. *Km* determination was performed at R5P concentrations in a range between 3.1 and 50 mM in Tris/HCl (pH 7.6). For 4-PEH inhibition mechanism characterization, the experiment was performed in the presence of 0.5 μg of enzyme and 0.1, 0.4, 0.7 or 1 mM of inhibitor. All inhibitors were tested in the presence of 3.1 mM R5P. A negative control was made using heat inactivated enzyme. The *Tc*RpiB enzyme was used as a positive control [31]. A calibration curve for Ru5P, using the referred method, was established to determine enzyme activity. An absorbance of 0.0381 at 290 nm was considered for 1 mM Ru5P. To determine the *Km* for Ru5P and to test 4-PEH inhibition as well, a modification of Dische's Cysteine-Carbazole method was used [32]. To determine *Km*, an incubation mixture contained 5 μl of 0.05 μg of enzyme in buffer A [100 mM Tris/HCl (pH 8.4), 1 mM EDTA and 0.5 mM 2-mercaptoethanol] plus 5 μl of Ru5P, giving final concentrations between 0.625 and 10 mM Ru5P, was used. For inhibition assay, Ru5P concentration used was 1.25 mM. Incubation was done for 10 min at room temperature. Following incubation, 15 μl of 0.5% cysteinium chloride, 125 μl of 75% (v/v) sulfuric acid and 5 μl of a 0.1% solution of carbazole in ethanol were added. After 30 min standing at room temperature, the A_{546} was determined. A blank without enzyme was run for each substrate or inhibitor concentration. Reaction linearity was checked varying enzyme concentration and time. To estimate the remaining Ru5P, a calibration curve was generated. In this assay conditions, 1 mM of Ru5P gave an A_{546} of 0.270 in a final reaction volume of 155 μl.

Immunofluorescence

For anti-*Tb*RpiB antibodies validation, cells from log-phase cultures of *T. brucei* RNAi cell lines and wt strain were centrifuged and resuspended at 10^6/ml in PBS. The cells were fixed in μ-Chamber 12 well (Ibidi) for 15 min, at room temperature, in PBS containing 4% p-formaldehyde, washed twice with PBS, and then permeabilized in PBS containing 0.1% of Triton X-100. The coverslips were incubated in PBS containing 10% FCS during 60 min, at room temperature, in a humidified atmosphere and washed twice with PBS/2% FCS. Then, incubated with primary rat or rabbit polyclonal antibodies against *Tb*RpiB (1:100 and 1:1000 respectively, both diluted in blocking solution) overnight, at 4°C, followed by two washes with PBS/2% FCS (5 min each one). Subsequently, cells were incubated with Alexa Fluor 647 conjugated goat anti-rat or Alexa Fluor 488 conjugated goat anti-rabbit secondary antibodies (Molecular probes from Life technologies) (1:500 diluted in blocking solution) for 1 h at room temperature in an humidified atmosphere, then washed twice with PBS. The coverslips were then stained and mounted with Vectashield-DAPI (Vector Laboratories, Inc.). Images were captured using fluorescence microscope AxioImager Z1 and software Axiovision 4.7 (Carl Zeiss, Germany). Pseudo-coloring of images were carried out using ImageJ software (version 1.43u). In case of *Tb*RpiB immunolocalization, bloodstream form *T. brucei* wt cells were probed using primary rat anti-*Tb*RpiB (1:100 diluted in blocking solution) and primary rabbit polyclonal antibody against aldolase (glycosome marker, 1:5000 diluted in blocking solution). Cells were then incubated with biotin conjugated goat anti-rat (1:500 diluted in blocking solution) (BD Pharmingen) for 1 h room temperature in a humidified atmosphere, then washed twice with PBS/2% FCS. Subsequently, cells were incubated with Alexa Fluor 647 conjugated goat anti-rabbit (Molecular probes, Life technologies) and Streptavidin-FITC (BD Pharmingen) secondary antibodies (1:1000 diluted in blocking solution) for 1 h at room temperature in an humidified atmosphere, then washed twice with PBS. Vertical stacks were captured, using an confocal microscope Leica TCS SP5II and LAS 2.6 software (Leica Microsystems, Germany). Mean fluorescence intensity of aldolase and RpiB was determined in each stack for the projected co-localization areas. Quantifications were carried out using ImageJ software (version 1.43u).

Digitonin permeabilization

For each sample condition, bloodstream cells were washed once with cold trypanosome homogenisation buffer (THB), composed by 25 mM Tris, 1 mM EDTA and 10% sucrose, pH = 7.8. Just before cell lyses, leupeptin (final concentration of 2 μg/ml) and different digitonin quantities (final concentrations of 5, 12.5, 25, 50, 100, 150 and 200 ug/ml) were added to 500 μl of cold THB, for cell pellet resuspension. Untreated cells (0 μg/ml of digitonin) and those completely permeabilized (total release, the result of incubation in 0.5% Triton X-100) were used for comparison. Each sample condition was incubated 60 min on ice, and then centrifuged at 2000 rpm, 4°C, for 10 min. Supernatants were taken and 500 μl of cold THB was added to each pellet. All fractions were analysed through Western blot for Rpi (10^8 cells per well; 1:1000 polyclonal rabbit anti-*Tb*RpiB as primary antibody), enolase (10^7 cells per well; 1:5000 polyclonal rabbit anti-enolase as primary antibody) and aldolase (10^7 cells per well; 1:5000 polyclonal rabbit anti-aldolase as primary antibody). HRP-conjugated goat anti-rabbit (1:5000) was used as secondary antibody.

Generation of transgenic RNAi cell lines

TbRPIB fragment (sense oligo with a BglII – SphI linker 5′ – GAGAAGATCTGCATGCGCGCAAGGTGGCTATCGGTG - 3′, and an antisense oligo with a ClaI – SalI 5′ – GCTAGCTA-CAGCTGACGGTCCTCCCCGCTGTATG – 3′) was cloned twice in opposite direction on either sides of a "stuffer" of the pHD1144 vector. The resulting construct obtained through HindIII and BglII digestion was cloned into pHD1145. The final construct was transfect into bloodstream forms with pHD1313, and stable individual clones were selected with 7.5 μg/ml of hygromycin. For functional complementation, *TcRPIB* fragment (sense oligo with a HindIII linker 5′ - GAAGCTTAT-GACGCGCCGAGTCGCAAT - 3′, and an antisense oligo with a BglII linker 5′ - AGATCTTCATTTTACCCCTTTGTTCC - 3′), was cloned in pHD1034 vector (digested with HindIII and BamHI). After transfection [33], individual clones were selected with 0.2 μg/ml of puromycin.

In vitro and *in vivo* analysis of *Tb*RpiB RNAi

For *in vitro* growth curves, cell lines were seeded at 2×10^5 parasites/ml of complete HMI-9 medium, in the absence and presence of 100 ng/ml of tetracycline (tet). Every 24 h, until day 10, cell growth was monitored microscopically. For *in vivo* infections, after 24 h in the absence of selective drugs, and then a further 48 h of tet induction, 10^4 wt and transgenic parasites were inoculated intraperitoneally in 6–8 weeks old BALB/c mice (n = 3–8). 48 h prior infection, the RNAi induced mice were treated with 1 mg/ml doxycycline hyclate and 5% sucrose containing water [34], while RNAi non-induced mice were given standard water. Parasitaemia was measured daily from the six day post-infection through tail blood extraction, during a period which all mice in the group were alive.

Northern blot analysis

Total RNA was isolated from ≈2×10^7 bloodstream forms using Trizol reagent (Life Technologies). 10 μg RNA were directly separated by overnight formaldehyde agarose-gel electrophoresis, transferred onto a nylon membrane by capillarity and fixed by UV irradiation. The membrane was prehybridized in a hybridization bottle in 5× SSC, 0.5% SDS with salmon sperm DNA (200 μg/ml) and 1× Denhardt's solution for 2 hours at 65°C. *TbRPIB* and signal recognition particle (*SRP*; Tb927.8.2861_7SL) probes were generated by PCR in the presence of [^{32}P]-labelled dCTP using Prime-It RmT random primer labelling kit (Stratagene) followed by purification using QIAquick Nucleotide Removal Kit (QIAGEN). Denaturated radioactive probes were added to the prehybridization solution at 65°C and incubated overnight. After rinsing the membrane twice for 5 min. with 2× SSC/0.1% SDS, the probes were washed out with two washes of 30 minutes in 0.1× SSC/0.1% SDS at 65°C and the membrane exposed on a Fugifilm FLA-3000 reader screen. ImageJ software (version 1.43u) was used for RNA quantification.

Protein extracts and western blot analysis

Cell free extracts were obtained in RIPA buffer (20 mM Tris-HCl (pH 7.5), 150 mM NaCl, 1 mM Na_2EDTA, 1 mM EGTA, 1% NP-40, 1% sodium deoxycholate, 2.5 mM sodium pyrophosphate, 1 mM b-glycerophosphate, 1 mM Na_3VO_4), with freshly-added complete protease inhibitor cocktail (Roche Applied Science). The total protein amount was quantified using Biorad Commercial Kit (Reagents A, B and S) and the samples were then kept at -80°C. For analysis of parasites collected from mice, trypanosomes were purified from mouse blood using a DE-52 (Whatman) column [35].

For Western blotting, 10 μg of recombinant *Tb*RpiB and *Tc*RpiB proteins were resolved in 15% SDS/PAGE (Tris-Tricine gel), while 30 μg of total soluble cell extract and 10^7 parasites were resolved in 12% Tris-Glycine SDS/PAGE, and all were then transferred on to a nitrocellulose Hy-bond ECL membrane (Amersham Biosciences). The membrane was blocked in 5% (w/v) non-fat dried skimmed milk in PBS/0.1% Tween-20 (blocking solution), followed by incubation with an anti-His-tag rabbit antibody (MicroMol-413) (1:1000) or a combination of an anti-*Tb*RpiB rabbit antibody (1:1000) with an anti-aldolase rabbit antibody (1:5000) in blocking solution at 4°C overnight, respectively. Blots were washed with PBS/0.1% Tween-20 (3 times 15 min). Horseradish peroxidase-conjugated goat anti-rabbit IgG (Amersham) (1:5000 for 1 h, at room temperature) was used as the secondary antibody. The membranes were developed using SuperSignal WestPico Chemiluminescent Substrate (Pierce). ImageJ software (version 1.43u) was used for protein bands semi-quantification.

Statistical analysis

Student's t-test and Graphpad Prism Software (version 5.0) were used. p values ≤0.05 were considered to be statistically significant (* $p\leq0.05$, ** $p\leq0.01$, *** $p\leq0.001$).

Results

*Tb*RpiB biochemical properties

An open reading frame with sequence similarity to RpiB was identified both in *T. brucei* (Tb927.11.8970) and in *T. cruzi* (Tc00.1047053508601.119) genomes. Protein sequence alignment using ClustalW [25] revealed 67% identity for *Tb*RpiB *versus* *Tc*RpiB, and both proteins show no similarity with human ribose 5–phosphate isomerase A. *Tc*RpiB and *Tb*RpiB contain 159 and 155 amino acids residues per monomer, respectively. Protein multiple sequence alignment of RpiB from *T. cruzi* CL Brener Esmeraldo-like (Tc00.1047053509199.24; PDB accession code 3K7S [36]), *T. cruzi* CL Brener Non-Esmeraldo-like (Tc00.1047053508601.119) and *T. brucei* (Tb927.11.8970) is shown in S1A Fig. The scale colour, from cyan (low-similarity residues) to red (high-similarity residues), underlines the degree of similarity between the three protein sequences, also seen in the *Tc*RpiB (Esmeraldo like strain) ribbon representation (S1B Fig.). The superposition of *Tc*RpiB (Esmeraldo like strain) structure (grey) (PDB code 3K7S), with the homology models generated for *Tc*RpiB (Non Esmeraldo like strain) (purple) and *Tb*RpiB (blue) show a high structural homology and strict conservation of the residues involved in R5P binding pocket (S1A, C Fig.).

Biochemical studies were performed using histidine-tagged fusion *Tb*RpiB and *Tc*RpiB (positive control) proteins expressed in *E. coli* and purified under non-denaturing conditions (Figs. 1A, S2A). The *T. brucei* and *T. cruzi* [31] enzymes have *in vitro* ribose 5-phosphate isomerase activity, as these proteins can use both R5P and Ru5P as substrates. For R5P, *T. brucei* protein showed a significantly higher K_m (2.8 fold increase, $p<0.05$), but not a lower maximum velocity (V_{max}) or catalytic constant (k_{cat}) compared to *T. cruzi* enzyme (Table 1 and S2B Fig.). For Ru5P, the K_m of the *T. brucei* protein was not significantly different from that of the *T. cruzi* enzyme value, but the V_{max} and k_{cat} were higher (≈1.5 fold, $p<0.05$) (Table 1 and S2B Fig.). Both the *T. brucei* and the *T. cruzi* enzymes exhibited significant lower K_ms for Ru5P than for R5P, (5.2 fold, $p<0.05$ and 3.7 fold, $p<0.01$, respectively), suggesting the reaction occurs preferentially from Ru5P to R5P. The turnover values (k_{cat}) were found to be significantly higher for Ru5P than for R5P, in both *T. brucei* ($p = 0.001$) and *T. cruzi* ($p< 0.001$) enzymes (Table 1 and S2B Fig.).

The reaction mechanism of ribose 5-phosphate isomerase involves two steps: an initial opening of the furanose ring of R5P, followed by the aldolase-ketose isomerisation, via a cis-enediolate high energy intermediate [31]. 4-PEH has been described to act as a competitive inhibitor which compromises the binding of 1,2-*cis*-enediolate intermediate [37]. The inhibitory capability of 4-PEH was screened *in vitro*, resulting in an IC50 of 0.8 mM and 0.7 mM for *Tb*RpiB (Fig. 1B) and *Tc*RpiB (S2C Fig.), respectively, with K_i values of 2.2 (Fig. 1C) and 1.6 mM (S2D Fig.). 4-PEH showed, as expected, a competitive inhibition behaviour, once using increasing concentrations of inhibitor, a progressive increase in the K_m for R5P without V_{max} alteration was observed (Figs. 1D, S2E). The inhibitor behaviour, and also the IC_{50} and the K_i values are in agreement to what was described before for *T. cruzi* enzyme [31,36]. 4-PEH was also reported as a potent inhibitor against *Mycobacterium tuberculosis* RpiB [37].

Undoubtedly, *Tb*RpiB has isomerase activity and uses preferentially ribulose 5-phosphate as a substrate.

*Tb*RpiB expression and subcellular localization

Rabbit and rat polyclonal antibodies were generated against the *Tb*RpiB recombinant protein. Antibody specificity was validated, as induction of RpiB RNAi resulted in a decrease in the fluorescence intensity of bloodstreams when compared to non-induced parasites (S3A, B, C Fig.). Similarly a significant decrease on RpiB levels in the extracts of *Tb*RpiB RNAi induced parasites is shown by Western blot. Rat and rabbit antibodies specificity against RpiB can be appreciated on the whole Western blot membranes (S3D, E Fig.). Using rabbit polyclonal antibody against parasite extracts, *Tb*RpiB was found more abundant in procyclic forms than in bloodstream forms (Fig. 2A). To ascertain RpiB subcellular localization in bloodstream forms,

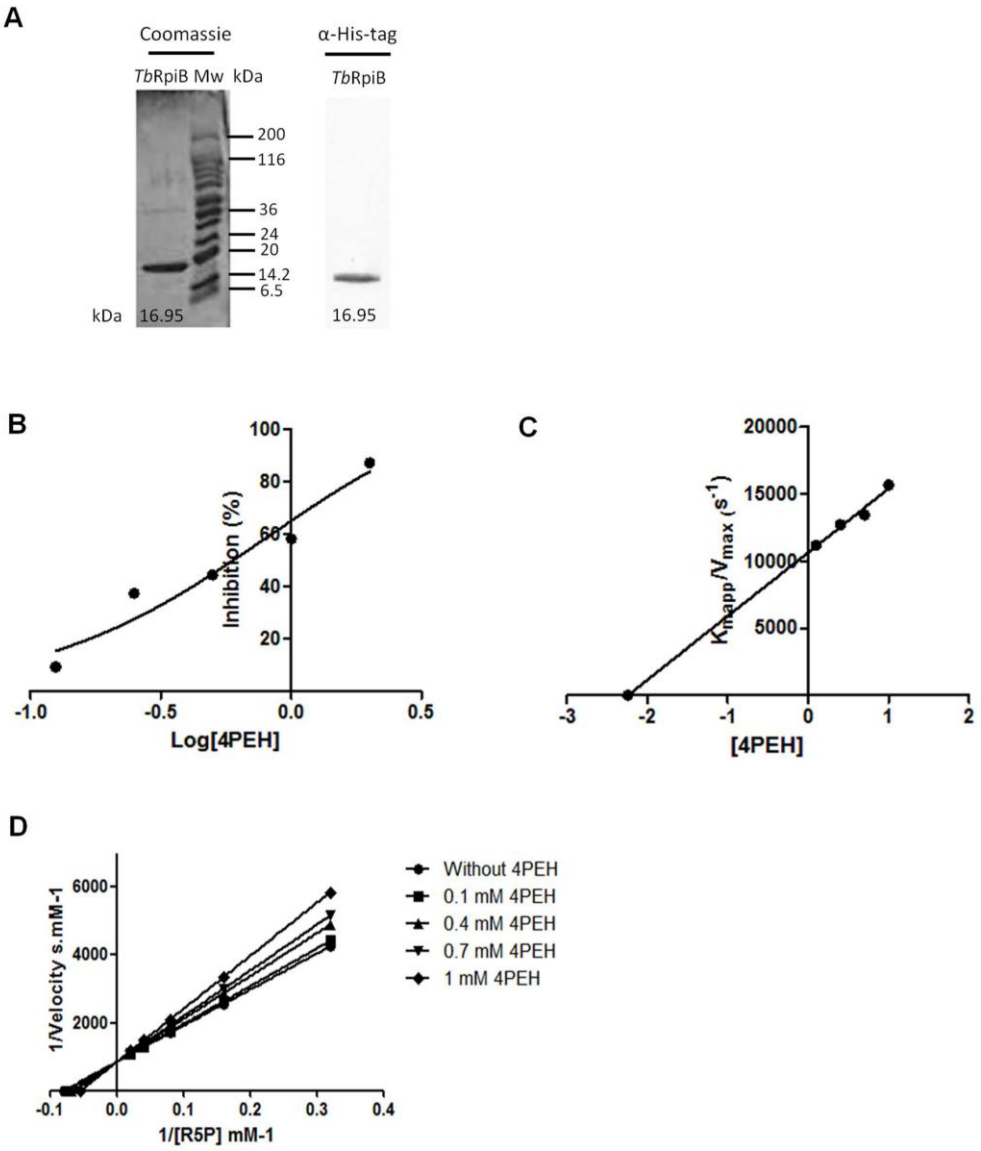

Fig. 1. Biochemical properties of *Tb*RpiB expressed in *E. coli*. (A) 10 μg of *Tb*RpiB recombinant protein analyzed by SDS-PAGE and Coomassie blue staining. Mw, molecular weight marker. Western blot analysis of his-tagged recombinant protein probed with rabbit anti-histidine monoclonal antibody (MicroMol-413) (1:1000). (B) Inhibition (%) of *Tb*RpiB activity by 4PEH. (C) Plot of K_{mapp}/V_{max} *versus* 4PEH concentrations; K_i corresponds to the symmetric value of the X-axis intersection. (D) Plots showing the effect of different 4PEH concentrations on the inverse of the initial velocity *versus* the inverse of several concentrations of R5P. (B–D) The values correspond to the means ± standard deviation of two replicates, and data is representative of three independent experiments.
doi:10.1371/journal.pntd.0003430.g001

two complementary approaches, immunofluorescence and digitonin fractionation, were performed. Fluorescent confocal microscopy analysis suggests that *Tb*RpiB despite being localized mainly in the cytosol can be also found in glycosomes due to colocalization with the glycosomal marker, aldolase [38] (Fig. 2B). Upon digitonin fractionation, RpiB showed an intermediate pattern between the glycosomal marker, aldolase (still partially in the pellet after 200 μg/ml digitonin treatment) and the cytosolic marker, enolase (almost all in supernatant with 25 μg/ml digitonin), being practically released with 100 μg/ml digitonin (Fig. 2C). In conclusion, RpiB localizes mainly in the cytosol of bloodstream forms.

In vitro and *in vivo* analysis of *Tb*RpiB RNAi

To assess if *Tb*RpiB targeting affects *in vitro* bloodstream forms growth, RNAi against RpiB was induced. This resulted in a lower

Table 1. *Tb*RpiB kinetic parameters.

	R5P to Ru5P	Ru5P to R5P
K_m (mM)	12.50±4.43	2.39±0.94
V_{max} $\times 10^{-3}$(mM.s^{-1})	1.17±0.16	5.84±0.79
k_{cat} (s^{-1})	12.00±1.58	39.44±5.32
k_{cat}/K_m ($M^{-1}.s^{-1}$)	9.60×10^2	1.64×10^4

The values are the means ± standard deviation obtained from 3 independent experiments.
doi:10.1371/journal.pntd.0003430.t001

mRNA and protein levels 1 and 2 days post-induction (Fig. 3A and B, respectively). Using ImageJ software we estimate a decrease of approximately 93% of protein levels at 48 h RNAi post-induction. The growth of *Tb*RpiB RNAi tet(-) and wt tet(-) cell lines was shown to be similar (Fig. 3C). A significant decrease of *in vitro* cell proliferation of induced *versus* non-induced RNAi cell lines was seen only after day 4 of the cumulative growth curve (Fig. 3C).

To test the importance of RpiB for parasite infectivity in a disease model, two groups of BALB/c mice were inoculated with the wt parental cell line and other two groups with the RNAi cell line. Some mice were fed with water containing doxycycline (Dox) to induce downregulation of *Tb*RpiB, whilst the remaining mice were kept as non-induced controls. A Western blot confirmed the reduction of the protein level in 48 h RNAi induced parasites used for mice infections (Fig. 4A). Blood samples were taken from all mice at daily intervals to chart parasitaemia (Fig. 4B). Animals achieving a parasitaemia greater than 10^8 trypanosomes per millilitre were euthanized. *In vivo* growth of the *Tb*RpiB RNAi Dox(-) trypanosomes was not significantly different from that of wt Dox(-) parasites. However a significant decrease in the parasitaemia of induced *versus* non-induced RNAi cell lines was seen. Within 6 days of inoculation, contrary to mice infected with induced RNAi cell line (in which overall parasitaemias remained below the detection limit, 5×10^4 trypanosomes/ml), mice infected with control parasites developed high levels of parasitaemia. As a consequence, and in contrast to mice infected with wt and *Tb*RpiB RNAi Dox(-) parasites, which were culled sooner (between eighth to thirteenth day post-infection), *Tb*RpiB RNAi Dox(+) were euthanized from the eighteenth day post-infection (Fig. 4C). Eventually parasitaemia also increased in the *Tb*RpiB RNAi Dox(+) mice, due to the emergence of "RNAi revertants" (Fig. 4D) [39–42]. In this way, ribose 5-phosphate isomerase B despite being dispensable *in vitro*, confers optimal *in vitro* growth and is highly relevant for mice infections.

Complementation of *Tb*RpiB RNAi phenotype

Functional complementation of *T. brucei* RNAi cell lines with the *T. cruzi* homologue was performed, since *Tc*RpiB has *in vitro* isomerase activity and *TcRPIB* nucleotide sequence is sufficiently different to avoid *Tb*RpiB RNAi. Western blot analysis confirmed *Tb*RpiB downregulation only in induced RNAi parasites, and *Tc*RpiB expression exclusively in complemented parasites (Fig. 5A). Cells with RNAi and complemented with *Tc*RpiB grew equally *in vitro* (Fig. 5B), and were almost as virulent *in vivo* (Fig. 5C, D), as the wild-type. RNAi revertants appeared during the course of infection in induced *Tb*RpiB RNAi infected mice, but not in induced complemented *Tb*RpiB RNAi infected mice (Fig. 5E). As a result, complementation restored *in vitro* and *in vivo* phenotypes.

Discussion

In this study we demonstrated that *Tb*RpiB, like the related *Tc*RpiB and *Leishmania donovani* RpiB (*Ld*RpiB) enzymes, has *in vitro* ribose 5-phosphate isomerase activity [31,43]. Based on the theoretical homology model, *Tb*RpiB is predicted to be dimeric. Although the dimer comprises a complete functional unit, tetramers are observed in all available RpiB structures except that of *Mycobacterium tuberculosis* RpiB [36]. Similarly to *T. cruzi*, *Clostridium thermocellum* and *Pisum sativum* Rpi enzymes, *Tb*RpiB has the ability of using both R5P or Ru5P as substrates, but with remarkable preference for Ru5P [31,44,45]. However, the differences in affinity are more pronounced in trypanosomes enzymes. Indeed, these differences were higher for *Tb*RpiB compared to *Tc*RpiB. Analysis of the three enzymes from trypanosomatids (*Tc*RpiB, *Ld*RpiB and *Tb*RpiB) shows that *Tb*RpiB and *Ld*RpiB have the highest K_m and k_{cat} value for R5P substrate, respectively [31,43]. Nevertheless, we can speculate that such differences may result in part by the fact that parasite enzymes were expressed and purified as recombinant proteins in bacteria and not purified directly from trypanosomes extracts. Consequently, differences in protein post-transcriptional processing and/or changes in protein conformation cannot be excluded.

RpiB is expressed on *T. brucei* procyclic and bloodstream forms, and our data indicate its higher expression in procyclics. Interestingly, a previous study has shown higher levels of *TbRPIB* mRNA (Tb927.11.8970) in logarithmic phase procyclic forms compared to bloodstream forms [46]. However, its biological meaning, if any, remains to be elucidated.

Regarding RpiB subcellular localization in bloodstream forms, the protein despite found mainly in the cytosol is also present in glycosomes. This might explain why a previous proteomic analysis failed to find *Tb*RpiB enzyme in purified glycosomes [47]. The glycosomal localization observed within the dual-localization can be justified by the presence of a peroxisomal targeting signal, PTS2 (-KVAIGADHI-), at the N-terminus [48]. Moreover, other enzymes of the hexose-monophosphate pathway, although present in glycosomes, were also found mainly within the cytosol (e.g. glucose-6-phosphate dehydrogenase, 6-phosphogluconolactonase and transketolase) [49,50].

*Tb*RpiB is clearly needed for optimal *in vitro* parasite growth, although we do not know whether it is essential for survival since some protein remained after RNAi. Nevertheless, our results show that *Tb*RpiB is important for parasites infectivity *in vivo*, through the appearance of RNAi revertants and reversion of the phenotype in complemented parasites. Infectivity defects of bloodstreams with reduced levels of *Tb*RpiB were shown on a monomorphic *T. brucei* strain. This strain is abnormally virulent and typically mice do not survive longer than ≈10 days. In the future, it would be interesting to test the role of RpiB in a more chronic infection, as the one caused by pleomorphic strains. Interfering with the PPP

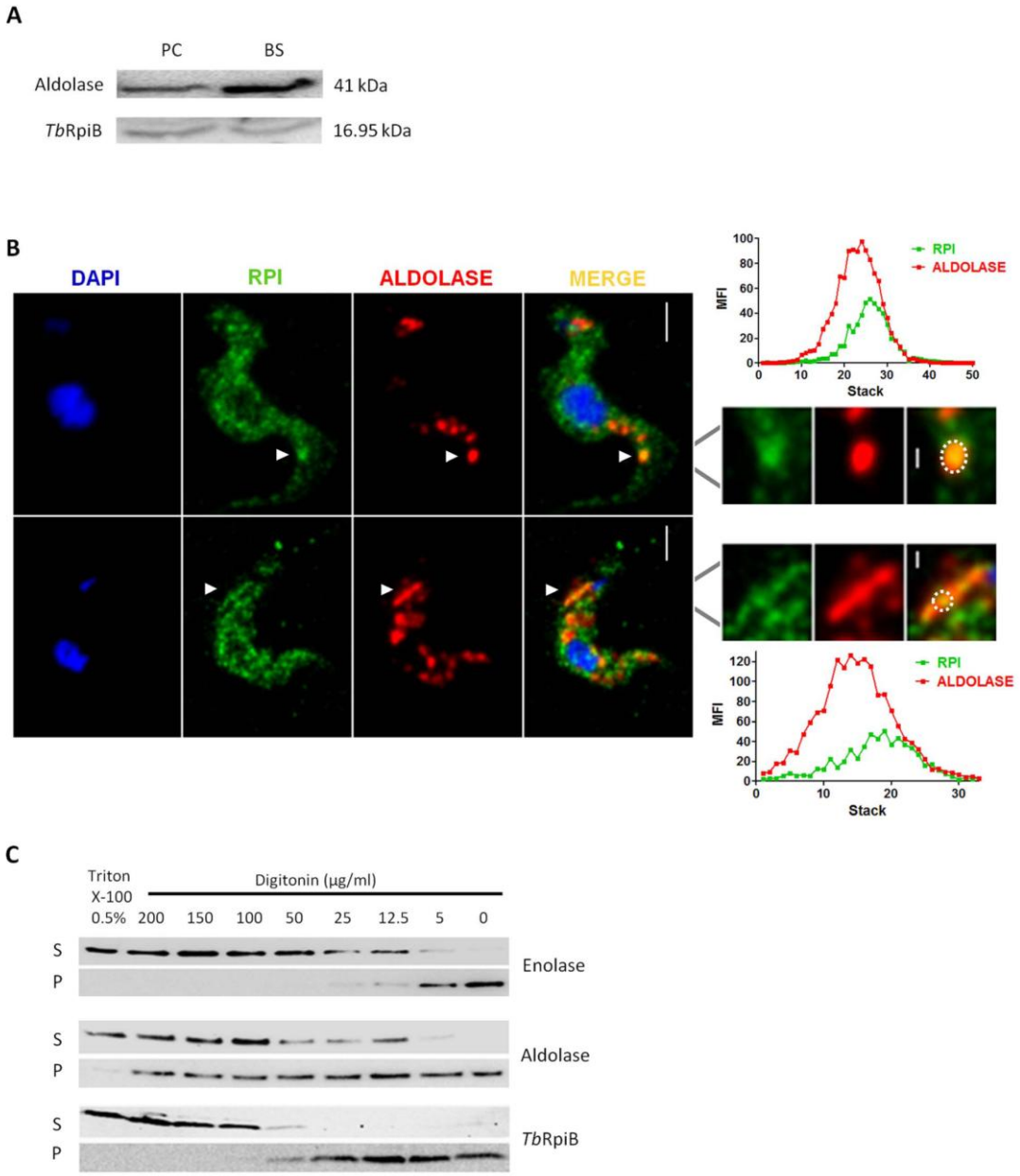

Fig. 2. *Tb*RpiB expression within life cycle stages and localization in bloodstream forms. (A) RpiB expression in *T. brucei* life-cycle stages; 30 µg of protein from bloodstream (BS) and procyclic (PC) total lysates was analysed by Western blot probed with rabbit anti-*Tb*RpiB (1:1000) and anti-aldolase (loading control; 1:5000) polyclonal antibodies. Data is representative of three independent experiments. (B) Immunofluorescence analysis by confocal microscopy of bloodstream forms *Tb*RpiB. Nuclear and kinetoplast DNA labelled by DAPI staining (blue). RpiB (green) and aldolase (red) were labelled respectively with rat anti-*Tb*RpiB (1:100) and rabbit anti-aldolase (1:5000) antibodies. White arrowheads indicate RpiB and aldolase co-localization areas that are magnified in the right panels. Mean fluorescence intensity (MFI) of aldolase (red) and RpiB (green) in these co-localization areas (white dotted circle) were determine for each stack. Images are maximal Z-projections of 50 and 33 contiguous stacks separated by 0.1 µm. Scale Bars: 2.5 (top left panel), 5 (below left panel), 0.5 (top right panel) and 1 µm (below right panel). (C) Supernatant (S) and pellet (P) fractions obtained with different concentrations of digitonin were subjected to Western blot analysis and probed with rabbit antibodies against *Tb*RpiB (1:1000), enolase (cytoplasmic marker; 1:5000), and aldolase (glycosome marker; 1:5000). Data is representative of two independent experiments. Untreated cells and those completely permeabilized by incubation with 0.5% Triton X-100 [total release (TR)] were used as controls. doi:10.1371/journal.pntd.0003430.g002

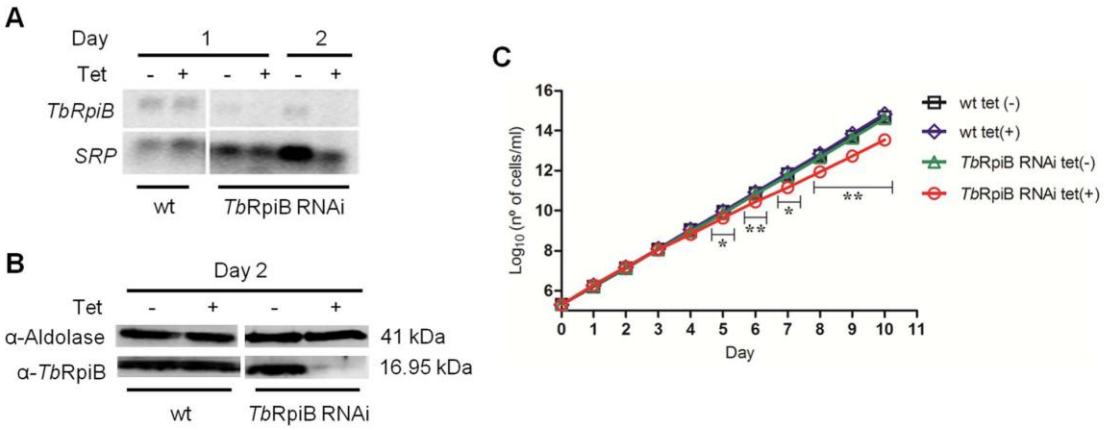

Fig. 3. *In vitro* effect of RNAi-mediated RpiB downregulation on *T. brucei* bloodstream forms. (A) Northern and (B) Western blot analysis of mRNA and protein levels, respectively, upon RpiB RNAi. *SRP* and aldolase used as loading controls, respectively. Rabbit anti-*Tb*RpiB (1:1000) and anti-aldolase (1:5000) polyclonal antibodies were used as primary antibodies. (C) Growth curve of a wt *versus* a representative RpiB RNAi cell line. Black squares and blue diamonds represent wt growth in the absence or presence of tetracycline (tet) while green triangles and red circles represent RpiB RNAi clone growth in the absence or presence of tet, respectively. Cumulative cell numbers (product of cell number and total dilution) are plotted. Values represent averages from three independent experiments using one representative RpiB RNAi clone and error bars indicate standard deviation. Statistical differences between non-induced and induced *Tb*RpiB RNAi clone are depicted (* $p \leq 0.05$, ** $p \leq 0.01$).
doi:10.1371/journal.pntd.0003430.g003

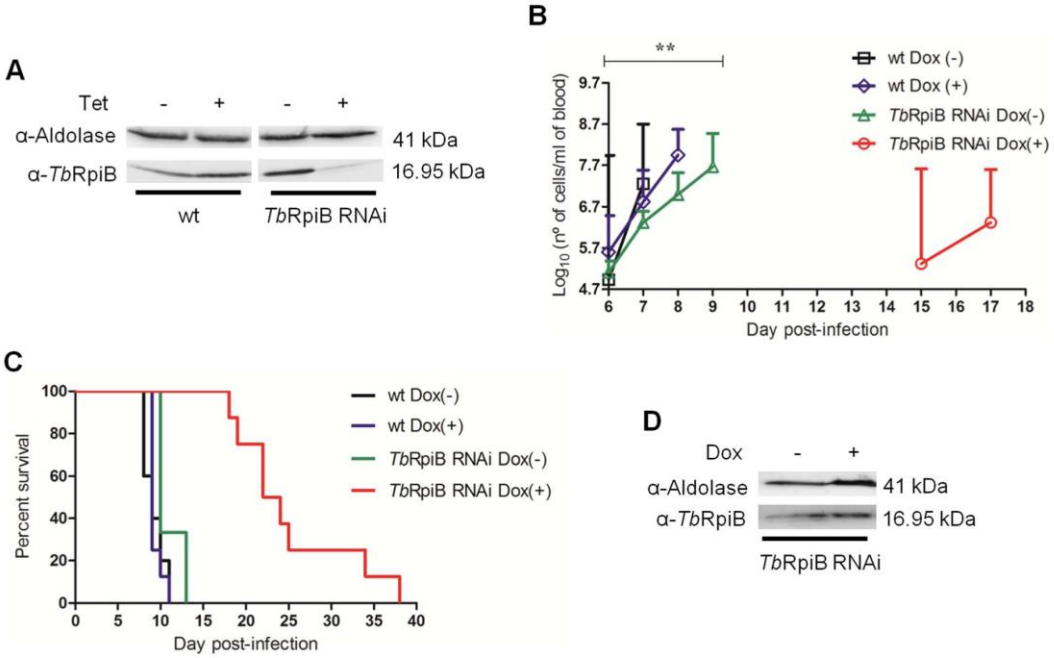

Fig. 4. *In vivo* effect of RNAi-mediated RpiB downregulation on *T. brucei* bloodstream forms. (A) Western blot analysis of Rpi protein levels in bloodstream forms 48 h after tet induction, which were used for mice infections. (B) Groups of mice (n = 3–7) were infected intraperitoneally with 10^4 control wt (black squares and blue diamonds) or a representative RNAi clone (green triangles and red circles). The mice were either untreated (black squares and green triangles) or treated with 1 mg/ml Dox (blue diamonds and red circles) in the water supply. Parasitaemias of each group are shown for the period of time in which there is no mice death. Values are means and errors bars indicate + standard deviation. 5×10^4 trypanosomes/ml of blood is the detection limit. Mice were culled when parasitaemia reached 10^8 cells/ml. (C) Kaplan–Meier survival analysis of mice infected with non-induced and induced wt cell line (black and blue line, respectively) *versus* a non-induced and induced representative RNAi clone (green and red line, respectively). Parasitaemias and survival curve are representative of two independent experiments using two different RNAi clones. (D) Western blot analysis of RpiB levels in a representative non-induced and Dox-induced RNAi clone collected from mice before being euthanized confirmed the appearance of RNAi revertants. Statistical differences between non-induced and induced *Tb*RpiB RNAi clone are depicted (** $p \leq 0.01$).
doi:10.1371/journal.pntd.0003430.g004

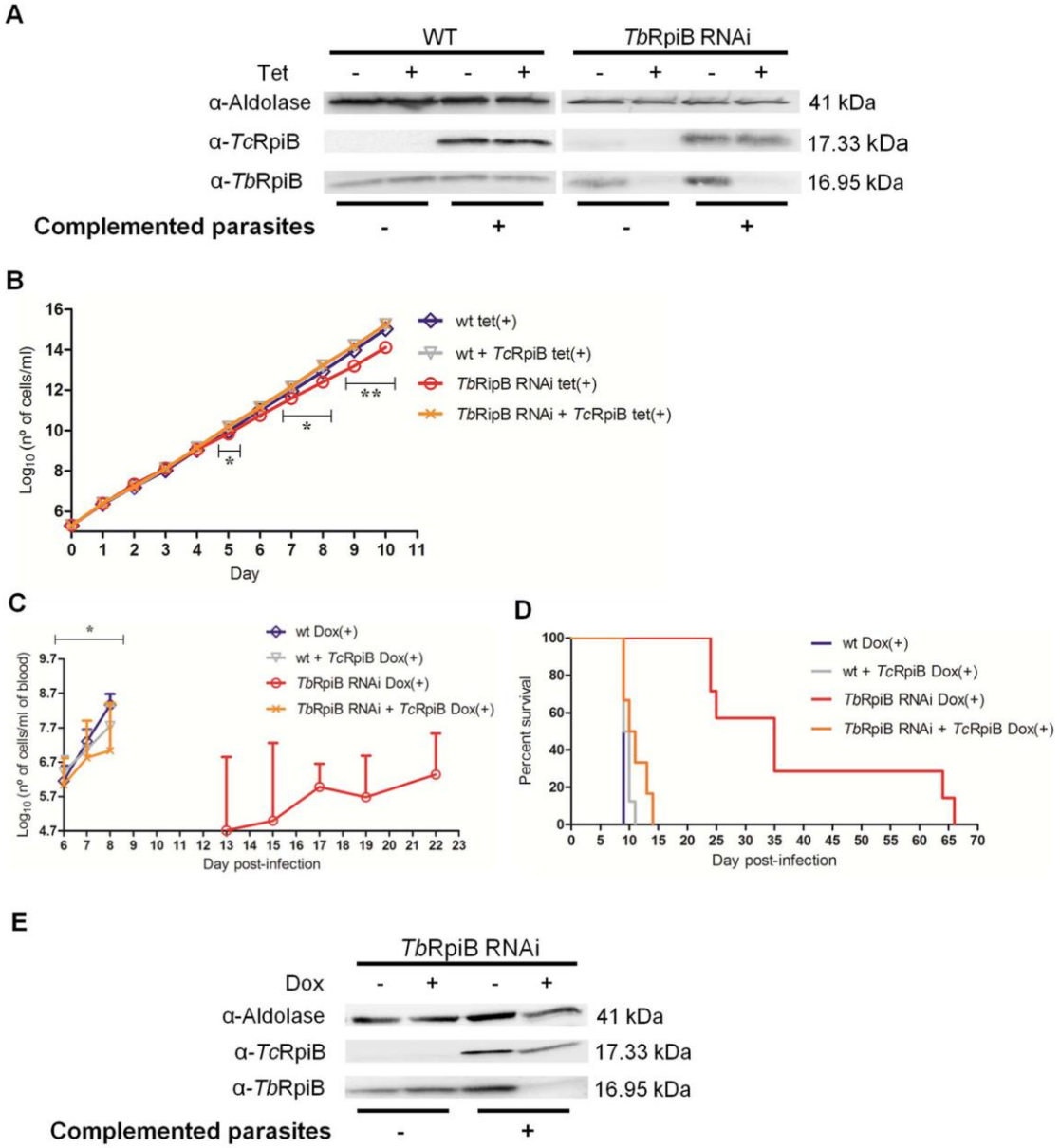

Fig. 5. Rescue of RpiB RNAi mediated defect by expression of *Tc*RpiB. (A) Western blot analysis of *Tb*RpiB and *Tc*RpiB levels in bloodstream forms 48 h after tetracycline (tet) induction reveal a decrease of RpiB in non-complemented and complemented *Tb*RpiB RNAi cells, contrary to wt controls. Parasite extracts were probed sequentially, with rabbit anti-*Tb*RpiB (1:1000) and anti-aldolase (loading control; 1:5000), and with anti-*Tc*RpiB (1:1000) primary antibodies. (B) *In vitro* cumulative growth of induced non-complemented and complemented wt bloodstream forms (blue diamond and grey down triangle, respectively) *versus* an induced non-complemented and complemented representative *Tb*RpiB RNAi clone (red circle and orange cross, respectively). Values represent an average of parasite numbers ± standard deviation of two independent experiments from a representative RNAi clone. (C) Groups of mice (n = 6–8) were infected intraperitoneally with 1×10^4 RNAi induced non-complemented and complemented wt parental cell line (blue diamond and grey down triangle, respectively) *versus* non-complemented and complemented representative *Tb*RpiB RNAi clone (red circle and orange cross, respectively). Mice were treated with 1 mg/ml Dox in the water supply. Mice were culled when parasitaemia reached 10^8 cells/ml. The mean value of the parasitaemias for each group of mice + standard deviation is shown. (D) Kaplan–Meier survival analysis of mice infected with Dox induced non-complemented and complemented wt cell line (blue and grey lines, respectively) *versus* induced non-complemented and complemented representative *Tb*RpiB RNAi clone (red and orange lines, respectively). Data are representative of two independent experiments of two different RNAi clones. (E) Western blot analysis of RpiB levels in a representative non-complemented and complemented *Tb*RpiB RNAi clone isolated from mice blood before being euthanized, showing the emergence of RNAi revertants only in induced non-complemented RNAi clones. Statistical differences between non-complemented and complemented induced *Tb*RpiB RNAi clone are depicted (* $p \leq 0.05$, ** $p \leq 0.01$).
doi:10.1371/journal.pntd.0003430.g005

non-oxidative branch showed to be detrimental under host pressure, in these highly proliferative parasitic forms, which can be due to a defective production of ribose 5-phosphate towards nucleotide and nucleic acid synthesis. Moreover, another enzyme capable of producing ribose 5-phosphate, ribokinase, is essential for parasites survival since attempts to remove the two alleles were unsuccessful [51].

*Tb*RpiB is not the first protein reported as dispensable under standard laboratory culture conditions but crucial for parasites growth in the animal host [52,53]. In rich culture conditions, parasites may uptake essential nutrients from the extracellular medium, which may not be as available in blood. Moreover, *in vivo*, parasites need to deal with pressure from the host immune response.

As for other proteins [54,55], our *in vitro* results differ from the ones achieved in RNA interference target sequencing (RITseq) screen [56]. Indeed, proteins described to be significantly important for parasites fitness by Alsford and colleagues [56] were not in others studies [54,55]. Despite large-scale RNAi screens have already proved useful, caution should be taken due to some level of false negatives and positives, inherent to high-throughput approaches and more importantly due to off-target effects [57]. Furthermore, variations between different large-scale RNAi screenings were already been reported and explained by the use of different *T. brucei* strains, RNAi constructs and methods for assessing cell growth highlighting the importance of using complementary approaches in such studies [58]. Despite all, both studies are in agreement and show a role for *Tb*RpiB on parasites growth.

To further investigate if bloodstream forms deleted of RpiB are completely cleared in mice, studies with gene knockout parasites should be done.

Overall our results clearly show a role of RpiB for bloodstream *in vitro* optimal growth and more importantly *in vivo* infectivity, but also suggest a conserved role among different *Trypanosoma* species. In conclusion *Tb*RpiB emerges as a new potential therapeutic target against African sleeping sickness.

Supporting Information

S1 Fig. Sequence alignment and ribbon representation of RpiB protein from trypanosomes. (A) ClustalW alignment of RpiB from *T. cruzi* CL Brener Esmeraldo-like (Tc00.1047053509199.24; PDB accession code 3K7S), *T. cruzi* CL Brener Non-Esmeraldo-like (Tc00.1047053508601.119) and *T. brucei* (Tb927.11.8970). The residues are colored according to ALSCRIPT Calcons (Aline version 011208) using a predefined colour scheme (red: identical residues; orange to blue: scale of conservation of amino acid properties; white: dissimilar residues). Secondary structure of *Tc*RpiB crystallographic model (PDB code 3K7S) (grey) and the theoretical homology models *Tc*RpiB (Tc00.1047053508601.119) (purple) and *Tb*RpiB (Tb927.11.8970) (blue) are depicted above the alignment. Black circles indicate R5P binding residues. (B) Ribbon representation of *Tc*RpiB Esmeraldo-like (PDB code 3K7S) colored according to the sequence similarity with *Tc*RpiB Non-Esmeraldo-like and *Tb*RpiB as shown in (A). (C) Superposition of *Tc*RpiB structure (PDB code 3K7S) (grey) with *Tc*RpiB (Tc00.1047053508601.119) (purple) and *Tb*RpiB (Tb927.11.8970) (blue) homology models. Ligand color scheme: R5P is shown in yellow (oxygen, pink; phosphorous orange).
(TIF)

S2 Fig. Biochemical properties of *Tc*RpiB (Tc00.1047053508601.119) expressed in *E. coli*. (A) 10 μg of *Tc*RpiB recombinant protein analyzed by SDS-PAGE and Coomassie blue staining. Mw, molecular weight marker. Western blot analysis of his-tagged recombinant protein probed with rabbit anti-histidine monoclonal antibody (MicroMol-413) (1:1000). (B) Kinetic parameters of direct (R5P to Ru5P) and inverse (Ru5P to R5P) reaction. The values are the means ± standard deviation obtained from 3 independent experiments. (C) Inhibition (%) of *Tc*RpiB activity by 4PEH. (D) Plot of K_{mapp}/V_{max} *versus* 4PEH concentrations; K_i corresponds to the symmetric value of the X-axis intersection. (E) Plot showing the effect of different 4PEH concentrations on the inverse of the initial velocity *versus* the inverse of several concentrations of R5P. (C–E) The values correspond to the means ± standard deviation of two replicates, and data is representative of three independent experiments.
(TIF)

S3 Fig. Validation of antibodies against *Tb*RpiB. Immunofluorescence analysis of *T. brucei* wt or a representative Rpi RNAi clone in the presence or absence of tetracycline (tet). RNAi induced and uninduced cells were grown for 48 h, then fixed and probed with rat polyclonal anti-*Tb*RpiB (A) or rabbit polyclonal anti-*Tb*RpiB (B) antibody and co-stained with DAPI. Bars, 5 μm. (C) Quantification of *Tb*RpiB fluorescence levels in induced cells [Rpi RNAi tet(+), $n = 30$] and uninduced cells [Rpi RNAi tet(−), $n = 30$], using the rat and the rabbit polyclonal anti-*Tb*RpiB antibodies. Data representative of two independent experiments using two different clones. ImageJ software (version 1.43u) was used for fluorescence quantification. p value was calculated by Student's t test (*** $p \leq 0.001$, for both $p < 0.001$). (D, E) Whole membrane resulting from Western blot analysis of RpiB levels, in *T. brucei* wt or a representative Rpi RNAi clone, in the presence or absence of tet. The membrane was probed with rat anti-*Tb*RpiB (1:100) (D) or rabbit anti-*Tb*RpiB (1:1000) (E), and after membrane stripping, with rabbit anti-aldolase (1:5000) for loading control.
(TIF)

Acknowledgments

We would like to thank Dr. Paul Michels from Université catholique de Louvain, Belgium, for sending us enolase antibody and Dr. Laurent Salmon from Laboratoire de Chimie Universite de Paris-Sud XI, France for providing 4-deoxy-4-phospho-D-erythronohydroxamic acid (4-PEH) inhibitor. We also thank Claudia Helbig for assistance in Heidelberg.

Author Contributions

Conceived and designed the experiments: IL JF JT ACdS. Performed the experiments: IL JF JT. Analyzed the data: IL JF SMR CC JT ACdS NS. Contributed reagents/materials/analysis tools: CC SMR NR NS. Wrote the paper: IL JF CC SMR JT ACdS.

References

1. MacGregor P, Szoor B, Savill NJ, Matthews KR (2012) Trypanosomal immune evasion, chronicity and transmission: an elegant balancing act. Nat Rev Microbiol 10: 431–438.
2. Radwanska M, Guirnalda P, De Trez C, Ryffel B, Black S, et al. (2008) Trypanosomiasis-induced B cell apoptosis results in loss of protective anti-parasite antibody responses and abolishment of vaccine-induced memory responses. PLoS Pathog 4: e1000078.
3. Lejon V, Mumba Ngoyi D, Kestens L, Boel L, Barbe B, et al. (2014) Gambiense human african trypanosomiasis and immunological memory: effect on phenotypic lymphocyte profiles and humoral immunity. PLoS Pathog 10: e1003947.

4. Clayton CE, Michels P (1996) Metabolic compartmentation in African trypanosomes. Parasitol Today 12: 465–471.
5. Hellemond JJ, Bakker BM, Tielens AG (2005) Energy metabolism and its compartmentation in Trypanosoma brucei. Adv Microb Physiol 50: 199–226.
6. Albert MA, Haanstra JR, Hannaert V, Van Roy J, Opperdoes FR, et al. (2005) Experimental and in silico analyses of glycolytic flux control in bloodstream form Trypanosoma brucei. J Biol Chem 280: 28306–28315.
7. Chambers JW, Fowler ML, Morris MT, Morris JC (2008) The anti-trypanosomal agent lonidamine inhibits Trypanosoma brucei hexokinase 1. Mol Biochem Parasitol 158: 202–207.
8. Willson M, Sanejouand YH, Perie J, Hannaert V, Opperdoes F (2002) Sequencing, modeling, and selective inhibition of Trypanosoma brucei hexokinase. Chem Biol 9: 839–847.
9. Chudzik DM, Michels PA, de Walque S, Hol WG (2000) Structures of type 2 peroxisomal targeting signals in two trypanosomatid aldolases. J Mol Biol 300: 697–707.
10. Azema L, Lherbet C, Baudoin C, Blonski C (2006) Cell permeation of a Trypanosoma brucei aldolase inhibitor: evaluation of different enzyme-labile phosphate protecting groups. Bioorg Med Chem Lett 16: 3440–3443.
11. Caceres AJ, Michels PA, Hannaert V (2010) Genetic validation of aldolase and glyceraldehyde-3-phosphate dehydrogenase as drug targets in Trypanosoma brucei. Mol Biochem Parasitol 169: 50–54.
12. Helfert S, Estevez AM, Bakker B, Michels P, Clayton C (2001) Roles of triosephosphate isomerase and aerobic metabolism in Trypanosoma brucei. Biochem J 357: 117–125.
13. Aronov AM, Suresh S, Buckner FS, Van Voorhis WC, Verlinde CL, et al. (1999) Structure-based design of submicromolar, biologically active inhibitors of trypanosomatid glyceraldehyde-3-phosphate dehydrogenase. Proc Natl Acad Sci U S A 96: 4273–4278.
14. Subramaniam C, Veazey P, Redmond S, Hayes-Sinclair J, Chambers E, et al. (2006) Chromosome-wide analysis of gene function by RNA interference in the african trypanosome. Eukaryot Cell 5: 1539–1549.
15. Bressi JC, Choe J, Hough MT, Buckner FS, Van Voorhis WC, et al. (2000) Adenosine analogues as inhibitors of Trypanosoma brucei phosphoglycerate kinase: elucidation of a novel binding mode for a 2-amino-N(6)-substituted adenosine. J Med Chem 43: 4135–4150.
16. Cordeiro AT, Thiemann OH, Michels PA (2009) Inhibition of Trypanosoma brucei glucose-6-phosphate dehydrogenase by human steroids and their effects on the viability of cultured parasites. Bioorg Med Chem 17: 2483–2489.
17. Dardonville C, Rinaldi E, Barrett MP, Brun R, Gilbert IH, et al. (2004) Selective inhibition of Trypanosoma brucei 6-phosphogluconate dehydrogenase by high-energy intermediate and transition-state analogues. J Med Chem 47: 3427–3437.
18. Cronin CN, Nolan DP, Voorheis HP (1989) The enzymes of the classical pentose phosphate pathway display differential activities in procyclic and bloodstream forms of Trypanosoma brucei. FEBS Lett 244: 26–30.
19. Comini MA OC, Cazzulo JJ (2013) Drug Targets in Trypanosomal and Leishmanial Pentose Phosphate Pathway. In: Jäger T KO, Flohé L, editor. Trypanosomatid Diseases: Molecular Routes to Drug Discovery. Wiley-VCH Verlag GmbH & Co. KGaA, Weinheim, Germany. pp. 297–313.
20. Husain A, Sato D, Jeelani G, Soga T, Nozaki T (2012) Dramatic increase in glycerol biosynthesis upon oxidative stress in the anaerobic protozoan parasite Entamoeba histolytica. PLoS Negl Trop Dis 6: e1831.
21. Ralser M, Wamelink MM, Kowald A, Gerisch B, Heeren G, et al. (2007) Dynamic rerouting of the carbohydrate flux is key to counteracting oxidative stress. J Biol 6: 10.
22. Sorensen KI, Hove-Jensen B (1996) Ribose catabolism of Escherichia coli: characterization of the rpiB gene encoding ribose phosphate isomerase B and of the rpiR gene, which is involved in regulation of rpiB expression. J Bacteriol 178: 1003–1011.
23. Schlecker T, Schmidt A, Dirdjaja N, Voncken F, Clayton C, et al. (2005) Substrate specificity, localization, and essential role of the glutathione peroxidase-type tryparedoxin peroxidases in Trypanosoma brucei. J Biol Chem 280: 14385–14394.
24. Alibu VP, Storm L, Haile S, Clayton C, Horn D (2005) A doubly inducible system for RNA interference and rapid RNAi plasmid construction in Trypanosoma brucei. Mol Biochem Parasitol 139: 75–82.
25. Larkin MA, Blackshields G, Brown NP, Chenna R, McGettigan PA, et al. (2007) Clustal W and Clustal X version 2.0. Bioinformatics 23: 2947–2948.
26. Bond CS, Schuttelkopf AW (2009) ALINE: a WYSIWYG protein-sequence alignment editor for publication-quality alignments. Acta Crystallogr D Biol Crystallogr 65: 510–512.
27. Arnold K, Bordoli L, Kopp J, Schwede T (2006) The SWISS-MODEL workspace: a web-based environment for protein structure homology modelling. Bioinformatics 22: 195–201.
28. Kiefer F, Arnold K, Kunzli M, Bordoli L, Schwede T (2009) The SWISS-MODEL Repository and associated resources. Nucleic Acids Res 37: D387–392.
29. Peitsch MC, Wells TN, Stampf DR, Sussman JL (1995) The Swiss-3DImage collection and PDB-Browser on the World-Wide Web. Trends Biochem Sci 20: 82–84.
30. Wood T (1970) Spectrophotometric ass for D-ribose-5-phosphateketol-isomerase and for D-ribulose-5-phosphate 3-epimerase. Anal Biochem 33: 297–306.
31. Stern AL, Burgos E, Salmon L, Cazzulo JJ (2007) Ribose 5-phosphate isomerase type B from Trypanosoma cruzi: kinetic properties and site-directed mutagenesis reveal information about the reaction mechanism. Biochem J 401: 279–285.
32. Domagk GF, Alexander WR, Doering KM (1974) Protein structure and enzymatic activity, XIV. Purification and properties of ribosephosphate isomerase from skeletal muscle. Hoppe Seylers Z Physiol Chem 355: 781–786.
33. Burkard G, Fragoso CM, Roditi I (2007) Highly efficient stable transformation of bloodstream forms of Trypanosoma brucei. Mol Biochem Parasitol 153: 220–223.
34. Rothberg KG, Burdette DL, Pfannstiel J, Jetton N, Singh R, et al. (2006) The RACK1 homologue from Trypanosoma brucei is required for the onset and progression of cytokinesis. J Biol Chem 281: 9781–9790.
35. Lanham SM (1968) Separation of trypanosomes from the blood of infected rats and mice by anion-exchangers. Nature 218: 1273–1274.
36. Stern AL, Naworyta A, Cazzulo JJ, Mowbray SL (2011) Structures of type B ribose 5-phosphate isomerase from Trypanosoma cruzi shed light on the determinants of sugar specificity in the structural family. FEBS J 278: 793–808.
37. Roos AK, Burgos E, Ericsson DJ, Salmon L, Mowbray SL (2005) Competitive inhibitors of Mycobacterium tuberculosis ribose-5-phosphate isomerase B reveal new information about the reaction mechanism. J Biol Chem 280: 6416–6422.
38. Clayton CE (1987) Import of fructose bisphosphate aldolase into the glycosomes of Trypanosoma brucei. J Cell Biol 105: 2649–2654.
39. Chen Y, Hung CH, Burderer T, Lee GS (2003) Development of RNA interference revertants in Trypanosoma brucei cell lines generated with a double stranded RNA expression construct driven by two opposing promoters. Mol Biochem Parasitol 126: 275–279.
40. Lecordier L, Walgraffe D, Devaux S, Poelvoorde P, Pays E, et al. (2005) Trypanosoma brucei RNA interference in the mammalian host. Mol Biochem Parasitol 140: 127–131.
41. Jetton N, Rothberg KG, Hubbard JG, Wise J, Li Y, et al. (2009) The cell cycle as a therapeutic target against Trypanosoma brucei: Hesperadin inhibits Aurora kinase-1 and blocks mitotic progression in bloodstream forms. Mol Microbiol 72: 442–458.
42. Loureiro I, Faria J, Clayton C, Ribeiro SM, Roy N, et al. (2013) Knockdown of asparagine synthetase A renders Trypanosoma brucei auxotrophic to asparagine. PLoS Negl Trop Dis 7: e2578.
43. Kaur PK, Dinesh N, Soumya N, Babu NK, Singh S (2012) Identification and characterization of a novel Ribose 5-phosphate isomerase B from Leishmania donovani. Biochem Biophys Res Commun 421: 51–56.
44. Yoon RY, Yeom SJ, Kim HJ, Oh DK (2009) Novel substrates of a ribose-5-phosphate isomerase from Clostridium thermocellum. J Biotechnol 139: 26–32.
45. Skrukrud CL, Gordon IM, Dorwin S, Yuan XH, Johansson G, et al. (1991) Purification and characterization of pea chloroplastic phosphoriboisomerase. Plant Physiol 97: 730–735.
46. Jensen BC, Sivam D, Kifer CT, Myler PJ, Parsons M (2009) Widespread variation in transcript abundance within and across developmental stages of Trypanosoma brucei. BMC Genomics 10: 482.
47. Colasante C, Ellis M, Ruppert T, Voncken F (2006) Comparative proteomics of glycosomes from bloodstream form and procyclic culture form Trypanosoma brucei brucei. Proteomics 6: 3275–3293.
48. Opperdoes FR, Szikora JP (2006) In silico prediction of the glycosomal enzymes of Leishmania major and trypanosomes. Mol Biochem Parasitol 147: 193–206.
49. Stoffel SA, Alibu VP, Hubert J, Ebikeme C, Portais JC, et al. (2011) Transketolase in Trypanosoma brucei. Mol Biochem Parasitol 179: 1–7.
50. Duffieux F, Van Roy J, Michels PA, Opperdoes FR (2000) Molecular characterization of the first two enzymes of the pentose-phosphate pathway of Trypanosoma brucei. Glucose-6-phosphate dehydrogenase and 6-phosphogluconolactonase. J Biol Chem 275: 27559–27565.
51. Kerkhoven EJ, Achcar F, Alibu VP, Burchmore RJ, Gilbert IH, et al. (2013) Handling uncertainty in dynamic models: the pentose phosphate pathway in Trypanosoma brucei. PLoS Comput Biol 9: e1003371.
52. Ong HB, Sienkiewicz N, Wyllie S, Patterson S, Fairlamb AH (2013) Trypanosoma brucei (UMP synthase null mutants) are avirulent in mice, but recover virulence upon prolonged culture in vitro while retaining pyrimidine auxotrophy. Mol Microbiol 90: 443–455.
53. Vigueira PA, Paul KS (2011) Requirement for acetyl-CoA carboxylase in Trypanosoma brucei is dependent upon the growth environment. Mol Microbiol 80: 117–132.
54. Signorell A, Rauch M, Jelk J, Ferguson MA, Butikofer P (2008) Phosphatidylethanolamine in Trypanosoma brucei is organized in two separate pools and is synthesized exclusively by the Kennedy pathway. J Biol Chem 283: 23636–23644.
55. Mackey ZB, Koupparis K, Nishino M, McKerrow JH (2011) High-throughput analysis of an RNAi library identifies novel kinase targets in Trypanosoma brucei. Chem Biol Drug Des 78: 454–463.
56. Alsford S, Turner DJ, Obado SO, Sanchez-Flores A, Glover L, et al. (2011) High-throughput phenotyping using parallel sequencing of RNA interference targets in the African trypanosome. Genome Res 21: 915–924.
57. Mohr SE, Perrimon N (2012) RNAi screening: new approaches, understandings, and organisms. Wiley Interdiscip Rev RNA 3: 145–158.
58. Jones NG, Thomas EB, Brown E, Dickens NJ, Hammarton TC, et al. (2014) Regulators of Trypanosoma brucei cell cycle progression and differentiation identified using a kinome-wide RNAi screen. PLoS Pathog 10: e1003886.

Supplementary Figures

Figure S1

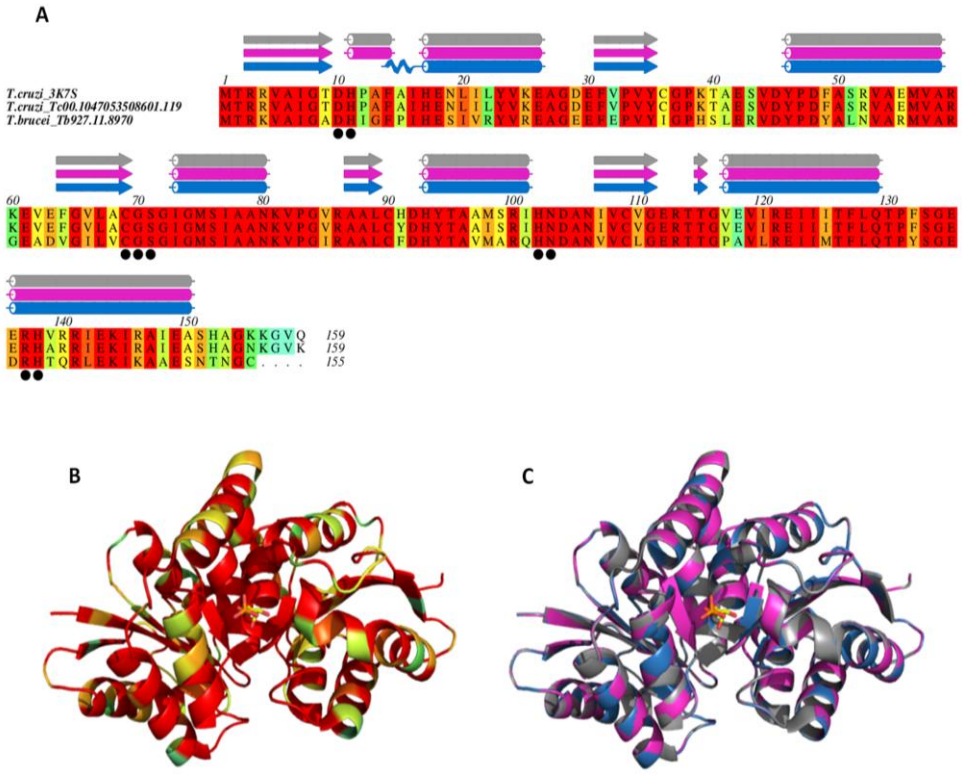

Figure S1. Sequence alignment and ribbon representation of RpiB protein from trypanosomes. (A) ClustalW alignment of RpiB from *T. cruzi* CL Brener Esmeraldo-like (Tc00.1047053509199.24; PDB accession code 3K7S), *T. cruzi* CL Brener Non-Esmeraldo-like (Tc00.1047053508601.119) and *T. brucei* (Tb927.11.8970). The residues are colored according to ALSCRIPT Calcons (Aline version 011208) using a predefined colour scheme (red: identical residues; orange to blue: scale of conservation of amino acid properties; white: dissimilar residues). Secondary structure of *Tc*RpiB crystallographic model (PDB code 3K7S) (grey) and the theoretical homology models *Tc*RpiB (Tc00.1047053508601.119) (purple) and *Tb*RpiB (Tb927.11.8970) (blue) are depicted above the alignment. Black circles indicate R5P binding residues. (B) Ribbon representation of *Tc*RpiB Esmeraldo-like (PDB code 3K7S) colored according to the sequence similarity with *Tc*RpiB Non-Esmeraldo-like and *Tb*RpiB as shown in (A). (C) Superposition of *Tc*RpiB structure (PDB code 3K7S) (grey) with *Tc*RpiB (Tc00.1047053508601.119) (purple) and *Tb*RpiB (Tb927.11.8970) (blue) homology models. Ligand color scheme: R5P is shown in yellow (oxygen, pink; phosphorous orange).

Figure S2

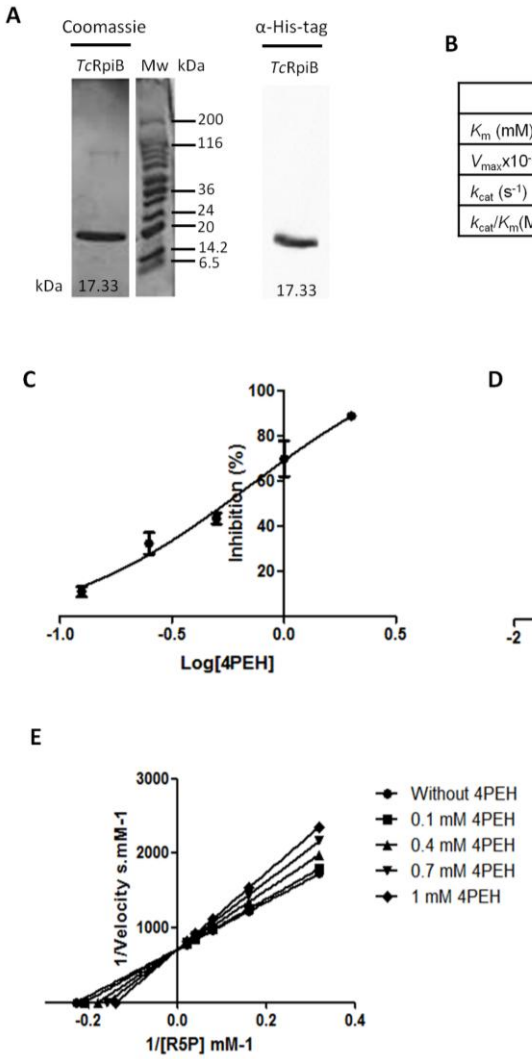

	R5P to Ru5P	Ru5P to R5P
K_m (mM)	4.41±0.70	1.19±0.39
V_{max}x10^{-3} (mM.s^{-1})	1.39±0.06	3.93±0.33
k_{cat} (s^{-1})	14.44±0.64	27.22±2.32
k_{cat}/K_m(M^{-1}.s^{-1})	3.28x10^3	2.34x10^4

Figure S2. Biochemical properties of *Tc*RpiB (Tc00.1047053508601.119) expressed in *E. coli*. (A) 10 µg of *Tc*RpiB recombinant protein analyzed by SDS-PAGE and Coomassie blue staining. Mw, molecular weight marker. Western blot analysis of his-tagged recombinant protein probed with rabbit anti-histidine monoclonal antibody (MicroMol-413) (1:1000). (B) Kinetic parameters of direct (R5P to Ru5P) and inverse (Ru5P to R5P) reaction. The values are the means ± standard deviation obtained from 3 independent experiments. (C) Inhibition (%) of *Tc*RpiB activity by 4PEH. (D) Plot of K_{mapp}/V_{max} *versus* 4PEH concentrations; K_i corresponds to the symmetric value of the X-axis intersection. (E) Plot showing the effect of different 4PEH concentrations on the inverse of the initial velocity *versus* the inverse of several concentrations of R5P. (C-E) The values correspond to the means ± standard deviation of two replicates, and data is representative of three independent experiments.

Figure S3

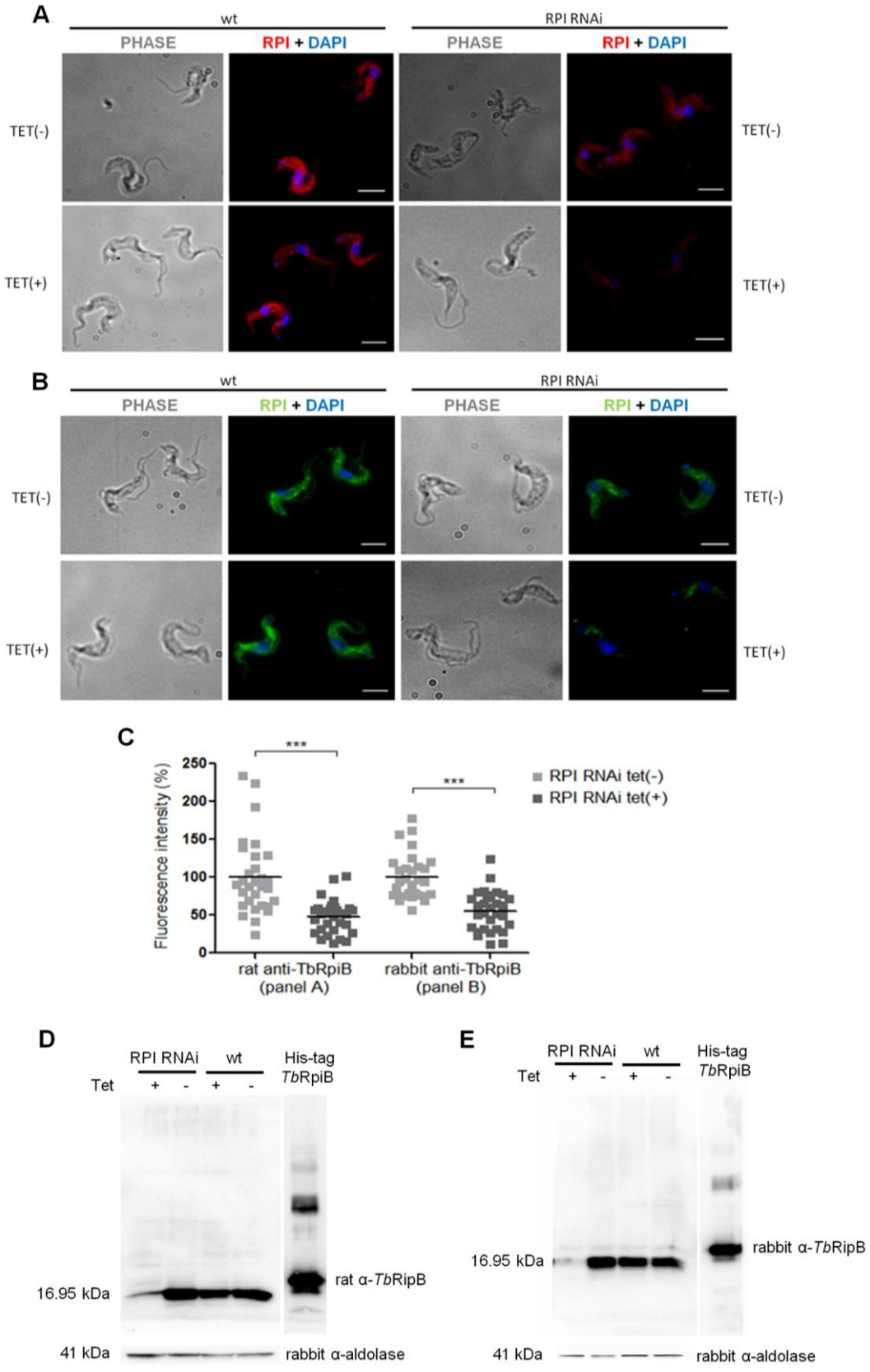
A
wt
RPI RNAi
PHASE
RPI + DAPI
PHASE
RPI + DAPI
TET(-)
TET(+)
TET(-)
TET(+)
B
wt
RPI RNAi
PHASE
RPI + DAPI
PHASE
RPI + DAPI
TET(-)
TET(+)
TET(-)
TET(+)
C
***
***
Fluorescence intensity (%)
250
200
150
100
50
0
RPI RNAi tet(-)
RPI RNAi tet(+)
rat anti-TbRpiB
(panel A)
rabbit anti-TbRpiB
(panel B)
D
RPI RNAi
wt
His-tag
TbRpiB
Tet
+
-
+
-
16.95 kDa
rat α-TbRipB
41 kDa
rabbit α-aldolase
E
RPI RNAi
wt
His-tag
TbRpiB
Tet
+
-
+
-
16.95 kDa
rabbit α-TbRipB
41 kDa
rabbit α-aldolase

Figure S3. Validation of antibodies against *Tb*RpiB. Immunofluorescence analysis of *T. brucei* wt or a representative Rpi RNAi clone in the presence or absence of tetracycline (tet). RNAi induced and uninduced cells were grown for 48h, then fixed and probed with rat polyclonal anti-*Tb*RpiB (A) or rabbit polyclonal anti-*Tb*RpiB (B) antibody and co-stained with DAPI. Bars, 5µm. (C) Quantification of *Tb*RpiB fluorescence levels in induced cells [Rpi RNAi tet(+), *n*=30] and uninduced cells [Rpi RNAi tet(-), *n*=30], using the rat and the rabbit polyclonal anti-*Tb*RpiB antibodies. Data representative of two independent experiments using two different clones. ImageJ software (version 1.43u) was used for fluorescence quantification. *p* value was calculated by Student's t test (*** $p \leq 0.001$, for both $p < 0.001$). (D, E) Whole membrane resulting from Western blot analysis of RpiB levels, in *T. brucei* wt or a representative Rpi RNAi clone, in the presence or absence of tet. The membrane was probed with rat anti-*Tb*RpiB (1:100) (D) or rabbit anti-*Tb*RpiB (1:1000) (E), and after membrane stripping, with rabbit anti-aldolase (1:5000) for loading control.

2.2.2 Unsuccessful attempts to generate *Trypanosoma brucei* ribose 5-phosphate isomerase B double knockout

Ribose 5-phosphate isomerase catalyzes the interconversion of ribulose 5-phosphate and ribose 5-phosphate within the non-oxidative branch of the pentose phosphate pathway. There are two types of ribose 5-phosphate isomerases, namely A and B. Trypanosomatids including *Trypanosoma brucei*, the agent of Human African trypanosomiasis, have a type B ribose 5-phosphate isomerase. This enzyme represents a potential drug target since it is absent from humans, which instead have a type A ribose 5-phosphate isomerase. We have recently shown using RNAi that ribose 5-phosphate isomerase B confers bloodstream forms optimal growth *in vitro* and more important, is detrimental for mice infectivity. To further evaluate ribose 5-phosphate isomerase essentiality we tried to engineer a double knockout cell line. While single knockout cell lines can be generated in a first attempt, null mutants were never obtained. As expected, infections with the single knockout lines showed a reduced infectivity *in vivo*. In conclusion, our data reinforces ribose 5-phosphate isomerase B as a promising drug target against *T. brucei* and demonstrates the need of using a conditional knockout system to ultimately prove its essentiality.

Unpublished data.

SHORT COMMUNICATION

Unsuccessful attempts to generate *Trypanosoma brucei* ribose 5-phosphate isomerase B double knockout

Inês Loureiro[1], Joana Tavares[1†*] & Anabela Cordeiro da Silva[1,2†*]

[1] Parasite Disease Group, Instituto de Biologia Molecular e Celular da Universidade do Porto, Rua do Campo Alegre, 823, 4150-180 Porto, Portugal

[2] Departamento de Ciências Biológicas, Faculdade de Farmácia da Universidade do Porto, Rua de Jorge Viterbo Ferreira, 228, 4050-313 Porto, Portugal

[†]These authors contributed equally to this work.

*corresponding authors e-mail: cordeiro@ibmc.up.pt; jtavares@ibmc.up.pt

Abstract

Ribose 5-phosphate isomerase catalyzes the interconversion of ribulose 5-phosphate and ribose 5-phosphate within the non-oxidative branch of the pentose phosphate pathway. There are two types of ribose 5-phosphate isomerases, namely A and B. Trypanosomatids including *Trypanosoma brucei*, the agent of Human African trypanosomiasis, have a type B ribose 5-phosphate isomerase. This enzyme represents a potential drug target since it is absent from humans, which instead have a type A ribose 5-phosphate isomerase. We have recently shown using RNAi that ribose 5-phosphate isomerase B confers bloodstream forms optimal growth *in vitro* and more important, is detrimental for mice infectivity. To further evaluate ribose 5-phosphate isomerase essentiality we tried to engineer a double knockout cell line. While single knockout cell lines can be generated in a first attempt, null mutants were never obtained. As expected, infections with the single knockout lines showed a reduced infectivity *in vivo*. In conclusion, our data reinforces ribose 5-phosphate isomerase B as a promising drug target against *T. brucei* and demonstrates the need of using a conditional knockout system to ultimately prove its essentiality.

Introduction

The pentose phosphate pathway (PPP) takes part of the carbohydrate metabolism and is divided into an oxidative and a non-oxidative branch. The oxidative PPP is

considered unidirectional and converts glucose 6-phosphate into ribulose 5-phosphate and NADPH, whereas the bidirectional non-oxidative branch metabolizes glycolytic intermediates yielding ribose 5-phosphate [1]. The importance of the non-oxidative branch is mainly attributed to the production of ribose 5-phosphate (R5P), a precursor for nucleic acids biosynthesis [2]. Within the non-oxidative PPP, ribose-5-phosphate isomerase (Rpi) catalyzes the interconversion of ribulose 5-phosphate into ribose 5-phosphate. There are two distinct forms of Rpi, termed A and B. The type B enzyme is present in Trypanosomatids, including in *Trypanosoma brucei* (*T. brucei*) parasites, while type A exists in humans. Although both enzymes catalyze the same reaction, they show no sequence or overall structural homology [3], which open up the possibility of considering *T. brucei* ribose 5-phosphate isomerase B (*Tb*RpiB) as a new potential drug target against Human African trypanosomiasis. This disease relies exclusively on chemotherapy for control since vaccines are unlike to be suitable [4,5]. Moreover, we showed recently that *Tb*RpiB mRNA knockdown through RNAi, is detrimental for parasites infectivity in mice [6], supporting the idea of a very promising therapeutic target. To further dissect the importance and role of RpiB in *T. brucei* parasites, targeted gene-disruption experiments were performed.

Materials and methods

Parasite growth

T. brucei brucei Lister 427 bloodstream forms were cultivated in HMI-9 medium, as previously described [7].

Generation of DNA constructs and transfection

Three different DNA cassettes were generated (Figure 1). The DNA fragments consisted in open reading frames (ORF) of the resistance genes (hygromycin, bleomycin and neomycin), flanked by the same 5' and 3' untranslated regions (UTRs) that flank the *TbRPIB* gene.

For the generation of single knockout (sKO) mutants, the plasmid used was the *pGL345-HYG* plasmid [8,9] modified with the 5′ (924 bp) and 3' (997 bp) *RPIB* flanks obtained through PCR from T. brucei genomic DNA template. PCR conditions were as follows: initial denaturation (2 min at 94ºC), 35 cycles of denaturation (15s at 94ºC), annealing (30s at 59ºC), elongation (1 min at 72ºC) and a final extension step (10 min at 72ºC). The primers contained *Hin*dIII/*Sal*I and *Sma*I/*Bgl*II restriction sites (Table 1) were

used for cloning into the appropriately pre-digested *pGL345-HYG* (Figure 1). Thereafter the final plasmid was digested with HindIII and BglII to obtain the final DNA fragment for transfection. The transfection [10], using the 10 µg of DNA, resulted in stable hygromycin-resistant parasites selected with 7.5 µg/ml of hygromycin.

To remove the second allele**,** *pGL345-BLEO* or *pGL345-NEO* plasmids were constructed by replacing the hygromycin with bleomycin or neomycin resistance gene ORF, respectively, in the plasmid used to obtain the sKOs, employing *Spe*I/*Bam*HI restriction enzymes (Figure 1). Ten micrograms of the final constructs, again obtained by digestion with HindIII and BglII restriction enzymes, were then transfected for double knockout (DKO) mutants achievement. The dose of 7.5 µg/ml, 0.2 µg/ml and 5 ug/ml of hygromycin, bleomycin and neomycin, respectively were used to select the resistant parasites.

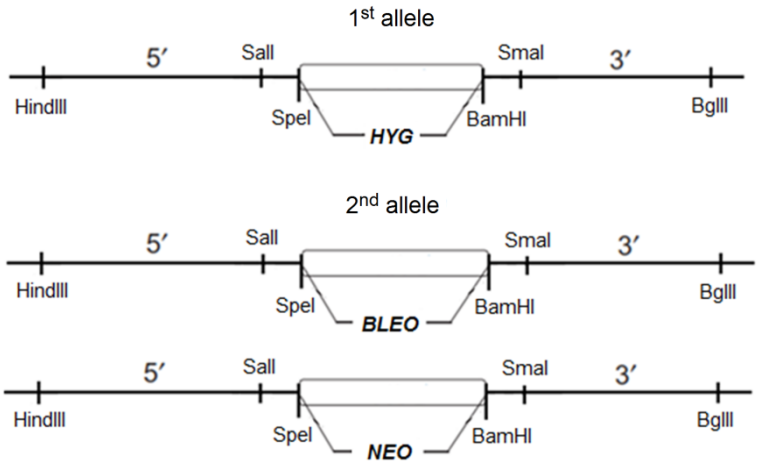

Figure 1. Graphic representation of the three constructs used for targeted disruption of *TbRPIB*. Drawings of the *HYG* fragment [used in the first attempt to generate single knockouts (sKO) (top)], of the *BLEO* fragment [used in the first two attempts to generate double knockouts (DKO) (center)], and *NEO* fragment [used in the third and fourth tries to obtain DKOs (bottom)] are depicted. Restriction enzymes used to insert the selectable marker (SpeI and BamHI), the 5' UTR (HindIII and SalI) and 3' UTR (SmaI and BglII) are charted.

PCR analysis

DNA was extracted using DNAzol reagents (Invitrogen) from wt and sKO cells lines. For sKO mutants resistant to hygromycin, PCR analysis was conducted using a forward primer complementary to a region 51-71 bp upstream the HindIII restriction site of the 5' UTR of *TbRPIB*, and a reverse primer complementary to a region 61-82 bp

downstream the ATG of the hygromycin ORF (Table 1). PCR products were run in 1% (w/v) agarose gel. PCR conditions were as follows: initial denaturation (2 min at 94ºC), 35 cycles of denaturation (30s at 94ºC), annealing (30s at 63ºC), elongation (2 min at 72ºC) and a final extension step (10 min at 72ºC). For sKO mutants resistant to neomycin PCR analysis was conducted using a forward primer complementary to a region 51-71 bp upstream the HindIII restriction site of the 5' UTR of *TbRPIB*, and a reverse primer complementary to a region 2347 bp downstream the ATG of the bleomycin ORF (Table 1). PCR products were run in 1% (w/v) agarose gel. PCR conditions were as follows: initial denaturation (2 min at 94ºC), 35 cycles of denaturation (30s at 94ºC), annealing (30s at 62ºC), elongation (2 min 30s at 72ºC) and a final extension step (10 min at 72ºC).

Table 1. Primers used to amplify 5' and 3' *RPIB* flanks.

	5' UTR
Primer F	5' - CGAAGCTTTAAGCGGTGATTGAGCGT - 3'
Primer R	5' - CGGTCGACTGTTGATTGTAAAAGGA - 3'
	3' UTR
Primer F	5' - CGCCCGGGATATTTGGTAAATGATAATC - 3'
Primer R	5' - CGAGATCTGCATACGTTCAGTGGTTGTT - 3'
	PCR analysis (*HYH* cassette)
Primer F	5' - AACATGCCCCACCCCTCCCC - 3'
Primer R	5' - GCTGCATCAGGTCGGAGACGC - 3'
	PCR analysis (*NEO* cassette)
Primer F	5' - AACATGCCCCACCCCTCCCC - 3'
Primer R	5' - GTGGTCGAATGGGCAGGTAG - 3'

Southern blot analysis

The 3′ UTR of *TbRPIB* was amplified by PCR (using the primers previously described) and labelled using the Kit Amersham AlkPhos Direct Labeling and Detection System with CDP-Star (GE Healthcare). The resulting labelled product was used as a probe. Genomic DNA preparations (10 µg) from wt and *TbRPIB* sKO cells were digested with BspHI and separated in a 0.8% (w/v) agarose gel. The DNA fragments were transferred onto Hybond-N^+ positively charged nylon membrane (GE Healthcare). Membrane hybridization, washes, and chemiluminescent detection were done according to the kit manufacture instructions.

Western blot analysis

For Western blotting, 10^7 of wt and sKO parasites were resolved in 12% Tris-Glycine SDS/PAGE, and then transferred on to a nitrocellulose Hy-bond ECL membrane

(Amersham Biosciences). The membrane was blocked in 5% (w/v) non-fat dried skimmed milk in PBS/0.1% Tween-20 (blocking solution), followed by incubation with a combination of rabbit anti-*Tb*RpiB (1:1000) [6] with rabbit anti-aldolase (1:5000) (kindly provided by Christine Clayton, ZMBH, University of Heidelberg, Germany) antibodies in blocking solution at 4ºC overnight, respectively. Blots were washed with PBS/0.1% Tween-20 (3 times, 15 min). Horseradish peroxidase-conjugated goat anti-rabbit IgG (Amersham) (1:5000 for 1h, at room temperature) was used as the secondary antibody. The membranes were developed using SuperSignal WestPico Chemiluminescent Substrate (Pierce). ImageJ software (version 1.43u) was used for protein bands semi-quantification.

In vitro and *in vivo* analysis of *TbRPIB* sKO

For *in vitro* growth curves, cell lines were seeded at 10^5 parasites/ml of complete HMI-9 medium, after 48h in the absence of selective drugs. Every 24h, until day 10, cell growth was monitored microscopically. For *in vivo* infections, after 48h in the absence of selective drugs, 10^4 wt and sKO parasites were inoculated intraperitoneally in 6–8 weeks old BALB/c mice (n=3). Parasitaemia was measured at fourth, fifth and sixth day post-infection through tail blood extraction.

Results and discussion

To obtain *TbRPIB* null mutants, sKO lines were firstly generated and were achieved right in the first attempt. After *HYG* cassette transfection, one *TbRPIB* wt allele was replaced through homologous recombination by the hygromycin selectable marker, giving rise to *TbRPIB* single-allele (null/+) knockout mutants. PCR and Southern blot confirmed the correct insertion of the cassette (Figure 2A and B, respectively), and Western blot shows a decrease in *Tb*RpiB protein levels of approximately 50% in sKO cell lines compared to wt lines (Figure 2C). No significant differences were found on the *in vitro* growth of *TbRPIB* sKO bloodstream forms compared to wt (Figure 2D). This differs from our previous results where a statistically significant difference on the *in vitro* cumulative growth of induced *versus* non-induced RNAi *Tb*RpiB cell lines was seen after day 4 [6]. The higher levels of RpiB down-regulation achieved with RNAi might explain the different phenotypes. When used to infect mice, *TbRPIB* sKO showed as expected, reduced infectivity evaluated by the parasitaemia (Figure 2E) and by the increase of mice life span (Figure 2F) when compared to wt parasites. Again, the defective phenotype observed *in vivo* was less pronounced when compared to the one achieved with RNAi [6].

Nevertheless, our data shows that 50% of RpiB down-regulation is sufficient to compromise parasites infectivity.

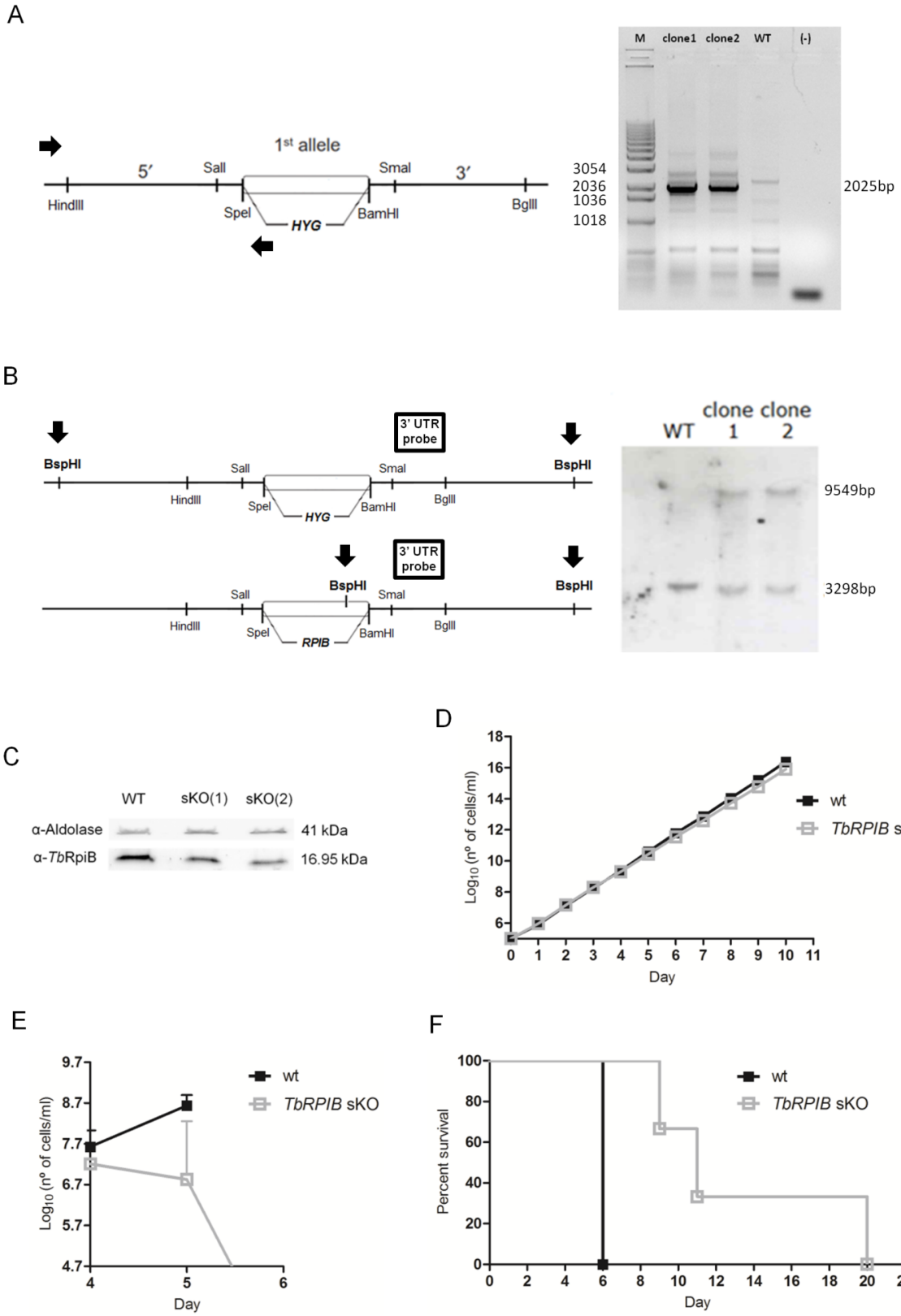

Figure 2. Analysis of bloodstream *TbRPIB* sKO (*HYG* marker). (A) PCR analysis of parental wt and two sKOs to evaluate hygromycin cassette integration on the *RPIB* genomic locus. The amplified 2025 bp region is depicted. A PCR mix without genomic DNA, was used as a negative control. (B) Southern blot analysis of BspHI digested genomic DNA (≈10 µg) from wt cells and two *TbRPIB* sKO clones (*HYG* selectable marker) probed with 3' UTR of *TbRPIB*. (C) Western blot analysis of whole-cell extracts from wt and two sKO clones. Proteins were detected with rabbit anti-*Tb*RpiB antibody. Aldolase was used as loading control. (D) Growth curve of a wt *versus* a representative sKO cell line. Black and grey squares represent wt and sKO growth, respectively. Cumulative cell numbers (product of cell number and total dilution) are plotted. Values represent averages from two independent experiments using one representative sKO clone and ± error bars indicate standard deviation. (E) Groups of mice (n=3) were infected intraperitoneally with 10^4 control wt (black squares) or a representative sKO clone (grey squares). Parasitaemias of each group are shown from 4^{th} to 6^{th} day post-infection. Values are means and errors bars indicate + standard deviation. 5×10^4 trypanosomes/ml of blood is the detection limit. For *TbRPIB* sKO, the mean of parasitaemia at day 6 was below the detection limit and therefore not seen in the graphic. Mice were culled when parasitaemia reached 10^8 cells/ml. (F) Kaplan–Meier survival analysis of mice infected with wt *versus* a representative sKO clone (black and grey line, respectively). Parasitaemias and survival curve are representative of two independent experiments using two different sKO clones.

For the generation of *TbRPIB* double-allele knockout mutants, the hygromycin-resistant cell line was subjected to a second round of transfection using a construct with a different selectable marker (bleomycin). Two attempts to cultivate transfectants in the presence of both hygromycin and bleomycin, did not result in the outgrowth of cells resistant to both antibiotics. In a third attempt, the construct was modified. The selectable marker was changed to neomycin. Again, cells resistant to both antibiotics did not grow. The neomycin construct reliability was assessed by simultaneous transfection of wt and sKO cell line. Resistant parasites were only obtained for the wt but not for the sKO cell line (Figure 3). This result strongly suggests that a functional copy of *TbRPIB* gene is essential for parasites survival.

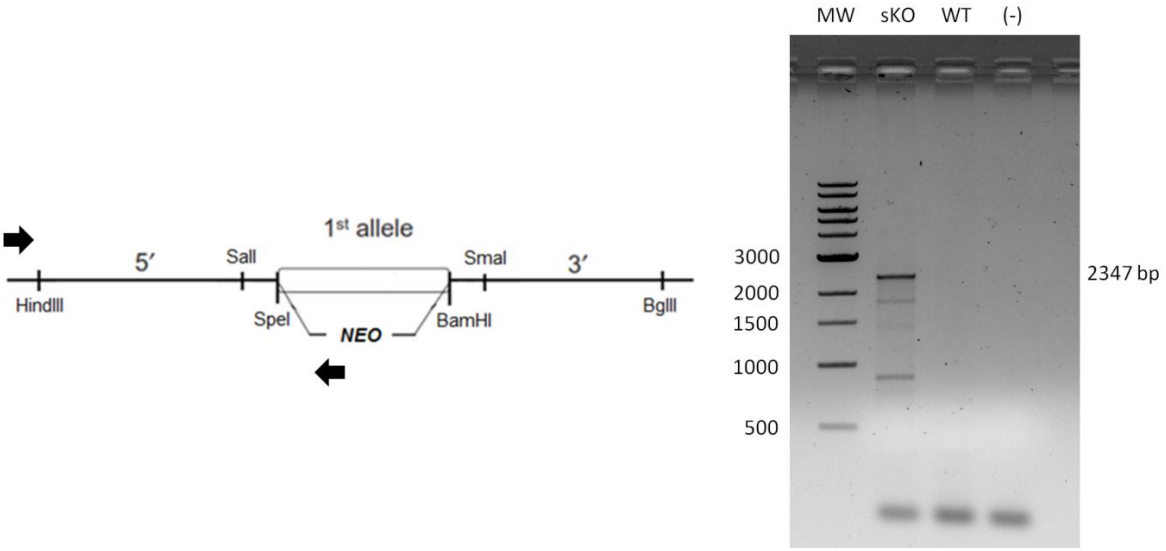

Figure 3. Analysis of bloodstream *TbRPIB* sKO (*NEO* marker). (A) PCR analysis of parental wt and sKO to evaluate neomycin cassette integration in the *RPIB* genomic locus. The amplified 2347 bp region is depicted. A PCR without genomic DNA (-), was used as a negative amplification control.

To ultimately prove the gene essentiality, a *TbRPIB* conditional knockout should be pursued. Using this system, parasites are engineered to express a regulatable allele of the gene and a gene is proved essential when parasites die upon removal of tetracycline (which represses transcription of the regulatable allele in null mutants) [11].

With our results RpiB gains strength as a potential therapeutic target against *T. brucei* infections.

Funding

This work was funded by FEDER funds through the Operational Competitiveness Program – COMPETE and by National Funds through FCT – Fundação para a Ciência e a Tecnologia under the project PEst-C/SAU/LA0002/2011. IL was supported by a FCT fellowship, reference SFRH/BD/64528/2009. JT is an Investigator FCT funded by National funds through FCT and co-funded through European Social Fund within the Human Potential Operating Programme. The research leading to these results has also received funding from the European Community's Seventh Framework Programme under grant agreement No. 602773 (Project KINDReD). The COST Action CM0801 "New drugs for neglected diseases" and CM1307 "Targeted chemotherapy towards diseases caused by endoparasites", and TRICONT project under ERA-NET New INDIGO have also

contributed for this work. The funders had no role in study design, data collection and analysis, decision to publish, or preparation of the manuscript.

Acknowledgements

We would like to thank Dr. Christine Clayton from Zentrum für Molekulare Biologie der Universität Heidelberg (ZMBH) for the scientific advices. We also thank Nuno Santarém and Joana Faria for the assistance.

References

1. Stincone A, Prigione A, Cramer T, Wamelink MM, Campbell K, et al. (2014) The return of metabolism: biochemistry and physiology of the pentose phosphate pathway. Biol Rev Camb Philos Soc.
2. Comini MA, Ortíz C, Cazzulo JJ (2013) Drug Targets in Trypanosomal and Leishmanial Pentose Phosphate Pathway. In: Jäger T KO, Flohé L, editor. Trypanosomatid Diseases: Molecular Routes to Drug Discovery. Wiley-VCH Verlag GmbH & Co. KGaA, Weinheim, Germany. pp. 297-313.
3. Zhang RG, Andersson CE, Skarina T, Evdokimova E, Edwards AM, et al. (2003) The 2.2 A resolution structure of RpiB/AlsB from Escherichia coli illustrates a new approach to the ribose-5-phosphate isomerase reaction. J Mol Biol 332: 1083-1094.
4. Babokhov P, Sanyaolu AO, Oyibo WA, Fagbenro-Beyioku AF, Iriemenam NC (2013) A current analysis of chemotherapy strategies for the treatment of human African trypanosomiasis. Pathog Glob Health 107: 242-252.
5. Radwanska M, Guirnalda P, De Trez C, Ryffel B, Black S, et al. (2008) Trypanosomiasis-induced B cell apoptosis results in loss of protective anti-parasite antibody responses and abolishment of vaccine-induced memory responses. PLoS Pathog 4: e1000078.
6. Loureiro I, Faria J, Clayton C, Macedo-Ribeiro S, Santarém N, et al. (2015) Ribose 5-Phosphate Isomerase B Knockdown Compromises Trypanosoma brucei Bloodstream Form Infectivity. PLoS Negl Trop Dis 9: e3430.
7. Schlecker T, Schmidt A, Dirdjaja N, Voncken F, Clayton C, et al. (2005) Substrate specificity, localization, and essential role of the glutathione peroxidase-type tryparedoxin peroxidases in Trypanosoma brucei. J Biol Chem 280: 14385-14394.

8. Williams RA, Smith TK, Cull B, Mottram JC, Coombs GH (2012) ATG5 is essential for ATG8-dependent autophagy and mitochondrial homeostasis in Leishmania major. PLoS Pathog 8: e1002695.
9. Mottram JC, Souza AE, Hutchison JE, Carter R, Frame MJ, et al. (1996) Evidence from disruption of the lmcpb gene array of Leishmania mexicana that cysteine proteinases are virulence factors. Proc Natl Acad Sci U S A 93: 6008-6013.
10. Burkard G, Fragoso CM, Roditi I (2007) Highly efficient stable transformation of bloodstream forms of Trypanosoma brucei. Mol Biochem Parasitol 153: 220-223.
11. Wyllie S, Oza SL, Patterson S, Spinks D, Thompson S, et al. (2009) Dissecting the essentiality of the bifunctional trypanothione synthetase-amidase in Trypanosoma brucei using chemical and genetic methods. Mol Microbiol 74: 529-540.

Chapter IV

Discussion and conclusions

1 Asparagine synthetase A

1.1 Trypanosomatids asparagine synthetase A peculiarities

Asparaginyl-tRNA synthetases and non-discriminating aspartyl-tRNA synthetases are involved in asparagine metabolism and have been subjected to a considerable number of studies (Becker & Kern, 1998; Blaise et al, 2011; Min et al, 2002; Pham et al, 2014; Raczniak et al, 2001; Roy et al, 2003) however, very few have been done in trypanosomatids (Gowri et al, 2012; Kalidas et al, 2014). AS-A is a tRNA synthetase paralog containing only the synthetase domain to perform asparagine biosynthesis (Gowri et al, 2012). While *ASB* genes are reported from all the three domains of life, *ASA* genes have been reported from prokaryotes (Nakamura et al, 1981), archaea (Blaise et al, 2011), and more recently from eukaryotic pathogens including, Trypanosomatids, *Trichomonas vaginalis*, *Entamoeba histolytica and Cryptosporidium spp* (Gowri et al, 2012; Heinz et al, 2012). In trypanosomatids, such *T. cruzi, T. brucei* and *L. donovani*, the *ASA* gene encodes a functional AS-A enzyme (Loureiro et al, 2013; Manhas et al, 2014).

Several AS-A 3D structures are available, including from *E. coli* (PDB 11AS and 12AS), *Pyrococcus abyssi* (PDB 3P8T, 3P8V, 3P8Y, 3REX, 3REU and 3RL6), and of an AS-A peptide from *Pyrococcus furiosus* (PDB 1NNH) (Blaise et al, 2011; Nakatsu et al, 1998) and more recently, also from *T. brucei* (Manhas et al, 2014). Analysis of *Ec*AS-A crystal structure reveals a class II catalytic core of aminoacyl tRNA synthetases (Nakatsu et al, 1998). Structure-based sequence comparison of *Ec*AS-A with the catalytic domain of yeast aspartyl tRNA synthetase showed a high conservation of catalytic residues. Despite the substrates of these two enzymes are the same, the activation of carboxyl groups on the aspartyl residues is different. *Saccharomyces cerevisiae* aspartyl tRNA synthetase activates the α carboxyl group of the substrate while *Ec*AS-A activates the β carboxyl group (Nakatsu et al, 1998). The recent crystal structure of archaeal *Pyrococcus abyssi* AS-A helped to uncover how the active site of ancestral aspartyl-tRNA synthetase rearranged throughout evolution to transform an enzyme activating α carboxyl group into an enzyme that is able to activate the β carboxyl group and can react with ammonia instead of tRNA (Blaise et al, 2011). Trypanosomes AS-A have the highest amino acid sequence identity with *Ec*AS-A and a sequence-based phylogenetic analysis followed by structural modeling suggests close evolutionary origin of kinetoplastid AS-A with the prokaryotic rather than the archael enzyme (Gowri et al, 2012; Loureiro et al, 2013). The crystal structure of apo-*Tb*AS-A was solved by molecular replacement using *Ec*AS-A

(PDB code 11AS) as the search model (Manhas et al, 2014). Expectedly, the overall fold of *Tb*AS-A was hence very similar to *E*cAS-A. This appears also to happen for the other trypanosomatids, *T. cruzi* and *L. donovani*. Interestingly, it still remains unclear the functional and structural significance of the small divergent region present in trypanosomatids enzymes but absent in *EcAS-A* and archaeal AS-A (Manhas et al, 2014). Also interesting is the fact that these residue insertions seem to have little sequence conservation between trypanosomes and *L. donovani* AS-A (*Ld*AS-A); in *Tb*AS-A sequence this insertion is: QVVFPRTSKPIPTMNSLSS; in *Tc*AS-A is: DITFPCGDPTMNSLAS, and in *Ld*AS-A is: KIGFPTADDEKPSVNTIMS). The apo form of *Tb*AS-A structure shows no significant deviation from its *E. coli* counterpart except a ~9Å displacement near α-helices 6 and 7 (Manhas et al, 2014). This study also confirmed that the active site residues involved in L-asparagine and AMP recognition are conserved between *Ec*AS-A, *Tb*AS-A and *Ld*AS-A. Nevertheless, small different features within the active sites, like the Y218 residue in *Ec*AS-A though conserved, is disordered in *Tb*AS-A and can be exploited to screen specific inhibitors that can selectively target parasite enzymes. In this line, and as predicted by the initial bioinformatics analysis, the amino acid sequence and structure similarity between trypanosomes AS-A and human AS-B showed to be very low. It was determined less than 15% of sequence identity (clustalw) (Larkin et al, 2007), and using Dali program (Holm & Rosenstrom, 2010), we were not able to structurally superimposed trypanosomes sequences with human AS-B. The common AS-A protein active sites present in the three trypanosomatids sequences are different from those found in human AS-B protein, therefore, it is theoretically possible to design a common inhibitor that will act against these and not against human protein.

AS type A enzymes are known for catalyzing the ATP dependent conversion of aspartate into asparagine, using strictly ammonia as the nitrogen source (Cedar & Schwartz, 1969a; Cedar & Schwartz, 1969b; Reitzer & Magasanik, 1982). AS type B enzymes detain the ability of using both ammonia and glutamine as substrates, with remarkable preference for the second (Boehlein et al, 1994; Ciustea et al, 2005; Duff et al, 2011; Horowitz & Meister, 1972; Patterson & Orr, 1968; Ramos & Wiame, 1979) (except for human enzyme which has similar affinity for glutamine and ammonia) (Ciustea et al, 2005). We have demonstrated that recombinant *Tb*AS-A and *Tc*AS-A have *in vitro* AS type A activity, as proteins were able to generate asparagine using aspartate, ATP and ammonia, in the presence of magnesium, which is an essential cofactor. To our knowledge, we reported for the first time, AS type A enzymes able to use not only ammonia but also glutamine as a nitrogen donor, however with preference for ammonia

(Loureiro et al, 2013). This hybrid activity was only previously demonstrated for type B enzymes (Boehlein et al, 1994; Ciustea et al, 2005; Duff et al, 2011; Horowitz & Meister, 1972; Patterson & Orr, 1968; Ramos & Wiame, 1979). In agreement with our study, a more recent paper also shows that *L. donovani* is capable of using glutamine as nitrogen source (Manhas et al, 2014). It is important to point that papers about AS-A biochemical characterization from bacteria are old papers, which resorted to technology available at that time (Cedar & Schwartz, 1968; Cedar & Schwartz, 1969a; Reitzer & Magasanik, 1982). Gene fusion technology and affinity chromatography is now widely used for the improvement of soluble protein production and/or purification in *E. coli*, which were not available at that time. The background activity seen in the absence of substrates corroborates some level of contamination in the purified enzymes, which may have led to misleading results (Cedar & Schwartz, 1969a). Therefore, the paradigm that AS-A enzymes are strictly ammonia dependent should be reevaluated. Nevertheless, the hybrid activity of trypanosomatids AS-A was detected using enzymes expressed on heterologous systems. Ideally this activity should be also demonstrated using the enzymes purified directly from parasites extracts. Another important aspect is the fact that, despite the residues involved in the binding of aspartate/asparagine and ATP/AMP are well described in type A enzymes, where and when does ammonia bind remains unknown (Blaise et al, 2011). In trypanosomatids AS-A, this issue also arises for glutamine. Unless the crystallographic structure is solved at very high resolution (~1Å), the hydrogen atoms are generally not visible in the electron density maps, and the ammonia nitrogen atom is not easily distinguishable from the oxygen atom in a water molecule. Thus, the cocrystallization of AS-A enzymes with ammonia will probably not allow the unambiguous determination of the ammonia binding site. The cocrystallization of trypanosomatids enzymes with glutamine, although difficult, may give information about the nitrogen donor binding site, therefore should be pursued.

In *Klebsiella aerogenes*, the nitrogen enrichment or impoverishment of the medium was proved to trigger the expression of AS-A or AS-B respectively (Reitzer & Magasanik, 1982). Trypanosomatids AS-A ability to use either ammonia or glutamine as nitrogen donors may reflect parasites need to adapt to changes in nitrogen content and availability (Loureiro et al, 2013; Manhas et al, 2014). Interestingly, the difference on affinity found in *Tb*AS-A and *Tc*AS-A for both substrates, ammonia or glutamine (1.5 and 2 folds difference, respectively), is lower than the difference found in most AS-B type enzymes (except for human AS-B, as mentioned above) (Ciustea et al, 2005; Duff et al, 2011; Horowitz & Meister, 1972; Patterson & Orr, 1968; Ramos & Wiame, 1979).

1.2 The promising *T. brucei* asparagine synthetase A is unlikely to be suitable as a drug target against human African trypanosomiasis

Our genetic studies showed that *Tb*AS-A is unlikely to be used as a target for the development of HAT new chemotherapeutic drugs. Parasites with down regulated levels of AS-A were able not only to growth as the wt *in vitro*, but also to equally infect mice. A defective growth phenotype and cell cycle arrest in G0/G1 was only observed when parasites with downregulated levels of AS-A were grown on asparagine-free medium. This phenotype was reverted when exogenous asparagine was added to the medium (Loureiro et al, 2013). Other studies also established a link between low levels of asparagine and *in vitro* cell cycle arrest. *Helycobacter pylori* L-asparaginase induces cell-cycle arrest *in vitro* of fibroblasts and gastric cell lines, in an extent that correlates with asparagine synthetase levels (Scotti et al, 2010). Moreover, removal of L-asparagine from the culture of L5178Y leukemia cells (lack a functional asparagine synthetase), by *E. coli* L-asparaginase leads to DNA fragmentation, cells cycle arrest in G1 phase, and apoptosis (Ueno et al, 1997). Similarly to *in vitro* experiments, the infectivity of bloodstream forms with reduced levels of AS-A was only affected when mice were simultaneously treated with *E. coli* L-asparaginase. The appearance of RNAi revertants, both *in vitro* and *in vivo* experiments, was a powerful sign of a stressful situation for the parasites. *T. brucei* can become irresponsive to tetracycline induction and consequently resume a normal growth efficiency through the deletion of the integrated target gene fragment and apparently by other unclear mechanisms, such as mutations at the T7 promotor/tetracyclin operator (Chen et al, 2003). Overall, our results suggest that bloodstream parasites rely on two major sources of asparagine to ensure normal proliferation: uptake from the extracellular medium and biosynthesis by AS-A. More importantly, parasites growth is only significantly affected when both sources of asparagine are compromised (Loureiro et al, 2013).

Its noteworthy to mention that in trypanosomes genome there is a second open reading frame (Tb927.3.4060) coding for a putative AS domain. However, this is apparently not a classical AS, despite the presence of a good Pfam AS domain (PF0073) at the C-terminus. A BLASTp search using the *T. brucei* sequence revealed a variety of proteins of unknown function that aligned not only across the AS domain, but also in the N-terminal region, which contains N-terminal aminohydrolase domains. Best matches originate from extremely diverse eukaryotes including a plant, an alga, a member of the fungi and an amoeba. BLASTp against the *Saccharomyces cerevisiae* predicted proteome yielded YML096W, and the reciprocal BLASTp on the trypanosome genome indeed gave

Tb927.3.4060 as best match. The function of YML096W is not known. Moreover, our results indirectly suggest that this protein may have no significant contribution for asparagine biosynthesis at least in *T. brucei* bloodstream forms (Loureiro et al, 2013).

Based on our results, a therapy that simultaneously inhibits *T. brucei* asparagine synthetase activity A, by using a AS-A specific inhibitor, and abrogates asparagine uptake, through L-asparaginase which decrease asparagine blood levels or through an asparagine transporter inhibitor which prevents the parasite to uptake extracellular asparagine, might be an option. Interfering with asparagine levels in the blood, through the administration of L-asparaginase, is currently used on the treatment of acute lymphoblastic leukemia (Pieters et al., 2011). These therapies rely on the fact that some malignant cells are dependent on exterior supplies of L-asparagine, because on their own exhibit a particular low level of AS expression (Asselin & Kurtzburg, 2003; Rizzari, 2003), and are also incapable of a rapid AS protein up-regulation response. Both aspects make these cells highly sensitive to L-asparaginase (Aslanian et al, 2001; Su et al, 2008). In contrast to leukemic cells which die when deprived of exogenous asparagine, most solid tumors express AS-B and synthesize asparagine *de novo* (Balasubramanian et al, 2013), therefore L-asparaginase alone has not proven to be an effective therapy. AS-B inhibition together with L-asparaginase administration might be a new strategy for the treatment pancreatic, ovarian, hepatic and breast tumours with high AS expression (Dufour et al, 2012; Lorenzi et al, 2008; Lorenzi et al, 2006; Yang et al, 2014). But still, L-asparaginase treatment requires parenteral administration and leads to serious adverse events, such as pancreatitis, severe hyperlipidaemia, altered liver function, severe allergic reactions, and thrombosis (Appel et al, 2008; Cohen et al, 2010; van den Berg, 2011). Once the actual chemotherapy against HAT is already highly toxic and expensive for developing countries, we need to developed new non-toxic and cheaper therapies of easy administration, rather than parenteral. Therefore is questionable the benefit of the suggested combination therapy over the existing HAT therapies. With regard to the second strategy, the functional redundancy in amino acid transporter repertoire, does not offer much of viable drug targets (Ebikeme, 2007). However exceptions exist, a recent study showed that in *Francisella tularensis* infection, the depletion of an amino acid transporter (AnsP) involved in asparagine and aspartate transport, lead to a severe intracellular growth defect and impact systemic dissemination of bacteria in mice. Remarkably, the intracellular growth and *in vivo* virulence defect of the mutants were fully and specifically reversed when asparagine, asparagine-containing dipeptides or simultaneous aspartic acid and ammonium were added at high concentrations and alternative amino acid permeases

assured their transport. These facts confirmed that the multiplication defect of the null *ansP* mutants is due to an asparagine uptake defect when the bacteria are localized in the cytosol of infected cells. Thus it is reasonable to assume that in these cases transporters can constitute attractive targets (Gesbert et al, 2014). However, interfering with asparagine uptake in *T. brucei* is unlikely to be achievable, once a family of 46 genes encoding amino acid transporters is present in the *T. brucei* genome making it the largest, and most diverse, family of transporters encoded in the genome (Ebikeme, 2007).

1.3 The controversy on the essentiality of asparagine synthetase A in trypanosomatids

In *T. brucei* bloodstream forms immunolocalization studies indicate AS-A is localized in the cytosol (Loureiro et al., 2013). In contrast, in *L. donovani* promastigotes AS-A was localized not only in the cytosol but also in the mitochondria of parasites engineered to express an episomal GFP-tagged AS-A. Indeed in this work, protein localization studies were performed on AS-A overexpressing parasites, an artificial condition that may have an impact on the protein distribution (Manhas et al, 2014). *L. major* AS-A appears to have a mitochondrial (PSORT II) and cytosolic (MARSPred) localization prediction however, mitochondria targeting signal peptide sequences and cleavage sites could not be predicted by computational tools (Manhas et al, 2014). These aspects combined with a poor and inaccurate mitochondria labeling warrant new AS-A localization studies in *Leishmania*. The same study also describes *ASA* as an essential gene for *Leishmania* based on failed attempts to delete the second copy of the gene (Manhas et al, 2014). However, to be fully convincing, attempts to remove the second allele should have been made in complemented parasites that are then left in culture without drug. The maintenance of the episomal copy in complemented null mutants cultured without drug pressure is the ultimate proof the gene is essential since in *Leishmania* no cKOs are yet possible. The authors mentioned that chromosomal null mutants could not be obtained as the double transfectant mutants showed aneuploidy, but experimental data regarding ploidy levels was not shown (Manhas et al, 2014). A slight growth delay *in vitro* was shown for *LdASA* sKOs compared to wt parasites, however this difference was not proved to be statistically significant (Manhas et al, 2014). Experiments to analyze the infectivity of sKO parasites would be also important and already indicative of AS-A relevance, since authors argue that this protein is a therapeutic target. Overall, the conclusion of *Leishmania ASA* as an essential gene requires a careful reevaluation.

1.4 Does the function of asparagine synthetase and its product, asparagine, goes beyond protein biosynthesis in *T. brucei*?

Depletion of any individual or several amino acids in the cells triggers the activation of the amino acid response (AAR) pathway (Gong et al, 1991; Hutson & Kilberg, 1994). Within this pathway, amino acid deprivation causes an increased abundance of the corresponding uncharged tRNA that binds to and activates the general control non-depressible 2 (GCN2) kinase (Kilberg et al, 2009) which in turns phosphorylates the eukaryotic translation initiation factor-2 alpha (eIF2α). The eIF2α is a general sensor of exogenous and endogenous stress signals and therefore a substrate for several other kinases, which are in turn activated by several stress events and that are summarized on figure 18. Phosphorylated eIF2α signals down-regulate global protein synthesis by repressing translation initiation (Baird & Wek, 2012), but simultaneously, up-regulate the translation of a subset of mRNA molecules involved in stress response, including the activating transcription factor 4 (ATF4) (Kilberg et al, 2009). Consequently ATF4 activates specific genes via C/EBP-ATF response element (CARE), including *AS* gene (Kilberg et al, 2009). The magnitude of the up-regulation of various ATF4 transcriptional targets, including AS, vary depending on the amino acid and on the cell line (Fomina-Yadlin et al, 2014). Reduced translation conserves energy and nutrients, allowing time for the cell to adapt appropriately to the stress conditions.

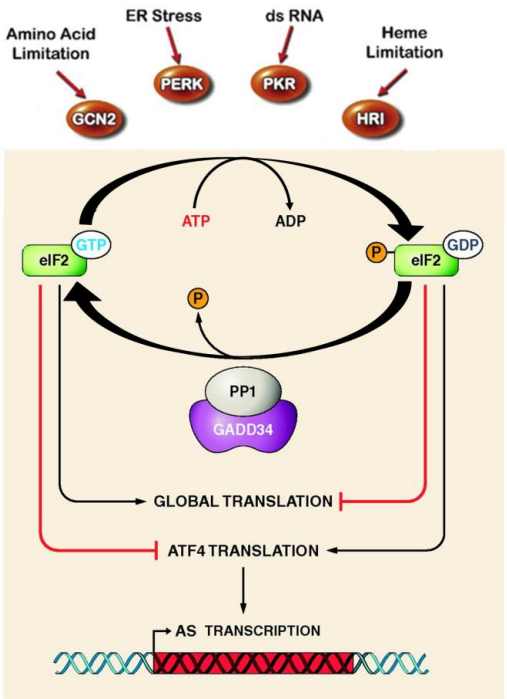

Figure 18. Phosphorylation of eIF2α is mediated by different kinases that respond to specific environmental stresses: 1) GCN2 which is activated during amino acid starvation; 2) protein kinase R (PKR), which plays a key role in the cellular anti-viral response; 3) protein kinase RNA-like endoplasmic reticulum kinase (PERK), which responds to protein misfolding in the endoplasmic reticulum; and 4) HRI that limits protein synthesis during heme-deficiency. Phosphorylated eIF2α suppresses global translation, but leads to a paradoxical increase in translation of specific mRNA species, such as that for ATF4, which consequently enhanced AS transcription, one of the hundreds of ATF4 target genes. [Adapted from (Balasubramanian et al, 2013; Kilberg et al, 2009)].

The activation of the GCN2-eIF2-ATF4 signalling pathway, leading to increased expression of AS was proved to be a component of solid tumor adaptation to nutrient deprivation and/or hypoxia (Ye et al, 2010). What is curious in this study, is the fact that supplementation of small hairpin ATF4-expressing tumor cells with asparagine, but no other amino acid, reversed the increased apoptosis and authophagy leading to increased cell survival. Moreover, another study proposed that the function of AS up-regulation in response to low glucose is to protect pancreatic cancer cells from apoptosis. In addition to greater tolerance for glucose limitation, pancreatic cancer cells over-expressing AS exhibited increased resistance to apoptosis induced by cisplatin (Cui et al, 2007).

AS protein's name directs the focus to its function, the synthesis of asparagine, however the reaction impact the cellular levels of glutamine as well (Scofield et al, 1990). Given the critical function of glutamine as an oxidizable energy source, a key nitrogen carrier, and a mammalian target of rapamycin (mTOR) regulator, glutamine homeostasis should also be considered when evaluating the impact of the activity of these enzymes. With respect to deprivation of glutamine, curiously a very recent paper using SV40-transformed mouse embryonic fibroblasts, neuroblastoma and human glioblastoma cell lines demonstrated that suppression of citrate synthase, the first tricarboxylic acid cycle (TCA) cycle enzyme, prevented glutamine-withdrawal-induced apoptosis, which was a bit surprising once many cancer cells consume large quantities of glutamine to maintain TCA cycle anaplerosis and cell survival (Zhang et al, 2014). Citrate synthase suppression reduced TCA cycle activity and diverted oxaloacetate into production of aspartate, and ultimately asparagine (Figure 19).

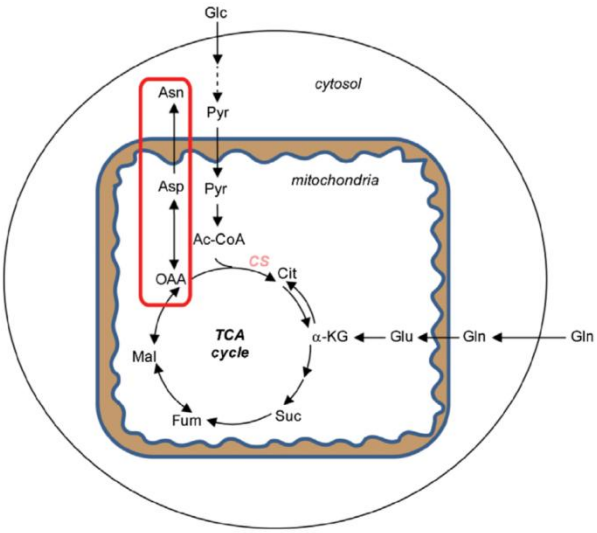

Figure 19. Citrate synthase knockdown redirects oxaloacetate to aspartate and asparagine biosynthesis. Abbreviations are as follows: Glc, glucose; Pyr, pyruvate; Ac-CoA, acetyl-CoA; CS, citrate synthase; Gln, glutamine; Glu, glutamate; Cit, citrate; a-KG, a-ketoglutarate; Suc, succinate; Fum, fumarate; Mal, malate; OAA, oxaloacetate; Asp, aspartate; Asn, asparagine. [Adaped from (Zhang et al, 2014)].

Subsequent experiments within this study demonstrated that asparagine can maintain the viability of glutamine-deprived cells without restoration of anaplerosis or the levels of other nonessential amino acids. The rescue of survival by asparagine was specific to depletion of the nonessential amino acid, glutamine, once exogenous asparagine had no effect on cell death induced either by depletion of essential amino acids, including leucine, threonine, or phenylalanine, or by glucose depletion or DNA topoisomerase inhibition. Interestingly, while sustained levels of asparagine promote cellular adaptation to depletion of glutamine and other nonessential amino acids, intracellular depletion of asparagine through AS knockdown, induces apoptosis even in the face of an abundant supply of glutamine and other nonessential amino acids, only being reversed by addition of exogenous asparagine. Surprisingly, only the addition of asparagine can specifically suppress that apoptosis through the suppression of CHOP induction without altering the upstream signaling cascade, including eIF2a phosphorylation and ATF4 accumulation. Zhang J et al. (2014) results showed that exogenous asparagine had no effect on cell death induced by glucose depletion contradicting the study above from Cui H at el. (2007). Nevertheless,all together the data proposes an unexpected role of AS-A and/or asparagine in regulating cell survival. Protein synthesis seems too simplistic, as other

amino acid synthesis pathways are not as highly regulated, and other amino acids do not appear to play as critical a role.

The response to stress via phosphorylation of eIF2α is conserved from yeast to mammals and plays a significant role when cells must respond to environmental stresses (Murguia & Serrano, 2012). Previous work indicated that trypanosomes encode three potential eIF2 kinases (eIF2K1-K3) being one of them, *Tb*eIF2K1, a possible GCN2 orthologue. *T. brucei Tb*eIF2K2, was able to phosphorylate yeast and mammalian eIF2α. It also phosphorylates an unusual form of eIF2α found in trypanosomes (Moraes et al, 2007). Phosphorylation of eIF2α has been shown to mediate translational control in response to nutritional stress and underlie cell differentiation in protozoan parasites. In *Toxoplasma gondii,* phosphorylation of eIF2α by different stress stimulus results in the differentiation into quiescent stages, which are responsible for microbial persistence and latent infection (Narasimhan et al, 2008). Also, phosphorylation of *Plasmodium falciparum* eIF2α is required in the formation of sporozoites in the salivary gland of the insect vector (Zhang et al, 2010). In the case of *Leishmania*, promastigotes with impaired eIF2α phosphorylation upon ER stress, showed delayed differentiation into amastigotes either within axenic cultures or macrophages (Chow et al, 2011). In *T. cruzi* differentiation of epimastigotes into the infective form, trypomastigotes, requires the inhibition of translation by phosphorylation of eIF2α that is triggered by nutritional deprivation (Chow et al, 2011). Unfortunately, neither of the above studies determined whether an increase of AS protein levels or asparagine occurs in stresses stimulus-response.

All these facts suggest that key features of eIF2-signalling pathway are probably conserved in parasites and raised a relevant question: is it possible that AS or asparagine serves another role, perhaps as a signaling molecule in *T. brucei*? In our study, bloodstream forms with down-regulated levels of AS-A had growth defects only in limiting asparagine environments suggesting that asparagine production is the main function of *Tb*AS-A. However, an involvement of AS-A in a stress-response signaling pathway can't be completely excluded since residual levels of AS-A upon RNAi induction might be sufficient for that potential function.

2 Ribose 5-phosphate isomerase B

2.1 Ribose 5-phosphate isomerase B has a critical role in *T. brucei* infectivity in mice

The PPP is an important pathway that branches from glycolysis and uses glucose-6-phosphate in reactions that ultimately produce NADPH and R5P. The connections between glycolysis, amino acid/lipid biosynthesis, and sugar/redox metabolism, place PPP central to the metabolic network. Involved in the non-oxidative branch of PPP, RpiB has been pointed in several pathogens as a potential therapeutic target (Edwards et al, 2011; Kaur et al, 2012; Roos et al, 2008; Stern et al, 2007; Wang & Yang, 2013) due to the very low sequence identity with its human counterpart RpiA. Presumably, both enzymes represent an example of convergent evolution as RpiA occur in most eukaryotes and some bacteria, while RpiB exist almost exclusively in prokaryotes, with few exceptions in lower eukaryotes, including trypanosomatids, other parasitic protozoa, and some fungi (Stern et al, 2011). In organisms where both genes are found, such as *E. coli*, RpiA plays the main role in the isomerazation of R5P and Ru5P (Skinner & Cooper, 1974) while RpiB might be involved on the isomerization of a different sugar phosphate, like D-allose-6-phosphate (Roos et al, 2008). Interestingly, *E. coli* RpiB is slightly worse at catalyzing the isomerization of D-allose-6-phosphate than R5P suggesting that if for some reason RpiA stops functioning, RpiB can take over its activity (Roos, 2007). Structural studies explained why larger 6-carbon sugar phosphate could be accommodated by *E. coli* RpiB and not by *Mycobacterium tuberculosis* (*M. tuberculosis*) RpiB enzyme. In the latter the active site has no space for a linear 6-carbon compound (Roos et al, 2008). Moreover since this sugar is extremely rare in nature, the reason why *E. coli* has an operon devoted to allose metabolism remains a mystery. In trypanosomes and other organisms where only an RpiB is encountered, the role of this enzyme must be mainly of R5P and Ru5P isomerization.

To date, the crystal structures of RpiB enzymes from *E. coli* (PDB 1NN4 and 2VVR) (Becker & Kern, 1998; Zhang et al, 2003), *M. tuberculosis* (PDB 2VVP, 2VVQ, 2VVO, 2BET, 2BES and 1USL) (Becker & Kern, 1998; Curnow et al, 1998; Roos et al, 2005), *Coccidioides immintis* (PDB 3QD5, 3SDW and 3SGW) (Min et al, 2002), *Anaplasma phagocytophilum* (PDB 4EM8), *Clostridium thermocellium* (PDB 3PH3, 3PH4 3HEE, and 3HE8) (Jung et al, 2011), *Giardia lamblia* (PDB 3S5P), *T. cruzi* (PDB 3K7P, 3M1P, 3K7O, 3K8C and 3K7S) (Stern et al, 2011), and *Thermotoga maritima* (1O1X)

(Gatti & Tzagoloff, 1991) have been determined. Multiple sequence alignment and structural superposition showed a huge similarity within the *Tc*RpiB (CL Brener Esmeraldo like strain), *Tc*RpiB (CL Brener Non-Esmeraldo like strain) and *Tb*RpiB sequences (Loureiro et al, 2015). Sequence and structure similarities between trypanosomes and human RipA enzymes were confirmed to be very low (<15%). Thus, it should be possible to design compounds that only bind to RpiB enzymes.

From X-ray structures and site-directed mutagenesis studies, it is consensual a main role for His102 in the furanose ring opening step, and was suggested Glu75 in the *M. tuberculosis* enzyme, Cys66 from *E. coli*, and Cys69 in *T. cruzi* as the catalytic base for the isomerization (Roos et al, 2004; Roos et al, 2005; Stern et al, 2007; Zhang et al, 2003). Additionally, His10 in *E. coli* and His11 in *T. cruzi* were proposed to be important in the stabilization of the protein (Stern et al, 2007; Zhang et al, 2003). The complete conservation of crucial amino acid residues in *Tb*RpiB warrants the *in vitro* RpiB activity. As in *Tc*RpiB (Stern et al, 2007), *T. brucei* enzyme detains the ability of using both R5P and Ru5P as substrates, with remarkable preference for the second (Loureiro et al, 2015).

As far as we know a *rpiB* knockout was only described in *E. coli*. But in this case both type A and B are equally efficient in catalyzing the isomerization step and therefore the construction of double mutants was needed to fully prevent this reaction. The Rpi dKO lacking both *rpiA* and *rpiB* showed severely impaired growth phenotype (Sorensen & Hove-Jensen, 1996). In contrast and as already mentioned, *T. brucei* lacks RpiA, therefore Rpi activity is very likely confined to the type B enzyme.

RNAi was firstly performed for *Tb*RpiB genetic validation. *In vitro* RNAi induction leads to a significant decrease of bloodstream forms proliferation after day 4. Most important is when RNAi was induced *in vivo*, and the infectivity of induced RNAi cells was substantially affected leading to a decrease in parasitaemia and a prolonged mice survival. Mice infected with RNAi induced parasites eventually die due to the emergence of RNAi revertants. The occurrence of any off target effect was excluded since *in vitro* and *in vivo* phenotypes were reverted in *Tc*RpiB complemented parasites (Loureiro et al, 2015). To further investigate if bloodstream forms deleted of RpiB are completely cleared in mice, we tried to generate knockout parasites. Despite several attempts we did not succeed to obtain null mutants suggesting the need of using a cKO system to unequivocally prove *Tb*RpiB essentiality. Studies conducted with sKO lines were in agreement with the previous RNAi results. Expectedly *in vivo* phenotypes, including parasitaemia and mice life span, were not so strong as the ones obtained in RNAi. A possible explanation is due to differences on the level of RpiB downregulation, which was

higher in RNAi than in the sKO clones (Loureiro et al, *unpublished*). To better understand why mice infected with sKO parasites had reduced parasitaemias and increased survival compared to wt, we propose to follow infections in mice using live imaging system and bioluminescent wt and sKO parasites.

2.2 Inquiries on the role of pentose phosphate pathway in *T. brucei*

An enhanced PPP activity has been reported in highly proliferative cells, such as pluripotent stem cells and cancer cells. In stem cells, an up-regulation of gene-products involved in glucose uptake and glucose phosphorylation to glucose 6-phosphate was observed comparatively to somatic cells. However, the expression levels of some genes coding glycolytic enzymes downstream glucose 6-phosphate were reduced, while the level of genes involved in the non-oxidative PPP (*RPIA* and *TKT*) increased (Prigione et al, 2011; Varum et al, 2011). Also, not only G6PDH is increased in various human cancer types when compared to the respective benign control tissue (Bezwoda et al, 1985; Pedersen, 1975; Zampella et al, 1982), but also an enhanced PPP activity occurs in the human breast cancer cell line MCF7 when compared to non-transformed mammary epithelial cells (Meadows et al, 2008). Therefore, the role of the PPP is particularly evident in cells or tissues that undergo proliferation. The fact that RPE and TKT enzymes are not detected in *T. brucei* bloodstream forms (Cronin et al, 1989) suggests that in these highly proliferative forms, the PPP is constrained to the production of NADPH and R5P (Comini et al, 2013). During proliferation, it is predictable that cells restructure their central carbon metabolism in order to adapt to the rise in metabolic demands. In our study we observed a stronger phenotype *in vivo* than *in vitro* which can be explained by the fact that, contrary to culture conditions, *in vivo* parasites may do not have access to essential nutrients, which are usually available in culture media. Moreover, parasites need to deal with pressure from the host immune response. To prevent a collapse of the metabolic network, parasites need to adapt their metabolism in order to ensure proper functionality upon environmental changes. A paradigm example of a transcriptional regulation of the PPP is the case of G6PDH in yeast. In a deficient NADPH producing yeast, due to *zwf1* (codes G6PDH) deletion, the NADPH-producing role of G6PDH is compensated by other NADP-oxidizing enzymes under normal growth conditions. On the other hand, the $NADP^+$/NADPH ratio collapses upon H_2O_2 exposure, rendering G6PDH null cells highly oxidant sensitive (Nogae & Johnston, 1990). The PPP plays pivotal roles in response to anabolic intermediates needs and in counteracting oxidative stress. It is mainly implicated

in (1) maintaining metabolic and redox homeostasis via $NADP^+$ to NADPH reduction, (2) synthesizing R5P used in nucleotide biosynthesis (increased synthesis is required upon DNA damage stress), and (3) activating stress-responsive gene expression (Figure 20) (Stincone et al, 2014).

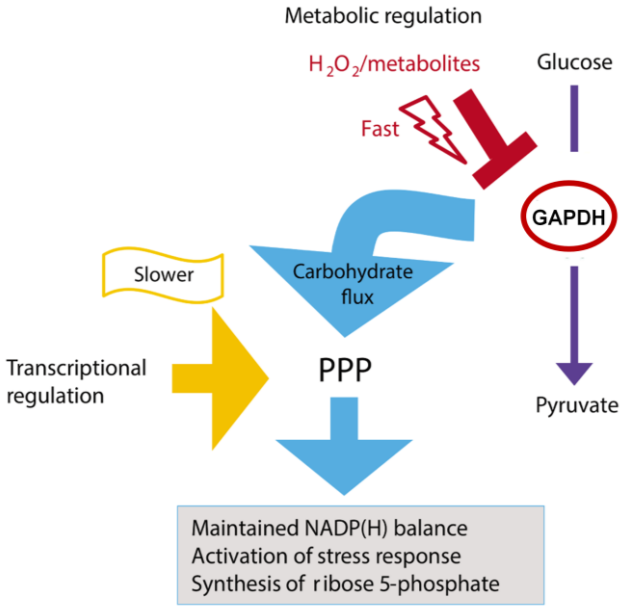

Figure 20. Induction of glycolysis/PPP transition during oxidative stress. In a stress situation, activity of the PPP is increased through orchestrated allosteric/post-translational and transcriptional regulation. The fastest response is made through oxidative inhibition of GAPDH and consequently forward glycolytic reactions, while PPP remains active. This process is also supported by post-translational modifications that increase G6PDH activity, a process comparatively slower but that allows cellular adaptation to stress in a long(er)-term response. [Adapted from (Stincone et al, 2014)].

It was previously demonstrated that the main role of PPP in *Plasmodium spp.* erythrocytic stages seems to be the NADPH supply, once R5P can be obtained from the uptake and degradation of host purines (Preuss et al, 2012). In *T. cruzi*, oxidative stress not only regulates kinetically, but also increases its protein level (Igoillo-Esteve & Cazzulo, 2006). In *T. brucei* G6PDH RNAi leads to growth arrest and reduced tolerance to H_2O_2, and in *L. mexicana* PPP flux increases when parasites were exposed to the oxidative stress inducer methylene blue (Maugeri et al, 2003). Also kinetic models of glycolysis and PPP reactions in *T. brucei* corroborated the importance of PPP in response to oxidative stress (Achcar et al, 2012; Albert et al, 2005; Kerkhoven et al, 2013). Additionally, 6PGDH

knockout (enzyme from the oxidative branch) leads to a lethal phenotype (Barrett, 1997) while in contrast, procyclics TKL null mutants (enzyme from the non-oxidative branch) do not have any effect on cell growth (Stoffel et al, 2011). Taken together, these results indicate that also in trypanosomatids, including *T. brucei*, the main role of the PPP appears to be in the defence against oxidative stress. Once $NADP^+$/NADPH take part of the oxidative PPP, supposedly the NADPH-dependent PPP antioxidant response will not be affected upon RpiB downregulation. However, it was already proposed in other organisms the occurrence of a NADPH-independent PPP antioxidant response, in which the underlying molecular mechanism is still unknown. This was based on the observations that: (1) in yeast double mutant deleted for both the oxidative PPP enzyme G6PDH (*zwf1*) and the non-oxidative PPP enzyme TAL (*tal1*) was more sensitive to H_2O_2 than the parent mutants deleted for either *zwf1* or *tal1* alone (Kruger et al, 2011), (2) also in yeast an increased oxidant resistance was obtained when the metabolite load of the non-oxidative pathway was augmented due to expression of the mammalian sedoheptulokinase (Kardon et al, 2008; Kruger et al, 2011); and (3) in *Entamoeba histolytica,* which has an alternative PPP pathway absent of G6PDH, 6PGDH and TAL, when exposed to oxidative stress, metabolites of the non-oxidative PPP increased (Husain et al, 2012). These facts impose the following question: does *T. brucei* parasite have an equal antioxidant response when the non-oxidative branch PPP is disturbed but the oxidative PPP remains fully active?

The detrimental effect of RpiB downregulation *in vivo* is most likely due to the inability of the parasite to respond to a much higher requirement of R5P for proliferation and/or DNA repair under host pressure. It is now crucial to understand if the quantity of R5P decreases in induced *Tb*RpiB RNAi relative to non-induced parasites, and if in fact *in vivo* the non-oxidative PPP flux into R5P does not operate. To measure oxidative relative to non-oxidative PPP flux into R5P, one possible method involves separate feeding experiments with, 1-^{13}C-glucose and 6-^{13}C-glucose and the measure of R5P labelling by mass spectrometry. Indeed, R5P produced via oxidative PPP is labelled with 6-^{13}C but not with 1-^{13}C-glucose (Fan et al, 2014). Another possibility involves feeding with 1,2-^{13}C-glucose and look for single *versus* double labelled R5P, with the former made by the oxidative PPP and the latter by the non-oxidative PPP (Lee et al, 1998) (Figure 21).

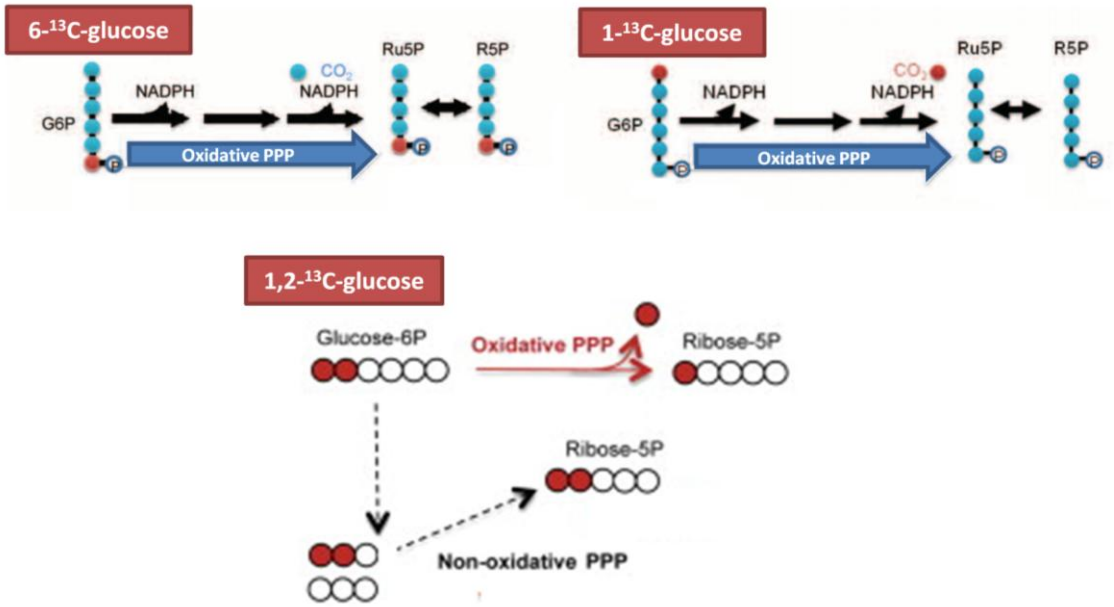

Figure 21. Glucose labelled on the sixth, first and both first and second carbons can be used to determine relative flux through the oxidative and non-oxidative PPP by assessment of singly, doubly and non-labelled downstream intermediates. [Adapted from (Fan et al, 2014; Metallo & Vander Heiden, 2013)].

In the case of *in vivo* experiments, mass spectrometry based methods are not applicable. Recently a new described NMR technique, termed hyperpolarization (Ardenkjaer-Larsen et al, 2003), can be used to measure PPP flux *in vivo* but the major limitation of the technique is the relatively short life time of the spin polarization, which means that only relatively rapid metabolic processes can be imaged (Stincone et al, 2014).

2.3 Do "alternative pathways" to generate ribose 5-phosphate exist?

A well described ribose transport is the one present in *E. coli* being taken by the *rbsACB* gene product (Figure 22A) (Roos, 2007). Phosphorylation of ribose by ribokinase is the first reaction in the metabolism of exogenous ribose and is required for keeping ribose inside the cell. Once phosphorylated it is trapped within the cell due to added negative charge, which prevents it from leaking back across the membrane. In *T. brucei*, a specific transport system for ribose was not yet identified, even though this parasite has a ribokinase gene (Kerkhoven et al, 2013). Interestingly, a previous study knockdown the ribokinase levels on *T. brucei* and no growth defect was observed. However attempts to generate null mutants failed in spite of numerous rounds of transfection. The cKO was generated with inducible expression of an exogenous copy of the ribokinase gene, but

again no growth phenotype could be observed, even if the ectopic copy was switched off. It was therefore concluded that ribokinase activity is essential but that residual levels in RNAi and leaky expression in the cKO were sufficient to fulfil its essential role. Therefore, if ribose can be uptaken by a not yet described transporter, ribokinase activity might be an alternative way of generating R5P.

As mentioned above *Plasmodium spp.* parasites are able to and depend on the uptake of host purines via an equilibrative nucleoside transporter (Figure 22B). The nucleosides can subsequently be degraded by nucleoside phosphorylases yielding ribose-1-phosphate, which might be isomerized by phosphoglucomutase to R5P (Downie et al, 2008). This alternative route does not appear to exist in *T. brucei* since the latest enzyme is absent (Bandini et al, 2012).

Both the non-oxidative PPP and the Calvin cycle share some important reactions. While the classical non-oxidative PPP uses TAL to make sedoheptulose 7-phosphate, the Calvin cycle uses the glycolytic enzyme ALD to convert erythrose 4-phosphate plus dihydroxyacetone phosphate into sedoheptulose 1,7-bisphosphate, which in turn is hydrolysed by the enzyme sedoheptulose-1,7-bisphosphatase to yield sedoheptulose 7-phosphate. This hydrolysis step provides the thermodynamic driving force, pushing the Calvin cycle towards R5P, and ultimately Ru5P (Figure 22C). Until recently, sedoheptulose-1,7-bisphosphatase enzymatic activity was thought to be specific of photosynthetic organisms, however metabolomic screening of yeast strains lacking genes of unknown function, revealed a strain with elevated sedoheptulose 1,7-bisphosphate. The associated gene was subsequently shown to encode an enzyme with sedoheptulose-1,7-bisphosphatase activity involved in a novel variant of the non-oxidative PPP that follows yet more closely the Calvin cycle reaction sequences (Figure 22D) (Clasquin et al, 2011). This variant of the non-oxidative PPP is termed riboneogenesis. R5P biosynthesis *via* riboneogenesis can be used when demand for ribose exceeds that for NADPH. In such cases, it is presumably advantageous to have a thermodynamically driven alternative to the standard oxidative towards non-oxidative PPP, and to avoid an over-reduction of the NADPH pool. Till now, sedoheptulose-1,7-bisphosphatase activity was proved to have a role only in plant and yeast metabolisms. In *T. brucei*, the presence of sedoheptulose-1,7-bisphosphatase coding gene was already confirmed (Hannaert et al, 2003b). Sequence alignment of trypanosome with plant and algal sequences indicated that all residues essential for catalysis have been conserved, suggesting that *T. brucei* encodes a functional protein, however it remains to be demonstrated. Also remains to be elucidated if this alternative non-oxidative PPP can constitute a salvage pathway for R5P.

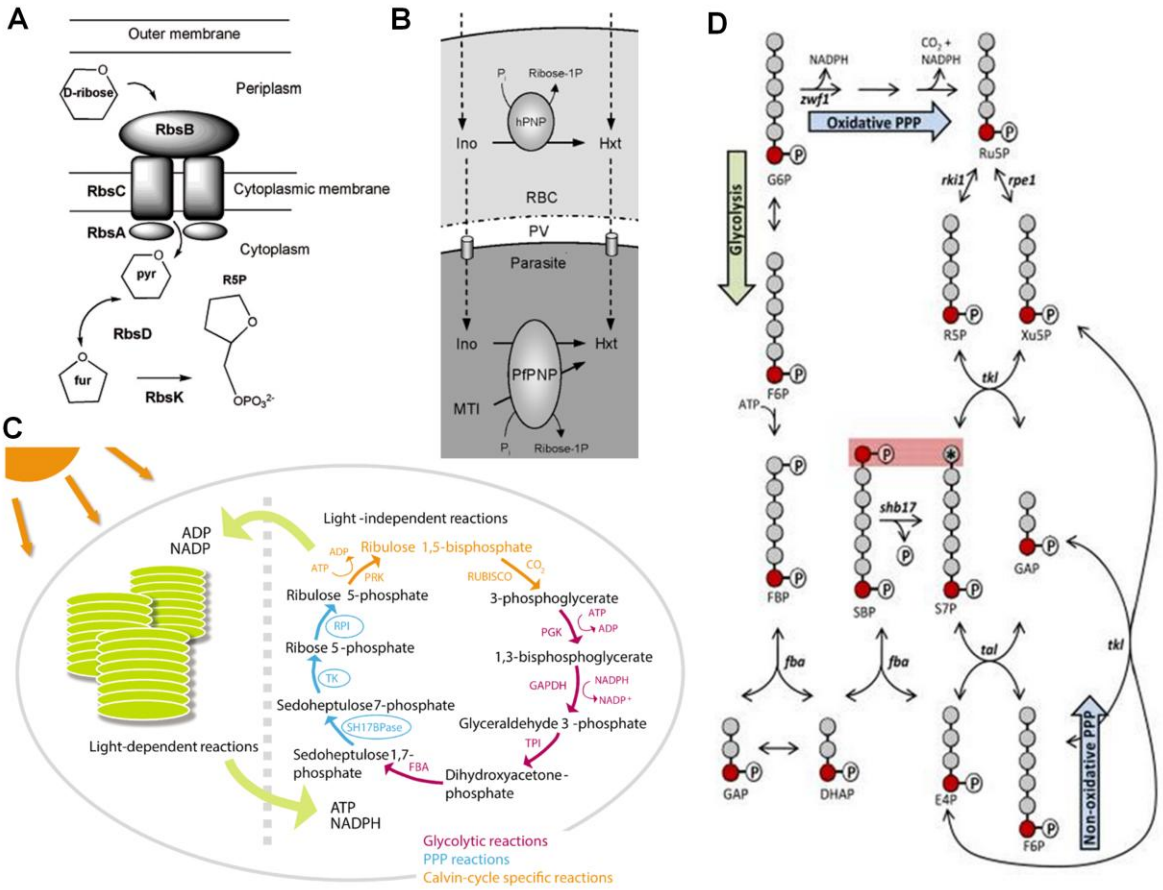

Figure 22. Alternative pathways to generate R5P bypassing the oxidative PPP. (A) The path from D-ribose to R5P in *E. coli*. RbsA a cytoplasmic ATPase, RbsC a membrane permease, RbsB the periplasmic ribose binding protein, RbsD is a mutarotase, that converts the pyranose form of ribose to the furanose form, and RbsK or ribokinase binds specifically the α-furanose form of ribose for its phosphorylation leading to R5P. (B) Ribose-1P synthesis within *Plasmodium* infected erythrocytes. (C) The light-independent reactions of carbon fixation in the Calvin cycle share enzymes and reactions with the PPP and glycolysis. (D) Yeast Shb17 feeds carbon into the non-oxidative PPP. The cells were fed with glucose labelled selectively at the 6-position with carbon 13 (6-^{13}C-glucose). Flux through Shb17 into S7P can be measured using [6-$^{13}C_1$]-glucose. [6-$^{13}C_1$]-glucose leads to [7-$^{13}C_1$]-S7P when S7P is made via the oxidative PPP or the non-oxidative PPP. However, when S7P is produced from SBP via Shb17, a fraction of the S7P pool is doubly labelled: [1,7-$^{13}C_2$]-S7P. This labelling pattern was observed preferentially when yeast cells were grown on media that decreased their need for NADPH (e.g. by providing them with lipids). Abbreviations: G6P, glucose-6-phosphate; F6P, frutose 6-phosphate; FBA or *fba*, fructose biphosphate aldolase; GAPDH, glyceraldehyde 3-phosphate dehydrogenase; GAP,

glyceraldehyde 3-phosphate; DHAP, dihydroxyacetone phosphate; TPI, triosephosphate isomerase; E4P, erythrose 4-phosphate; SBP, sedoheptulose-1,7-bisphosphate; S7P, sedoheptulose 7-phosphate; *shb17* or SH17BPase, sedoheptulose-1,7-bisphosphatase; *tal*, transaldolase; TK or *tkl*, transketolase; RPI or *rki1*, ribose phosphate isomerase; *rpe1*, ribose phosphate epimerase; R5P, ribose 5-phosphate; Ru5P, ribulose 5-phosphate; Xu5P, xylulose 5-phosphate; PGK, phosphoglycerate kinase; PRK, phosphoribulokinase; hPNP, human purine nucleoside phosphorylase; PfPNP, purine nucleoside phosphorylase; Ino, inosine; Hxt, hypoxanthine; RBC, red blood cell; PV, parasitophorous vacuole; MTI, methylthioinosine. [Adapted from (Clasquin et al, 2011; Downie et al, 2008; Roos, 2007; Stincone et al, 2014)].

2.4 Challenges on *T. brucei* ribose 5-phosphate isomerase B druggability

Despite genetic studies demonstrated *Tb*RpiB as a highly promising drug target (Loureiro et al, 2015); Loureiro et al, *unpublished*), two important aspects concerning inhibition studies and possible RpiB redundancy should be kept in mind. 4-PEH is the strongest inhibitor described against RpiB enzymes (Roos et al, 2005; Stern et al, 2007), being also active against the *T. brucei* enzyme (Loureiro et al, 2015). However, 4-PEH mediated inhibition of *Tb*RpiB not only requires concentrations on the milimolar range (Loureiro et al, 2015) but also lacks selectivity, since it also inhibits the spinach type A enzyme (Roos et al, 2005). Future structure-based drug design studies are needed to design potent and selective inhibitors. Another concern, despite speculative, is that under drug pressure, “alternative pathways” to generate R5P may overcome the detrimental effect of RipB inhibition.

In conclusion, there is still a long way until RipB is considered an ideal drug target against HAT.

Chapter V

Publications outside the scope of the thesis

OPEN ACCESS Freely available online

PLoS NEGLECTED TROPICAL DISEASES

Impact of Continuous Axenic Cultivation in *Leishmania infantum* Virulence

Diana Moreira[1☯], Nuno Santarém[1☯], Inês Loureiro[1], Joana Tavares[1,2], Ana Marta Silva[1], Ana Marina Amorim[1], Ali Ouaissi[1,3], Anabela Cordeiro-da-Silva[1,2¶], Ricardo Silvestre[1*¶]

1 Parasite Disease Group, IBMC - Instituto de Biologia Molecular e Celular, Universidade do Porto, Porto, Portugal, **2** Departamento de Ciências Biológicas, Faculdade de Farmácia, Universidade do Porto, Porto, Portugal, **3** INSERM, UMR, CNRS 5235, Université Montpellier II, Montpellier, France

Abstract

Experimental infections with visceral *Leishmania* spp. are frequently performed referring to stationary parasite cultures that are comprised of a mixture of metacyclic and non-metacyclic parasites often with little regard to time of culture and metacyclic purification. This may lead to misleading or irreproducible experimental data. It is known that the maintenance of *Leishmania* spp. *in vitro* results in a progressive loss of virulence that can be reverted by passage in a mammalian host. In the present study, we aimed to characterize the loss of virulence in culture comparing the *in vitro* and *in vivo* infection and immunological profile of *L. infantum* stationary promastigotes submitted to successive periods of *in vitro* cultivation. To evaluate the effect of axenic *in vitro* culture in parasite virulence, we submitted *L. infantum* promastigotes to 4, 21 or 31 successive *in vitro* passages. Our results demonstrated a rapid and significant loss of parasite virulence when parasites are sustained in axenic culture. Strikingly, the parasite capacity to modulate macrophage activation decreased significantly with the augmentation of the number of *in vitro* passages. We validated these *in vitro* observations using an experimental murine model of infection. A significant correlation was found between higher parasite burdens and lower number of *in vitro* passages in infected Balb/c mice. Furthermore, we have demonstrated that the virulence deficit caused by successive *in vitro* passages results from an inadequate capacity to differentiate into amastigote forms. In conclusion, our data demonstrated that the use of parasites with distinct periods of axenic *in vitro* culture induce distinct infection rates and immunological responses and correlated this phenotype with a rapid loss of promastigote differentiation capacity. These results highlight the need for a standard operating protocol (SOP) when studying *Leishmania* species.

Citation: Moreira D, Santarém N, Loureiro I, Tavares J, Silva AM, et al. (2012) Impact of Continuous Axenic Cultivation in *Leishmania infantum* Virulence. PLoS Negl Trop Dis 6(1): e1469. doi:10.1371/journal.pntd.0001469

Editor: Shaden Kamhawi, National Institutes of Health, United States of America

Received April 22, 2011; **Accepted** November 20, 2011; **Published** January 24, 2012

Funding: This work was supported by Fundação para a Ciência e Tecnologia (FCT) and FEDER Ciência 2010, project numbers PTDC/SAU-FCF/101017/2008, PTDC/SAU-FCF/100749/2008, program Ciência 2008 and FCT grants SFRH/BDP/48340/2008, SFRH/BD/64528/2009, SFRH/BD/37352/2007. The funders had no role in study design, data collection and analysis, decision to publish, or preparation of the manuscript.

Competing Interests: The authors have declared that no competing interests exist.

* E-mail: rleal@ibmc.up.pt

☯ These authors contributed equally to this work.

¶ These authors also contributed equally to this work.

Introduction

Protozoan parasites of the genus *Leishmania* undergo several developmental transitions during their life cycle. Ingestion of infected macrophages during a blood meal by the sandfly vector leads to the release of intracellular amastigotes into the vector's midgut. This abrupt change in environment induces the transformation into extracellular procyclic promastigotes. The procyclic form within the vector midgut replicates and ultimately transforms into virulent metacyclic promastigotes, in a complex process that encompass parasite migration towards the upper gut of sandfly vector [1]. In laboratory conditions, it is possible to achieve indefinite promastigote growth outside the sandfly using several established media; the procyclic forms correspond to promastigotes in exponential phase of growth that will eventually pass into a stationary phase, a fraction of these stationary parasites differentiates into the metacyclic form, with properties resembling those of sand fly promastigotes [2,3]. Although stationary-phase promastigotes with undefined *in vitro* passages are commonly used without limitations, it has been demonstrated that continuous culture over time induces loss of virulence. In fact, long-term *in vitro* culture of promastigotes was one of the first empirical approaches to efficiently identify parasite virulence genes leading to the experimental development of attenuated strains [4]. Similarly, long-term *in vitro* growth of drug-resistant parasites was suggested to mediate a loss of the resistance phenotype [5]. This can be due to either loss of virulence factors induced by the lack of a survival pressure or due to disadvantageous adaptations to the media resulting in phenomena similar to clonal selection [6]. Either way, alterations in the physiology of the parasite that are induced by long-term growth in these media may lead to misinterpretation and contradictory results. Thus, one must carefully consider the influence of the different laboratorial factors in order to minimize these variables.

The current study is based upon the hypothesis that maintenance of *Leishmania* spp. in axenic *in vitro* culture results in a progressive loss of virulence quickly generating a significant bias towards the experimental data. We have compared the *in vitro* and

Author Summary

Protozoan of the genus *Leishmania* undergo several developmental transitions during its life cycle. *Leishmania* alternates between two morphologically distinct forms, promastigotes (insect stage) and amastigotes (vertebrate stage). Most of the available information about *Leishmania* spp. has been obtained from studying *in vitro* cultured promastigotes, an excellent experimental model for the different developmental stages present in the insect vector. Although promastigotes are grown in a controlled environment, the maintenance of long term culture results in loss of virulence, which can lead to a misinterpretation and often contradictory experimental results. It is then of great interest to unravel the defects arising from sustained axenic parasite culture in laboratory settings. The authors demonstrate a correlation between the maintenance of parasite culture with a growing defect of the promastigote form to differentiate in the mammalian amastigote form. This research provides a biological explanation for the loss of virulence due to sustained parasite culture and discusses the impact for all experimental work done with visceral *Leishmania* species.

in vivo infections and focused on the influence that axenic parasite growth and long-term maintenance can have on *in vitro* infections outcome. Our results demonstrate, for the first time, that the loss of virulence caused by the maintenance of axenic promastigotes in culture can be the result of a growing inability to differentiate into amastigote forms. Moreover, the induction of differentiation from promastigote to amastigote and then back to promastigote forms both *in vitro* and *in vivo* was capable to restore parasite virulence. Overall, our study demonstrated the need of a standard operating protocol (SOP) to study visceral *Leishmania* spp. highlighting the crucial importance for proper control of parasite cultures in studies focusing on the mammalian stage, such as drug development or vaccine trials.

Materials and Methods

Animals and parasites

Ten to twelve-week-old female Balb/c mice were obtained from Instituto de Biologia Molecular e Celular (IBMC; Porto, Portugal) animal facilities. Under laboratory conditions, the animals were maintained in sterile cabinets and allowed food and water *ad libitum*. Animal care and procedures were in accordance with institutional guidelines. All conducted experiments were done in accordance with the IBMC.INEB Animal Ethics Committee and the Portuguese Veterinary Director General guidelines. RS has an accreditation for animal research given from Portuguese Veterinary Direction (Ministerial Directive 1005/92). A cloned line of virulent *L. infantum* (MHOM/MA/67/ITMAP-263) was grown at 26°C in RPMI 1640 medium (Lonza, Swtzerland) supplemented with 10% heat-inactivated Fetal Bovine Serum - FBS (Lonza, Switzerland), 2 mM L-glutamine, 100 U/ml penicillin, 100 mg/ml streptomycin and 20 mM HEPES buffer. The MHOM/MA/67/ITMAP-263 clone (zymodeme MON-1) was originally isolated from the bone marrow of a human patient in Morocco and cloned by micromanipulation. In some experiments, a previously uncharacterized field attenuated *L. infantum* strain was used (species confirmed by pteridine reductase 1 sequencing and currently under ongoing characterization in our laboratory). To minimize the possibility of clonal bias, we have performed three independent recoveries of parasite from Balb/c mice for these experiments. All cultures were initiated at 10^6 parasites/ml and passed each 5 days. Promastigote to amastigote differentiation was achieved by culturing 10^7 stationary phase promastigotes/ml at 37°C in a cell free culture medium (MAA20) [7]. Amastigote to promastigote differentiation was performed by culturing 10^7 axenic amastigotes/ml in complete RPMI medium for 4 days at 27°C. In alternative, spleens of infected Balb/c mice were placed in similar culture conditions for 7 days.

Ficoll density purification assay

Metacyclic promastigotes were purified from cultures with 3, 5 or 9 days or from 5-day cultures with 4, 21 and 31 (P4, P21 and P31) *in vitro* passages by Ficoll density gradient, as previously described [8]. Briefly, 6 ml of 40% Ficoll was overlaid by 6 ml of 10% Ficoll in RPMI base. Then, 6 ml of PBS containing 1.2×10^9 parasites was placed at the top of the Ficoll gradient. The step gradient was centrifuged for 10 minutes at 370 g at room temperature without brake. The metacyclics promastigotes were recovered from the layer between 0% and 10% Ficoll solution. Metacyclic promastigotes, identified by morphological criteria, *i.e.*, short and slender with a long flagellum twice the body length using phase contrast on a Nikon Eclipse 80i.

qPCR analysis

Total RNA was isolated from cells with the Trizol® reagent (Invitrogen, Barcelona, Spain), according to the manufacturer's instructions. Briefly, parasites were washed with ice-cold phosphate-buffered saline (PBS), harvested and homogenized in 800 µl of Trizol by pipetting vigorously. After addition of 160 µl of chloroform, the samples were vortexed, incubated for 2 min at room temperature and centrifuged at 12.000 g, for 15 min, at 4°C. The aqueous phase containing RNA was transferred to a new tube and RNA precipitated with 400 µl of isopropanol for at least 10 min at room temperature. Following a 10 min centrifugation at 12.000 g, the pellet was washed with 1 ml of 75% ethanol and resuspended in 10 µl of 60°C heated RNase free water. The RNA concentration was determined by using a Nanodrop spectrophotometer (Wilmington, DE, USA) and quality was inspected for absence of RNA degradation or genomic DNA contamination, using the Experion RNA StdSens Chips in the ExperionTM automated microfluidic electrophoresis system (BioRad Hercules, CA, USA). RNA was stored at −80°C until use. RT was performed with equal amounts of total extracted RNA (1 µg) obtained from parasites recovered from different experimental conditions by using Superscript II RT (Gibco BRL) and random primers (Stratagene). Real-Time quantitative PCR (qPCR) reactions were run in duplicate for each sample on a Bio-Rad My Cycler iQ5 (BioRad, Hercules, CA, USA). Primers sequences were obtained from Stabvida (Portugal) and thoroughly tested. qPCR was performed in a 20 µl volume containing 5 µl of complementary cDNA (50 ng), 10 µl of 2× Syber Green Supermix (BioRad, Hercules, CA, USA), 2 µl of each primer (250 nM) and 1 µl H_2O PCR grade. Specific primers for histone H4 (forward: 5′ ACACCGAGTATGCG -3′; reverse: 5′- TAGCCGTAGAGGATG-3′; LinJ35.1400 histone H4: Gene ID 5073031), Small Hydrophilic Endoplasmic Reticulum-associated Protein (SHERP) (forward: 5′ CAATGCGCACAACAAGAT -3′; reverse: 5′-TACGAGCCGCCGCTTA-3′; LinJ23.1190 SHERP: Gene ID 5069222) and rRNA45 (forward: 5′CCTACCATGCCGTGTCCTTCTA -3′; reverse: 5′- AACGACCCCTGCAGCAATAC -3′) [9] were used for amplification. After amplification, a threshold was set for each gene and cycle threshold-values (Ct-values) were calculated for all samples. Gene expression changes were analyzed using the built-in iQ5 Optical system software v2.1

(Bio-Rad laboratories, Inc). The results were normalized using as reference gene the rRNA45 rRNA sequence [9].

Viability analysis

Purified and non-purified promastigotes at a density of 10^5/ml were washed and suspended in Annexin V binding buffer. Parasites were incubated at room temperature for 15 minutes with AnnexinV-Cy5 (BD Pharmingen, San Diego, CA) and 7-AAD (Sigma). Parasites subjected to Ultra Violet light during 30 minutes and kept in culture for 4 hours were used as positive control. In amastigote differentiation, 2×10^6 cells with 1 µM of propidium iodide (PI) were used. Data were collected in a BD FACScalibur cytometer (20.000 gated events) and analyzed by FlowJo software (Ashland, OR).

Promastigote CFSE-labeling

Purified and non-purified promastigotes (6×10^7/ml) were washed two times, suspended in PBS containing 5 µM of carboxyfluorescein succinimidyl ester (CFSE) (Invitrogen Molecular probes, Eugene, Oregon) and incubated at 37°C for 10 minutes. Labeled parasites were washed, incubated at 4°C for 5 minutes. Parasites were washed again to remove the exceed CFSE dye and suspended in culture medium before proceeding to macrophage infections. For promastigote to amastigote differentiation and proliferation analysis, 10^7 CFSE-labeled promastigotes were placed on 1 ml of MAA20. Each day, 100 µl of culture added with 1 µM of PI was analyzed by flow cytometry. Axenic amastigotes, identified by the absence of visible flagella and oval shape body, were observed in phase contrast on a Nikon Eclipse 80i.

In vitro macrophage infection

Cell suspension of bone marrow was obtained by flushing the femurs of susceptible Balb/c mice. The cell suspension was cultured in Dulbecco's modified Eagle's medium (DMEM) (Lonza, Switzerland), supplemented with 10% heat-inactivated FBS (Lonza, Switzerland), 2 mM L-glutamine, 100 U/ml penistreptomycin and 1 mM sodium pyruvate. After overnight incubation at 37°C, non-adherent cells were recovered (300 g for 10 min, at room temperature) and cultured in 24-well culture dishes at 2×10^5cells/ml in supplemented DMEM. For bone-marrow derived macrophages (BMMø) differentiation 10% L-929 cell conditioned medium (LCCM) was added at days 0 and 4. At day 7 of culture, CFSE labeled promastigotes were incubated with the BMMø at a 10:1 ratio. After 4 hours, infection was stopped the infection rates were determined at 4, 24 and 48 hours post-infection by a BD FACScalibur cytometer and analyzed by FlowJo software. In some experiments, BMMø were infected and submitted to lipopolysaccharide (LPS) stimulus. Briefly, four hours after infection, infection was stopped and 1 µg/ml of LPS (Sigma) added. Twenty-four hours post-infection, BMMø culture supernatants were collected for cytokine quantification by Enzyme-Linked Immunosorbent Assay - ELISA (TNF-α, IL-12p40, IL-6 and IL-10), using commercial sandwich immunoassay kits (Biolegend and BD, San Diego, CA). Also, BMMø were recovered at 24 hours post-infection for surface co-stimulatory markers analysis. Thus, BMMø were stained with CD40-PE and MHCII-APC at 4°C, during 30 minutes in the dark. The cells were then washed in PBS and suspended in 200 µl of PBS-2% FBS. Data were collected by a BD FACScalibur cytometer and analyzed by FlowJo software.

Animal experiments and parasite quantification

Promastigotes recovered from stationary culture with 4, 21 and 31 *in vitro* passages stationary-culture were collected, washed and suspended in sterile PBS. A volume of 200 µl of PBS containing 10^8 parasites was injected intraperitoneally. Mice of each group were sacrificed at 56 days post-infection. The parasite burden in the spleen and liver was determined by limiting dilution as previously described [10].

Statistical analysis

The data was analyzed using the non-parametric Kruskal-Wallis test followed by Dunn posttest for multiple comparisons when necessary.

Results

The maintenance of *L. infantum* promastigotes in axenic cultures results in diminished virulence

We started by clarifying our *in vitro* model of *L. infantum* infection in relation to the parasite development stage. *L. infantum* parasites recovered from the spleen of infected Balb/c mice were used to start axenic cultures at a 10^6 parasites/ml. The first task was to clearly define the culture time frame in which we can recover stationary parasites. Performing basic cell cycle analysis we excluded the use of the parasites until 2 days of culture because there was still significant active division (Fig. S1A). In order to evaluate the infectivity of stationary *L. infantum*, we used CFSE-labeled stationary promastigotes recovered at 3, 5 and 9 days of *in vitro* growth and BMMø as infection cellular target. Our data demonstrate that 3rd culture-day *L. infantum* promastigotes were significantly less infectious when compared with the 5th and 9th days of culture (Fig. S1B). These differences were already observed at 4 hours post-infection indicating a deficient parasite uptake with 3rd culture-day *L. infantum* promastigotes. Intraphagolysosomal adaptation mechanisms do not appear to be involved in the infection differences since similar infection percentages reductions were found between 4 and 24 hours (15.6 ± 0.4 for 3rd culture-day; 15.0 ± 1.2 for 5th culture-day; 18.1 ± 1.1 for 9th culture-day, when comparing 4 with 24 hours post-infection). Many reports now relate virulence with parasites culture viability [11,12]. In order to lay down the hypothesis that differences in infectivity could be attributed to non-viable parasites, we evaluated the percentages of apoptotic or necrotic parasites by AnnV/7AAD labeling [13]. Nevertheless, no significant differences were found between all culture days (data not shown).

Several groups have already reported that long-term *in vitro* cultivation (more than 12 months) of *Leishmania* spp. leads to a totally avirulent promastigote population [6,14]. According to these findings, we decided to evaluate if the sustained maintenance of *L. infantum* promastigotes in axenic culture at shorter time periods lead to distinct BMMø *in vitro* infection rates with distinctive immunologic phenotypes. In order to accomplish this, we maintained *L. infantum* promastigotes recovered from the spleen of infected mice for 4, 21 and 31 passages, which are equivalent to 20, 105 and 155 division events, considering simple exponential growth. The long-term maintenance of *L. infantum* in culture did not modify the promastigote growth behavior (Fig. 1A) neither their viability that was always superior to 90% (data not shown). Taking into account the distinct infection profiles depicted in Fig. S1B, we chose 5-day culture promastigotes to compare infectivity. When non-purified parasite cultures were used to *in vitro* infect BMMø, a marginal but significant loss of infectivity at 48 hours for P21 and P31 when compared to P4 was observed (Fig. 1B). Metacyclic forms have been understood to be the most infective parasite form [8,15]. Therefore, we enriched the promastigote culture recovered from P4, P21 and P31 in metacyclics recovered by Ficoll density gradient, herein referred as Ficoll-purified

promastigotes [16], and analyzed their infectivity in primary BMMø cells (Fig. 1C). When Ficoll-purified metacyclic promastigotes from these cultures were used, differences were abrogated irrespective of the passage used (Fig. 1C). To confirm the enrichment of metacyclic promastigotes in this fraction and as an internal control of our experimental conditions, we analyzed the expression of two genes, SHERP and histone H4 that can be used to evaluate metacyclogenesis. SHERP gene is found to be up-regulated in infective metacyclic promastigotes [17]. On the other hand, higher expression of histone H4 is associated with exponential phase promastigotes [18]. Indeed, the qPCR analysis demonstrated a significant increase in the SHERP mRNA transcripts in Ficoll-purified promastigotes when compared with non-purified parasite cultures (Fig. S2). These results suggested that the maintenance of *L. infantum* in axenic cultures resulted in a virulence leakage affecting their infectivity probably by the loss of metacyclic parasites. Nevertheless, no significant differences were found between the percentage of Ficoll-purified promastigote recovery from each culture (P4: 6.6±0.1%; P21: 3.4±1.6%; P31: 4.0±0.9%).

Maintenance of long-term axenic *L. infantum* cultures decrease parasite capacity to modulate host cell functions in an inflammatory context

We have above demonstrated that the BMMø infection by *L. infantum* promastigotes depends not only upon the days of culture but is significantly modulated by their axenic culture period. However, we were unable to detect any major changes on macrophage activation status when submitted to *L. infantum* infection (data not shown), which can be explained by the *Leishmania* silent entry mechanism [19]. Therefore, we hypothesized that, when facing an inflammatory stimulus, axenic cultures with high passage number should be less successful in subverting macrophage effector functions being less capable of promoting infection. In order to investigate this hypothesis, we incubated BMMø cells with Ficoll-purified or non-purified parasites from distinct culture periods, which were 4 hours later submitted to LPS stimulation. As before, we observed a decrease of the infection rate with the augmentation of parasite *in vitro* passages (Fig. 2A). This difference was minimized if Ficoll-purified promastigotes were used instead, although it was still statistically significant at 48 hours post-infection (Fig. 2B). LPS stimulation rapidly induces a surface up-regulation of MHCII molecules and co-stimulatory marker CD40. The analysis of these markers demonstrated that high passage number parasites had lower capacities to counteract the LPS activation stimulus (Fig. 2C). Once again, these differences were abrogated when metacyclic-enriched populations were used (Fig. 2C). We have also evaluated the levels of secreted IL-6, IL-12p40 and TNF-α and of the anti-inflammatory IL-10 cytokine. We found that the capacity to control LPS-induced cytokines was variable depending on the number of parasite passages, likely reflecting its distinct virulence. While significant differences were found with P31 parasites in the BMMø secretion levels of IL-6 and TNF-α (Fig. S3A and S3B, respectively), the major modifications were observed at the IL-12p40 and IL-10 levels (Fig. S3C and S3D, respectively). Indeed, P4 parasites were more capable to down-regulate IL-12p40 secretion induced by LPS stimulus, while increasing IL-10 cytokine secretion. This demonstrates that high passage parasites failed to counteract the secretion of pro-inflammatory cytokines induced by LPS in a similar manner. Moreover, if a pro-inflammatory/IL-10 ratio is constructed, a strong correlation was observed between shorter axenic culture maintenance periods and lower pro-inflammatory/IL-10 ratios (Table 1). Since the metacyclic enrichment diminished the differences observed in parasite infection rate and co-stimulatory markers found with stationary-phase promastigotes in different passages, we further investigated whether the cytokine bias was similarly altered. Indeed, the use of Ficoll-purified metacyclic enriched promastigotes, whatever their source, shifted the cytokine environment towards an anti-inflammatory ratio. Although some statistical differences were found between Ficoll-purified promastigotes from different passages, all displayed lower pro-inflammatory/IL-10 ratios when compared with LPS stimulation (Table 1). Overall, these data suggests that when *Leishmania*-infected BMMø are faced with an inflammatory stimulus, there is a specific overall loss of modulatory capacity that seems to be related to the highly immunoregulatory population of metacyclic parasites.

Sustained culture of *L. infantum* promastigotes results in an *in vivo* loss of virulence

We have above demonstrated that sustained axenic parasite culture results in a rapid loss of *in vitro* virulence. Previous reports demonstrating an *in vivo* loss of virulence were based on long-term, usually more than 1 year, parasite maintenance [6,14]. However, we have observed a clear *in vitro* defect after only 21 passages. Therefore, we decided to validate the observed phenotype by performing *in vivo* infections using the susceptible Balb/c mice model. Six weeks after the infectious challenge with non-purified stationary-phase promastigotes recovered from P4, P21 or P31 cultures, a significant difference was found between P4 and high passage number parasite infections in the liver (Fig. 3A). Similarly, we have observed a significant lower parasite burden in the spleen of P31 infected mice that P4 infections (Fig. 3B). These results confirm the observed *in vitro* loss of virulence with parasite culture maintenance.

Loss of virulence originates from inadequate capacity to differentiate into amastigote forms

To elucidate the biological mechanisms that account for the loss of virulence due to long term parasite culture, we started by hypothesizing two major potential reasons: decrease number of metacyclic promastigotes or inadequate differentiation into amastigote forms. The quantification of Ficoll-purified promastigotes described above did not show any significant differences among the passages suggesting similar metacyclic quantities. However, the Ficoll density gradient assay is not a specific and sensible test for the quantification of metacyclic promastigotes in a culture but rather a method for its enrichment. Thus, to evaluate the hypothetical deficit on the generation of metacyclic promastigotes, we have performed *in vitro* infections using BMMø as targets, where we substitute 5% or 10% of non-purified stationary-phase promastigotes from each passage with similar percentages of Ficoll-purified fractions of P4 cultures to increase the total percentage of metacyclic promastigote. As a positive control, we used a naturally attenuated *L. infantum* from which we were unable to recover metacyclic promastigotes. Indeed, although the promastigotes of this *L. infantum* strain presents a similar axenic growth curve (Fig. S4), we were always unable to recover by Ficoll density gradient relevant number of promastigotes (lower that 0.1% of initial culture) from stationary-phase cultures. The quantification of CFSE-positive BMMø demonstrated that increasing the percentage of Ficoll-purified promastigotes did not significantly enhance, at any time point, the percentage of infected BMMø for P4 (Fig. 4A), P21 (Fig. 4B) or P31 (Fig. 4C) promastigotes. However, the opposite was observed with the naturally attenuated strain, where a significant increase of infected

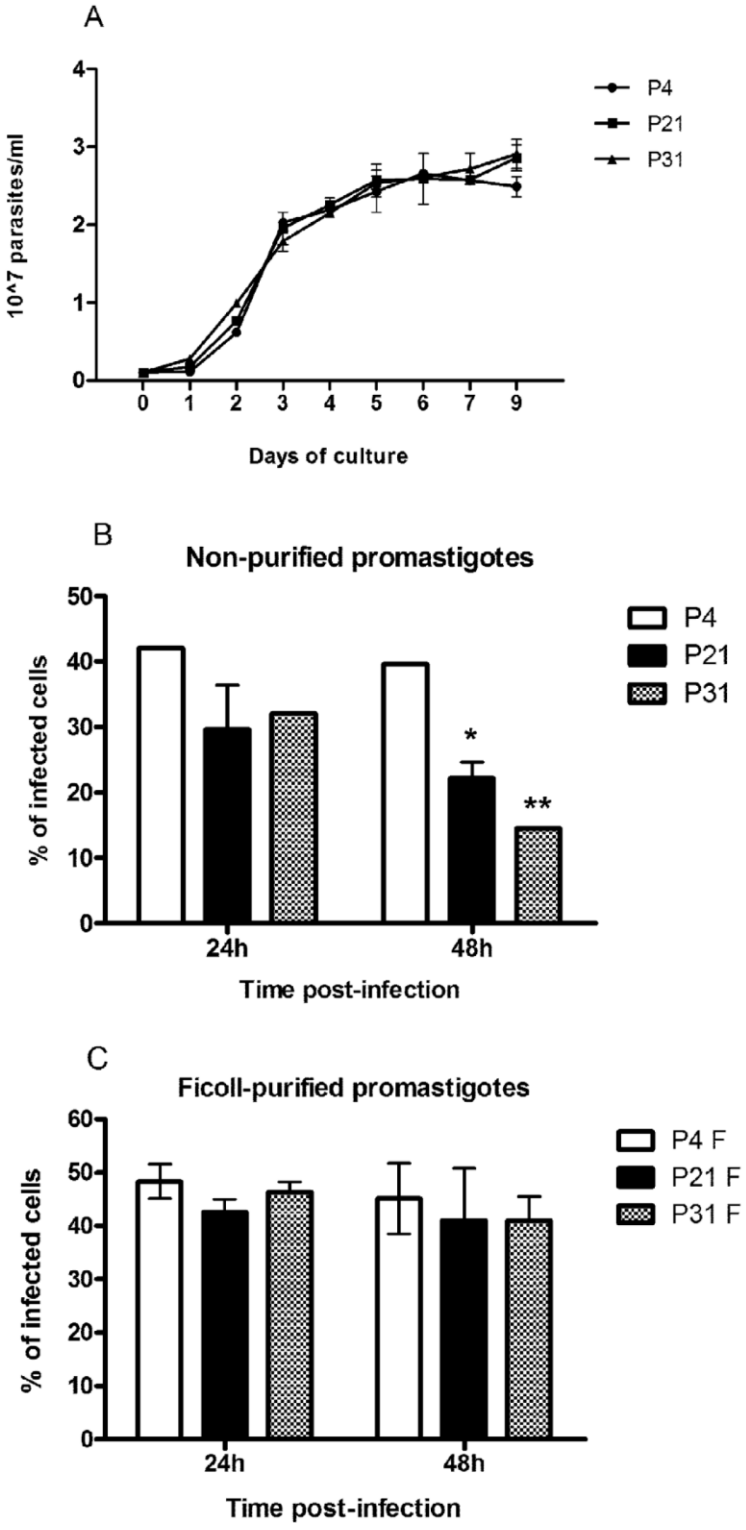
A
10^7 parasites/ml
Days of culture
P4
P21
P31
B
Non-purified promastigotes
% of infected cells
Time post-infection
24h
48h
*
**
P4
P21
P31
C
Ficoll-purified promastigotes
% of infected cells
Time post-infection
24h
48h
P4 F
P21 F
P31 F

Figure 1. Long-term *in vitro* maintenance of *L. infantum* promastigotes does not alter parasite growth. *L. infantum* growth curves were performed by neubauer chamber counting (**A**). BMMø were infected at a 1:10 (cell/parasite) ratio with non-purified (**B**) and Ficoll-purified (**C**) promastigotes labeled with CFSE. Data were acquired by FACScalibur cytometer and analyzed by FlowJo software. Three independent experiments were performed; one representative experiment is shown. The mean and standard deviation are shown. *$P<0,05$, **$P<0,01$, ***$P<0,001$ statistical significance relatively to P4.
doi:10.1371/journal.pntd.0001469.g001

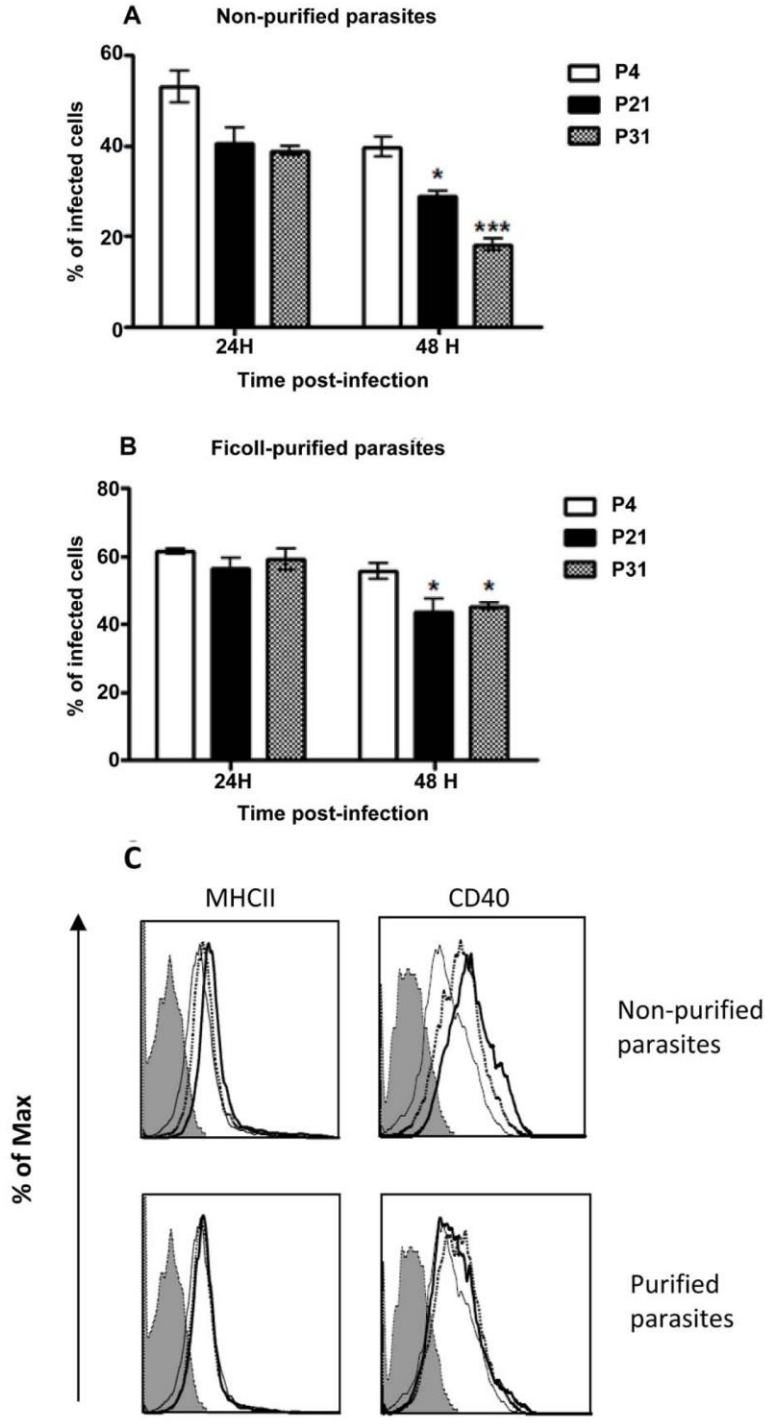

Figure 2. Long-term *in vitro* maintenance of *L. infantum* promastigotes results in loss of virulence *in vitro*. BMMø were submitted to LPS stimulation 4 hours after infection with non-purified (**A**) or Ficoll-purified (**B**) CFSE-labeled promastigotes at a 1:10 (cell/parasite) ratio. The percentage of infected cells was determined by the number of CFSE-positive cells in a FACScalibur cytometer. Expression of MHCII and co-stimulatory molecule CD40 at 24 hours post-infection. Thick line – P31, dotted line - P4, thin line - LPS and shadded hystogram - isotype control (**C**). Two independent experiments were performed; one representative experiment is shown. The mean and standard deviation are shown. *$P<0,05$; **$P<0,01$ statistical significance relatively to P4.
doi:10.1371/journal.pntd.0001469.g002

macrophages was observed at 48 hours post-infection (Fig. 4D). These results demonstrated that the lack of virulence originated from sustained parasite culture cannot be reverted by the addition of enriched-metacyclic fractions. This excludes a defect in the capacity to generate metacyclic promastigotes as the inherent biological cause for the virulence loss. Therefore, we investigated the potential role of inadequate capacity to differentiate in the amastigote form. CFSE-labeled stationary-phase promastigotes recovered from each passage were placed on MAA20 [7] and followed for three days. We evaluated the promastigote differentiation by light microscopy, axenic amastigotes proliferation by CFSE labeling and overall viability by PI staining. All cultures presented axenic amastigotes-like cells after 3 days of differentiation (data not shown). However, high passage number promastigotes displayed a striking decrease of differentiated cells. To quantify these differences, we have assessed the progressive diminution in the intensity of CFSE staining after the differentiation process. In fact, while P4 promastigotes progressively diminished CFSE fluorescence (Fig. 5A and B), high passage number promastigotes exhibit a severe defect to proliferate as amastigotes forms, as observed in both histogram curves (Fig. 5A) and quantification of mean fluorescence CFSE intensity (Fig. 5B). Moreover, this defect was not correlated with a difference on cell death, since similar percentages of viable parasites were found for all cultures during the differentiation process (Fig. 5C). Interestingly, the naturally attenuated strain did not display any significant change to differentiate when compared with P4 promastigotes, suggesting a distinct mechanism of loss of virulence that is not related with the capacity to generate axenic amastigotes.

L. infantum virulence is restored after full differentiation to amastigote forms

It is a current empirical methodology to pass *Leishmania* spp. promastigotes in experimental models to maintain virulence. We have hypothesized that the differentiation process from promastigotes to amastigotes forms would select the most virulent parasites in a heterogeneous culture assuring the continuity of competent and adapted parasites. Therefore, to explore this assumption we have differentiated promastigotes from each passage number in amastigotes both in axenic and *in vivo* conditions. Axenic amastigotes were obtained by differentiating promastigotes in MAA20 medium [7] for a period of 3 days. The viable axenic amastigotes were maintained axenically in culture for 10 days, after which were re-differentiated to promastigotes forms. In alternative, we recovered *L. infantum* parasites from the spleen of infected Balb/c mice by allowing amastigote to promastigote differentiation for a period of 7 days. All these promastigotes were sub-cultured for 4 passages and used to infect BMMø. Remarkably, we did not observe any difference between infections whatever the initial parasite source used (Fig. 6A and B). Again, we used as a control the naturally attenuated *L. infantum* strain. Although an increase of virulence was observed after the differentiation protocol (Fig. 6A), when compared to non-differentiated parasites (Fig. 4D), we observed a general lower infection percentage with the exception of 4 hours post-infection. Overall, these results demonstrate that the defect on virulence due to sustained parasite maintenance can be recovered either by *in vitro* or *in vivo* full differentiation to amastigote and back to promastigotes forms.

Discussion

Visceral *Leishmania* infections studies have been the center of some controversy which can occasionally be traced back to the use of distinct *in vitro* promastigotes culture conditions. The plasticity of the *Leishmania* genome [20] is an important variable to consider when axenic promastigotes are used for *in vitro* or *in vivo* studies. Thus, parasite phenotypic plasticity allows it to adapt to the environment generating discrepancies between studies in different laboratories even when using the same *Leishmania* strain.

Table 1. Ratio of several pro-inflammatory cytokines/IL-10 quantified by ELISA on cell supernatants of 24 hours infected BMMø.

		IL-12p40/IL-10	IL-6/IL-10	TNF-α/IL-10
Non - purified	**LPS**	1,15 ± 0,13	3,46 ± 0,14	6,74 ± 0,40
	LPS P4	0,80± 0,01[a,b]	0,40 ± 0,003*** [a,b]	0,30 ± 0,016*** [a,b]
	LPS P21	2,41 ± 0,04*	1,39 ± 0,10*	1,09 ± 0,06*
	LPS P31	1,95 ± 0,72	1,15 ± 0,13*	0,84 ±0,07*
Ficoll - purified	**LPS P4**	0,18 ± 0,00*** [c,d]	0,15 ± 0,01*** [c,d]	0,09 ± 0,01*** [c,d]
	LPS P21	0,45 ± 0,02***	0,39 ± 0,01**	0,19 ± 0,03**
	LPS P31	0,40 ± 0,01***	0,40 ± 0,01**	0,18 ± 0,01**

The values are expressed in arbitrary units. One representative experiment out of two is shown. The mean and standard deviation are shown.
*P<0.05,
**P<0.01,
***P<0.001 statistical significant relatively to LPS and between passages of culture presented.
[a]*P < 0.05 between LPS P4 and LPS P21,
[b]*P < 0.05 between LPS P4 and LPS P31,
[c]*P < 0.05 between LPS P4 and LPS P21 and,
[d]*P < 0.05 between LPS P4 and LPS P31. All Ficoll-purified ratios are significantly different (at least *P < 0.05) from the related non-purified population.
doi:10.1371/journal.pntd.0001469.t001

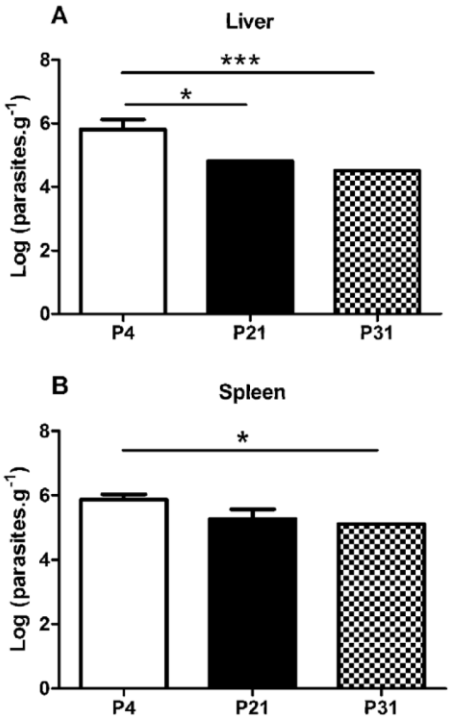

Figure 3. Long-term *in vitro* maintenance of *L. infantum* promastigotes results in loss of virulence *in vivo*. Balb/c mice were infected with stationary phase promastigotes submitted to 4, 21 or 31 successive *in vitro* passages. After 6 weeks post-infection, the parasite load was determined in liver (**A**) and spleen (**B**) by limiting dilution. The mean and standard deviation are shown. *$P<0,05$; **$P<0,01$; ***$P<0,001$.
doi:10.1371/journal.pntd.0001469.g003

In the current work, we have started by investigating in our *in vitro* model of *L. infantum* infection the relation between the parasite development stage and its infectivity. The first step was to discard logarithmic parasites because they are not ultimately responsible for the infection [3], so we used a basic cell cycle analysis to discard multiplying parasites (less than 10% of total population are in S/G2 phase after the third day of culture). This data correlated clearly with basic morphological visualization. Stationary *L. infantum* cultures in day 5 and 9 induced higher BMMø infection rates than day 3 parasites. This difference in infectivity might translate the time frame required for becoming truly metacyclic parasites [21], which was also corroborated by the less amount of metacyclic recovered (data not shown). Since the presence of apoptotic parasites is essential for a virulent inoculum of *Leishmania* promastigotes [22], we decided to quantify the percentage of apoptotic and dead parasites in each case to remove this possible bias from our analysis. In fact, for all time frames tested, the differences in infectivity were not related to apoptotic or dead parasites in the non-purified or Ficoll-purified populations, with culture viability always higher than 90%.

Some authors described that *in vitro* maintenance for long periods constitute an important factor for the loss of virulence in *L. infantum* [14] and *L. major* [6] promastigotes. Nonetheless, this loss of virulence is a reversible phenomenon, since serial passages on susceptible mice allow the parasite to recover a virulence phenotype [23]. In the present study, we complemented the previous observations by comparing the impact of continuous *in vitro* culture on *Leishmania* promastigote virulence and also into the capacity of host macrophage manipulation. Our data clearly demonstrated a loss of *L. infantum* virulence related to the augmentation of *in vitro* culture periods although no modification was observed in the axenic promastigote growth behavior. This significant loss of infectivity was observed as soon as 105 days of successive (21 passages) culture and worsened with parasite maintenance in culture. In fact, 20 passages was the soonest time point where we could have a significant reproducible loss of

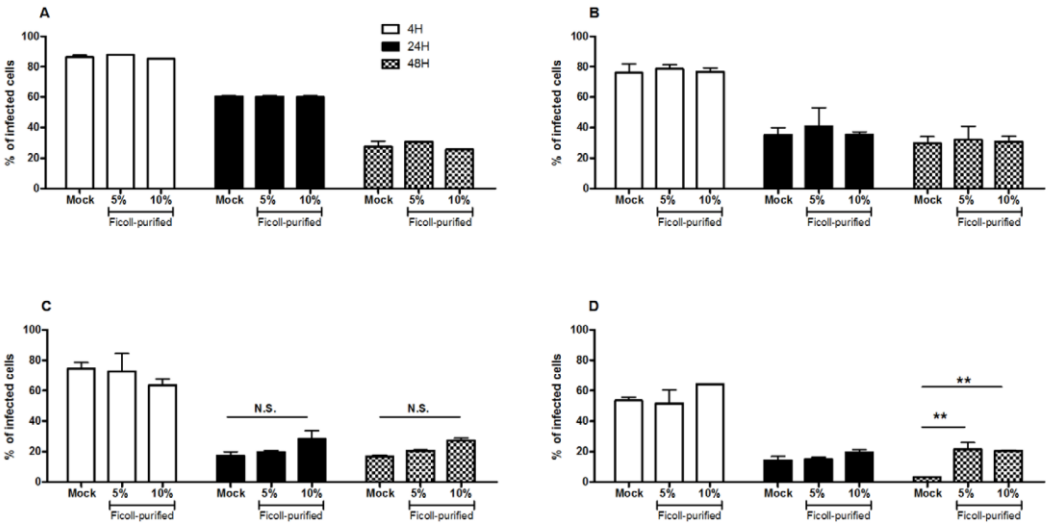

Figure 4. Decreased capacity to infect is not correlated with a loss of metacyclic promastigotes. BMMø were infected at a 1:10 (cell/parasite) ratio with non-purified promastigotes submitted to 4 (**A**), 21 (**B**) or 31 (**C**) successive *in vitro* passages with 5% or 10% of Ficoll-purified parasites or without (Mock). As a control, BMMø were infected with a naturally attenuated strain in the same conditions (**D**). Data were acquired by FACScalibur cytometer and analyzed by FlowJo software. Two independent experiments were performed; one representative experiment is shown. The mean and standard deviation are shown. **$P<0,01$.
doi:10.1371/journal.pntd.0001469.g004

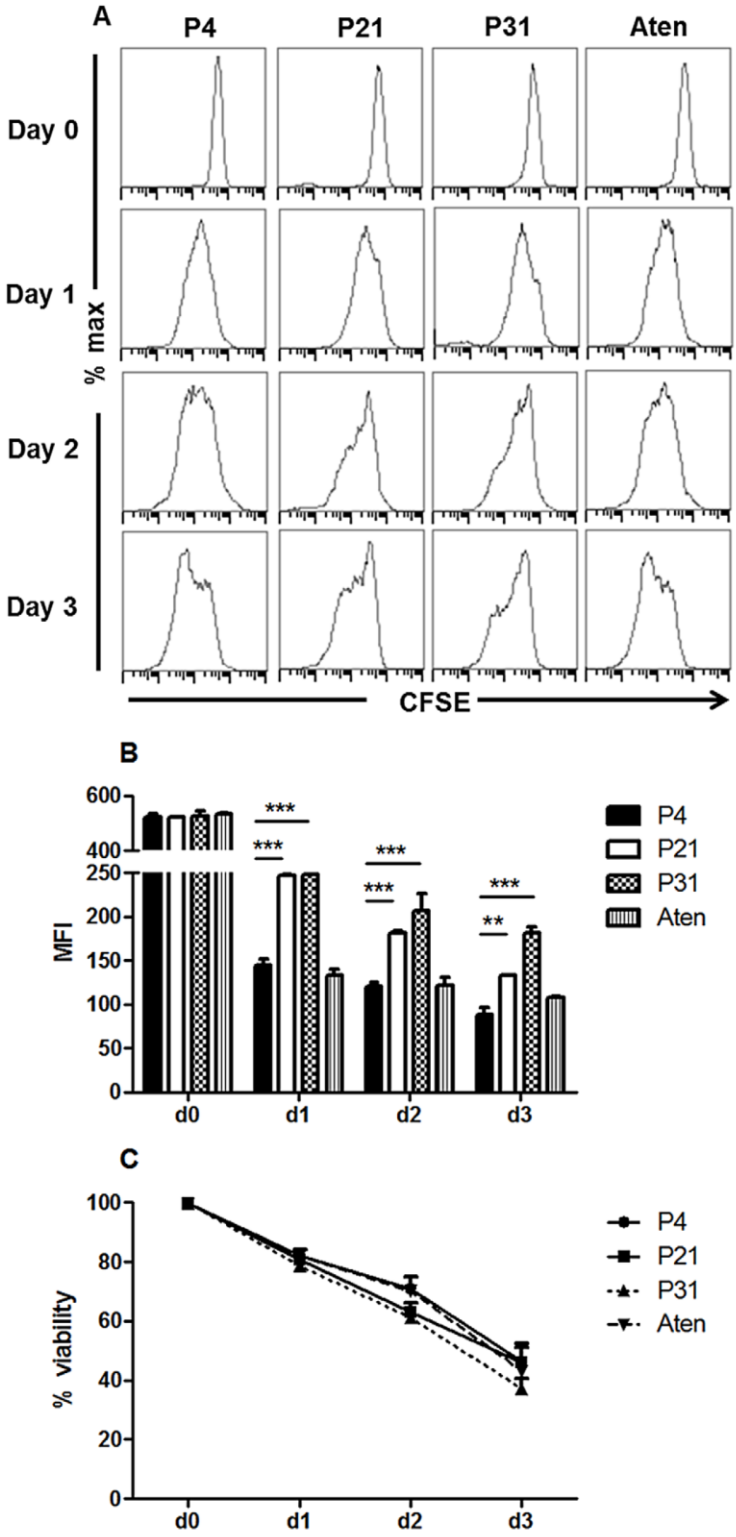
A
P4
P21
P31
Aten
Day 0
Day 1
Day 2
Day 3
% max
CFSE
B
MFI
600
400
250
200
150
100
50
0
***
**
d0
d1
d2
d3
P4
P21
P31
Aten
C
% viability
100
80
60
40
20
0
d0
d1
d2
d3
P4
P21
P31
Aten

Figure 5. Diminished capacity of long-term cultured *L. infantum* promastigotes to differentiate and proliferate as axenic amastigotes. CFSE-labeled non-purified promastigotes submitted to 4, 21 or 31 successive *in vitro* passages or from a field recovered naturally attenuated strain (Aten) were cultured in MAA20 for 3 days to induce differentiation into the amastigote form. (**A**) Parasite multiplication was followed by FACScalibur quantification of CFSE fluorescence. (**B**) For each time, the mean fluorescence intensity (MFI) was calculated. The mean and standard deviation are shown. $^{**}P<0,01$; $^{***}P<0,001$ (**C**) At the same time, parasite viability was followed by propidium iodide (PI) incorporation.
doi:10.1371/journal.pntd.0001469.g005

infection. There is a grey area between passage 9 and passage 20 where we can have variation of infection in a manner that probably reflects the initial parasite inoculum recovered from the mammal. This was also observed after *in vivo* infection where we had a significant decrease in parasite burden after 21 and 31 passages, confirming the *in vitro* observations.

The percentage of metacyclic in a heterogeneous stationary-phase is an important factor in the parasite infectivity since they are significantly more infective than the non-purified population. We used a Ficoll density gradient methodology to enrich the percentage of metacyclic promastigotes [24]. Beyond the morphological changes, during the *Leishmania* spp. differentiation process, modifications also occur in gene expression and in the composition of parasite surface that help to characterize metacyclic promastigotes. Thus, we have evaluated the enrichment of metacyclic promastigotes in the Ficoll-purified fraction by microscopy (data not shown) and through qPCR analysis of the SHERP and histone H4 gene expression. The augmentation of SHERP gene expression in Ficoll-purification supported an enriched metacyclic population. The use of Ficoll-purified promastigotes abolished the differences found among the different passages. Yet, significant differences were found for P21 and P31, at 48 hours post-infection when facing an inflammatory stimulus, showing that the phenomenon of loss of virulence, although less prominent in the metacyclic-enriched parasites, was not restricted to the unpurified culture. Since the differences at the infection level were significant, we examined if there was a potential effect on the macrophage activation status. In the presence of a strong inflammatory stimulus, *L. infantum* is able to suppress certain LPS-derived pro-inflammatory cytokine responses in an active parasite-specific process while it augments the production of some anti-inflammatory cytokines (Silvestre et al, unpublished data). Indeed, the addition of LPS to *Leishmania* spp. infected cells was demonstrated to synergistically induce the secretion of the anti-inflammatory IL-10 cytokine in monocytes [25] and in macrophages [26]. The functional polarization of macrophages into IL-10 producers characterized as M2 cells [27] has been long understood to play a crucial role in the success of parasite infection process [28]. Our results demonstrated a growing defect of high passage parasites to modulate the LPS stimulatory effect. Furthermore, it is clear from the inflammatory profile depicted in Table 1 that metacyclic enriched fractions are always significantly more effective in abrogating a macrophage response to the inflammatory stimuli than their non-purified counterparts

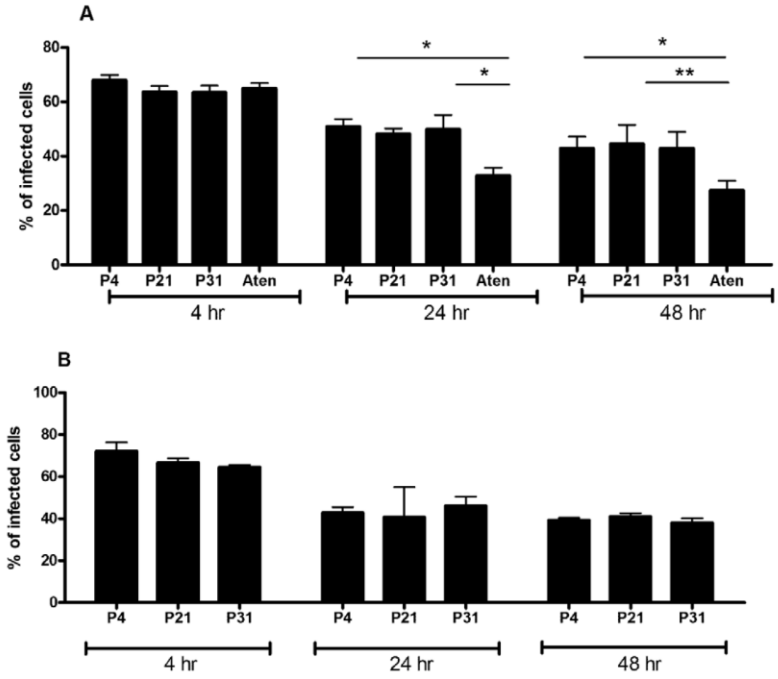

Figure 6. Virulence is recovered after *in vitro* or *in vivo* promastigote-amastigote differentiation process. BMMø were infected at a 1:10 (cell/parasite) ratio with non-purified promastigotes differentiated from *in vitro* axenic amastigotes (**A**) or *ex-vivo* intracellular amastigotes (**B**). As a control, a naturally attenuated strain (Aten) was submitted to the same experimental conditions. Data were acquired by FACScalibur cytometer and analyzed by FlowJo software. Three independent experiments were performed; one representative experiment is shown. The mean and standard deviation are shown. $^{*}P<0,05$; $^{**}P<0,01$.
doi:10.1371/journal.pntd.0001469.g006

revealing the metacyclic parasites as a highly immunomodulatory population with a distinct profile from the non-purified population. There is a distinct and significant loss of immunomodulatory properties from P4 to P21 that becomes stable after P21. This loss of immunomodulatory properties seems reminiscent of phenomenon of transient gene expression similar to what happens under drug pressure [29], being lost upon the terminus of immunological pressure. Indeed, this might be happening in just a few passages of axenic culture. In an attempt to explain the loss of virulence mechanism, some authors referred to a reduction of metallo and cysteine peptidases activity, important for virulence, in *L. braziliensis* [30,31] and in *L. amazonensis* [32] or mitochondrial defects [33] during long-term culture. However, others have been unable to detect any differences in the parasite enzymatic profile with long *in vitro* periods of cultivation [34,35].

One can speculate that the overall loss of immunomodulatory properties over time, and in consequence loss of virulence might reflect a diminution of the number of metacyclic parasites in the population. Although the percentage of Ficoll-recovered promastigotes was quite similar among the three tested passages, these fractions do not constitute a pure metacyclic population, so we decided to complement older passage parasites with Ficoll recovered metacyclic promastigotes to access if the loss of virulence could be reverted by exogenous addition of metacyclic parasites from an early passage. No improvement in the overall infection was observed, although, when these same metacyclic parasites were added to an avirulent field strain, from which we were unable to recover metacyclics, there was an improvement on the infection.

Another possibility to explain the virulence loss was the possibility of a defective promastigote to amastigote differentiation. Our data clearly demonstrated that high passage number promastigotes displayed decrease capacity in differentiating, which was not correlated with decreased cellular viability. This incapacity translates into fewer parasites able to differentiate leading to a less capable population to face host cell response. Ultimately, this results in lower parasite burdens *in vitro* and *in vivo*. Moreover, these axenic amastigotes recovered after differentiation were morphologically indistinguishable and retained similar growth capacity (data not shown). To ultimately state and confirm the importance of promastigote to amastigote differentiation as a driving selective force for virulence, we showed that parasites passed through the amastigote stage, either *in vitro* or *in vivo*, revert the loss of virulence. This fact in conjunction with the remarkable loss of immunomodulatory properties leads to the early loss of virulence detected in our model.

We do not rule out metacyclogenesis related defects as a driving force for a virulence. In relation to metacyclogenesis it has been argued that a successful and complete differentiation is dependent on the presence of large amount of metacyclic promastigotes [36]. However, it is still not clear whether this process is an essential step in the differentiation *in vitro*, since procyclic promastigotes appear to differentiate with equal efficiency as metacyclics [37–40]. Indeed, our results with the naturally attenuated strain support this notion. Our data do not rule out that P21 or P31 metacyclic promastigotes could not display any sort of biochemical or protein expression defect that may impact the differentiation process. Similarly, we cannot reject the idea of longer periods of sustained cultured originating defective metacyclic cultures. However, during our study, the loss of virulence was related to a specific defect on promastigote to amastigote differentiation.

Overall, our data demonstrated that the loss of virulence is linked with decreased capacity to differentiate in amastigote forms, which may probably be originated from the absence of a complete life cycle. Therefore, special care must be taken when performing experiments with axenic *Leishmania* promastigotes. The systematic and rigorous control of *Leishmania* culture conditions should be considered as a keystone for each experimental protocol. The differences found in infectivity accompanied by disparate effects at the macrophage activation levels point to significant differences at biochemical and structural level, enlarging the effects of careless parasite maintenance to other experimental fields. This information is extremely relevant especially for those developing new drug and vaccine approaches. In such cases the immune response to the parasite is the essence of the experimental procedure.

Supporting Information

Figure S1 Cell cycle analysis and *in vitro* virulence of *L. infantum* recovered in distinct culture days. *L. infantum* promastigotes were cultured at a 10^6/ml. Each day, 2×10^6 promastigotes were recovered and the cell cycle analyzed by PI staining (**A**). BMMø were incubated with non-purified CFSE labeled *L. infantum* promastigotes at a ratio of 1:10 (cell/parasite). The percentage of infected cells was obtained by quantifying the number of CFSE-positive cells (**B**). Data were acquired at 4 and 24 hours post-infection in a FACScalibur cytometer and analysed by FlowJo software. Three independent experiments were performed; one representative experiment is shown. The mean and standard deviation are shown. *$P<0,05$, **$P<0,01$ statistical significance relatively to 3rd day of parasite growth.
(TIF)

Figure S2 Indirect quantification of metacyclic promastigotes in heterogenous and Ficoll-purified cultures by gene transcription analysis. Transcription profile of SHERP and Histone H4 genes obtained by qPCR, for non-purified and Ficoll-purified promastigotes. Normalizations were made against the reference gene rRNA45. Three independent experiments were performed, each performed in duplicate; one representative experiment is shown. The mean and standard deviation are shown. *$P<0,05$.
(TIF)

Figure S3 Long-term cultured *L. infantum* promastigotes show decrease capacity to modulate an inflammatory stimulus *in vitro*. BMMø were submitted to LPS stimulation 4 hours after infection with non-purified promastigotes. The levels of IL-6 (**A**), TNF-α (**B**), IL-12p40 (**C**) and IL-10 (**D**) were quantified 24 hours post-infection on BMMø supernatants by ELISA. Three independent experiments were performed; one representative experiment is shown. The mean and standard deviation are shown. *$P<0,05$; **$P<0,01$; ***$P<0,001$ statistical differences relative to LPS unless depicted by a bar.
(TIF)

Figure S4 Naturally attenuated *L. infantum* strain has a similar axenic growth in comparison to WT strain. *L. infantum* growth curves were performed by neubauer chamber counting. The mean and standard deviation are shown.
(TIF)

Author Contributions

Conceived and designed the experiments: NS RS. Performed the experiments: DM NS AMA RS. Analyzed the data: DM NS AO RS ACdS. Contributed reagents/materials/analysis tools: IL JT AMS. Wrote the paper: DM NS RS.

References

1. Bates PA (2007) Transmission of *Leishmania* metacyclic promastigotes by phlebotomine sand flies. Int J Parasitol 37: 1097–1106.
2. Sacks DL, Perkins PV (1984) Identification of an infective stage of *Leishmania* promastigotes. Science 223: 1417–1419.
3. Sacks DL, Perkins PV (1985) Development of infective stage *Leishmania* promastigotes within phlebotomine sand flies. Am J Trop Med Hyg 34: 456–459.
4. Mitchell GF, Handman E, Spithill TW (1984) Vaccination against cutaneous leishmaniasis in mice using nonpathogenic cloned promastigotes of *Leishmania major* and importance of route of injection. Aust J Exp Biol Med Sci 62(Pt 2): 145–153.
5. Hadighi R, Mohebali M, Boucher P, Hajjaran H, Khamesipour A, et al. (2006) Unresponsiveness to Glucantime treatment in Iranian cutaneous leishmaniasis due to drug-resistant *Leishmania tropica* parasites. PLoS Med 3: e162.
6. Segovia M, Artero JM, Mellado E, Chance ML (1992) Effects of long-term in vitro cultivation on the virulence of cloned lines of *Leishmania major* promastigotes. Ann Trop Med Parasitol 86: 347–354.
7. Sereno D, Lemesre JL (1997) Axenically cultured amastigote forms as an in vitro model for investigation of antileishmanial agents. Antimicrob Agents Chemother 41: 972–976.
8. Yao C, Chen Y, Sudan B, Donelson JE, Wilson ME (2008) *Leishmania chagasi*: homogenous metacyclic promastigotes isolated by buoyant density are highly virulent in a mouse model. Exp Parasitol 118: 129–133.
9. Ouakad M, Bahi-Jaber N, Chenik M, Dellagi K, Louzir H (2007) Selection of endogenous reference genes for gene expression analysis in *Leishmania major* developmental stages. Parasitol Res 101: 473–477.
10. Silvestre R, Cordeiro-Da-Silva A, Santarem N, Vergnes B, Sereno D, et al. (2007) SIR2-deficient *Leishmania infantum* induces a defined IFN-gamma/IL-10 pattern that correlates with protection. J Immunol 179: 3161–3170.
11. Wanderley JL, Moreira ME, Benjamin A, Bonomo AC, Barcinski MA (2006) Mimicry of apoptotic cells by exposing phosphatidylserine participates in the establishment of amastigotes of *Leishmania (L) amazonensis* in mammalian hosts. J Immunol 176: 1834–1839.
12. Wanderley JL, Pinto da Silva LH, Deolindo P, Soong L, Borges VM, et al. (2009) Cooperation between apoptotic and viable metacyclics enhances the pathogenesis of Leishmaniasis. PLoS One 4: e5733.
13. El-Fadili AK, Zangger H, Desponds C, Gonzalez IJ, Zalila H, et al. (2010) Cathepsin B-like and cell death in the unicellular human pathogen *Leishmania*. Cell Death Dis 1: e71.
14. Grimm F, Brun R, Jenni L (1991) Promastigote infectivity in *Leishmania infantum*. Parasitol Res 77: 185–191.
15. Louassini M, Adroher FJ, Foulquie MR, Benitez R (1998) Investigations on the in vitro metacyclogenesis of a visceral and a cutaneous human strain of *Leishmania infantum*. Acta Trop 70: 355–368.
16. Spath GF, Beverley SM (2001) A lipophosphoglycan-independent method for isolation of infective *Leishmania* metacyclic promastigotes by density gradient centrifugation. Exp Parasitol 99: 97–103.
17. Knuepfer E, Stierhof YD, McKean PG, Smith DF (2001) Characterization of a differentially expressed protein that shows an unusual localization to intracellular membranes in *Leishmania major*. Biochem J 356: 335–344.
18. Soto M, Quijada L, Alonso C, Requena JM (1997) Molecular cloning and analysis of expression of the *Leishmania infantum* histone H4 genes. Mol Biochem Parasitol 90: 439–447.
19. Silvestre R, Santarem N, Tavares J, Silva AM, Cordeiro-Da-Silva A (2009) Recognition of *Leishmania* parasites by innate immunity. Immun, Endoc & Metab Agents in Med Chem 9: 106–127.
20. Bastien P, Blaineau C, Pages M (1992) *Leishmania*: sex, lies and karyotype. Parasitol Today 8: 174–177.
21. Sadlova J, Price HP, Smith BA, Votypka J, Volf P, et al. (2010) The stage-regulated HASPB and SHERP proteins are essential for differentiation of the protozoan parasite *Leishmania major* in its sand fly vector, Phlebotomus papatasi. Cell Microbiol 12: 1765–1779.
22. van Zandbergen G, Bollinger A, Wenzel A, Kamhawi S, Voll R, et al. (2006) *Leishmania* disease development depends on the presence of apoptotic promastigotes in the virulent inoculum. Proc Natl Acad Sci U S A 103: 13837–13842.
23. Katakura K, Kobayashi A (1985) Enhancement of infectivity of *Leishmania donovani* promastigotes by serial mouse passages. J Parasitol 71: 393–394.
24. Saraiva EM, Pinto-da-Silva LH, Wanderley JL, Bonomo AC, Barcinski MA, et al. (2005) Flow cytometric assessment of *Leishmania* spp metacyclic differentiation: validation by morphological features and specific markers. Exp Parasitol 110: 39–47.
25. Meddeb-Garnaoui A, Zrelli H, Dellagi K (2009) Effects of tropism and virulence of *Leishmania* parasites on cytokine production by infected human monocytes. Clin Exp Immunol 155: 199–206.
26. Lapara NJ, 3rd, Kelly BL (2010) Suppression of LPS-induced inflammatory responses in macrophages infected with *Leishmania*. J Inflamm (Lond) 7: 8.
27. Mantovani A, Sica A, Sozzani S, Allavena P, Vecchi A, et al. (2004) The chemokine system in diverse forms of macrophage activation and polarization. Trends Immunol 25: 677–686.
28. Cunningham AC (2002) Parasitic adaptive mechanisms in infection by *leishmania*. Exp Mol Pathol 72: 132–141.
29. Ubeda JM, Legare D, Raymond F, Ouameur AA, Boisvert S, et al. (2008) Modulation of gene expression in drug resistant *Leishmania* is associated with gene amplification, gene deletion and chromosome aneuploidy. Genome Biol 9: R115.
30. Bates PA, Robertson CD, Coombs GH (1994) Expression of cysteine proteinases by metacyclic promastigotes of *Leishmania mexicana*. J Eukaryot Microbiol 41: 199–203.
31. Lima AK, Elias CG, Souza JE, Santos AL, Dutra PM (2009) Dissimilar peptidase production by avirulent and virulent promastigotes of *Leishmania braziliensis*: inference on the parasite proliferation and interaction with macrophages. Parasitology 136: 1179–1191.
32. Chaudhuri G, Chang KP (1988) Acid protease activity of a major surface membrane glycoprotein (gp63) from *Leishmania mexicana* promastigotes. Mol Biochem Parasitol 27: 43–52.
33. Nasyrova RM, Kallinikova VD, Vafakulov S, Nasyrov F (1993) [The virulence and cytochemical properties of *Leishmania major* during long-term cultivation]. Parazitologiia 27: 233–241.
34. Cuervo P, Santos AL, Alves CR, Menezes GC, Silva BA, et al. (2008) Cellular localization and expression of gp63 homologous metalloproteases in *Leishmania (Viannia) braziliensis* strains. Acta Trop 106: 143–148.
35. Soares RP, Macedo ME, Ropert C, Gontijo NF, Almeida IC, et al. (2002) *Leishmania chagasi*: lipophosphoglycan characterization and binding to the midgut of the sand fly vector Lutzomyia longipalpis. Mol Biochem Parasitol 121: 213–224.
36. Cysne-Finkelstein L, Temporal RM, Alves FA, Leon LL (1998) *Leishmania amazonensis*: long-term cultivation of axenic amastigotes is associated to metacyclogenesis of promastigotes. Exp Parasitol 89: 58–62.
37. Barak E, Amin-Spector S, Gerliak E, Goyard S, Holland N, et al. (2005) Differentiation of *Leishmania donovani* in host-free system: analysis of signal perception and response. Mol Biochem Parasitol 141: 99–108.
38. Goyard S, Segawa H, Gordon J, Showalter M, Duncan R, et al. (2003) An in vitro system for developmental and genetic studies of *Leishmania donovani* phosphoglycans. Mol Biochem Parasitol 130: 31–42.
39. Debrabant A, Joshi MB, Pimenta PF, Dwyer DM (2004) Generation of *Leishmania donovani* axenic amastigotes: their growth and biological characteristics. Int J Parasitol 34: 205–217.
40. Saar Y, Ransford A, Waldman E, Mazareb S, Amin-Spector S, et al. (1998) Characterization of developmentally-regulated activities in axenic amastigotes of *Leishmania donovani*. Mol Biochem Parasitol 95: 9–20.

The American Journal of Pathology, Vol. 177, No. 6, December 2010

DOI: 10.2353/ajpath.2010.100367

Immunopathology and Infectious Diseases

Activation of Phosphatidylinositol 3-Kinase/Akt and Impairment of Nuclear Factor-κB

Molecular Mechanisms Behind the Arrested Maturation/Activation State of Leishmania infantum*-Infected Dendritic Cells*

Bruno Miguel Neves,*† Ricardo Silvestre,‡ Mariana Resende,‡ Ali Ouaissi,‡§ Joana Cunha,‡ Joana Tavares,‡¶ Inês Loureiro,‡ Nuno Santarém,‡ Ana Marta Silva,‡ Maria Celeste Lopes,*† Maria Teresa Cruz,*† and Anabela Cordeiro da Silva‡¶

From the Faculdade de Farmácia, and Centro de Neurociências e Biologia Celular,† Universidade de Coimbra, Coimbra, Portugal; the Parasite Disease Group,‡ and Faculdade de Farmácia,¶ Instituto de Biologia Molecular e Celular, Universidade do Porto, Porto, Portugal; and INSERM,§ UMR CNRS 5235, Université Montpellier II, Montpellier, France*

Understanding the complex interactions between *Leishmania* and dendritic cells (DCs) is central to the modulation of the outcome of this infection, given that an effective immune response against *Leishmania* is dependent on the successful activation and maturation of DCs. We report here that *Leishmania infantum* promastigotes successfully infect mouse bone marrow-derived DCs without triggering maturation, as shown by a failure in the up-regulation of CD40 and CD86 expression, and that parasites strongly counteract the lipopolysaccharide-triggered maturation of DCs. A small increase in interleukin (IL)-12 and IL-10 transcription and secretion and a decrease in IL-6 were observed in infected cells. This arrested DC maturation state is actively promoted by parasites because heat-killed or fixed parasites increased cytokine and costimulatory molecule expression. At a molecular level, *L. infantum* rapidly induced activation of phosphatidylinositol 3-kinase/Akt and extracellular signal-regulated kinase 1/2, whereas no effect was observed in the c-Jun N-terminal kinase and p38 mitogen-activated protein kinase proinflammatory pathways. Moreover, parasites actively promoted cleavage of the nuclear factor-κB p65^{RelA} subunit, causing its impairment. The blockade of phosphatidylinositol 3-kinase/Akt by either treatment of bone marrow-derived DCs with wortmannin or transfection with an Akt dominant-negative mutant resulted in a strong decrease in infection rates, revealing for the first time a crucial role of this pathway on *Leishmania* engulfment by DCs. Overall, our data indicate that activation of Akt and impairment of nuclear factor-κB are responsible for immunogenicity subversion of *L. infantum*-infected DCs. ***(Am J Pathol 2010, 177:2898–2911; DOI: 10.2353/ajpath.2010.100367)***

Visceral leishmaniasis is a vector-borne parasite infection caused by species of the genus *Leishmania* (*Leishmania donovani* and *Leishmania infantum*/*Leishmania chagasi*) that disseminate hematogenously, infecting mononuclear phagocytic cells in the spleen, liver, lymph nodes, and bone marrow.[1] A protective response against all forms of leishmaniasis is dependent on interleukin (IL)-12 production by antigen-presenting cells, which leads to the differentiation and proliferation of $CD4^+$ Th_1 cells with interferon-γ and tumor necrosis factor (TNF)-α production.[2–4] Although *Leishmania*-infected neutrophils are believed to

Supported by Fundação para a Ciência e a Tecnologia (FCT) and Fundo Europeu de Desenvolvimento Regional (FEDER) Ciência 2010 (project numbers PTDC/SAU-FCF/67351/2006 and PTDC/SAU-FCF/101017/2008 and FCT grants SFRH/BD/30563/2006, SFRH/BD/48626/2008, SFRH/BDP/48340/2008, SFRH/BD/64528/2009, SFRH/BD/37352/2007, and SFRH/BD/28316/2006).

Accepted for publication August 5, 2010.

Supplemental material for this article can be found on *http://ajp.amjpathol.org*.

Address reprint requests to Bruno Neves, Ph.D., Centro de Neurociências e Biologia Celular, Universidade de Coimbra, Azinhaga de Santa Comba, Celas 3000-548 Coimbra, Portugal. E-mail: neves_bruno@sapo.pt.

constitute one of the earliest sources of IL-12 in resistant C57BL/6 mice,[5] it is currently believed that dendritic cells (DCs) are the critical source of early IL-12 production after *Leishmania* infection.[6,7]

DCs are specialized antigen-presenting cells that play a crucial role in driving adaptive immune responses.[8] Depending on their maturation/activation state, DCs have the ability to polarize distinct T-cell subsets (T-helper cells [Th_1, Th_2, and Th_{17}], regulatory T cells, and cytotoxic T cells), controlling the outcome of an infection. Recently, research focused on the role played by DCs during leishmaniasis and DC-based vaccination for the control of this infection has gained special attention. Although there is consensus that DCs play a critical role in the progression or resolution of leishmaniasis (reviewed in 9, 10), the data obtained in these studies have often generated conflicting results. Early *in vitro* experiments demonstrated that on phagocytosis of *Leishmania major* promastigote or amastigote, DCs became activated as determined by increased expression levels of costimulatory surface markers, IL-12p40 secretion, and their potential for priming primary $CD4^+$-T lymphocytes.[11] Nevertheless, studies performed with New World cutaneous and mucocutaneous *Leishmania* species are more controversial, because although *Leishmania braziliensis* uptake was shown to ultimately induce DC maturation,[12,13] infection with *Leishmania amazonensis* or *Leishmania mexicana* parasites dramatically impaired the differentiation and function of DCs, irrespective of the parasite form used.[14–17] Furthermore, the role played by DCs during visceral leishmaniasis is still poorly understood and needs further elucidation. A few studies have demonstrated that DC infection with visceral *Leishmania* species triggers, within minutes, the release of preformed membrane-associated IL-12p70.[18] Nevertheless, the production of IL-12p40 was shown to be weak and transient[6] and occurs in the absence of DC maturation.[19–21]

To date, the early molecular mechanisms by which *Leishmania* parasites control the DC activation/maturation state and thus their immunostimulatory abilities remain unclear. The DC maturation process is a well coordinated series of events tightly controlled by the balance of particular intracellular signaling pathways. Among these pathways, the nuclear factor-κB (NF-κB) signaling system is considered the master regulator of innate immunity and inflammatory responses and phosphoinositide 3-kinase (PI3K) has been regarded as an internal safety mechanism to control extensive inflammation, by limiting IL-12 production and enhancing the synthesis of the anti-inflammatory IL-10. Likewise the three primary kinases members of the mitogen-activated protein kinase (MAPK) family, p38, c-Jun N-terminal kinase (JNK), and extracellular signal regulated kinase (ERK), have been implicated in the regulation of several aspects of phenotypic and functional maturation of DCs, as well as cytokine production.[22]

Therefore, in the present study, we examined the ability of mouse bone marrow-derived DCs to phagocyte *L. infantum* promastigotes and assessed the effects of infection on the three major MAPKs pathways and the PI3K/Akt and the NF-κB signaling cascades. The impact of early infection on the DC phenotype and cytokine release profile was also analyzed. In addition, we investigated the ability of the parasite to subvert the lipopolysaccharide (LPS)-triggered DC maturation/activation process. Finally, we used specific inhibitors to understand the relevance of each pathway in the *L. infantum* promastigote-induced events in DCs. Our results clearly demonstrate that the uptake of visceral *L. infantum* promastigotes actively arrests the activation/maturation of bone-marrow DCs, thus promoting a silent infection through the biased modulation of PI3K/Akt and NF-κB pathways.

Materials and Methods

Materials

LPS from *Escherichia coli* (serotype 026:B6) was obtained from Sigma Chemical Co. (St. Louis, MO). SB203580 and SP600125 were from Calbiochem (San Diego, CA), PD098059 was obtained from RBI (Natick, MA) and wortmannin was from Sigma Chemical Co.

Animals and Parasites

Ten- to 12-week-old female BALB/c mice were obtained from Instituto de Biologia Molecular e Celular (Porto, Portugal) animal facilities. Animal care was in accordance with institutional guidelines. A cloned line of virulent *L. infantum* (MHOM/MA/67/ITMAP-263) was maintained by weekly subpassages (less than 10) in complete RPMI 1640 (RPMIc) supplemented with 10% heat-inactivated fetal bovine serum, 100 U/ml penicillin, 100 mg/ml streptomycin, and 2 mmol/L HEPES (BioWhittaker, Walkersville, MD). In some experiments, the cloned line of virulent *L. infantum* promastigotes expressing monomeric green fluorescent protein (GFP) was used. *L. infantum* recombinant parasites overexpressing GFP genes and the neomycin phosphotransferase gene (*neo*) as a dominant positive selection marker conferring resistance to G418, were generated by transfection of the expression vector pSPαNEOαGFP. Expression of the GFP and *neo* genes in vector pSPαNEOαGFP is driven by the α-tubulin intergenic region of *Leishmania enriettii*.[23] Transfection experiments were done as described elsewhere,[24] and transfectants were selected and grown in the presence of G418 (100 μg/ml).

Bone Marrow-Derived Dendritic Cells

Bone marrow-dendritic cells (BMDCs) were derived as described previously.[25] In brief, bone marrow from femurs and tibiae of 10- to 12-week-old BALB/c mice were flushed with RPMI 1640, using syringes and 25-gauge needles. The tissue was resuspended, and BMDCs were obtained by seeding 5×10^6 bone marrow cells in 25 ml of RPMIc supplemented with 50 μmol/L 2-mercaptoethanol (Sigma Chemical Co.) and 200 U/ml of granulocyte macrophage–colony-stimulating factor (GM-CSF) (PeproTech, Rocky Hill, NJ) (DC medium).

Cells were cultured at 37°C and 5% CO_2 for 3 days, after which the same amount of DC medium was added to each flask. At days 6 and 8, half of the culture supernatant was collected and centrifuged, and the cell pellet was resuspended in the same amount of fresh DC medium and put back into the original flasks. At day 10, the same procedure was performed but with use of only 100 U/ml of GM-CSF. BMDCs obtained after 12 days of culture displayed a phenotype highly enriched in $CD11c^+$ cells (~95%).

In Vitro *Stimulation and Infection of Dendritic Cells*

For *in vitro* infection, 12-day nonadherent BMDCs were seeded at 1×10^6 cells/ml of RPMIc containing 3 U/ml of GM-CSF in 24-well plates (for flow cytometry and enzyme-linked immunosorbent assay [ELISA] assays), at 2×10^5/200 μl in chamber slides (for infection quantification) or at 2×10^6cells/ml in 6-well plates (for Western blots and quantitative PCR assays). After an overnight incubation period, stationary-phase *L. infantum* promastigotes were added to the culture at an infection ratio of 10:1 (parasites/cell). Parallel experiments were also performed using polystyrene beads (FACS AccuDrop beads, 6 μm in diameter) and heat-killed (30 minutes at 56°C) or fixed parasites (10 minutes in glutaraldehyde). For Western blot assays, the cells were exposed to parasites for 10, 30, or 60 minutes and then immediately lysed in radioimmunoprecipitation buffer. For further experiments noninternalized parasites were removed by gently washing after 4 hours of infection, and fresh RPMIc supplemented with 3 U/ml of GM-CSF was added to the wells. Cells were immediately recovered or maintained for 24 hours (for flow cytometry and ELISA assays). When specific inhibitors of the different signaling pathways were used (500 nmol/L wortmannin, 20 μmol/L SB203580, 20 μmol/L PD098059, 2 μmol/L SP600125, or 10 μmol/L BAY 11-7082), cells were pretreated with the respective drugs for 1 hour and then submitted to infection as described above. BMDCs stimulated with LPS (1 μg/ml) were used as a positive control for DC activation/maturation. When indicated as LPS + infection, the cells were simultaneously exposed to LPS and parasites for 30 minutes (for Western blot assays) or pretreated with LPS for 1 hour and then infected (LPS → infection) for the indicated times (for flow cytometry and ELISA assays).

Determination of Percentage of Infected Cells

BMDCs cultured in chamber slides (Lab-Tek Chamber Slides, Nunc GmbH&Co. KG, Wiesbaden, Germany) were infected for a 4-hour period at a 10:1 (parasites/cell) ratio. After three washing steps, cells were immediately prepared or maintained in culture for additional 12, 24, 48, or 72 hours. Afterward, BMDCs were washed with PBS, fixed with 2% paraformaldehyde for 30 minutes and finally permeabilized with 0.1% (v/v) Triton X-100 in PBS for 10 minutes at 4°C. Cells were then mounted in Vectashield with the nuclear label 4′,6-diamidino-2-phenylindole (Vector Laboratories, Burlingame, CA) and analyzed with a fluorescent microscope (Axioskop-Carl Zeiss, Jena, Germany) at ×1000 magnification. Images were captured with a digital camera (Spot 2, Diagnostic Instruments, Sterling Heights, MI) and the software Spot 3.1 (Diagnostic Instruments). In some experiments, the percentage of infected BMDCs was determined by flow cytometry evaluation of GFP-positive cells on infection with GFP-recombinant parasites. In brief, BMDCs were infected for a 4-hour period at a 10:1 (parasites/cell) ratio and after washing steps were analyzed in a FACScan cytometer equipped with FlowJo software (TreeStar Inc., Ashland, OR) to evaluate BMDCs presenting a GFP-positive signal.

Cell Lysate Preparation

Cells were washed in ice-cold PBS and harvested in radioimmunoprecipitation lysis buffer (50 mmol/L Tris-HCl, pH 8.0, 1% Nonidet P-40, 150 mmol/L NaCl, 0.5% sodium deoxycholate, 0.1% SDS, 2 mmol/L EDTA, and 1 mmol/L dithiothreitol) freshly supplemented with protease and phosphatase inhibitor cocktails (Roche, Mannheim, Germany). The nuclei and the insoluble cell debris were removed by centrifugation at 12,000 × *g* for 10 minutes at 4°C. The extracts were collected and used as total cell lysates. Nuclear and cytosolic fractions were prepared using the Nuclear Extract Kit (Active Motif Inc., Carlsbad, CA) according to the manufacturer's instructions. The protein concentration was determined using the bicinchoninic acid method, and the cell lysates were denatured at 95°C for 5 minutes in sample buffer (0.125 mmol/L Tris, pH 6.8, 2% w/v SDS, 100 mmol/L dithiothreitol, 10% glycerol, and bromphenol blue) for further use in Western blot analysis.

Western Blot Analysis

Western blots were performed to evaluate the levels of phospho-IκB-α, IκB-α, $p65^{RelA}$, phospho-ERK1/ERK2, phospho-p38 MAPK, phospho-stress activated protein kinase (SAPK)/JNK, and phospho-Akt. In brief, 50 μg of protein was electrophoretically separated on a 12% (v/v) SDS-polyacrylamide gel, and transferred to a polyvinylidene difluoride membrane (Millipore Corporation, Bedford, MA). The membranes were blocked with 5% (w/v) fat-free dry milk in Tris-buffered saline containing 0.1% (v/v) Tween 20 (TBS-T) for 1 hour at room temperature. Blots were then incubated overnight at 4°C with the primary antibodies against the different proteins to be studied: phospho-IκB-α (1:1000), IκB-α (1:1000), $p65^{RelA}$ (1:1000), phospho-ERK1/ERK2 (1:1000), phospho-p38 MAPK (1:1000), phospho-JNK (1:1000), and phospho-Akt (1:500). The membranes were then washed for 25 minutes with TBS-T and incubated for 1 hour at room temperature with alkaline phosphatase-conjugated anti-rabbit or anti-mouse antibodies (1:20,000) (GE Healthcare, Chalfont St. Giles, UK). The immune complexes were detected by membrane exposure to the ECF reagent for 5 minutes, followed by scanning for blue

excited fluorescence on the Storm 860 imager (GE Healthcare). The generated signals were analyzed using ImageQuant TL software. To test whether similar amounts of protein for each sample were loaded, the membranes were stripped and reprobed with antibodies to total ERK1/2, SAPK/JNK, p38 MAPK, and Akt or with an anti-actin antibody, and blots were developed with alkaline phosphatase-conjugated secondary antibodies and visualized by enhanced chemifluorescence. Antibodies against phospho-IκB-α, IκB-α, p65^{RelA}, phospho-p44/p42 MAPK (ERK1/ERK2), phospho-p38 MAPK, phospho-SAPK/JNK, and phospho-Akt (Ser473) were from Cell Signaling Technology (Danvers, MA). The pan anti-JNK antibody was from R&D Systems (Minneapolis, MN), and pan anti-ERK, p38 and Akt were from Cell Signaling Technology. The anti-actin antibody was purchased from Millipore Corporation.

Flow Cytometry Determination

For the analysis of surface costimulatory markers, 2×10^5 BMDCs were incubated for 20 minutes with saturating concentrations of fluorescein isothiocyanate-conjugated monoclonal antibodies to either CD40 (clone 3/23), CD86 (clone GL1), or anti CD11c-PE (clone HL3). Mouse isotype controls were used when necessary. All of the antibodies were obtained from BioLegend (San Diego, CA), except for anti-CD11c-PE antibody, which was obtained from BD Pharmingen (San Diego, CA). After two washing steps with PBS/2% fetal bovine serum, the cells were analyzed by flow cytometry in a FACScan cytometer equipped with FlowJo software. Cells were selected on the basis of forward scatter/side scatter values; BMDCs were gated on CD11c$^+$ and dead cells were excluded from all samples by propidium iodide labeling.

Determination of Cytokines by ELISA

The levels of IL-12p40, TNF-α, IL-6, and IL-10 were measured in the culture supernatants by ELISA. All cytokine quantification was done according to the manufacturer's recommendations (BD Pharmingen for IL-10 and BioLegend for IL12p40, TNF-α, and IL-6). Samples were assayed in triplicate, and the data are expressed as the average and SD of each cytokine assayed.

RNA Extraction and Real-Time RT-PCR

Total RNA was isolated from cells with TRIzol reagent (Invitrogen, Barcelona, Spain), according to the manufacturer's instructions. The RNA concentration was determined by OD_{260} measurement using a NanoDrop spectrophotometer (Thermo Scientific, Wilmington, DE), and quality was inspected for the absence of degradation or genomic DNA contamination, using Experion RNA StdSens Chips in the Experion automated microfluidic electrophoresis system (Bio-Rad, Hercules, CA). RNA was stored in RNA Storage Solution (Ambion, Foster City, CA) at −80°C until use. Real-time RT-PCR reactions were run in duplicate for each sample on a Bio-Rad MyCycler iQ5. Primer sequences (Table 1) were designed using Beacon Designer software (version 7.2, PREMIER Biosoft International, Palo Alto, CA) and thoroughly tested. In brief, 1 μg of total RNA was reverse-transcribed using the iScript Select cDNA Synthesis Kit (Bio-Rad). Real-time PCR was performed as described previously.[26] After amplification, a threshold was set for each gene and C_t values were calculated for all samples. Gene expression changes were analyzed using the built-in iQ5 Optical system software (version 2). The results were normalized using a reference gene, *HPRT-1*, de-

Table 1. Primer Sequences for Targeted cDNAs

Targeted cDNA	Primer sequence	Reference sequence identification
HPRT1		
Forward	5′-GTTGAAGATATAATTGACACTG-3′	
Reverse	5′-GGCATATCCAACAACAAAC-3′	NM_013556
CD40		
Forward	5′-GCCACTGAGACCACTGATAC-3′	
Reverse	5′-TCTGACTCGTTCCTTTCTGTAG-3′	NM_011611
CD86		
Forward	5′-TATCTCCAACAGCCTCTC-3′	
Reverse	5′-TGTAATCTCCTTCCAATACG-3′	NM_019388
IL-12p40		
Forward	5′-CTCAGGATGGAAGAGTCC-3′	
Reverse	5′-CAAGTGGAATGCTAGAATATC-3′	NM_008352
TNF-α		
Forward	5′-CAAGGGACTAGCCAGGAG-3′	
Reverse	5′-TGCCTCTTCTGCCAGTTC-3′	NM_013693
IL-6		
Forward	5′-TTCCATCCAGTTGCCTTC-3′	
Reverse	5′-TTCTCATTTCCACGATTTCC-3′	NM_031168
IL-10		
Forward	5′-CCCTTTGCTATGGTGTCCTTTC-3′	
Reverse	5′-ATCTCCCTGGTTTCTCTTCCC-3′	NM_010548

termined with Genex software (MultiD Analyses AB, Göteberg, Sweden) as the most stable for the treatment conditions used.

Calculation of Real-Time RT-PCR Results

Because the real-time RT-PCR results are presented as ratios of treated samples over untreated (control) or LPS-treated cells, the data do not follow a normal distribution. A two-base logarithmic transformation was therefore used to make observations symmetric and closer to a normal distribution. If x represents the fold change of a gene in one sample, then the two-base logarithmic transformation is $\log_2(x) = \ln(x1)/\ln(2)$. This way, fold changes of 2 and 0.5 correspond to mean $\log_2$ values of 1 and −1, respectively.

Plasmid Preparation

Plasmids coding for a dominant-negative form of Akt, HA-Akt DN (K179M)[27] or for a constitutively active form, HA-Akt CA (myr-HA-AKT), were obtained from Addgene (Cambridge, MA, plasmid numbers 16243 and 16244, respectively). An endotoxin-free Plasmid Purification Kit (Qiagen, Hilden, Germany) was used according to the manufacturer's instructions to purify HA-Akt DN and HA-Akt CA. The DNA concentration was determined by OD_{260} measurement using a NanoDrop spectrophotometer.

Cell Transfection

Nucleofection of BMDCs was performed in the Amaxa Nucleofector according to the manufacturer's instructions. In brief, the BMDCs were collected and washed twice in PBS and subsequently 2×10^5 cells were resuspended in 100 μl of Nucleofector solution. Plasmid DNA coding for pmaxGFP (2 μg), HA-Akt DN (2 μg), or HA-Akt CA (2 μg) was added to 2×10^5 cells, and the samples were transferred into certified cuvettes and nucleofected by using program Y-001. Immediately after transfection, 400 μl of medium previously warmed to 37°C, was added to each cuvette. The DCs were collected, dispensed in the wells of Lab-Tek Chamber Slides, and incubated at 37°C and 5% CO_2 for 48 hours. Cells were then infected, and the rates of infection were determined was described above. For image acquisition, the actin network of cells was stained with Alexa Fluor 555 phalloidin (Invitrogen). Images were acquired in a confocal laser scanning microscope (Zeiss LSM 510 Meta). The filter set used included an excitation filter of 560 nm and an emission filter of 575 nm. The settings for contrast, brightness, pinhole, acquisition mode, and scanning time were maintained throughout the work.

Statistical Analysis

The results are presented as means ± SD, and the statistical difference between two groups was determined by the two-sided unpaired Student's *t*-test. For multiple group comparisons, the one-way analysis of variance test, with a Bonferroni multiple comparison posttest was used. The tests were performed using GraphPad Prism (version 5.02; GraphPad Software, San Diego, CA). Statistically significant values are as follows: $^*P < 0.05$, $^{**}P < 0.01$, and $^{***}P < 0.001$.

Results

Visceral L. infantum *Promastigotes Successfully Infect Murine BMDCs*

Leishmania manipulates host immune responses to protect itself from elimination. Here, in an attempt to unravel the molecular mechanisms involved in DCs manipulation by visceral *Leishmania* parasites, primary murine BMDCs from susceptible BALB/c mice were infected *in vitro* with *L. infantum* promastigotes. Because *Leishmania* exhibits a strong tropism for macrophage, it was of major importance to ensure the high purity of BMDCs population submitted to infection. Flow cytometry analyses revealed a small population expressing the macrophage marker F4/80, which was excluded from all subsequent analyses. In addition, we did not observe any contamination with T-cell (CD3) or B-cell (B220) populations (data not shown). After a differentiation period of 12 days in the presence of GM-CSF, BMDCs were phenotypically characterized as $CD4^-CD8^-CD11b^+CD11c^+DEC205^-$ DCs.

We first examined whether *L. infantum* promastigotes could infect and survive within murine BMDCs. Cells were incubated with *L. infantum* promastigotes at a parasite/cell ratio of 10:1 for 4 hours, after which the parasite internalization was determined. As shown in Figure 1A, after 4 hours of parasite-cell incubation, between 50 and 60% of immature BMDCs were successfully infected by *L. infantum* promastigotes with an average of 3 parasites/cell (3.2 ± 1.1). The infection rate was confirmed by flow cytometry evaluation of GFP-*L. infantum* promastigotes (Figure 1B). After removal of nonphagocytosed parasites, infected BMDCs were maintained in culture for 12, 24, 48, or 72 hours to evaluate parasite development. The number of cells presenting intracellular parasites dropped significantly from 4 to 12 hours ($P = 0.044$), and the mean number of parasites per infected cell also presented a slight yet not significant decrease (Figure 1A). The infection rate seemed to stabilize after 24 hours, with no significant differences between 24 and 48 hours or 24 and 72 hours (Figure 1A). After the slight decrease observed at 12 hours, the number of parasites per cell showed an increasing tendency in posterior time points, being significant at 48 and 72 hours ($P = 0.012$ and 0.015, respectively). These results clearly suggest that the first 12 hours led to the resolution of a large part of the infection, which nevertheless did not induce the complete elimination of the parasite. Indeed, after this critical period, the infection remained stable for at least 72 hours, and parasites subsisted within cells thus showing that infections are not abortive.

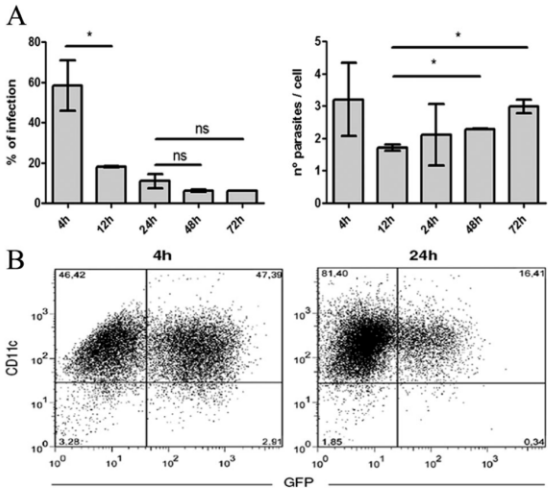

Figure 1. Kinetic analyses of visceral *L. infantum* infection. **A:** Cells were infected with promastigotes at a 10:1 (parasites/cell) ratio for 4 hours. BMDCs were immediately recovered or left in culture for an additional 12, 24, 48, or 72 hours. A fluorescent nuclear label, 4′,6-diamidino-2-phenylindole, was added to the cells, and the number of infected cells as well as the number of parasite per cell was counted with a fluorescence microscope at ×1000. Results are representative of three independent experiments. **B:** BMDCs infected with GFP-*L. infantum* promastigotes at a 10:1 (parasites/cell) ratio were recovered after 4 hours of incubation or left in culture for an additional 24 hours after the end of the infection. The cells were analyzed by flow cytometry, and the percentage of GFP-positive BMDCs was quantified. Each value represents the mean ± SD from three independent experiments. NS, not significant; $^*P < 0.05$.

L. infantum *Promastigotes Silently Infect Murine BMDCs and Counteract LPS-Triggered BMDC Activation/Maturation Process*

It was previously demonstrated that several *Leishmania* species suppress the up-regulation of costimulatory molecules in infected macrophages.[28,29] However, the data generated using DCs as main infection targets for *Leishmania* are often incoherent and conflicting, depending on the type of DCs, species, and developmental stage of the parasite used. Hence, we investigated the activation status of murine BMDCs that were infected with *L. infantum* promastigotes by analyzing the transcription and surface expression of the DC maturation markers CD40 and CD86 by quantitative PCR (qPCR) and flow cytometry, respectively. As shown in Figure 2, A and C, and Table 2, *L. infantum* promastigotes failed to up-regulate the transcription and surface expression of CD40 and CD86 costimulatory molecules in BMDCs. Given that a significant variation in the percentage of infected BMDCs was observed during the time course of the experiment (Figure 1A), to avoid bias due to different parasite load, we evaluated the expression pattern of costimulatory molecules through the duration of the experiment. Nevertheless, the expression of the surface markers after infection was always similar to that of noninfected BMDCs (data not shown). To access the active involvement of parasites in the arrested maturation of infected BMDCs and to discard an unspecific phagocytic process, parallel experiments were performed with polystyrene beads and heat-killed or glutaraldehyde-fixed parasites. Surprisingly and in contrast to viable parasites, the exposure of BMDCs to killed *L. infantum* promastigotes or to the beads significantly increased the transcription (Supplemental Figure S1, see *http://ajp.amjpathol.org*) and expression of CD40 and CD86 (Table 2). These results show that the arresting of BMDCs maturation after engulfment of *L. infantum* promastigotes is a parasite-specific process that requires the active involvement of viable parasites.

We next tested the ability of parasites to manipulate the LPS-triggered maturation status of dendritic cells. Lipopolysaccharide is a TLR4 agonist that has long been used as a potent inducer of DC maturation.[30] As expected, LPS stimulation induced the maturation of BMDCs, as judged by the increased transcription and expression of CD40 and CD86 (Figure 2, A and C). However, in LPS-stimulated BMDCs that were subsequently submitted to *L. infantum* infection, mRNA levels of CD40 were significantly decreased (Figure 2B). These data were corroborated by flow cytometry experiments that showed a decrease on the surface expression of this molecule (Figure 2C). Taken together, these observations confirm silent infection of murine BMDCs by visceral *L. infantum* promastigotes and show the ability of parasites to counteract the maturation/activation process triggered by other inflammatory stimuli.

L. infantum *Promastigotes Induce Marginal Production of IL-12p40 and IL-10 and Manipulate the LPS-Induced Cytokine Profile in BMDCs*

In response to intracellular pathogens, DCs secrete cytokines that will dictate the nature of the T-cell response. The quality of this immune response is influenced by the balance between the secretion of pro- and anti-inflammatory cytokines, in particular IL-12 and IL-10, respectively. Consequently, complementary experiments were performed to examine the effect of *L. infantum* promastigotes on BMDC cytokine production and on the ability of parasites to manipulate the LPS-induced cytokine profile. The transcription and secretion of proinflammatory (IL-6, IL12, and TNF-α) and anti-inflammatory (IL-10) cytokines were assessed by qPCR and ELISA, respectively. As shown in Figure 3A, the internalization of *L. infantum* promastigotes slightly induced transcription of IL-12p40 and IL-10, with mean $\log_2$ values of 1.9 ± 0.8 ($P < 0.05$) and 1.4 ± 0.3 ($P < 0.01$), respectively. Nevertheless, this effect was seen to be transient, because 24 hours after infection the mRNA levels of these cytokines in infected cells were not significantly different from those of noninfected BMDCs. In contrast, the transcription of the *IL-6* gene was found to be significantly decreased in a time-sustained manner (Figure 3A). No significant differences were found for the TNF-α mRNA levels after infection. The consequences of these transcriptional changes were then evaluated at the protein level by ELISA assays performed in the culture supernatants obtained 24 hours postinfection. In accordance with qPCR results, *L. infantum* significantly increased the secretion of IL-12p40 ($P <$

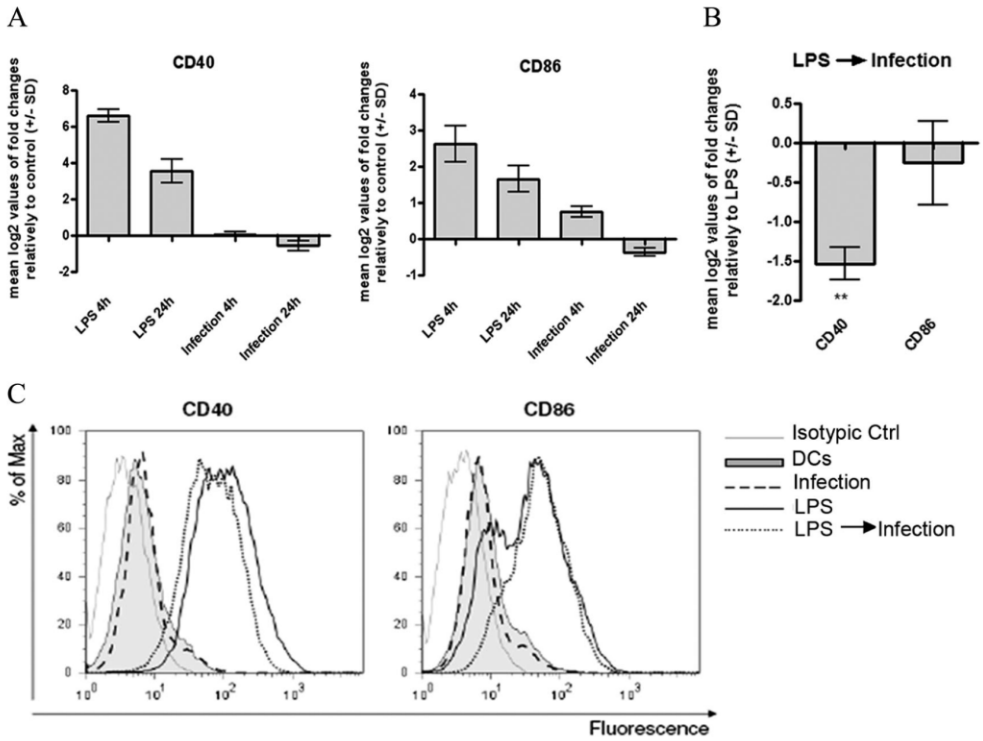

Figure 2. Effects of *L. infantum* infection on BMDC CD40 and CD86 costimulatory molecule expression. **A:** BMDCs plated at 2×10^6 cells/well were infected with *L. infantum* promastigotes in a 10:1 (parasites/cell) ratio for 4 hours. Cells were immediately recovered or left in culture for an additional 24 hours after the end of the infection. As a control, BDMCs were stimulated with 1 μg/ml LPS for 4 and 24 hours. The mRNA levels were assessed by qPCR for CD40 and CD86. Gene expression is indicated as mean $\log_2$ values of fold changes relative to untreated cells. **B:** BMDCs were treated with 1 μg/ml LPS or pretreated for 1 hour with LPS and then infected with *L. infantum* promastigotes in a 10:1 (parasites/cell) ratio, (LPS → Infection). After 4 hours of culture, cells were harvested, and the CD40 and CD86 mRNA levels were assessed by qPCR. Gene expression is indicated as mean $\log_2$ values of fold changes relative to LPS-treated cells. **C:** Cells were infected, treated with 1 μg/ml LPS or pretreated during 1 hour with LPS and then infected (LPS → Infection). After 24 hours, the surface expression of CD40 and CD86 was measured on gated $CD11c^+$ cells by flow cytometry. As negative control, cells were incubated in RPMIc (DCs) for a similar time. Each value represents the mean ± SD from three independent experiments. $^{**}P < 0.01$.

0.001) and caused a slight 1.6-fold decrease in the IL-6 protein level (not statistically significant) (Figure 3B). Although there was an infection-induced increase in *IL-10* gene transcription, no increase in IL-10 secretion was observed. This discrepancy might be explained by the low gene induction and by the lower sensitivity of the ELISA assay compared with the qPCR technique. This pattern of cytokine expression is specific and actively modulated by viable parasites, given that exposure to killed parasites or beads caused a different cytokine profile (Supplemental Figure S2, see *http://ajp.amjpathol.org*). Of particular interest is the difference in the amounts of IL-12 produced. Cells exposed to killed parasites showed a significantly higher transcription of IL-12 than cells exposed to viable promastigotes. This finding indicates that although some IL-12 was produced during DC infection, parasites actively limit the production of this cytokine, avoiding the triggering of a strong proinflammatory response.

Table 2. Effect of Viable and Killed *L. infantum* Promastigotes on BMDC CD40 and CD86 Surface Expression

Cell Treatment	CD40	CD86
Cells	14.73 ± 4.39	34.30 ± 2.63
L. infantum	12.32 ± 1.78 (NS)	31.25 ± 2.44 (NS)
Heat-killed *L. infantum*	28.64 ± 1.20**	44.41 ± 8.68 (NS)
Fixed *L. infantum*	37.57 ± 1.67***	89.46 ± 19.18 (NS)
Beads	36.96 ± 5.02***	281.50 ± 74.54***

BMDCs were infected with *L. infantun* promastigotes at an infection ratio of 10:1 (parasites/cell). In parallel, cells were exposed to polystyrene beads and heat-killed or glutaraldehyde-fixed parasites in the same ratio as that used for infection. After 24 hours, the surface expression of CD40 and CD86 was measured on gated $CD11c^+$ cells by flow cytometry. Each value represents the geometric mean ± SD from three independent experiments: NS, not significant; $^{**}P < 0.01$; $^{***}P < 0.001$.

We also assessed the ability of parasites to manipulate the LPS-induced cytokine profile. LPS potently induced the transcription and secretion of IL-12p40, IL-6, TNF-α, and IL-10; however, this secretion profile was substantially altered by infection with *L. infantum* promastigotes. The infection caused a significant decrease in the transcription and secretion of the LPS-induced proinflammatory cytokines IL-12p40 (qPCR -0.76 ± 0.3, $P < 0.05$; ELISA $P < 0.05$) and IL-6 (qPCR -0.76 ± 0.3, $P < 0.05$; ELISA $P < 0.01$), whereas no significant effect was found for TNF-α (Figure 3, B and C). In contrast, the mRNA and protein levels of the anti-inflammatory cytokine IL-10 were significantly increased in LPS-treated cells exposed to

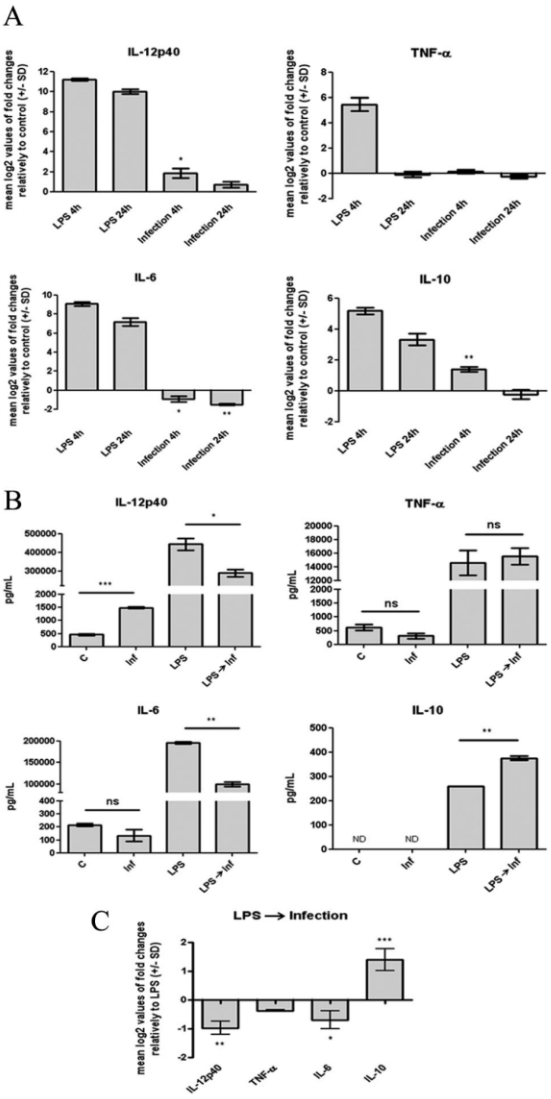

Figure 3. Effects of *L. infantum* infection on BMDC cytokine production. **A:** Cells plated at 2×10^6 cells/well were infected with *L. infantum* promastigotes in a 10:1 (parasites/cell) ratio or stimulated with 1 μg/ml LPS during the indicated times at 37°C with 5% CO_2. The mRNA levels were assessed by real-time qPCR for IL-12p40, TNF-α, IL-6, and IL-10. Gene expression is indicated as mean $\log_2$ values of fold changes relative to untreated cells. **B:** The levels of IL-12p40, TNF-α, IL-6, and IL-10 were quantified by ELISA on 24-hour culture supernatants of 1×10^6 BMDCs that were either infected with *L. infantum* promastigotes (Inf), stimulated with 1 μg/ml LPS, or pretreated for 1 hour with LPS and then infected (LPS→ Inf). C, control. **C:** BMDCs (2×10^6/well) were stimulated with 1 μg/ml LPS or infected for 1 hour after LPS stimulation. Four hours after infection, the mRNA levels of IL-12p40, TNF-α, IL-6, and IL-10 were assessed by real-time qPCR. Gene expression is indicated as mean $\log_2$ values of fold changes relative to LPS-treated cells. Each value represents the mean ± SD from three independent experiments. $^*P < 0.05$; $^{**}P < 0.01$; $^{***}P < 0.001$; ns, not significant.

parasites (qPCR 1.41 ± 0.4, $P < 0.001$; ELISA $P < 0.01$). Overall these results show that in BMDCs *L. infantum* promastigotes slightly induce the transcription and secretion of IL-12p40 and IL-10 while reducing IL-6 levels. In addition, our data indicate that parasites are able to shift the levels of cytokines induced by LPS to a more parasite-convenient anti-inflammatory status.

L. infantum *Promastigotes Induce a Rapid Phosphorylation of ERK1/2 and Akt While They Actively Promote a Cleavage on NF-κB p65^{RelA} Subunit*

The initial interaction between host mononuclear phagocytes and *Leishmania* parasites results in the induction of intracellular signaling pathways that connect receptor-mediated events to nuclear transcription responses. To investigate these molecular mechanisms, we examined the effect of infection on the phosphorylated forms of MAPKs (ERK1/ERK2, SAPK/JNK, and p38 MAPK) and of Akt, which correspond to the active forms of the enzymes. The involvement of the transcription factor NF-κB was also evaluated by measuring the levels of its inhibitory protein, IκB-α, in both phosphorylated and nonphosphorylated forms and by assessing the nuclear translocation of the p65^{RelA} subunit. As shown in Figure 4, A and D, infection of BMDCs with *L. infantum* promastigotes caused a rapid activation of ERK1/ERK2 and Akt. In contrast, SAPK/JNK and p38 pathways were not modulated by parasites (Figure 4, B and C). The NF-κB transcription factor cascade was not activated, at least by its canonical way, as evaluated by the absence of phosphorylation and subsequent degradation of the inhibitory protein IκB-α (Figure 4E). Interestingly, and not reported until now in DCs, parasites induced a rapid cleavage of the NF-κB p65^{RelA} subunit, resulting a major new fragment of approximately 35 kDa (Figure 4F). The presence of this fragment on cytoplasmic and nuclear extracts of parasite-exposed cells indicates that cleavage may occur in cytoplasm and is followed by immediate translocation into the nucleus. Moreover, this cleavage was not observed with heat-killed or fixed promastigotes, pointing to a specific process that requires the activity of protein structures and viability of the parasite (Supplemental Figure S3F, see *http://ajp.amjpathol.org*). Similar results for all pathways assayed were obtained in another dendritic cell model, a fetal skin-derived dendritic cell line (data not shown).

L. infantum *Promastigotes Repress LPS-Induced NF-κB Activation and Exert a Synergistic Effect on ERK1/2 and Akt Phosphorylation*

Further experiments were conducted to evaluate whether parasites were able to subvert/counteract, at signaling pathway levels, the effects of the effective maturation stimulus LPS. We exposed the cells simultaneously to LPS and *L. infantum* promastigotes for 30 minutes and analyzed the effects on NF-κB, MAPKs, and PI3K/Akt pathways (Figure 5, A–D). On LPS stimulation all of the pathways studied were activated and when BMDCs were coincubated with LPS and parasites, the phosphorylated forms of ERK and Akt were increased over the LPS-

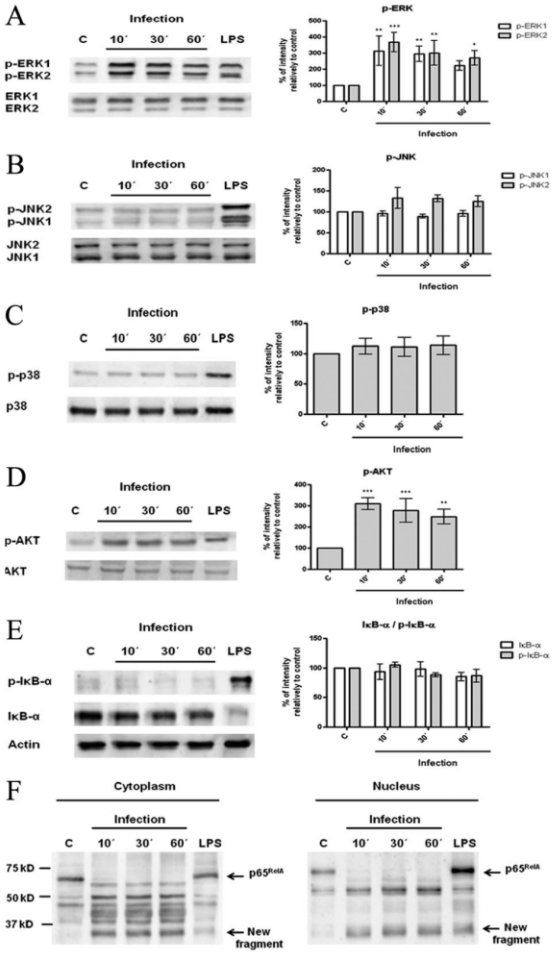

Figure 4. Interaction of *L. infantum* promastigotes with PI3K/Akt, MAPKs, and NF-κB signaling pathways. BMDCs were infected with *L. infantum* promastigotes in a cell/parasite ratio of 1:10, and cell lysates were prepared after 10, 30, or 60 minutes of infection. As a positive control, BMDCs were stimulated with 1 μg/ml of LPS for 30 minutes. The activation of specific intracellular signaling pathways was examined by Western blot analysis using specific antibodies to the phosphorylated (p-) forms of ERK1/2 (**A**), SAPK/JNK (**B**), p38 MAPK (**C**), Akt (**D**), and IκB-α (**E**). NF-κB activation was also evaluated by determination of the levels of its inhibitory protein IκB-α and by assessment of nuclear translocation of the NF-κB $p65^{RelA}$ subunit (**F**). Equal protein loading was assessed using antibodies to total ERK1/2, SAPK/JNK, p38 MAPK, and Akt or with an anti-actin antibody. The optical densities of the bands were obtained by scanning the membranes in a fluorescence scanner and then were analyzed with ImageQuant TL Software. The results are expressed as % intensity relative to control (C). Each value represents the mean ± SD from three independent experiments. $^{*}P < 0.05$; $^{**}P < 0.01$; $^{***}P < 0.001$.

induced levels, revealing a synergistic effect (Figure 5, A and D). Nevertheless, the most striking effect of the co-incubation of BMDCs with LPS and parasites was observed in the NF-κB transcription factor cascade. The phosphorylation of IκB-α was just slightly decreased, whereas the levels of total IκB-α remained approximately the same (Figure 5E); however, the NF-κB $p65^{RelA}$ subunit was dramatically affected. As reported above, the parasites seemed to actively promote the cleavage of the $p65^{RelA}$ subunit and in cells simultaneously exposed to parasites and LPS, this effect is clearly exacerbated (Figure 5F). This result suggests that LPS-triggered activation of NF-κB may somehow facilitate the cleavage promoted by the parasites. These events are currently under investigation in our laboratory.

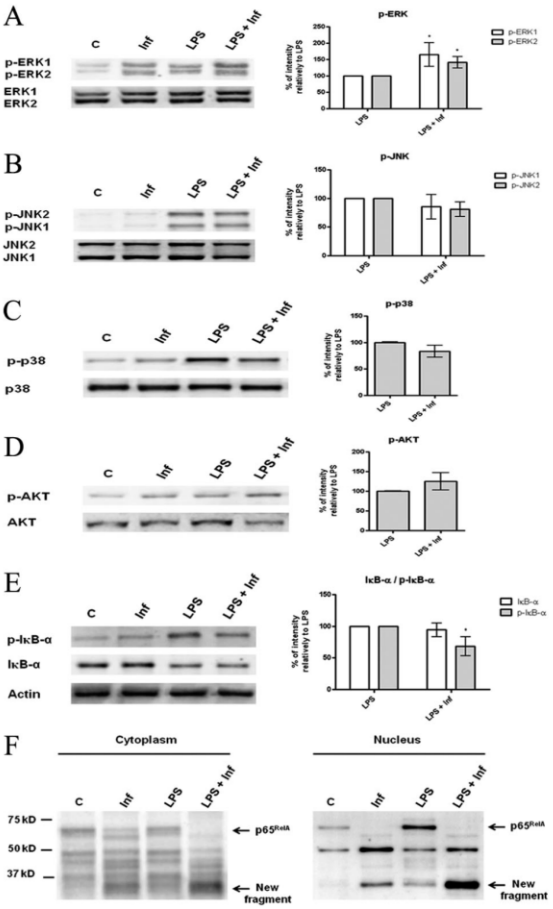

Figure 5. Effects of *L. infantum* infection on LPS-triggered signaling pathways. BMDCs were infected with *L. infantum* promastigotes for 30 minutes. *infantum*). In some experiments, infected BMDCs were simultaneously stimulated with 1 μg/ml LPS (LPS + Inf). Nonstimulated cells (C) or LPS-stimulated cells (LPS) were used as negative and positive controls, respectively. Cell extracts were analyzed by Western blot using specific antibodies to the phosphorylated (p-) forms of ERK1/2 (**A**), SAPK/JNK (**B**), p38 MAPK (**C**), Akt (**D**), and IκB-α (**E**) and for total IκB-α and NF-κB $p65^{RelA}$ (**F**). Equal protein loading was evaluated with antibodies to total ERK1/2, SAPK/JNK, p38 MAPK, and Akt or with an anti-actin antibody. The optical densities of the bands were obtained by scanning the membranes in a fluorescence scanner and then were analyzed with ImageQuant TL software. The results are expressed as % intensity relative to control. Each value represents the mean ± SD from three independent experiments. $^{*}P < 0.05$; $^{**}P < 0.01$; $^{***}P < 0.001$.

Taken together, these data show that *L. infantum* promastigotes are able to manipulate the LPS-triggered signaling cascades at different levels.

Inhibition of PI3K/Akt Blocks L. infantum *Infection in BMDCs*

The way *Leishmania* parasites signal to gain entry and survive in their host is not completely understood. In this study we provided clear evidence that *L. infantum* pro-

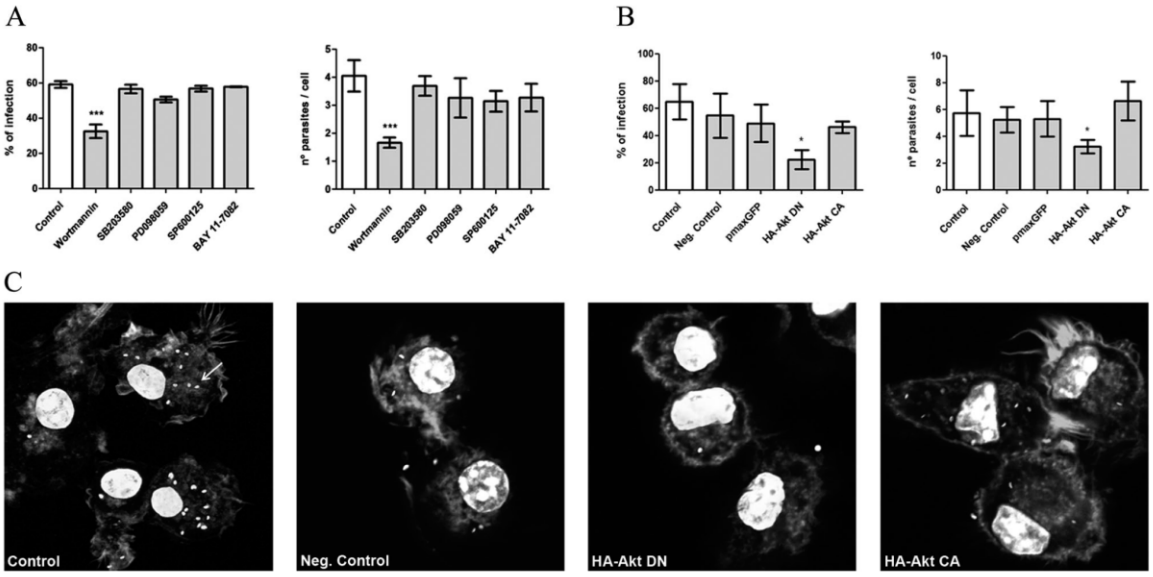

Figure 6. Relevance of PI3K/Akt, MAPKs, and NF-κB signaling pathways on the engulfment of parasites by BMDCs. **A:** BMDCs previously treated with specific inhibitors for Akt (wortmannin), p38 MAPK (SB203580), ERK1/2 (PD098059), SAPK/JNK (SP600125), or NF-κB (Bay 11-7082) were incubated with *L. infantum* parasites for 4 hours. **B:** BMDCs were submitted to electroporation without any plasmid DNA (negative control) or transfected with pmaxGFP, a dominant-negative mutant of Akt (HA-Akt DN), or with a constitutively activated form of Akt (HA-Akt CA). After 48 hours, BMDCs were infected with *L. infantum* parasites. Four hours after infection, cells were stained with 4′,6-diamidino-2-phenylindole, and the numbers of infected cells as well as the numbers of parasites per cells were counted with a fluorescence microscope at ×1000. **C:** Images representative of fields of the different transfection experiments (original magnification: ×630) were acquired with a confocal laser scanning microscope (Zeiss LSM 510 Meta). Parasites were distributed in cytoplasm, and one of them is indicated by an **arrow**. Each value represents the mean ± SD from three independent experiments. $^{*}P < 0.05$; $^{**}P < 0.01$; $^{***}P < 0.001$.

mastigotes interact and modulate different signaling systems in BMDCs. Thus, we decided to analyze the relevance of PI3K/Akt, MAPKs, and NF-κB pathways for *L. infantum* promastigotes uptake by cells. BMDCs were preincubated for 1 hour with wortmannin (PI3K/Akt inhibitor), SB203580 (p38MAPK inhibitor), PD098059 (ERK1/ERK2 inhibitor), or SP600125 (SAPK/JNK inhibitor) and then were exposed to parasites for 4 hours. To evaluate the role of NF-κB, cells were similarly treated with BAY 11-7082, an irreversible inhibitor of IκB-α phosphorylation.[31] Preliminary experiments were conducted to evaluate and select the nontoxic concentrations of each inhibitor that efficiently inhibited the phosphorylation of the respective kinase mediator (data not shown). The effects of the different inhibitors on infection rates were checked by assessing the number of infected cells and number of parasites per cell.

As shown in Figure 6A, the engulfment of *L. infantum* promastigotes was significantly inhibited in the presence of wortmannin (32.53 ± 1.9%; $P < 0.001$), demonstrating for the first time that PI3K/Akt activation is required for the uptake of *L. infantum* parasites. This mechanism seemed to be specific for PI3K, because none of the other tested inhibitors altered parasite uptake so drastically. Because of this crucial role of the PI3K/Akt pathway on the entry of parasites, we decided to confirm these data by using a molecular approach that consisted of transient transfection of BMDCs with a dominant-negative mutant of Akt, HA-Akt DN (K179M). The results obtained supported the data from the pharmacological approach. The cells transfected with the negative mutant (HA-Akt DN) showed a 2.9 decrease in the parasite uptake and a 1.8 decrease in the number of parasites per cell compared with mock-transfected cells (negative control). In contrast, cells transfected with pmaxGFP or with a constitutively activated form of Akt (HA-Akt CA) did not showed significant differences in infection rates (Figure 6, B and C).

Activation of PI3K/Akt and Impairment of NF-κB by L. infantum *Promastigotes Limit BMDC Maturation Status and the Release of Proinflammatory Cytokines*

To assess the relevance of PI3K/Akt, MAPKs, and NF-κB pathways in the *L. infantum* modulation of BMDC functions, we used specific inhibitors of each pathway and checked their effects on the transcription of costimulatory molecules CD40 and CD86 and of the cytokines IL-6, IL-12p40, TNF-α, and IL-10. As shown in Figure 7, we found that the inhibition of PI3K/Akt by wortmannin before BMDC infection caused a slight increase in the transcription of costimulatory molecules CD40 and CD86 and proinflammatory cytokines IL-12p40 and IL-6. Remarkably, the opposite effect was observed for anti-inflammatory IL-10, which was found to be significantly repressed (−1.04 ± 0.3, $P < 0.001$). In contrast, pretreatment with PD098059 (inhibitor of ERK) marginally increased IL-10 transcription (0.53 ± 0.1, $P < 0.05$), suggesting a minor role for ERK in controlling the expression of this cytokine.

Transcription of the costimulatory molecules CD40 and CD86 as well as the proinflammatory cytokines IL-12p40,

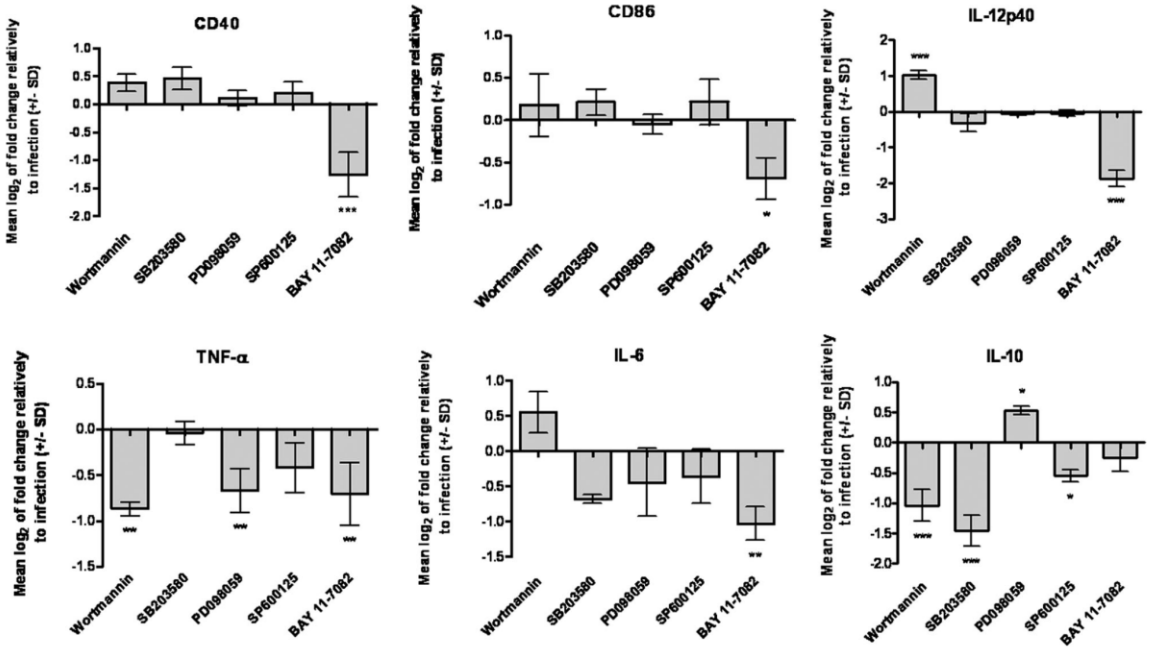

Figure 7. Relevance of PI3K/Akt, MAPKs, and NF-κB signaling pathways on the expression of costimulatory molecules and cytokines by infected BMDCs. *L. infantum* parasites were incubated with BMDCs previously treated with specific inhibitors for Akt (wortmannin), p38 MAPK (SB203580), ERK1/2 (PD098059), SAPK/JNK (SP600125), or NF-κB (Bay 11-7082). The CD40, CD86, IL-12p40, TNF-α, IL-6, and IL-10 mRNA levels were assessed by qPCR 4 hours postinfection. Gene expression is indicated as mean $\log_2$ values of fold changes relative to *L. infantum*-infected cells. Each value represents the mean ± SD from three independent experiments. $^{*}P < 0.05$; $^{**}P < 0.01$; $^{***}P < 0.001$.

TNF-α, and IL-6 was significantly reduced by the NF-κB inhibitor BAY 11-7082. Because we showed that parasites do not activate this transcription factor and may even cause its impairment, these results have to be interpreted as the effects of inhibition over the basal activation state of the pathway, being evident the involvement of the NF-κB cascade in the transcriptional control of the above molecules. Therefore, we can postulate that the nonactivation/impairment of this pathway by *L. infantum* promastigotes justifies the lack of or weak expression of costimulatory and proinflammatory molecules by infected BMDCs. Overall, these data suggest that PI3K/Akt activation and nonactivation/impairment of NF-κB transcription factor are dominant mechanisms by which the parasite orchestrates and manipulates the inflammatory/maturation status of DCs.

Discussion

The molecular mechanisms by which *Leishmania* parasites evade/impair DC biological functions remain incompletely understood. These facts prompted us to study the interaction between visceral *L. infantum* promastigotes and DCs at multiple levels. Our data showed that murine BMDCs rapidly internalize *L. infantum* promastigotes and that a large part of the infection is cleared in the first 12 hours postinfection, a period after which the number of parasites per cell starts to increase. Concerning the ability of parasites to activate DCs, discrepant observations are found in literature, with some studies showing DC activation[32–35] and others showing a silent infection.[14,36] These discrepant results might be due to the use of different parasite species and life-cycle stages as well as different sources of DCs. In this study, we showed that *L. infantum* promastigotes were able to infect DCs, avoiding the induction of CD40 and CD86 expression in a specific process that was dependent viability, because killed parasites strongly induced these maturation markers.

In agreement with previous studies performed with *L. major*,[11,37] *L. amazonensis,*[17] *L. donovani*,[6] and *L. infantum* promastigotes,[7] we observed in our model a transient induction of the transcription of IL-12p40 and IL-10 that dropped dramatically at 24 hours postinfection. In contrast with recent reports that described the production of high levels of TNF-α by *L. braziliensis*-infected mouse DCs[12] or *L. infantum*-infected human DCs,[38] in our DC model *L. infantum* promastigotes were unable to up-regulate TNF-α and induced a time-sustained impairment of the transcription and secretion of the IL-6 cytokine. As observed for the expression of surface molecules, this cytokine profile of infected cells is specific for viable parasites. Of particular relevance was the fact that killed parasites induced a significantly higher transcription and secretion of IL-12 than cells exposed to viable parasites, indicating that *L. infantum* promastigotes actively limit the production of this proinflammatory cytokine. Given that in our model not all of the DCs are infected, the slight increase in IL-12 that we observed in cells exposed to viable promastigotes may result from the activity of noninfected bystander DCs, in a process similar to the one

described by Carvalho et al.[12] In fact, experiments performed in our laboratory by Ricardo Silvestre, Mariana Resende, Bruno Neves, Ali Ouaissi, Maria Teresa Cruz and Anabela Cordeiro da Silva with isolated populations of infected and bystander DCs showed that IL-12 is exclusively produced by the bystander DC population (manuscript in preparation).

As previously observed in macrophages,[39–42] our data provide evidences that *L. infantum* promastigotes actively counteract the LPS-induced maturation process in dendritic cells. We observed that parasites significantly decrease the LPS-induced CD40 surface expression in BMDCs and that the levels of LPS-induced cytokines were also considerably affected after infection. The expression of the proinflammatory cytokines IL-6 and IL-12 was significantly reduced in LPS-treated cells infected with *L. infantum* promastigotes and in contrast, the LPS-induced expression of the anti-inflammatory cytokine IL-10 was synergistically enhanced by exposure to parasites. These results further support the evidence that *L. infantum* is able to bias the cytokine release profile toward a more parasite-convenient immunosuppressive profile.

At molecular level we showed that *L. infantum* promastigotes rapidly induced a time-sustained activation of PI3K/Akt and ERK1/2 signaling cascades, whereas the NF-κB transcription factor seems to be impaired. The available data regarding the involvement of the NF-κB signaling system in *Leishmania* infection of DCs are limited, although recent studies showed that *L. mexicana* lipophosphoglycan[43] and *L. major* infection[44] activate this family of transcription factors in human monocyte-derived DCs. The data obtained in this study demonstrated that *L. infantum* promastigotes are unable to "canonically" activate the NF-κB transcription factor, as shown by the inability of parasites to promote phosphorylation and posterior degradation of the NF-κB inhibitory protein, IκB-α. Surprisingly, parasites induced a cleavage on the NF-κB $p65^{RelA}$ subunit, resulting in a major new fragment of approximately 35 kDa. This cleavage was not observed in cells exposed to heat-killed or fixed parasites, indicating that protein structures of the parasite are directly involved in this process. Given the role of NF-κB on the activation/maturation process of DCs,[45] its impairment by viable parasites provides an explanation for the maintenance of infected cells in an incomplete mature state. A similar observation was reported in a recent study performed in macrophages, showing that infection with *Leishmania* promastigotes induced a specific cleavage of the NF-κB $p65^{RelA}$ subunit.[46] The authors postulated that the resulting $p35^{RelA}$ fragment may represent an important mediator by which *Leishmania* promastigotes induce several chemokines without inducing other NF-κB-regulated genes, such as *iNOS* and *IL-12* that are detrimental for parasite survival. Moreover, we showed that *Leishmania* actively counteract the LPS-triggered activation of NF-κB cascade by reducing IκB-α phosphorylation and extensively cleaving the NF-κB $p65^{RelA}$ subunit. Because parasite-promoted cleavage seems to be somehow facilitated by LPS, we hypothesize that the cleavage still occurs in NF-κB-IκB-α complexes but is facilitated in LPS-treated cells because of the release of NF-κB from IκB-α. Supporting this hypothesis, Gregory et al[46] have shown that the inhibition of IκB-α proteasomal degradation decreases the appearance of the $p35^{RelA}$ fragment in infected nuclei.

Regarding the other signaling pathways analyzed in this study, we observed that among the members of the MAPK family, only ERK was clearly activated by *L. infantum* promastigotes, whereas JNK and p38 were not affected. The MAPKs transduction pathways are understood to play positive as well as negative regulatory roles in inflammatory cytokine production[22] and several reports indicate that activation of ERK can prevent proper DC maturation and cause a shift through a Th_2 DC-polarizing cytokine/chemokine profile.[26,47,48] However, our results indicated that the ERK pathway plays a minor role in *L. infantum*-induced DC costimulatory molecules and cytokine release profile. Treatment of cells with PD098059, a specific inhibitor of ERK1/2, minimally affected transcription of genes encoding CD40, CD86, or the studied cytokines. Interestingly we found that, in contrast to the observed effect for NF-κB, p38, and JNK, *Leishmania* synergizes with LPS to induce ERK activation.

For the first time, we provide evidence that infection of murine DCs by *L. infantum* promastigotes led to the activation of PI3K/Akt pathway. We verified that the activation of this signaling cascade by *Leishmania* parasites plays a major role in their ability to impair the transcription of proinflammatory cytokines. Preincubation of cells with wortmannin, a specific inhibitor of PI3K, followed by infection, caused an increase in the transcription of CD40, IL-12p40, and IL-6 encoding genes. In contrast, the parasite-induced IL-10 expression was strongly repressed. Further, a recent report indicated that inhibition of Akt in *L. amazonensis* promastigote-infected macrophages increased IL-12p40 production at the transcriptional level.[49] As observed for ERK, the PI3K/Akt pathway was synergistically activated in BMDCs coincubated with LPS and *L. infantum* promastigotes. This synergism on Akt phosphorylation might explain at a molecular level the observed decrease in IL-12p40 and the increase in IL-10 expression in cells treated with LPS before infection.

We also showed that the integrity of the PI3K/Akt pathway is essential for the capacity of *L. infantum* promastigotes to infect cells. Treatment of BMDCs with wortmannin or transfection with a dominant-negative mutant of Akt profoundly impairs the infection rates, reducing the percentage of infected cells and the number of parasites per cell. Modulation of host cell PI3K-dependent signaling by microbial pathogens is becoming recognized as an important strategy for establishment of infection and intracellular survival of microorganisms.[50–52] Interestingly, similar to our observations for *Leishmania*, *Trypanosoma cruzi,* an intracellular protozoan parasite of the same family as *Leishmania*, activates the PI3K/Akt pathway in host cells, this activation being crucial for the entry of parasites.[53–55]

In summary, this study demonstrated for the first time that a visceral *Leishmania* species can differentially target PI3K/Akt, MAPKs, and NF-κB to modulate the maturation, activation, and immunostimulatory abilities of DCs. Overall, our results show that the activation of the PI3k/Akt pathway and the impairment of NF-κB transcription factor

are crucial strategies by which *Leishmania* parasites subvert DC immunostimulatory abilities. Knowledge of the intracellular signaling profile triggered by *Leishmania* parasites in host immune cells sheds light on the mechanisms leading to immune evasion. This awareness will surely reveal new potential targets for the development of therapeutic strategies against visceral leishmaniasis.

Acknowledgment

We thank Marc Ouellette for providing the pSP expression vector.

References

1. Kaye PM, Svensson M, Ato M, Maroof A, Polley R, Stager S, Zubairi S, Engwerda CR: The immunopathology of experimental visceral leishmaniasis. Immunol Rev 2004, 201:239–253
2. Ghalib HW, Whittle JA, Kubin M, Hashim FA, el-Hassan AM, Grabstein KH, Trinchieri G, Reed SG: IL-12 enhances Th1-type responses in human Leishmania donovani infections. J Immunol 1995, 154:4623–4629
3. Liew FY, Parkinson C, Millott S, Severn A, Carrier M: Tumour necrosis factor (TNFα) in leishmaniasis. I. TNFα mediates host protection against cutaneous leishmaniasis. Immunology 1990, 69:570–573
4. Murray HW, Hariprashad J: Interleukin 12 is effective treatment for an established systemic intracellular infection: experimental visceral leishmaniasis. J Exp Med 1995, 181:387–391
5. Charmoy M, Megnekou R, Allenbach C, Zweifel C, Perez C, Monnat K, Breton M, Ronet C, Launois P, Tacchini-Cottier F: Leishmania major induces distinct neutrophil phenotypes in mice that are resistant or susceptible to infection. J Leukoc Biol 2007, 82:288–299
6. Gorak PM, Engwerda CR, Kaye PM: Dendritic cells, but not macrophages, produce IL-12 immediately following Leishmania donovani infection. Eur J Immunol 1998, 28:687–695
7. Schleicher U, Liese J, Knippertz I, Kurzmann C, Hesse A, Heit A, Fischer JA, Weiss S, Kalinke U, Kunz S, Bogdan C: NK cell activation in visceral leishmaniasis requires TLR9, myeloid DCs, and IL-12, but is independent of plasmacytoid DCs. J Exp Med 2007, 204:893–906
8. Steinman RM, Hemmi H: Dendritic cells: translating innate to adaptive immunity. Curr Top Microbiol Immunol 2006, 311:17–58
9. Antoine JC, Prina E, Courret N, Lang T: Leishmania spp.: on the interactions they establish with antigen-presenting cells of their mammalian hosts. Adv Parasitol 2004, 58:1–68
10. Soong L: Modulation of dendritic cell function by Leishmania parasites. J Immunol 2008, 180:4355–4360
11. Konecny P, Stagg AJ, Jebbari H, English N, Davidson RN, Knight SC: Murine dendritic cells internalize Leishmania major promastigotes, produce IL-12 p40 and stimulate primary T cell proliferation in vitro. Eur J Immunol 1999, 29:1803–1811
12. Carvalho LP, Pearce EJ, Scott P: Functional dichotomy of dendritic cells following interaction with Leishmania braziliensis: infected cells produce high levels of TNF-α, whereas bystander dendritic cells are activated to promote T cell responses. J Immunol 2008, 181:6473–6480
13. Vargas-Inchaustegui DA, Xin L, Soong L: Leishmania braziliensis infection induces dendritic cell activation. ISG15 transcription, and the generation of protective immune responses J Immunol 2008, 180:7537–7545
14. Bennett CL, Misslitz A, Colledge L, Aebischer T, Blackburn CC: Silent infection of bone marrow-derived dendritic cells by Leishmania mexicana amastigotes. Eur J Immunol 2001, 31:876–883
15. Boggiatto PM, Jie F, Ghosh M, Gibson-Corley KN, Ramer-Tait AE, Jones DE, Petersen CA: Altered dendritic cell phenotype in response to Leishmania amazonensis amastigote infection is mediated by MAP kinase, ERK. Am J Pathol 2009, 174:1818–1826
16. Favali C, Tavares N, Clarencio J, Barral A, Barral-Netto M, Brodskyn C: Leishmania amazonensis infection impairs differentiation and function of human dendritic cells. J Leukoc Biol 2007, 82:1401–1406
17. Xin L, Li K, Soong L: Down-regulation of dendritic cell signaling pathways by Leishmania amazonensis amastigotes. Mol Immunol 2008, 45:3371–3382
18. Quinones M, Ahuja SK, Melby PC, Pate L, Reddick RL, Ahuja SS: Preformed membrane-associated stores of interleukin (IL)-12 are a previously unrecognized source of bioactive IL-12 that is mobilized within minutes of contact with an intracellular parasite. J Exp Med 2000, 192:507–516
19. Campos-Martín Y, Colmenares M, Gozalbo-Lopez B, Lopez-Nunez M, Savage PB, Martinez-Naves E: Immature human dendritic cells infected with Leishmania infantum are resistant to NK-mediated cytolysis but are efficiently recognized by NKT cells. J Immunol 2006, 176:6172–6179
20. Caparrós E, Serrano D, Puig-Kroger A, Riol L, Lasala F, Martinez I, Vidal-Vanaclocha F, Delgado R, Rodriguez-Fernandez JL, Rivas L, Corbi AL, Colmenares M: Role of the C-type lectins DC-SIGN and L-SIGN in Leishmania interaction with host phagocytes. Immunobiology 2005, 210:185–193
21. Tejle K, Lindroth M, Magnusson KE, Rasmusson B: Wild-type Leishmania donovani promastigotes block maturation, increase integrin expression and inhibit detachment of human monocyte-derived dendritic cells—the influence of phosphoglycans. FEMS Microbiol Lett 2008, 279:92–102
22. Nakahara T, Moroi Y, Uchi H, Furue M: Differential role of MAPK signaling in human dendritic cell maturation and Th1/Th2 engagement. J Dermatol Sci 2006, 42:1–11
23. Laban A, Tobin JF, Curotto de Lafaille MA, Wirth DF: Stable expression of the bacterial neor gene in Leishmania enriettii. Nature 1990, 343:572–574
24. Papadopoulou B, Roy G, Ouellette M: A novel antifolate resistance gene on the amplified H circle of Leishmania. EMBO J 1992, 11:3601–3608
25. Lutz MB, Kukutsch N, Ogilvie AL, Rossner S, Koch F, Romani N, Schuler G: An advanced culture method for generating large quantities of highly pure dendritic cells from mouse bone marrow. J Immunol Methods 1999, 223:77–92
26. Neves BM, Cruz MT, Francisco V, Garcia-Rodriguez C, Silvestre R, Cordeiro-da-Silva A, Dinis AM, Batista MT, Duarte CB, Lopes MC: Differential roles of PI3-Kinase. MAPKs and NF-κB on the manipulation of dendritic cell T_h1/T_h2 cytokine/chemokine polarizing profile Mol Immunol 2009, 46:2481–2492
27. Zhou BP, Hu MC, Miller SA, Yu Z, Xia W, Lin SY, Hung MC: HER-2/neu blocks tumor necrosis factor-induced apoptosis via the Akt/NF-κB pathway. J Biol Chem 2000, 275:8027–8031
28. Reiner NE, Ng W, McMaster WR: Parasite-accessory cell interactions in murine leishmaniasis. II. Leishmania donovani suppresses macrophage expression of class I and class II major histocompatibility complex gene products. J Immunol 1987, 138:1926–1932
29. Saha B, Das G, Vohra H, Ganguly NK, Mishra GC: Macrophage-T cell interaction in experimental visceral leishmaniasis: failure to express costimulatory molecules on Leishmania-infected macrophages and its implication in the suppression of cell-mediated immunity. Eur J Immunol 1995, 25:2492–2498
30. Poltorak A, He X, Smirnova I, Liu MY, Van Huffel C, Du X, Birdwell D, Alejos E, Silva M, Galanos C, Freudenberg M, Ricciardi-Castagnoli P, Layton B, Beutler B: Defective LPS signaling in C3H/HeJ and C57BL/10ScCr mice: mutations in Tlr4 gene. Science 1998, 282:2085–2088
31. Pierce JW, Schoenleber R, Jesmok G, Best J, Moore SA, Collins T, Gerritsen ME: Novel inhibitors of cytokine-induced IκBα phosphorylation and endothelial cell adhesion molecule expression show anti-inflammatory effects in vivo. J Biol Chem 1997, 272:21096–21103
32. Flohé SB, Bauer C, Flohé S, Moll H: Antigen-pulsed epidermal Langerhans cells protect susceptible mice from infection with the intracellular parasite Leishmania major. Eur J Immunol 1998, 28:3800–3811
33. Henri S, Curtis J, Hochrein H, Vremec D, Shortman K, Handman E: Hierarchy of susceptibility of dendritic cell subsets to infection by Leishmania major: inverse relationship to interleukin-12 production. Infect Immun 2002, 70:3874–3880
34. McDowell MA, Marovich M, Lira R, Braun M, Sacks D: Leishmania priming of human dendritic cells for CD40 ligand-induced interleukin-12p70 secretion is strain and species dependent. Infect Immun 2002, 70:3994–4001
35. von Stebut E, Belkaid Y, Nguyen BV, Cushing M, Sacks DL, Udey MC: Leishmania major-infected murine Langerhans cell-like dendritic cells from susceptible mice release IL-12 after infection and vaccinate

against experimental cutaneous Leishmaniasis. Eur J Immunol 2000, 30:3498–3506
36. Prina E, Abdi SZ, Lebastard M, Perret E, Winter N, Antoine JC: Dendritic cells as host cells for the promastigote and amastigote stages of Leishmania amazonensis: the role of opsonins in parasite uptake and dendritic cell maturation. J Cell Sci 2004, 117:315–325
37. Xin L, Li Y, Soong L: Role of interleukin-1β in activating the CD11c(high) CD45RB-dendritic cell subset and priming Leishmania amazonensis-specific $CD4^+$ T cells in vitro and in vivo. Infect Immun 2007, 75:5018–5026
38. Garg R, Barat C, Ouellet M, Lodge R, Tremblay MJ: Leishmania infantum amastigotes enhance HIV-1 production in cocultures of human dendritic cells and CD4 T cells by inducing secretion of IL-6 and TNF-α. PLoS Negl Trop Dis 2009, 3:e441
39. Cameron P, McGachy A, Anderson M, Paul A, Coombs GH, Mottram JC, Alexander J, Plevin R: Inhibition of lipopolysaccharide-induced macrophage IL-12 production by Leishmania mexicana amastigotes: the role of cysteine peptidases and the NF-κB signaling pathway. J Immunol 2004, 173:3297–3304
40. Chandra D, Naik S: Leishmania donovani infection down-regulates TLR2-stimulated IL-12p40 and activates IL-10 in cells of macrophage/monocytic lineage by modulating MAPK pathways through a contact-dependent mechanism. Clin Exp Immunol 2008, 154:224–234
41. Kaye PM, Rogers NJ, Curry AJ, Scott JC: Deficient expression of co-stimulatory molecules on Leishmania-infected macrophages. Eur J Immunol 1994, 24:2850–2854
42. Olivier M, Gregory DJ, Forget G: Subversion mechanisms by which Leishmania parasites can escape the host immune response: a signaling point of view. Clin Microbiol Rev 2005, 18:293–305
43. Argueta-Donohué J, Carrillo N, Valdes-Reyes L, Zentella A, Aguirre-Garcia M, Becker I, Gutierrez-Kobeh L: Leishmania mexicana: participation of NF-κB in the differential production of IL-12 in dendritic cells and monocytes induced by lipophosphoglycan (LPG). Exp Parasitol 2008, 120:1–9
44. Jayakumar A, Donovan MJ, Tripathi V, Ramalho-Ortigao M, McDowell MA: Leishmania major infection activates NF-κB and interferon regulatory factors 1 and 8 in human dendritic cells. Infect Immun 2008, 76:2138–2148
45. Ardeshna KM, Pizzey AR, Devereux S, Khwaja A: The PI3 kinase, p38 SAP kinase, and NF-κB signal transduction pathways are involved in the survival and maturation of lipopolysaccharide-stimulated human monocyte-derived dendritic cells. Blood 2000, 96:1039–1046
46. Gregory DJ, Godbout M, Contreras I, Forget G, Olivier M: A novel form of NF-κB is induced by Leishmania infection: involvement in macrophage gene expression. Eur J Immunol 2008, 38:1071–1081
47. Puig-Kröger A, Relloso M, Fernandez-Capetillo O, Zubiaga A, Silva A, Bernabeu C, Corbi AL: Extracellular signal-regulated protein kinase signaling pathway negatively regulates the phenotypic and functional maturation of monocyte-derived human dendritic cells. Blood 2001, 98:2175–2182
48. Rescigno M, Martino M, Sutherland CL, Gold MR, Ricciardi-Castagnoli P: Dendritic cell survival and maturation are regulated by different signaling pathways. J Exp Med 1998, 188:2175–2180
49. Ruhland A, Kima PE: Activation of PI3K/Akt signaling has a dominant negative effect on IL-12 production by macrophages infected with Leishmania amazonensis promastigotes. Exp Parasitol 2009, 122:28–36
50. Duclos S, Desjardins M: Subversion of a young phagosome: the survival strategies of intracellular pathogens. Cell Microbiol 2000, 2:365–377
51. Fratti RA, Backer JM, Gruenberg J, Corvera S, Deretic V: Role of phosphatidylinositol 3-kinase and Rab5 effectors in phagosomal biogenesis and mycobacterial phagosome maturation arrest. J Cell Biol 2001, 154:631–644
52. Coombes BK, Mahony JB: Identification of MEK- and phosphoinositide 3-kinase-dependent signalling as essential events during Chlamydia pneumoniae invasion of HEp2 cells. Cell Microbiol 2002, 4:447–460
53. Woolsey AM, Sunwoo L, Petersen CA, Brachmann SM, Cantley LC, Burleigh BA: Novel PI 3-kinase-dependent mechanisms of trypanosome invasion and vacuole maturation. J Cell Sci 2003, 116:3611–3622
54. Todorov AG, Einicker-Lamas M, de Castro SL, Oliveira MM, Guilherme A: Activation of host cell phosphatidylinositol 3-kinases by Trypanosoma cruzi infection. J Biol Chem 2000, 275:32182–32186
55. Wilkowsky SE, Barbieri MA, Stahl P, Isola EL: Trypanosoma cruzi: phosphatidylinositol 3-kinase and protein kinase B activation is associated with parasite invasion. Exp Cell Res 2001, 264:211–218

Pharm Res
DOI 10.1007/s11095-010-0268-6

RESEARCH PAPER

In Vitro and *In Vivo* Anticancer Activity of a Novel Nano-sized Formulation Based on Self-assembling Polymers Against Pancreatic Cancer

Clare Hoskins • Mehdi Ouaissi • Sofia Costa Lima • Woei Ping Cheng • Inês Loureirio • Eric Mas • Dominique Lombardo • Anabela Cordeiro-da-Silva • Ali Ouaissi • Paul Kong Thoo Lin

Received: 8 July 2010 / Accepted: 30 August 2010

ABSTRACT

Purpose To evaluate the *in vitro* and *in vivo* pancreatic anticancer activity of a nano-sized formulation based on novel polyallylamine grafted with 5% mole cholesteryl pendant groups (CH_5-PAA).

Methods Insoluble novel anticancer drug, Bisnaphthalimido-propyldiaaminooctane (BNIPDaoct), was loaded into CH_5-PAA polymeric self-assemblies by probe sonication. Hydrodynamic diameters and polydispersity index measurements were determined by photon correlation spectroscopy. The *in vitro* cytotoxicity evaluation of the formulation was carried out by the sulforhodamine B dye assay with human pancreatic adenocarcinoma BxPC-3 cells, while for the *in vivo* study, Xenograff mice were used. *In vitro* apoptotic cell death from the drug formulation was confirmed by flow cytometric analysis.

Results The aqueous polymer-drug formulation had a mean hydrodynamic size of 183 nm. The drug aqueous solubility was increased from negligible concentration to 0.3 mg mL^{-1}. CH_5-PAA polymer alone did not exhibit cytotoxicity, but the new polymer-drug formulation showed potent *in vitro* and *in vivo* anticancer activity. The mode of cell death in the *in vitro* study was confirmed to be apoptotic. The *in vivo* results revealed that the CH_5-PAA alone did not have any anti-proliferative effect, but the CH_5-PAA-drug formulation exhibited similar tumour reduction efficacy as the commercial drug, gemcitabine.

Conclusions The proposed formulation shows potential as pancreatic cancer therapeutics.

KEY WORDS amphiphilic polyallylamine · apoptosis · Bisnaphthalimidopropyl-diaminooctane · BxPC-3 cells · nanoparticles · pancreatic cancer · self-assembling polymers

C. Hoskins • P. Kong Thoo Lin (✉)
School of Pharmacy and Life Sciences, Robert Gordon University
St. Andrew Street
Aberdeen AB25 1HG Scotland, UK
e-mail: p.kong@rgu.ac.uk

M. Ouaissi • E. Mas • D. Lombardo
INSERM, UMR-911 CRO2, Faculté de Médecine
27 Blv Jean MOULIN
13385 Marseille Cedex 05, France

S. C. Lima • I. Loureirio • A. Cordeiro-da-Silva • A. Ouaissi
IBMC—Instituto de Biologia Molecular e Celular
Universidade do Porto
Rua do Campo Alegre 823
4150-180 Porto, Portugal

W. P. Cheng
School of Pharmacy, University of Hertfordshire
College Lane
Hatfield AL10 9AB, UK

A. Ouaissi
INSERM, CNRS, UMR 5235, Universite de Montpellier 2
Batiment 24-CC 107, Pl. Eugene Bataillon
34095 Montpellier Cedex 5, France

M. Ouaissi
Faculté de Médecine, Université Aix Marseille
Marseille 13000, France

Published online: 25 September 2010

INTRODUCTION

Ductal adenocarcinoma of the pancreas is the fourth causative death from malignant disease in Western countries (1). Because of its aggressiveness, it usually leads to death. Pancreatic resection currently remains the only chance to cure patients, with a 5-year overall survival rate between 7% and 34% compared to a median survival of 3–11 months for unresected cancer patients (2–4). Despite the application of a new combination of chemotherapy and radiation therapy, prognosis remains very poor (5). Gemcita-

bine is currently the drug of choice for treatment and has a response rate of 23.8% in pancreatic cancer patients (6). However, the relatively low response of gemcitabine means that there is still an urgent need for new and more efficient therapies. One group of compounds which has shown promise as potential anticancer agents is the Bisnaphthalimidopropyl (BNIP) diaminoalkylamines. In our laboratory, BNIP derivatives, Bisnaphthalimidopropyldiaminooctane (BNIPDaoct), were designed and synthesised to exhibit good *in vitro* cytotoxicity against colon, breast and leukaemia cells (Fig. 1). Although cell death in those cell lines was confirmed to be apoptotic, the precise mode of action of those compounds is yet to be determined, although DNA damage is implicated (7–10). The lack of aqueous solubility associated with this group of compounds has made *in vitro* and *in vivo* testing extremely difficult (11). Many approaches have been attempted to address this issue. Chemical modifications of the bisnaphthalimides both at the naphthalimido rings and the linker alkyl chains has been attempted but with limited success (11,12).

Since BNIPDaoct showed negligible aqueous solubility, harsh solvents such as DMSO have to be used to get the drug into solution (7). Recently, Thompson and colleagues reported the fabrication of novel comb-shaped polymers based on the hydrophobic and hydrophilic modification of a water-soluble polymer backbone, poly(allylamine) (PAA) (13). The polymer forms nano self-assemblies upon the aggregation of the hydrophobic pendant groups in aqueous media and has shown to encapsulate hydrophobic probes (13). To date, the use of self-assembling polymers for the delivery of hydrophobic anticancer agents has been extensively studied (14). These nano-containers have shown to encapsulate poorly soluble anticancer drugs, such as paclitaxel, etoposide within their lipophilic core via hydrophobic interactions (15–17). During their *in vivo* journey, the nano-carriers protect the drugs from enzymatic degradation, resulting in an effective delivery to the target site (18). The advantages of using nano-carriers in chemotherapy include increased drug solubility, prolonged drug exposure time, tumour-selective drug delivery via enhanced permeability and retention effect, improved therapeutic efficacy, decreased side effects, and lower drug resistance (19–21). However, most of the self-assembling polymers consist of block copolymers which are formed mainly via copolymerisation of hydrophobic and hydrophilic monomers (18,19,21). In this report, we used a novel self-assembling polymer based on modification of 15 kDa water-soluble polymer, polyallylamine (PAA) with cholesteryl moieties. There are limited studies on this type of polymer construct in drug delivery. To date, only a few reports using hydrophobically modified polyethylenimine (20), glycol chitosan (22), have shown promising potential in hydrophobic drug delivery. The cross-linked polyallylamine (PAA) has been used clinically as an oral phosphate binder (23); however, hydrophobically modified PAA as a delivery system for hydrophobic drugs has not been reported before. Furthermore, the use of modified PAA for biomedical application includes attachment of hydrophilic moiety (methyl glycolate) (24) or histidine to PAA for gene delivery (25), and the use of thiolated PAA as an intestinal permeation enhancer (26). None of the work thus far has attempted to attach a cholesteryl pendant group to PAA for hydrophobic drug delivery. Therefore, the novelty of this work lies in the *in vitro* and *in vivo* characterisation of a novel biomaterial for the delivery of an insoluble novel therapeutic agent. In this study, a formulation using the cationic PAA grafted with cholesteryl groups in 5% molar ratio (CH_5-PAA, Fig. 2) was applied to enhance the aqueous solubility of BNIPDaoct. The CH_5-PAA formulation incorporating BNIPDaoct was characterised, and the anticancer properties of such a formulation was studied both *in vitro* and *in vivo* using pancreatic BxPC-3 cancerous cells. The mechanism by which *in vitro* cell death occurs was explored using standard molecular approaches.

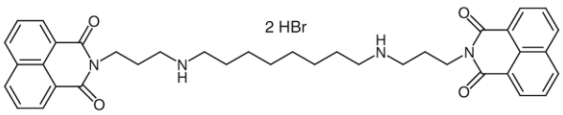

Fig. 1 Chemical structure of BNIPDaoct.

MATERIALS AND METHODS

Materials

Poly(allylamine) hydrochloride, cholesterol chloroformate, triethylamine, octane sulfonic acid, anhydrous sodium acetate, gemcitabine, carbonyl cyanide m-chlorophenylhydrazone and nonenzymatic cell-dissociation solution were from Sigma-Aldrich chemical company (UK). Thiopental was bought from

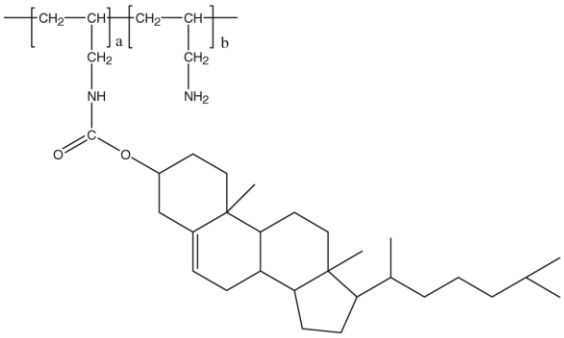

Fig. 2 Chemical structure of Cholesteryl-PAA (CH-PAA).

Sigma, St. Louis, MO. Visking tubing membranes were from Medicell International Ltd. (London, UK). GDX PVDF filters were purchased from Whatman, UK. DMSO, methanol and diethyl ether were from Fisher Scientific (UK). RPMI 1640 media, 10% heat-inactivated fetal bovine serum, 1% glutamine, L-gluthamine, penicillin, streptomycin and amphotericine B were from BioWhitaker (Belgium). TCA (trichloroacetic acid) and 2% saponin were purchased from Fluka (Switzerland). Tetramethylrodamine methyl ester was purchased from Molecular probes. FITC-conjugated annexin detection kit was from R&D Systems.

Methods

Synthesis and Characterisation of 5% Cholesteryl-PAA

Synthesis of 5% mole modification of Cholesteryl-PAA (CH_5-PAA, Fig. 2) was carried out as described by Thompson and colleagues (30). Briefly, 15 kDa PAA-HCl (10 g, Sigma-Aldrich) salt was dissolved in doubly distilled water. Sodium hydroxide pellets were added slowly until a pH of 13 was achieved, and the mixture was stirred for 1 h. The polymer was exhaustively dialysed against water using 7000 Dalton membrane for 24 h with six water changes (at 2 h intervals for first 8 h). The solution was recovered from the dialysis tubing and freeze-dried on a 48 h cycle. The free amino PAA (2 g) was dissolved in 100 mL chloroform:methanol (1:1 *v/v*). Triethylamine (2 mL) was added, and the mixture was stirred for 0.5 h. Cholesteryl chloroformate (0.6678 g) was dissolved in 20 mL chloroform:methanol (1:1 *v/v*) and then added drop-wise to the polymer solution over 2 h at 37°C. The mixture was then left stirring for 24 h at 37°C.

After 24 h, the solvent was removed using a rotary film evaporator, and the residue washed with diethyl ether (3× 100 mL). The dry residue was dissolved in doubly distilled water (50 mL), and the solution was exhaustively dialysed (molar weight cut-off = 7 kDa) against 5 L doubly distilled water for 24 h (6 water changes were made). The solution was freeze dried for 48 h, and the product was recovered as white cotton-like solid (2.2 g, 79% yield). The polymer was characterised by ^{1}HNMR (Bruker UltraShield 400 MHz) and elemental analysis (Strathclyde University, Glasgow, UK). BNIPDaoct was synthesised as previously reported (12).

Preparation of CH_5-PAA, BNIPDaoct Formulation

CH_5-PAA polymer solution (1 mg mL^{-1}) was prepared by dissolving the polymer in water followed by probe sonication (10 min). BNIPDaoct (1 mg mL^{-1}) was added to the Ch_5-PAA solution and sonicated for a further 10 min to ensure maximum drug solubilisation had occurred. The solution was filtered using 0.45 µm syringe filters with prefilters to remove any excess undissolved drug (20).

Characterisation of Novel CH_5-PAA, BNIPDaoct Formulation

Solubilisation of BNIPDaoct

BNIPDaoct concentration in self-assemblies was analysed using RP Zorbax ODS 250 mm×46 mm×5 µm HPLC column (Hichrom, UK). The mobile phase consisted of 55:45 (*v/v*) buffer:acetonitrile, and the flow rate was 1 mL min^{-1}. The buffer for the mobile phase was made up of 0.432 g octane sulfonic acid and 1.64 g anhydrous sodium acetate made up to 200 mL with deionised water; the solution was subsequently pH adjusted to pH 4.5. The column eluent was monitored at 234 nm excitation and 394 nm emission, using a fluorescent detector (Shimadzu prominence UFLC, UK). The samples were diluted with the mobile phase, and 20 µL was injected onto the column; the resultant peak at 10 min was analysed. A calibration was carried out by dissolving BNIPDaoct in DMSO:water (50:50 *v/v*) (39–625 µg mL^{-1}), R^2=0.999. The drug loading efficiency was calculated using the following formula:

$$\text{Drug loading efficiency} = \text{encapsulated drug analysed by HPLC/initial drug weight} \times 100$$

Sizing of Nano-aggregates

Hydrodynamic diameters and polydispersity index measurements were carried out on the CH_5-PAA alone and in polymer drug formulation using a photon correlation spectroscopy (PCS) (Zetasizer Nano-ZS, Malvern Instruments, UK). All measurements were conducted in triplicate at 25°C, and an average value was determined.

Cell Culture

Human pancreatic adenocarcinoma cell line BxPC-3 (ATCC) was maintained at 37°C in a humid atmosphere with 5% CO_2. The cells were grown in RPMI 1640 supplemented with 10% heat-inactivated fetal bovine serum, 1% glutamine, 2 mM L-gluthamine, 100 U ml^{-1} penicillin, 100 µg mL^{-1} streptomycin and amphotericine B.

Cytotoxic Activity

Cell viability was evaluated using the sulforhodamine B dye assay (SRB; Sigma-Aldrich) (38). Cells were seeded on 96-well plates at a density of 2×10^4 cells/well and incubated for 24 h at 37°C in 5% CO_2 atmosphere prior to the addition of different drugs and formulation. Cells were then treated with CH_5-PAA alone (0–30 µg/mL) and in CH_5-PAA-BNIPDaoct aqueous formulation (30 µg/mL polymer

and 0.04–10 μM drug); neat BNIPDaoct was dissolved in DMSO (50%) and gemcitabine in PBS, pH 7.4. The final concentration of DMSO used as control was 0.01%. After 48 h, the cells were fixed *in situ* by the addition of 50 μL of cold 50% (*w*/*v*) TCA (final concentration, 10% TCA) and incubated for 1 h at 4°C. Supernatants were discarded, and the plates were washed five times with water and air-dried. SRB solution (100 μL) at 0.4% (*w*/*v*) in 1% acetic acid was added to each well, and plates incubated for 10 min at room temperature. After staining, unbound dye was removed by five washes with 1% acetic acid, and then the plates were air dried. Bound SRB was subsequently solubilised with 200 μL of 10 mM Tris-base solution (pH 10.5) by agitating the plate on a shaker until the colour became homogeneous. SRB bound to the cellular protein content was determined by colorimetric measurement on an automated plate reader (515 nm). The IC_{50} values, defined as the drug concentration that inhibits 50% of growth compared to untreated cells, were then determined for each drug, polymer and formulation using the dose-dependent curves.

Detection of Apoptosis

Flow Cytometric Analysis of External Phosphatidylserine Exposure

Cells were seeded in 24-well plates at a density of 1×10^5 cells/well and allowed to adhere for 24 h followed by incubation with CH_5-PAA, CH_5-PAA-BNIPDaoct formulation, BNIPDaoct or gemcitabine (1 or 10 μM) for 24 h. Cells were collected and labelled with FITC-conjugated annexin V for 15 min, at room temperature, in a Ca^{2+}-enriched binding buffer (apoptosis detection kit, R&D Systems). PI (propidium iodide) (0.5 μg mL^{-1}) was added to exclude the necrotic cells with disrupted plasma membrane permeability, and the cells were analyzed by flow cytometry. Staurosporine-exposed cells (1 μM) were used as a positive control. All data were analyzed using CellQuest software (BD Biosciences, USA).

Measurement of Mitochondrial Membrane Potential

Tetramethylrhodamine methyl ester (TMRE) is a cationic lipophilic dye that readily accumulates in active mitochondria. For the determination of mitochondrial membrane potential ($\Delta\Psi$), the cells were seeded in 24-well plates at a density of 1×10^5 cells/well and allowed to adhere for 24 h followed by incubation with CH_5-PAA, CH_5-PAA-BNIPDaoct formulation, BNIPDaoct or gemcitabine (1 or 10 μM) for 24 h. Drug-treated or non-treated cells were washed in PBS and incubated with 200 nM of TMRE for 30 min at 37°C and 5% CO_2 and analyzed by flow cytometry on the FL2-H channel. PI (4 μg mL^{-1}) was used before the last acquisition to exclude dead cells and recorded on FL3-H channel. As a positive control, cells already labelled with TMRE for 30 min were treated during 20 min at 37°C with 200 μM final concentration of carbonyl cyanide m-chlorophenylhydrazone (CCCP), which depolarizes mitochondria by abolishing the proton gradient across the inner mitochondrial membrane (27).

Flow Cytometric Analysis of DNA Fragmentation

The DNA content of 1×10^5 cells/well incubated with 1 or 10 μM of CH_5-PAA, CH_5-PAA-BNIPDaoct formulation, BNIPDaoct or gemcitabine during 24 h was determined by flow cytometry using PI (0.5 μg mL^{-1}), after the cells were permeabilized with 50 μL of 2% saponin solution in PBS (28). After permeabilization, drug-treated or non-treated cells were washed in PBS and then analyzed by flow cytometry on the FL3-H channel.

In Vivo Effect of CH_5-PAA-BNIPDaoct Formulation on Xenograff Mice (Mice Implanted Subcutaneously with BxPC-3 Tumor Cells)

Female NMRI Nu/Nu mice, six weeks of age, (le Genest-St.-Isle, France) were kept in pathogen-free conditions (weight of mice was 24–30 g). All surgical procedures and animal care were carried out according to accreditation number 13416 given by the French ministry of agriculture. Human pancreatic cancer cell line BxPC-3 was cultured to 90% confluence in RPMI 1640 supplemented with 10% heat-inactivated fetal bovine serum, 2 mM L-glutamine, 100 U mL^{-1} penicillin, 100 μg mL^{-1} streptomycin and amphotericine B. The cells were washed twice with cold PBS and harvested with nonenzymatic cell-dissociation solution for 10 min at 37°C. The cells were washed three times with PBS and kept on ice until injection. Mice were transiently anesthetized (<30 s) with a low dose (2.5 mg) of thiopental to place them in the restraining tube. The tumour cell suspension (1.8×10^6 cells in 100 μL of PBS) was injected subcutaneously (s.c.) in the right flank of each mouse. When the tumour became palpable (two weeks), measurements in two dimensions with vernier calipers were carried out once a week and volume tumours calculated according to the formula $(\pi/6)\times(a\times b^2)$, where a is the largest and b the smallest diameter of the tumour.

Drug treatments were performed twice per week for four weeks. Four groups of mice were studied: Group 1 mice (n=13) received intraperitoneal injections (i.p.) of 1 mg kg^{-1} CH_5-PAA, 0.3 mg kg^{-1} BNIPDaoct aqueous formulation in a volume of 100 μL; Group 2 mice (n=6) received i.p. injections of 1 mg kg^{-1} CH_5-PAA aqueous solution in a volume of 100 μL; Group 3 mice (n=11)

received i.p. injections of 2.5 mg kg^{-1} of gemcitabine dissolved in PBS.

The treatment efficacy was evaluated by the change in tumour volume during the treatment period. The measurement for the tumour volume was performed twice per week for four weeks. After five weeks of treatment, the mice were sacrificed. Differences between the means of unpaired samples were evaluated by the Mann Whitney test, and the results were considered statistically different when $p<0.05$.

RESULTS

Synthesis and Characterisation of CH_5-PAA

The ^{1}HNMR confirmed the synthesis, and the elemental analysis showed the cholesteryl grafting value (4.7% mole) was in close agreement with the initial molar feed ratios (13). The proton assignments for CH_5-PAA are: $\delta_{0.75}$, $\delta_{0.9}$, $\delta_{1.0}$, $\delta_{1.1}$ = CH_3 (cholesteryl), $\delta_{1.1–2.1}$ = CH_2 (cholesteryl and PAA), $\delta_{2.3}$ = CH_2 (cholesteryl), $\delta_{2.4–3.2}$ = CH_2 (PAA), $\delta_{4.4}$ = CH–O (cholesteryl), $\delta_{5.4}$ = CH (cholesteryl).

Characterisation of Novel CH_5-PAA-BNIPDaoct Formulation

At 1 mg mL^{-1}, CH_5-PAA formed a clear colourless solution. The self-assemblies formed had a hydrodynamic radius of 167 nm (Table 1); the low polydispersity index indicated that the aggregates formed were mostly uniform in size. CH_5-PAA possessed a critical aggregation concentration (CAC) at 0.02 mg mL^{-1}; this was the lowest polymer concentration required for spontaneous self-assembly formation to occur (13). The CAC value was previously determined with the use of a hydrophobic methyl orange probe, whereby a hypsochromic shift was observed on encapsulation into the self-assemblies driven by non-covalent hydrophobic interactions (13).

The drug powder clumped together when it was mixed with water. Filtered BNIPDaoct aqueous solution showed negligible aqueous solubility as it was not detectable by HPLC. However, CH_5-PAA was capable of solubilising 0.3 mg mL^{-1} of the BNIPDaoct at 1 mg mL^{-1} polymer concentration using 1:1 initial drug:polymer loading weight ratio. Filtration removed the excess undissolved drug in the formulation. Before filtration, the undissolved drug was clearly visible as yellowish solids clumped together at the top of the solution. Once filtered, the final solution was an optically clear yellowish solution indicating the encapsulation of the drug in the polymeric self-assemblies. The hydrodynamic radius of the polymeric self-assemblies increased from 167 nm to 183 nm in the presence of BNIPDaoct. The low PDI indicates uniform size population in the formulation (Table 1).

Table 1 Hydrodynamic Radius and Polydispersity Index of CH_5-PAA Polymer Solution and CH_5-PAA-BNIPDoact Formulation Determined by Photon Correlation Spectroscopy

Polymer/Formulation	Size (nm)	Polydispersity index (PDI)
CH_5-PAA	167 ± 3	0.190 ± 0.100
CH_5-PAA-BNIPDaoct	183 ± 2	0.167 ± 0.001

All solutions was tested at 1 mg mL^{-1} polymer concentration ($n = 3 \pm$SD).

In Vitro Cytotoxic Activity

The human pancreatic cells (BxPC-3) were subjected to CH_5-PAA, CH_5-PAA-BNIPDaoct formulation, BNIPDaoct or gemcitabine treatments. The anti-proliferative effects were evaluated with final concentrations ranging from 0.04 to 10 μM for 48 h, resulting in a dose-dependent inhibition of cell growth, quantified by SRB dye assay (Fig. 3). The polymer (CH_5-PAA) alone up to 30 μ mg/mL and DMSO (0.01%) had no cytoxicity on the pancreatic cancer cells, while CH_5-PAA-BNIPDaoct formulation and BNIPDaoct had a half maximal inhibitory concentration (IC_{50}) of 1.06 ± 0.13 μM and 1.11 ± 0.12 μM, respectively. The presence of polymer did not alter the cytotoxicity effect of BNIPDaoct. BxPC-3 cells exhibited a notably lower sensitivity to gemcitabine with an IC_{50} value of 8.5 ± 0.18 μM, indicating that gemcitabine is less effective than BNIPDaoct.

In Vitro Apoptotic Analysis

Mediated CH_5-PAA-BNIPDaoct formulation and BNIPDaoct apoptosis were studied by the combination of a number of assays. Flow cytometry experiments were carried out at least three times and in duplicates (Figs. 4, 5, and 6). Although drug concentration of 5 μM was attempted, similar results were obtained with 1 and 10 μM drug concentrations (data not shown). With the exception of the DNA fragmentation assay, the cells analysed were gated for the live population. In general, the best results were obtained with compounds at 10 μM concentration.

In apoptotic cells, the membrane phospholipid phosphatidylserine (PS) is translocated from the inner to the outer leaflet of the plasma membrane, thereby exposing PS to the external cellular environment. Substantial increase in phosphatidylserine exposure induced by CH_5-PAA-BNIPDaoct formulation (80%) and BNIPDaoct (90%) was observed using Annexin V/PI assays (Fig. 4) at 10 μM drug concentration when compared with the positive control staurosporine (1 μM). It is interesting to note that at 10 μM drug concentration, both CH_5-PAA and gemcitabine showed similar levels of annexin V-positive

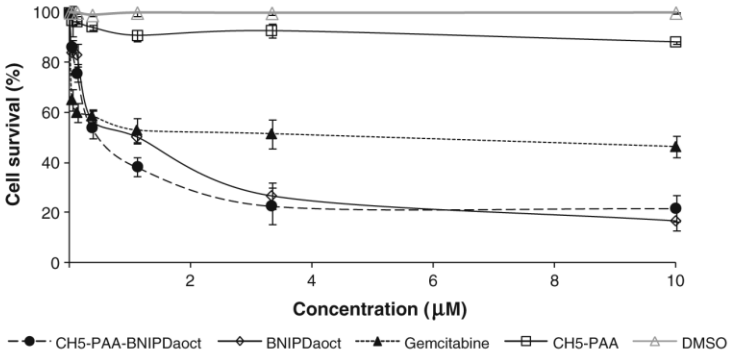

Fig. 3 Dose-dependent inhibition of BxPC-3 cell growth by CH_5-PAA-BNIPDaoct formulation, BNIPDaoct or gemcitabine (0–10 μM). The CH_5-PAA concentration used in all formulations was 30 μg/mL. CH_5-PAA alone was tested from 0 to 30 μmg/mL and DMSO was at 0.01% concentration. Cells (2×10^4/well) were seeded in 96-well plates and incubated overnight. Compounds were added at various concentrations, and cells were further incubated for 48 h. Cell proliferation was determined by SRB assay. The data is representative of three experiments carried out independently.

cells. No significant effect was detected with 1 μM drug concentration.

Mitochondrial damage as a result of depolarized Δψm, is often observed during the early apoptotic stages and may be a prerequisite for cytochrome *c* release (28). Therefore, experiments were carried out to determine whether drug-treated tumour cells induced a decrease in Δψm. The results shown in Fig. 5 demonstrated a significant increase in the percentage of cells exhibiting reduced Δψm upon drug treatment during 24 h with 1 or 10 μM of either CH_5-PAA-BNIPDaoct formulation or BNIPDaoct. The effect obtained was comparable to that observed with the positive control treatment using CCCP and higher than that of the standard drug gemcitabine.

The above observations prompted us to investigate the changes occurring in the nuclear material of drug-treated cells by flow cytometry analysis after cell permeabilization and the labelling with PI. As shown in Fig. 6, both CH_5-PAA-BNIPDaoct formulation and BNIPDaoct at 10 μM concentrations and after 24 h exposure induced DNA fragmentation in BxPC-3 cells at a level significantly higher than that shown when using Staurosporine as a positive control. Furthermore those effects were five times the mean

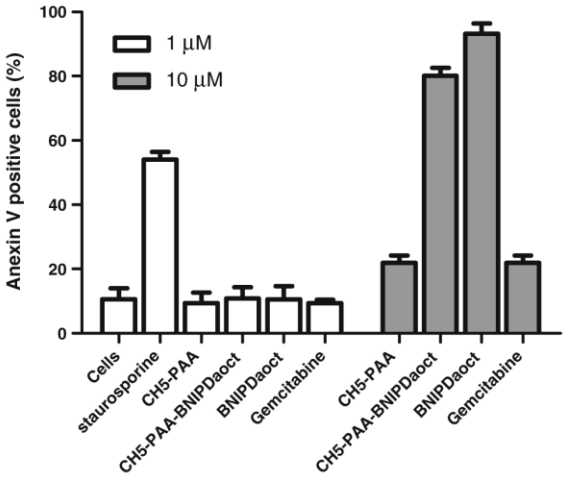

Fig. 4 Effect of CH_5-PAA, CH_5-PAA-BNIPDaoct formulation, BNIP-Daoct or gemcitabine on phosphatidylserine exposure to BxPC-3 cells. Cells were treated during 24 h with either 1 or 10 μM drug. After PBS washing, cells were stained with annexin V-FITC and propidium iodide and analyzed by cytometry. Staurosporine (1 μM, 24 h) treatment was used as a positive control. Data are representative of three independent experiments. PI-positive cells were excluded.

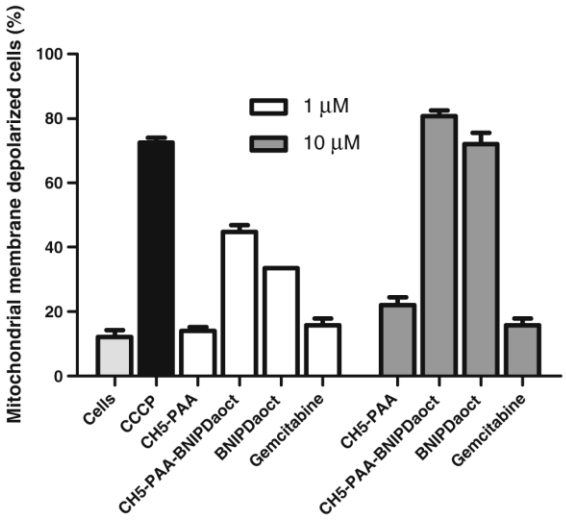

Fig. 5 Flow cytometry analysis of mitochondrial membrane depolarisation in BxPC-3 cells after 24 h treatment with 1 or 10 μM of either CH_5-PAA, CH_5-PAA-BNIPDaoct formulation, BNIPDaoct or gemcitabine. The percentage of cells exhibiting reduced ΔΨM was determined by flow cytometry using TMRE. CCCP was used as a positive control. Data are representative of three independent experiments. PI-positive cells were excluded.

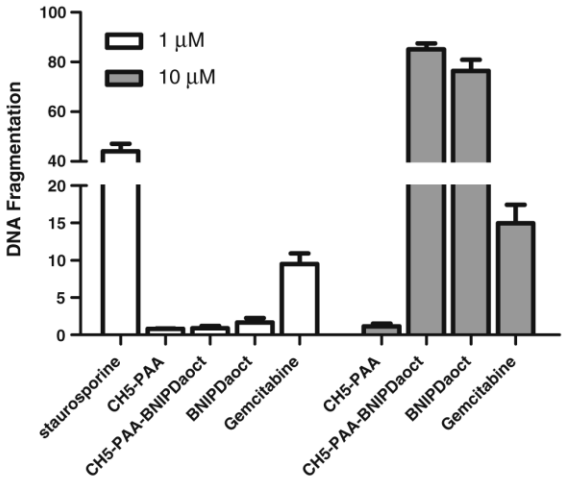

Fig. 6 Flow cytometry analysis of DNA fragmentation in tumor cells after incubation with CH_5-PAA, CH_5-PAA-BNIPDaoct formulation, BNIPDaoct or gemcitabine (1 or 10 μM). Cells with or without the drug treatment during 24 h were permeabilized with saponin, stained with propidium iodide and analyzed by cytometry. The positive control consisted of cells treated with 1 μM Staurosporine during 24 h. Data are representative of three independent experiments.

value observed when using 10 µM concentration of gemcitabine. Interestingly, in this experiment, polymer CH_5-PAA exhibited negligible DNA fragmentation, hence confirming the low toxicity of the polymer.

In Vivo Effect of CH_5-PAA-BNIPDaoct Formulation on Xenograff Tumour (BxPC-3 Cell Line Implanted)

To further analyze the anti-proliferative activity of the drug-formulation, the effect of BNIP derivative was assessed on mice which were implanted subcutaneously with BxPC-3 tumour cells. Figure 7 presents a scatter plot of mean tumour volumes after administration of drugs. All formulations were well tolerated with no gross toxicity reaction observed. Statistical analysis using the Mann Whitney test showed significant difference in tumour size between CH_5-PAA-BNIPDaoct formulation and CH_5-PAA-treated mice after 6, 9, 12, 16 days treatment (*p values = 0.028, 0.01, 0.003, 0.028 respectively). This indicates that CH_5-PAA itself did not exhibit any anti-proliferative activity. After the third injection, statistically significant difference in tumour size between CH_5-PAA-BNIPDaoct formulation and gemcitabine-treated mice was observed (p = 0.006) (at day 6 after the beginning of IP treatment). Note that in this experiment the *in vivo* data showed the effectiveness of CH_5-PAA-BNIPDaoct formulation in reducing tumour growth in mice. The CH_5-PAA polymer alone was used as a negative control, i.e. tumour size keeps increasing with time, whereas Gemcitabine, a known anticancer drug currently used in the clinic against pancreatic cancer, was used as a positive control. It is noteworthy to mention that there was no effect on tumor growth when mice were treated with PBS alone (data not shown).

At the end of the *in vivo* study termination, the mean tumour volume of each group was determined (Fig. 8). The Mann Whitney test was then applied to compare the values for each group. The group of mice treated with CH_5-PAA alone did not experience a reduction in tumour growth, while mice treated with both BNIPDaoct formulation (p = 0.0159) and gemcitabine (p = 0.0138) had a statistically significant decrease in tumour size compared to CH_5-PAA. This strongly supports that CH_5-PAA-BNIPDaoct formulation is at least as efficient as gemcitabine. Indeed, there is no statistical difference between the CH_5-PAA-BNIPDaoct formulation and gemcitabine (Fig. 8).

DISCUSSION

Most pancreatic cancers are not diagnosed until after they have metastasized. Standard treatments for advanced disease include radiotherapy and/or chemotherapy regimens. However, radiotherapy is often toxic, and the chemotherapy which includes drugs such as 5-fluorouracil (5-FU) and gemcitabine is either ineffective or effective for only a short duration. Although gemcitabine has been shown to provide an improvement in the life quality (29), high intrinsic resistance of pancreatic cancer to currently available agents might explain the failure of gemcitabine alone and gemcitabine-based combination chemotherapy to achieve great success (30–32). Therefore, new therapeutic strategies are urgently needed. The search for means to interfere with the tumour cell proliferation led to the identification of a large number of natural and synthetic compounds that could revert the cell morphology of various cancer cells to apparently normal phenotype (33). Interestingly, some of these molecules exhibited histone deacetylase inhibitory activity. For instance, pancreatic adenocarcinoma cell lines IMIM-PC-1, IMIM-PC2 and RWP-1 have been shown to be highly sensitive to the apoptosis-inducing effect of Trichostatin (TSA) and suberoylanilide hydroxamid (SAHA) (34). Moreover, it has been reported that TSA could synergize with gemcitabine (35) or proteasome inhibitor PS-341 to induce apoptosis of pancreatic tumor cell lines (36). We have recently reported that a number of class I, II and III deacetylase inhibitors, bisnaphthalimidopropyl (BNIPDaoct) could induce apoptosis of various human pancreatic cancer cell lines *in vitro* (38,39). The above observations provide a rationale to investigate further the anti-pancreatic tumour properties of BNIPDaoct. The bulky multi-ring structures and long alkyl chains of BNIPDaoct are

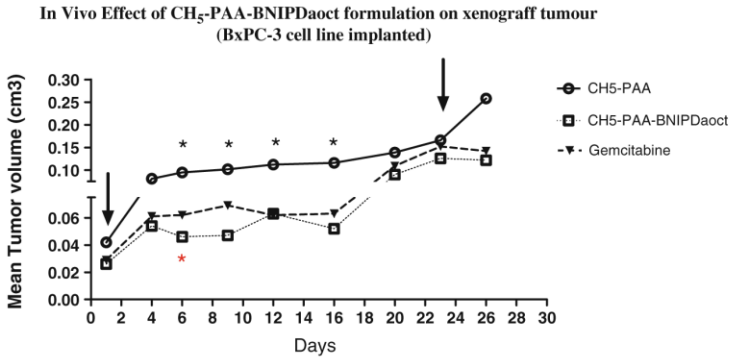

Fig. 7 Scatter plot of mean tumour volume in mice implanted with BxPC-3 cell line and treated with CH_5-PAA, CH_5-PAA-BNIPDaoct formulation, or gemcitabine. Treatment was started after 2 weeks of xenograff when tumour was palpable as described under Materials and Methods section. *Error bars* are SD. (*$P < 0.05$, CH_5-PAA-BNIP-Daoct formulation *vs* CH_5-PAA; **$P < 0.05$, CH_5-PAA,BNIPDaoct formulation *vs* gemcitabine). *Arrows* indicate the first and the last injection.

essential to preserve the activity of the drug. However, at the same time, this has resulted in undesirable physico-chemical properties of the drug. Negligible concentration of BNIPDaoct was obtained when the drug was dissolved in aqueous solution. As a result, *in vitro* assays were conducted using harsh solvents such as DMSO reported in our previous work (39). The poor aqueous solubility of the drug also restricts *in vivo* investigations, since a drug is commonly dissolved in aqueous media for *in vivo* parenteral administration.

Using the nano-carriers formed by amphiphilic polymer CH_5-PAA, an aqueous formulation of CH_5-PAA-BNIP-Daoct was successfully prepared with a drug loading efficiency of 30%. Upon incorporation of the novel anticancer drug BNIPDaoct into the polymeric self-assembly, a slight increase in aggregate size was observed. The size increased from 167 nm (unloaded CH_5-PAA) to 183 nm in the presence of the drug (Table 1). This increase in hydrodynamic radius can be attributed to expansion of the hydrophobic core in order to accommodate the BNIPDoact molecules (40). The polydispersity index was slightly lower for the CH_5-PAA-BNIPDaoct formulations (0.167) than for the Ch_5-PAA (0.190), indicating the drug-loaded aggregates were of a more uniform size distribution. The size of 178 nm is ideal, since it has been reported the size of <183 nm is important to ensure long circulation time *in vivo* (19)—the reason being, at this size, the nanoparticles are able to avoid the uptake of mononuclear phagocytic system (MPS) present in the liver and spleen. As a result, prolonged circulation will lead to accumulation at the tumour through the enhanced permeation and retention (EPR) effect (19).

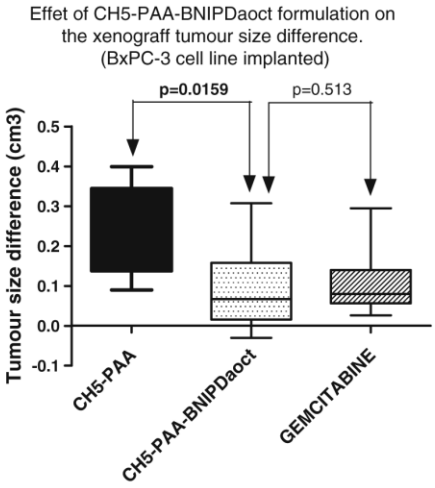

Fig. 8 The tumour size differences for each group were calculated using the following formula: tumour size at the end-tumour size at the start of treatment.

When human pancreatic (BxPC-3) cells were exposed to the novel CH_5-PAA-BNIPDaoct formulation *in vitro*, they possessed a notably lower IC_{50} than that of commercially available gemcitabine (8.50 μM), demonstrating that BxPC-3 cells are more sensitive to the cytotoxic effect of the polymer-drug formulation. The difference between the IC_{50} of the free drug dissolved in DMSO and the CH_5-PAA-BNIPDaoct formulation was negligible. This indicated that the polymer did not enhance the cytotoxic effect of the drug on the cells, and this corresponds with the non-cytotoxic profile of CH_5-PAA at the concentrations tested. However, the formulation is still advantageous for *in vivo* administration as it is desirable to eliminate the use of harsh solvents which can cause toxic side effects to the patient. The non-volatile nature of the formulation will result in greater dose reproducibility and ease of administration. *In vitro* analysis of the CH_5-PAA-BNIPDaoct formulation and BNIPDaoct alone confirm that both caused cell death by apoptosis. Interestingly, the data demonstrated that CH_5-PAA had negligible toxicity toward the tumor cell line. Furthermore, the CH_5-BNIP-Daoct formulation administered *in vivo* to nude tumour bearing mice was capable of reducing tumour growth rate when compared to CH_5-PAA alone.

Although the BNIPDaoct dose used in the formulation is eight-fold less than gemcitabine, the reduction in tumour growth was comparable to the current commercially

available drug gemcitabine for anticancer treatment. The reduction in tumour size was significant using the CH_5-PAA-BNIPDaoct formulation ($p<0.05$) compared to the polymer alone, CH_5-PAA. It has been reported that glycol chitosan modified with sterol structure, cholanic acid, was able to entrap docetaxel with the particle size of 320 nm and exhibited higher antitumour efficacy in lung cancer cell-bearing mice than free docetaxel. The authors showed reduced *in vivo* anticancer drug toxicity compared to free docetaxel and attributed this effect to the ability of nano-sized particles to preferentially localized in tumour tissues (22). Chytil and colleagues demonstrated that N-(2-hydroxypropyl)methacrylamide (HPMA)-doxorubicin conjugate modified with cholesteryl pendant groups resulted in significant tumour regression with long-term survival in mice bearing EL-4T cell lymphoma compared to other alkyl chains substituents such as dodecyl and oleic acid (40). This indicates that the presence of cholesterol moieties is beneficial, although the exact mechanism is not known. In this study, comparison between free drug and the formulation was not possible due to the insolubility of the drug in aqueous solution for *in vivo* administration. Based on other similar work, it is hypothesized that EPR effect resulted in the antitumour efficacy observed in this study.

CONCLUSION

Pancreatic cancer remains an untreatable disease, which in most cases is uniformly lethal. Here we show that polyallylamine grafted with cholesteryl moieties (CH_5-PAA) was able to increase the water solubility of a practically insoluble anticancer agent, BNIPDaoct. The drug-loaded self-assembled aggregates had a mean diameter of 178 nm with a narrow size distribution. This formulation showed a greater cytotoxic effect *in vitro* on human pancreatic carcinoma cells than the leading drug gemcitabine in human pancreatic cancer cells, BxPC-3, while the polymer itself was non-cytotoxic. Although the BNIPDaoct dose was eight-fold less than gemcitabine, the formulation was able to reduce tumour growth in xenograft mice with results comparable to gemcitabine. The results of this study indicate that CH_5-PAA-BNIPDaoct has great potential as a suitable therapeutic alternative to gemcitabine for treatment of pancreatic cancer.

ACKNOWLEDGEMENTS

SCL is supported by a fellowship from FCT (SFRH/BPD/37880/2007). Clare Hoskins was funded by Robert Gordon University, Research Development Initiative scheme.

Conflict of Interest The authors do not have any conflicts of interest to report.

REFERENCES

1. Lowenfels AB, Maisonneuve P. Epidemiology and prevention of pancreatic cancer. Jpn J Clin Oncol. 2004;34:238–44.
2. Sarkar FH, Li Y, Wang Z, Kong D. Pancreatic cancer stem cells and EMT in drug resistance and metastasis. Minerva Chir. 2009;64:489–500.
3. Jemal A, Thomas A, Murray T, Thun M. Cancer statistics. Cancer J Clin. 2002;52:23–47.
4. Sa Cunha A, Rault A, Laurent C, Adhoute X, Vendrely V, Bellannee G, *et al.* Surgical resection after radiochemotherapy in patients with unresectable adenocarcinoma of the pancreas. J Am Coll Surg. 2005;201(3):359–65.
5. Lockhart AC, Rothenberg ML, Berlin JD. Treatment for pancreatic cancer: current therapy and continued progress. Gastroenterology. 2005;128:1642–54.
6. Novarino I, Chiappin GF, Bertelli A, Heouaine G, Ritorto A, Addeo G, *et al.* Phase II study of cisplatin, gemcitabine and 5-fluorouracil in advanced pancreatic cancer. Ann Oncol. 2004;15:474–7.
7. Oliveira J, Ralton L, Tavares J, Codeiro-da-Silva A, Bestwick C, McPherson A, *et al.* The synthesis and the in vitro cytotoxicity studies of bisnaphthalimidoproply polyamine derivatives against colon cancer cells and parasite *Leishmania infantum*. Bioorganic Med Chem. 2007;15:541–5.
8. Dance A-M, Ralton L, Fuller Z, Milne L, Duthie S, Bestwick C, *et al.* Synthesis and biological activities of bisnaphthalimido polyamines derivatives: cytotoxicity, DNA binding, DNA damage and drug localization in breast cancer MCF 7 cells. Biochem Pharmacol. 2005;69:19–27.
9. Kong Thoo Lin P, Dance A-M, Bestwick C, Milne L. The biological activities of new polyamine derivatives as potential therapeutic agents. Biochem Soc Trans. 2003;31:407–10.
10. Ralton L, Bestwick CS, Milne L, Duthie S, Kong Thoo Lin P. The study of Bisnaphthalimidopropyl Spermidine and Spernine on DNA damage and repair within Colon Carcinoma Cells. Chem-Biol Interact. 2009;177:1–6.
11. Brana MF, Ramos A. Naphthalimides as anti-cancer agents: synthesis and biological activity. Curr Med Chem Anti-Canc Agents. 2001;1:237–55.
12. Kong Thoo Lin P, Pavlov VA. The synthesis and *in vitro* cytotoxic studies of novel Bis-naphthalimidopropyl polyamine derivatives. Bioorg Med Chem Lett. 2000;10:1609–12.
13. Thompson C, Ding C, Qu X, Yang Z, Uchegbu IF, Tetley L, *et al.* The effect of polymer architecture on the nano self-assemblies based on novel comb-shaped amphiphilic poly(allylamine). Colloid Polym Sci. 2008;286:1511–26.
14. Qiu L, Zheng C, Jin Y, Zhu K. Polymeric micelles as nanocarriers for drug delivery. Expert Opin Ther Pat. 2007;17:819–30.
15. Branco MC, Schneider JP. Self-assembling materials for therapeutic delivery. Acta Biomaterialia. 2009;5:817–3.
16. Letchford K, Burt H. A review of the formation and classification of amphiphilic block copolymer nanoparticulate structures: micelles, nanospheres, nanocapsules and polymersomes. Eur J Pharm Biopharm. 2007;65:259–69.
17. Nishiyama N, Kataoka K. Current state, achievements and future prospects of polymeric micelles as nanocarriers for drug and gene delivery. Pharmacol Ther. 2006;112:630–48.
18. Kwon G, Okano T. Polymeric micelles as new drug carriers. Adv Drug Deliv Rev. 1996;21:107–16.
19. Qui L, Zheng C, Jin Y, Zhu K. Polymeric micelles as nanocarriers for drug delivery. Expert Opin Ther Pat. 2007;17:819–30.
20. Cheng WP, Gray AI, Tetley L, Hang TLB, Schätzlein AG, Uchegbu IF. Polyelectrolyte nanoparticles with high drug loading enhance the oral uptake of hydrophobic compounds. Biomacromolecules. 2006;7:1509–20.

21. Kwon G, Kataoka K. Block Copolymer micelles as long-circulating drug vehicles. Adv Drug Deliv Rev. 1995;16:295–309.
22. Hwang H-Y, Kim I-S, Kwon IC, Kim Y-H. Tumour targetability and antitumor effect of docetaxel-loaded hydrophobically modified glycol chitosan nanoparticles. J Control Release. 2008;128:23–31.
23. Albaaj F, Hutchison AJ. Hyperphosphataemia in renal failure: causes, consequences and current management. Drugs. 2003;63:577–96.
24. Boussif O, Delair T, Brua C, Veron L, Pavirani A, Kolbe HVJ. Synthesis of polyallylamine derivatives and their use as gene transfer vectors *in vitro*. Bioconjug Chem. 1999;10:877–83.
25. Chung YC, Hsieh WY, Young TH. Polycation/DNA complexes coated with oligonucleotides for gene delivery. Biomaterials. 2010;31:4194–203.
26. Vigl C, Leithner K, Albrecht K, Bernkop-Schnurch A. The effluc pump inhibitory properties of (thiolated) polyallylamines. J Drug Deliv Sci Technol. 2009;19:405–11.
27. Scaduto Jr RC, Grotyohann LW. Measurement of mitochondrial membrane potential using fluorescent rhodamine derivatives. Biophys J. 1999;76:469–77.
28. Nicoletti I, Migliorati G, Pagliacei MC, Grignani F, Riccardi C. A rapid and simple method for measuring thymocyte apoptosis by propidium iodide staining and flow cytometry. J Immunol Methods. 1991;139:271–9.
29. Mignotte B, Vayssiere JL. Mitochondria and apoptosis. Eur J Biochem. 1998;252:1–15.
30. Burris HA, Moore MJ, Andersen J, Green MR, Rothenberg ML, Modiano MR, *et al.* Improvements in survival and clinical benefit with gemcitabine as first-line therapy for patients with advanced pancreas cancer: a randomized trial. J Clin Oncol. 1997;15:2403–13.
31. von Wichert G, Seufferlein T, Adler G. Palliative treatment of pancreatic cancer. J Dig Dis. 2008;9:1–7.
32. O'Reilly EM, Abou-Alfa GK. Cytotoxic therapy for advanced pancreatic adenocarcinoma. Semin Oncol. 2007;34:347–53.
33. Burris H, Rocha-Lima III C. New therapeutic directions for advanced pancreatic cancer: targeting the epidermal growth factor and vascular endothelial growth factor pathways. Oncologist. 2008;13:289–98.
34. Mei S, Ho AD, Mahlknecht U. Role of histone deacetylase inhibitors in the treatment of cancer. Int J Oncol. 2004;25:1509–19.
35. Garcia-Morales P, Gomez-Martinez A, Carrato A, Martinez-Lacaci I, Barbera VM, Soto JL, *et al.* Histone deacetylase inhibitors induced caspase-independent apoptosis in human pancreatic adenocarcinoma cell lines. Mol Cancer Ther. 2005;4:1222–30.
36. Donadelli M, Costanzo C, Beghelli S, Scupoli MT, Dandrea M, Bonora A, *et al.* Synergistic inhibition of pancreatic adenocarcinoma cell growth by trichostatin A and gemcitabine. Biochim Biophys Acta. 2007;1773:1095–106.
37. Bai J, Demirjian A, Sui J, Marasc W, Callery MP. Histone deacetylase trichostatin A and proteasome inhibitor PS-341 synergistically induce apoptosis in pancreatic cancer cells. Biochim Biophys Res Comm. 2006;348:1245–53.
38. Ouaïssi M, Cabral S, Tavares J, Cordeiro da Silva A, Mathieu-Daude F, Mas E, *et al.* Histone deacetylase (HDAC) encoding gene expression in pancreatic cancer cell lines and cell sensitivity to HDAC inhibitors. Cancer Biol Ther. 2008;7:523–31.
39. Tavares J, Ouaissi A, Kong Thoo Lin P, Loureiro I, Kaur S, Roy N, *et al.* Bisnaphthalimidopropyl derivatives as inhibitors of Leishmania SIR2 related protein 1. ChemMedChem. 2010;5:140–7.
40. Chytil P, Etrych T, Konak C, Sirova M, Mrkvan T, Boucek J, *et al.* New HPMA copolymer-based drug carriers with covalently bound hydrophobic substituents for solid tumour targeting. J Control Release. 2008;127:121–30.

DOI: 10.1002/cmdc.200900367

Bisnaphthalimidopropyl Derivatives as Inhibitors of *Leishmania* SIR2 Related Protein 1

Joana Tavares,[a] Ali Ouaissi,[a, b] Paul Kong Thoo Lin,[c] Inês Loureiro,[a] Simranjeet Kaur,[d] Nilanjan Roy,[d] and Anabela Cordeiro-da-Silva*[a]

The NAD^+-dependent deacetylases, namely sirtuins, are involved in the regulation of a variety of biological processes such as gene silencing, DNA repair, longevity, metabolism, apoptosis, and development. An enzyme from the parasite *Leishmania infantum* that belongs to this family, LiSIR2RP1, is a NAD^+-dependent tubulin deacetylase and an ADP-ribosyltransferase. This enzyme's involvement in *L. infantum* virulence and survival underscores its potential as a drug target. Our search for selective inhibitors of LiSIR2RP1 has led, for the first time, to the identification of the antiparasitic and anticancer bisnaphthalimidopropyl (BNIP) alkyl di- and triamines (IC_{50} values in the single-digit micromolar range for the most potent compounds). Structure–activity studies were conducted with 12 BNIP derivatives that differ in the length of the central alkyl chain, which links the two naphthalimidopropyl moieties. The most active and selective compound is the BNIP diaminononane (BNIPDanon), with IC_{50} values of 5.7 and 97.4 μM against the parasite and human forms (SIRT1) of the enzyme, respectively. Furthermore, this compound is an NAD^+-competitive inhibitor that interacts differently with the parasite and human enzymes, as determined by docking analysis, which might explain its selectivity toward the parasitic enzyme.

Introduction

Proteins that belong to the silent information regulator 2 (SIR2) family, also known as sirtuins, are present in a variety of organisms from bacteria to humans.[1] They are involved in the regulation of a number of biological processes such as heterochromatin formation, gene silencing, DNA repair, development, longevity, metabolism, adipogenesis, and apoptosis (reviewed in reference [2]). Indeed, these proteins are classified as class III histone deacetylases, owing to their dependence on NAD^+ to deacetylate lysine residues of histones and non-histone substrates.[3–5] Apart from the deacetylase activity, some sirtuins also exhibit ADP-ribosyltransferase activity.[6,7]

Recent findings suggest a direct link between the activity of sirtuins and diseases such as cancer, HIV, and Parkinson's disease.[8–12] The first reports on sirtuin inhibitors identified, apart from the physiological inhibitor nicotinamide, synthetic inhibitors such as sirtinol and splitomicin (Figure 1).[13,14] Because these three compounds exhibit weak inhibitory properties, subsequent structure–activity studies led to the identification of more potent derivatives such as HR73 and β-phenylsplitomicin.[8,15,16] Furthermore, high-throughput screening against the human sirtuin SIRT1 led to the identification of an indole derivative (see Figure 1) as the most potent ($IC_{50} < 0.1$ μM) and selective inhibitor over two other NAD^+-dependent deacetylases, SIRT2 and SIRT3, described so far.[17] In addition, drugs that mimic adenosine (suramin) or that target enzymes or receptors, such as kinases, that bind to adenosine-containing cofactors or ligands have been identified as human SIR2 inhibitors.[18,19] Moreover, the recently reported co-crystal structure of a SIRT5–suramin complex has shed more light on the molecular nature of SIRT5 enzyme inhibition.[20]

Leishmaniasis is a parasitic disease caused by the protozoan parasites of the genus *Leishmania*, and is characterized by diverse clinical manifestations varying from localized ulcerative skin lesions to disseminated visceral infection. The latter is fatal when left untreated. *Leishmania* infects vertebrate hosts via the bite of a sand fly (*Phlebotomus* and *Lutzomya* spp.) during a blood meal, through the inoculation of infective flagellated promastigotes that invade or are phagocytosed by local or recruited host cells. In the phagolysosomes, the promastigotes differentiate into non-flagellated amastigotes, which multiply

[a] *Dr. J. Tavares, Dr. A. Ouaissi, I. Loureiro, Prof. Dr. A. Cordeiro-da-Silva*
IBMC – Instituto de Biologia Molecular e Celular
Universidade do Porto
Rua do Campo Alegre 823, 4150-180 Porto (Portugal)
and
Laboratório de Bioquímica
Faculdade de Farmácia da Universidade do Porto
R. Aníbal Cunha no. 164, 4050-047 Porto (Portugal)
Fax: (+351) 226 099 157
E-mail: cordeiro@ibmc.up.pt

[b] *Dr. A. Ouaissi*
INSERM, CNRS, UMR 5235, Université de Montpellier 2
Bâtiment 24-CC 107, Pl. Eugène Bataillon
34095 Montpellier Cedex 5 (France)

[c] *Prof. Dr. P. Kong Thoo Lin*
The Robert Gordon University
School of Pharmacy and Life Sciences
St. Andrew Street, Aberdeen AB25 1HG, Scotland (UK)

[d] *S. Kaur, Dr. N. Roy*
Centre of Pharmacoinformatics
National Institute of Pharmaceutical Education and Research
Sector 67, SAS Nagar 160062, Punjab (India)

Supporting information for this article is available on the WWW under http://dx.doi.org/10.1002/cmdc.200900367.

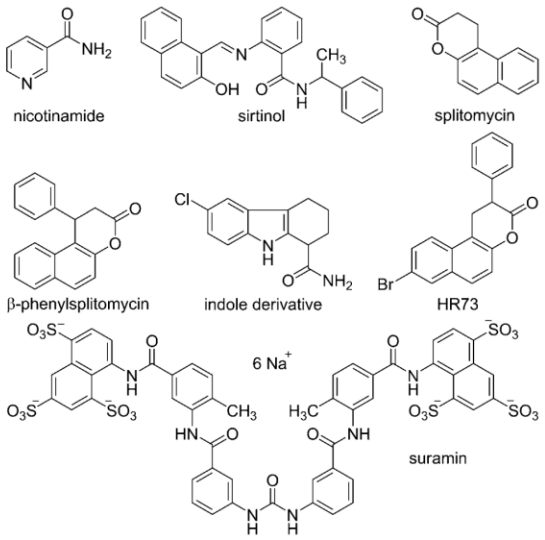

Figure 1. Examples of NAD^+-dependent SIR2 inhibitors.

and are able to infect other adjacent or distant macrophages. The classical treatment is currently unsatisfactory owing to side effects, the emergence of resistance, and the need for increased efficacy in immunosuppressed patients, especially due to HIV co-infection. During the past few years we have been interested in the protozoan parasite *Leishmania infantum* SIR2-related protein 1 (LiSIR2RP1) due to its role in the survival and virulence of the parasite.[21,22] Indeed, this cytosolic parasite protein, partially associated with the microtubule network, is a NAD^+-dependent tubulin deacetylase and an ADP-ribosyltransferase.[23]

In previous studies we have shown that bisnaphthalimidopropyl (BNIP) polyamine derivatives exert anti-leishmanial activity in vitro, inducing the death of promastigote forms by apoptosis.[24] The search for target-specific SIR2 inhibitors led us to evaluate whether BNIP derivatives can selectively inhibit the parasitic enzyme.[24–26]

Herein we report the first structure–activity relationship study of 12 BNIP derivatives with regard to their activity against human SIRT1 (hSIRT1) and the parasitic enzyme, LiSIR2RP1. The compounds differed in the length of the central alkyl chains, with 2, 3, or 4 nitrogen atoms, linking the two naphthalimidopropyl groups. We found that the most potent and selective inhibitor of LiSIR2RP1 is the BNIP diaminononane **6**, which has an alkyl linker containing nine methylene groups and two NH groups. Furthermore, this compound is an NAD^+-competitive inhibitor, and results from our molecular docking analysis suggest how it interferes differently with LiSIR2RP1 than with hSIRT1; this could explain the greater selectivity of compound **6** toward the parasitic enzyme.

Results and Discussion

Chemistry

We previously reported the synthesis of compounds such as (bisnaphthalimidopropyl)putrescine (BNIPPut), -spermidine (BNIPSpd), -spermine (BNIPSpm), and the bisnaphthalimidopropyl di- and triamines such as BNIPDaoct, BNIPDanon, BNIPDadec, BNIPDeta, and BNIPDpta.[25–27] The same methodology was used to carry out the synthesis of new compounds BNIPDapen (**2**), BNIPDahex (**3**), BNIPDahep (**4**), and BNIPDadodec (**8**).

The synthesis essentially involves a three-step reaction. Penta-, hexa-, hepta- and dodeca-diamines were first mesitylated with mesityl chloride in pyridine at room temperature. N-alkylation between the *N*-mesityl alkyl diamines and *o*-tosylpropylnaphthalimide[26] gave the corresponding protected compounds, which upon treatment with hydrobromic acid/glacial acetic acid yielded their respective products in high yields (80–94%; Scheme 1)

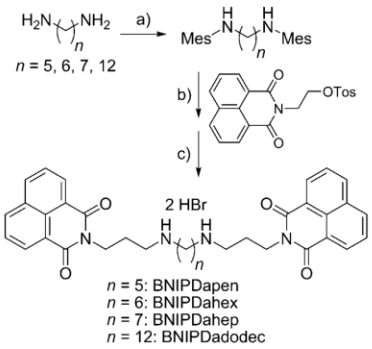

Scheme 1. Reagents and conditions: a) MesCl/pyridine, room temperature; b) DMF/Cs_2CO_3, 85 °C, 12 h; c) HBr/glacial acetic acid, CH_2Cl_2, room temperature, 12 h.

Enzyme inhibition

All BNIP derivatives and some of the commercially available sirtuin inhibitors such as nicotinamide, sirtinol, and suramin were tested in vitro for their ability to inhibit the *L. infantum* (LiSIR2RP1) and human (hSIRT1) forms of sirtuin. Experiments were conducted with a commercially available fluorimetric deacetylase assay. This coupled enzymatic assay uses a dual fluorophore- and quencher-labeled peptide that contains an acetylated lysine as substrate. After the peptide is deacetylated by sirtuin activity, it becomes a substrate for proteolysis by lysyl endopeptidase, resulting in separation of the quencher from the fluorophore; the ensuing fluorescence is then measured (see scheme S1, Supporting Information). To determine if the apparent inhibitory activity observed for the compounds tested is not due to inhibition of the intermediate proteolysis step, we measured the effect of each compound on this lysyl endopeptidase with a deacetylated peptide in place of the

acetylated one. None of the compounds was able to inhibit lysyl endopeptidase, confirming that inhibition is due to their interference with the NAD^+-dependent deacetylase activity of LiSIR2RP1 or hSIRT1 (see figure S1, Supporting Information).

We recently demonstrated that LiSIR2RP1 is an ADP-ribosyltransferase and an NAD^+-dependent deacetylase that can be inhibited in a noncompetitive manner by nicotinamide.[23] The mechanism by which nicotinamide inhibits the deacetylase activity of sirtuins is already known. In fact, nicotinamide inhibits these enzymes by interfering with an intermediate reaction. The positively charged *O*-alkyl amidate intermediate and nicotinamide are generated after the nucleophilic attack of the acetyl lysine carbonyl oxygen on the C1′ to the nicotinamide ribose of NAD^+.[6,28,29] When nicotinamide binds to the enzyme containing the *O*-alkyl amidate intermediate, both can react in a process known as nicotinamide exchange, in which the NAD^+ and the acetylated peptide are reformed.[6,28,30] In the presence of high concentrations of nicotinamide, this reaction occurs at the expense of deacetylation. The results listed in Table 1 indicate that LiSIR2RP1 is more sensitive to nicotinamide inhibition ($IC_{50} = 39.4 \pm 5.0$ μM) than hSIRT1 ($IC_{50} = 118.3 \pm 23.6$ μM). This could be due to differences in the flexible loop

Table 1. Inhibition of *L. infantum* SIR2RP1 (LiSIR2RP1) and human SIRT1 (hSIRT1) by known sirtuin inhibitors.

Compound	IC_{50} [μM][a] LiSIR2RP1	hSIRT1	SI[b]
nicotinamide	39.4 ± 5.0	118.3 ± 23.6	3.00
sirtinol	193.8 ± 31.8	245.5 ± 3.5	1.28
suramin	6.8 ± 0.7	2.4 ± 0.5	0.35

[a] Concentration of drug required to inhibit 50% of enzymatic activity relative to control; data are reported as the mean ± SD of at least three independent experiments. [b] Selectivity index = $(IC_{50\,hSIRT1})/(IC_{50\,LiSIR2RP1})$.

of the respective enzymes, which seems to be involved in the recognition of different substrates, and its close contact with the C pocket. Indeed, Avalos and colleagues[31] disclosed the mechanism of sirtuin inhibition by nicotinamide, highlighting the role of the C pocket. A structure-based mechanism was proposed, in which nicotinamide can be present in either a reactive or an entrapped conformation, and the *O*-alkyl amidate intermediate can exist in a contracted or extended conformation; these seem to be key factors for deacetylation or the nicotinamide exchange reaction. Furthermore, varying sensitivities to nicotinamide inhibition were reported for the yeast SIR2 in complexes with different proteins.[32]

Sirtinol has low inhibitory potency toward the *L. infantum* enzyme, with an IC_{50} value of 193.8 ± 31.8 μM (Table 1). The IC_{50} value toward hSIRT1 determined in this study (245.5 ± 3.5 μM, Table 1) is higher than that reported by others.[15] This could be due to its low aqueous solubility, although no significant difference in sirtinol's potency toward the parasite and human sirtuin forms was observed.

Suramin is a symmetric polyanionic naphthylurea originally used to treat sleeping sickness and onchocerciasis. Several other biological functions have been attributed to this compound and its derivatives, such as antiproliferative and antiviral activities.[33] Although suramin has been shown to interfere with numerous proteins, we thought it would be interesting to investigate whether it can act as a inhibitor of LiSIRTRP1 versus hSIRT1. Indeed, we show herein that suramin is a more active inhibitor of hSIRT1 ($IC_{50} = 2.4 \pm 0.5$ μM) than of LiSIRTRP1 ($IC_{50} = 6.8 \pm 0.7$ μM; Table 1). The inhibitory activity toward hSIRT1 agrees with the results reported by Schuetz and colleagues.[20] Furthermore, the structural basis of hSIRT5 inhibition by suramin reveals that this molecule interacts with the B and C pockets of the NAD^+ binding site as well as with the substrate binding site. Additionally, suramin acts as a linker molecule, leading to the dimerization of hSIRT5.[20] A similar mechanism of inhibition has been suggested by molecular docking and analysis of favorable interactions with human SIRT1 and SIRT2.[19]

A series of bisnaphthalimidopropyldiamine derivatives containing an alkyl linker with 4 (compound **1**) to 11 (compound **8**) methylene units were synthesized. We reasoned that with increasing length of the alkyl chain, the two naphthalimido rings are less likely to undergo π–π stacking interactions. The effect of introducing positive charges, through nitrogen atoms, on the bisnaphthalimido linker was also evaluated with compounds **9**–**12**. All of the tested bisnaphthalimidopropyl derivatives are capable of inhibiting the NAD^+-dependent deacetylase activity of LiSIR2RP1, with IC_{50} values < 55 μM. The most active compound against this enzyme, compound **6**, exhibited an IC_{50} value in the single-digit micromolar range (5.7 ± 0.2 μM; Table 2). On the other hand, the least effective compound was **12**, with an IC_{50} value of 54.7 ± 15.7 μM (Table 2). The selectivity index, which is the ratio of the inhibitory potencies of the BNIP derivatives toward LiSIR2RP1 versus hSIRT1, appears to depend on the length and net charge of the linker group. Indeed, BNIP diamine derivatives containing 4–7 methylene units (compounds **1**–**4**) in the linker are less active than those containing 8–12 methylene units (compounds **5**–**8**). The optimal distance between the two naphthalimidopropylamine groups that results in the most potent inhibitory activity toward LiSIR2RP1 was observed with compound **6**, the linker group of which contains nine methylene units. The introduction of positive charges in the linker does not improve potency. For example, compound **9** has eight atom units in the linker, of which seven are carbon and one is a nitrogen atom, and it is less active ($IC_{50} = 17.9 \pm 1.6$ μM) than compound **5**, which contains eight carbons ($IC_{50} = 9.2 \pm 1.4$ μM; Table 2).

All BNIP derivatives were less potent against hSIRT1 than toward the LiSIR2RP1. The IC_{50} values obtained with hSIRT1 vary between 43.1 and 182.8 μM (Table 2).

In contrast to our observations with LiSIR2RP1, changes in the linker do not significantly affect the potency of these compounds toward hSIRT1. Indeed, the most active compound on this enzyme is **11**, with an IC_{50} value of 43.1 ± 9.3 μM. These results suggest a certain degree of selectivity in some BNIP derivatives toward the parasite enzyme. The highest selectivity for

Table 2. Inhibition of *L. infantum* SIR2RP1 (LiSIR2RP1) and human SIRT1 (hSIRT1) by BNIP derivatives.

R =

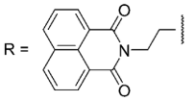

	Compound	Structure	IC_{50} [μM][a] LiSIR2RP1	hSIRT1	SI[b]
1	BNIPDabut	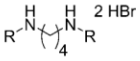	35.0 ± 5.8	73.1 ± 14.9	2.1*
2	BNIPDapen	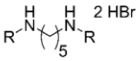	37.7 ± 6.9	82.2 ± 16.4	2.2*
3	BNIPDahex	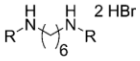	43.3 ± 9.5	93.5 ± 7.8	2.2**
4	BNIPDahep	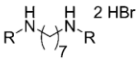	52.7 ± 5.2	127.5 ± 31.9	2.4*
5	BNIPDaoct	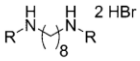	9.2 ± 1.4	116.5 ± 23.3	12.7**
6	BNIPDanon	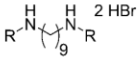	5.7 ± 0.2	97.4 ± 4.9	17.0***
7	BNIPDadec	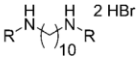	11.2 ± 1.6	113.8 ± 22.7	10.2**
8	BNIPDadodec	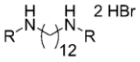	10.1 ± 1.2	94.7 ± 23.7	9.4**
9	BNIPSpd	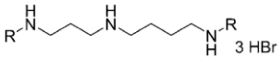	17.9 ± 1.6	94.8 ± 23.7	5.3**
10	BNIPSpm	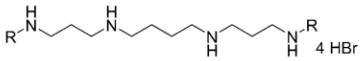	39.5 ± 6.5	102.2 ± 31.9	2.6**
11	BNIPDpta	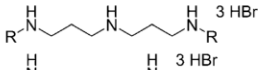	32.8 ± 2.4	43.1 ± 9.3	1.3
12	BNIPDeta	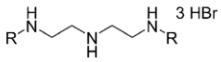	54.7 ± 15.7	182.8 ± 22.2	3.3**

[a] Data are reported as the mean ± SD of at least three independent experiments. [b] Selectivity index = $(IC_{50\,hSIRT1})/(IC_{50\,LiSIR2RP1})$; *$p < 0.05$, **$p < 0.01$, ***$p < 0.001$ between LiSIR2RP1 and hSIRT1.

LiSIR2RP1 was observed with compound **6**, followed by compounds **5** and **7**, as they are respectively 17-, 12.7-, and 10.2-fold more active against LiSIR2RP1 than hSIRT1.

In parallel, we examined the potential of BNIP molecules to exert anti-leishmanial activity particularly toward the form of the parasite that is present in the human host. The data show that the molecules indeed exert an efficient anti-intracellular amastigote activity, with IC_{50} values ranging from 1.01 ± 0.39 to 9.52 ± 0.56 μM (Table 3). It is not surprising that we observed no straight correlation between the inhibitory activities of BNIP compounds toward the enzymatic activity of LiSIR2RP1 and intracellular amastigote proliferation. Indeed, the enzyme assays were conducted with 0.25 μg of recombinant LiSIR2RP1 (rLiSIR2RP1), whereas LiSIR2RP1 is only weakly expressed in wild-type parasites. In fact, in a previous study, in order to co-immunoprecipitate a sufficient quantity of interacting LiSIR2RP1 partner(s) for identification by mass spectrometry, we were compelled to use transfected parasites overexpressing LiSIR2RP1.[34] Therefore, this might explain the discrepancies between the IC_{50} values.

Complementary experiments were done using an alternative method to evaluate the inhibitory effect of the BNIP derivatives on the NAD^+-dependent deacetylase activity of LiSIR2RP1. In a previous report we showed that, in the presence of NAD^+, LiSIR2RP1 deacetylates purified tubulin.[23] The reaction could be inhibited by nicotinamide and visualized by western blot using specific antibodies raised against either total α-tubulin or its acetylated form.[23] Figure 2 shows the effect of increasing concentrations of nicotinamide or compound **7** (each at 0.125, 0.25 and 0.5 mM) on NAD^+-dependent deacetylation of tubulin (0.5 μg) mediated by rLiSIR2RP1 (0.5 μg). Because DMSO was used to dissolve compound **7**, increasing amounts of DMSO (0.25, 0.5 and 1%) corresponding to the percentage present in each assay were used as controls. As expected, none of the DMSO concentrations inhibited tubulin deacetylation by LiSIR2RP1. In contrast, increasing amounts of compound **7** or nicotinamide were capable of inhibiting tubulin deacetylation mediated by LiSIR2RP1.

Table 3. Effect of BNIP derivatives on the intracellular development of *L. infantum* amastigotes.

	Compound	IC_{50} [μM][a]
1	BNIPDabut	4.53 ± 0.54
2	BNIPDapen	1.26 ± 0.18
3	BNIPDahex	3.46 ± 0.48
4	BNIPDahep	1.12 ± 0.0084
5	BNIPDaoct	2.43 ± 0.19
6	BNIPDanon	6.03 ± 0.67
7	BNIPDadec	1.02 ± 0.41
8	BNIPDadodec	1.01 ± 0.39
11	BNIPDpta	4.22 ± 1.07
12	BNIPDeta	9.52 ± 0.56

[a] PMA-differentiated THP-1 cells infected with amastigotes were incubated with a series of compound concentrations over 3 days. The growth inhibitory effect of the compounds was determined by luciferase assay, and IC_{50} values were determined by linear regression analysis; each experiment was performed in triplicate, and values represent the mean ± SD obtained for at least three independent experiments.

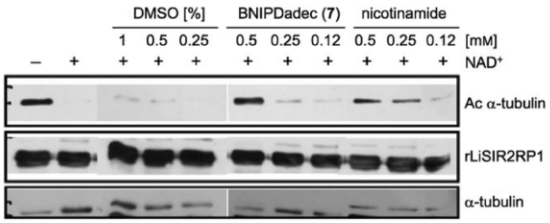

Figure 2. Compound **7** inhibits the deacetylation of α-tubulin by LiSIR2RP1: Purified tubulin dimers were incubated overnight at room temperature with purified rLiSIR2RP1 in the presence or absence of NAD^+ (1 mM) and nicotinamide or compound **7** (each at 0.5, 0.25, 0.125, 0 mM). The percentage of DMSO (1, 0.5, and 0.25%) present in each concentration of compound **7** was also evaluated. The reaction products were analyzed by western blot with specific antibodies to acetylated α-tubulin, α-tubulin, and LiSIR2RP1 as indicated.

To further analyze the inhibitory activity of BNIP derivatives, kinetics studies were performed with rLiSIR2RP1 and its most active inhibitor, **6**, by combining various drug and NAD^+ concentrations (Figure 3). A similar approach was conducted using increasing amounts of acetylated peptide substrate; the results are shown as Lineweaver–Burk plots. Compound **6** did not act as a competitive inhibitor of the LiSIR2RP1 substrate (Figure 3a). Its inhibitory effect on LiSIR2RP1 deacetylase activity is due to competition with NAD^+ (Figure 3b). The K_M values obtained for NAD^+ differed in the presence of compound **6** at 0, 3, or 6 μM (K_M = 45.0, 78.14, and 149.9 μM, respectively), while no significant differences were observed between their respective V_{max} values (138.9, 140.8, and 112.4 $F_{340/440}\,min^{-1}$). Based on these data, we hypothesize that **6** interacts with the NAD^+ binding site of the enzyme, or at least close enough to induce structural changes that interfere with NAD^+ binding.

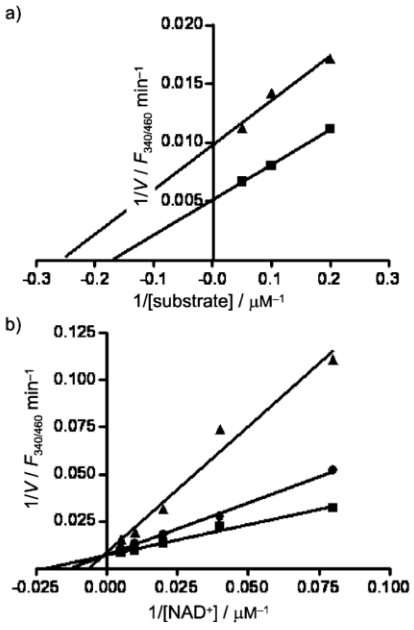

Figure 3. Kinetics of inhibition of LiSIR2RP1 by compound **6**: The rate of substrate deacetylation in the CycLex SIRT1/Sir2 deacetylase fluorimetric kit was measured in the presence (▲, ●) or absence (■) of compound **6** (7.5 μM); the concentration of substrate was fixed at 10 μM. a) Inhibition by compound **6** as a function of substrate concentration; the concentration of NAD^+ was fixed at 200 μM. b) Inhibition by **6** at 6 μM (▲) and at 3 μM (●) as a function of NAD^+ concentration (12.5, 25, 50, 100, and 200 μM).

Suramin and other related adenosine receptor antagonists, such as kinase inhibitors, were reported to be sirtuin inhibitors.[18–20,35] In fact, the screen of a library of kinase inhibitors led to the identification of a disubstituted bis(indol)maleimide as a potent and competitive inhibitor of NAD^+ (IC_{50} values of 3.5 and 0.8 μM against hSIRT1 and hSIRT2, respectively).[18]

Examination of the inhibitor binding site

To determine the potential structural differences between LiSIR2RP1 and hSIRT1, a homology model of both proteins was built and analyzed. The homology model of LiSIR2RP1 showed 40% identity with the template human SIRT2 as reference (PDB code: 1J8F).[36] The region showing 41% identity with the template (residues 242–525) was modeled out of a total of 747 amino acids in hSIRT1. The evaluation of these models using PROCHECK revealed that 93% of the residues are in the most favored regions of the Ramachandran plot for both models, with 0.4% of the residues in disallowed regions for hSIRT1. No residue was in the disallowed regions of the Ramachandran plot for LiSIR2RP1. The overall quality factor of the models was 78% for hSIRT1 and 66% for LiSIR2RP1. Based on this information, the homology models were considered to be reliable.

Four BNIP derivatives, (compounds **6**, **7**, and **8**, with low IC_{50} values) and compound **3** (with a high IC_{50} value), were selected for docking to validate the inhibitory action of these inhibitors on LiSIR2RP1. It was found that all of these compounds acting at the NAD^+ binding pocket, hence showing competition with NAD^+ (data not shown), which is in agreement with our experimental data. Compound **6** was found to be the best suited as an inhibitor among all other BNIP derivatives, owing to its lowest docking score and higher interaction with the target. Structural comparison of the binding pockets of LiSIR2RP1 and hSIRT1 revealed a highly conserved NAD^+ binding site; however, the binding mode of compound **6** differed considerably between the two proteins (Figure 4). The docking scores of compound **6** on LiSIR2RP1 and hSIRT1 are −17.2 and −15.8, and the numbers of hydrogen bonds formed are six and five, respectively. In hSIRT1, compound **6** interacts with Arg 274, Ser 442, and Asn 465 in the A pocket, and with Gln 345 in the B pocket; it is directed away from the C pocket, as shown in Figure 4. Compound **6** shows an interaction with the adenine sub-pocket (A pocket) and C pocket (NAD^+ hydrolysis region) in LiSIR2RP1. The residues involved in hydrogen bonding with **6** in LiSIR2RP1 include Ala 40, Gly 216, and Asn 241 present in the A pocket, and Asn 125 in the C pocket. The C pocket comprises residues Ser 43, His 106, Asp 127 and Asn 125, and is reported to be involved in the polarization and hydrolysis of the NAD^+ glycosidic bond, leading to the formation of the enzyme–ADP-ribose intermediate, as cited for human SIRT2.[37] The interaction of **6** with C pocket residues may interfere with

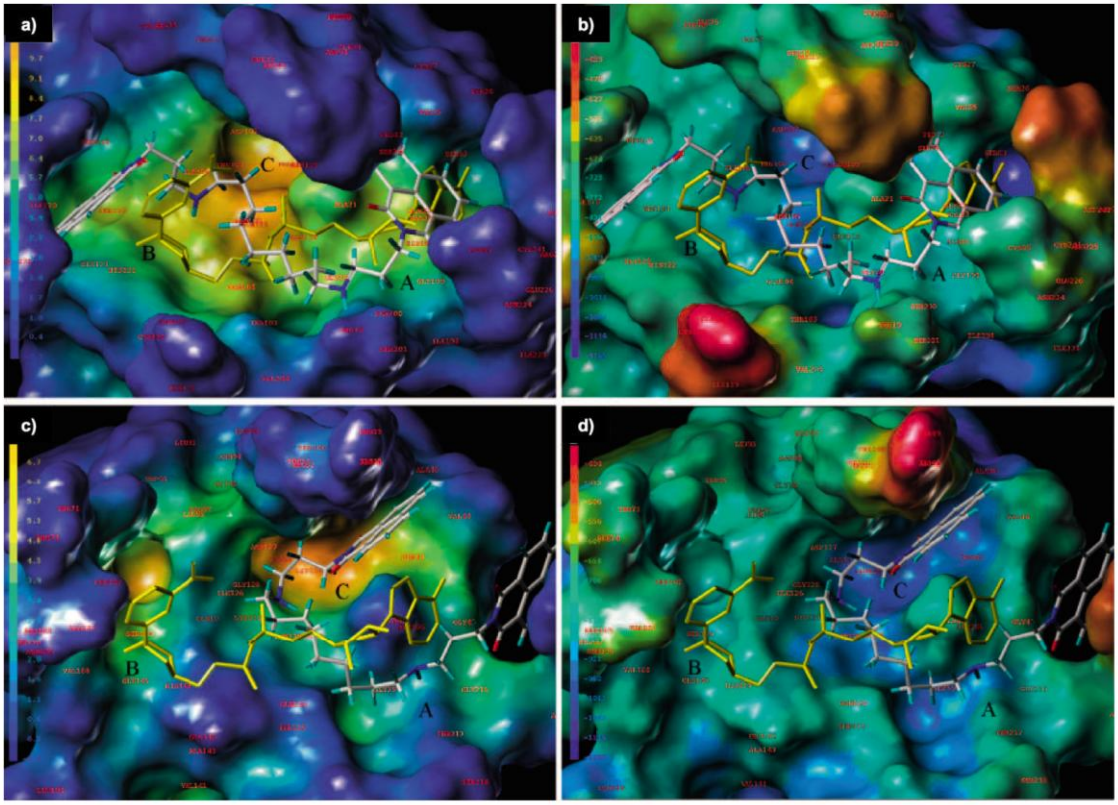

Figure 4. Cavity depth (a, c) and electrostatic surface analysis (b, d) for the binding pockets of: a, b) hSIRT1 and c, d) LiSIR2RP1. The NAD^+ molecule is shown in yellow, and compound **6** is colored by atom type. The A, B, and C pockets of the NAD^+ binding site are indicated (black letters). The numbers of hydrogen bonds formed are six and five in LiSIR2RP1 and hSIRT1, respectively. In hSIRT1, compound **6** interacts with Arg 274, Ser 442, and Asn 465 in the A pocket and Gln 345 in the B pocket, and is directed away from the C pocket. In LiSIR2RP1 **6** interacts with the adenine sub-pocket (A pocket) and the NAD^+ hydrolysis region (C pocket). The residues involved in hydrogen bonding with compound **6** in LiSIR2RP1 include Ala 40, Gly 216, and Asn 241 present in the A pocket, and Asn 125 in the C pocket. The interaction with the residues of the C pocket may interfere with NAD^+ hydrolysis, and thereby explains its action as an inhibitor.

NAD^+ hydrolysis, and therefore explains its action as an inhibitor. Furthermore, based on a detailed computational analysis, subtle differences in the catalytic and ligand binding domains between LmSIR2 and hSIR2 were recently reported, opening the possibility of selectively targeting the parasite enzyme.[36] However, co-crystal structure data are needed to establish the binding mode beyond doubt.

Conclusions

For the first time, BNIP derivatives have been identified as a new class of NAD^+-competitive SIR2 inhibitors that preferentially inhibit the *L. infantum* form of sirtuin (LiSIR2RP1). Furthermore, this study shows that despite the well-conserved catalytic core domain of SIR2 enzymes, subtle structural differences in the inhibitors can provide selective targeting. However, concerns about enzyme selectivity and inhibitory potency, which might be influenced by cellular NAD^+ concentrations, remain the key factors in the development of NAD^+-competitive SIR2 inhibitors.

Experimental Section

Chemistry

All reagents for syntheses were obtained from Sigma–Aldrich and Fluka, and were used without purification. Thin-layer chromatography (TLC) was performed on Kieselgel 60 F_{254} plates (Merck) in $CHCl_3/CH_3OH$ (97:3 or 99:1). FAB MS data were obtained on a VG Analytical AutoSpec instrument (25 Kv), and low-resolution EC/CI mass spectra were collected on a Micromass Quattro II. For accurate mass, ESI spectra were obtained on Finnigan MAT 900 XLT or 95T spectrometers. ^1H and ^{13}C NMR spectra were recorded on JEOL JNM-EX90 FT and Bruker 400 MHz instruments.

All compounds used in this work, with the exception of (bisnaphthalimidopropyldiamino)pentane (BNIPDapen), -hexane (BNIPDahex), -heptane (BNIPDahep), and -dodecane (BNIPDadodec), have been described previously.[25,26] The synthesis of these compounds is described below.

Step 1: Corresponding diaminopentane, -hexane, -heptane and -dodecane were dissolved in anhydrous pyridine, followed by the addition of mesityl chloride (MesCl; 2.1-fold molar excess). The resulting solution was stirred at room temperature for 4 h. Removal

of the pyridine followed by addition of cold H_2O resulted in the formation of a precipitate. The latter was filtered off and washed thoroughly with H_2O. The crude product was recrystallized from absolute EtOH.

Step 2: Mesitylated diamines (0.651 mmol) were dissolved in anhydrous *N*,*N*-dimethylformamide (DMF; 13.5 mL) followed by the addition of *O*-tosylpropylnaphthalimide[26] (0.13 mmol) and Cs_2CO_3 (1.06 g). The solution was left overnight at 80 °C. Completion of the reaction was monitored by TLC. DMF was removed in vacuo, and the residue was poured into cold H_2O. The resulting precipitate was filtered and washed thoroughly with H_2O. After drying, the crude product was recrystallized from EtOH to give the fully protected pure product in high yield (75–85%).

Step 3: The fully protected polyamine derivatives (0.222 mmol) were dissolved in anhydrous CH_2Cl_2 (10 mL), followed by the addition of hydrobromic acid/glacial acetic acid (1 mL). The solution was left to stir at room temperature for 24 h. The yellow precipitate formed was filtered off and washed with CH_2Cl_2, EtOAc and Et_2O.

BNIPDapen (83%), ^{1}H NMR ([D$_6$]DMSO): $\delta = 8.48–7.88$ (arom), 4.11 (2×N-CH$_2$), 3.01 (2×N-CH$_2$), 2.87 (N-CH$_2$), 2.02 (2×CH$_2$), 1.60 (2×CH$_2$), 1.34 ppm (-CH$_2$-); ^{13}C NMR ([D$_6$]DMSO): $\delta = 22.91$ (2×CH$_2$), 24.46 (CH$_2$), 24.79 (CH$_2$), 36.70 (CH$_2$), 44.72 (N-CH$_2$), 46.27 (N-CH$_2$), 121.99, 127.13, 130.62, 131.21, 134.31 (arom), 163.61 ppm (C=O); HRMS (FAB) calcd for $C_{35}H_{38}N_4O_4Br_2$: 577.2809 [M−2HBr+H]$^+$, found: 577.2827 [M−2HBr+H]$^+$

BNIPDahex (91%), ^{1}H NMR ([D$_6$]DMSO): $\delta = 8.48–7.88$ (arom), 4.09 (2×N-CH$_2$), 2.99 (2×N-CH$_2$), 2.86 (N-CH$_2$), 2.02 (2×CH$_2$), 1.56 (2×CH$_2$), 1.27 ppm (2×-CH$_2$-); ^{13}C NMR ([D$_6$]DMSO): $\delta = 24.52$ (CH$_2$), 25.21 (CH$_2$), 25.39 (CH$_2$), 36.72 (CH$_2$), 44.81 (N-CH$_2$), 46.54 (N-CH$_2$), 121.99, 127.13, 130.62, 131.21, 134.31 (arom), 163.61 ppm (C=O); HRMS (FAB) calcd for $C_{36}H_{40}N_4O_4Br_2$: 752.510, 671.2227 [M−Br]$^+$, found: 671.2221 [M−Br]$^+$.

BNIPDahep (94%), ^{1}H NMR ([D$_6$]DMSO): $\delta = 8.48–7.87$ (arom), 4.11 (2×N-CH$_2$), 2.99 (2×N-CH$_2$), 2.86 (N-CH$_2$), 2.02 (2×CH$_2$), 1.54 (2×CH$_2$), 1.25 ppm (3×-CH$_2$-); ^{13}C NMR ([D$_6$]DMSO): $\delta = 24.46$ (CH$_2$), 25.30 (CH$_2$), 25.66 (CH$_2$), 27.84, (CH$_2$), 36.70 (CH$_2$), 44.72 (N-CH$_2$), 46.60 (N-CH$_2$), 121.99, 127.13, 130.62, 131.21, 134.31 (arom), 163.58 ppm (C=O); HRMS (FAB): calcd for $C_{37}H_{42}N_4O_4Br_2$: 760.74, 605.3122 [M−2HBr+H]$^+$, found: 605.3126 [M−2HBr+H]$^+$.

BNIPDadodec (80%), ^{1}H NMR ([D$_6$]DMSO): $\delta = 8.47–7.87$ (arom), 4.11 (2×N-CH$_2$), 3.00 (2×N-CH$_2$), 2.85 (N-CH$_2$), 2.04 (2×CH$_2$), 1.55 (2×CH$_2$), 1.22 ppm (4×-CH$_2$-); ^{13}C NMR ([D$_6$]DMSO): $\delta = 24.46$ (CH$_2$), 25.39 (CH$_2$), 25.84 (CH$_2$), 28.40 (CH$_2$), 28.73 (CH$_2$), 28.82, (CH$_2$), 36.70 (CH$_2$), 44.72 (N-CH$_2$), 46.60 (N-CH$_2$), 121.99, 127.13, 130.62, 131.21, 134.31 (arom), 163.64 ppm (C=O): HRMS (FAB): calcd for $C_{42}H_{52}N_4O_4Br_2$: 836.709, 755.3166 [M−Br]$^+$, found: 755.3168 [M−Br]$^+$.

Compounds: Sirtinol, nicotinamide, and suramin were purchased from Sigma. Stock solutions of nicotinamide and suramin were prepared in phosphate-buffered saline (PBS), and the other compounds in DMSO, and they were all stored at −20 °C. Working solutions were freshly diluted in the enzyme reaction buffer to reach the desired final concentrations.

Biological assays

Fluorimetric deacetylase assay of rLiSIR2RP1 and hSIRT1: LiSIR2RP1 (N-terminal His$_6$ tag) was expressed in *E. coli* and purified by affinity chromatography, as previously reported by our research group.[23] The effects of the compounds on NAD$^+$-dependent deacetylase activity of the parasite (LiSIR2RP1) and human (SIRT1) forms of the enzyme were assessed by using a commercially available CycLex SIRT1/Sir2 deacetylase fluorimetric kit (CycLex Co. Ltd., Nagano, Japan). This assay system allows the detection of a fluorescent signal upon deacetylation of the peptide substrate, followed by cleavage through the action of a protease. Fluorescence was measured in a fluorimetric microplate reader (Synergy HT, BIOTEK) with excitation and emission wavelengths set at 340 and 440 nm, respectively. Reactions were performed in the presence of 200 μM NAD$^+$, 10 μM acetylated peptide, and each of the inhibitors at a range of various concentrations.

The inhibitory effect of the drugs on rLiSIR2RP1 and hSIRT1 activity is expressed as a percentage, and was calculated according to the ratio between the rates of the enzymatic reaction in the first 20 min in the presence and absence of the inhibitor.

Growth inhibition assays: The growth of LUC-expressing amastigotes in the human leukemia monocyte cell line (THP-1 cells) was evaluated according to Sereno et al.[38] with some modifications. Briefly, THP-1 cells were cultured in RPMI 1640 medium (Cambrex) supplemented with 10% heat-inactivated fetal bovine serum (FBS; Cambrex), 2 mM L-glutamine (Cambrex), 100 U mL^{-1} penicillin (Cambrex), and 100 μg mL^{-1} streptomycin (Cambrex). Log-phase THP-1 cells were differentiated by incubation for 2 days in medium containing 20 ng mL^{-1} PMA (Sigma). Once differentiated, the cells became adherent and were washed with pre-warmed medium and then infected with stationary axenic amastigotes expressing LUC at a parasite/macrophage ratio of 3:1 for 4 h at 37 °C under an atmosphere containing 5% CO_2. Non-internalized parasites were removed, and serial dilutions of each drug were added. After 3 days of incubation at 37 °C under 5% CO_2, the cells were washed and the luciferase activity was determined.

The luciferase activity of the LUC-expressing parasites was determined as described elsewhere,[39] and the values were expressed as relative light units (RLU). The percentage of growth inhibition was calculated as (1−RLU of drug-treated parasites)/(RLU drug-untreated parasites)×100. The IC_{50} values (concentration required to inhibit growth by 50%) were determined by linear regression analysis.

All compounds were initially tested in uninfected THP-1 cells before being incubated with macrophages harboring intracellular amastigotes, and the cytotoxicity was evaluated by MTT assay. Indeed, drug concentrations that were toxic toward uninfected macrophages were not used in the assays to determine IC_{50} values against intracellular amastigotes (data not shown).

Tubulin deacetylation assay: The deacetylation reactions in which tubulin was used as a substrate were performed with purified tubulin (Pure, Cytoskeleton Inc). The reactions were carried out in deacetylase buffer (10 mM Tris-HCl pH 8.0, 10 mM NaCl) containing 0.5 μg of either tubulin and LiSIR2RP1, in the presence or absence of 1 mM NAD$^+$, and left overnight with constant agitation at room temperature. The inhibitors, **7** and nicotinamide, were tested at concentrations of 0, 0.125, 0.250, and 0.5 mM. The amount of DMSO present in the tested concentrations for compound **7** was included as a control. The reactions were stopped by adding 5× Laemmli sample buffer; the proteins were separated by 10% SDS-PAGE and then subjected to western blot. The nitrocellulose membrane was probed with the following antibodies: mouse monoclonal anti-(acetylated tubulin) antibody (clone 6-11B-1) from Sigma; mouse monoclonal anti-(α-tubulin) antibody (clone DM1A) from

NeoMarkers, and the mouse monoclonal antibody IIIG4, produced as described by Vergnes and colleagues.[21]

Computational methods

Modeling and docking of inhibitors: Homology modeling was done for hSIRT1 and LiSIR2RP1 by using the comparative protein modeling program MODELLER. The crystal structure of human SIRT2 (PDB code: 1J8F) was used as a template in both cases. Sequences were aligned with the align2d command in MODELLER. The optimization of the models was done using molecular dynamics (MD) with the simulated annealing (SA) method in MODELLER. Out of the five models generated for each protein, the best model was evaluated based on the lowest MODELLER Objective function. The quality and geometry of models was checked using the program PROCHECK and VERIFY_3D in SAVES server. The NAD^+ molecule was added to the models using MOE. These models were then subjected to further refinement and energy minimization using the Biopolymer module in Sybyl. Molecular surface was generated using the Molcad module in Sybyl to analyze and compare the binding pocket of NAD^+ in both structures. Four BNIP derivatives—**3**, **6**, **7**, and **8**—showing a range of IC_{50} values, were selected to perform docking for LiSIR2RP1 and hSIRT1 using the FlexX module in Sybyl.

Statistical analysis: The data were analyzed using Student's *t* test.

Acknowledgements

This work was funded by the Fundação para a Ciência e Tecnologia (FCT) POCI 2010 and co-funded by FEDER grant number POCI/SAU-FCF/59837/2004, Centre Franco Indien pour la promotion de la recherche avancée; Indo–French Centre for the promotion of advanced research (CEFIPRA/IFCPAR) grant number 3603, and INSERM. Thanks to the EPSRC National Mass Spectrometry Service Centre at Swansea University, Swansea (UK) for mass spectral analysis, and the Treaty of Windsor Anglo–Portuguese Joint Research Programme for funding. J.T. is supported by a fellowship from FCT number SFRH/BD/18137/2004. The authors thank A. Ferreira for the English revision of the manuscript.

Keywords: docking · NAD^+-dependent deacetylases · protozoa · sirtuin inhibitors

[1] C. B. Brachmann, J. M. Sherman, S. E. Devine, E. E. Cameron, L. Pillus, J. D. Boeke, *Genes Dev.* **1995**, *9*, 2888–2902.
[2] K. Zhao, R. Marmorstein, in *Histone Deacetylases: Transcriptional Regulation and Other Cellular Functions* (Ed.: E. Verdin), Humana, Totowa NJ, **2006**, 203–217.
[3] S. Imai, C. M. Armstrong, M. Kaeberlein, L. Guarente, *Nature* **2000**, *403*, 795–800.
[4] B. J. North, B. L. Marshall, M. T. Borra, J. M. Denu, E. Verdin, *Mol. Cell* **2003**, *11*, 437–444.
[5] V. J. Starai, I. Celic, R. N. Cole, J. D. Boeke, J. C. Escalante-Semerena, *Science* **2002**, *298*, 2390–2392.
[6] A. A. Sauve, V. L. Schramm, *Curr. Med. Chem.* **2004**, *11*, 807–826.
[7] G. Liszt, E. Ford, M. Kurtev, L. Guarente, *J. Biol. Chem.* **2005**, *280*, 21313–21320.
[8] S. Pagans, A. Pedal, B. J. North, K. Kaehlcke, B. L. Marshall, A. Dorr, C. Hetzer-Egger, P. Henklein, R. Frye, M. W. McBurney, H. Hruby, M. Jung, E. Verdin, M. Ott, *PLoS Biol.* **2005**, *3*, e41.
[9] H. Vaziri, S. K. Dessain, E. Ng Eaton, S. I. Imai, R. A. Frye, T. K. Pandita, L. Guarente, R. A. Weinberg, *Cell* **2001**, *107*, 149–159.
[10] O. R. Bereshchenko, W. Gu, R. Dalla-Favera, *Nat. Genet.* **2002**, *32*, 606–613.
[11] H. Ota, E. Tokunaga, K. Chang, M. Hikasa, K. Iijima, M. Eto, K. Kozaki, M. Akishita, Y. Ouchi, M. Kaneki, *Oncogene* **2006**, *25*, 176–185.
[12] T. F. Outeiro, E. Kontopoulos, S. M. Altmann, I. Kufareva, K. E. Strathearn, A. M. Amore, C. B. Volk, M. M. Maxwell, J. C. Rochet, P. J. McLean, A. B. Young, R. Abagyan, M. B. Feany, B. T. Hyman, A. Kazantsev, *Science* **2007**, *317*, 516–519.
[13] C. M. Grozinger, E. D. Chao, H. E. Blackwell, D. Moazed, S. L. Schreiber, *J. Biol. Chem.* **2001**, *276*, 38837–38843.
[14] A. Bedalov, T. Gatbonton, W. P. Irvine, D. E. Gottschling, J. A. Simon, *Proc. Natl. Acad. Sci. USA* **2001**, *98*, 15113–15118.
[15] A. Mai, S. Massa, S. Lavu, R. Pezzi, S. Simeoni, R. Ragno, F. R. Mariotti, F. Chiani, G. Camilloni, D. A. Sinclair, *J. Med. Chem.* **2005**, *48*, 7789–7795.
[16] R. C. Neugebauer, U. Uchiechowska, R. Meier, H. Hruby, V. Valkov, E. Verdin, W. Sippl, M. Jung, *J. Med. Chem.* **2008**, *51*, 1203–1213.
[17] A. D. Napper, J. Hixon, T. McDonagh, K. Keavey, J. F. Pons, J. Barker, W. T. Yau, P. Amouzegh, A. Flegg, E. Hamelin, R. J. Thomas, M. Kates, S. Jones, M. A. Navia, J. O. Saunders, P. S. DiStefano, R. Curtis, *J. Med. Chem.* **2005**, *48*, 8045–8054.
[18] K. T. Howitz, K. J. Bitterman, H. Y. Cohen, D. W. Lamming, S. Lavu, J. G. Wood, R. E. Zipkin, P. Chung, A. Kisielewski, L. L. Zhang, B. Scherer, D. A. Sinclair, *Nature* **2003**, *425*, 191–196.
[19] J. Trapp, R. Meier, D. Hongwiset, M. U. Kassack, W. Sippl, M. Jung, *ChemMedChem* **2007**, *2*, 1419–1431.
[20] A. Schuetz, J. Min, T. Antoshenko, C. L. Wang, *Structure* **2007**, *15*, 377–389.
[21] B. Vergnes, D. Sereno, N. Madjidian-Sereno, J. L. Lemesre, A. Ouaissi, *Gene* **2002**, *296*, 139–150.
[22] B. Vergnes, D. Sereno, J. Tavares, A. Cordeiro-da-Silva, L. Vanhille, N. Madjidian-Sereno, D. Depoix, A. Monte-Alegre, A. Ouaissi, *Gene* **2005**, *363*, 85–96.
[23] J. Tavares, A. Ouaissi, N. Santarém, D. Sereno, B. Vergnes, P. Sampaio, A. Cordeiro-da-Silva, *Biochem. J.* **2008**, *415*, 377–386.
[24] J. Tavares, A. Ouaissi, P. K. T. Lin, A. Tomás, A. Cordeiro-da-Silva, *Int. J. Parasitol.* **2005**, *35*, 637–646.
[25] P. K. T. Lin, V. A. Pavlov, *Bioorg. Med. Chem. Lett.* **2000**, *10*, 1609–1612.
[26] J. Oliveira, L. Ralton, J. Tavares, A. Codeiro-da-Silva, C. S. Bestwick, A. McPherson, P. K. Thoo Lin, *Bioorg. Med. Chem.* **2007**, *15*, 541–545.
[27] A. M. Dance, L. Ralton, Z. Fuller, L. Milne, S. Duthie, C. S. Bestwick, P. K. T. Lin, *Biochem. Pharmacol.* **2005**, *69*, 19–27.
[28] A. A. Sauve, I. Celic, J. Avalos, H. Deng, J. D. Boeke, V. L. Schramm, *Biochemistry* **2001**, *40*, 15456–15463.
[29] J. M. Denu, *Trends Biochem. Sci.* **2003**, *28*, 41–48.
[30] M. D. Jackson, M. T. Schmidt, N. J. Oppenheimer, J. M. Denu, *J. Biol. Chem.* **2003**, *278*, 50985–50998.
[31] J. L. Avalos, K. M. Bever, C. Wolberger, *Mol. Cell* **2005**, *17*, 855–868.
[32] J. C. Tanny, D. S. Kirkpatrick, S. A. Gerber, S. P. Gygi, D. Moazed, *Mol. Cell. Biol.* **2004**, *24*, 6931–6946.
[33] T. E. Voogd, E. L. Vansterkenburg, J. Wilting, L. H. Janssen, *Pharmacol. Rev.* **1993**, *45*, 177–203.
[34] A. Monte-Alegre, A. Ouaissi, D. Sereno, *Kinetoplastid Biol. Dis.* **2006**, *23*, 5–6.
[35] J. Trapp, A. Jochum, R. Meier, L. Saunders, B. Marshall, C. Kunick, E. Verdin, P. Goekjian, W. Sippl, M. Jung, *J. Med. Chem.* **2006**, *49*, 7307–7316.
[36] R. U. Kadam, V. M. Kiran, N. Roy, *Bioorg. Med. Chem. Lett.* **2006**, *16*, 6013–6018.
[37] M. S. Finnin, J. R. Donigian, N. P. Pavletich, *Nat. Struct. Biol.* **2001**, *8*, 621–625.
[38] D. Sereno, G. Roy, J. L. Lemesre, B. Papadopoulou, M. Ouellette, *Antimicrob. Agents Chemother.* **2001**, *45*, 1168–1173.
[39] G. Roy, C. Dumas, D. Sereno, Y. Wu, A. K. Singh, M. J. Tremblay, M. Ouellette, M. Olivier, B. Papadopoulou, *Mol. Biochem. Parasitol.* **2000**, *110*, 195–206.

Received: September 3, 2009
Revised: October 29, 2009
Published online on ■■ ■■, 2009

FULL PAPERS

We have identified a new class of NAD^+-competitive SIR2 inhibitors that preferentially inhibit the *L. infantum* form of sirtuin (LiSIR2RP1). Despite the well-conserved catalytic core domain of SIR2 enzymes, subtle structural differences in the inhibitors can provide selective targeting.

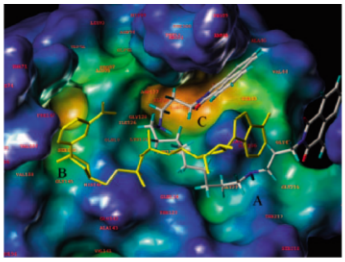

*J. Tavares, A. Ouaissi, P. Kong Thoo Lin, I. Loureiro, S. Kaur, N. Roy, A. Cordeiro-da-Silva**

■■ – ■■

Bisnaphthalimidopropyl Derivatives as Inhibitors of *Leishmania* SIR2 Related Protein 1

Chapter VI

Bibliography

Abdulla MH, O'Brien T, Mackey ZB, Sajid M, Grab DJ, McKerrow JH (2008) RNA interference of *Trypanosoma brucei* cathepsin B and L affects disease progression in a mouse model. *PLoS neglected tropical diseases* **2:** e298

Achcar F, Kerkhoven EJ, SilicoTryp C, Bakker BM, Barrett MP, Breitling R (2012) Dynamic modelling under uncertainty: the case of *Trypanosoma brucei* energy metabolism. *PLoS computational biology* **8:** e1002352

Adams MJ, Ellis GH, Gover S, Naylor CE, Phillips C (1994) Crystallographic study of coenzyme, coenzyme analogue and substrate binding in 6-phosphogluconate dehydrogenase: implications for NADP specificity and the enzyme mechanism. *Structure* **2:** 651-668

Agranoff D, Stich A, Abel P, Krishna S (2005) Proteomic fingerprinting for the diagnosis of human African trypanosomiasis. *Trends in parasitology* **21:** 154-157

Albert MA, Haanstra JR, Hannaert V, Van Roy J, Opperdoes FR, Bakker BM, Michels PA (2005) Experimental and in silico analyses of glycolytic flux control in bloodstream form *Trypanosoma brucei*. *The Journal of biological chemistry* **280:** 28306-28315

Ali BR, Pal A, Croft SL, Taylor RJ, Field MC (1999) The farnesyltransferase inhibitor manumycin A is a novel trypanocide with a complex mode of action including major effects on mitochondria. *Molecular and biochemical parasitology* **104:** 67-80

Alibu VP, Storm L, Haile S, Clayton C, Horn D (2005) A doubly inducible system for RNA interference and rapid RNAi plasmid construction in *Trypanosoma brucei*. *Molecular and biochemical parasitology* **139:** 75-82

Alirol E, Schrumpf D, Amici Heradi J, Riedel A, de Patoul C, Quere M, Chappuis F (2013) Nifurtimox-eflornithine combination therapy for second-stage gambiense human African trypanosomiasis: Medecins Sans Frontieres experience in the Democratic Republic of the Congo. *Clinical infectious diseases : an official publication of the Infectious Diseases Society of America* **56:** 195-203

Allsopp R (2001) Options for vector control against trypanosomiasis in Africa. *Trends in parasitology* **17:** 15-19

Alsford S, Eckert S, Baker N, Glover L, Sanchez-Flores A, Leung KF, Turner DJ, Field MC, Berriman M, Horn D (2012) High-throughput decoding of antitrypanosomal drug efficacy and resistance. *Nature* **482:** 232-236

Alsford S, Field MC, Horn D (2013) Receptor-mediated endocytosis for drug delivery in African trypanosomes: fulfilling Paul Ehrlich's vision of chemotherapy. *Trends in parasitology* **29:** 207-212

Alsford S, Kawahara T, Glover L, Horn D (2005) Tagging a *T. brucei* RRNA locus improves stable transfection efficiency and circumvents inducible expression position effects. *Molecular and biochemical parasitology* **144:** 142-148

Alsford S, Turner DJ, Obado SO, Sanchez-Flores A, Glover L, Berriman M, Hertz-Fowler C, Horn D (2011) High-throughput phenotyping using parallel sequencing of RNA interference targets in the African trypanosome. *Genome research* **21:** 915-924

Andrulis IL, Chen J, Ray PN (1987) Isolation of human cDNAs for asparagine synthetase and expression in Jensen rat sarcoma cells. *Molecular and cellular biology* **7:** 2435-2443

Andrulis IL, Shotwell M, Evans-Blackler S, Zalkin H, Siminovitch L, Ray PN (1989) Fine structure analysis of the Chinese hamster AS gene encoding asparagine synthetase. *Gene* **80:** 75-85

Appel IM, Hop WC, van Kessel-Bakvis C, Stigter R, Pieters R (2008) L-Asparaginase and the effect of age on coagulation and fibrinolysis in childhood acute lymphoblastic leukemia. *Thrombosis and haemostasis* **100:** 330-337

Ardenkjaer-Larsen JH, Fridlund B, Gram A, Hansson G, Hansson L, Lerche MH, Servin R, Thaning M, Golman K (2003) Increase in signal-to-noise ratio of > 10,000 times in liquid-state NMR. *Proceedings of the National Academy of Sciences of the United States of America* **100:** 10158-10163

Arnau J, Lauritzen C, Petersen GE, Pedersen J (2006) Current strategies for the use of affinity tags and tag removal for the purification of recombinant proteins. *Protein expression and purification* **48:** 1-13

Aronov AM, Suresh S, Buckner FS, Van Voorhis WC, Verlinde CL, Opperdoes FR, Hol WG, Gelb MH (1999) Structure-based design of submicromolar, biologically active inhibitors of trypanosomatid glyceraldehyde-3-phosphate dehydrogenase. *Proceedings of the National Academy of Sciences of the United States of America* **96:** 4273-4278

Aslanian AM, Fletcher BS, Kilberg MS (2001) Asparagine synthetase expression alone is sufficient to induce l-asparaginase resistance in MOLT-4 human leukaemia cells. *The Biochemical journal* **357:** 321-328

Asselin BL, Kurtzburg J (2003) Asparaginase Treatment of Acute Leukemias: Humana Press

Azema L, Lherbet C, Baudoin C, Blonski C (2006) Cell permeation of a *Trypanosoma brucei* aldolase inhibitor: evaluation of different enzyme-labile phosphate protecting groups. *Bioorganic & medicinal chemistry letters* **16:** 3440-3443

Babokhov P, Sanyaolu AO, Oyibo WA, Fagbenro-Beyioku AF, Iriemenam NC (2013) A current analysis of chemotherapy strategies for the treatment of human African trypanosomiasis. *Pathogens and global health* **107:** 242-252

Bacchi CJ (1993) Resistance to clinical drugs in African trypanosomes. *Parasitol Today* **9:** 190-193

Bacchi CJ, Brun R, Croft SL, Alicea K, Buhler Y (1996) In vivo trypanocidal activities of new S-adenosylmethionine decarboxylase inhibitors. *Antimicrobial agents and chemotherapy* **40:** 1448-1453

Bacchi CJ, Yarlett N (1993) Effects of antagonists of polyamine metabolism on African trypanosomes. *Acta tropica* **54:** 225-236

Baetselier PD, Namangala B, Noel W, Brys L, Pays E, Beschin A (2001) Alternative versus classical macrophage activation during experimental African trypanosomosis. *International journal for parasitology* **31:** 575-587

Bailey JW, Smith DH (1992) The use of the acridine orange QBC technique in the diagnosis of African trypanosomiasis. *Trans R Soc Trop Med Hyg* **86:** 630

Baird TD, Wek RC (2012) Eukaryotic initiation factor 2 phosphorylation and translational control in metabolism. *Advances in nutrition* **3:** 307-321

Baker N, Alsford S, Horn D (2011) Genome-wide RNAi screens in African trypanosomes identify the nifurtimox activator NTR and the eflornithine transporter AAT6. *Molecular and biochemical parasitology* **176:** 55-57

Baker N, Glover L, Munday JC, Aguinaga Andres D, Barrett MP, de Koning HP, Horn D (2012) Aquaglyceroporin 2 controls susceptibility to melarsoprol and pentamidine in African trypanosomes. *Proceedings of the National Academy of Sciences of the United States of America* **109:** 10996-11001

Bakker BM, Mensonides FI, Teusink B, van Hoek P, Michels PA, Westerhoff HV (2000) Compartmentation protects trypanosomes from the dangerous design of glycolysis. *Proceedings of the National Academy of Sciences of the United States of America* **97:** 2087-2092

Bakker BM, Walsh MC, ter Kuile BH, Mensonides FI, Michels PA, Opperdoes FR, Westerhoff HV (1999) Contribution of glucose transport to the control of the glycolytic flux in *Trypanosoma brucei*. *Proceedings of the National Academy of Sciences of the United States of America* **96:** 10098-10103

Balana-Fouce R, Reguera RM (2007) RNA interference in *Trypanosoma brucei*: a high-throughput engine for functional genomics in trypanosomatids? *Trends in parasitology* **23:** 348-351

Balasegaram M, Harris S, Checchi F, Ghorashian S, Hamel C, Karunakara U (2006) Melarsoprol versus eflornithine for treating late-stage Gambian trypanosomiasis in the Republic of the Congo. *Bulletin of the World Health Organization* **84:** 783-791

Balasubramanian MN, Butterworth EA, Kilberg MS (2013) Asparagine Synthetase: Regulation by Cell Stress and Involvement in Tumor Biology. *American journal of physiology Endocrinology and metabolism*

Balmer O, Beadell JS, Gibson W, Caccone A (2011) Phylogeography and taxonomy of *Trypanosoma brucei*. *PLoS neglected tropical diseases* **5:** e961

Bandini G, Marino K, Guther ML, Wernimont AK, Kuettel S, Qiu W, Afzal S, Kelner A, Hui R, Ferguson MA (2012) Phosphoglucomutase is absent in *Trypanosoma brucei* and redundantly substituted by phosphomannomutase and phospho-N-acetylglucosamine mutase. *Molecular microbiology* **85:** 513-534

Baral TN (2010) Immunobiology of African trypanosomes: need of alternative interventions. *Journal of biomedicine & biotechnology* **2010:** 389153

Barkhuizen M, Magez S, Ryffel B, Brombacher F (2008) Interleukin-12p70 deficiency increases survival and diminishes pathology in *Trypanosoma congolense* infection. *The Journal of infectious diseases* **198:** 1284-1291

Barnes RL, Shi H, Kolev NG, Tschudi C, Ullu E (2012) Comparative genomics reveals two novel RNAi factors in *Trypanosoma brucei* and provides insight into the core machinery. *PLoS pathogens* **8:** e1002678

Barrett MP (1997) The pentose phosphate pathway and parasitic protozoa. *Parasitol Today* **13:** 11-16

Barrett MP, Boykin DW, Brun R, Tidwell RR (2007) Human African trypanosomiasis: pharmacological re-engagement with a neglected disease. *British journal of pharmacology* **152:** 1155-1171

Barrett MP, Burchmore RJ, Stich A, Lazzari JO, Frasch AC, Cazzulo JJ, Krishna S (2003) The trypanosomiases. *Lancet* **362:** 1469-1480

Barrett MP, Mottram JC, Coombs GH (1999) Recent advances in identifying and validating drug targets in trypanosomes and leishmanias. *Trends in microbiology* **7:** 82-88

Barrett MP, Vincent IM, Burchmore RJ, Kazibwe AJ, Matovu E (2011) Drug resistance in human African trypanosomiasis. *Future microbiology* **6:** 1037-1047

Barry JD, Hajduk SL, Vickerman K, Le Ray D (1979) Detection of multiple variable antigen types in metacyclic populations of *Trypanosoma brucei*. *Trans R Soc Trop Med Hyg* **73:** 205-208

Becker HD, Kern D (1998) Thermus thermophilus: a link in evolution of the tRNA-dependent amino acid amidation pathways. *Proceedings of the National Academy of Sciences of the United States of America* **95:** 12832-12837

Benko PV, Wood TC, Segel IH (1969) Multiplicity and regulation of amino acid transport in Penicillium chrysogenum. *Archives of biochemistry and biophysics* **129:** 498-508

Berrang-Ford L, Berke O, Sweeney S, Abdelrahman L (2010) Sleeping sickness in southeastern Uganda: a spatio-temporal analysis of disease risk, 1970-2003. *Vector borne and zoonotic diseases* **10:** 977-988

Berriman M, Ghedin E, Hertz-Fowler C, Blandin G, Renauld H, Bartholomeu DC, Lennard NJ, Caler E, Hamlin NE, Haas B, Bohme U, Hannick L, Aslett MA, Shallom J, Marcello L, Hou L, Wickstead B, Alsmark UC, Arrowsmith C, Atkin RJ, Barron AJ, Bringaud F, Brooks K, Carrington M, Cherevach I, Chillingworth TJ, Churcher C, Clark LN, Corton CH, Cronin A, Davies RM, Doggett J, Djikeng A, Feldblyum T, Field MC, Fraser A, Goodhead I, Hance Z, Harper D, Harris BR, Hauser H, Hostetler J, Ivens A, Jagels K, Johnson D, Johnson J, Jones K, Kerhornou AX, Koo H, Larke N, Landfear S, Larkin C, Leech V, Line A, Lord A, Macleod A, Mooney PJ, Moule S, Martin DM, Morgan GW, Mungall K,

Norbertczak H, Ormond D, Pai G, Peacock CS, Peterson J, Quail MA, Rabbinowitsch E, Rajandream MA, Reitter C, Salzberg SL, Sanders M, Schobel S, Sharp S, Simmonds M, Simpson AJ, Tallon L, Turner CM, Tait A, Tivey AR, Van Aken S, Walker D, Wanless D, Wang S, White B, White O, Whitehead S, Woodward J, Wortman J, Adams MD, Embley TM, Gull K, Ullu E, Barry JD, Fairlamb AH, Opperdoes F, Barrell BG, Donelson JE, Hall N, Fraser CM, Melville SE, El-Sayed NM (2005) The genome of the African trypanosome *Trypanosoma brucei*. *Science* **309:** 416-422

Besteiro S, Barrett MP, Riviere L, Bringaud F (2005) Energy generation in insect stages of *Trypanosoma brucei*: metabolism in flux. *Trends in parasitology* **21:** 185-191

Bezwoda WR, Derman DP, See N, Mansoor N (1985) Relative value of oestrogen receptor assay, lactoferrin content, and glucose-6-phosphate dehydrogenase activity as prognostic indicators in primary breast cancer. *Oncology* **42:** 7-12

Biebinger S, Rettenmaier S, Flaspohler J, Hartmann C, Pena-Diaz J, Wirtz LE, Hotz HR, Barry JD, Clayton C (1996) The PARP promoter of *Trypanosoma brucei* is developmentally regulated in a chromosomal context. *Nucleic acids research* **24:** 1202-1211

Bitonti AJ, Cross-Doersen DE, McCann PP (1988) Effects of alpha-difluoromethylornithine on protein synthesis and synthesis of the variant-specific glycoprotein (VSG) in *Trypanosoma brucei* brucei. *The Biochemical journal* **250:** 295-298

Blaise M, Frechin M, Olieric V, Charron C, Sauter C, Lorber B, Roy H, Kern D (2011) Crystal structure of the archaeal asparagine synthetase: interrelation with aspartyl-tRNA and asparaginyl-tRNA synthetases. *Journal of molecular biology* **412:** 437-452

Blangy D, Buc H, Monod J (1968) Kinetics of the allosteric interactions of phosphofructokinase from *Escherichia coli*. *Journal of molecular biology* **31:** 13-35

Blattner FR, Plunkett G, 3rd, Bloch CA, Perna NT, Burland V, Riley M, Collado-Vides J, Glasner JD, Rode CK, Mayhew GF, Gregor J, Davis NW, Kirkpatrick HA, Goeden MA, Rose DJ, Mau B, Shao Y (1997) The complete genome sequence of *Escherichia coli* K-12. *Science* **277:** 1453-1462

Blum J, Nkunku S, Burri C (2001) Clinical description of encephalopathic syndromes and risk factors for their occurrence and outcome during melarsoprol treatment of human African trypanosomiasis. *Tropical medicine & international health : TM & IH* **6:** 390-400

Bochud-Allemann N, Schneider A (2002) Mitochondrial substrate level phosphorylation is essential for growth of procyclic *Trypanosoma brucei*. *The Journal of biological chemistry* **277:** 32849-32854

Bockstal V, Guirnalda P, Caljon G, Goenka R, Telfer JC, Frenkel D, Radwanska M, Magez S, Black SJ (2011) *T. brucei* infection reduces B lymphopoiesis in bone marrow and truncates compensatory splenic lymphopoiesis through transitional B-cell apoptosis. *PLoS pathogens* **7:** e1002089

Boehlein SK, Nakatsu T, Hiratake J, Thirumoorthy R, Stewart JD, Richards NG, Schuster SM (2001) Characterization of inhibitors acting at the synthetase site of *Escherichia coli* asparagine synthetase B. *Biochemistry* **40:** 11168-11175

Boehlein SK, Richards NG, Schuster SM (1994) Glutamine-dependent nitrogen transfer in *Escherichia coli* asparagine synthetase B. Searching for the catalytic triad. *The Journal of biological chemistry* **269:** 7450-7457

Boehlein SK, Stewart JD, Walworth ES, Thirumoorthy R, Richards NG, Schuster SM (1998) Kinetic mechanism of *Escherichia coli* asparagine synthetase B. *Biochemistry* **37:** 13230-13238

Bour T, Akaddar A, Lorber B, Blais S, Balg C, Candolfi E, Frugier M (2009) Plasmodial aspartyl-tRNA synthetases and peculiarities in *Plasmodium falciparum*. *The Journal of biological chemistry* **284:** 18893-18903

Bouteille B, Buguet A (2012) The detection and treatment of human African trypanosomiasis. *Research and Reports in Tropical Medicine* **3:** 35-45

Bowyer PW, Tate EW, Leatherbarrow RJ, Holder AA, Smith DF, Brown KA (2008) N-myristoyltransferase: a prospective drug target for protozoan parasites. *ChemMedChem* **3:** 402-408

Bray PG, Barrett MP, Ward SA, de Koning HP (2003) Pentamidine uptake and resistance in pathogenic protozoa: past, present and future. *Trends in parasitology* **19:** 232-239

Bridges DJ, Gould MK, Nerima B, Maser P, Burchmore RJ, de Koning HP (2007) Loss of the high-affinity pentamidine transporter is responsible for high levels of cross-resistance between arsenical and diamidine drugs in African trypanosomes. *Molecular pharmacology* **71:** 1098-1108

Brimacombe KR, Walsh MJ, Liu L, Vasquez-Valdivieso MG, Morgan HP, McNae I, Fothergill-Gilmore LA, Michels PA, Auld DS, Simeonov A, Walkinshaw MD, Shen M, Boxer MB (2014) Identification of ML251, a Potent Inhibitor of *T. brucei* and *T. cruzi* Phosphofructokinase. *ACS medicinal chemistry letters* **5:** 12-17

Bruce D. (1895) Preliminary report on the tsetse fly disease or nagana in Zululand Durban. In Davis Ba (ed.).

Brun R, Blum J, Chappuis F, Burri C (2010) Human African trypanosomiasis. *Lancet* **375:** 148-159

Brun R, Schonenberger M (1981) Stimulating effect of citrate and cis-Aconitate on the transformation of *Trypanosoma brucei* bloodstream forms to procyclic forms in vitro. *Zeitschrift fur Parasitenkunde* **66:** 17-24

Brun R, Schumacher R, Schmid C, Kunz C, Burri C (2001) The phenomenon of treatment failures in Human African Trypanosomiasis. *Tropical medicine & international health : TM & IH* **6:** 906-914

Brysk MM, Corpe WA, Hankes LV (1969) Beta-cyanoalanine formation by *Chromobacterium violaceum*. *Journal of bacteriology* **97:** 322-327

Buguet A, Bisser S, Josenando T, Chapotot F, Cespuglio R (2005) Sleep structure: a new diagnostic tool for stage determination in sleeping sickness. *Acta tropica* **93:** 107-117

Buguet A, Bouteille B, Mpandzou G. (2009) La recherche sur la maladie du sommeil (trypanosomose humaine africaine) en République du Congo de 2004 à 2009. Brazzaville:Editions Les Manguiers.

Burri C, Brun R (2003) Eflornithine for the treatment of human African trypanosomiasis. *Parasitology research* **90 Supp 1:** S49-52

Caceres AJ, Michels PA, Hannaert V (2010) Genetic validation of aldolase and glyceraldehyde-3-phosphate dehydrogenase as drug targets in *Trypanosoma brucei*. *Molecular and biochemical parasitology* **169:** 50-54

Campillo N, Carrington M (2003) The origin of the serum resistance associated (SRA) gene and a model of the structure of the SRA polypeptide from *Trypanosoma brucei rhodesiense*. *Molecular and biochemical parasitology* **127:** 79-84

Capewell P, Clucas C, DeJesus E, Kieft R, Hajduk S, Veitch N, Steketee PC, Cooper A, Weir W, MacLeod A (2013) The TgsGP gene is essential for resistance to human serum in *Trypanosoma brucei gambiense*. *PLoS pathogens* **9:** e1003686

Carter NS, Berger BJ, Fairlamb AH (1995) Uptake of diamidine drugs by the P2 nucleoside transporter in melarsen-sensitive and -resistant *Trypanosoma brucei brucei*. *The Journal of biological chemistry* **270:** 28153-28157

Castric PA, Farnden KJ, Conn EE (1972) Cyanide metabolism in higher plants. V. The formation of asparagine from -cyanoalanine. *Archives of biochemistry and biophysics* **152:** 62-69

Castric PA, Strobel GA (1969) Cyanide metabolism by *Bacillus megaterium*. *The Journal of biological chemistry* **244:** 4089-4094

CDC. (2012) Parasites African Trypanosomiasis (also known as Sleeping Sickness). Centers for Disease Control and Prevention, http://www.cdc.gov/parasites/sleepingsickness/ Vol. 2014.

Cedar H, Schwartz JH (1968) Production of L-asparaginase II by *Escherichia coli*. *Journal of bacteriology* **96:** 2043-2048

Cedar H, Schwartz JH (1969a) The asparagine synthetase of *Escherichia coli*. I. Biosynthetic role of the enzyme, purification, and characterization of the reaction products. *J Biol Chem* **244:** 4112-4121

Cedar H, Schwartz JH (1969b) The asparagine synthetase of *Escherichia coli*. II. Studies on mechanism. *The Journal of biological chemistry* **244:** 4122-4127

Chambers JW, Fowler ML, Morris MT, Morris JC (2008) The anti-trypanosomal agent lonidamine inhibits *Trypanosoma brucei* hexokinase 1. *Molecular and biochemical parasitology* **158:** 202-207

Chappuis F, Loutan L, Simarro P, Lejon V, Buscher P (2005a) Options for field diagnosis of human african trypanosomiasis. *Clinical microbiology reviews* **18:** 133-146

Chappuis F, Udayraj N, Stietenroth K, Meussen A, Bovier PA (2005b) Eflornithine is safer than melarsoprol for the treatment of second-stage *Trypanosoma brucei* gambiense human African trypanosomiasis. *Clinical infectious diseases : an official publication of the Infectious Diseases Society of America* **41:** 748-751

Chawla B, Madhubala R (2010) Drug targets in *Leishmania*. *Journal of parasitic diseases : official organ of the Indian Society for Parasitology* **34:** 1-13

Chen Y, Hung CH, Burderer T, Lee GS (2003) Development of RNA interference revertants in *Trypanosoma brucei* cell lines generated with a double stranded RNA expression construct driven by two opposing promoters. *Molecular and biochemical parasitology* **126:** 275-279

Chow C, Cloutier S, Dumas C, Chou MN, Papadopoulou B (2011) Promastigote to amastigote differentiation of *Leishmania* is markedly delayed in the absence of PERK eIF2alpha kinase-dependent eIF2alpha phosphorylation. *Cellular microbiology* **13:** 1059-1077

Ciustea M, Gutierrez JA, Abbatiello SE, Eyler JR, Richards NG (2005) Efficient expression, purification, and characterization of C-terminally tagged, recombinant human asparagine synthetase. *Archives of biochemistry and biophysics* **440:** 18-27

Clasquin MF, Melamud E, Singer A, Gooding JR, Xu X, Dong A, Cui H, Campagna SR, Savchenko A, Yakunin AF, Rabinowitz JD, Caudy AA (2011) Riboneogenesis in yeast. *Cell* **145:** 969-980

Claustre S, Denier C, Lakhdar-Ghazal F, Lougare A, Lopez C, Chevalier N, Michels PA, Perie J, Willson M (2002) Exploring the active site of *Trypanosoma brucei* phosphofructokinase by inhibition studies: specific irreversible inhibition. *Biochemistry* **41:** 10183-10193

Clayton CE, Michels P (1996) Metabolic compartmentation in African trypanosomes. *Parasitol Today* **12:** 465-471

Cleland WW (1967) Enzyme kinetics. *Annual review of biochemistry* **36:** 77-112

Cohen H, Bielorai B, Harats D, Toren A, Pinhas-Hamiel O (2010) Conservative treatment of L-asparaginase-associated lipid abnormalities in children with acute lymphoblastic leukemia. *Pediatric blood & cancer* **54:** 703-706

Coley AF, Dodson HC, Morris MT, Morris JC (2011) Glycolysis in the african trypanosome: targeting enzymes and their subcellular compartments for therapeutic development. *Molecular biology international* **2011:** 123702

Coller SP, Mansfield JM, Paulnock DM (2003) Glycosylinositolphosphate soluble variant surface glycoprotein inhibits IFN-gamma-induced nitric oxide production via reduction in STAT1 phosphorylation in African trypanosomiasis. *J Immunol* **171:** 1466-1472

Coller SP, Paulnock DM (2001) Signaling pathways initiated in macrophages after engagement of type A scavenger receptors. *Journal of leukocyte biology* **70:** 142-148

Comini MA, Guerrero SA, Haile S, Menge U, Lunsdorf H, Flohe L (2004) Validation of *Trypanosoma brucei* trypanothione synthetase as drug target. *Free radical biology & medicine* **36:** 1289-1302

Comini MA, Ortíz C, Cazzulo JJ (2013) Drug Targets in Trypanosomal and Leishmanial Pentose Phosphate Pathway. In *Trypanosomatid Diseases: Molecular Routes to Drug Discovery*, Jäger T KO, Flohé L (ed), pp 297-313. Wiley-VCH Verlag GmbH & Co. KGaA, Weinheim, Germany

Cooper AJ (1977) Asparagine transaminase from rat liver. *The Journal of biological chemistry* **252:** 2032-2038

Cordeiro AT, Thiemann OH, Michels PA (2009) Inhibition of *Trypanosoma brucei* glucose-6-phosphate dehydrogenase by human steroids and their effects on the viability of cultured parasites. *Bioorganic & medicinal chemistry* **17:** 2483-2489

Coruzzi GM (2003) Primary N-assimilation into Amino Acids in Arabidopsis. In *Arabidopsis Book* Vol. 2, 2003/01/01 edn, p e0010.

Coustou V, Besteiro S, Biran M, Diolez P, Bouchaud V, Voisin P, Michels PA, Canioni P, Baltz T, Bringaud F (2003) ATP generation in the *Trypanosoma brucei* procyclic form: cytosolic substrate level is essential, but not oxidative phosphorylation. *The Journal of biological chemistry* **278:** 49625-49635

Cox FE (2004) History of sleeping sickness (African trypanosomiasis). *Infectious disease clinics of North America* **18:** 231-245

Cronin CN, Nolan DP, Voorheis HP (1989) The enzymes of the classical pentose phosphate pathway display differential activities in procyclic and bloodstream forms of *Trypanosoma brucei*. *FEBS letters* **244:** 26-30

Cross GA (1975) Identification, purification and properties of clone-specific glycoprotein antigens constituting the surface coat of *Trypanosoma brucei*. *Parasitology* **71:** 393-417

Crowe JS, Barry JD, Luckins AG, Ross CA, Vickerman K (1983) All metacyclic variable antigen types of *Trypanosoma congolense* identified using monoclonal antibodies. *Nature* **306:** 389-391

Cui H, Darmanin S, Natsuisaka M, Kondo T, Asaka M, Shindoh M, Higashino F, Hamuro J, Okada F, Kobayashi M, Nakagawa K, Koide H, Kobayashi M (2007) Enhanced expression of asparagine synthetase under glucose-deprived conditions protects pancreatic cancer cells from apoptosis induced by glucose deprivation and cisplatin. *Cancer research* **67:** 3345-3355

Curnow AW, Tumbula DL, Pelaschier JT, Min B, Soll D (1998) Glutamyl-tRNA(Gln) amidotransferase in *Deinococcus radiodurans* may be confined to asparagine biosynthesis. *Proceedings of the National Academy of Sciences of the United States of America* **95:** 12838-12843

Czichos J, Nonnengaesser C, Overath P (1986) *Trypanosoma brucei*: cis-aconitate and temperature reduction as triggers of synchronous transformation of bloodstream to procyclic trypomastigotes in vitro. *Experimental parasitology* **62:** 283-291

Dagenais TR, Freeman BE, Demick KP, Paulnock DM, Mansfield JM (2009) Processing and presentation of variant surface glycoprotein molecules to T cells in African trypanosomiasis. *J Immunol* **183:** 3344-3355

Dardonville C, Rinaldi E, Barrett MP, Brun R, Gilbert IH, Hanau S (2004) Selective inhibition of *Trypanosoma brucei* 6-phosphogluconate dehydrogenase by high-energy intermediate and transition-state analogues. *Journal of medicinal chemistry* **47:** 3427-3437

Dardonville C, Rinaldi E, Hanau S, Barrett MP, Brun R, Gilbert IH (2003) Synthesis and biological evaluation of substrate-based inhibitors of 6-phosphogluconate dehydrogenase as potential drugs against African trypanosomiasis. *Bioorganic & medicinal chemistry* **11:** 3205-3214

DaRocha WD, Otsu K, Teixeira SM, Donelson JE (2004) Tests of cytoplasmic RNA interference (RNAi) and construction of a tetracycline-inducible T7 promoter system in *Trypanosoma cruzi*. *Molecular and biochemical parasitology* **133:** 175-186

de A S Navarro MV, Gomes Dias SM, Mello LV, da Silva Giotto MT, Gavalda S, Blonski C, Garratt RC, Rigden DJ (2007) Structural flexibility in *Trypanosoma brucei* enolase revealed by X-ray crystallography and molecular dynamics. *The FEBS journal* **274:** 5077-5089

De Koning HP (2001) Uptake of pentamidine in *Trypanosoma brucei brucei* is mediated by three distinct transporters: implications for cross-resistance with arsenicals. *Molecular pharmacology* **59:** 586-592

de la Fuente J, Rodriguez M, Redondo M, Montero C, Garcia-Garcia JC, Mendez L, Serrano E, Valdes M, Enriquez A, Canales M, Ramos E, Boue O, Machado H, Lleonart R, de Armas CA, Rey S, Rodriguez JL, Artiles M, Garcia L (1998) Field studies and cost-effectiveness analysis of vaccination with Gavac against the cattle tick Boophilus microplus. *Vaccine* **16:** 366-373

De Raadt P (1976) African sleeping sickness today. *Trans R Soc Trop Med Hyg* **70:** 114–116

Dean S, Marchetti R, Kirk K, Matthews KR (2009) A surface transporter family conveys the trypanosome differentiation signal. *Nature* **459:** 213-217

Deborggraeve S, Claes F, Laurent T, Mertens P, Leclipteux T, Dujardin JC, Herdewijn P, Buscher P (2006) Molecular dipstick test for diagnosis of sleeping sickness. *Journal of clinical microbiology* **44:** 2884-2889

Delarue M, Duclert-Savatier N, Miclet E, Haouz A, Giganti D, Ouazzani J, Lopez P, Nilges M, Stoven V (2007) Three dimensional structure and implications for the catalytic mechanism of 6-phosphogluconolactonase from *Trypanosoma brucei*. *Journal of molecular biology* **366:** 868-881

Delespaux V, de Koning HP (2007) Drugs and drug resistance in African trypanosomiasis. *Drug resistance updates : reviews and commentaries in antimicrobial and anticancer chemotherapy* **10:** 30-50

Dempsey WL, Mansfield JM (1983) Lymphocyte function in experimental African trypanosomiasis. VI. Parasite-specific immunosuppression. *J Immunol* **130:** 2896-2898

den Boer ML, Evans WE, Pieters R (2005) TELAML1-positive ALL: a discordant genotype. *Cell cycle* **4:** 997-998

Devine DV, Falk RJ, Balber AE (1986) Restriction of the alternative pathway of human complement by intact *Trypanosoma brucei* subsp. gambiense. *Infection and immunity* **52:** 223-229

Dickens F, Glock GE (1951) Direct oxidation of glucose-6-phosphate, 6-phosphogluconate and pentose-5-phosphates by enzymes of animal origin. *The Biochemical journal* **50:** 81-95

Dodson HC, Lyda TA, Chambers JW, Morris MT, Christensen KA, Morris JC (2011) Quercetin, a fluorescent bioflavanoid, inhibits *Trypanosoma brucei* hexokinase 1. *Experimental parasitology* **127:** 423-428

Doua F, Miezan TW, Sanon Singaro JR, Boa Yapo F, Baltz T (1996) The efficacy of pentamidine in the treatment of early-late stage *Trypanosoma brucei gambiense* trypanosomiasis. *The American journal of tropical medicine and hygiene* **55:** 586-588

Downie MJ, Kirk K, Mamoun CB (2008) Purine salvage pathways in the intraerythrocytic malaria parasite *Plasmodium falciparum*. *Eukaryotic cell* **7:** 1231-1237

Doyle JJ, Hirumi H, Hirumi K, Lupton EN, Cross GA (1980) Antigenic variation in clones of animal-infective *Trypanosoma brucei* derived and maintained in vitro. *Parasitology* **80:** 359-369

Drain J, Bishop JR, Hajduk SL (2001) Haptoglobin-related protein mediates trypanosome lytic factor binding to trypanosomes. *The Journal of biological chemistry* **276:** 30254-30260

Drennan MB, Stijlemans B, Van den Abbeele J, Quesniaux VJ, Barkhuizen M, Brombacher F, De Baetselier P, Ryffel B, Magez S (2005) The induction of a type 1 immune response following a *Trypanosoma brucei* infection is MyD88 dependent. *J Immunol* **175:** 2501-2509

Drew ME, Morris JC, Wang Z, Wells L, Sanchez M, Landfear SM, Englund PT (2003) The adenosine analog tubercidin inhibits glycolysis in *Trypanosoma brucei* as revealed by an RNA interference library. *The Journal of biological chemistry* **278:** 46596-46600

Duclert-Savatier N, Poggi L, Miclet E, Lopes P, Ouazzani J, Chevalier N, Nilges M, Delarue M, Stoven V (2009) Insights into the enzymatic mechanism of 6-phosphogluconolactonase from *Trypanosoma brucei* using structural data and molecular dynamics simulation. *Journal of molecular biology* **388:** 1009-1021

Duff SM, Qi Q, Reich T, Wu X, Brown T, Crowley JH, Fabbri B (2011) A kinetic comparison of asparagine synthetase isozymes from higher plants. *Plant physiology and biochemistry : PPB / Societe francaise de physiologie vegetale* **49:** 251-256

Duffieux F, Van Roy J, Michels PA, Opperdoes FR (2000) Molecular characterization of the first two enzymes of the pentose-phosphate pathway of *Trypanosoma brucei*. Glucose-6-phosphate dehydrogenase and 6-phosphogluconolactonase. *The Journal of biological chemistry* **275:** 27559-27565

Dufour E, Gay F, Aguera K, Scoazec JY, Horand F, Lorenzi PL, Godfrin Y (2012) Pancreatic tumor sensitivity to plasma L-asparagine starvation. *Pancreas* **41:** 940-948

Durand-Dubief M, Bastin P (2003) TbAGO1, an argonaute protein required for RNA interference, is involved in mitosis and chromosome segregation in *Trypanosoma brucei*. *BMC biology* **1:** 2

Eastman RT, Buckner FS, Yokoyama K, Gelb MH, Van Voorhis WC (2006) Thematic review series: lipid posttranslational modifications. Fighting parasitic disease by blocking protein farnesylation. *Journal of lipid research* **47:** 233-240

Eberle C, Burkhard JA, Stump B, Kaiser M, Brun R, Krauth-Siegel RL, Diederich F (2009) Synthesis, inhibition potency, binding mode, and antiprotozoal activities of fluorescent inhibitors of trypanothione reductase based on mepacrine-conjugated diaryl sulfide scaffolds. *ChemMedChem* **4:** 2034-2044

Eberle C, Lauber BS, Fankhauser D, Kaiser M, Brun R, Krauth-Siegel RL, Diederich F (2011) Improved inhibitors of trypanothione reductase by combination of motifs: synthesis, inhibitory potency, binding mode, and antiprotozoal activities. *ChemMedChem* **6:** 292-301

Ebikeme C (2007) Amino Acid Transporters & Amino Acid Metabolism in *Trypanosoma brucei* brucei. Doctor of Philosophy Thesis, Division of Infection & Immunity Faculty of Biomedical & Life Sciences-University of Glasgow

Edwards TE, Abramov AB, Smith ER, Baydo RO, Leonard JT, Leibly DJ, Thompkins KB, Clifton MC, Gardberg AS, Staker BL, Van Voorhis WC, Myler PJ, Stewart LJ (2011) Structural characterization of a ribose-5-phosphate isomerase B from the pathogenic fungus *Coccidioides immitis*. *BMC structural biology* **11:** 39

El-Sayed NM, Myler PJ, Bartholomeu DC, Nilsson D, Aggarwal G, Tran AN, Ghedin E, Worthey EA, Delcher AL, Blandin G, Westenberger SJ, Caler E, Cerqueira GC, Branche C, Haas B, Anupama A, Arner E, Aslund L, Attipoe P, Bontempi E, Bringaud F, Burton P, Cadag E, Campbell DA, Carrington M, Crabtree J, Darban H, da Silveira JF, de Jong P, Edwards K, Englund PT, Fazelina G, Feldblyum T, Ferella M, Frasch AC, Gull K, Horn D, Hou L, Huang Y, Kindlund E, Klingbeil M, Kluge S, Koo H, Lacerda D, Levin MJ, Lorenzi H, Louie T, Machado CR, McCulloch R, McKenna A, Mizuno Y, Mottram JC, Nelson S, Ochaya S, Osoegawa K, Pai G, Parsons M, Pentony M, Pettersson U, Pop M, Ramirez JL, Rinta J, Robertson L, Salzberg SL, Sanchez DO, Seyler A, Sharma R, Shetty J, Simpson AJ, Sisk E, Tammi MT, Tarleton R, Teixeira S, Van Aken S, Vogt C, Ward PN, Wickstead B, Wortman J, White O, Fraser CM, Stuart KD, Andersson B (2005) The genome sequence of *Trypanosoma cruzi*, etiologic agent of Chagas disease. *Science* **309:** 409-415

Emmer BT, Daniels MD, Taylor JM, Epting CL, Engman DM (2010) Calflagin inhibition prolongs host survival and suppresses parasitemia in *Trypanosoma brucei* infection. *Eukaryotic cell* **9:** 934-942

Emmer BT, Souther C, Toriello KM, Olson CL, Epting CL, Engman DM (2009) Identification of a palmitoyl acyltransferase required for protein sorting to the flagellar membrane. *Journal of cell science* **122:** 867-874

Engstler M, Pfohl T, Herminghaus S, Boshart M, Wiegertjes G, Heddergott N, Overath P (2007) Hydrodynamic flow-mediated protein sorting on the cell surface of trypanosomes. *Cell* **131:** 505-515

Esposito D, Chatterjee DK (2006) Enhancement of soluble protein expression through the use of fusion tags. *Current opinion in biotechnology* **17:** 353-358

Esser KM, Schoenbechler MJ, Gingrich JB (1982) *Trypanosoma rhodesiense* blood forms express all antigen specificities relevant to protection against metacyclic (insect form) challenge. *J Immunol* **129:** 1715-1718

Fairlamb AH (2003) Chemotherapy of human African trypanosomiasis: current and future prospects. *Trends in parasitology* **19:** 488-494

Fairlamb AH, Blackburn P, Ulrich P, Chait BT, Cerami A (1985) Trypanothione: a novel bis(glutathionyl)spermidine cofactor for glutathione reductase in trypanosomatids. *Science* **227:** 1485-1487

Fairlamb AH, Cerami A (1992) Metabolism and functions of trypanothione in the Kinetoplastida. *Annual review of microbiology* **46:** 695-729

Fairlamb AH, Henderson GB, Bacchi CJ, Cerami A (1987) In vivo effects of difluoromethylornithine on trypanothione and polyamine levels in bloodstream forms of *Trypanosoma brucei*. *Molecular and biochemical parasitology* **24:** 185-191

Fairlamb AH, Henderson GB, Cerami A (1989) Trypanothione is the primary target for arsenical drugs against African trypanosomes. *Proceedings of the National Academy of Sciences of the United States of America* **86:** 2607-2611

Fairlamb AH, Smith K, Hunter KJ (1992) The interaction of arsenical drugs with dihydrolipoamide and dihydrolipoamide dehydrogenase from arsenical resistant and sensitive strains of *Trypanosoma brucei brucei*. *Molecular and biochemical parasitology* **53:** 223-231

Fan J, Ye J, Kamphorst JJ, Shlomi T, Thompson CB, Rabinowitz JD (2014) Quantitative flux analysis reveals folate-dependent NADPH production. *Nature* **510:** 298-302

Feng L, Yuan J, Toogood H, Tumbula-Hansen D, Soll D (2005) Aspartyl-tRNA synthetase requires a conserved proline in the anticodon-binding loop for tRNA(Asn) recognition in vivo. *The Journal of biological chemistry* **280:** 20638-20641

Ferrante A, Allison AC (1983) Alternative pathway activation of complement by African trypanosomes lacking a glycoprotein coat. *Parasite immunology* **5:** 491-498

Ferrari S, Losasso V, Saxena P, Costi MP (2013) Targeting the Trypanosomatidic Enzymes Pteridine Reductase and Dihydrofolate Reductase. In *Trypanosomatid Diseases: Molecular Routes to Drug Discovery*, Timo Jäger OKaLF (ed), 24, pp 445-472. Wiley-VCH Verlag GmbH & Co. KGaA

Field MC, Carrington M (2009) The trypanosome flagellar pocket. *Nature reviews Microbiology* **7:** 775-786

Flohe L (2012) The trypanothione system and its implications in the therapy of trypanosomatid diseases. *International journal of medical microbiology : IJMM* **302:** 216-220

Fomina-Yadlin D, Gosink JJ, McCoy R, Follstad B, Morris A, Russell CB, McGrew JT (2014) Cellular responses to individual amino-acid depletion in antibody-expressing and parental CHO cell lines. *Biotechnology and bioengineering* **111:** 965-979

Franco JR, Simarro PP, Diarra A, Jannin JG (2014) Epidemiology of human African trypanosomiasis. *Clinical epidemiology* **6:** 257-275

Frearson JA, Brand S, McElroy SP, Cleghorn LA, Smid O, Stojanovski L, Price HP, Guther ML, Torrie LS, Robinson DA, Hallyburton I, Mpamhanga CP, Brannigan JA, Wilkinson AJ, Hodgkinson M, Hui R, Qiu W, Raimi OG, van Aalten DM, Brenk R, Gilbert IH, Read KD, Fairlamb AH, Ferguson MA, Smith DF, Wyatt PG (2010) N-myristoyltransferase inhibitors as new leads to treat sleeping sickness. *Nature* **464:** 728-732

Friedheim EA (1949) Mel B in the treatment of human trypanosomiasis. *The American journal of tropical medicine and hygiene* **29:** 173-180

Furuya T, Kessler P, Jardim A, Schnaufer A, Crudder C, Parsons M (2002) Glucose is toxic to glycosome-deficient trypanosomes. *Proceedings of the National Academy of Sciences of the United States of America* **99:** 14177-14182

Gamarro F, Yu PL, Zhao J, Edman U, Greene PJ, Santi D (1995) *Trypanosoma brucei* dihydrofolate reductase-thymidylate synthase: gene isolation and expression and characterization of the enzyme. *Molecular and biochemical parasitology* **72:** 11-22

Gatti DL, Tzagoloff A (1991) Structure and evolution of a group of related aminoacyl-tRNA synthetases. *Journal of molecular biology* **218:** 557-568

Gaufichon L, Masclaux-Daubresse C, Tcherkez G, Reisdorf-Cren M, Sakakibara Y, Hase T, Clement G, Avice JC, Grandjean O, Marmagne A, Boutet-Mercey S, Azzopardi M, Soulay F, Suzuki A (2013) *Arabidopsis thaliana* ASN2 encoding asparagine synthetase is involved in the control of nitrogen assimilation and export during vegetative growth. *Plant, cell & environment* **36:** 328-342

Geiger A, Simo G, Grebaut P, Peltier JB, Cuny G, Holzmuller P (2011) Transcriptomics and proteomics in human African trypanosomiasis: current status and perspectives. *Journal of proteomics* **74:** 1625-1643

Geiser F, Luscher A, de Koning HP, Seebeck T, Maser P (2005) Molecular pharmacology of adenosine transport in *Trypanosoma brucei*: P1/P2 revisited. *Molecular pharmacology* **68:** 589-595

Gesbert G, Ramond E, Rigard M, Frapy E, Dupuis M, Dubail I, Barel M, Henry T, Meibom K, Charbit A (2014) Asparagine assimilation is critical for intracellular replication and dissemination of *Francisella*. *Cellular microbiology* **16:** 434-449

Gibson W (2007) Resolution of the species problem in African trypanosomes. *International journal for parasitology* **37:** 829-838

Gibson WC (1986) Will the real *Trypanosoma b. gambiense* please stand up. *Parasitol Today* **2:** 255-257

Gibson WC, de CMTF, Godfrey DG (1980) Numerical analysis of enzyme polymorphism: a new approach to the epidemiology and taxonomy of trypanosomes of the subgenus Trypanozoon. *Advances in parasitology* **18:** 175-246

Giffin BF, McCann PP, Bitonti AJ, Bacchi CJ (1986) Polyamine depletion following exposure to DL-alpha-difluoromethylornithine both in vivo and in vitro initiates morphological alterations and mitochondrial activation in a monomorphic strain of *Trypanosoma brucei brucei*. *The Journal of protozoology* **33:** 238-243

Ginger ML, Fairlamb, A.H. & Opperdoes, F.R. (2007) Comparative genomics of trypanosome metabolism. In *Trypanosomes : after the genome*, JD Barry JM, R McCulloch & A Acosta-Serrano (ed), pp 373-417. London: Horizon Bioscience

Glaser L, Brown DH (1955) Purification and properties of d-glucose-6-phosphate dehydrogenase. *The Journal of biological chemistry* **216:** 67-79

Gong SS, Guerrini L, Basilico C (1991) Regulation of asparagine synthetase gene expression by amino acid starvation. *Molecular and cellular biology* **11:** 6059-6066

Gouzy A, Larrouy-Maumus G, Bottai D, Levillain F, Dumas A, Wallach JB, Caire-Brandli I, de Chastellier C, Wu TD, Poincloux R, Brosch R, Guerquin-Kern JL, Schnappinger D, Sorio de Carvalho LP, Poquet Y, Neyrolles O (2014) *Mycobacterium tuberculosis* exploits asparagine to assimilate nitrogen and resist acid stress during infection. *PLoS pathogens* **10:** e1003928

Gowri VS, Ghosh I, Sharma A, Madhubala R (2012) Unusual domain architecture of aminoacyl tRNA synthetases and their paralogs from *Leishmania major*. *BMC genomics* **13:** 621

Grant IF (2001) Insecticides for tsetse and trypanosomiasis control: is the environmental risk acceptable? *Trends in parasitology* **17:** 10-14

Grishin NV, Osterman AL, Brooks HB, Phillips MA, Goldsmith EJ (1999) X-ray structure of ornithine decarboxylase from *Trypanosoma brucei*: the native structure and the structure in complex with alpha-difluoromethylornithine. *Biochemistry* **38:** 15174-15184

Guler JL, Kriegova E, Smith TK, Lukes J, Englund PT (2008) Mitochondrial fatty acid synthesis is required for normal mitochondrial morphology and function in *Trypanosoma brucei*. *Molecular microbiology* **67:** 1125-1142

Gull K (2002) The cell biology of parasitism in *Trypanosoma brucei*: insights and drug targets from genomic approaches? *Current pharmaceutical design* **8:** 241-256

Gupta S, Cordeiro AT, Michels PA (2011) Glucose-6-phosphate dehydrogenase is the target for the trypanocidal action of human steroids. *Molecular and biochemical parasitology* **176:** 112-115

Gutierrez JA, Pan YX, Koroniak L, Hiratake J, Kilberg MS, Richards NG (2006) An inhibitor of human asparagine synthetase suppresses proliferation of an L-asparaginase-resistant leukemia cell line. *Chemistry & biology* **13:** 1339-1347

Haanstra JR, Kerkhoven EJ, van Tuijl A, Blits M, Wurst M, van Nuland R, Albert MA, Michels PA, Bouwman J, Clayton C, Westerhoff HV, Bakker BM (2011) A domino effect in drug action: from metabolic assault towards parasite differentiation. *Molecular microbiology* **79:** 94-108

Haanstra JR, van Tuijl A, Kessler P, Reijnders W, Michels PA, Westerhoff HV, Parsons M, Bakker BM (2008) Compartmentation prevents a lethal turbo-explosion of glycolysis in trypanosomes. *Proceedings of the National Academy of Sciences of the United States of America* **105:** 17718-17723

Haberkorn A, Harder A, Greif G (2001) Milestones of protozoan research at Bayer. *Parasitology research* **87:** 1060-1062

Hainard A, Tiberti N, Robin X, Lejon V, Ngoyi DM, Matovu E, Enyaru JC, Fouda C, Ndung'u JM, Lisacek F, Muller M, Turck N, Sanchez JC (2009) A combined CXCL10, CXCL8 and H-FABP panel for the staging of human African trypanosomiasis patients. *PLoS neglected tropical diseases* **3:** e459

Hajduk SL, Moore DR, Vasudevacharya J, Siqueira H, Torri AF, Tytler EM, Esko JD (1989) Lysis of *Trypanosoma brucei* by a toxic subspecies of human high density lipoprotein. *The Journal of biological chemistry* **264:** 5210-5217

Hall BS, Bot C, Wilkinson SR (2011) Nifurtimox activation by trypanosomal type I nitroreductases generates cytotoxic nitrile metabolites. *The Journal of biological chemistry* **286:** 13088-13095

Hall JP, Wang H, Barry JD (2013) Mosaic VSGs and the scale of *Trypanosoma brucei* antigenic variation. *PLoS pathogens* **9:** e1003502

Hanau S, Rinaldi E, Dallocchio F, Gilbert IH, Dardonville C, Adams MJ, Gover S, Barrett MP (2004) 6-phosphogluconate dehydrogenase: a target for drugs in African trypanosomes. *Current medicinal chemistry* **11:** 2639-2650

Hannaert V, Bringaud F, Opperdoes FR, Michels PA (2003a) Evolution of energy metabolism and its compartmentation in Kinetoplastida. *Kinetoplastid biology and disease* **2:** 11

Hannaert V, Saavedra E, Duffieux F, Szikora JP, Rigden DJ, Michels PA, Opperdoes FR (2003b) Plant-like traits associated with metabolism of Trypanosoma parasites. *Proceedings of the National Academy of Sciences of the United States of America* **100:** 1067-1071

Hanrahan O, Webb H, O'Byrne R, Brabazon E, Treumann A, Sunter JD, Carrington M, Voorheis HP (2009) The glycosylphosphatidylinositol-PLC in *Trypanosoma brucei* forms a linear array on the exterior of the flagellar membrane before and after activation. *PLoS pathogens* **5:** e1000468

Hargrove JW, Omolo S, Msalilwa JS, Fox B (2000) Insecticide-treated cattle for tsetse control: the power and the problems. *Medical and veterinary entomology* **14:** 123-130

Harris TH, Cooney NM, Mansfield JM, Paulnock DM (2006) Signal transduction, gene transcription, and cytokine production triggered in macrophages by exposure to trypanosome DNA. *Infection and immunity* **74:** 4530-4537

Hassell AM, An G, Bledsoe RK, Bynum JM, Carter HL, 3rd, Deng SJ, Gampe RT, Grisard TE, Madauss KP, Nolte RT, Rocque WJ, Wang L, Weaver KL, Williams SP, Wisely GB, Xu R, Shewchuk LM (2007) Crystallization of protein-ligand complexes. *Acta crystallographica Section D, Biological crystallography* **63:** 72-79

Heby O, Persson L, Rentala M (2007) Targeting the polyamine biosynthetic enzymes: a promising approach to therapy of African sleeping sickness, Chagas' disease, and leishmaniasis. *Amino acids* **33:** 359-366

Heby O, Roberts SC, Ullman B (2003) Polyamine biosynthetic enzymes as drug targets in parasitic protozoa. *Biochemical Society transactions* **31:** 415-419

Heinz E, Williams TA, Nakjang S, Noel CJ, Swan DC, Goldberg AV, Harris SR, Weinmaier T, Markert S, Becher D, Bernhardt J, Dagan T, Hacker C, Lucocq JM, Schweder T, Rattei T, Hall N, Hirt RP, Embley TM (2012) The genome of the obligate intracellular parasite *Trachipleistophora hominis*: new insights into microsporidian genome dynamics and reductive evolution. *PLoS pathogens* **8:** e1002979

Heise N, Opperdoes FR (1999) Purification, localisation and characterisation of glucose-6-phosphate dehydrogenase of *Trypanosoma brucei*. *Molecular and biochemical parasitology* **99:** 21-32

Helfert S, Estevez AM, Bakker B, Michels P, Clayton C (2001) Roles of triosephosphate isomerase and aerobic metabolism in *Trypanosoma brucei*. *The Biochemical journal* **357:** 117-125

Hide G, Cattand P, LeRay D, Barry JD, Tait A (1990) The identification of *Trypanosoma brucei* subspecies using repetitive DNA sequences. *Molecular and biochemical parasitology* **39:** 213-225

Hinchman SK, Henikoff S, Schuster SM (1992) A relationship between asparagine synthetase A and aspartyl tRNA synthetase. *The Journal of biological chemistry* **267:** 144-149

Hofreuter D, Novik V, Galan JE (2008) Metabolic diversity in *Campylobacter jejuni* enhances specific tissue colonization. *Cell host & microbe* **4:** 425-433

Holm L, Rosenstrom P (2010) Dali server: conservation mapping in 3D. *Nucleic acids research* **38:** W545-549

Hong Y, Kinoshita T (2009) Trypanosome glycosylphosphatidylinositol biosynthesis. *The Korean journal of parasitology* **47:** 197-204

Horn D (2014) Antigenic variation in African trypanosomes. *Molecular and biochemical parasitology* **195:** 123-129

Horowitz B, Meister A (1972) Glutamine-dependent asparagine synthetase from leukemia cells. Chloride dependence, mechanism of action, and inhibition. *The Journal of biological chemistry* **247:** 6708-6719

Huang XH, H.M.; and Raushel, F. (2001) Channeling of substrates and intermediates in enzyme-catalyzed reactions. *Annual Review in Biochemistry* **70:** 149-180

Hudson KM, Byner C, Freeman J, Terry RJ (1976) Immunodepression, high IgM levels and evasion of the immune response in murine trypanosomiasis. *Nature* **264:** 256-258

Humbert R, Simoni RD (1980) Genetic and biomedical studies demonstrating a second gene coding for asparagine synthetase in *Escherichia coli*. *Journal of bacteriology* **142:** 212-220

Hunter DR, Segel IH (1971) Acidic and basic amino acid transport systems of *Penicillium chrysogenum*. *Archives of biochemistry and biophysics* **144:** 168-183

Hunter DR, Segel IH (1973) Control of the general amino acid permease of *Penicillium chrysogenum* by transinhibition and turnover. *Archives of biochemistry and biophysics* **154:** 387-399

Husain A, Sato D, Jeelani G, Soga T, Nozaki T (2012) Dramatic increase in glycerol biosynthesis upon oxidative stress in the anaerobic protozoan parasite *Entamoeba histolytica*. *PLoS neglected tropical diseases* **6:** e1831

Hutchinson OC, Webb H, Picozzi K, Welburn S, Carrington M (2004) Candidate protein selection for diagnostic markers of African trypanosomiasis. *Trends in parasitology* **20:** 519-523

Hutson RG, Kilberg MS (1994) Cloning of rat asparagine synthetase and specificity of the amino acid-dependent control of its mRNA content. *The Biochemical journal* **304 (Pt 3):** 745-750

Igoillo-Esteve M, Cazzulo JJ (2006) The glucose-6-phosphate dehydrogenase from *Trypanosoma cruzi*: its role in the defense of the parasite against oxidative stress. *Molecular and biochemical parasitology* **149:** 170-181

Inoue N, Otsu K, Ferraro DM, Donelson JE (2002) Tetracycline-regulated RNA interference in *Trypanosoma congolense*. *Molecular and biochemical parasitology* **120:** 309-313

Ireland RJ, Joy KW (1983) Purification and properties of an asparagine aminotransferase from *Pisum sativum* leaves. *Archives of biochemistry and biophysics* **223:** 291-296

Iten M, Mett H, Evans A, Enyaru JC, Brun R, Kaminsky R (1997) Alterations in ornithine decarboxylase characteristics account for tolerance of *Trypanosoma brucei rhodesiense* to D,L-alpha-difluoromethylornithine. *Antimicrobial agents and chemotherapy* **41:** 1922-1925

Jacobs RT, Nare B, Phillips MA (2011) State of the art in African trypanosome drug discovery. *Current topics in medicinal chemistry* **11:** 1255-1274

Jamonneau V, Ilboudo H, Kabore J, Kaba D, Koffi M, Solano P, Garcia A, Courtin D, Laveissiere C, Lingue K, Buscher P, Bucheton B (2012) Untreated human infections by *Trypanosoma brucei gambiense* are not 100% fatal. *PLoS neglected tropical diseases* **6:** e1691

Jamonneau V, Ravel S, Garcia A, Koffi M, Truc P, Laveissiere C, Herder S, Grebaut P, Cuny G, Solano P (2004) Characterization of *Trypanosoma brucei* s.l. infecting asymptomatic sleeping-sickness patients in Cote d'Ivoire: a new genetic group? *Annals of tropical medicine and parasitology* **98:** 329-337

Janne J, Alhonen-Hongisto L, Seppanen P, Siimes M (1981) Use of polyamine antimetabolites in experimental tumours and in human leukemia. *Medical biology* **59:** 448-457

Jones GE (1978) L-Asparagine auxotrophs of Saccharomyces cerevisiae: genetic and phenotypic characterization. *Journal of bacteriology* **134:** 200-207

Jones SM, Urch JE, Brun R, Harwood JL, Berry C, Gilbert IH (2004) Analogues of thiolactomycin as potential anti-malarial and anti-trypanosomal agents. *Bioorganic & medicinal chemistry* **12:** 683-692

Jung J, Kim JK, Yeom SJ, Ahn YJ, Oh DK, Kang LW (2011) Crystal structure of *Clostridium thermocellum* ribose-5-phosphate isomerase B reveals properties critical for fast enzyme kinetics. *Applied microbiology and biotechnology* **90:** 517-527

Kalidas S, Cestari I, Monnerat S, Li Q, Regmi S, Hasle N, Labaied M, Parsons M, Stuart K, Phillips MA (2014) Genetic validation of aminoacyl-tRNA synthetases as drug targets in *Trypanosoma brucei*. *Eukaryotic cell* **13:** 504-516

Kardon T, Stroobant V, Veiga-da-Cunha M, Schaftingen EV (2008) Characterization of mammalian sedoheptulokinase and mechanism of formation of erythritol in sedoheptulokinase deficiency. *FEBS letters* **582:** 3330-3334

Karioti A, Skaltsa H, Linden A, Perozzo R, Brun R, Tasdemir D (2007) Anthecularin: a novel sesquiterpene lactone from *Anthemis auriculata* with antiprotozoal activity. *The Journal of organic chemistry* **72:** 8103-8106

Kathir KM, Kumar TK, Rajalingam D, Yu C (2005) Time-dependent changes in the denatured state(s) influence the folding mechanism of an all beta-sheet protein. *The Journal of biological chemistry* **280:** 29682-29688

Kaur PK, Dinesh N, Soumya N, Babu NK, Singh S (2012) Identification and characterization of a novel Ribose 5-phosphate isomerase B from *Leishmania donovani*. *Biochemical and biophysical research communications* **421:** 51-56

Kaushik RS, Uzonna JE, Zhang Y, Gordon JR, Tabel H (2000) Innate resistance to experimental African trypanosomiasis: differences in cytokine (TNF-alpha, IL-6, IL-10 and IL-12) production by bone marrow-derived macrophages from resistant and susceptible mice. *Cytokine* **12:** 1024-1034

Kayembe D, Wery M (1972) [Observations on the diamidine sensitivity of strains of *Trypanosoma gambiense* recently isolated in the Republic of Zaire]. *Annales de la Societe belge de medecine tropicale* **52:** 1-8

Kazibwe AJ, Nerima B, de Koning HP, Maser P, Barrett MP, Matovu E (2009) Genotypic status of the TbAT1/P2 adenosine transporter of *Trypanosoma brucei gambiense* isolates from Northwestern Uganda following melarsoprol withdrawal. *PLoS neglected tropical diseases* **3:** e523

Kennedy PG (2008) Diagnosing central nervous system trypanosomiasis: two stage or not to stage? *Trans R Soc Trop Med Hyg* **102:** 306-307

Kennedy PG (2010) Novel biomarkers for late-stage human African trypanosomiasis--the search goes on. *The American journal of tropical medicine and hygiene* **82:** 981-982

Kennedy PG (2013) Clinical features, diagnosis, and treatment of human African trypanosomiasis (sleeping sickness). *The Lancet Neurology* **12:** 186-194

Kerkhoven EJ, Achcar F, Alibu VP, Burchmore RJ, Gilbert IH, Trybilo M, Driessen NN, Gilbert D, Breitling R, Bakker BM, Barrett MP (2013) Handling uncertainty in dynamic models: the pentose phosphate pathway in *Trypanosoma brucei*. *PLoS computational biology* **9:** e1003371

Kessler PS, Parsons M (2005) Probing the role of compartmentation of glycolysis in procyclic form *Trypanosoma brucei*: RNA interference studies of PEX14, hexokinase, and phosphofructokinase. *The Journal of biological chemistry* **280:** 9030-9036

Khow O, Suntrarachun S (2012) Strategies for production of active eukaryotic proteins in bacterial expression system. *Asian Pacific journal of tropical biomedicine* **2:** 159-162

Kilberg MS, Shan J, Su N (2009) ATF4-dependent transcription mediates signaling of amino acid limitation. *Trends in endocrinology and metabolism: TEM* **20:** 436-443

Kinyua JK, Nguu EK, Mulaa F, Ndung'u JM (2005) Immunization of rabbits with *Glossina pallidipes* tsetse fly midgut proteins: effects on the fly and trypanosome transmission. *Vaccine* **23:** 3824-3828

Kobayakawa T, Louis J, Izui S, Lambert PH (1979) Autoimmune response to DNA, red blood cells, and thymocyte antigens in association with polyclonal antibody synthesis during experimental African trypanosomiasis. *J Immunol* **122:** 296-301

Koffi M, Solano P, Barnabe C, de Meeus T, Bucheton B, Cuny G, Jamonneau V (2007) Genetic characterisation of *Trypanosoma brucei* s.l. using microsatellite typing: new perspectives for the molecular epidemiology of human African trypanosomiasis. *Infection, genetics and evolution : journal of molecular epidemiology and evolutionary genetics in infectious diseases* **7:** 675-684

Koizumi M, Nakatsu T, Kato H, Oda J (1999) A Potent Transition-State Analogue Inhibitor of *Escherichia coli* Asparagine Synthetase A. *J Am Chem Soc* **121:** 5799-5800

Kolev NG, Tschudi C, Ullu E (2011) RNA interference in protozoan parasites: achievements and challenges. *Eukaryotic cell* **10:** 1156-1163

Krauth-Siegel RL, Comini MA (2008) Redox control in trypanosomatids, parasitic protozoa with trypanothione-based thiol metabolism. *Biochimica et biophysica acta* **1780:** 1236-1248

Krauth-Siegel RL, Meiering SK, Schmidt H (2003) The parasite-specific trypanothione metabolism of trypanosoma and leishmania. *Biological chemistry* **384:** 539-549

Krieger S, Schwarz W, Ariyanayagam MR, Fairlamb AH, Krauth-Siegel RL, Clayton C (2000) Trypanosomes lacking trypanothione reductase are avirulent and show increased sensitivity to oxidative stress. *Molecular microbiology* **35:** 542-552

Kruger A, Gruning NM, Wamelink MM, Kerick M, Kirpy A, Parkhomchuk D, Bluemlein K, Schweiger MR, Soldatov A, Lehrach H, Jakobs C, Ralser M (2011) The pentose phosphate pathway is a metabolic redox sensor and regulates transcription during the antioxidant response. *Antioxidants & redox signaling* **15:** 311-324

Kuboki N, Inoue N, Sakurai T, Di Cello F, Grab DJ, Suzuki H, Sugimoto C, Igarashi I (2003) Loop-mediated isothermal amplification for detection of African trypanosomes. *Journal of clinical microbiology* **41:** 5517-5524

Kullas AL, McClelland M, Yang HJ, Tam JW, Torres A, Porwollik S, Mena P, McPhee JB, Bogomolnaya L, Andrews-Polymenis H, van der Velden AW (2012) L-asparaginase II produced by *Salmonella typhimurium* inhibits T cell responses and mediates virulence. *Cell host & microbe* **12:** 791-798

Lalmanach G, Boulange A, Serveau C, Lecaille F, Scharfstein J, Gauthier F, Authie E (2002) Congopain from *Trypanosoma congolense*: drug target and vaccine candidate. *Biological chemistry* **383:** 739-749

Langousis G, Hill KL (2014) Motility and more: the flagellum of *Trypanosoma brucei*. *Nature reviews Microbiology* **12:** 505-518

Lanteri CA, Tidwell RR, Meshnick SR (2008) The mitochondrion is a site of trypanocidal action of the aromatic diamidine DB75 in bloodstream forms of *Trypanosoma brucei*. *Antimicrobial agents and chemotherapy* **52:** 875-882

Larkin MA, Blackshields G, Brown NP, Chenna R, McGettigan PA, McWilliam H, Valentin F, Wallace IM, Wilm A, Lopez R, Thompson JD, Gibson TJ, Higgins DG (2007) Clustal W and Clustal X version 2.0. *Bioinformatics* **23:** 2947-2948

Le Ray D, Barry JD, Vickerman K (1978) Antigenic heterogeneity of metacyclic forms of *Trypanosoma brucei*. *Nature* **273:** 300-302

Lee SH, Stephens JL, Englund PT (2007) A fatty-acid synthesis mechanism specialized for parasitism. *Nature reviews Microbiology* **5:** 287-297

Lee SH, Stephens JL, Paul KS, Englund PT (2006) Fatty acid synthesis by elongases in trypanosomes. *Cell* **126:** 691-699

Lee WN, Boros LG, Puigjaner J, Bassilian S, Lim S, Cascante M (1998) Mass isotopomer study of the nonoxidative pathways of the pentose cycle with [1,2-13C2]glucose. *The American journal of physiology* **274:** E843-851

Legros D, Evans S, Maiso F, Enyaru JC, Mbulamberi D (1999) Risk factors for treatment failure after melarsoprol for *Trypanosoma brucei* gambiense trypanosomiasis in Uganda. *Trans R Soc Trop Med Hyg* **93:** 439-442

Lejon V, Boelaert M, Jannin J, Moore A, Buscher P (2003a) The challenge of *Trypanosoma brucei gambiense* sleeping sickness diagnosis outside Africa. *The Lancet infectious diseases* **3:** 804-808

Lejon V, Buscher P (2005) Review Article: cerebrospinal fluid in human African trypanosomiasis: a key to diagnosis, therapeutic decision and post-treatment follow-up. *Tropical medicine & international health : TM & IH* **10:** 395-403

Lejon V, Buscher P, Magnus E, Moons A, Wouters I, Van Meirvenne N (1998) A semi-quantitative ELISA for detection of *Trypanosoma brucei gambiense* specific antibodies in serum and cerebrospinal fluid of sleeping sickness patients. *Acta tropica* **69:** 151-164

Lejon V, Legros D, Richer M, Ruiz JA, Jamonneau V, Truc P, Doua F, Dje N, N'Siesi FX, Bisser S, Magnus E, Wouters I, Konings J, Vervoort T, Sultan F, Buscher P (2002) IgM quantification in the cerebrospinal fluid of sleeping sickness patients by a latex card agglutination test. *Tropical medicine & international health : TM & IH* **7:** 685-692

Lejon V, Mumba Ngoyi D, Kestens L, Boel L, Barbe B, Kande Betu V, van Griensven J, Bottieau E, Muyembe Tamfum JJ, Jacobs J, Buscher P (2014) Gambiense human african trypanosomiasis and immunological memory: effect on phenotypic lymphocyte profiles and humoral immunity. *PLoS pathogens* **10:** e1003947

Lejon V, Reiber H, Legros D, Dje N, Magnus E, Wouters I, Sindic CJ, Buscher P (2003b) Intrathecal immune response pattern for improved diagnosis of central nervous system involvement in trypanosomiasis. *The Journal of infectious diseases* **187:** 1475-1483

Leppert BJ, Mansfield JM, Paulnock DM (2007) The soluble variant surface glycoprotein of African trypanosomes is recognized by a macrophage scavenger receptor and induces I kappa B alpha degradation independently of TRAF6-mediated TLR signaling. *J Immunol* **179:** 548-556

Li F, Hua SB, Wang CC, Gottesdiener KM (1996) Procyclic *Trypanosoma brucei* cell lines deficient in ornithine decarboxylase activity. *Molecular and biochemical parasitology* **78:** 227-236

Li F, Hua SB, Wang CC, Gottesdiener KM (1998) *Trypanosoma brucei brucei*: characterization of an ODC null bloodstream form mutant and the action of alpha-difluoromethylornithine. *Experimental parasitology* **88:** 255-257

Li SQ, Fung MC, Reid SA, Inoue N, Lun ZR (2007) Immunization with recombinant beta-tubulin from *Trypanosoma evansi* induced protection against *T. evansi*, *T. equiperdum* and *T. b. brucei* infection in mice. *Parasite immunology* **29:** 191-199

Li SQ, Yang WB, Ma LJ, Xi SM, Chen QL, Song XW, Kang J, Yang LZ (2009) Immunization with recombinant actin from *Trypanosoma evansi* induces protective immunity against *T. evansi*, *T. equiperdum* and *T. b. brucei* infection. *Parasitology research* **104:** 429-435

Lillig CH, Holmgren A (2007) Thioredoxin and related molecules--from biology to health and disease. *Antioxidants & redox signaling* **9:** 25-47

Lopez R, Demick KP, Mansfield JM, Paulnock DM (2008) Type I IFNs play a role in early resistance, but subsequent susceptibility, to the African trypanosomes. *J Immunol* **181:** 4908-4917

Lorenzi PL, Llamas J, Gunsior M, Ozbun L, Reinhold WC, Varma S, Ji H, Kim H, Hutchinson AA, Kohn EC, Goldsmith PK, Birrer MJ, Weinstein JN (2008) Asparagine synthetase is a predictive biomarker of L-asparaginase activity in ovarian cancer cell lines. *Molecular cancer therapeutics* **7:** 3123-3128

Lorenzi PL, Reinhold WC, Rudelius M, Gunsior M, Shankavaram U, Bussey KJ, Scherf U, Eichler GS, Martin SE, Chin K, Gray JW, Kohn EC, Horak ID, Von Hoff DD, Raffeld M, Goldsmith PK, Caplen NJ, Weinstein JN (2006) Asparagine synthetase as a causal, predictive biomarker for L-asparaginase activity in ovarian cancer cells. *Molecular cancer therapeutics* **5:** 2613-2623

Louis FJ, Simarro PP (2005) [Rough start for the fight against sleeping sickness in French equatorial Africa]. *Medecine tropicale : revue du Corps de sante colonial* **65:** 251-257

Loureiro I, Faria J, Clayton C, Macedo-Ribeiro S, Santarém N, Roy N, Cordeiro-da-Siva A, Tavares J (2015) Ribose 5-Phosphate Isomerase B Knockdown Compromises *Trypanosoma brucei* Bloodstream Form Infectivity. *PLoS neglected tropical diseases* **9:** e3430

Loureiro I, Faria J, Clayton C, Ribeiro SM, Roy N, Santarem N, Tavares J, Cordeiro-da-Silva A (2013) Knockdown of asparagine synthetase A renders *Trypanosoma brucei* auxotrophic to asparagine. *PLoS neglected tropical diseases* **7:** e2578

Lubega GW, Byarugaba DK, Prichard RK (2002) Immunization with a tubulin-rich preparation from *Trypanosoma brucei* confers broad protection against African trypanosomosis. *Experimental parasitology* **102:** 9-22

Luehr CA, Schuster SM (1985) Purification and characterization of beef pancreatic asparagine synthetase. *Archives of biochemistry and biophysics* **237:** 335-346

Lumsden WH, Kimber CD, Evans DA, Doig SJ (1979) *Trypanosoma brucei*: Miniature anion-exchange centrifugation technique for detection of low parasitaemias: Adaptation for field use. *Trans R Soc Trop Med Hyg* **73:** 312-317

Lye LF, Owens K, Shi H, Murta SM, Vieira AC, Turco SJ, Tschudi C, Ullu E, Beverley SM (2010) Retention and loss of RNA interference pathways in trypanosomatid protozoans. *PLoS pathogens* **6:** e1001161

MacGregor P, Szoor B, Savill NJ, Matthews KR (2012) Trypanosomal immune evasion, chronicity and transmission: an elegant balancing act. *Nature reviews Microbiology* **10:** 431-438

MacLean L, Odiit M, Sternberg JM (2001) Nitric oxide and cytokine synthesis in human African trypanosomiasis. *The Journal of infectious diseases* **184:** 1086-1090

Magez S, Caljon G, Tran T, Stijlemans B, Radwanska M (2010) Current status of vaccination against African trypanosomiasis. *Parasitology* **137:** 2017-2027

Magez S, Radwanska M, Drennan M, Fick L, Baral TN, Allie N, Jacobs M, Nedospasov S, Brombacher F, Ryffel B, De Baetselier P (2007) Tumor necrosis factor (TNF) receptor-1 (TNFp55) signal transduction and macrophage-derived soluble TNF are crucial for nitric oxide-mediated *Trypanosoma congolense* parasite killing. *The Journal of infectious diseases* **196:** 954-962

Magez S, Stijlemans B, Baral T, De Baetselier P (2002) VSG-GPI anchors of African trypanosomes: their role in macrophage activation and induction of infection-associated immunopathology. *Microbes and infection / Institut Pasteur* **4:** 999-1006

Magez S, Stijlemans B, Radwanska M, Pays E, Ferguson MA, De Baetselier P (1998) The glycosyl-inositol-phosphate and dimyristoylglycerol moieties of the glycosylphosphatidylinositol anchor of the trypanosome variant-specific surface glycoprotein are distinct macrophage-activating factors. *J Immunol* **160:** 1949-1956

Magnus E, Vervoort T, Van Meirvenne N (1978) A card-agglutination test with stained trypanosomes (C.A.T.T.) for the serological diagnosis of *T. b. gambiense* trypanosomiasis. *Annales de la Societe belge de medecine tropicale* **58:** 169-176

Malvy D, Chappuis F (2011) Sleeping sickness. *Clinical microbiology and infection : the official publication of the European Society of Clinical Microbiology and Infectious Diseases* **17:** 986-995

Manhas R, Tripathi P, Khan S, Sethu Lakshmi B, Lal SK, Gowri VS, Sharma A, Madhubala R (2014) Identification and functional characterization of a novel bacterial type asparagine synthetase A: a tRNA synthetase paralog from *Leishmania donovani*. *The Journal of biological chemistry* **289:** 12096-12108

Martin KL, Smith TK (2006) Phosphatidylinositol synthesis is essential in bloodstream form *Trypanosoma brucei*. *The Biochemical journal* **396:** 287-295

Maser P, Sutterlin C, Kralli A, Kaminsky R (1999) A nucleoside transporter from *Trypanosoma brucei* involved in drug resistance. *Science* **285:** 242-244

Matovu E, Geiser F, Schneider V, Maser P, Enyaru JC, Kaminsky R, Gallati S, Seebeck T (2001) Genetic variants of the TbAT1 adenosine transporter from African trypanosomes in relapse infections following melarsoprol therapy. *Molecular and biochemical parasitology* **117:** 73-81

Matovu E, Stewart ML, Geiser F, Brun R, Maser P, Wallace LJ, Burchmore RJ, Enyaru JC, Barrett MP, Kaminsky R, Seebeck T, de Koning HP (2003) Mechanisms of arsenical and diamidine uptake and resistance in *Trypanosoma brucei*. *Eukaryotic cell* **2:** 1003-1008

Maudlin I, Turner MJ, Dukes P, Miller N (1984) Maintenance of *Glossina morsitans morsitans* on antiserum to procyclic trypanosomes reduces infection rates with homologous and heterologous *Trypanosoma congolense* stocks. *Acta tropica* **41:** 253-257

Maugeri DA, Cazzulo JJ, Burchmore RJ, Barrett MP, Ogbunude PO (2003) Pentose phosphate metabolism in *Leishmania mexicana*. *Molecular and biochemical parasitology* **130:** 117-125

Maul DM, Schuster SM (1986) Kinetic properties and characteristics of mouse liver mitochondrial asparagine aminotransferase. *Archives of biochemistry and biophysics* **251:** 585-593

McCulloch R, Horn D (2009) What has DNA sequencing revealed about the VSG expression sites of African trypanosomes? *Trends in parasitology* **25:** 359-363

Meadows AL, Kong B, Berdichevsky M, Roy S, Rosiva R, Blanch HW, Clark DS (2008) Metabolic and morphological differences between rapidly proliferating cancerous and normal breast epithelial cells. *Biotechnology progress* **24:** 334-341

Mehlitz D, Zillmann U, Scott CM, Godfrey DG (1982) Epidemiological studies on the animal reservoir of Gambiense sleeping sickness. Part III. Characterization of trypanozoon stocks by isoenzymes and sensitivity to human serum. *Tropenmedizin und Parasitologie* **33:** 113-118

Meister A, Fraser PE (1954) Enzymatic formation of L-asparagine by transamination. *The Journal of biological chemistry* **210:** 37-43

Merchant SS, Prochnik SE, Vallon O, Harris EH, Karpowicz SJ, Witman GB, Terry A, Salamov A, Fritz-Laylin LK, Marechal-Drouard L, Marshall WF, Qu LH, Nelson DR, Sanderfoot AA, Spalding MH, Kapitonov VV, Ren Q, Ferris P, Lindquist E, Shapiro H, Lucas SM, Grimwood J, Schmutz J, Cardol P, Cerutti H, Chanfreau G, Chen CL, Cognat V, Croft MT, Dent R, Dutcher S, Fernandez E, Fukuzawa H, Gonzalez-Ballester D, Gonzalez-Halphen D, Hallmann A, Hanikenne M, Hippler M, Inwood W, Jabbari K, Kalanon M, Kuras R, Lefebvre PA, Lemaire SD, Lobanov AV, Lohr M, Manuell A, Meier I, Mets L, Mittag M, Mittelmeier T, Moroney JV, Moseley J, Napoli C, Nedelcu AM, Niyogi K, Novoselov SV, Paulsen IT, Pazour G, Purton S, Ral JP, Riano-Pachon DM, Riekhof W, Rymarquis L, Schroda M, Stern D, Umen J, Willows R, Wilson N, Zimmer SL, Allmer J, Balk J, Bisova K, Chen CJ, Elias M, Gendler K, Hauser C, Lamb MR, Ledford H, Long JC, Minagawa J, Page MD, Pan J, Pootakham W, Roje S, Rose A, Stahlberg E, Terauchi AM, Yang P, Ball S, Bowler C, Dieckmann CL, Gladyshev VN, Green P, Jorgensen R, Mayfield S, Mueller-Roeber B, Rajamani S, Sayre RT, Brokstein P, Dubchak I, Goodstein D, Hornick L, Huang YW, Jhaveri J, Luo Y, Martinez D, Ngau WC, Otillar B, Poliakov A, Porter A, Szajkowski L, Werner G, Zhou K, Grigoriev IV, Rokhsar DS, Grossman AR (2007) The Chlamydomonas genome reveals the evolution of key animal and plant functions. *Science* **318:** 245-250

Merritt C, Stuart K (2013) Identification of essential and non-essential protein kinases by a fusion PCR method for efficient production of transgenic *Trypanosoma brucei*. *Molecular and biochemical parasitology* **190:** 44-49

Meshnick SR, Blobstein SH, Grady RW, Cerami A (1978) An approach to the development of new drugs for African trypanosomiasis. *The Journal of experimental medicine* **148:** 569-579

Metallo CM, Vander Heiden MG (2013) Understanding metabolic regulation and its influence on cell physiology. *Molecular cell* **49:** 388-398

Michalska K, Jaskolski M (2006) Structural aspects of L-asparaginases, their friends and relations. *Acta biochimica Polonica* **53:** 627-640

Michels PA, Bringaud F, Herman M, Hannaert V (2006) Metabolic functions of glycosomes in trypanosomatids. *Biochimica et biophysica acta* **1763:** 1463-1477

Miclet E, Stoven V, Michels PA, Opperdoes FR, Lallemand JY, Duffieux F (2001) NMR spectroscopic analysis of the first two steps of the pentose-phosphate pathway elucidates the role of 6-phosphogluconolactonase. *The Journal of biological chemistry* **276:** 34840-34846

Min B, Pelaschier JT, Graham DE, Tumbula-Hansen D, Soll D (2002) Transfer RNA-dependent amino acid biosynthesis: an essential route to asparagine formation. *Proceedings of the National Academy of Sciences of the United States of America* **99:** 2678-2683

Mina JG, Pan SY, Wansadhipathi NK, Bruce CR, Shams-Eldin H, Schwarz RT, Steel PG, Denny PW (2009) The *Trypanosoma brucei* sphingolipid synthase, an essential enzyme and drug target. *Molecular and biochemical parasitology* **168:** 16-23

Mitschke L, Parthier C, Schroder-Tittmann K, Coy J, Ludtke S, Tittmann K (2010) The crystal structure of human transketolase and new insights into its mode of action. *The Journal of biological chemistry* **285:** 31559-31570

Mobley DL, Dill KA (2009) Binding of small-molecule ligands to proteins: "what you see" is not always "what you get". *Structure* **17:** 489-498

Molyneux DH (1980) Host-trypanosomes interactions in Glossina. *Insect Science and its Application* **1:** 39-46

Mony BM, MacGregor P, Ivens A, Rojas F, Cowton A, Young J, Horn D, Matthews K (2014) Genome-wide dissection of the quorum sensing signalling pathway in *Trypanosoma brucei*. *Nature* **505:** 681-685

Moraes MC, Jesus TC, Hashimoto NN, Dey M, Schwartz KJ, Alves VS, Avila CC, Bangs JD, Dever TE, Schenkman S, Castilho BA (2007) Novel membrane-bound eIF2alpha kinase in the flagellar pocket of *Trypanosoma brucei. Eukaryotic cell* **6:** 1979-1991

Moreno T, Pous J, Subirana JA, Campos JL (2010) Coiled-coil conformation of a pentamidine-DNA complex. *Acta crystallographica Section D, Biological crystallography* **66:** 251-257

Morgan HP, McNae IW, Nowicki MW, Zhong W, Michels PA, Auld DS, Fothergill-Gilmore LA, Walkinshaw MD (2011) The trypanocidal drug suramin and other trypan blue mimetics are inhibitors of pyruvate kinases and bind to the adenosine site. *The Journal of biological chemistry* **286:** 31232-31240

Morris JC, Wang Z, Drew ME, Englund PT (2002) Glycolysis modulates trypanosome glycoprotein expression as revealed by an RNAi library. *The EMBO journal* **21:** 4429-4438

Motyka SA, Zhao Z, Gull K, Englund PT (2004) Integration of pZJM library plasmids into unexpected locations in the *Trypanosoma brucei* genome. *Molecular and biochemical parasitology* **134:** 163-167

Mpamhanga CP, Spinks D, Tulloch LB, Shanks EJ, Robinson DA, Collie IT, Fairlamb AH, Wyatt PG, Frearson JA, Hunter WN, Gilbert IH, Brenk R (2009) One scaffold, three binding modes: novel and selective pteridine reductase 1 inhibitors derived from fragment hits discovered by virtual screening. *Journal of medicinal chemistry* **52:** 4454-4465

Mugasa CM, Adams ER, Boer KR, Dyserinck HC, Buscher P, Schallig HD, Leeflang MM (2012) Diagnostic accuracy of molecular amplification tests for human African trypanosomiasis--systematic review. *PLoS neglected tropical diseases* **6:** e1438

Murguia JR, Serrano R (2012) New functions of protein kinase Gcn2 in yeast and mammals. *IUBMB life* **64:** 971-974

Musoke AJ, Barbet AF (1977) Activation of complement by variant-specific surface antigen of *Trypanosoma brucei*. *Nature* **270:** 438-440

Nakamura M, Yamada M, Hirota Y, Sugimoto K, Oka A, Takanami M (1981) Nucleotide sequence of the asnA gene coding for asparagine synthetase of *E. coli* K-12. *Nucleic acids research* **9:** 4669-4676

Nakatsu T, Kato H, Oda J (1998) Crystal structure of asparagine synthetase reveals a close evolutionary relationship to class II aminoacyl-tRNA synthetase. *Nature structural biology* **5:** 15-19

Namangala B (2012) Contribution of innate immune responses towards resistance to African trypanosome infections. *Scandinavian journal of immunology* **75:** 5-15

Namangala B, Brys L, Magez S, De Baetselier P, Beschin A (2000a) *Trypanosoma brucei brucei* infection impairs MHC class II antigen presentation capacity of macrophages. *Parasite immunology* **22:** 361-370

Namangala B, De Baetselier P, Beschin A (2009) Both type-I and type-II responses contribute to murine trypanotolerance. *The Journal of veterinary medical science / the Japanese Society of Veterinary Science* **71:** 313-318

Namangala B, de Baetselier P, Brijs L, Stijlemans B, Noel W, Pays E, Carrington M, Beschin A (2000b) Attenuation of *Trypanosoma brucei* is associated with reduced immunosuppression and concomitant production of Th2 lymphokines. *The Journal of infectious diseases* **181:** 1110-1120

Namangala B, Sugimoto C, Inoue N (2007) Effects of exogenous transforming growth factor beta on *Trypanosoma congolense* infection in mice. *Infection and immunity* **75:** 1878-1885

Namangala B, Yokoyama N, Ikehara Y, Taguchi O, Tsujimura K, Sugimoto C, Inoue N (2008) Effect of CD4+CD25+ T cell-depletion on acute lethal infection of mice with *Trypanosoma congolense*. *The Journal of veterinary medical science / the Japanese Society of Veterinary Science* **70:** 751-759

Nantulya VM, Doyle JJ, Jenni L (1980) Studies on *Trypanosoma (nannomonas) congolense* IV. Experimental immunization of mice against tsetse fly challenge. *Parasitology* **80:** 133-137

Narasimhan J, Joyce BR, Naguleswaran A, Smith AT, Livingston MR, Dixon SE, Coppens I, Wek RC, Sullivan WJ, Jr. (2008) Translation regulation by eukaryotic initiation factor-2 kinases in the development of latent cysts in *Toxoplasma gondii*. *The Journal of biological chemistry* **283:** 16591-16601

Nerima B, Matovu E, Lubega GW, Enyaru JC (2007) Detection of mutant P2 adenosine transporter (TbAT1) gene in *Trypanosoma brucei gambiense* isolates from northwest Uganda using allele-specific polymerase chain reaction. *Tropical medicine & international health : TM & IH* **12:** 1361-1368

Newsholme EA, Rolleston FS, Taylor K (1967) Inhibition of brain hexokinase by glucose 6-phosphate. *The Biochemical journal* **104:** 47P

Ngaira JM, Nantulya VM, Musoke AJ, Hirumi K (1983) Phagocytosis of antibody-sensitized *Trypanosoma brucei* in vitro by bovine peripheral blood monocytes. *Immunology* **49:** 393-400

Ngo H, Tschudi C, Gull K, Ullu E (1998) Double-stranded RNA induces mRNA degradation in *Trypanosoma brucei*. *Proceedings of the National Academy of Sciences of the United States of America* **95:** 14687-14692

Njiru ZK, Mikosza AS, Matovu E, Enyaru JC, Ouma JO, Kibona SN, Thompson RC, Ndung'u JM (2008) African trypanosomiasis: sensitive and rapid detection of the sub-genus Trypanozoon by loop-mediated isothermal amplification (LAMP) of parasite DNA. *International journal for parasitology* **38:** 589-599

Nogae I, Johnston M (1990) Isolation and characterization of the ZWF1 gene of *Saccharomyces cerevisiae*, encoding glucose-6-phosphate dehydrogenase. *Gene* **96:** 161-169

Nogge G, Giannetti M (1980) Specific antibodies: a potential insecticide. *Science* **209:** 1028-1029

Noireau F, Lemesre JL, Nzoukoudi MY, Louembet MT, Gouteux JP, Frezil JL (1988) Serodiagnosis of sleeping sickness in the Republic of the Congo: comparison of indirect immunofluorescent antibody test and card agglutination test. *Trans R Soc Trop Med Hyg* **82:** 237-240

Nowicki MW, Tulloch LB, Worralll L, McNae IW, Hannaert V, Michels PA, Fothergill-Gilmore LA, Walkinshaw MD, Turner NJ (2008) Design, synthesis and trypanocidal activity of lead compounds based on inhibitors of parasite glycolysis. *Bioorganic & medicinal chemistry* **16:** 5050-5061

Nwagwu M, Opperdoes FR (1982) Regulation of glycolysis in *Trypanosoma brucei*: hexokinase and phosphofructokinase activity. *Acta tropica* **39:** 61-72

Olsson T, Bakhiet M, Edlund C, Hojeberg B, Van der Meide PH, Kristensson K (1991) Bidirectional activating signals between *Trypanosoma brucei* and CD8+ T cells: a trypanosome-released factor triggers interferon-gamma production that stimulates parasite growth. *European journal of immunology* **21:** 2447-2454

Opigo J, Woodrow C (2009) NECT trial: more than a small victory over sleeping sickness. *Lancet* **374:** 7-9

Opperdoes FR, Szikora JP (2006) In silico prediction of the glycosomal enzymes of Leishmania major and trypanosomes. *Molecular and biochemical parasitology* **147:** 193-206

Outchkourov NS, Roeffen W, Kaan A, Jansen J, Luty A, Schuiffel D, van Gemert GJ, van de Vegte-Bolmer M, Sauerwein RW, Stunnenberg HG (2008) Correctly folded Pfs48/45 protein of *Plasmodium falciparum* elicits malaria transmission-blocking immunity in mice. *Proceedings of the National Academy of Sciences of the United States of America* **105:** 4301-4305

Owino AV, Masiga KD, Limo KM (2008) RNA interference: a pathway to drug target identification and validation in trypanosome. *African Journal of Biochemistry Research* **2** 066-073

Oza SL, Ariyanayagam MR, Aitcheson N, Fairlamb AH (2003) Properties of trypanothione synthetase from *Trypanosoma brucei*. *Molecular and biochemical parasitology* **131:** 25-33

Paindavoine P, Pays E, Laurent M, Geltmeyer Y, Le Ray D, Mehlitz D, Steinert M (1986) The use of DNA hybridization and numerical taxonomy in determining relationships between *Trypanosoma brucei* stocks and subspecies. *Parasitology* **92 (Pt 1):** 31-50

Paindavoine P, Rolin S, Van Assel S, Geuskens M, Jauniaux JC, Dinsart C, Huet G, Pays E (1992) A gene from the variant surface glycoprotein expression site encodes one of several transmembrane adenylate cyclases located on the flagellum of *Trypanosoma brucei*. *Molecular and cellular biology* **12:** 1218-1225

Pal A, Hall BS, Field MC (2002) Evidence for a non-LDL-mediated entry route for the trypanocidal drug suramin in *Trypanosoma brucei*. *Molecular and biochemical parasitology* **122:** 217-221

Pall ML (1970) Amino acid transport in *Neurospora crassa*. 3. Acidic amino acid transport. *Biochimica et biophysica acta* **211:** 513-520

Pan W, Ogunremi O, Wei G, Shi M, Tabel H (2006) CR3 (CD11b/CD18) is the major macrophage receptor for IgM antibody-mediated phagocytosis of African trypanosomes: diverse effect on subsequent synthesis of tumor necrosis factor alpha and nitric oxide. *Microbes and infection / Institut Pasteur* **8:** 1209-1218

Panethymitaki C, Bowyer PW, Price HP, Leatherbarrow RJ, Brown KA, Smith DF (2006) Characterization and selective inhibition of myristoyl-CoA:protein N-myristoyltransferase from *Trypanosoma brucei* and *Leishmania major*. *The Biochemical journal* **396:** 277-285

Papadopoulos MC, Abel PM, Agranoff D, Stich A, Tarelli E, Bell BA, Planche T, Loosemore A, Saadoun S, Wilkins P, Krishna S (2004) A novel and accurate diagnostic test for human African trypanosomiasis. *Lancet* **363:** 1358-1363

Patterson MKJ, Orr GR (1968) Asparagine biosynthesis by the Novikoff Hepatoma isolation, purification, property, and mechanism studies of the enzyme system. *J Biol Chem* **243:** 376-380

Paul ML, Kaur A, Geete A, Sobhia ME (2014) Essential gene identification and drug target prioritization in *Leishmania* species. *Molecular bioSystems* **10:** 1184-1195

Paulnock DM, Coller SP (2001) Analysis of macrophage activation in African trypanosomiasis. *Journal of leukocyte biology* **69:** 685-690

Pays E, Vanhollebeke B, Uzureau P, Lecordier L, Perez-Morga D (2014) The molecular arms race between African trypanosomes and humans. *Nature reviews Microbiology* **12:** 575-584

Peacock L, Bailey M, Carrington M, Gibson W (2014) Meiosis and haploid gametes in the pathogen *Trypanosoma brucei. Current biology : CB* **24:** 181-186

Peacock L, Ferris V, Sharma R, Sunter J, Bailey M, Carrington M, Gibson W (2011) Identification of the meiotic life cycle stage of *Trypanosoma brucei* in the tsetse fly. *Proceedings of the National Academy of Sciences of the United States of America* **108:** 3671-3676

Pedersen SN (1975) The glycolytic enzyme activity of the human cervix uteri. *Cancer* **35:** 469-474

Pellecchia M, Bertini I, Cowburn D, Dalvit C, Giralt E, Jahnke W, James TL, Homans SW, Kessler H, Luchinat C, Meyer B, Oschkinat H, Peng J, Schwalbe H, Siegal G (2008) Perspectives on NMR in drug discovery: a technique comes of age. *Nature reviews Drug discovery* **7:** 738-745

Pepin J, Meda HA (2001) The epidemiology and control of human African trypanosomiasis. *Advances in parasitology* **49:** 71-132

Perez-Morga D, Vanhollebeke B, Paturiaux-Hanocq F, Nolan DP, Lins L, Homble F, Vanhamme L, Tebabi P, Pays A, Poelvoorde P, Jacquet A, Brasseur R, Pays E (2005) Apolipoprotein L-I promotes trypanosome lysis by forming pores in lysosomal membranes. *Science* **309:** 469-472

Pham JS, Dawson KL, Jackson KE, Lim EE, Pasaje CF, Turner KE, Ralph SA (2014) Aminoacyl-tRNA synthetases as drug targets in eukaryotic parasites. *International journal for parasitology Drugs and drug resistance* **4:** 1-13

Phillips C, Dohnalek J, Gover S, Barrett MP, Adams MJ (1998) A 2.8 A resolution structure of 6-phosphogluconate dehydrogenase from the protozoan parasite *Trypanosoma brucei*: comparison with the sheep enzyme accounts for differences in activity with coenzyme and substrate analogues. *Journal of molecular biology* **282:** 667-681

Phillips MA (2012) Stoking the drug target pipeline for human African trypanosomiasis. *Molecular microbiology* **86:** 10-14

Pink R, Hudson A, Mouries MA, Bendig M (2005) Opportunities and challenges in antiparasitic drug discovery. *Nature reviews Drug discovery* **4:** 727-740

Piotrowski M, Volmer JJ (2006) Cyanide metabolism in higher plants: cyanoalanine hydratase is a NIT4 homolog. *Plant molecular biology* **61:** 111-122

Poulin R, Lu L, Ackermann B, Bey P, Pegg AE (1992) Mechanism of the irreversible inactivation of mouse ornithine decarboxylase by alpha-difluoromethylornithine. Characterization of sequences at the inhibitor and coenzyme binding sites. *The Journal of biological chemistry* **267:** 150-158

Preuss J, Jortzik E, Becker K (2012) Glucose-6-phosphate metabolism in *Plasmodium falciparum. IUBMB life* **64:** 603-611

Price HP, Menon MR, Panethymitaki C, Goulding D, McKean PG, Smith DF (2003) Myristoyl-CoA:protein N-myristoyltransferase, an essential enzyme and potential drug target in kinetoplastid parasites. *The Journal of biological chemistry* **278:** 7206-7214

Prigione A, Lichtner B, Kuhl H, Struys EA, Wamelink M, Lehrach H, Ralser M, Timmermann B, Adjaye J (2011) Human induced pluripotent stem cells harbor homoplasmic and heteroplasmic

mitochondrial DNA mutations while maintaining human embryonic stem cell-like metabolic reprogramming. *Stem cells* **29:** 1338-1348

Priotto G, Kasparian S, Mutombo W, Ngouama D, Ghorashian S, Arnold U, Ghabri S, Baudin E, Buard V, Kazadi-Kyanza S, Ilunga M, Mutangala W, Pohlig G, Schmid C, Karunakara U, Torreele E, Kande V (2009) Nifurtimox-eflornithine combination therapy for second-stage African *Trypanosoma brucei gambiense* trypanosomiasis: a multicentre, randomised, phase III, non-inferiority trial. *Lancet* **374:** 56-64

Priotto G, Pinoges L, Fursa IB, Burke B, Nicolay N, Grillet G, Hewison C, Balasegaram M (2008) Safety and effectiveness of first line eflornithine for *Trypanosoma brucei gambiense* sleeping sickness in Sudan: cohort study. *Bmj* **336:** 705-708

Proto WR, Castanys-Munoz E, Black A, Tetley L, Moss CX, Juliano L, Coombs GH, Mottram JC (2011) *Trypanosoma brucei* metacaspase 4 is a pseudopeptidase and a virulence factor. *The Journal of biological chemistry* **286:** 39914-39925

Qian G, Liu C, Wu G, Yin F, Zhao Y, Zhou Y, Zhang Y, Song Z, Fan J, Hu B, Liu F (2013) AsnB, regulated by diffusible signal factor and global regulator Clp, is involved in aspartate metabolism, resistance to oxidative stress and virulence in *Xanthomonas oryzae pv. oryzicola*. *Molecular plant pathology* **14:** 145-157

Raczniak G, Becker HD, Min B, Soll D (2001) A single amidotransferase forms asparaginyl-tRNA and glutaminyl-tRNA in *Chlamydia trachomatis*. *The Journal of biological chemistry* **276:** 45862-45867

Radwanska M, Guirnalda P, De Trez C, Ryffel B, Black S, Magez S (2008) Trypanosomiasis-induced B cell apoptosis results in loss of protective anti-parasite antibody responses and abolishment of vaccine-induced memory responses. *PLoS pathogens* **4:** e1000078

Radwanska M, Magez S, Michel A, Stijlemans B, Geuskens M, Pays E (2000) Comparative analysis of antibody responses against HSP60, invariant surface glycoprotein 70, and variant surface glycoprotein reveals a complex antigen-specific pattern of immunoglobulin isotype switching during infection by *Trypanosoma brucei*. *Infection and immunity* **68:** 848-860

Ramey K, Eko FO, Thompson WE, Armah H, Igietseme JU, Stiles JK (2009) Immunolocalization and challenge studies using a recombinant Vibrio cholerae ghost expressing *Trypanosoma brucei* Ca(2+) ATPase (TBCA2) antigen. *The American journal of tropical medicine and hygiene* **81:** 407-415

Ramos F, Wiame JM (1979) Synthesis and activation of asparagine in asparagine auxotrophs of *Saccharomyces cerevisiae*. *European journal of biochemistry / FEBS* **94:** 409-417

Ramos F, Wiame JM (1980) Two asparagine synthetases in *Saccharomyces cerevisiae*. *European journal of biochemistry / FEBS* **108:** 373-377

Raper J, Fung R, Ghiso J, Nussenzweig V, Tomlinson S (1999) Characterization of a novel trypanosome lytic factor from human serum. *Infection and immunity* **67:** 1910-1916

Rasooly R, Balaban N (2004) Trypanosome microtubule-associated protein p15 as a vaccine for the prevention of African sleeping sickness. *Vaccine* **22:** 1007-1015

Reitzer LJ, Magasanik B (1982) Asparagine synthetases of *Klebsiella aerogenes*: properties and regulation of synthesis. *Journal of bacteriology* **151:** 1299-1313

Richards NG, Schuster SM (1998) Mechanistic issues in asparagine synthetase catalysis. *Advances in enzymology and related areas of molecular biology* **72:** 145-198

Rifkin MR (1978) Identification of the trypanocidal factor in normal human serum: high density lipoprotein. *Proceedings of the National Academy of Sciences of the United States of America* **75:** 3450-3454

Rizzari C (2003) *Asparaginase Treatment*, Treatment of Acute Leukemias: Humana Press

Rizzari C, Conter V, Stary J, Colombini A, Moericke A, Schrappe M (2013) Optimizing asparaginase therapy for acute lymphoblastic leukemia. *Current opinion in oncology* **25 Suppl 1:** S1-9

Robello C, Navarro P, Castanys S, Gamarro F (1997) A pteridine reductase gene ptr1 contiguous to a P-glycoprotein confers resistance to antifolates in *Trypanosoma cruzi. Molecular and biochemical parasitology* **90:** 525-535

Roberts J, Holcenberg JS, Dolowy WC (1972) Isolation, crystallization, and properties of *Achromobacteraceae* glutaminase-asparaginase with antitumor activity. *The Journal of biological chemistry* **247:** 84-90

Robertson JG (2005) Mechanistic basis of enzyme-targeted drugs. *Biochemistry* **44:** 5561-5571

Robinette D, Neamati N, Tomer KB, Borchers CH (2006) Photoaffinity labeling combined with mass spectrometric approaches as a tool for structural proteomics. *Expert review of proteomics* **3:** 399-408

Robinson KA, Beverley SM (2003) Improvements in transfection efficiency and tests of RNA interference (RNAi) approaches in the protozoan parasite *Leishmania*. *Molecular and biochemical parasitology* **128:** 217-228

Rogers DJ, Randolph SE (2002) A response to the aim of eradicating tsetse from Africa. *Trends in parasitology* **18:** 534-536

Roos AK (2007) Structural and Functional Studies of Ribose-5-phosphate isomerase B. Doctor of Phylosophy Thesis, Deparment of Cell and Molecular Biology, Uppsala Universitet,

Roos AK, Andersson CE, Bergfors T, Jacobsson M, Karlen A, Unge T, Jones TA, Mowbray SL (2004) *Mycobacterium tuberculosis* ribose-5-phosphate isomerase has a known fold, but a novel active site. *Journal of molecular biology* **335:** 799-809

Roos AK, Burgos E, Ericsson DJ, Salmon L, Mowbray SL (2005) Competitive inhibitors of *Mycobacterium tuberculosis* ribose-5-phosphate isomerase B reveal new information about the reaction mechanism. *The Journal of biological chemistry* **280:** 6416-6422

Roos AK, Mariano S, Kowalinski E, Salmon L, Mowbray SL (2008) D-ribose-5-phosphate isomerase B from Escherichia coli is also a functional D-allose-6-phosphate isomerase, while the *Mycobacterium tuberculosis* enzyme is not. *Journal of molecular biology* **382:** 667-679

Rotureau B, Subota I, Buisson J, Bastin P (2012) A new asymmetric division contributes to the continuous production of infective trypanosomes in the tsetse fly. *Development* **139:** 1842-1850

Roy H, Becker HD, Reinbolt J, Kern D (2003) When contemporary aminoacyl-tRNA synthetases invent their cognate amino acid metabolism. *Proceedings of the National Academy of Sciences of the United States of America* **100:** 9837-9842

Ruda GF, Campbell G, Alibu VP, Barrett MP, Brenk R, Gilbert IH (2010a) Virtual fragment screening for novel inhibitors of 6-phosphogluconate dehydrogenase. *Bioorganic & medicinal chemistry* **18:** 5056-5062

Ruda GF, Wong PE, Alibu VP, Norval S, Read KD, Barrett MP, Gilbert IH (2010b) Aryl phosphoramidates of 5-phospho erythronohydroxamic acid, a new class of potent trypanocidal compounds. *Journal of medicinal chemistry* **53:** 6071-6078

Russo DC, Williams DJ, Grab DJ (1994) Mechanisms for the elimination of potentially lytic complement-fixing variable surface glycoprotein antibody-complexes in *Trypanosoma brucei*. *Parasitology research* **80:** 487-492

Salmon D, Vanwalleghem G, Morias Y, Denoeud J, Krumbholz C, Lhomme F, Bachmaier S, Kador M, Gossmann J, Dias FB, De Muylder G, Uzureau P, Magez S, Moser M, De Baetselier P, Van Den Abbeele J, Beschin A, Boshart M, Pays E (2012) Adenylate cyclases of *Trypanosoma brucei* inhibit the innate immune response of the host. *Science* **337:** 463-466

Sanderson L, Dogruel M, Rodgers J, De Koning HP, Thomas SA (2009) Pentamidine movement across the murine blood-brain and blood-cerebrospinal fluid barriers: effect of trypanosome infection, combination therapy, P-glycoprotein, and multidrug resistance-associated protein. *The Journal of pharmacology and experimental therapeutics* **329:** 967-977

Sands M, Kron MA, Brown RB (1985) Pentamidine: a review. *Reviews of infectious diseases* **7:** 625-634

Saraiva EM, de Figueiredo Barbosa A, Santos FN, Borja-Cabrera GP, Nico D, Souza LO, de Oliveira Mendes-Aguiar C, de Souza EP, Fampa P, Parra LE, Menz I, Dias JG, Jr., de Oliveira SM, Palatnik-de-Sousa CB (2006) The FML-vaccine (Leishmune) against canine visceral leishmaniasis: a transmission blocking vaccine. *Vaccine* **24:** 2423-2431

Schenk G, Duggleby RG, Nixon PF (1998) Properties and functions of the thiamin diphosphate dependent enzyme transketolase. *The international journal of biochemistry & cell biology* **30:** 1297-1318

Schleifer KW, Filutowicz H, Schopf LR, Mansfield JM (1993) Characterization of T helper cell responses to the trypanosome variant surface glycoprotein. *J Immunol* **150:** 2910-2919

Schmid C, Richer M, Bilenge CM, Josenando T, Chappuis F, Manthelot CR, Nangouma A, Doua F, Asumu PN, Simarro PP, Burri C (2005) Effectiveness of a 10-day melarsoprol schedule for the treatment of late-stage human African trypanosomiasis: confirmation from a multinational study (IMPAMEL II). *The Journal of infectious diseases* **191:** 1922-1931

Schofield CJ, Maudlin I (2001) Trypanosomiasis control. *International journal for parasitology* **31:** 614-619

Schopf LR, Filutowicz H, Bi XJ, Mansfield JM (1998) Interleukin-4-dependent immunoglobulin G1 isotype switch in the presence of a polarized antigen-specific Th1-cell response to the trypanosome variant surface glycoprotein. *Infection and immunity* **66:** 451-461

Schumann Burkard G, Jutzi P, Roditi I (2011) Genome-wide RNAi screens in bloodstream form trypanosomes identify drug transporters. *Molecular and biochemical parasitology* **175:** 91-94

Schwarz F, Aebi M (2011) Mechanisms and principles of N-linked protein glycosylation. *Current opinion in structural biology* **21:** 576-582

Scofield MA, Lewis WS, Schuster SM (1990) Nucleotide sequence of *Escherichia coli* asnB and deduced amino acid sequence of asparagine synthetase B. *The Journal of biological chemistry* **265:** 12895-12902

Scotti C, Sommi P, Pasquetto MV, Cappelletti D, Stivala S, Mignosi P, Savio M, Chiarelli LR, Valentini G, Bolanos-Garcia VM, Merrell DS, Franchini S, Verona ML, Bolis C, Solcia E, Manca R, Franciotta D, Casasco A, Filipazzi P, Zardini E, Vannini V (2010) Cell-cycle inhibition by *Helicobacter pylori* L-asparaginase. *PloS one* **5:** e13892

Semballa S, Geffard M, Daulouede S, Malvy D, Veyret B, Lemesre JL, Holzmuller P, Mnaimneh S, Vincendeau P (2004) Antibodies directed against nitrosylated neoepitopes in sera of patients with human African trypanosomiasis. *Tropical medicine & international health : TM & IH* **9:** 1104-1110

Seyfang A, Duszenko M (1991) Specificity of glucose transport in *Trypanosoma brucei*. Effective inhibition by phloretin and cytochalasin B. *European journal of biochemistry / FEBS* **202:** 191-196

Seyfang A, Mecke D, Duszenko M (1990) Degradation, recycling, and shedding of *Trypanosoma brucei* variant surface glycoprotein. *The Journal of protozoology* **37:** 546-552

Sharlow E, Golden JE, Dodson H, Morris M, Hesser M, Lyda T, Leimgruber S, Schroeder CE, Flaherty DP, Weiner WS, Simpson D, Lazo JS, Aubé J, Morris JC (2011) Identification of Inhibitors of *Trypanosoma brucei* Hexokinases. *Probe Reports from the NIH Molecular Libraries Program* **41:** 1859-1866

Sharlow ER, Lyda TA, Dodson HC, Mustata G, Morris MT, Leimgruber SS, Lee KH, Kashiwada Y, Close D, Lazo JS, Morris JC (2010) A target-based high throughput screen yields *Trypanosoma brucei* hexokinase small molecule inhibitors with antiparasitic activity. *PLoS neglected tropical diseases* **4:** e659

Shelton MD, Chock PB, Mieyal JJ (2005) Glutaredoxin: role in reversible protein s-glutathionylation and regulation of redox signal transduction and protein translocation. *Antioxidants & redox signaling* **7:** 348-366

Sheng C, Ji H, Miao Z, Che X, Yao J, Wang W, Dong G, Guo W, Lu J, Zhang W (2009) Homology modeling and molecular dynamics simulation of N-myristoyltransferase from protozoan parasites: active site characterization and insights into rational inhibitor design. *Journal of computer-aided molecular design* **23:** 375-389

Sheppard J, Nielsen K, Tizard I, Holmes W (1978) Direct activation of complement by trypanosomes. *The Journal of parasitology* **64:** 544-546

Shi H, Chamond N, Djikeng A, Tschudi C, Ullu E (2009) RNA interference in *Trypanosoma brucei*: role of the n-terminal RGG domain and the polyribosome association of argonaute. *The Journal of biological chemistry* **284:** 36511-36520

Shi H, Djikeng A, Tschudi C, Ullu E (2004a) Argonaute protein in the early divergent eukaryote *Trypanosoma brucei*: control of small interfering RNA accumulation and retroposon transcript abundance. *Molecular and cellular biology* **24:** 420-427

Shi H, Tschudi C, Ullu E (2006a) An unusual Dicer-like1 protein fuels the RNA interference pathway in *Trypanosoma brucei*. *Rna* **12:** 2063-2072

Shi H, Ullu E, Tschudi C (2004b) Function of the *Trypanosome* Argonaute 1 protein in RNA interference requires the N-terminal RGG domain and arginine 735 in the Piwi domain. *The Journal of biological chemistry* **279:** 49889-49893

Shi M, Pan W, Tabel H (2003) Experimental African trypanosomiasis: IFN-gamma mediates early mortality. *European journal of immunology* **33:** 108-118

Shi M, Wei G, Pan W, Tabel H (2006b) Experimental African trypanosomiasis: a subset of pathogenic, IFN-gamma-producing, MHC class II-restricted CD4+ T cells mediates early mortality in highly susceptible mice. *J Immunol* **176:** 1724-1732

Shi MQ, Wei GJ, Tabel H (2007) *Trypanosoma congolense* infections: MHC class II-restricted immune responses mediate either protection or disease, depending on IL-10 function. *Parasite immunology* **29:** 107-111

Shiba K, Motegi H, Yoshida M, Noda T (1998) Human asparaginyl-tRNA synthetase: molecular cloning and the inference of the evolutionary history of Asx-tRNA synthetase family. *Nucleic acids research* **26:** 5045-5051

Shibayama K, Takeuchi H, Wachino J, Mori S, Arakawa Y (2011) Biochemical and pathophysiological characterization of *Helicobacter pylori* asparaginase. *Microbiology and immunology* **55:** 408-417

Sidoli C, Molteni A, Bellanti B, Redaelli L, Iuzzolino L, Rubino M, Arioli P, Nardese V, Carettoni D (2006) Biochemical assay development for drug discovery: a sequential optimization from protein expression to enzymatic activity. *Microbial Cell Factories* **5:** 1-2

Sienkiewicz N, Jaroslawski S, Wyllie S, Fairlamb AH (2008) Chemical and genetic validation of dihydrofolate reductase-thymidylate synthase as a drug target in African trypanosomes. *Molecular microbiology* **69:** 520-533

Sienkiewicz N, Ong HB, Fairlamb AH (2010) *Trypanosoma brucei* pteridine reductase 1 is essential for survival in vitro and for virulence in mice. *Molecular microbiology* **77:** 658-671

Silva MS, Prazeres DM, Lanca A, Atouguia J, Monteiro GA (2009) Trans-sialidase from *Trypanosoma brucei* as a potential target for DNA vaccine development against African trypanosomiasis. *Parasitology research* **105:** 1223-1229

Skinner AJ, Cooper RA (1974) Genetic studies on ribose 5-phosphate isomerase mutants of *Escherichia coli* K-12. *Journal of bacteriology* **118:** 1183-1185

Smith TK, Butikofer P (2010) Lipid metabolism in *Trypanosoma brucei*. *Molecular and biochemical parasitology* **172:** 66-79

Smith TK, Crossman A, Borissow CN, Paterson MJ, Dix A, Brimacombe JS, Ferguson MA (2001) Specificity of GlcNAc-PI de-N-acetylase of GPI biosynthesis and synthesis of parasite-specific suicide substrate inhibitors. *The EMBO journal* **20:** 3322-3332

Snijder HJ, Van Eerde JH, Kingma RL, Kalk KH, Dekker N, Egmond MR, Dijkstra BW (2001) Structural investigations of the active-site mutant Asn156Ala of outer membrane phospholipase A: function of the Asn-His interaction in the catalytic triad. *Protein science : a publication of the Protein Society* **10:** 1962-1969

Solano P, Torr SJ, Lehane MJ (2013) Is vector control needed to eliminate gambiense human African trypanosomiasis? *Frontiers in cellular and infection microbiology* **3:** 33

Sorensen KI, Hove-Jensen B (1996) Ribose catabolism of *Escherichia coli*: characterization of the rpiB gene encoding ribose phosphate isomerase B and of the rpiR gene, which is involved in regulation of rpiB expression. *Journal of bacteriology* **178:** 1003-1011

Spinks D, Ong HB, Mpamhanga CP, Shanks EJ, Robinson DA, Collie IT, Read KD, Frearson JA, Wyatt PG, Brenk R, Fairlamb AH, Gilbert IH (2011) Design, synthesis and biological evaluation of novel inhibitors of *Trypanosoma brucei* pteridine reductase 1. *ChemMedChem* **6:** 302-308

Spinks D, Shanks EJ, Cleghorn LA, McElroy S, Jones D, James D, Fairlamb AH, Frearson JA, Wyatt PG, Gilbert IH (2009) Investigation of trypanothione reductase as a drug target in *Trypanosoma brucei*. *ChemMedChem* **4:** 2060-2069

Stams WA, den Boer ML, Holleman A, Appel IM, Beverloo HB, van Wering ER, Janka-Schaub GE, Evans WE, Pieters R (2005) Asparagine synthetase expression is linked with L-asparaginase resistance in TEL-AML1-negative but not TEL-AML1-positive pediatric acute lymphoblastic leukemia. *Blood* **105:** 4223-4225

Stanghellini A, Josenando T (2001) The situation of sleeping sickness in Angola: a calamity. *Tropical medicine & international health : TM & IH* **6:** 330-334

Stephens JL, Lee SH, Paul KS, Englund PT (2007) Mitochondrial fatty acid synthesis in *Trypanosoma brucei*. *The Journal of biological chemistry* **282:** 4427-4436

Stephens NA, Hajduk SL (2011) Endosomal localization of the serum resistance-associated protein in African trypanosomes confers human infectivity. *Eukaryotic cell* **10:** 1023-1033

Stern AL, Burgos E, Salmon L, Cazzulo JJ (2007) Ribose 5-phosphate isomerase type B from *Trypanosoma cruzi*: kinetic properties and site-directed mutagenesis reveal information about the reaction mechanism. *The Biochemical journal* **401:** 279-285

Stern AL, Naworyta A, Cazzulo JJ, Mowbray SL (2011) Structures of type B ribose 5-phosphate isomerase from *Trypanosoma cruzi* shed light on the determinants of sugar specificity in the structural family. *The FEBS journal* **278:** 793-808

Sternberg JM, Rodgers J, Bradley B, Maclean L, Murray M, Kennedy PG (2005) Meningoencephalitic African trypanosomiasis: Brain IL-10 and IL-6 are associated with protection from neuro-inflammatory pathology. *Journal of neuroimmunology* **167:** 81-89

Stevens DR, Moulton JE (1978) Ultrastructural and immunological aspects of the phagocytosis of *Trypanosoma brucei* by mouse peritoneal macrophages. *Infection and immunity* **19:** 972-982

Steverding D (2008) The history of African trypanosomiasis. *Parasites & vectors* **1:** 3

Stewart ML, Burchmore RJ, Clucas C, Hertz-Fowler C, Brooks K, Tait A, Macleod A, Turner CM, De Koning HP, Wong PE, Barrett MP (2010) Multiple genetic mechanisms lead to loss of functional TbAT1 expression in drug-resistant trypanosomes. *Eukaryotic cell* **9:** 336-343

Stijlemans B, Baral TN, Guilliams M, Brys L, Korf J, Drennan M, Van Den Abbeele J, De Baetselier P, Magez S (2007) A glycosylphosphatidylinositol-based treatment alleviates trypanosomiasis-associated immunopathology. *J Immunol* **179:** 4003-4014

Stincone A, Prigione A, Cramer T, Wamelink MM, Campbell K, Cheung E, Olin-Sandoval V, Gruening NM, Krueger A, Tauqeer Alam M, Keller MA, Breitenbach M, Brindle KM, Rabinowitz JD, Ralser M (2014) The return of metabolism: biochemistry and physiology of the pentose phosphate pathway. *Biological reviews of the Cambridge Philosophical Society*

Stoffel SA, Alibu VP, Hubert J, Ebikeme C, Portais JC, Bringaud F, Schweingruber ME, Barrett MP (2011) Transketolase in *Trypanosoma brucei*. *Molecular and biochemical parasitology* **179:** 1-7

Su N, Pan YX, Zhou M, Harvey RC, Hunger SP, Kilberg MS (2008) Correlation between asparaginase sensitivity and asparagine synthetase protein content, but not mRNA, in acute lymphoblastic leukemia cell lines. *Pediatric blood & cancer* **50:** 274-279

Subramaniam C, Veazey P, Redmond S, Hayes-Sinclair J, Chambers E, Carrington M, Gull K, Matthews K, Horn D, Field MC (2006) Chromosome-wide analysis of gene function by RNA interference in the african trypanosome. *Eukaryotic cell* **5:** 1539-1549

Sugiyama A, Kato H, Nishioka T, Oda J (1992) Overexpression and purification of asparagine synthetase from *Escherichia coli*. *Bioscience, biotechnology, and biochemistry* **56:** 376-379

Sunter J, Webb H, Carrington M (2013) Determinants of GPI-PLC localisation to the flagellum and access to GPI-anchored substrates in trypanosomes. *PLoS pathogens* **9:** e1003566

Swinney DC (2004) Biochemical mechanisms of drug action: what does it take for success? *Nature reviews Drug discovery* **3:** 801-808

Szathmary E (1999) The origin of the genetic code: amino acids as cofactors in an RNA world. *Trends in genetics : TIG* **15:** 223-229

Tachado SD, Gerold P, Schwarz R, Novakovic S, McConville M, Schofield L (1997) Signal transduction in macrophages by glycosylphosphatidylinositols of *Plasmodium*, *Trypanosoma*, and *Leishmania*: activation of protein tyrosine kinases and protein kinase C by inositolglycan and diacylglycerol moieties. *Proceedings of the National Academy of Sciences of the United States of America* **94:** 4022-4027

Tait A, Babiker EA, Le Ray D (1984) Enzyme variation in *Trypanosoma brucei spp*. I. Evidence for the sub-speciation of *Trypanosoma brucei gambiense*. *Parasitology* **89 (Pt 2):** 311-326

Takayanagi T, Kawaguchi H, Yabu Y, Itoh M, Appawu MA (1987) Contribution of the complement system to antibody-mediated binding of *Trypanosoma gambiense* to macrophages. *The Journal of parasitology* **73:** 333-341

Tasdemir D, Guner ND, Perozzo R, Brun R, Donmez AA, Calis I, Ruedi P (2005) Anti-protozoal and plasmodial FabI enzyme inhibiting metabolites of *Scrophularia lepidota* roots. *Phytochemistry* **66:** 355-362

Tasdemir D, Topaloglu B, Perozzo R, Brun R, O'Neill R, Carballeira NM, Zhang X, Tonge PJ, Linden A, Ruedi P (2007) Marine natural products from the Turkish sponge Agelas oroides that inhibit the enoyl reductases from *Plasmodium falciparum*, *Mycobacterium tuberculosis* and *Escherichia coli*. *Bioorganic & medicinal chemistry* **15:** 6834-6845

Taylor MC, Kaur H, Blessington B, Kelly JM, Wilkinson SR (2008) Validation of spermidine synthase as a drug target in African trypanosomes. *The Biochemical journal* **409:** 563-569

Tetley L, Turner CM, Barry JD, Crowe JS, Vickerman K (1987) Onset of expression of the variant surface glycoproteins of *Trypanosoma brucei* in the tsetse fly studied using immunoelectron microscopy. *Journal of cell science* **87 (Pt 2):** 363-372

Tielens AG, Van Hellemond JJ (1998) Differences in energy metabolism between trypanosomatidae. *Parasitol Today* **14:** 265-272

Tirados I, Esterhuizen J, Rayaisse JB, Diarrassouba A, Kaba D, Mpiana S, Vale GA, Solano P, Lehane MJ, Torr SJ (2011) How do tsetse recognise their hosts? The role of shape in the responses of tsetse (*Glossina fuscipes* and *G. palpalis*) to artificial hosts. *PLoS neglected tropical diseases* **5:** e1226

Torrie LS, Wyllie S, Spinks D, Oza SL, Thompson S, Harrison JR, Gilbert IH, Wyatt PG, Fairlamb AH, Frearson JA (2009) Chemical validation of trypanothione synthetase: a potential drug target for human trypanosomiasis. *The Journal of biological chemistry* **284:** 36137-36145

Truc P, Tibayrenc M (1993) Population genetics of *Trypanosoma brucei* in central Africa: taxonomic and epidemiological significance. *Parasitology* **106 (Pt 2):** 137-149

Tulloch LB, Martini VP, Iulek J, Huggan JK, Lee JH, Gibson CL, Smith TK, Suckling CJ, Hunter WN (2010) Structure-based design of pteridine reductase inhibitors targeting African sleeping sickness and the leishmaniases. *Journal of medicinal chemistry* **53:** 221-229

Tumbula-Hansen D, Feng L, Toogood H, Stetter KO, Soll D (2002) Evolutionary divergence of the archaeal aspartyl-tRNA synthetases into discriminating and nondiscriminating forms. *The Journal of biological chemistry* **277:** 37184-37190

Tumbula DL, Becker HD, Chang WZ, Soll D (2000) Domain-specific recruitment of amide amino acids for protein synthesis. *Nature* **407:** 106-110

Ueno T, Ohtawa K, Mitsui K, Kodera Y, Hiroto M, Matsushima A, Inada Y, Nishimura H (1997) Cell cycle arrest and apoptosis of leukemia cells induced by L-asparaginase. *Leukemia : official journal of the Leukemia Society of America, Leukemia Research Fund, UK* **11:** 1858-1861

Urwyler S, Studer E, Renggli CK, Roditi I (2007) A family of stage-specific alanine-rich proteins on the surface of epimastigote forms of *Trypanosoma brucei*. *Molecular microbiology* **63:** 218-228

Uzonna JE, Kaushik RS, Gordon JR, Tabel H (1999) Cytokines and antibody responses during *Trypanosoma congolense* infections in two inbred mouse strains that differ in resistance. *Parasite immunology* **21:** 57-71

Uzureau P, Uzureau S, Lecordier L, Fontaine F, Tebabi P, Homble F, Grelard A, Zhendre V, Nolan DP, Lins L, Crowet JM, Pays A, Felu C, Poelvoorde P, Vanhollebeke B, Moestrup SK, Lyngso J, Pedersen JS, Mottram JC, Dufourc EJ, Perez-Morga D, Pays E (2013) Mechanism of *Trypanosoma brucei gambiense* resistance to human serum. *Nature* **501:** 430-434

Van Den Abbeele J, Caljon G, De Ridder K, De Baetselier P, Coosemans M (2010) *Trypanosoma brucei* modifies the tsetse salivary composition, altering the fly feeding behavior that favors parasite transmission. *PLoS pathogens* **6:** e1000926

Van Den Abbeele J, Claes Y, van Bockstaele D, Le Ray D, Coosemans M (1999) *Trypanosoma brucei* spp. development in the tsetse fly: characterization of the post-mesocyclic stages in the foregut and proboscis. *Parasitology* **118 (Pt 5):** 469-478

van den Berg H (2011) Asparaginase revisited. *Leukemia & lymphoma* **52:** 168-178

van Hellemond JJ, Tielens AG (2006) Adaptations in the lipid metabolism of the protozoan parasite *Trypanosoma brucei*. *FEBS letters* **580:** 5552-5558

Van Schaftingen E, Opperdoes FR, Hers HG (1987) Effects of various metabolic conditions and of the trivalent arsenical melarsen oxide on the intracellular levels of fructose 2,6-bisphosphate and

of glycolytic intermediates in Trypanosoma brucei. *European journal of biochemistry / FEBS* **166:** 653-661

Vanhamme L, Paturiaux-Hanocq F, Poelvoorde P, Nolan DP, Lins L, Van Den Abbeele J, Pays A, Tebabi P, Van Xong H, Jacquet A, Moguilevsky N, Dieu M, Kane JP, De Baetselier P, Brasseur R, Pays E (2003) Apolipoprotein L-I is the trypanosome lytic factor of human serum. *Nature* **422:** 83-87

Vanhollebeke B, De Muylder G, Nielsen MJ, Pays A, Tebabi P, Dieu M, Raes M, Moestrup SK, Pays E (2008) A haptoglobin-hemoglobin receptor conveys innate immunity to *Trypanosoma brucei* in humans. *Science* **320:** 677-681

Vansterkenburg EL, Coppens I, Wilting J, Bos OJ, Fischer MJ, Janssen LH, Opperdoes FR (1993) The uptake of the trypanocidal drug suramin in combination with low-density lipoproteins by *Trypanosoma brucei* and its possible mode of action. *Acta tropica* **54:** 237-250

Varum S, Rodrigues AS, Moura MB, Momcilovic O, Easley CAt, Ramalho-Santos J, Van Houten B, Schatten G (2011) Energy metabolism in human pluripotent stem cells and their differentiated counterparts. *PloS one* **6:** e20914

Vassella E, Probst M, Schneider A, Studer E, Renggli CK, Roditi I (2004) Expression of a major surface protein of *Trypanosoma brucei* insect forms is controlled by the activity of mitochondrial enzymes. *Molecular biology of the cell* **15:** 3986-3993

Vernet T, Tessier DC, Chatellier J, Plouffe C, Lee TS, Thomas DY, Storer AC, Menard R (1995) Structural and functional roles of asparagine 175 in the cysteine protease papain. *The Journal of biological chemistry* **270:** 16645-16652

Vickerman K (1985) Developmental cycles and biology of pathogenic trypanosomes. *British medical bulletin* **41:** 105-114

Vickerman K, Luckins AG (1969) Localization of variable antigens in the surface coat of *Trypanosoma brucei* using ferritin conjugated antibody. *Nature* **224:** 1125-1126

Vincendeau P, Gobert AP, Daulouede S, Moynet D, Mossalayi MD (2003) Arginases in parasitic diseases. *Trends in parasitology* **19:** 9-12

Vincent IM, Creek D, Watson DG, Kamleh MA, Woods DJ, Wong PE, Burchmore RJ, Barrett MP (2010) A molecular mechanism for eflornithine resistance in African trypanosomes. *PLoS pathogens* **6:** e1001204

Vreysen MJ (2001) Principles of area-wide integrated tsetse fly control using the sterile insect technique. *Medecine tropicale : revue du Corps de sante colonial* **61:** 397-411

Vreysen MJ, Saleh KM, Ali MY, Abdulla AM, Zhu ZR, Juma KG, Dyck VA, Msangi AR, Mkonyi PA, Feldmann HU (2000) *Glossina austeni* (Diptera: Glossinidae) eradicated on the island of Unguja, Zanzibar, using the sterile insect technique. *Journal of economic entomology* **93:** 123-135

Walsh MJ, Brimacombe KR, Vasquez-Valdivieso MG, Auld DS, Simeonov A, Morgan HP, Fothergill-Gilmore LA, Michels PAM, Walkinshaw MD, Shen M, Boxer MB (2010) Identification of Selective Inhibitors of Phosphofructokinase as Lead Compounds Against Trypanosomiasis. In *Probe Reports from the NIH Molecular Libraries Program*. Bethesda (MD)

Wang CC (1995) Molecular mechanisms and therapeutic approaches to the treatment of African trypanosomiasis. *Annual review of pharmacology and toxicology* **35:** 93-127

Wang J, Yang W (2013) Concerted proton transfer mechanism of *Clostridium thermocellum* ribose-5-phosphate isomerase. *The journal of physical chemistry B* **117:** 9354-9361

Wang Z, Morris JC, Drew ME, Englund PT (2000) Inhibition of *Trypanosoma brucei* gene expression by RNA interference using an integratable vector with opposing T7 promoters. *The Journal of biological chemistry* **275:** 40174-40179

Wastling SL, Welburn SC (2011) Diagnosis of human sleeping sickness: sense and sensitivity. *Trends in parasitology* **27:** 394-402

Webb H, Carnall N, Carrington M (1994) The role of GPI-PLC in *Trypanosoma brucei*. *Brazilian journal of medical and biological research = Revista brasileira de pesquisas medicas e biologicas / Sociedade Brasileira de Biofisica [et al]* **27:** 349-356

Webb H, Carnall N, Vanhamme L, Rolin S, Van Den Abbeele J, Welburn S, Pays E, Carrington M (1997) The GPI-phospholipase C of *Trypanosoma brucei* is nonessential but influences parasitemia in mice. *The Journal of cell biology* **139:** 103-114

Wei G, Tabel H (2008) Regulatory T cells prevent control of experimental African trypanosomiasis. *J Immunol* **180:** 2514-2521

WHO. (1998) Control and surveillance of African trypanosomiasis. In Committee RoaWE (ed.), *WHO technical report series 881*. World Health Organization, Geneva.

Widener J, Nielsen MJ, Shiflett A, Moestrup SK, Hajduk S (2007) Hemoglobin is a co-factor of human trypanosome lytic factor. *PLoS pathogens* **3:** 1250-1261

Wiemer EA, Michels PA, Opperdoes FR (1995) The inhibition of pyruvate transport across the plasma membrane of the bloodstream form of *Trypanosoma brucei* and its metabolic implications. *The Biochemical journal* **312 (Pt 2):** 479-484

Wilkinson SR, Taylor MC, Horn D, Kelly JM, Cheeseman I (2008) A mechanism for cross-resistance to nifurtimox and benznidazole in trypanosomes. *Proceedings of the National Academy of Sciences of the United States of America* **105:** 5022-5027

Willadsen P, Bird P, Cobon GS, Hungerford J (1995) Commercialisation of a recombinant vaccine against Boophilus microplus. *Parasitology* **110 Suppl:** S43-50

Willert EK, Fitzpatrick R, Phillips MA (2007) Allosteric regulation of an essential trypanosome polyamine biosynthetic enzyme by a catalytically dead homolog. *Proceedings of the National Academy of Sciences of the United States of America* **104:** 8275-8280

Willert EK, Phillips MA (2008) Regulated expression of an essential allosteric activator of polyamine biosynthesis in African trypanosomes. *PLoS pathogens* **4:** e1000183

Williams DJ, Taylor K, Newson J, Gichuki B, Naessens J (1996) The role of anti-variable surface glycoprotein antibody responses in bovine trypanotolerance. *Parasite immunology* **18:** 209-218

Willis RC, Woolfolk CA (1975) L-asparagine uptake in *Escherichia coli*. *Journal of bacteriology* **123:** 937-945

Willson M, Sanejouand YH, Perie J, Hannaert V, Opperdoes F (2002) Sequencing, modeling, and selective inhibition of *Trypanosoma brucei* hexokinase. *Chemistry & biology* **9:** 839-847

Wirtz E, Clayton C (1995) Inducible gene expression in trypanosomes mediated by a prokaryotic repressor. *Science* **268:** 1179-1183

Wirtz E, Hoek M, Cross GA (1998) Regulated processive transcription of chromatin by T7 RNA polymerase in Trypanosoma brucei. *Nucleic acids research* **26:** 4626-4634

Wirtz E, Leal S, Ochatt C, Cross GA (1999) A tightly regulated inducible expression system for conditional gene knock-outs and dominant-negative genetics in *Trypanosoma brucei*. *Molecular and biochemical parasitology* **99:** 89-101

Woese CR, Olsen GJ, Ibba M, Soll D (2000) Aminoacyl-tRNA synthetases, the genetic code, and the evolutionary process. *Microbiology and molecular biology reviews : MMBR* **64:** 202-236

Wolf YI, Aravind L, Grishin NV, Koonin EV (1999) Evolution of aminoacyl-tRNA synthetases--analysis of unique domain architectures and phylogenetic trees reveals a complex history of horizontal gene transfer events. *Genome research* **9:** 689-710

Wolf YI, Rogozin IB, Grishin NV, Tatusov RL, Koonin EV (2001) Genome trees constructed using five different approaches suggest new major bacterial clades. *BMC evolutionary biology* **1:** 8

Woo PT (1970) The haematocrit centrifuge technique for the diagnosis of African trypanosomiasis. *Acta tropica* **27:** 384-386

Wurst M, Robles A, Po J, Luu VD, Brems S, Marentije M, Stoitsova S, Quijada L, Hoheisel J, Stewart M, Hartmann C, Clayton C (2009) An RNAi screen of the RRM-domain proteins of *Trypanosoma brucei*. *Molecular and biochemical parasitology* **163:** 61-65

Wyllie S, Oza SL, Patterson S, Spinks D, Thompson S, Fairlamb AH (2009) Dissecting the essentiality of the bifunctional trypanothione synthetase-amidase in *Trypanosoma brucei* using chemical and genetic methods. *Molecular microbiology* **74:** 529-540

Xiao Y, McCloskey DE, Phillips MA (2009) RNA interference-mediated silencing of ornithine decarboxylase and spermidine synthase genes in *Trypanosoma brucei* provides insight into regulation of polyamine biosynthesis. *Eukaryotic cell* **8:** 747-755

Xong HV, Vanhamme L, Chamekh M, Chimfwembe CE, Van Den Abbeele J, Pays A, Van Meirvenne N, Hamers R, De Baetselier P, Pays E (1998) A VSG expression site-associated gene confers resistance to human serum in *Trypanosoma rhodesiense*. *Cell* **95:** 839-846

Yang H, He X, Zheng Y, Feng W, Xia X, Yu X, Lin Z (2014) Down-regulation of asparagine synthetase induces cell cycle arrest and inhibits cell proliferation of breast cancer. *Chemical biology & drug design* **84:** 578-584

Yarlett N, Bacchi CJ (1988) Effect of DL-alpha-difluoromethylornithine on methionine cycle intermediates in *Trypanosoma brucei brucei. Molecular and biochemical parasitology* **27:** 1-10

Ye J, Kumanova M, Hart LS, Sloane K, Zhang H, De Panis DN, Bobrovnikova-Marjon E, Diehl JA, Ron D, Koumenis C (2010) The GCN2-ATF4 pathway is critical for tumour cell survival and proliferation in response to nutrient deprivation. *The EMBO journal* **29:** 2082-2096

Young SA, Smith TK (2010) The essential neutral sphingomyelinase is involved in the trafficking of the variant surface glycoprotein in the bloodstream form of *Trypanosoma brucei*. *Molecular microbiology* **76:** 1461-1482

Yun O, Priotto G, Tong J, Flevaud L, Chappuis F (2010) NECT is next: implementing the new drug combination therapy for *Trypanosoma brucei gambiense* sleeping sickness. *PLoS neglected tropical diseases* **4:** e720

Zampella EJ, Bradley EL, Jr., Pretlow TG, 2nd (1982) Glucose-6-phosphate dehydrogenase: a possible clinical indicator for prostatic carcinoma. *Cancer* **49:** 384-387

Zhang J, Fan J, Venneti S, Cross JR, Takagi T, Bhinder B, Djaballah H, Kanai M, Cheng EH, Judkins AR, Pawel B, Baggs J, Cherry S, Rabinowitz JD, Thompson CB (2014) Asparagine plays a critical role in regulating cellular adaptation to glutamine depletion. *Molecular cell* **56:** 205-218

Zhang M, Fennell C, Ranford-Cartwright L, Sakthivel R, Gueirard P, Meister S, Caspi A, Doerig C, Nussenzweig RS, Tuteja R, Sullivan WJ, Jr., Roos DS, Fontoura BM, Menard R, Winzeler EA, Nussenzweig V (2010) The *Plasmodium* eukaryotic initiation factor-2alpha kinase IK2 controls the latency of sporozoites in the mosquito salivary glands. *The Journal of experimental medicine* **207:** 1465-1474

Zhang Q, Lee J, Pandurangan S, Clarke M, Pajak A, Marsolais F (2013) Characterization of *Arabidopsis* serine:glyoxylate aminotransferase, AGT1, as an asparagine aminotransferase. *Phytochemistry* **85:** 30-35

Zhang RG, Andersson CE, Skarina T, Evdokimova E, Edwards AM, Joachimiak A, Savchenko A, Mowbray SL (2003) The 2.2 A resolution structure of RpiB/AlsB from *Escherichia coli* illustrates a new approach to the ribose-5-phosphate isomerase reaction. *Journal of molecular biology* **332:** 1083-1094

Zheng S, Haselkorn R (1996) A glutamate/glutamine/aspartate/asparagine transport operon in *Rhodobacter capsulatus*. *Molecular microbiology* **20:** 1001-1011

Ziegelbauer K, Overath P (1993) Organization of two invariant surface glycoproteins in the surface coat of *Trypanosoma brucei. Infection and immunity* **61:** 4540-4545

Zillmann U, Mehlitz D, Sachs R (1984) Identity of Trypanozoon stocks isolated from man and a domestic dog in Liberia. *Tropenmedizin und Parasitologie* **35:** 105-108